NEW ANALYTICAL METHODS FOR DETERMINING TRACE ELEMENTS IN COAL

Leslie S. Dale and Kenneth W. Riley
CSIRO Division of Coal and Energy Technology,
Sydney, NSW, 2234, Australia

Keywords: Coal, trace elements, analytical methods.

ABSTRACT

New and improved analytical methods, based on modern spectroscopic techniques, have been developed to provide more reliable data on the levels of environmentally significant elements in Australian bituminous thermal coals. Arsenic, selenium and antimony are determined using hydride generation atomic absorption or fluorescence spectrometry, applied to an Eschka fusion of the raw coal. Boron is determined on the same digest using inductively coupled plasma atomic emission spectrometry (ICPAES). ICPAES is also used to determine beryllium, chromium, cobalt, copper, manganese, molybdenum, nickel, lead and zinc, after fusion of a low temperature ash with lithium borate. Other elements of concern including cadmium, uranium and thorium are analysed by inductively coupled plasma mass spectrometry on a mixed acid digest of a low temperature ash. This technique was also suitable for determining elements analysed by the ICPAES. Improved methods for chlorine and fluorine have also been developed. Details of the methods will be given and results of validation trials discussed on some of the methods which are anticipated to be designated Australian standard methods.

INTRODUCTION

Increasing attention is being focussed on the potential environmental impact of trace elements, particularly those of environmental concern, associated with electricity production from coal-fired power plants. As a consequence the impact of trace elements on the surrounding ecology from atmospheric emissions and mobilisation in ash dams is coming under increased scrutiny.

Trace elements of concern to the environment and health have been identified by the United States National Research Council[1]. More recently the levels of trace elements in coal have received greater attention with the introduction of legislation, in some countries, which imposes atmospheric discharge limits on a range of environmentally sensitive trace elements. Details of these limits in Australia, Austria, Germany, Italy and the United States of America are given by Clarke and Sloss[2]. Of most significance relating to the impact of trace elements on the environment was the recent amendments to the US Clean Air Act, 1991, which greatly expanded the role of the US Environmental Protection Agency to regulate trace element emissions. Included in the list of 190 hazardous air pollutants were arsenic, antimony, beryllium, cadmium, cobalt, chromium, chlorine, fluorine, mercury, manganese, nickel, lead and selenium together with radionuclides including radon. Although the power industry is not included in the list of source categories, the amendments require the measurement of mercury emissions from coal-fired power plants. The Electric Power Research Institute (EPRI) in the US has carried out a field monitoring project to measure a range of trace elements in the process and discharge streams of power plants to determine the efficiency of control devices to reduce emissions of air toxics[3].

The imposition of stricter controls by regulatory bodies on emissions has focussed attention on the levels of environmentally sensitive elements, particularly those designated as air toxics, in thermal coals. As a consequence of this there is an increasing need to accurately specify the levels of these trace elements to satisfy contractual requirements. Australia is the world's largest exporter of coal and the implications of regulations on trace element emissions are for the development of better quality assurance procedures in the specification of the levels of key environmental trace elements in export thermal coals.

Quality assurance requires the application of validated standard methods which guarantee the accuracy and reliability of the analytical data. The problem is that, in most cases, current standard methods do not have the necessary accuracy to specify the levels of environmentally sensitive trace elements at the concentrations normally present in Australian product thermal coals. One reason for this inadequacy of current standard methods is that they are based on long established analytical techniques such as atomic absorption spectrometry (AAS) which lack the sensitivity to provide the necessary quality assurance. AAS is also a single element technique which, in terms of the number of elements identified as environmentally significant, makes it less cost effective than newer multi-element, simultaneous techniques such as inductively coupled plasma atomic emission spectrometry (ICPAES). Over the past decade this technique has become more readily available in commercial laboratories and its suitability for determining many of the designated trace elements has been established.

In view of the pressing requirements for better quality assurance, new analytical methods based on ICPAES has been developed. The current standard methods based on hydride generation-AAS for arsenic and selenium has been revisited and an improved method, based on atomic fluorescence spectrometry, has provided increased sensitivity for these trace elements. These methods are undergoing validation trials with the anticipation that they will be adopted as new Australian standard methods.

Other techniques have also been used to develop reliable methods. These include inductively coupled plasma mass spectrometry (ICPMS) for a range of trace elements including cadmium, nickel, lead, molybdenum, thorium and uranium. Proton induced gamma ray emission (PIGE) has been applied to the determination of fluorine and X-ray fluorescence spectrometry (XRF) for chlorine.

CURRENT STATUS OF STANDARD METHODS

The performance of current standard methods is shown in table 1 where the lower limits of determination of the methods are compared with the means and range values for the key environmental trace elements in Australian export thermal coals as given by Dale and Fardy[4]. In most cases the current methods are inadequate for determinations at the low range values. For cadmium, cobalt, molybdenum, uranium and thorium no standard methods exist.

Table 1. Mean and Range Values for Trace Elements of Environmental Concern in Australian Export Thermal Coals Compared with Lower Limit of Determination (LLD) of Available Standard Methods

		mg/kg				
		Range		LLD*		
Element	Mean*	Low	High	AS	ASTM	ISO
As	2	<1	7	0.5	1	1
B	17	<5	40	20	-	-
Cd	0.09	<0.05	0.22	-	-	-
Hg	0.06	0.01	0.14	0.01	0.01	-
Mo	1.6	0.25	5.5	-	-	-
Pb	7.5	2.5	13	40	10	-
Se	1	<1	2	-	1	-
Mn	30	3	110	30	-	-
Cr	12	5	27	20	5	-
Cu	12	4	23	50	5	-
Ni	14	<9	39	20	10	-
V	26	10	63	100	10	-
Zn	19	3	53	80	50	-
F	120	40	200	50	10	-
Co	5.3	1.6	14	-	-	-
Cl	200	20	630	100	200	-
Sb	0.54	<0.05	1.5	-	-	-
Be	1.4	0.25	5.5	2	0.5	-
U	1.1	0.3	2.1	-	-	-
Th	3.5	1.1	7.7	-	-	-

* AS - Australian Standard
ASTM - American Society for Testing Materials
ISO - International Organisation for Standardisation

METHOD FOR ARSENIC, SELENIUM AND ANTIMONY

This method is based on the current US standard (ASTM D4606-87) which involves the fusion of the raw coal using Eschka's mixture. The elements arsenic and selenium are determined by hydride generation-AAS using matrix matched standards. The new method uses similar conditions for generation of the hydride. However advantage is taken of the higher sensitivity obtained with atomic fluorescence spectrometry. The method has also been found satisfactory for determining antimony and has been validated by analysis of certified reference materials as shown in Table 2.

Table 2. Results for Arsenic, Selenium and Antimony Obtained on Certified Reference Materials using Hydride Generation Atomic Fluorescence Spectrometry

CRM	Arsenic		Selenium		Antimony	
	mg/kg					
	Certified	Found	Found	Certified	Found	Certified
NIST 1632b	3.70 ± 0.28	3.72 ± 0.12	1.30 ± 0.12	1.29 ± 0.11	0.28 ± 0.02	(0.24)
SARM 19	7.65 ± 0.10	7 ± 1	1.12 ± 0.06	1	-	-
SARM 20	-	-	0.75 ± 0.04	0.8 ± 0.2	-	-

This method is currently undergoing validation tests in an interlaboratory trial and is anticipated to be adopted as an Australian standard method.

METHOD FOR BORON

The method developed is based on the Eschka fusion procedure used for arsenic, selenium and antimony. The element is determined using ICPAES using matrix matched standards. The method was validated using South African reference coals as demonstrated by the following results.

Table 3. Results for Boron Obtained on an SARM Reference Coal

	mg/kg	
CRM	Found	Indicated*
18	28	30
19	94	90
20	84	90

* Values are not certified.

This method is also undergoing validation tests and is anticipated to be adopted as an Australian standard.

ICPAES METHOD FOR TRACE ELEMENTS

This method is based on fusion of a 450°C ash of the coal with a mixture of 1 part lithium metaborate to 3 parts lithium tetraborate. The elements chromium, copper, zinc, vanadium, manganese, nickel, cobalt, molybdenum, lead and beryllium are determined using ICPAES with matrix matched standards.

The method has been validated using NIST 1632b and is currently undergoing validation tests in an interlaboratory trial. It is anticipated to be adopted as an Australian standard method.

TRACE ELEMENTS BY ICPMS

This technique has gained popularity over the past decade because of its very high sensitivity and multi-element capability. It has been applied, in this laboratory, to the determination of a wide range of trace elements in coal. The method developed is based on dissolution of a 450°C ash of the coal using a mixture of nitric-hydrochloric-hydrofluoric acids. The elements are determined using appropriate internal standard elements (indium, thallium and enriched stable isotopes of chromium-53 and zinc-68).

This technique has been found suitable for determining a wide range of environmental trace elements including uranium, thorium, cadmium, antimony, lead, nickel, arsenic, beryllium, chromium, cobalt, copper, zinc, vanadium and molybdenum. Of particular significance is the ability to analyse for cadmium, uranium, and thorium (detection limits 0.01, 0.005 and 0.005 mg/kg respectively). There are no standard methods available for these elements because of their low abundances in coal and the lack of sensitivity of more conventional techniques. Cadmium however could possibly be analysed by graphite furnace-AAS.

Although ICPMS instruments are expensive the technique is finding increased popularity in commercial laboratories. It is expected that its application to the determination of trace elements

in coal will receive greater attention because of its high sensitivity and multi-element capability which makes it cost effective.

METHOD FOR CHLORINE

Current methods for chlorine are based on oxygen bomb digestion or fusion followed by determination by ion-selective electrode (AS 1038.8.1, ASTM D4208). There are however, recognised problems with these methods. These relate to the recovery of the chlorine during the sample destruction and the lack of sensitivity of the ion-selective measurement. Evidence of the problems has been highlighted in international interlaboratory comparisons such as the CANSPECS program organised by Energy Resources Canada. The extreme variability of results by laboratories using the same standard method suggests that these methods lack the reliability required by standard methods. This variability is of great concern to Australian coal producers because of disputes that occur between suppliers and buyers.

In recognition of the problems with current methods, a procedure is being developed based on X-ray fluorescence spectrometry (XRF). This procedure has the advantage that it analyses the raw coal and is therefore non-destructive thereby overcoming one of the main deficiencies of current methods.

The suitability of the XRF procedure has been verified by comparison with results obtained by instrumental neutron activation analysis (see Table 4). The lower limit of determination of the XRF method is 30 mg/kg which is below the low range value for Australian coals. Analysis of the NIST 1632b CRM gave a value of 1190 mg/kg which compares favourably with the indicated value of 1230 mg/kg. The new method requires minimal sample preparation (grinding to less than 75 μm and the addition of an internal standard) and is cost effective on the basis of its high sample throughput compared to current standard methods.

Table 4 - Comparison of Chlorine Results Obtained on Coals by XRF and INAA

	Cl (mg/kg)	
Sample	XRF	INAA
1	250	235
2	450	410
3	505	495
4	670	610
5	970	1075

METHOD FOR FLUORINE

The standard method for determining this element is based on destruction of the raw coal by pyrohydrolysis followed by determination with an ion-selective electrode (AS 1038.10.4). This method has limitations in that the problems are associated with the liberation of the fluorine from the sample and the rather poor sensitivity of the ion-selective electrode at the levels normally encountered in coals.

The method used in our laboratory is based on proton induced gamma ray emission using the 2MV van der Graaf accelerator available through the Australian Nuclear Science and Technology Organisation. Previous work[5] has verified the application of this technique to the analysis of coal for fluorine. It is based on the irradiation of the raw coal with high energy protons in which the fluorine atoms produce characteristic g-rays. It is therefore non-destructive. Analysis of the NIST 1632a CRM gave a mean value of 183 mg/kg with a standard deviation of 10 mg/kg (12 determinations). The accepted value for this CRM is 178 mg/kg. The detection limit is 5 mg/kg.

PERFORMANCE OF NEW METHODS

The new methods provide the necessary sensitivity to meet the requirements for determining a range of key environmental trace elements in Australian coals. This is demonstrated in Table 5 which compares the lower limit of determination of the new methods and the current standard methods. For most elements, the new methods provide the capability for reliably analysing Australian coals at the levels normally present.

Validation trials are currently in progress involving a number of participating commercial laboratories. Preliminary data suggests that the methods for arsenic, selenium and antimony based on the hydride generation-AFS technique will meet the requirements for acceptance as a standard method as required by Standards Australia. Similar agreement between laboratories for

the boron and ICPAES methods suggests that these will become standard methods. Future efforts will be directed towards the establishment of an Australian standard method based on ICPMS which would account for cadmium, uranium and thorium.

The methods used for chlorine and fluorine are presently considered as reference methods. There needs to be a revision of current methods in view of the discrepancies which occur between laboratories.

Table 5 - Lower Limits of Determination (LLD) for Trace Elements with New Analytical Methods Compared with Standard Methods and the Means and Range Values in Australian Export Thermal Coals

	mg/kg				
	Mean	Range		LLD	
Element		Low	High	New Method	Standard Method
As	2	<1	7	0.03	0.4
B	17	<5	40	3	20
Cd	0.09	<0.05	0.22	0.01	-
Mo	1.6	0.25	5.5	0.2	-
Pb	7.5	2.5	13	0.2	10
Se	1	<1	2	0.03	1
Mn	30	3	110	0.02	-
Cr	12	5	27	0.1	5
Cu	12	4	23	0.2	5
Ni	14	<9	39	2	10
V	26	10	63	0.2	10
Zn	19	3	53	0.2	50
Co	5.3	1.6	14	0.2	-
Cl	200	20	650	50	200
Sb	0.54	<0.05	1.5	0.03	-
Be	1.4	0.25	5.5	0.01	-
U	1.1	0.3	2.1	0.03	-
Th	3.5	1.1	7.7	0.03	-
F	120	40	200	20	50

SUMMARY

The new methods provide adequate sensitivity to reliably determine a range of key environmental trace elements in Australian coals. These methods are based on modern instrumentation which is generally available in commercial laboratories. These new methods address the need for better quality assurance in the specification of trace elements in export coals. This has been as a direct result of increasing concern on the environmental impact of trace elements from coal-fired power plants.

ACKNOWLEDGEMENT

This work was supported by a grant from the Australian Coal Association Research Program (Grant No. C3015).

REFERENCES

1. United States National Research Council. PECH Report, National Academic Press, Washington, D.C. 1980.
2. Clarke, L.B and Sloss, L.L., International Energy Agency Report IEACR/49, London, 1992.
3. Boutacoff, D., EPRI Journal, 5-13, Mar. 1991.
4. Dale, L.S., Lavrencic, S.A. and Fardy, J.J., NERDDP Report EG91/1005, 1991.
5. Clayton, E. and Dale, L.S., Anal. Lett., 18, 1533-1538, 1985.

INVESTIGATION OF THE BEHAVIOR OF POTENTIALLY HAZARDOUS TRACE ELEMENTS IN KENTUCKY COALS AND COMBUSTION BYPRODUCTS

J.D. Robertson, L.J. Blanchard, S. Srikantapura,
B. K. Parekh, and C.J. Lafferty
Department of Chemistry and Center for Applied Energy Research
University of Kentucky
Lexington, KY 40506-0055

Keywords: Trace elements, coal cleaning, PIXE

INTRODUCTION

The minor- and trace-element content of coal is of great interest because of the potentially hazardous impact on human health and the environment resulting from their release during coal combustion. Of the one billion tons of coal mined annually in the United States, 85-90% is consumed by coal-fired power plants.[1] Potentially toxic elements present at concentrations as low as a few µg/g can be released in large quantities from combustion of this magnitude. Of special concern are those trace elements that occur naturally in coal which have been designated as potential hazardous air pollutants (HAPs) in the 1990 Amendments to the Clean Air Act.[2]

The principle objective of this work was to investigate a combination of physical and chemical coal cleaning techniques to remove 90 percent of HAP trace elements at 90 percent combustibles recovery from Kentucky #9 coal. Samples of this coal were first subjected to physical separation by flotation in a Denver cell. The float fraction from the Denver cell was then used as feed material for hydrothermal leaching tests in which the efficacy of dilute alkali (NaOH) and acid (HNO_3) solutions at various temperatures and pressures was investigated. The combined column flotation and mild chemical cleaning strategy removed 60-80% of trace elements with greater than 85% recovery of combustibles from very finely ground (-325 mesh) coal. The elemental composition of the samples generated at each stage was determined using particle induced X-ray emission (PIXE) analysis. PIXE is a rapid, instrumental technique that, in principle, is capable of analyzing all elements from sodium through uranium with sensitivities as low as 1 µg/g.

EXPERIMENTAL PROCEDURE

Sample Preparation

A sample of run of mine coal from the Kentucky #9 seam was collected at the mine site, and split into subsamples as needed. Each subsample was then ground to -325 mesh and a 5% (w/v) slurry was prepared. The slurry was subjected to Denver floatation, and the float fraction was employed as the feed sample for hydrothermal leaching using either a NaOH or HNO_3 solution in a 1 liter autoclave reactor. The duration, temperature, and pressure of the chemical leaching process were varied to ascertain their influence, if any, on the removal of trace elements. Each clean coal sample was dried at 50°C overnight, and pressed into a 1 mm x 19 mm pellet for elemental analysis.

PIXE Analysis

A schematic of the PIXE analysis system at Element Analysis Corporation is shown in Figure 1. A dual energy irradiation is performed on each sample with the X-ray detector in two positions for data collection. During the high-energy (2.1 MeV) irradiation, the detector is in a close-in position with a thick absorber and during the low-energy (1.6 MeV) irradiation, the detector is in a backed-out position with no absorber. Variable charge collection at these two energies/positions allows for spectrum balance and flexibility in the analysis on either the high- or low-energy ends of the X-ray spectrum.

Protons enter the target chamber by passing through a 0.30 mil Kapton window and the X-rays exit through a 0.1 mil Mylar window that is at 45 degrees relative to the beam. The beam, which is at an angle of 23° relative to the sample surface, is swept over the target to irradiate a 16 mm diameter area. The sample chamber is flushed with helium at atmospheric pressure to reduce sample heating and charging and each sample is irradiated for 15 minutes. A typical PIXE spectrum of a coal sample is shown in Figure 2. Data analysis is performed using a modified version of the GUPIX[3] PC-based software package. In order that the accuracy and precision of the measurements may be assessed, the results for the PIXE analysis of 7 samples of the NIST 1635a Subbituminous Coal standard reference material are presented in Table 1.

RESULTS & DISCUSSION

In general, HNO_3 was more effective than NaOH in reducing elemental concentrations for all elements except V and Ga. The increase in the concentration of Cu and Cr in certain tests was attributed to corrosion of fittings in the autoclave reactor.

Table 1. Results for NIST SRM 1635a Subbituminous Coal

Element	PIXE Result[a]	Certified Value[b]
Sodium	0.21 ± 0.02 %	(0.24 ± 0.02 %)
Magnesium	760 ± 71 ppm	(1040 ± 130 ppm)
Aluminum	0.30 ± 0.02 %	(0.29 ± 0.03 %)
Silicon	0.60 ± 0.03 %	(0.59 ± 0.05 %)
Sulfur	0.39 ± 0.02 %	0.33 ± 0.03 %
Potassium	113 ± 11 ppm	(96 ± 16 ppm)
Calcium	0.69 ± 0.02 %	(0.54 ± 0.03 %)
Titanium	213 ± 8 ppm	(202 ± 6 ppm)
Chromium	1.2 ± 0.9 ppm	2.5 ± 0.3 ppm
Manganese	19.8 ± 1.2 ppm	21.4 ± 1.5 ppm
Iron	0.23 ± 0.01 %	0.239 ± 0.005 %
Nickel	Below LOD	1.74 ± 0.10 ppm
Copper	3.1 ± 0.2 ppm	3.6 ± 0.3 ppm
Zinc	4.6 ± 0.9 ppm	4.7 ± 0.5 ppm
Selenium	Below LOD	0.9 ± 0.3 ppm
Bromine	1.3 ± 0.3 ppm	(1.4 ± 0.4 ppm)
Strontium	129 ± 9 ppm	(121 ± 19 ppm)

[a]Average and standard deviation of the analysis of 7 samples
[b]Values in parentheses are the recommended or consensus values

The degree to which elements are removed by coal cleaning processes depends to a great extent on their mode of occurrence or chemical association in the coal. Although the exact composition can vary greatly from one coal to the next, generalizations have been made concerning common modes of occurrence for trace elements in coal.[4] For example, the fact that Mg, Ca, Mn, and Sr have a carbonate association would explain their efficient removal since the solubilities of carbonates increase in acidic solutions. Moreover, elements known to have an association with pyrite, Fe, S, As, Zn, Ni, and Ga, all show a significant decrease in concentration. Similarly, a considerable reduction in elements known to be strongly associated with silicates, Si, Al, Mg, and K, was observed. Elements thought to have a significant organic association were removed less efficiently by HNO_3. In these samples, those elements were V, Cr, Ti, and Cu. X-ray absorption fine structure spectroscopy of Kentucky #9 coal has indicated a partial organic association for V, Cr, and Ti. Although the association of Cu has not been determined in these samples, Cu is known to have partial organic associations in other coals.

An increase in the duration and pressure of the hydrothermal leaching process showed negligible improvement in the reduction of elemental concentrations for some elements and only slight improvements for others. Thus, it appears these variables have minimal impact on the effectiveness of this coal cleaning process.

SUMMARY

The variable with the greatest impact on hydrothermal leaching appears to be the leaching agent itself. A significant reduction in the concentration of many elements was observed with the use of 2% HNO_3. On the other hand, increasing the reaction time from 15 minutes to 1 hour and/or the vessel pressure from 100 psi to 300 psi had only a slight impact on the removal of hazardous elements in coal.

ACKNOWLEDGEMENTS

This work was supported by the U. S. DOE and the Kentucky EPSCoR Program. In addition, the authors would like to thank Element Analysis Corporation for the use of their PIXE system.

REFERENCES

1. 1992 Keystone Coal Industry Manual, MacLean Hunter Publications, Chicago, IL (1992).

2. Amendments to the Clean Air Act, U.S. Public Law 101-549; U.S. Government Printing Office: Washington DC, Nov. 15, 1990, 314 pp.

3. Maxwell, J. A.; Campbell, J. L.; Teesdale, W. J. *Nuclear Instrumentation and Methods* **1989**, *B43*, 218.

4. Finkelman, R. B. *Fuel Processing Technology* **1994**, *39*, 21.

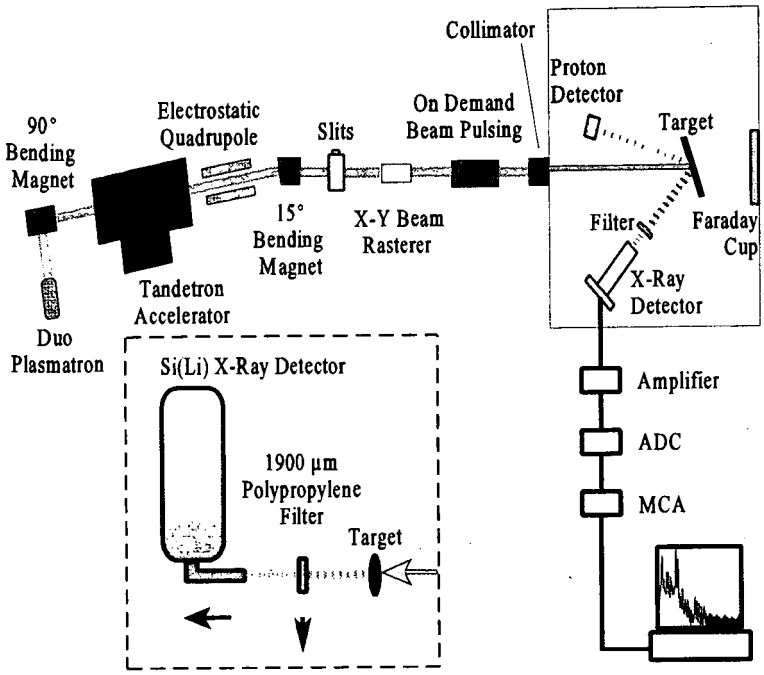

Figure 1. Schematic diagram of PIXE system.

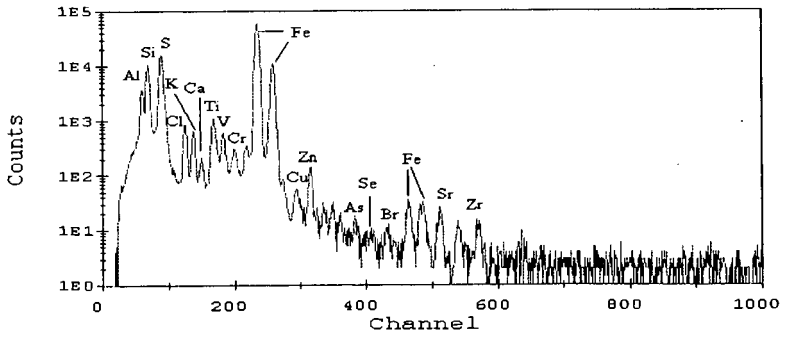

Figure 2. Typical PIXE spectrum of coal.

XANES SPECTROSCOPIC CHARACTERIZATION OF SELECTED ELEMENTS IN DEEP-CLEANED FRACTIONS OF KENTUCKY #9 COAL

Frank E. Huggins[1], Srikanta Srikantapura[1,2], B. K. Parekh[2],
Lori Blanchard[3], and J. David Robertson[2,3]

[1]Department of Chemical and Materials Engineering,
[2]Center for Applied Energy Research, and [3]Department of Chemistry,
University of Kentucky, Lexington, KY 40506

Keywords: Trace elements in coal, modes of occurrence, XAFS spectroscopy

INTRODUCTION

Cleaning of pulverized (-200 mesh) coal is a potentially cost-effective strategy for removing mineral matter and associated minor and trace elements from coal prior to combustion, thereby minimizing the release of pollutants to the atmosphere during combustion. Of special concern are those trace elements designated as potential hazardous air pollutants (HAPs) in the 1990 Amendments to the Clean Air Act[1]. Various physical and chemical cleaning methods have been examined with regard to their efficiency for removal of trace elements from coal. Although the mode of occurrence is recognized to be a key factor in determining the behavior of a given element with respect to a specific cleaning method, no study, as far as we are aware, has attempted to include such information.

In this study, a finely ground sample of Kentucky #9 coal from the Illinois coal basin region in western Kentucky has been subjected to a combination of physical cleaning and chemical leaching methods. Each generated fraction has then been characterized using proton-induced X-ray emission (PIXE) spectroscopy to determine the bulk chemical composition and X-ray absorption fine structure (XAFS) spectroscopy to determine information relevant to the elemental mode of occurrence for selected elements. As we will show, inclusion of the mode of occurrence information explains much of the variable efficiency exhibited with respect to the cleaning process by different elements. Conversely, the superior efficiency of column flotation for removal of mineral matter from clean coal provides samples in which the elements exist almost entirely in organic association. Such samples have proven to be invaluable for generating the XAFS spectral signatures for elements in organic association.

EXPERIMENTAL

(a) Coal Cleaning Studies: A 50 kilogram sample of Kentucky #9 coal was made available for this study by the Big Rivers Utility company. The coal, originally consisting of 1" lumps, was dried and crushed to 28 mesh. A representative kilogram sample of the 28 mesh coal was then ground to 80% passing 60 mesh, from which two head samples of 150 grams each were prepared and submitted for analysis. Samples were then prepared for gravity separation testing and release analysis, the results of which are described elsewhere[2].

A representative sample was then ground to 90% passing 325 mesh to constitute the fine coal sample. Aliquots of this sample were subjected to separation by flotation in a Denver cell and also in a 2"-diameter "Ken-Flote" column[3] into float and tailings fractions. The float fraction from the Denver cell was then used as feed for hydrothermal leaching tests that were conducted in a 1 liter autoclave at 110°C and 300 psi. Four samples were prepared: samples were exposed for 15 and 60 minutes to either a 10% acid (H_3PO_4) or basic (NaOH) medium. The overall sample scheme and sample labelling notation are shown in Figure 1. Sufficient samples of each fraction were obtained for proximate analysis, chemical analysis by PIXE spectroscopy, and element speciation analysis by XAFS spectroscopy.

(b) PIXE Spectroscopic Analysis: Each generated sample in the scheme shown in Figure 1 was analyzed by thick-target PIXE spectroscopy using the dual-energy irradiation procedure[4]. NIST coal and fly-ash SRMs were used to monitor the accuracy and precision of the trace element measurements. Results for the SRMs and detection limits for the PIXE measurements are given elsewhere[4]; further details of PIXE analysis can be found in the preceding paper in this volume.

(c) XAFS Spectroscopic Analysis: XAFS spectroscopy of selected elements in the samples generated according to the scheme shown in Figure 1 was carried out either at the National Synchrotron Light Source (NSLS) in Brookhaven National Laboratory, NY, or at the Stanford Synchrotron Radiation Laboratory (SSRL) at Stanford University, CA. Similar experimental procedures were used at both of these facilities; these procedures have been described in detail in previous publications[5,6]. The XAFS spectra from elements in coal were collected in fluorescence geometry using a thirteen-element germanium detector developed principally for

trace element investigation[7]. Spectra were obtained typically from 100 eV below the K-edge of the element under investigation to as much as 500 eV above the edge. As is usually done, the XAFS spectra were subdivided into separate X-ray absorption near-edge structure (XANES) and extended X-ray absorption fine structure (EXAFS) regions. In many instances, particularly when the concentration of the element was less than about 50 parts-per-million (ppm), the EXAFS signal was too weak to be reliably interpreted and interpretation of the mode of occurrence of an element was based exclusively on the XANES region.

The XANES spectra shown in this paper have been prepared from the raw XAFS spectroscopic data in the usual manner: the spectra are first normalized to the edge step and any slope in the data is removed by fitting spline functions to the pre-edge and post-edge regions and subtracting the pre-edge background extended beneath the overall spectrum. Each spectrum shows a zero-point of energy that is defined by the position of the same absorption edge in a standard material, the spectrum of which is collected at the same time as the spectrum from the coal. For the elements discussed in this paper, these zero points are defined in standard materials as follows: potassium (3608.4 eV, KCl), calcium (4038.1, calcite $CaCO_3$), titanium (4966 eV, Ti metal foil), vanadium (5465 eV, V metal foil), chromium (5989 eV, Cr in stainless steel), manganese (6539 eV, Mn metal foil), arsenic (11867 eV, As_2O_3). ^{57}Fe Mössbauer spectroscopy, rather than Fe XAFS spectroscopy, was used to examine the different forms of iron in some of the fractions shown in Figure 1 because this method is more definitive for elucidating details regarding the iron minerals present in coal.

Table 1: PIXE Analytical Data for Head, Float and Tailings Samples from Denver Cell and "Ken-Flote" Column Flotation Tests

	Sample				
	Head	DC-1	DC-2	CF3-1	CF3-2
Wt fraction, wt%	100.00	72.33	27.67	83.17	16.83
Ash content, wt%	18.29	5.69	50.88	3.56	84.20
Sulfur, wt%	2.96	2.25	5.49	2.94	6.29
Elements in ppm					
Na	5010	2523	--	4233	5852
Mg	5392	2381	10006	3456	20743
Al	19463	8479	57138	11705	103127
Si	45258	15197	129760	17462	222744
S	29095	22446	54905	19432	62873
Cl	3632	1113	--	1529	244
K	4181	1418	10019	1135	15962
Ca	2597	1592	34524	1107	41068
Ti	1249	931	2430	711	2797
V	159	59	187	36	133
Cr	40	31	84	19	98
Mn	37	43	491	21	401
Fe	18173	13465	78278	8612	55967
Ni	21	25	67	19	55
Cu	8	17	47	12	44
Zn	47	20	154	13	108
Ga	7	5	11	3	10
As	10	14	100	10	50
Br	22	26	27	12	12
Sr	41	21	75	15	23

RESULTS AND DISCUSSION

A. Cleaning Efficiency:

Coal characterization data and PIXE analysis data on elemental concentrations are summarized for the different float and tailings fractions in Table 1. The two flotation methods are both efficient at separating the inorganic matter from organic matter, but the column flotation test is definitely the better of the two methods. This is also illustrated in Figure 2, which provides a direct comparison of the two methods. In general, the float/tailings difference indicators in this figure are longer for the column flotation method than for the Denver cell method for most of the elements. It is also instructive to examine the tailings/float concentration ratio for individual elements (or equivalently comparing the length of the indicators in Figure 2) to that for the

overall ash. The elements that exceed or equal the overall ash ratio are Ca and Mn; those that are slightly less than the overall ash ratio are Al, Si, K, and Zn in both tests, and Fe along with As in the case of the Denver cell test. Not surprisingly, sulfur shows a small value for the ratio because over 40% of the element is organically bound. However, there is a group of elements consisting of Ti, V, Cr, Ni, Ga, that also have relatively short indicators, suggesting that significant fractions of these elements might also be in organic association.

Attempts to mass balance individual elements in these flotation experiments vary from good to poor and certainly the differences for a number of elements are much larger than can be attributed to experimental errors in the PIXE analysis. The most significant problem would appear to be segregation of the heavy minerals (pyrite, calcite) in the feed sample as the largest variations between the flotation experiments are exhibited by calcium, manganese and iron. In particular, the calculated feed composition for the column flotation experiment has significantly lesser amounts of these elements and somewhat more Al and Si (derived from excess clays?) than that for the Denver cell flotation test.

B. The Lithophile Elements:
XANES spectra of Ti, V, Cr, and Mn showed quite different spectra for the float and tailings fractions (e.g for Mn, Figure 3). Whereas the XANES spectra of the tailings fractions could be attributed to principally (>80%) illite for Ti, V and Cr, and to a mixed mineralogical occurrence for Mn (25% Mn/illite and 75% Mn/calcite), the spectra of the float fractions did not match the spectra of any mineral standard examined and distinct organically associated forms were inferred to exist for these four elements. For Ti and Cr, the closest matches appeared to be a poorly crystalline oxide or oxyhydroxide, a possibility raised in earlier studies[8] of V in Kentucky #9 coal. For Mn, the spectrum of the float fraction was altered significantly by application of both the base and acid leaching tests and the Mn content was also reduced in both tests. This suggested the presence of two organically associated forms of Mn: one that was soluble in acid; the other soluble in base.

Examination of the XANES spectra of calcium, a major element, also showed distinctly different spectra for the tailings and float fractions. The spectra of the tailings fractions were clearly dominated by Ca as calcite, whereas the spectra of the float fractions were similar to that observed for carboxyl-bound Ca in low-rank coals[9]. Interestingly, K XANES spectra of all fractions, whether float or tailings, were identical to that of K in illite. The fact that illitic Ti, V, and Cr spectra were only seen for the tailings fraction and not for the float fraction suggests that there are two generations of illite in the coal: one generation is coarse and/or easily separated from the coal (e.g. partings) and contains all of the minor elements; the other generation is fine, can not be separated easily from the organic matter, and is essentially devoid of significant Ti, V, and Cr. These two illite forms might represent coarse detrital and fine-grained authigenic generations of illite in the coal, respectively.

C. The Chalcophile Elements:
In contrast to the lithophile elements, the two chalcophile elements examined, Fe and As, were found in the same forms in both the tailings and float fractions. Both Fe and As are found in association with pyrite and its oxidation products in all fractions. Arsenic occurs as a substitutional replacement for sulfur in the pyrite structure and as arsenate. The arsenate form is more prevalent in the float fractions (Figure 4), consistent with the fact that smaller particle sizes of pyrite are both more likely to be found in the float fractions and to be more oxidized than large particle sized pyrite. The Mössbauer data for iron tells a very similar story. Iron in oxidized form (principally jarosite) is relatively more common compared to iron as pyrite in the float fractions than in the tailings fractions. There is an approximate linear correlation between the fraction of oxidized arsenic and the fraction of Fe as jarosite for all the samples examined. This relationship would imply perhaps that the arsenate is incorporated in the jarosite structure, presumably by substitution of the arsenate group for the sulfate group in the jarosite structure.

CONCLUSIONS

The results of this study demonstrate convincingly that Ca, Ti, V, Cr and Mn in Kentucky #9 coal occur in both a mineralogical and an organic association. For Ti, V, and Cr the mineralogical association consists principally of substitution in the cation layers in the clay mineral illite, whereas Mn substitutes mainly for Ca in calcite, which is the major mineral occurrence for calcium. The organic association has not been so clearly identified, but is consistent with the elements present in oxygen coordination, either at individual isolated ion-exchange sites on maceral surfaces, or in microparticles of poorly crystalline oxide or oxyhydroxide minerals. For Ti, V, and Cr, this organic association represents approximately 50% of the occurrence of these elements in this particular sample of Kentucky #9 coal. In contrast to the five lithophile elements, the chalcophile elements, Fe and As, appear to occur almost

exclusively in pyrite or its oxidation products in all fractions of this coal. Such occurrences readily explain the relatively poor separation of some of these elements (Ti, V, Cr) in flotation tests.

Finally, this investigation demonstrates that information on elemental modes of occurrence from XAFS spectroscopy is a very useful supplement for the interpretation and understanding of results from coal cleaning studies. Conversely, the mineral-rich and mineral-poor fractions generated in the course of such studies provide the means for a much better understanding of elemental occurrences based on XAFS spectroscopy. This serendipitous relationship will be exploited for investigation of other coals and cleaning processes.

ACKNOWLEDGEMENTS

This work is supported by a grant from the Commonwealth of Kentucky/U.S. Department of Energy EPSCoR program. FEH gratefully acknowledges the assistance of M. Najih, J. Zhao, N. Shah, and F. Lu with the XAFS data collection at NSLS and SSRL, and of K.R.P.M. Rao with the Mössbauer measurements. Element Analysis Corporation is acknowledged for the use of their accelerator for the PIXE measurements. The U.S. Department of Energy is further acknowledged for its support of the synchrotron facilities at both NSLS and SSRL.

REFERENCES

1. Amendments to the Clean Air Act, *U.S. Public Law 101-549*; U.S. Government Printing Office: Washington DC, Nov. 15, 1990; 314 pp.
2. Srikantapura, S. "*Removal of Trace Elements from Coal by Advanced Physical and Chemical Techniques*", M.Sc. Thesis, University of Kentucky, 1996.
3. Parekh, B.K.; Stotts, W.F.; Groppo, J.G. In *Processing and Utilization of High-Sulfur Coals III, Coal Science and Technology*, **16**, Elsevier: Amsterdam, 1990, 197-208.
4. Blanchard, L.J.; Robertson, J.D.; Srikantapura, S.; Parekh, B.K.; Huggins, F.E. *Preprints, ACS Div. Fuel Chem.* **40(4)**, *1995*, 828-832.
5. Huggins, F.E.; Shah, N.; Zhao, J.; Lu, F.; Huffman, G.P. *Energy Fuels* **7**, *1993*, 482-489.
6. Huffman, G.P.; Huggins, F.E.; Shah, N.; Zhao, J. *Fuel Proc. Technol.* **39**, *1994*, 47-62.
7. Cramer, S.P.; Tench, O.; Yocum, N.; George, G.N. *Nucl. Instrum. Meth.* **A266**, *1988*, 586-591.
8. Maylotte, D.H.; Wong, J.; St. Peters, R.L.; Lytle, F.W.; Greegor, R.B. *Science*, **214**, *1981*, 554-556.
9. Huffman, G.P.; Huggins, F.E. In *The Chemistry of Low-Rank Coals*; Schobert, H.H., Ed; ACS Symposium Series, **264**, *1984*, 159-174.

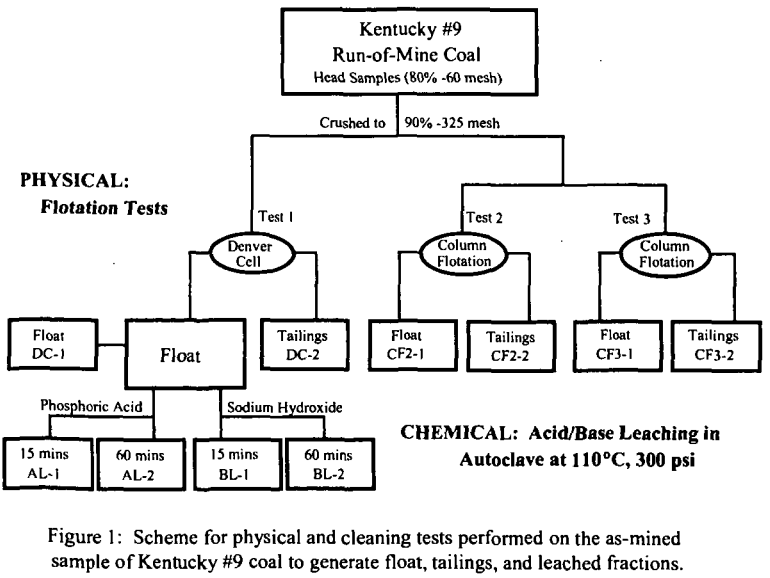

Figure 1: Scheme for physical and cleaning tests performed on the as-mined sample of Kentucky #9 coal to generate float, tailings, and leached fractions.

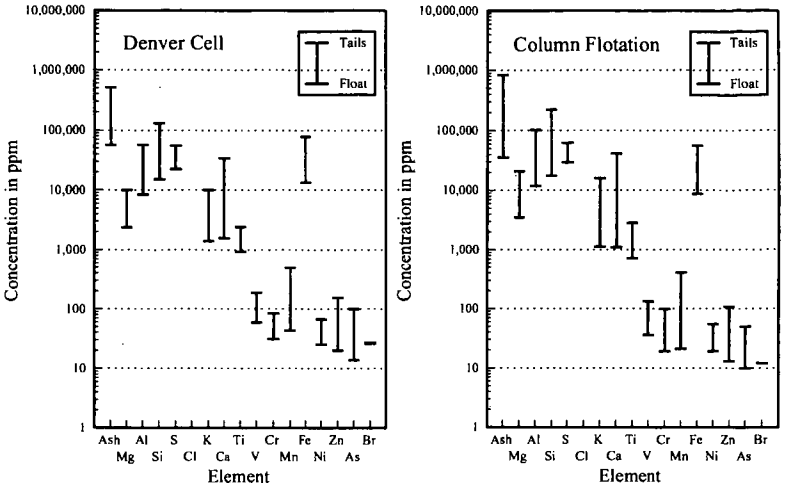

Figure 2: Comparison of the relative efficiency of the segregation of elements in Kentucky #9 coal between float and tailings fractions generated in the Denver cell test and in the "Ken-Flote" column flotation test.

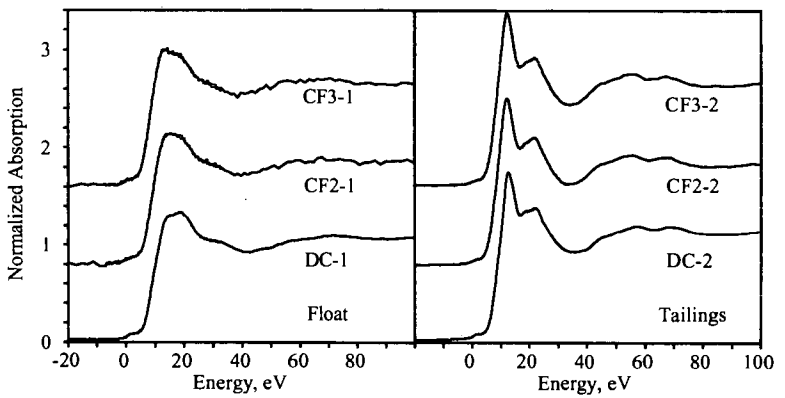

Figure 3: Mn XANES spectra of float and tailings fractions of Kentucky #9 coal.

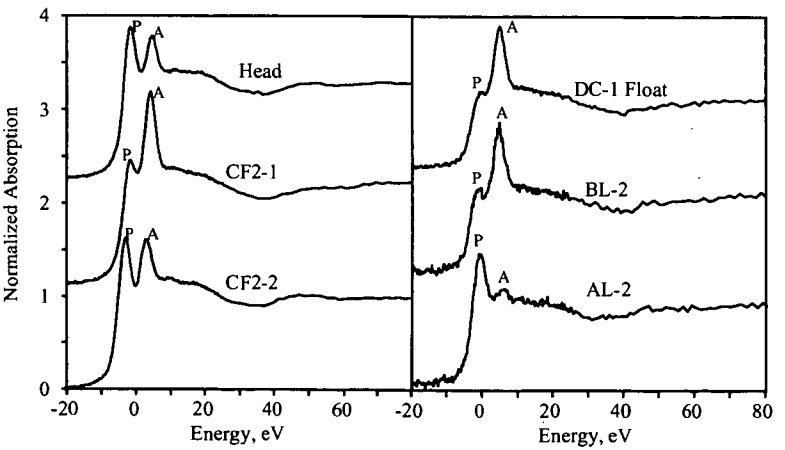

Figure 4: As XANES spectra of various fractions of Kentucky #9 coal.

WASHABILITY OF AIR TOXICS IN MARKETED ILLINOIS COALS

I. Demir[1], R. R. Ruch[1], R. A. Cahill[1], J. M. Lytle[1], and K. K. Ho[2]
[1]Illinois State Geological Survey, Champaign, IL 61820
[2]Illinois Clean Coal Institute, Carterville, IL 62918

Key words: hazardous air pollutants, Illinois coals, washability

INTRODUCTION AND BACKGROUND

The 1990 Clean Air Act Amendments (CAA) require that the health risks resulting from the atmospheric emissions of 189 hazardous air pollutants (HAPs) from various industrial sources be assessed and, if needed, emission limits be established [U.S. Public Law 101-549, 1990]. Of these 189 HAPs, 16 elements (As, Be, Cd, Cl, Co, Cr, F, Hg, Mn, Ni, P, Pb, Sb, Se, Th, U) occur in coal in trace or minor quantities, and may be emitted into the atmosphere during combustion. Electrical utilities are presently exempt from compliance with the CAA requirements for HAPs. This may, however, change after the U.S. Environmental Protection Agency (EPA) completes its risk analyses and promulgates emission standards as prescribed by law.

The U.S. Geological Survey (USGS) has a substantial amount of data on HAPs in channel samples of coals from various regions of the U.S. The U.S. EPA will use this database for its risk assessment of HAPs emissions from coal-fired power plants. Because Illinois coals shipped to utilities are cleaned at conventional preparation plants, and conventional cleaning decreases levels of most HAPs in marketed Illinois coals relative to channel samples [Demir et al., 1994a], the USGS data on channel samples would overestimate the emission of HAPs from combustion of these coals at utilities.

Recent reviews of the environmental aspects of trace and minor elements in coal (Swaine, 1989; Clarke and Sloss, 1992; Wesnor, 1993) indicated that (1) modern pollution control systems can trap up to more than 90% of fly ash generated during coal combustion and (2) trace elements that "escape" during combustion are either emitted in gas phase or attached to ultrafine fly ash particles that are not captured by the pollution control systems. Highly volatile HAP elements (Hg, Cl, F) are mostly or partially volatilized in the flue gas, while less volatile ones (As, Cd, Pb, P, Sb) generally vaporize, oxidize, and then, upon cooling, condense onto the fly ash particles (Fig. 1). The least volatile HAPs (Mn, Th) are enriched in bottom ash and slag. Other HAPs (Se, Be, Co, Cr, Ni, U) exhibit mixed behavior depending on their mode of occurrence in the feed coal, the characteristics of coal and mineral matter, and types and operational conditions of combustion units.

Coal cleaning is an attractive alternative to costly post-combustion control of air toxics emissions from power plants. Reviews that summarized progress in the removal of trace and minor elements, including HAPs, via coal cleaning include Mezey [1977], National Research Council [1979, 1980], Wheelock and Markuszewski [1981, 1984], Streeter [1986], Kaiser Engineers [1989], Jacobsen et al. [1992], and Norton et al. [1986, 1989, 1992]. These reviews show that physical coal cleaning can be economical and effective for significantly decreasing the content of most HAPs prior to combustion. In general, physical cleaning becomes efficient if a high degree of comminution is utilized to free mineral matter from the macerals. Those elements associated (either physically disseminated or bonded chemically) with the macerals are not easily removed; in some cases, their concentrations may actually be enhanced in the cleaned coal. Recent studies [Paul and Honaker,1994; Honaker and Reed 1994] indicated that mineral matter content of finely ground Illinois Basin coals can be effectively decreased using advanced gravity separators.

It has been generally recognized that the cleaning efficiency of gravity separators for fine-sized coal cannot be estimated from conventional, static float-sink (F-S) tests. Centrifugal F-S procedures, however, could successfully predict the cleanability of -28-mesh (<0.589-mm) size coal [Harrison, 1986; Franzidis and Harris, 1986; Cavallaro and Killmeyer, 1988; Ho and Warchol, 1988; Bosold and Glessner, 1988; Dumm and Hogg, 1988; Suardini, 1993].

The purpose of this study was to generate F-S washability data to estimate how much more the HAP content of marketed Illinois coals can be decreased if advanced gravity-based coal cleaning was used at coal preparation plants. Washability data for twelve HAP elements (As, Be, Co, Cr, Mn, Ni, P, Pb, Sb, Se, Th, U) in 27 coal samples ground to -100 mesh (<149 μm) and in 8 coal samples ground to -200 mesh (<74 μm) are reported and discussed.

EXPERIMENTAL

Samples and Sample Preparation

Each of the 27 samples of marketed coals was collected from a different coal preparation plant in Illinois. The samples are from five different regions of Illinois coal field (Fig. 2), and are preserved under nitrogen at the Illinois State Geological Survey (ISGS). Collection, preparation, and storage of the samples were described by Demir et al. [1994a,b].

Representative splits of the 27 samples were dry-ground in a hammer mill so that 90% of the particles were smaller than 100 mesh (149 μm). Also, eight of the 27 samples were wet-ground in a rod mill (700 grams coal + 700 mL tap water) generally for 30 minutes so that 90% of the particles were smaller than 200 mesh (74 μm). The coal slurry from the rod mill was filtered and air-dried. The -100 and -200 mesh samples were saved under nitrogen for the subsequent washability tests.

Washability Tests
A centrifugal float-sink (F-S) method based on the methods reported in Ho and Warchol [1988] and Cavallaro and Killmeyer [1988] was used to determine the washabilities of both ash and HAPs. The washability test procedure was as follows:

(1) Mix about 100-g of coal sample dried at 40°C overnight with 2 L of coalgrav® liquid (mixture of tetrachloroethylene and naphtha) with a specific gravity (s.g.) of 1.3 to generate a slurry containing about 5% coal. Add dispersing reagent (Aerosol OT) to the mixture to achieve a dosage of about 5 mg reagent per g of coal.
(2) Agitate the mixture with a mechanical stirrer for 6 to 10 minutes and then in an ultrasonic bath until no agglomeration persists (usually 2 to 10 minutes).
(3) Pour the slurry into 250-mL Teflon centrifuge bottles, tightly cap the bottles, and place the bottles in a centrifuge.
(4) Centrifuge the slurry at 2000 rpm (about 880 g force for the centrifuge used) for 20 minutes.
(5) Gently stir the float portion of the slurry in the bottles without disturbing the sink portion. Centrifuge the slurry again at 2000 rpm for 20 minutes.
(6) Repeat step 5.
(7) Gently pour the float out of the bottles onto a filter paper placed in a filter funnel. The pouring of the float portion usually does not significantly disturb the sink portion which becomes tightly compacted during the 1-hour centrifugation.
(8) Filter the float and then wash it thoroughly, first with 250 mL of ethanol, and then 1.5 L of deionized water, to remove residues of coalgrav® and dispersing agent. Dry the float overnight at 40°C and weigh it.
(9) Mix the sink from step 8 with 2 L of 1.4 s.g. coalgrav®, and repeat steps 2 through 8. A small amount of lower s.g. liquid trapped in the wet sink during the preceding step does not measurably alter the s.g. of the new suspension.
(10) Mix the sink from step 9 with 2 L of 1.6 s.g. coalgrav®, and repeat steps 2 through 8.
(11) Wash, dry, and weigh the sink as in step 8.
(12) Submit the <1.3, 1.3-1.4, 1.4-1.6, and >1.6 s.g. F-S fractions for chemical analysis.

Chemical Analysis and Preparation of Cleaned Composite Samples
The 27 samples of marketed coals were analyzed for the 12 HAPs and ash and all of their F-S fractions were analyzed for ash using well-established procedures for common coal analyses at the ISGS (Table 1). The combustible materials content of each F-S fraction was calculated by subtracting its ash and moisture contents from 100. Then a plot of %cumulative combustibles recovery vs cumulative weight of F-S fractions was constructed for each F-S test. Using these plots, the first two or three lightest fractions from each test were successively combined so that the composite sample contained 80% of the combustible materials in the parent coal. All 80%-combustibles recovery products were analyzed for the 12 HAPs and ash.

RESULTS AND DISCUSSION
The analytical data for the feed coals and their clean washability products (Table 2) were used to estimate the ability to remove HAP elements from finely-ground marketed Illinois coals through the use of advanced gravity separators. The ranges of average concentrations for 12 HAP elements in the 27 samples of marketed Illinois coals (Fig. 3) were as follows:

<2 mg/kg:	Be, Sb, Se, Th
2-10 mg/kg:	As, Co, U
10-20 mg/kg:	Cr, Ni, Pb
>20 mg/kg:	Mn, P

The concentrations of all HAPs, except Be, in the coals were decreased (with a few exceptions) as a result of F-S separation at ~100 mesh size (Table 3, Fig. 4). Some of the decreases (or enrichments) of element concentrations calculated for some individual samples may be erroneous if the difference between the concentration of a given element in the parent coal and that in its clean F-S product is not greater than the analytical precision for that particular element. Such decrease and enrichment errors, however, generally cancel each other when mean values for the entire sample set are computed. On average, Be was enriched in the -100 mesh washability products by 94% when compared with the parent coals. This suggests that Be was finely disseminated (perhaps organically associated) within the coal macerals. Because some of Be tends to stay with bottom ash and slag during coal combustion (Fig. 1), and because the mean concentration of Be in the marketed coals was only 1.3 mg/kg (Fig. 3), additional environmental risk due to an average of 94% enrichment of this element could be very small.

The decrease in ash content ranged from 37% to 75% with an average of 53% (Table 3, Fig 4). As a result, 9 of the 27 clean F-S products had ash contents of 2.77% to 3.86% (Table 2). The average decreases for As, Mn, and P exceeded that for ash, indicating that these three elements were somewhat enriched in relatively coarse mineral grains that were effectively removed during the F-S process; As was likely associated mainly with pyrite, Mn with calcite, and P with apatite. Precombustion removal of As from coal is important because of its relatively high atmospheric mobility during coal combustion (Fig. 1). The decrease of Se, another element with relatively

high atmospheric mobility (Fig. 1), was smaller than that of As but still significant (37%). The average decreases for Cr(20%), Sb(19%), and U(11%) were relatively small. Although Sb can be mobilized by attachment to air-borne fly ash particles, its small concentrations (Table 2, Fig. 3) could limit any environmental risk associated with Sb emission from combustion of marketed Illinois coals. Atmospheric emissions of Cr and U are expected to be small because they tend to be fixed in coarse ash and slag during coal combustion.

Grinding the 8 coals to -200 mesh (<74 μm) resulted in greater average decreases for Sb, Se, and Th and a smaller decrease for Mn when compared with decreases obtained for -100 mesh (<149 μm) samples of the same coals (Table 4, Fig. 5). The changes in the amount of decrease of other elements and ash for -200 mesh samples relative to -100 mesh samples were not significant. It should be noted that additional tests with varying centrifuge speed and amount and type of dispersant should be conducted to determine whether the F-S separation efficiency for -200 mesh samples can be increased.

The marketed coal products are currently ground to 70% passing 200 mesh (74 μm) size for utilization in pulverized coal boilers which comprise over 90% of the combustion units used in Illinois [Honaker et al., 1994]. Therefore, because there would be no extra cost for grinding, an advanced coal cleaning strategy that would substantially decrease HAPs, as well as ash and sulfur, in Illinois coals beyond conventional cleaning can be economical. Furthermore, as much as 10% of the production of many coal preparation plants in Illinois is fine coal waste. An efficient and low cost cleaning of this fine coal waste would generate additional clean coal and thus increase revenues from mined coal. Using clean coal would not only reduce atmospheric HAPs emissions but also slagging and fouling at coal-fired power plants.

SUMMARY AND CONCLUSIONS

Float-sink washability data on 27 samples of marketed Illinois coals indicated that, at -100 mesh (<149 μm) particle size and with an 80%-combustibles recovery, the ash contents of the coals can potentially be decreased by 37% to 75% with an average of 53%, beyond conventional cleaning, using advanced gravity-based coal cleaning. As a result, some of the clean products could have ash contents of less than 3%. Decreases in ash contents were accompanied by decreases in the levels of eleven HAPs (As, Co, Cr, Mn, Ni, P, Pb, Sb, Se, Th, U) investigated, with a few exceptions. The average decreases for As, Mn, and P exceeded that for ash. The average decrease of Se was smaller than that of ash but still significant (37%). Precombustion removal of As and Se from coal is important because of their relatively high atmospheric mobility during coal combustion. On average, Be was enriched in the washability products by 94% compared with the parent coals. Because of its low concentrations in the coals and its low atmospheric mobility, the enrichment of Be caused by fine coal cleaning could increase any related environmental risk only slightly. The average decreases for Cr(20%), Sb(19%), and U(11%) were relatively small. Although Sb can be enriched in air-borne fly ash particles, any environmental risk associated with atmospheric Sb emission could be small because marketed Illinois coals generally have Sb concentration of about 1 mg/kg or less. Most of Cr and U are expected to be fixed in coarse ash and slag rather than emitted into the atmosphere during coal combustion. The grinding of 8 of the coals to -200 mesh (<74 μm) increased the removal of Sb, Se, and Th, decreased that of Mn and did not significantly change those of other HAPs compared with the -100 mesh (<149 μm) samples of the same coals. An efficient and low-cost fine coal cleaning of marketed Illinois coals could reduce not only the atmospheric HAPs emissions but also slagging and fouling at coal-fired power plants.

ACKNOWLEDGEMENTS

We thank J. D. Steele, J. K. Frost, R. R. Frost, L. R. Henderson, C. Chaven, and K. M. Henry for analyzing the samples. We also thank C. C. Rohl for his help in carrying out the float-sink tests. This research was supported in part by the Illinois Department of Energy and Natural Resources (IDENR) through its Coal Development Board and the Illinois Clean Coal Institute (ICCI) and by the U.S. Department of Energy (DOE). Any opinions, findings, conclusions, or recommendations expressed herein are those of the authors and do not necessarily reflect the views of IDENR, ICCI, or DOE.

REFERENCES

ASTM, Petroleum Products, Lubricants, and Fossil Fuels: Vol. 05.05, (1992).

Bosold, R. C. and Glessner, D. M., Laboratory Guidelines and Procedures for Coal Analysis: Volume 1, Assessing the Cleanability of Fine Coal, EPRI Report EPRI-CS-5644-Vol. 1 (1988).

Cavallaro, J. A., and R. P. Killmeyer, J. Coal Quality, 7, 55 (1988).

Clarke L. B. and Sloss L. L., Trace Elements - Emission from Coal Combustion and Gasification. IEA Coal Research, IEACR/49, London (1992).

Demir, I., Harvey R. D., Ruch, R. R., Steele, J. D., and Ho, K. K., ACS Div. Fuel Chem. Preprints, 39(2), 530 (1994a).

Demir, I., Harvey R. D., Ruch, R. R., Damberger, H. H., Chaven, C., Steele, J. D., and Frankie, W. T., Characterization of Available (Marketed) Coals From Illinois Mines. Illinois State Geological Survey, Open File Series 1994-2 (1994b).

Dumm, T. F. and Hogg, R., Miner. Metall. Process., 5(1), 25 (1988).

Franzidis, J. P. and Harris, M. C., J. South. Afr. Inst. Min. Metall., 86(10), 409 (1986).

Harrison, C., J. Coal Quality, 5(3), 115 (1986).

Ho, K. K. and Warchol, J. J., Swell Technology for Deep Clean Coal. Alliance Research Center Report RDD:86:4373-01-01:01, Final Report for Ohio Coal Development Office, Grant No: OCDO/R-86-85 (1988).

Honaker, R. Q. and Reed, S., A Fine Coal Circuitry Study Using Column Flotation and Gravity Separation. Quarterly Technical Report (9/1-11/30/1994) to the Illinois Clean Coal Institute (1994).
Honaker, R. Q., Paul, B. C., and Wang, D., Advanced Physical Coal Cleaning To Comply with Potential Air Toxic Regulations. Quarterly Technical Report (9/1-11/30/1994) to the Illinois Clean Coal Institute (1994).
Jacobsen, P. S., Blinn, M. B., Wan, E. I., and Nowok, M. A., Proc. 9th Int. Coal Preparation and Exposition Conf., p. 82, Cincinnati, OH (1992).
Kaiser Engineers, Inc., Trace Elements in Coal and Coal Wastes, Interim Report, EPRI GS-6575, Palo Alto, CA (1989).
Mezey, E. J., Proc. Workshop, Accessory Elements in Coal, National Academy of Science, p. 34 (1977).
National Research Council, Redistribution of Accessory Elements in Mining and Mineral Processing, Part I, Coal and Oil Shale, p. 44. National Academy of Science, Washington, D.C. (1979).
National Research Council, Trace Element Geochemistry of Coal Resource Development Related to Environmental Quality and Health. National Academy of Science, Washington, D.C. (1980).
Norton, G. A., Markuszewski, R., and Buttermore, W. H., Proc. 2nd International Conf. on Elem. Anal. Coal and Its By-Products, p. 270 (1992).
Norton, G. A. and Markuszewski, R., Coal Preparation, 7, 55 (1989).
Norton, G. A., Markuszewski, R., and Araghi, H. G., ACS Symposia Series 319, 63, ACS, Washington, D.C. (1986).
Paul, B. C. and Honaker, R. Q., Production of Illinois Base Compliance Coal Using Enhanced Gravity Separation. Final Technical Report to the Illinois Clean Coal Institute (1994).
Streeter, R.C., Evaluation of the Effect of Coal Cleaning on Fugitive Elements. US DOE Report, DOE/PC/62690-T7 (1986).
Suardini, P. J., Proc. 10th International Coal Testing Conf., p. 33 (1993).
Swaine D. L., J. Coal Qual., 8, 67 (1989).
U.S. Public Law 101-549, Clean Air Act Amendments, Title 3, 104 Stat 2531-2535 (1990).
Wesnor J. D., EPRI/EPA SO_2 Conf., collection of papers, Boston, MA (1993).
Wheelock, T. D. and Markuszewski, R., American Institute of Physics Conf. Proceedings, 70, p. 357. American Inst. of Physics, NY (1981).
Wheelock, T. D. and Markuszewski, R., The Science and Technology of Coal and Coal Utilization, p. 47. Plenum Press, NY (1984).

Table 1. Relative precision and detection limits of methods commonly used for analyses of HAPs and ash in coal samples

Element	Relative precision %	Average detection limit	Methods* WDXRF	AAS	INAA	OEP	PyroIC
Major and minor oxides (%)							
MnO	ash 5	0.01	X				
P_2O_5	ash 5	0.02	X				
Trace elements (mg/kg)							
As	coal 7	1.0			X		
Be	ash 5	0.5				X	
Cd	ash 10	2.5		X			
Co	coal 5	0.3			X		
Cr	ash 2	7.0			X		
F	coal 10	20.0					X
Hg	coal 15	0.01		X**			
Ni	ash 10	15.0		X	X		
Pb	ash 20	25.0		X		X	
Sb	coal 10	0.2			X		
Se	coal 10	2.0			X		
Th	coal 5	0.4			X		
U	coal 15	3.0			X		

Constituent	Absolute precision (%)	Accuracy (%)	ASTM method (1992)
Ash	0.10	0.5	D5142-90

* WDXRF = wavelength-dispersive x-ray fluorescence spectrometry
AAS = atomic absorption spectrometry
INAA = instrumental neutron activation analysis
OEP = optical emission (photographic) spectrometry
PyroIC = pyrohydrolysis and ion chromatography
** Hg by cold vapor atomic absorption spectrometry

Table 2. Chemical composition of samples of marketed Illinois coals (feed) and their clean F-S fractions at 80% combustibles recovery (product). Ash values are in wt% and elemental values are in mg/kg (all values are on a dry basis). One-half the detection limit was used, for those values less than the detection limit, in the computations of means and standard deviations.*

FEED COAL NO.	REGION	MESH SIZE	Ash		As		Be		Co		Cr		Mn		Ni		P		Pb		Sb		Se		Th		U	
			coal	prod.	coal	prod.	coal	prod.	coal	prod.	coal	prod.	coal	prod.	coal	prod.	coal	prod.	coal	prod.	coal	prod.	coal	prod.	coal	prod.	coal	prod.
C32773	1	-100	8.72	5.01	1.3	0.5	1	1.0	2.3	2.0	12	11	39	13	11	10	44	22	<6	<5	0.2	0.2	1.9	1.2	1.2	1.0	1.7	<1
C32774	1	-100	7.07	2.77	20	9.1	4	11.0	3.1	0.9	5.8	4.4	18	5.0	15	4	87	52			1.2	0.8	1.2	0.9	0.8	0.6	<0.8	<1
C32777	1	-100	14.52	7.87	5.1	1.2	1.2	2.2	1.5	1.6	11	10	205	35	7	6	44	17	36	22	1.1	0.8	1.6	1.1	1.1	0.9	1.1	0.7
C32778	1	-100	9.8	4.79	10	2.9	2.2	4.8	4.6	3.8	12	9.4	38	12	31	25	87	39	14	9	2.2	2.2	1.5	1.0	1.5	1.2	0.9	1.3
C32782	1	-100	11.62	5.89	2.4	0.9	<1.0	2.2	1.6	1.2	14	9.7	55	15	7	7	87	26	<6	<5	0.5	0.4	1.9	1.0	1.1	0.9	1.3	1.4
C32785	1	-100	9.75	4.38	2.3	0.7			2.6	1.8	17	12	39	12	18	11	131	31			0.4	0.2	3.9	1.9	1.3	1.0	1.8	1.4
C32797	1	-100	10.29	5.59	4	1.1			3	2.3	13	11	32	12	16	14	87	31			0.6	0.6	1.4	1.0	1.5	1.1	1.9	1.8
C32814	1	-100	6	3.36	6.4	2.6	2	3.1	2.5	1.5	5.7	6.2	30	7.0	12	10	30	13	23	14	1.9	1.5	1.3	1.1	0.6	0.6	8.0	6.8
C32779	2	-100	9.63	3.86	1.7	0.8	<1.0	2.3	2	1.3	17	13	29	9.0	11	6	44	17	7	6	0.4	0.3	2.3	1.2	1.3	0.9	3.1	3.1
C32794	2	-100	10.52	4.32	2.3	0.8	1.1	2.3	2.8	2.1	12	12	40	11	14	8	44	17	15	7	0.3	0.2	1.9	1.1	1.4	1.1	2.0	1.8
C32798	2	-100	13.16	6.1	2.2	0.8	<1.0	1.1	3.3	1.9	23	14	54	16	18	17	87	35	12	<5	0.3	0.3	3.2	1.3	1.7	1.3	2.7	2.6
C32800	2	-100	11.39	7.23	2	1.0			2.8	2.3	23	17	30	14	16	9	87	35			0.4	0.4	2.8	1.5	1.6	1.2	2.9	2.3
C32813	2	-100	14.7	7.88	2.4	1.0	1.4	1.4	3.5	2.1	42	22	40	16	24	15	305	109	13	7	0.7	0.5	5.4	2.9	2.1	1.5	3.7	2.8
C32815	2	-100	12.03	5.01	3	0.9	<1.0	2.1	2.7	1.7	14	11	61	18	10	6	44	13	12	<5	0.6	0.4	2.1	1.0	1.7	1.2	1.9	1.9
C32784	3	-100	8.13	3.32	18	9.3	1.8	3.5	4.2	2.5	11	8.9	17	6.5	15	9	44	31			1.1	1.0	1.4	1.1	1.4	0.9	1.0	<1
C32795	3	-100	5.76	2.79	3.6	2.2	1	1.0	4.8	4.6	8.6	7.0	11	4.0	18	14	44	31	16	10	1.1	1.1	1.1	0.8	1.2	0.8	0.6	<.5
C32799	3	-100	11.42	3.48	17	1.6			4.4	4.0	12	8.6	64	5.0	15	13	436	275			3.6	3.0	1.3	0.9	1.6	0.9	0.7	0.7
C32801	3	-100	8.36	4.71	10	4.6			4.4	3.0	12	9.9	21	9.0	14	7	44	31			0.6	0.6	1.5	1.1	1.5	1.1	1.0	1.0
C32803	3	-100	9.19	5.25	4.1	1.8			2.7	2.1	12	11	28	10	13	7	44	17			0.4	0.3	1.5	0.9	1.6	1.3	1.1	1.3
C32661	4H	-100	8.17	4.01	3.4	1.5	1.6	2.5	3.9	1.8	16	13	20	7.0	14	5	44	17	19	12	0.5	0.3	2	1.0	1.5	1.0	7.5	6.3
C32665	4H	-100	9.39	3.8	4.4	1.3	1.2	1.0	3.6	2.1	13	12	25	6.0	11	5	44	13	19	6	0.4	0.3	1.7	0.9	1.6	1.1	5.7	5.6
C32771	4H	-100	12.57	4.29	3.7	0.9	1.1	1.6	4.1	1.9	14	12	36	8.0	10	9	44	17	22	13	0.3	0.2	1.4	0.8	1.8	1.1	2.2	2.1
C32776	4H	-100	9.27	4.16	2.7	1.0	1.5	1.4	3.6	2.3	15	13	38	10	12	7	44	17	10	13	0.6	0.5	1.7	1.2	1.4	0.9	1.8	1.9
C32662	4S	-100	7	3.67	14	5.2	1.4	2.7	4.4	2.8	10	7.8	15	6.0	17	12	175	74	23	11	1.0	0.8	1.3	0.9	1.9	1.2	1.9	1.6
C32772	4S	-100	9.33	4.34	8	2.6	1	1.0	3.9	2.3	9.2	8.2	39	8.0	13	9	87	44	27	23	0.7	0.6	1.3	1.0	1.3	1.0	<1.0	<1
C32781	4S	-100	9.71	5.19	4.3	1.4	<1.0	1.1	2.7	1.7	12	9.9	37	10	11	9	44	13	46	32	1.4	1.0	2.5	1.3	1.2	0.9	2.0	1.5
C32793	4S	-100	14.14	3.59	33	8.4	1.2	2.0	5.5	3.7	13	7.0	39	8.0	22	15	175	57	36	11	1.2	1.1	1.1	0.9	1.8	0.8	0.8	0.6
mean	all		10.06	4.69	7.1	2.4	1.3	2.4	3.4	2.3	14	11	41	11	15	10	92	41	19	11	0.9	0.7	1.9	1.1	1.4	1.0	2.2	2.0
stdev	all		2.37	1.35	7.3	2.5	0.8	2.1	1.0	0.9	6.7	3.4	35	6	5	5	89	51	11	8	0.7	0.6	0.9	0.4	0.3	0.2	1.9	1.7
C32773	1	-200	8.72	4.87	1.3	0.6	1	1.6	2.3	1.8	12	10	39	24	11	8	44	26	<6	<5	0.2	0.1	1.9	0.9	1.2	0.9	1.7	<1
C32774	1	-200	7.07	2.65	20	7.4	4	9.0	3.1	1.4	5.8	6.5	18	5.0	15	6	87	52			1.2	0.9	1.2	0.5	0.8	0.6	<0.8	<1
C32794	2	-200	10.52	5.69	2.3	1.0	1.1	2.1	2.8	1.8	12	7.9	40	19	14	6	44	26	15	<5	0.3	0.2	1.9	0.9	1.4	0.9	2	1.6
C32813	2	-200	14.7	5.67	2.4	0.8	1.4	2.7	3.5	2.3	42	21	40	17	24	12	305	96	13	5	0.7	0.6	5.4	1.6	2.1	1.2	3.7	3.2
C32784	3	-200	8.13	3.21	18	6.0	1.8	2.4	4.2	2.8	11	9.0	17	9.0	15	9	44	35	40	32	1.1	0.9	1.4	0.8	1.4	0.8	1	1.0
C32665	4H	-200	9.39	3.47	4.4	0.9	1.2	1.9	3.6	2.3	13	12	25	11	11	9	44	17	19	6	0.4	0.2	1.7	0.8	1.6	1.0	5.7	5.3
C32771	4H	-200	12.57	5.17	3.7	1.0	1.1	1.8	4.1	2.8	14	14	36	20	10	11	44	22	22	7	0.3	0.2	1.4	0.7	1.8	1.2	2.2	2.1
C32772	4S	-200	9.33	3.62	8	1.7	1	1.4	3.9	2.8	9.2	9.1	39	15	13	9	87	39	27	11	0.7	0.6	1.3	0.7	1.3	0.9	<1	<1
mean	all		10.05	4.29	7.5	2.4	1.6	2.9	3.4	2.3	15	11	32	15	14	9	87	39	32	37	0.6	0.5	2.0	0.9	1.5	0.9	2.6	2.3
stdev	all		2.33	1.12	6.9	2.5	0.9	2.4	0.6	0.5	10.5	4.3	9	6	4	2	84	24	28	71	0.4	0.3	1.3	0.3	0.4	0.2	2.2	1.9

* blank spaces indicate that no data were available at the time of this writing

Table 3. Percent changes in ash and HAPs contents as a result of F-S separation of 27 samples of marketed Illinois coals ground to -100 mesh. Each clean F-S product contained 80% of the combustible materials of its parent sample. Negative values indicate decreases and positive values enrichments. In the statistical computations, one-half the detection limit was used for all values below the detection limit.*

FEED COAL NO.	REGION	Ash	As	Be	Co	Cr	Mn	Ni	P	Pb	Sb	Se	Th	U
C32773	1	-43	-62	0	-13	-8	-67	-9	-50	-17	0	-37	-17	-71
C32774	1	-61	-55	175	-71	-24	-72	-73	-40		-33	-25	-25	25
C32777	1	-46	-76	-83	7	-9	-83	-14	-61	-39	-27	-31	-18	-36
C32778	1	-51	-71	118	-17	-22	-68	-19	-55	-36	0	-33	-20	44
C32782	1	-49	-63	340	-25	-31	-73	0	-70	-17	-20	-47	-18	8
C32785	1	-55	-70		-31	-29	-69	-39	-76		-50	-51	-23	-22
C32797	1	-46	-73		-23	-15	-63	-13	-64		0	-29	-27	-5
C32814	1	-44	-59	55	-40	9	-77	-17	-57	-39	-21	-15	0	-15
C32779	2	-60	-53	360	-35	-24	-69	-45	-61	-14	-25	-48	-31	0
C32794	2	-59	-65	109	-25	0	-73	-43	-61	-33	-33	-42	-21	-10
C32798	2	-54	-64	120	-42	-39	-70	-6	-60	-79	0	-59	-24	-4
C32800	2	-37	-50		-18	-26	-53	-44	-60		0	-46	-25	-21
C32813	2	-46	-58	0	-40	-48	-60	-38	-64	-46	-29	-46	-29	-24
C32815	2	-58	-70	320	-37	-21	-70	-40	-70	-79	-33	-52	-29	0
C32784	3	-59	-48	94	-40	-19	-62	-40	-30		-9	-21	-36	-50
C32795	3	-52	-39	0	-4	-19	-64	-22	-30	-38	0	-27	-33	-58
C32799	3	-70	-91		-9	-28	-92	-13	-37		-17	-31	-44	0
C32801	3	-44	-54		-32	-17	-57	-50	-30		0	-27	-27	0
C32803	3	-43	-56		-22	-8	-64	-46	-61		-25	-40	-19	18
C32661	4H	-51	-56	56	-54	-19	-65	-64	-61	-37	-40	-50	-33	-16
C32665	4H	-60	-70	-17	-42	-8	-76	-55	-70	-68	-25	-47	-31	-2
C32771	4H	-66	-76	45	-54	-14	-78	-10	-61	-41	-33	-43	-39	-5
C32776	4H	-55	-63	-7	-36	-13	-74	-42	-61	30	-14	-29	-36	6
C32662	4S	-48	-63	93	-36	-22	-60	-29	-58	-52	-20	-31	-37	-16
C32772	4S	-53	-68	0	-41	-11	-79	-31	-49	-15	-14	-23	-23	0
C32781	4S	-47	-67	120	-37	-17	-73	-18	-70	-30	-29	-48	-25	-25
C32793	4S	-75	-75	67	-33	-46	-79	-32	-67	-69	-8	-18	-56	-25
mean	all	-53	-64	94	-31	-20	-70	-32	-57	-38	-19	-37	-28	-11
stdev	all	9	10	117	16	12	8	18	13	25	14	12	10	24

* blank spaces indicate that no data were available at the time of this writing.

Table 4. Percent changes in ash and HAPs contents as a result of F-S separation of 8 samples of marketed Illinois coals ground to -100 and -200 mesh. Each clean F-S product contained 80% of the combustible materials of its parent sample. Negative values indicate decreases and positive values enrichments. In the statistical computations, one-half the detection limit was used for all values less than the detection limit.*

FEED COAL NO.	REGION	MESH SIZE	Ash	As	Be	Co	Cr	Mn	Ni	P	Pb	Sb	Se	Th	U
C32773	1	-100	-43	-62	0	-13	-8	-67	-9	-50	-17	0	-37	-17	-71
C32774	1	-100	-61	-55	175	-71	-24	-72	-73	-40		-33	-25	-25	25
C32794	2	-100	-59	-65	109	-25	0	-73	-43	-61	-33	-33	-42	-21	-10
C32813	2	-100	-46	-58	0	-40	-48	-60	-38	-64	-46	-29	-46	-29	-24
C32784	3	-100	-59	-48	94	-40	-19	-62	-40	-30		-9	-21	-36	-50
C32665	4H	-100	-60	-70	-17	-42	-8	-76	-55	-70	-68	-25	-47	-31	-2
C32771	4H	-100	-66	-76	45	-54	-14	-78	-10	-61	-41	-33	-43	-39	-5
C32772	4S	-100	-53	-68	0	-41	-11	-79	-31	-49	-15	-14	-23	-23	0
mean	all		-56	-63	51	-41	-17	-71	-37	-53	-37	-22	-36	-28	-17
stdev	all		7	8	64	16	14	7	20	13	18	12	10	7	29
C32773	1	-200	-44	-54	60	-22	-17	-38	-27	-41	-17	-50	-53	-25	-71
C32774	1	-200	-63	-63	125	-55	12	-72	-60	-40		-25	-58	-25	25
C32794	2	-200	-46	-57	91	-36	-34	-53	-57	-41	83	-33	-53	-36	-20
C32813	2	-200	-61	-67	93	-34	-50	-58	-50	-69	-81	-14	-70	-43	-14
C32784	3	-200	-61	-67	33	-33	-18	-47	-40	-20	-20	-18	-43	-43	0
C32665	4H	-200	-63	-80	58	-36	-8	-56	-18	-61	-68	-50	-53	-38	-7
C32771	4H	-200	-59	-73	64	-32	0	-44	10	-50	-68	-33	-50	-33	-5
C32772	4S	-200	-61	-79	40	-28	-1	-62	-31	-55	-59	-14	-46	-31	0
mean	all		-57	-68	71	-35	-15	-54	-34	-47	-33	-30	-53	-34	-12
stdev	all		7	9	29	9	19	10	22	14	53	14	8	7	26

* blank spaces indicate that no data were available at the time of this writing.

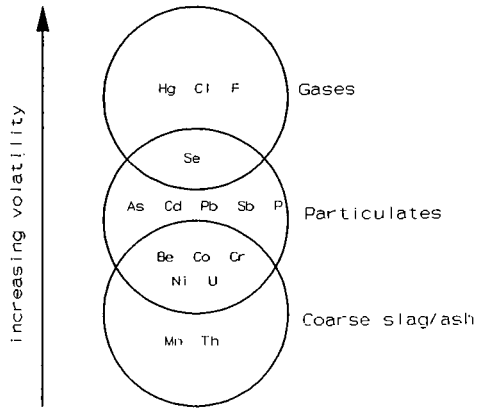

Figure 1. Enrichment of HAPs in different coal combustion and gasification products (after Clarke and Sloss, 1992).

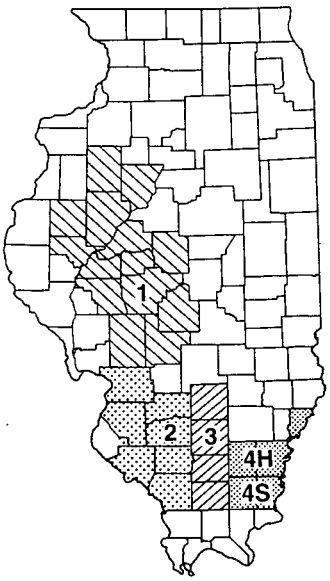

Figure 2. Sample regions of Illinois coal field. Region 4 was subdivided by seam into Herrin (H) and Springfield (S) coals.

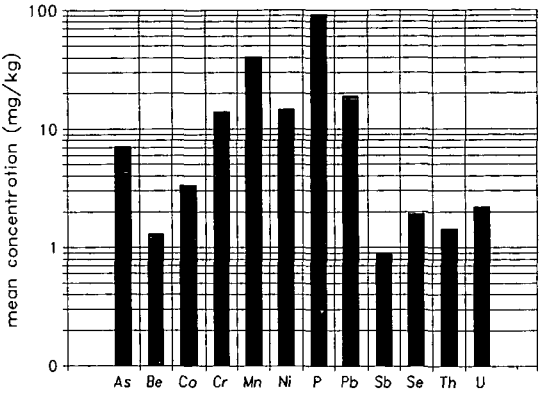

Figure 3. Mean concentrations of 12 HAPs in 27 samples of marketed Illinois coals.

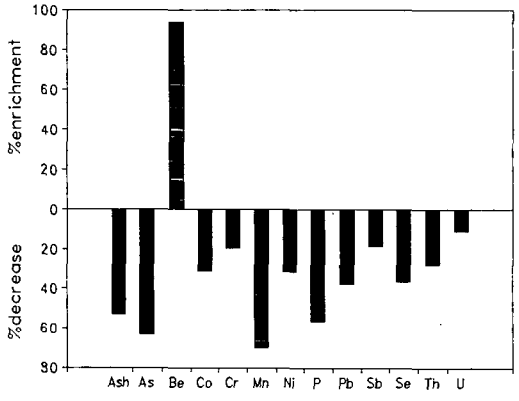

Figure 4. Average estimated changes in concentrations of 12 HAPs in 27 samples of marketed Illinois coals ground to -100 mesh if an advanced gravity separation process were applied and 80% of the combustible materials recovered from the process.

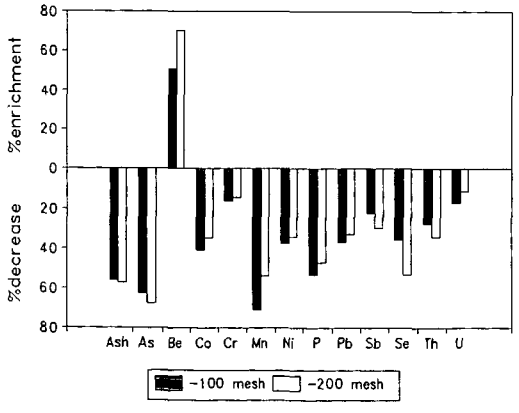

Figure 5. Average estimated changes in concentrations of 12 HAPs in 8 samples of marketed Illinois coals ground to -100 and -200 mesh if an advanced gravity separation process were applied and 80% of the combustible materials recovered from the process.

TRACE ELEMENT CONTENT OF CLEANED ILLINOIS BASIN COAL

Karen A. Katrinak, Raymond A. DeWall, and Ronald C. Timpe
Energy & Environmental Research Center
University of North Dakota
Grand Forks, North Dakota 58202

Keywords: Trace metals, coal, scanning electron microscopy

ABSTRACT

Illinois Basin coal samples treated to extract organic sulfur and selected hazardous air pollutants (HAPs) were examined for trace metal content using scanning electron microscopy with wavelength-dispersive spectrometry (SEM-WDS). The extraction process used subcritical water, defined as water held in the liquid state under sufficient pressure to remain liquid at temperatures greater than the normal boiling point, but below the supercritical point of water (218 atm and 374°C). The samples were sink-floated to remove pyrite prior to receiving the subcritical extraction treatment. Some mineral matter remains in the coal, including sulfates, aluminosilicates, and small amounts of pyrite. In individual mineral grains in the unextracted coal, mercury is found intermittently at levels up to 0.62 wt%, arsenic at up to 0.28 wt%, and selenium at up to 0.38 wt%. These occurrences appear to be localized concentrations.

INTRODUCTION

Scanning electron microscopy with wavelength-dispersive spectrometry (SEM-WDS) is useful for determining the trace metal content of materials in situations where high spatial resolution is desired. The technique is more time-consuming than atomic absorption or other methods used to determine bulk trace element content of materials, but the additional effort required provides information unobtainable through other means. For coal samples, use of SEM-WDS allows the associations of trace metals with particular minerals in coal to be determined. This approach is particularly important in gaining the information necessary to determine how coal-cleaning processes work.

METHODS

Samples were mounted in carnauba wax, cross-sectioned, polished, and carbon-coated to improve conductivity. Analyses were conducted on a JEOL 35C scanning electron microscope equipped with two JEOL wavelength-dispersive spectrometers with xenon-filler proportional counters and a Noran Instruments energy-dispersive spectrometer. The microscope is controlled by a Noran Instruments Voyager 2 computer system.

The microscope was operated at an accelerating voltage of 25 kV with a beam current of 100 nA. Wavelength-dispersive spectral peaks were counted for 100 s. Live time for each energy-dispersive spectrum used to obtain major-element chemistry was 30 s. Certified standards were used for calibration. The data were subjected to ZAF (atomic number, absorption, and fluorescence) corrections following collection. The detection limit for arsenic, selenium, and mercury using the SEM-WDS technique is approximately 0.01 wt%.

Four samples of Illinois Basin Coal were characterized: raw IBC-101, extracted IBC-101, raw IBC-102, and extracted IBC-102. The extracted coals were treated with subcritical water, defined as water held in the liquid state under sufficient pressure to remain liquid at temperatures greater than the normal boiling point, but below the supercritical point of water (218 atm and 374°C). The samples were sink-floated to remove pyrite prior to receiving the subcritical extraction treatment. Arsenic, selenium, and mercury were measured in individual mineral grains from each raw and extracted coal. Major element composition was also determined.

RESULTS AND DISCUSSION

Results show that trace metals are distributed irregularly throughout the mineral matter in the four samples. Data are presented in Tables 1 through 4 for the IBC-101 raw coal, IBC-101 extracted coal, IBC-102 raw coal, and IBC-102 extracted coal, respectively. The mineral grains analyzed represent a wide variety of compositions, including aluminosilicate, calcium sulfate, pyrite, and iron oxide. The copper-rich grains analyzed represent an additive used in the extraction process.

The most dramatic difference in major element composition between raw and extracted coal samples is for sulfur. Sulfur is abundant in both of the raw coal samples, but is almost entirely absent in the extracted samples, demonstrating that the extraction process is effective at removing this element. Iron is present at high levels in both raw and extracted samples.

Arsenic, selenium, and mercury occur in both raw and extracted samples, suggesting that the coal-cleaning process may not completely remove these trace metals. In the IBC-101 samples, mercury and selenium appear to have been reduced by the extraction process, but arsenic is more abundant in the extracted sample. In the case of the IBC-102 sample, the extraction process may have added mercury, as this element is present in a greater proportion of the mineral grains and in higher concentrations in the extracted sample than in the raw sample. Arsenic and selenium occur with roughly equivalent frequency and concentration in the raw and extracted IBC-102 samples. Most of the mineral grains analyzed contained one or more of these elements, although none of the grains contained all three of the trace metals measured.

CONCLUSIONS

Results presented here show that the distribution of trace metals in raw and extracted coals varies greatly. Arsenic, selenium, and mercury were found to be associated with a range of mineral compositions and are present even in low-pyrite cleaned coals. The extraction process appears to remove sulfur effectively, but some trace metals may remain in the coal after treatment.

TABLE 1

Elemental Composition of Individual Mineral Grains in IBC-101 Raw Coal

Point No.	Trace Metals, wt%			Major Elements, wt%						Total, wt%
	As	Se	Hg	Al	Si	P	S	Ca	Fe	
1	ND*	0.02	0.37	ND	ND	ND	36.11	ND	63.49	99.99
2	ND	0.38	0.13	ND	ND	ND	43.04	56.46	ND	100.01
3a	ND	0.01	0.04	ND	ND	2.12	40.05	57.79	ND	100.01
3b	ND	0.04	ND	ND	ND	ND	39.97	48.17	11.83	100.01
3c	ND	0.03	0.62	ND	ND	ND	42.24	57.12	ND	100.01
3d	ND	0.02	ND	ND	13.23	ND	40.92	45.83	ND	100.00
3e	0.02	0.01	ND	2.99	9.75	ND	34.51	34.01	18.71	100.00
3f	ND	0.03	ND	ND	ND	ND	44.34	55.64	ND	100.01
3g	ND	0.01	ND	ND	10.19	ND	32.72	17.58	39.51	100.01
3h	0.28	0.02	ND	8.73	28.70	ND	15.74	ND	44.35	100.00
3i	ND	0.01	ND	ND	ND	ND	44.03	55.97	ND	100.01
3j	ND	0.02	ND	6.41	20.19	ND	11.58	5.60	56.21	99.99
3k	0.01	0.02	ND	ND	ND	ND	12.43	ND	87.54	100.00
4a	ND	ND	ND	ND	ND	ND	20.25	ND	79.74	99.99
4b	ND	ND	ND	ND	ND	ND	20.43	ND	79.58	100.01
4c	0.01	ND	ND	ND	ND	ND	21.30	ND	78.68	99.99
4d	0.07	0.01	ND	7.73	14.45	ND	36.96	ND	40.77	99.99
4e	ND	ND	ND	17.01	21.42	ND	24.78	ND	36.80	100.01
4f	0.01	0.01	ND	35.45	64.53	ND	ND	ND	ND	100.00
4g	0.01	0.01	ND	ND	ND	ND	41.66	ND	58.33	100.01
4h	0.01	0.01	ND	34.62	65.37	ND	ND	ND	ND	100.01

* Not detected.

TABLE 2

Elemental Composition of Individual Mineral Grains in IBC-101 Extracted Coal

Point No.	Trace Metals, wt%			Major Elements, wt%								Total, wt%
	As	Se	Hg	Mg	Al	Si	S	Ca	Ti	Fe	Cu	
1	ND*	0.01	ND	ND	27.23	12.07	ND	ND	ND	60.68	ND	99.99
2	ND	ND	ND	ND	49.95	50.05	ND	ND	ND	ND	ND	100.00
3	ND	0.01	ND	ND	ND	ND	ND	ND	ND	99.99	ND	100.00
4	ND	ND	ND	ND	56.84	43.16	ND	ND	ND	ND	ND	100.00
5	0.03	0.02	ND	ND	ND	4.78	ND	ND	ND	ND	95.17	100.00
6	ND	0.03	ND	ND	ND	ND	ND	ND	ND	99.97	ND	100.00
7	ND	ND	ND	ND	ND	ND	ND	ND	ND	100.00	ND	100.00
8a	0.06	ND	ND	7.66	ND	26.11	ND	23.02	ND	43.15	ND	100.00
8b	0.14	ND	ND	3.78	ND	7.21	ND	24.47	ND	64.39	ND	99.99
8c	0.12	ND	ND	9.42	ND	32.32	ND	12.19	6.10	39.85	ND	100.00
8d	0.25	ND	ND	23.42	ND	51.39	ND	ND	ND	24.94	ND	100.00
8e	0.07	ND	ND	2.70	ND	26.98	ND	49.81	8.83	11.62	ND	100.01
8f	0.18	ND	ND	10.33	ND	24.13	ND	7.29	2.74	55.33	ND	100.00

* Not detected.

TABLE 3

Elemental Composition of Individual Mineral Grains in IBC-102 Raw Coal

Point No.	Trace Metals, wt% As	Se	Hg	Major Elements, wt% Al	Si	S	Ca	Ti	Fe	Zn	Total, wt%
1	ND*	0.03	ND	ND	ND	34.00	ND	ND	ND	65.96	99.99
2	ND	0.01	ND	ND	ND	37.94	ND	ND	62.05	ND	100.00
3	0.01	ND	ND	ND	ND	50.91	ND	ND	49.08	ND	99.99
4	ND	ND	ND	ND	ND	52.79	ND	ND	47.21	ND	100.00
5	ND	0.01	ND	ND	ND	46.74	ND	ND	53.25	ND	100.00
6	ND	ND	ND	ND	ND	50.66	ND	ND	49.33	ND	99.99
7	ND	ND	ND	ND	3.53	40.75	55.72	ND	ND	ND	100.00
8	ND	ND	ND	ND	ND	52.84	ND	ND	47.16	ND	100.00
9	ND	ND	ND	ND	0.93	55.84	ND	ND	43.23	ND	100.00
10	0.01	ND	ND	5.79	4.24	48.05	ND	ND	41.91	ND	100.00
11	0.02	ND	0.01	ND	ND	55.25	ND	ND	44.72	ND	100.00
12	ND	ND	ND	ND	ND	ND	100.00	ND	ND	ND	100.00
13	ND	ND	0.01	24.62	51.98	ND	ND	2.90	9.55	ND	100.01
14	0.03	ND	0.01	ND	ND	53.30	ND	ND	46.66	ND	100.00
15	0.01	ND	ND	16.69	40.93	19.90	ND	ND	12.62	ND	100.01
16	ND	ND	ND	ND	ND	53.25	ND	ND	46.75	ND	100.00
17	ND	ND	ND	ND	ND	54.71	ND	ND	45.29	ND	100.00

* Not detected.

TABLE 4

Elemental Composition of Individual Mineral Grains in IBC-102 Extracted Coal

Point No.	Trace Metals, wt% As	Se	Hg	Major Elements, wt% Al	Si	S	Mn	Fe	Cu	Total, wt%
1	0.01	0.01	ND*	ND	ND	ND	ND	99.98	ND	100.00
2	0.02	0.03	ND	ND	ND	ND	ND	99.94	ND	99.99
3	0.03	0.03	ND	ND	ND	ND	ND	99.93	ND	99.99
4	0.06	0.05	ND	ND	ND	ND	ND	99.89	ND	100.00
5	ND	ND	ND	ND	ND	ND	ND	ND	100.00	100.00
6	ND	ND	0.08	ND	ND	ND	ND	99.92	ND	100.00
7	ND	ND	0.01	ND	ND	ND	ND	99.99	ND	100.00
8	ND	ND	0.02	ND	ND	ND	ND	99.98	ND	100.00
9	ND	ND	ND	ND	ND	ND	ND	2.47	97.52	99.99
10	ND	ND	0.01	ND	ND	ND	ND	99.99	ND	100.00
11	ND	ND	ND	ND	ND	ND	ND	100.00	ND	100.00
12	ND	ND	0.08	ND	0.48	ND	0.60	98.84	ND	100.00
13	0.03	ND	0.06	ND	ND	0.52	ND	99.38	ND	99.99
14	ND	ND	0.05	ND	ND	ND	ND	99.95	ND	100.00
15	ND	ND	0.06	ND	ND	ND	ND	99.93	ND	100.00
16	ND	ND	ND	ND	ND	ND	ND	100.00	ND	100.00
17	ND	ND	0.05	ND	ND	ND	ND	99.95	ND	100.00
18	ND	ND	0.02	ND	ND	ND	ND	99.98	ND	100.00
19	ND	ND	0.03	ND	ND	ND	ND	99.97	ND	100.00
20	ND	ND	0.04	ND	ND	ND	ND	99.96	ND	100.00
21	ND	ND	0.01	ND	ND	ND	ND	99.99	ND	100.00

* Not detected.

CHROMIUM VALENCE FORMS OF COAL FLY ASH IN THE SOLID STATE AND LEACHATES

John L. Wong, Zhanling Shi, and Anhua Liu
Department of Chemistry, University of Louisville
Louisville, Kentucky 40292

Keywords: Cr speciation, solution chemistry of Cr in leachates, carbon paste electrode

INTRODUCTION. Speciation of chromium in fly ash is a significant and complicated issue. Huggins et al. [1] used a synchrotron X-ray method to show that most of the chromium in coal fly ash is Cr(III), an important finding that should be evaluated further. Also, questions pertaining to the bioavailability of Cr and its phase distribution in fly ash, whose determination is subject to the redox chemistry of fly ash, will need to be answered for risk assessment purpose.

METHODOLOGY. Cr(VI) in leachates was determined by cathodic stripping voltammetry (CSV), and Cr(III), Cr(total) as Cr(VI) after H_2O_2 treatment [2,3]. Independent analysis of Cr(III) and Cr(VI) was achieved by either separating Cr(III,VI) on Chelex 100 [4] prior to CSV or by using a diphenylcarbazide (DPCI)-modified carbon paste electrode (CPE) in cyclic voltammetry of the mixture [5]. By doping CPE with fly ash and/or standard and using it in a DPCI-containing electrolyte, the Cr valence forms in the solid state were quantitated. Fe(II,III) speciation was carried out spectrophotometrically [6]. The Tessler procedure modified for phase separation and digestion of Ni in fly ash [7] was adapted for Cr speciation. SRM 1633b was obtained from NIST and CFF ash samples from Dr. Huggins of the Univ. of Kentucky.

RESULTS AND DISCUSSION. Table 1 shows Cr(VI) to be 72-82% of total Cr in the 50% HF digest of 4 coal fly ash samples, contradicting the X-ray solid analysis by Huggins et al. [1]. The SRM ash was extracted sequentially and compared with total digestion for valence form and mass balance. As shown in Table 2, the water-soluble and bioavailable Cr (Step 1) is only Cr(III). No Cr was detected in the iron oxide matrix (Step 2). The electromagnetic Cr phase (Step 3) may be Ni-Cr alloy or CrO_2. In acid extractions, Cr(III) was 1.8 times of Cr(VI) in HCl, but Cr(VI) was 2.6 times of Cr(III) in HF. The summation of Cr(III) in extracts 1-5 was 41% vs. 27% in the total digest. Starting with the residue of Step 3 where the water-soluble, iron oxide, and magnetic phases were removed, Table 3 showed that the 2-step acid extraction yielded 35% of total remaining Cr as Cr(III) vs. 29% from the single step treatment. In all these extractions, the Cr mass balance was 99-100%. It seems likely that redox chemistry in different leachates may have effected these varying ratios of Cr valence forms.

To understand redox chemistry in Cr speciation, the Fe(II,III) species in the 5 sequential extracts of 1633b are shown in Table 4. The absence of Fe(II) in leachate 1 is indicative of the true origin of Cr(III) identified therein. Table 5 validates the reducing power of Fe(II) and FeS_2 in 3 extractants. For comparison, arsenite did not reduce Cr(VI) at pH 5 but gave partial reduction in acid (cf. Table 6). In leachates 4 and 5, there was no Fe(II) detected and Cr(VI) was observed. In Table 6 is shown the partial oxidation of Cr(III) by MnO_2 at pH5 and complete oxidation in acid. The latter may be responsible for generating Cr(VI) in the acid leachates of the coal fly ash.

Solid state voltammetric peaks of Cr(III) at 600 mV (Fig.1A) and Cr(VI) at -600 mV (Fig.1B) are diagnostic of Cr valence forms. Direct Cr speciation of 2 coal fly ash, Fig. 2 for SRM 1633b and Fig. 3 for LS102, revealed Cr(III) only, whose oxidation peak was enhanced by spiking with Cr_2O_3 (Fig.4,5). The quantitation of Cr(III) shown in Table 7 agrees to within 5% of the total Cr found in the HF-digested samples. In Fig. 6 is shown the emergence of the Cr(VI) peak at -600 mV in the residue of 1633b heated in 2N HCl for 2 h, which disappeared after heating it for 4 h. A similar phenomenon is seen in Fig. 7 for 1633b heated in 50% HF but the Cr peaks were broadened due to more extensive leaching. The Cr species in the solids and leachates of 1633b were determined to obtain closure. As shown in Table 8, Cr(III) in 1633b was either oxidized to Cr(VI) and detectable on the residue surface or dissolved and then partly oxidized in solution.

REFERENCES

1. Huggins, F.E.; Shah, N.; Zhao, J.; Lu, F.; Huffman, G.P. Energy & Fuels 1993, 7, 482-489.
2. Boussemart, M.; van der Berg, C.M.G. Anal. Proc. 1991, 28, 68-70.
3. Boussemart, M.; van der Berg, C.M.G.; Ghaddaf, M. Anal. Chim. Acta 1992, 262, 103-105.
4. Ou-Yang, G.L.; Jeu, J.F. Anal. Chim. Acta 1993, 279, 329-334.
5. Paniagua, A.R.; Vazquez, M.D.; Tascon, M.L.; Batanero, P.S. Electroanal. 1993, 5, 155-163.
6. Christian, G.D. in Analytical Chemistry, 2nd ed., 1977, Wiley, p.456.
7. Wong, J.L.; Qian, J.; Chen, C.H. Proc. 2nd Intl. Conf. on Managing Hazardous Air Pollutants, EPRI TR-104295, 1993, IV-1 - IV-19

Table 1. Voltammetric analysis of chromium valence states of HF digests of coal fly ash

Samples[a]	Cr(VI) ug/g	Cr Total ug/g	Cr(VI) / Cr Total %Total
CFF-LS100	116.3	155.1	75.0
CFF-LS102	112.1	137.4	81.6
CFF-LS100/FLT	108.8	140.8	77.3
SRM 1633b	142.0	196.4	72.3

[a] CFF samples were obtained from Dr. F.E. Huggins, Univ. of Kentucky, who showed Cr(III) to be the predominant species by XAFS spectroscopy.

Table 2. Chromium speciation of SRM 1633b by phase separation

Sequential Extraction	Cr(III) ug/g	Cr(III) %	Cr(VI) ug/g	Cr(VI) %	Cr(ttl) ug/g	Cr(ttl) % certified[a]
1. NaOAc, pH5	13.0	100.0	0.0	0.0	12.7	6.7
2. Na2S2O4-Citrate pH5	0.0	0.0	0.0	0.0	0.0	0.0
3. Electromagnet	-	-	-	-	5.9	3.0
4. 2N HCl, heat	30.2	64.9	16.4	35.1	46.8	24.0
5. 50% HF, heat	35.6	28.1	91.1	71.9	129.4	66.4
Extracts 1 to 5	78.8	41.0	107.5	59.0	194.8	100.1
50% HF (total digest)	53.5	26.9	145.4	73.1	196.4	99.1

[a] Cr certified 198.2 ug/g

Table 3. Comparison of chromium valence state of SRM 1633b by 2 extractions

A: Electromagnet residue ------ 2N HCl ------ 50% HF

B: Electromagnet residue ---------- 50% HF

Sequential Extractions	A Cr(III) ug / g	A Cr(VI) ug / g	A Cr(Tot) ug / g	B Cr(III) ug / g	B Cr(VI) ug / g	B Cr(Tot) ug / g
2N HCl	30.7	16.5	46.6			
CV%	4.0	3.1	2.6			
50% HF	30.9	97.7	127.8	50.3	123.8	175.3
CV%	4.8	2.9	2.3	3.0	2.8	4.6
Subtotal	61.6	114.2	174.4	50.3	123.8	175.3
% Valence	35.0	65.0		28.9	71.1	

Table 4. Mass balance of Fe determination in 5-step extraction of SRM 1633b

Extraction step	Fe2+ found (ug/g)	Fe3+ found (ug/g)	Fe(T) found (ug/g)	% Certified
1. NaOAc, pH 5	0.0	2076.8	2076.8	2.7
2. Na2S2O4-citrate, pH 5	6367.0	0.0	6367.0	8.2
3. electromagnet	5447.7	9990.2	15437.9	19.9
4. 2 N HCl, heat	0.0	8144.4	8144.4	10.5
5. 50 % HF, heat	0.0	45462.6	45462.6	58.7
Total	11814.7	65674.0	77488.7	100.0

Fe Certified in 1633b: 77800 ug/g

Table 5. Fate of Cr(VI) in the presence of Fe(II) and FeS2 in extractions

Extractant	A, Cr Recovered		B, Cr Recovered			
	Cr(III)		Cr(III)		Cr(VI)	
	ug	%	ug	%	ug	%
NaOAc, pH5 Bransonic	4.72	94.4	0.00	0.0	0.96	96.0
2N HCl, heat	4.91	98.2	0.96	96.0	0.00	0.0
50% HF, heat	4.88	97.6	1.05	105.0	0.00	0.0

A: 5 ug Cr(VI) + 50 ug Fe(II)

B: 1 ug Cr(VI) + 10 mg FeS2

Table 6. Fate of Cr(III) and Cr(VI) in the presence of arsenite and MnO2

Extractant	A, Cr Recovered				B, Cr Recovered			
	Cr(III)		Cr(VI)		Cr(III)		Cr(VI)	
	ug	%	ug	%	ug	%	ug	%
NaOAc, pH5 Bransonic	0	0	4.77	95.4	2.30	46.0	2.80	56.0
2N HCl, heat	2.35	4.7	2.47	49.4	0.00	0.0	4.76	95.2
50% HF, heat	2.31	46.2	2.44	48.8	0.00	0.0	4.80	96.0

A: 5 ug Cr(VI) + 5 ug As(III)

B: 5 ug Cr(III) + 10 mg As(V)

Table 7. Solid state Cr speciation of fly ash by CPE[a]

Fly Ash	Peak Current uA	Cr(III) found ug/g	CV %	Cr(total)[b] ug/g
SRM 1633b[c]	8.46	205.5	2.5	195
CFF-LS102	5.60	135.4	4.9	137

[a]Carbon paste electrode: fly ash-CPE in electrolyte: 0.002M H2SO4+0.5M KNO3+10-4M DPCI; single peak from anodic scan, no Cr(VI) peak in cathodic scan; CV from 3 seperate analysis

[b]Cr determined after digestion of fly ash in 50% HF

[c]Certified Cr 198.2 ug/g

Table 8. Chromium sepeciation of SRM 1633b in solids and leachates

Treatment	Cr in solids[a] (ug/g)		Cr in leachates[b] (ug/g)		Cr(sum) / Cr certified %
	Cr(III)	Cr(VI)	Cr(III)	Cr(VI)	
(None) before extraction	205.5	0	0	0	105.4
2N HCl, heat 2h	146.1	9.65	29.4	11.5	99.1
2N HCl, heat 4h	135.4	0	39.4	22.7	99.5
50% HF, heat 4h	0	0	53.9	149.2	102.2

[a]100 mg 1633b--1 g carbon as CPE in electrolyte 0.002M H2SO4+0.5M KNO3+10-4M DPCI

[b]DPCI--MCPE in electrolyte 0.002M H2SO4+0.5M KNO3

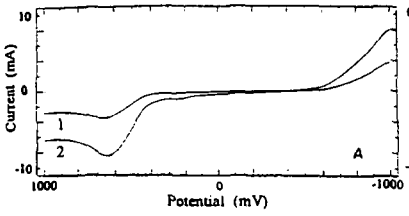

Fig. 1A *Oxidation voltammograms of Cr(III) in* carbon paste electrod in electrolyte: $2X10^{-3}$ M H_2SO_4+0.5 M KNO_3+10^{-4} M DPCI
1-- 100 mg $KCr(SO4)_2$/g carbon
2-- 100 mg Cr_2O_3/g carbon

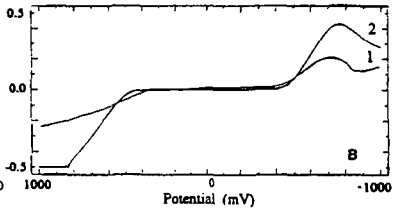

Fig. 1B Reduction voltammograms of Cr(VI) in carbon paste electrode in the above electrolyte.
1-- 100 mg $PbCrO_4$/g carbon
2--100 mg $BaCrO_4$/g carbon

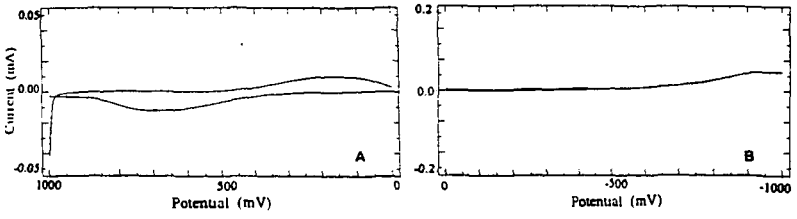

Fig. 2 Cyclic voltammograms of SRM 1633b in carbon paste electrode (100 mg/g) in the above electrolyte,
A--plotted 1000 mV--0 mV at ±50 μA B-- plotted -1000 mV--0 mV at ± 200 μA.

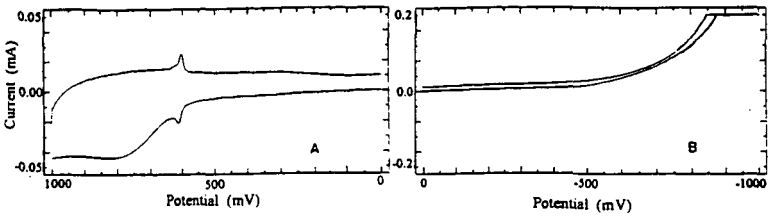

Fig. 3 Cyclic voltammograms of CFF-LS102 in carbon paste electrode (100 mg/g) in the above electrolyte, A–plotted 1000 mV–0 mV at ±50 μA B– polted -1000 mV–0 mV at ± 200 μA.

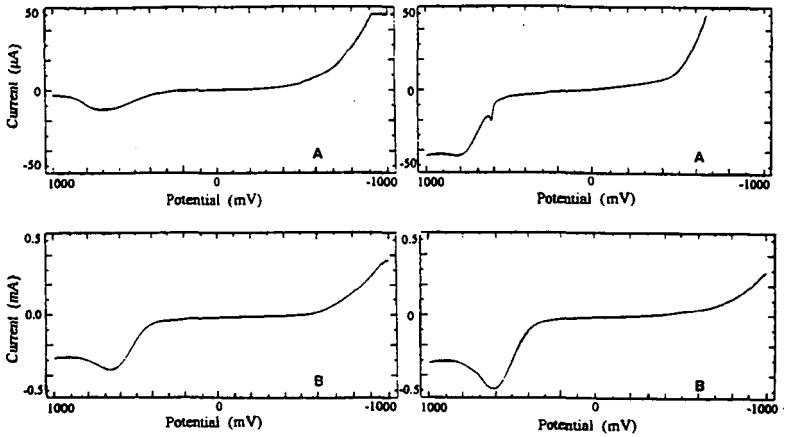

Fig. 4 Oxidation voltammograms of SRM 1633b spiked with Cr_2O_3 in carbon paste electrode in the above electrolyte
A–100 mg 1633b/g carbon
B–0.5 mg Cr_2O_3 added

Fig. 5 Oxidation voltammograms of CFF-LS102 spiked with Cr_2O_3 in carbon paste electrode in the above electrolyte
A–100 mg CFF-LS102 /g carbon
B–0.5 mg Cr_2O_3 added

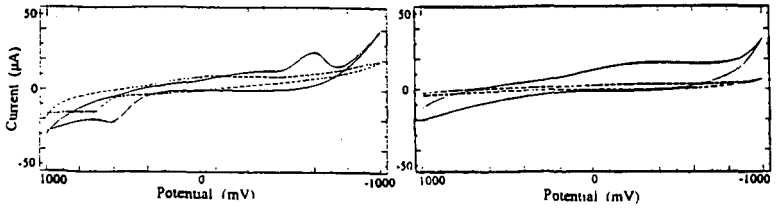

Fig. 6 Cyclic voltammograms of SRM 1633b residue of 2N HCl treatment in carbon paste electrode in the above electrolyte
(——)–140°C. 2 h.
(- - - -)–140°C. 4 h.

Fig. 7 Cyclic voltammograms of SRM 1633b residue of 50% HF treatment in carbon paste electrode in the above electrolyte
(——)–140°C 2 h.
(- - - -)–140°C 4 h.

A FUNDAMENTAL INVESTIGATION OF TOXIC SUBSTANCES FROM COAL COMBUSTION

C.L. Senior and L.E. Bool,
PSI Technologies
20 New England Business Center
Andover, MA 01886

G.P. Huffman and F.E. Huggins
University of Kentucky
Lexington, KY 40506

Keywords: air toxics, trace elements, coal, combustion

INTRODUCTION

The Clean Air Act Amendments of 1990 identify a number of hazardous air pollutants (HAPs) as candidates for regulation. Should regulations be imposed on HAP emissions from coal-fired power plants, a sound understanding of the fundamental principles controlling the formation and partitioning of toxic species during coal combustion will be needed. For this reason PSI Technologies, under the support of the U.S. DOE, the Electric Power Research Institute (EPRI), and the Technical Research of Finland (VTT), has teamed with researchers from the USGS and several leading universities to determine the dominant mechanisms that control trace element partitioning in combustion systems. The final objective of this program will be to develop a broadly applicable emissions model useful to regulators and utility planners.

This paper describes the need for this type of fundamentally based emissions model, and some of the important data required to develop such a model. Some of these data include the elemental modes of occurrence in coal of important trace elements, and how these modes of occurrence may control the partitioning of these elements in combustion systems. The current program to study these issues is presented, as are the results obtained to date. Four coals have been selected for their diversity in mineralogy and trace element composition. After a description of the rationale for the approach, preliminary data on coal composition and on modes of occurrence of trace elements in the coals are presented.

RATIONALE

Current understanding about toxic species transformations and partitioning in coal-fired combustion systems points to gaps in data that need to be filled in order to produce a model that will be useful for both new and existing combustion sources. The large amount of data accumulated from field and laboratory tests has defined the general behavior of toxic and trace species during coal combustion. One of the major efforts to collect field data is the Power Plant Integrated Systems Chemical Emissions Study (PISCES) led by EPRI. Within PISCES, EPRI performed an extensive literature search on the partitioning of toxic and trace species into the various output streams of power plants. Detailed field measurements were also made of the concentrations of 22 species in the effluent streams of power plants.[1] This effort has resulted in a large database of emissions of trace and toxic species.[2] Organic toxins may also be emitted from coal-fired systems. Field studies suggested that emissions of organic species from coal-fired plants are tied to the combustion efficiency and are typically much lower than emissions of inorganic species.[3-5]

There appears to be a consensus of opinion that the four most critical trace elements for coal combustion are Hg, As, Cr, and Se. Ni, Mn, and Pb are of lesser concern, while the remaining elements (Sb, Be, Co, Cd) appear to present little cause for concern for coal utilization because of their low abundance in coal and their insignificant contribution to pollution of the atmosphere in comparison to non-coal source.[6] Chlorine and the other halogens are also of concern. Chlorine, in particular, can be found at concentrations in excess of 1000 ppm in some bituminous coals. Thus for some power plants, either HCl or Cl_2 may exceed the 10 ton/y CAAA limit. Also chlorine may play a key role in determining the volatility of mercury.[7]

Messerole and Chow[8], using PISCES data, found that several elements, including As, Cd, Hg, and Se, typically vaporize in utility boilers. Some of these condense on flyash particles and are removed by pollution control devices. Others such as Hg, F, and Cl are emitted predominantly as vapors. However, significant variations in trace element behavior were noted, possibly caused by interactions with other minerals or differences in modes of occurrence in the parent coal. This was emphasized by Meij[7], who observed large differences in Hg and As partitioning as coal type was varied in one utility boiler unit. These difference were attributable to differences in the mode of occurrence and the combustion transformations of these metals. If the fundamental mechanisms that govern the behavior of these species were understood, the utility industry could better predict emission rates.

This need increases in importance when unique fuels, equipment configurations, and operating conditions are considered.

Other investigators have studied the behavior of trace elements in laboratory combustion systems as reviewed in recent papers.[10-12] Despite these efforts, mechanistic information is generally lacking. For example, Linak and Wendt[11] presented the results from several laboratory and field studies on the enrichment of trace elements in the submicron ash. Although the data set is not entirely consistent for all species, it does show enrichment of several elements in the submicron ash which is most likely to escape from particulate control devices. These elements include Sb, As, Cd, Cr, Pb, Hg, Ni, and Se. Other elements such as Cl were found to remain in the vapor phase.

Previous mineral matter transformation work has demonstrated the critical importance of the *forms* or *modes* of occurrence of trace elements in coal on their behavior during combustion.[12,13] The mode of occurrence of an element is important because of the tremendous diversity in which an element can be found in coal.[14,15] An element can be completely dispersed throughout the coal macerals or can exist within its own discrete mineral phase. Organically associated metals such as sodium typically vaporize during combustion. Metals contained in clays, on the other hand, typically do no vaporize. Bool and Helble showed that the volatility of a number of trace metals is dependent on elemental form in the coal.[12] Quann et al. noted the importance of form in a systematic study of twenty different coals burned under well-characterized conditions.[17]

One of the first methods developed for estimating emissions from power plants was the use of empirical emissions factors.[10,18] For example, based on data from five boilers, Brooks reports an average emission factor of 684 lb/10^{12} Btu for arsenic in uncontrolled dry-bottom pulverized coal boilers.[10] Although emissions factors are useful for preliminary calculations, they are clearly inappropriate for use in determining regulatory compliance or in predicting the effect of fuel and boiler modifications on partitioning and emissions. A more complex model to predict trace species partitioning, based on the PISCES database, has been developed by Rubin and co-workers.[18,19] This model uses a probabilistic analysis to predict the partitioning of a given element into the various output streams of a coal-fired utility boiler. Boiler configuration inputs are combined with trace element partitioning data from the PISCES database. The model predicts a range of emission values based on the uncertainties of the inputs (i.e., species concentrations in the coal). The model has been shown to predict emissions of several species for specific power plants with a reasonable degrec of accuracy.[20] Use of the model is best suited to well-defined configurations for which partitioning data are available. Since the PISCES project covered less than 5% of the approximately 1,750 utility boilers in the U.S., many existing facilities fall "outside" the data base. For novel fuels and boiler configurations, the uncertainty in predicted toxic species emission will be high.

The large amount of data accumulated from the field and from laboratory tests has defined the general behavior of toxic and trace species during coal combustion. Concentrations of toxic elements have been measured for many coals. A broad variation in elemental form has been reported for many elements with major data gaps existing. Very little information on the interactions of trace species with major coal minerals is available. The four most critical trace toxic metals that are emitted to the environment by coal combustion are Hg, As, Cr, and Se. Halogens, particularly Cl, are also of key importance. In order to meet the challenges of cleaner power production in the future, a new method is needed to predict emissions of toxic species from a wide range of fuels (and blends) and from many different kinds of combustion systems. The specific approach taken by the team is described below.

TECHNICAL APPROACH

The discussion in the preceding section illustrates the need to perform a comprehensive program to determine how the form of occurence of an element in coal and the combustion conditions control the partitioning of that element in combustion system. This information, if obtained as part of carefully planned combustion experimentation, will be crucial to better understand the partitioning data collected in full scale units, and to develop a model applicable to all types of coal fired combustion systems. With this objective, the PSIT-led team has begun a multi-year program to determine the forms of occurence in coal, and the effect of the combustion (and post combustion) environment on partitioning of these elements. Participants in the program include researchers from MIT, Princeton University, University of Arizona, University of Connecticut, University of Kentucky, USGS, and VTT. The following section describes many of the tools that will be used, and the combustion facilities that will be used, to address these issues.

Direct identification of the modes of occurrence of trace inorganic species in coal and ash using unique analytical techniques such as XAFS analysis and selective leaching forms a cornerstone of the approach. Elemental modes of occurrence will be established for the key elements using a combined microscopic/spectroscopic approach. XAFS spectroscopy is currently capable of

supplying information in the middle of the periodic table (Ti-Sn) with abundances in excess of 5 to 10 ppm.[15] Whereas XAFS spectroscopy will provide a specific signature of all modes of a given element in the coal in a single spectrum, the microscopic-based methods will provide valuable complementary information on the spatial distribution and association of the element. This combined approach, which has not been attempted before, should provide the more information than has been available previously about an element's mode of occurrence in coal. Elemental modes of occurrence will also be determined for trace species using an analytical procedure developed by USGS. This protocol combines low temperature ashing, chemical analysis, x-ray diffraction, coal segregation via flotation, leaching, electron microbeam measurements, and low and moderate temperature heating tests to elucidate forms of elements in coal.

Combustion testing will be used to determine the importance of each of four fundamental processes that may influence the speciation and partitioning of trace metals during combustion. These processes are (1) vaporization of metallic species, (2) gas-phase transformations of metallic species, (3) condensation of gaseous metallic species, and (4) solid transformations of metallic species. In general all four of these processes can take place simultaneously and in competition with each other.

A unique aspect of the program is an attempt to isolate and study these steps as much as possible while retaining the conditions that are typically present during coal combustion. *Fundamental bench scale studies* will be used to isolate vaporization and condensation of trace metals. Combustion of size and density-classified coal particles will allow a mechanistic interpretation of vaporization. Thermogravimetric studies of metal vapor-solid interactions will provide information on the interactions between gaseous species and ash particles post-combustion. *Integrated combustion experiments* using utility grind coal samples and realistic combustion stoichiometries will allow the evaluation of excluded mineral and combustion effects. *Self-sustained combustion experiments* using a 100,000 Btu/h coal-fired combustor with realistic heating and cooling rates permits the examination of trace metal partitioning when all the important mechanisms are combined.

A critical review of available field data provides guidance for the overall program direction and model validation. An analysis of steady state and transient organic emissions from field data will be conducted to determine whether organic toxic emissions pose a concern and should therefore be included in ToPEM. Inorganic emissions reported from recent comprehensive field sampling campaigns will also be reviewed and one or more sets of model validation data will be selected from DoE or EPRI field studies consisting of coal composition, combustion conditions, and concentrations of trace metals in solid and gaseous streams, including the effects of back end conditions on trace metal partitioning. The effect of coal type and combustion conditions on submicron ash morphology will also be assessed using data collected by VTT.

COAL CHARACTERIZATION

Four coals have been acquired for the Phase I baseline studies. All coals are currently being used by utilities in the United States and represent a diversity of coal and mineral types. The coals are (1) Illinois 6 (Burning Star No. 4 mine), (2) Washed Pittsburgh Seam (Blacksville mine), (3) Eastern Kentucky coal (Elkhorn and Hazard seams), and (4) Wyodak subbituminous (Black Thunder mine). All coals will be analyzed for trace element content (Instrumental Neutron Activation Analysis), for iron oxidation state (Mössbauer spectroscopy), mineral distribution (Computer Controlled Scanning Electron Microscopy), and for forms of trace elements (XAFS and selective leaching).

Preliminary work on the mode of occurrence of arsenic in two bituminous coals, Pittsburgh and Elkhorn/Hazard, has been completed. The form of occurrence of As in coal may have an effect on the vaporization behavior during combustion. Most As in U.S. coals is associated with the sulfide phase (i.e., pyrite).[21] Oxidation of the pyrite in coal will result in the formation of arsenates. Preliminary evidence suggests that arsenic associated with pyrite may volatilize more readily than arsenates.[22]

Mössbauer spectroscopy was used to assess the oxidation state of iron in the Pittsburgh and Elkhorn/Hazard coals. Virtually all the iron in the Pittsburgh coal is present as pyrite, whereas almost one-third of the iron in the Elkhorn/Hazard coal is present in other forms (clays, siderite, and jarosite). The presence of jarosite may be an indication of oxidation of pyrite in the coal. The Elkhorn/Hazard coal showed 12% of the iron as jarosite, while for the Pittsburgh coal only 2% jarosite was detected.

Based on a previous XAFS study of arsenic occurrence in U.S. bituminous coals,[22] three forms of As have been identified in these coals. Arsenical pyrite, in which As substitutes for Fe in FeS_2, is the most common. Arsenate compounds (AsO_4^{-3}) are the next most common and arsenopyrite (FeAsS) is the least common. Oxidation of arsenical pyrite has been shown to produce arsenate compounds. In the present work XANES spectroscopy for As was conducted on both coals as well

as on high density fractions (which are predominantly pyrite) separated by a float/sink technique using bromoform (Figure 1). The much better signal/noise ratio obtained in the high density fractions as compared to the raw coals suggests that As is strongly associated with the pyrite. It is also clear that the As in the Elkhorn/Hazard coal is significantly more oxidized than in the Pittsburgh coal since the arsenate peak (A) is relatively higher than the pyrite peak (P). This is consistent with the Mössbauer analysis which indicates that a significant amount of the pyrite in the Elkhorn/Hazard coal is oxidized. Combustion experiments are planned which will explore the relationship between forms of As in the coal and As vaporization during combustion.

A previous study of trace element partitioning in two of the program coals,[12] provides an indication of the combustion behavior of trace elements in the Pittsburgh and Wyodak coals. The two coals were subjected to a leaching analysis to determine the forms of selected trace metals (As, Se, Hg, Zn, Sb, Cr). Combustion experiments and equilibrium calculations were used to understand the mechanisms governing the combustion behavior. The form of the element in the coal was shown to have major impact on the combustion behavior. Those elements that were organically bound or associated with the sulfide minerals were shown to vaporize during combustion. Once in the vapor phase, these elements in some cases reacted with minerals present in the ash to form condensed phases. The size distribution of trace elements resulting from combustion was determined by whether or not the element reacted with mineral compounds in the ash.

ACKNOWLEDGMENTS

The XAFS spectra were obtained at the Stanford Synchrotron Radiation Laboratory. The work was supported by the U.S. Department of Energy under contract DE-AC22-95PC95101.

REFERENCES

1. Chow, W. and Torrens, I.M., Presented at the *American Power Conference*, Chicago, IL, 1994
2. Wetherhold, R.G. and Chow, W., Presented at the *International Conf. on Managing Hazardous Air Pollutants*, Palo Alto, CA, 1991.
3. Sage, P.W. and Williamson, J., Presented at the *2nd International Conf. on Managing Hazardous Air Pollutants*, Washington, D.C., 1993.
4. Miller, C.A., Sravistava, R.K., and Ryan, J.V., *Env. Sci. Tech.*, **1994**, *28*, 6.
5. Chu, P., Nott, B. and Chow, W., Presented at the *2nd International Conf. on Managing Hazardous Air Pollutants*, Washington, D.C, 1993.
6. Clarke, L.B. and Sloss, L.L., Trace Elements - Emissions from Coal Combustion and Gasification, IEA Coal Research Report IEACR/49, 1992.
7. Meij, R., *Fuel Proc. Technol.*, **1994**, *39*, 199.
8. Meserole, F.B. and Chow, W., Presented at the *International Conf. on Managing Hazardous Air Pollutants*, Palo Alto, CA, 1991.
9. Meij, R. and van der Kooj, J. Air Pollutant Emissions from Coal-Fired Power Stations, *KEMA Sci. Tech. Rep.* **1986**, *6*, 4.
10. Brooks, G., Estimating Air Toxics Emissions from Coal and Oil Combustion Sources, EPA Report PB89-194229, 1989.
11. Linak, W.P. and Wendt, J.O.L., *Prog. Energy Comb. Sci.*, **1993**, *19*, 145.
12. Bool, L.E. and Helble, J.J., *Energy & Fuels*, **1995**, *9*, 880.
13. Zygarlicke et al., Combustion Inorganic Transformations, University of North Dakota Energy and Environmental Research Center Final Report on Contract DE-FC21-86MC10637, 1991.
14. Swaine, D.J., *Trace Elements in Coal*, Butterworths, London, 1990.
15. Huggins, F.E., Zhao, J., Shah, N., and Huffman, G.P., Presented at *International Conf. on Coal Science*, Banff, Alberta, 1993.
16. Helble, J.J., *Fuel Proc. Technol.*, **1994**, *39*, 159.
17. Quann, R.J. and Sarofim, A.F., *Comb. Sci. Technol.*, **1990**, *74*.
18. Edwards, L.O., Muelah, C.A., Sawyer, R.E., Thompson, C.M., Williams, D.H., and Delleny, R.D., Trace Metals and Stationary Conventional Combustion Processes, EPA Report No. EPA-600/s7-80-155, 1981.
19. Rubin, E.S., Berkenpas, M.B., and Chow, W., Presented at the *Ninth Annual Pittsburgh Coal Conference*, Pittsburgh, PA, 1992.
20. Rubin, E.S., Berkenpas, M.B., Freu, H.C., and Toole-O;Neil, B. Presented at the *2nd International Conf. on Managing Hazardous Air Pollutants*, Washington, D.C, 1993.
21. Finkelman, R.B., Palmer, C.A., Krasnow, M.R., Aruscavage, P.J., Sellers, G.A., and Dulong, F.T, *Energy & Fuels*, **1990**, *4*, 755.
22. Huggins, F.E., Helble, J.J., Shah, N., Zhao, J., Srinivasachar, S., Morency, J.R., Lu, F., and Huffman, G.P., *Preprints of ACS Div. Fuel Chem.*, **1993**, *38*.

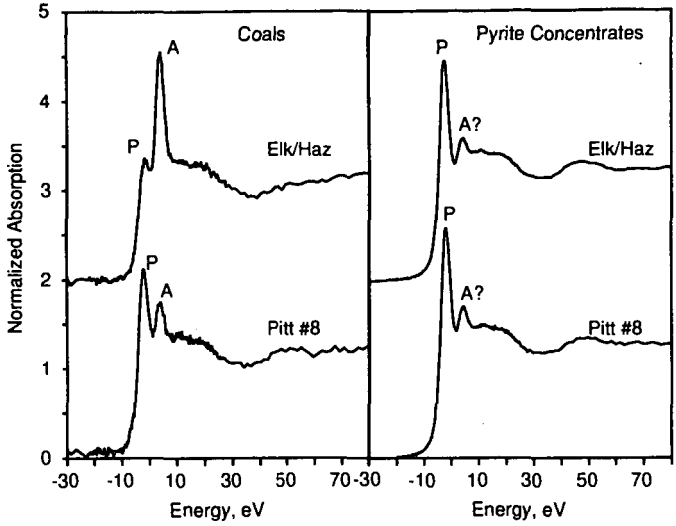

Figure 1. XANES spectra for arsenic: Pittsburgh and Elkhorn/Hazard coals and high density fractions. Peaks corresponding to arsenate (A) and pyrite-associated (P) species are indicated.

FATE OF TRACE ELEMENTS IN UK COALS DURING GASIFICATION PROCESSES

Andrew J. Bushell and Jim Williamson
Department of Materials, Imperial College of Science, Technology and Medicine,
London SW7 2BP, UK.

Keywords: UK coals, gasification, pilot plant

ABSTRACT

Five UK coals were selected to cover the range of mineral matter and ash contents typically encountered in UK bituminous coals. Trace element analysis was performed on both the whole coals and size separated fractions using ICP analysis for 21 trace elements, including Be, Cr, Co, Ni, As, Cd, Sb, Hg, and Pb, elements deemed to be the most environmentally hazardous.
Small quantities of each coal were gasified in a laboratory gasifier in an atmosphere of N_2 containing 15% O_2. Samples of bed ash, cyclone ash, and a fine gas-filtered ash were collected and analysed to determine the partition of the trace elements between the gasification products. Mass balance calculations showed that the recovery of the trace elements varied from 20 to 97%; the low recovery of some trace elements highlighting the difficulties of collecting representative samples from a laboratory system.
A parallel study on samples taken from a pilot plant gasifier showed significantly higher recovery rates, indicating the value of larger scale trials.

INTRODUCTION

The gasification of coal, and in particular the development of integrated gasification combined cycles systems (IGCC) holds the promise for coal conversion processes with both higher efficiencies and lower gaseous emissions. While such systems may meet the anticipated legislation for NO_X, SO_X and particulate emissions, it is essential that the fate of the trace elements and the heavy metals which are present in all coals is well established, since these elements may yet present further environmental hazards.

Coals contain most of the naturally occurring elements with widely varying concentrations depending on rank, geological origin and history. Coal combustion has been reported as being the main source of Hg, Ni, Sn and V emissions, and the second largest source of Cd, Se, and Tl (1). The 1990 US Clean Air Act identified eleven trace elements, namely Be, Cr, Mn, Co, Ni, As, Se, Cd, Sb, Hg and Pb as being the most environmentally hazardous. These elements are all found in coals at concentrations ranging from a few ppb for elements such as Sb and Hg, to several hundred ppm for Mn. The majority of the trace elements are associated with the mineral matter in the coal. This mineral matter consists primarily of clays (aluminosilicates) and quartz, with smaller amounts of carbonates, sulphides, sulphates and oxides. Trace elements may also be associated with the macerals, reflecting the inorganic species present in the vegetation from which the coal was formed. The exchange of ions between mineral matter and macerals following the coalification process gives added complexity to establishing the distribution and mode of occurrence of the trace elements in a coal.

The occurrence of trace elements has been extensively studied and reported by Swaine (2), with recent reviews by Clarke and Sloss (3), and Davidson and Clarke (4). These reviews have concentrated on the origins of the trace elements in coal and on the wide range of analytical techniques which are now available for their determination. Pyrite in coal is generally accepted as being a major source of many of the trace elements, and in particular those of environmental concern.

During combustion or gasification of a coal the trace elements partition between the ash residues and the gaseous emissions. The actual distribution will depend on the combustion or gasification conditions and the mode of occurrence of the trace elements in the coal. Trace elements may conveniently be divided into three groups depending on their volatility and the vapour pressure of simple compounds such as oxides and chlorides. Group I elements are the least volatile and remain with the ash residues. Group II elements are more volatile and partition between the residual ash and the gaseous phase, with condensation of vapour species on the surface of the fine ash particles as the gases cool. Group III elements have a high volatility and show little or no tendency to condense from the vapour phase. Many of the environmentally sensitive elements fall into groups II and III, highlighting the current concern. Dale (5) reported on the trace element partitioning in the stack emissions from pf fired power stations, stressing the importance of monitoring flue gas discharges which may contain some of the environmentally sensitive elements. Other studies, notably those carried out by KEMA in the Netherlands (4) have shown that, with the exception of Hg and Se, 95% or more of the trace elements may be recovered from the bottom ash and the electrostatic precipitators at a power station. Concern remains that the fine particulate matter, with surface enrichment in trace

elements, may escape the gas cleaning process.

Much less work has been reported on the fate of the trace elements during gasification processes. Here the conditions are much more reducing and thus the volatile species may be different from those which form in a combustion process. Benson et al (6) reported that elements such as As, Cd, Se and Pb all showed increased volatility as the C:O ratio decreased in a laboratory gasification study of three US coals. Bushell and Williamson (7) gave the results of a trace element survey for a selection of UK bituminous coals. This Showed that the elements with the strongest mineral associations were Ba, Co, Cr, Cu, La, Pb, Zn, and Zr, while those elements with a strong maceral association were Be, Sr and V.

This paper gives further details of the fate of the trace elements during gasification of coals from both a laboratory study and a pilot scale gasification process using UK coals.

EXPERIMENTAL

Five UK bituminous coals were selected from the UK Coal Data Bank , currently managed by CRE Group Ltd, Stoke Orchard. The coals provided the range of ash contents and mineralogy found in UK coals. Coals were supplied as partially washed <212μm coals. A high temperature ash (HTA) was prepared in a muffle furnace at 815°C and the major oxides and the trace elements present were analysed using a lithium borate fusion, followed by ICPS analysis. The elements As, Sb and Bi were determined by a hydride generation technique, and both the coals and ashes Hg was determined by a cold vapour generation process followed by ICPS.

A low temperature ash (LTA) was prepared in an O_2 plasma which left the mineral matter in a largely unaltered form. Mineral matter was identified by x-ray powder diffraction analysis of the LTA, and a quantitative estimate of the proportions of the minerals present was made by a normative analysis procedure, using the ash composition and the minerals known to be present.

Samples of each coal were ground to <38μm and then density separated into mineral-rich and coal-rich fractions using bromochloromethane (ρ = 1.99g cm^3). Each fraction was analysed for the trace elements and enrichment factors calculated, i.e. the concentration of an element in the separated fraction / concentration of the element in the original coal, to determine how the trace elements were partitioned between the macerals and the mineral matter.

Each coal was also separated into eight size fractions using a Gilsonic Siever with mesh sizes at 180, 150, 125, 106, 75, 53 and 38μm. Size fractions were high temperature ashed and the trace elements in each fraction determined to assess the distribution of the trace elements between the various size ranges.

The coals were gasified in a laboratory gasifier where 10 x 1g samples of coal were introduced into a pre-heated bed of fluidised sand at 950°C where the fluidising gas was 15% O_2 in N_2 . After gasification, samples of the bed ash, cyclones fines and fine gas-filtered particulates (10-0.1μm) taken from the gas stream were analysed for the trace elements.

The fate of the trace elements in the laboratory gasifier were compared to that in a pilot plant scale gasifier. Coal and ash residues were obtained from the air- blown gasifier (ABG) operated by British Coal at the Coal Research Establishment at Stoke Orchard. This gasifier operates at temperatures up to 1000°C and 20 bars pressure, with coal feed rates of 200-300 kg hr^{-1}. Some 70-80% of the coal is converted into a low calorific gas, with ash and char being continuously removed from the base of the reactor to a circulating fluidised bed combustor (CFBC), where the remaining char conversion takes place. Limestone may be added to the coal as a sulphur sorbent to retain the sulphur in the bed ash. Samples of coal feed, bed ash and ash from the primary cyclone were provided for analysis of the major oxides and the trace elements.

RESULTS AND DISCUSSION

The ash composition and the trace element concentrations in each of the coals used for the laboratory gasification studies are shown in Table 1. To a first approximation, the concentration of most of the trace elements is related to the amount of mineral matter in the coal and thus high ash coals showed higher concentrations of the trace elements. The coals all contained mixtures of clays (kaolinite and illites), quartz and pyrite in different proportions, and variable but smaller amounts of calcite, dolomite, ankerite, rutile and apaptite. Trace element concentrations were noticeably higher for coals with larger amounts of pyrite. Ash contents ranged from 3.9 wt% for the Daw Mill coal to 19 wt% for Longannet. Since Longannet has the lowest iron content, although the ash content is high, the trace element levels are still comparable with the other coals.

In general the ash contents of the size separated coals increased as the size range was reduced. The one exception to this was the Longannet coal, where the mineral matter was uniformly distributed across all the size ranges, and thus relatively uniform trace element concentrations were observed for each size fraction of the coal.

Samples of the bed ash, cyclone fines and the fine particulate ash filtered from the gas stream of the laboratory gasifier were analysed and a mass balance calculation performed to determine the distribution of the trace elements during the gasification process. The results with the Daw Mill coal (3.9 wt% ash) are shown in Table 2. With the exception of Cd and Zn, where virtually no recovery was recorded, 30 - 90% of most of the trace elements which entered the gasifier could be accounted for. Most of the trace elements were found in the cyclone fines, where the major oxide ash composition was close to that of the whole coal. A few percent of the trace elements were retained in the bed ash or found with the fine particulates filtered from the gas stream. This suggests that at the gasification temperatures most of the trace elements remain with the decomposed mineral matter, which is elutriated from the bed as the char is oxidised. Some trace elements may be volatilised under gasification conditions, to then recondense on the surface of the ash particles in or before entering the cyclone separator.

Similar results were obtained with the Longannet coal (19.0 wt% ash) as shown in Table 3. The mass balance calculations showed a higher recovery of the trace elements in the gasifier residues, with again the majority of the trace elements appearing in the cyclone fines. Significant amounts of Zn and La were found in the gas-filtered fines, which suggested that condensation of the Zn had occurred on the surface of the finest ash particles from the cooling vapours, while in addition the elutriation of very small La enriched particles (clays) from the fluidised bed may be a possible explanation of the high value for the La.

The results from the laboratory study were nevertheless disappointing, with substantial amounts of many of the trace elements unaccounted for in the mass balance calculations. The most likely source of error in the experimentation would appear to be in the sampling of the bed ash, since this is where many of the low volatile elements should appear. The difficulties in taking representative 1-2g samples from a 200g bed of sand are formidable when one realises that it may be just a few mineral grains, rich in trace elements, which are distributed somewhere in the bed. This raises the whole question of the problems and the suitability of laboratory studies for this type of research.

Residues from the British Coal air-blown gasifier consisted of a bed ash containing approximately 50% char, and fines collected from the primary, secondary and tertiary cyclones. Bed ash and primary cyclone fines constituted the bulk of the inorganic material introduced into the gasifier. Table 4. shows the distribution of the trace elements between the bed ash and the primary fines when Daw Mill coal was used as feedstock for the gasifier. An ash analysis showed that the primary fines were enriched in Fe, indicating possible preferential elutriation of fine particles of pyrite from the bed. Trace element analysis and mass balance calculations showed that 95% or more of the trace elements introduced into the gasifier could be accounted for. The trace elements partitioned relatively uniformly between the bed ash and the fines. The more volatile elements such as Be, Co, Cr, Cu, Mo, Ni, Pb, and V showing an enrichment in the fines, while the more refractory elements such as Ba, Sc, Y and Zr showed a slight preference to remain in the bed ash. The high levels of trace elements found in the cyclone fines from both the laboratory studies and the pilot scale gasification process suggests that the physical and chemical association of the trace elements with the decomposed mineral matter is perhaps as much , if not more important, than the volatility of the elements. Thus establishing the mode of occurrence of the trace elements in a given coal may be key factor in determining the fate of the trace elements on gasification.

CONCLUSIONS

Trace element concentrations in UK coals have been found to be closely related to the amount of mineral matter in the coal. In particular, many of the trace elements would appear to be associated with the pyrite. On gasification the trace elements are distributed between the residual ash and a cyclone ash, with condensation of the more volatile species on the surface of the finest ash particles. Pilot scale gasification has provided better mass balance data than the laboratory studies.

ACKNOWLEDGEMENTS

This work has been supported with grants from BCURA and the ECSC (Project No 7720-EC 01703). Technical support from the CRE Group Ltd, Cheltenham, Loughborough University and the Department of Geology, Imperial College has been much appreciated and is gratefully acknowledged.

REFERENCES
1. Nriagu, J.O. Environment, **32**, 7-33, 1990.
2. Swaine, D.J., "Trace Elements in Coal", Butterworths, London, 1990.
3. Clarke, L.B. and Sloss, L.L., Trace Element Emissions from Coal Combustion and Gasification, IEA Coal Research, London, Report No IEACR 149, 1992.
4. Davidson, R. and Clarke, L.L. Trace elements in Coal, IEA Coal Research, London, IEAPER/ 21, 1996.
5. Dale, L., 8th Int. Conf. Coal Science, Oviedo, Vol 2, pp 1975-1977, 1995.
6. Benson, S.A., Erikson, T.A.and Zygarlicke, C.J., 4th EPRI Conf. on "The Effects of Coal Quality on Power Plants", Charleston, USA, 1994.
7. Bushell, A.J. and Williamson, J., 8th Int. Conf. Coal Science, Oviedo, Vol 1, pp 167-170, 1995.

Table 1. Ash content, trace element concentrations and mineral matter in each coal used for laboratory gasification studies.

Coal	Kellingley	Longannet	Daw Mill	Thoresby	Nadins
ash content (wt%)	4.2	19.0	3.9	4.2	9.4
SiO_2	33.7	52.3	30.3	36.3	28.6
Al_2O_3	19.5	39.7	25.9	25.3	15.7
Fe_2O_3	23.9	1.4	14.4	25.5	26.4
MgO	0.8	0.5	3.2	0.7	2.9
CaO	9.6	0.9	13.7	2.1	10.6
Na_2O	3.6	0.2	0.8	5.6	0.3
K_2O	1.3	0.6	0.4	1.6	1.5
P_2O_5	5.0	0.9	0.3	0.2	0.7
TiO_2	0.8	1.5	1.0	0.9	0.6
MnO	0.2	0	0.5	0	0.3
Trace elements	(ppm)				
Ag	1	0	0	0	0
As	5	1	7	12	31
Ba	67	160	150	67	64
Be	1	3	0.6	2	4
Bi	0.1	0.4	0.2	0.2	0.1
Cd	0	0	0	0	0
Co	6	11	5	3	14
Cr	10	57	11	11	28
Cu	23	61	6	24	15
Hg	0.04	<0.01	0.07	0.07	0.1
La	4	43	4	5	6
Li	6	76	7	11	15
Mo	3	4	3	4	4
Ni	13	46	11	14	52
Pb	8	21	8	21	56
Sb	1	0.4	0.3	1.8	2.4
Sc	2	-	1	2	5
Sr	53	581	35	34	44
V	16	45	15	29	25
Zn	62	27	3	13	29
Zr	10	58	8	11	11
Mineral matter content of coals (wt%)					
kaolinite	28	85	54	38	34
illites	27	11		33	
quartz	5	3			9
pyrite	28		20	29	34
calcite			14		7
apatite	12				
rutile		1			
ankerite					16
dolomite			12		

Table 2. Distribution of trace elements between bed ash, cyclone ash and gas-filtered fines from the laboratory gasification of the Daw Mill coal.

	Input to gasifier (μg)	% elements recovered	Distribution of trace elements			
			Bed ash	Fines	Filter	Balance
Ag	1.1	86	5.5	80.7	0	13.8
Ba	1413	33	2.9	29.1	0.5	67.5
Be	5.5	35	2.3	32.6	0	65.1
Cd	5.7	0	0	0	0	100
Co	44	37	2.0	35.0	0	62.9
Cr	99	34	3.3	30.4	0	66.3
Cu	80	35	3.0	31.7	0.1	65.2
La	31	43	5.7	37.7	0	56.6
Li	47	47	5.6	41.4	0	52.9
Mo	30	31	2.5	28.3	0	69.3
Ni	97	33	2.0	31.2	0	66.8
Pb	80	100	7.0	72.3	20.6	-
Sr	288	43	4.4	38.7	0.3	56.6
V	146	40	2.3	37.4	0.1	60.2
Zn	296	0.3	0	0	0.3	99.7

Table 3. Distribution of trace elements between bed ash, cyclone ash and gas-filtered fines from the laboratory gasification of the Longannet coal.

	Input to gasifier(μg)	% elements recovered	Distribution of trace elements			
			Bed ash	Fines	Filter	Balance
Ag	8.3	36	5.7	27.9	2.0	64.4
Ba	1263	67	20.9	45.7	0	3.4
Be	26	56	5.7	49.8	0.7	43.8
Cd	7.2	52	11.0	39.7	1.0	48.3
Co	91	57	2.4	53.9	0.7	43.1
Cr	387	56	3.7	51.5	0.9	43.9
Cu	502	56	4.0	50.9	0.8	44.3
La	305	84	3.3	50.6	30.7	15.5
Li	642	68	17.1	50.4	0.4	32.2
Mo	31	48	5.2	41.5	1.7	51.6
Ni	384	63	11.0	50.7	0.8	37.5
Pb	154	64	12.1	47.1	5.0	35.8
Sr	4392	67	14.3	50.7	1.9	33.2
V	442	60	5.4	54.5	0.5	39.7
Zn	160	54	11.4	35.0	7.9	45.7

Table 4. Distribution of trace elements between bed ash and primary cyclone fines using Daw Mill coal in the pilot scale air-blown gasifier

Trace element input ($mg.hr^{-1}$)		Output of trace elements (mg.hr-1)			Distribution of trace elements	
		bed ash	Fines	Unaccounted	Bed ash (%)	Fines (%)
Ag	0.16	0.03	0.04	0.09	40	60
Ba	97	57	48	0	54	46
Be	0.25	0.05	0.11	0.09	32	68
Cd	0.17	0.05	0.04	0.08	51	49
Co	1.3	0.42	0.82	0.09	34	66
Cr	4.3	1.2	2.3	0.85	35	65
Cu	4.1	1.0	2.7	0.35	27	73
La	1.3	0.48	0.76	0.08	39	61
Li	3.8	1.6	2.0	0.24	44	56
Mo	0.64	0.17	0.48	0	26	74
Ni	4.5	1.2	2.4	1.0	33	67
Pb	3.7	0.54	1.3	1.32	29	71
Sc	0.91	0.14	0.05	0.72	73	27
Sr	11	2.6	6.3	2.04	29	71
V	5.2	1.9	3.9	0	32	68
Y	1.8	2.2	0.1	0	96	4
Zn	3.1	3.0	1.7	0	63	37
Zr	9.1	12.3	0.19	0	98	2

THE BEHAVIOR OF TRACE ELEMENTS IN FLUIDIZED BED COMBUSTION

Geima P. Suarez-Fernandez, Xavier Querol*, Jose L. Fernandez Turiel*, A. Benito Fuertes and M. Rosa Martinez-Tarazona.
Instituto Nacional del Carbón (CSIC), La Corredoria s/n, Apdo 73, 33080 Oviedo, Spain
*Institut de Ciéncies de la Terra (CSIC), Lluis Solé I Sabals s/n 08026 Barcelona, Spain

Keywords: Trace elements, Fluidized bed combustion

ABSTRACT
The present study focuses on the behavior of major, minor and trace elements during fluidized bed coal combustion, at 850ºC in a 0.14 m i.d. atmospheric reactor. The combustion ashes were continuously taken out of the bed. The rest were elutriated by the combustion gases and collected in two cyclones and a baghouse filter located at the outlet. A low volatile bituminous coal from the Asturian Central basin (North of Spain) was used for the experiments that comprised two tests; with and without addition of limestone. The concentrations of 57 elements were determined in the coal and in the different combustion ashes by ICP-MS, ICP-EAS, and XRF. Elements normally present in the combustion flue gases as vapor, such as Hg and As were sampled in impingners, and determined by cold vapor atomic absorption, and ISO R-601 standard method. Using these methods these elements were not detected in the gas phase. No major differences were observed on the behavior of trace elements during combustion with and without limestone addition. The results show a clear grain size segregation of elements of environmental concern such as As, Co, Cu, Hg, Mo, Ni, Pb, Sb and Se. These elements are enriched in the finest grain size fraction. The grain size partitioning could be attributed to the following processes: a) physical segregation of major and trace elements in the reactor, due to differences on the distribution of these elements in the feed coal and, b) chemical segregation due to volatilization and condensation from flue gas.

INTRODUCTION
Information about of relative contribution of "hazardous air pollutants" trace elements to the atmospheric emissions from coal combustion is important to evaluate the environmental impact of these contaminants. Future environmental regulation of these emissions will be more stringent. During pulverized coal combustion (PCC), trace elements are partitioned between the bottom ashes, fly ashes and vapor, according, not only to the operating conditions and furnace design, but also to their mode of occurrence. This mode of occurrence differs in coals from different origins. Trace element partitioning in PCC has been extensively studied and although there are some aspects related to their behavior that need to be clarified, some generalizations have been established[1-6]. A relative enrichment of trace elements in fly ashes, specially in the fine grain size fractions due to condensation of volatile species from the flue gases on the surface of fly ash particles has been found[1-6].

The fate of trace elements during fluidized bed combustion (FBC) has received less attention and information in the literature is scarce. It can be assumed that trace elements volatilization at the typical fluidized bed combustion temperatures (<900ºC) will occur in less extension than in pulverized coal combustion (>1400ºC). However, the expected reduction of trace element emissions in FBC could be partially offset by the longer residence times. Experimental data on the behavior of trace elements in FBC are inconclusive and depend on the type of coal and operating conditions. Most of the measurements of trace elements emissions from FBC have been obtained in atmospheric plants but some data are available for pressurized fluidized bed combustion[7]. Regarding the operating conditions, it has been observed that trace element emission in FBC can be reduced by changing the depth of the bed[3,8]. Thus, when the bed depth is reduced to half, emissions of selected trace elements decrease between 5% and 50%. When comparing the trace element behavior for PCC and FBC some differences have been found. For instance, it has been observed that in FBC systems, emissions of elements such as Hg, As, Pb, Sc, Co, Na and K are lower than in PCC[1], even be below the emission standards[9]. The enrichment of volatile elements in the finest ash particles, which occurs regularly in PCC, does not happen in some FBC systems[10]. However in other studies[3,11] it has been observed that trace element concentration increases with decreasing particle size. It should also be remarked that in some tests, Hg was the only element detected in the gas phase in flue gases from FBC[3], whereas in PCC other elements such as B, Cl, F, Se and As were frequently present. The effect of limestone, added to control of SO_2 emission, upon trace element behavior is not clear. Thus, it has been observed that As, Cd, Pb, and Se emissions were significantly reduced with limestone addition[2]. In the other hand, it has been reported that addition of limestone gave rise to an increase in Pb, Cd and Mn emissions, which was justified by the likely presence of these elements in the limestone[3]. In a study carried out in PFBC, it has been concluded that trace elements emissions with or without limestone addition is similar[7].

With the aim of contributing to the knowledge of the behavior of trace elements during fluidized bed combustion, in the present work, experiments with and without limestone addition, were carried out.

EXPERIMENTAL PART
Coal combustion was carried out in a laboratory-scale continuos fluidized bed reactor (0.14 m i.d.). The coal, ranging in size from 0.16 to 1.5 mm, was fed in continuously. Most of the ashes were continuously taken out of the bed. The rest were elutriated by the combustion gases and collected in two cyclones and a baghouse filter placed in the outlet. The experiments were carried out with a fluidization velocity of 0.7 m/s, an air excess of 30% and at combustion temperature of 850ºC.

The sampling train for recovering trace elements from flue gases, was similar to the equipment specified by the US Environmental Protection Agency (EPA). The reagent used in the impigners was 0.5 M HNO_3. The content of Hg and As in this solution were determined by cold vapor atomic absorption spectrometry, and the ISO R-601 standard method.

A low volatile bituminous coal from the Asturian Central basin (North of Spain) was used in this study. The proximate, elemental analyses and sulfur forms are given in Table 1. The concentrations of 57 elements in the coal, ashes from the bed (R), from the two cyclones (C1 and C2), and from the baghouse filter (BF), were analyzed by Inductively Coupled Plasma Mass Spectrometry (ICP-MS) and Inductively Coupled Plasma Emission Spectrometry (ICP-AES). A special two stage sample digestion method[12] for ICP analyses was used in this study in order to avoid the loss of volatile elements during sample treatment. Because sample preparation for ICP analysis involves digestion with HF, the Si content was determined by X-ray fluorescence spectrometry (XRF). Particle size distribution of the collected ashes was measured in a Counter Coulter apparatus. In order to analyze the effect of limestone addition upon the trace element emission, an experiment was carried out with limestone (coal/limestone weight ratio: 37). The limestone was fed into the reactor in sizes between 0,1 and 0,5 mm. This limestone sample does not contain significant trace element concentration with the exception of 1589 ppm of Sr.

RESULTS AND DISCUSSION

The concentrations of major, minor and trace elements in the coal and combustion ashes R, C1, C2 and BF are given in Table 2. Concentrations in the coal have been refered to ashes in order to normalized the results. Major and minor elements have been also determined in order to ensure a balance of volatile and non-volatile elements during the experiments. The accuracy of the mass balance depends upon the ash sampling in the reactor which involves some errors, but roughly allows to estimate that elements such as As, Be, Cd, Hg and Se, could be partially released in vapor phase or condensed in the cold parts of the system. In spite of that, Hg and As analyzed in the flue gases by the methods already described, were not detected in the gas phase. The concentration of most of the trace elements decreases in the bed ashes (R) and increases in the fly ashes, mainly in those from the C2 and BF. This segregation could be attributed to two different processes: one is the physical segregation of major and trace elements in the reactor due to differences on the distribution of these elements in the feed coal and the other, the chemical segregation due to volatilization and condensation from flue gas.

In a previous work, mineral matter composition in this coal has been analyzed[13]. Illite, chlorite, kaolinite, quartz, pyrite, calcite, dolomite and siderite were the major minerals identified. After coal combustion in the FBC, illite and quartz remained mostly unaltered in the ashes but the other phases were transformed in oxides and sulfates[13]. We should kept in mind that some of these minerals, are dispersed as fine particles of inherent mineral matter. Moreover, when the coal particles are burnt at the temperatures used in FBC (i.e. 850ºC)some particles of mineral matter retain their original size or can be fragmentate. The mineral species of finest particle sizes are preferentially elutriated with the flue gases and a depletion of their concentration in the R ashes is expected. Concerning to the major elements (Table 2), this depletion is more significant for the elements present as carbonates (Ca, Mg, Fe), and also occurs for trace elements with carbonate affinity, such as Ba and Sr.

In the other hand, volatile trace elements are preferably concentrated in the fly ash particles. This behavior is more remarkable for some elements such as As, Co, Cu, Hg, Mo, Ni, Pb, Sb, Se, Sr and Zn. The study of the particle size distribution in R, C1, C2 and BF ashes, has shown that the C1 ash particles have reached sizes up to 60 μm, although 90% of the total volume of this particles are smaller than 8 μm. Maximum size particles found in the C2 ashes are of 15 μm, 90% of the total volume being smaller than 2 μm, and in the BF the maximum size is of 10 μm but 90% of the volume is smaller than 2 μm. The study of the enrichment of some trace elements on finest fly ash particles is of special interest. In order to eliminate the variability of different ash product characteristics, the enrichment factors (EF) were normalized to the concentration of Al. The EF of an element x is related to the concentration c of Al in coal ashes or combustion ashes as follows:

$$EF = \frac{(C_x/C_{Al})_{combustion\ ashes}}{(C_x/C_{Al})_{coal\ ashes}}$$

Enrichment factors calculated for some trace elements of major environmental concern, in the experiments with and without limestone addition, are shown in Figure 1. The rest of the elements studied, can be classified in three groups according to the EF values, in a similar way that has been done for PCC systems[1-3]. (I) low volatile trace elements are those with no significant enrichment or depletion in all the ashes (R; C1; C2 and BF). Cs, Ga, Ge, Nb, Sc, Ti, Tl, V, Zr, and rare earth. (II) elements that vaporize during combustion and condense on the surface of the smaller fly ash particles (mainly in C2 and BF). As, Bi, Co, Cu, Hg, Mo, Ni, Pb, Sb, Se, Sn, Sr, W and Zn are in this group, (III) elements that remain mostly in the vapor phase, that have enrichment factor <1 in all the ashes. Be and Cd follow this behavior. Other elements that are included normally in this group such as Hg or Se, were in part retained in the ashes.

The comparison between the composition of the ashes obtained from the tests carried out with and without limestone addition, has shown that retention efficiencies for most elements are similar in both cases. We should note that most of the Ca from the added limestone is retained mainly in R and C1, but in C1 in less extension Particles rich in Ca, elutriated with the more fine fly ashes (C2 and BF), belong mainly to the carbonates originally present in the coal. Some elements such as Fe, Co, Cu, Sn and Zn are more concentrated in the fly ashes obtained with limestone addition. This

fact cannot be explained in terms of particle size and vaporization-condensation mechanism, such as has been done in other similar experiments[3]. According to the results of the Coulter Counter analysis, the size distribution of C1, C2 and BF obtained during the test carried out with limestone addition is similar to the size distribution in the test without limestone addition.

ACKNOWLEDGMENTS

The authors wish to thanks financial support from FICYT (Project PA-MAS92-06), and the help of Dr. J. Gonzalez Cañibano of HUNOSA, for providing the sample for this work.

REFERENCES

1. Lim, M. Y. IEA Coal Research London. Report ICTIS/TR05, 1979, 58 pp
2. Smith, I. M. IEA Coal Research London. Report IEA CR/01, 1987, 87 pp
3. Clarke, L. B. and Sloss, L. L IEA Coal Research, London. Report IEACR/49, 1992,111 pp.
4. Meij, R. Fuel Processing Technology, 1994, **39**, 199
5. Martinez-Tarazona, M. R., and Spears, D. A. Fuel Processing Technology (in press)
6. Davidson, R. M. and Clarke L. B. IEA Coal Research, London. Report IEAPER/21, 1996, 60 pp
7. Mojtahedi, W., Nieminen, M., Hulkonen, S. and Jahkola, A. Fuel Processing Tecnology, **26**, 1990, 83.
8. Clarke, L. B. Fuel **72**, 1993, 731
9. Huges, I.S.C and Littlejohn, R.F. International Journal of Energy Research, 12, 1988, 473
10. Littlejohn, R.F. Energy Research, **8**, 1984, 375
11. Gay A. J. and Davis P. B. in Coal Science and Chemistry. Ed by A.,Volborth, 1987, 221
12. Querol, X., Fdez-Turiel, J.L. and Lopez-Soler, A. Fuel **74**, 1995, 331
13. Suarez-Fernandez, G.P., Fuertes, A.B. and Martinez-Tarazona, M.R. (unpublished results)

Table 1- Analyses of coal

	content wt %
Proximate (db)	
Volatile Matter	9.62
High Temperature Ashes	31,1
Elemental (db)	
C	62.1
H	2.69
N	0.96
$S_{total\ db}$	0.60
O (by diff.)	2.55
Other (db)	
$S_{pyritic}$	0.21
$S_{sulfate}$	0.02
$S_{organic}$ (by diff.)	0,37
CO_2 (fron CO_3^{2-})	1,77

Table 2.- Element concentrations in the ashes obtained in the experiences carried out without and with limestone addition, analyzed by Inductively Coupled Plasma Mass Spectrometry (1), Inductively Coupled Plasma Emission Spectrometry (2), or both (3). Concentrations are in ppm except for those indicated.

	coal ashes		withouth limestone					with limestone			
			R	C1	C2	BF		R	C1	C2	BF
Ag[1]	5.6		2.2	5.9	3.8	2.6		1.8	4.8	2.5	2.0
Al[2] %	15.2		14.9	13.7	15.2	15.8		13.2	12.8	15.2	14.5
As[1]	48		18	57	98	93		24	46	86	69
B[3]	52		41	90	87	64		39	76	80	113
Ba[3]	860		678	973	1471	1714		573	880	1428	1483
Be[1]	32		13	23	17	17		12	20	16	15
Bi[1]	0.98		1.0	0.80	1.7	1.4		0.60	0.51	1.1	1.2
Ca[2] %	3.73		2.40	7.00	4.91	4.37		5.68	8.35	5.15	4.19
Cd[1]	3.0		1.2	2.8	2.2	1.9		1.1	1.8	1.7	2.2
Co[1]	40		24	53	67	82		22	49	65	117
Cr[2]	140		144	163	181	183		127	163	201	203
Cs[1]	23		22	17	19	19		17	15	17	16

Table 2 (cont.).-

	coal ashes	withouth limestone				with limestone			
		R	C1	C2	BF	R	C1	C2	BF
Cu[3]	76	55	96	75	108	53	92	80	169
Fe[2] %	4.50	3.75	5.48	5.20	5.57	3.41	5.13	5.15	8.82
Ga[1]	47	41	37	43	42	34	34	39	36
Ge[1]	7.3	4.3	6.1	4.3	6.4	3.5	5.5	5.4	5.7
Hf[1]	5.3	3.6	3.4	4.0	4.0	2.5	3.2	3.4	3.7
Hg[1]	0.68	0.23	0.38	4.0	3.5	0.33	0.57	4.0	3.5
K[2]%	3.37	3.52	2.60	2.76	2.86	3.07	2.46	2.80	2.63
Li[2]	257	219	253	282	291	199	234	263	269
Mg[2] %	1.05	0.90	1.22	1.18	1.17	0.84	1.18	1.17	1.04
Mo[1]	8.7	3.0	13	20	21	4.0	12	19	21
Na[2] %	0.54	0.56	0.51	0.55	0.55	0.49	0.48	0.55	0.52
Nb[1]	35	27	29	31	35	22	27	29	30
Ni[3]	100	66	105	132	160	57	102	159	195
P[2] %	0.03	0.04	0.05	0.07	0.04	0.03	0.04	0.05	0.07
Pb[3]	84	73	80	125	131	68	62	122	114
Rb[1]	247	184	175	156	155	155	162	156	142
S[2] %	1.52	0.57	1.92	2.03	1.78	1.04	1.67	1.96	1.78
Sb[1]	4.2	2.9	5.3	6.8	7.7	2.5	4.8	6.3	6.7
Sc[1]	48	33	42	46	47	30	41	42	37
Se[1]	23	5.3	19	25	24	6.6	29	24	22
Si %	23.1	23.0	20.5	-----	20.7	24.4	20.3	-------	19,6
Sn[1]	15	12	12	54	19	8	13	283	36
Sr[1]	371	280	566	795	924	374	572	773	808
Ta[1]	14	1.6	2.7	3.5	2.8	0.97	1.8	1.6	1.4
Te[1]	1.0	0.29	0.19	0.82	0.68	0.21	0.38	0.45	0.68
Ti[2] %	0.62	0.60	0.56	0.61	0.66	0.54	0.53	0.61	0.61
Tl[1]	1.3	1.4	1.2	1.6	1.3	0.95	1.1	1.1	0.87
V[3]	267	192	227	227	238	171	209	220	216
W[1]	8.1	3.9	6.9	7.3	8.1	2.9	4.9	6.1	15
Y[1]	47	31	48	56	62	27	46	53	53
Zn[2]	160	136	216	227	319	136	185	278	434
Zr[1]	144	87	100	102	114	70	94	99	97
Ce[1]	144	98	112	101	114	80	100	97	101
Dy[1]	8.8	6.7	9.6	11	12	5.1	8.1	9.5	9.8
Er[1]	4.9	3.2	4.7	5.5	5.5	2.4	3.9	4.5	4.9
Eu[1]	2.7	2.4	2.8	3.3	3.5	1.8	2.1	2.8	2.8
Gd[1]	12	10	11	13	15	7,2	10	11	12
Ho[1]	1.6	1.4	1.8	2.4	2.3	0.95	1.5	1.8	1.9
La[1]	74	63	63	68	75	54	56	65	67
Nd[1]	62	53	52	55	65	42	45	54	56
Pr[1]	18	17	14	17	20	13	13	16	17
Sm[1]	12	10	12	13	14	8	10	11	12
Tb[1]	1.7	1.5	1.9	2.3	2.2	1.1	1.5	1.7	1.8
Th[1]	32	27	26	27	31	21	23	26	28
U[1]	6.8	4.9	6.3	6.4	8.4	4.3	5.5	6.5	6.8
Yb[1]	4.7	3.2	4.4	4.4	4.7	2.3	3.5	3.7	3.9

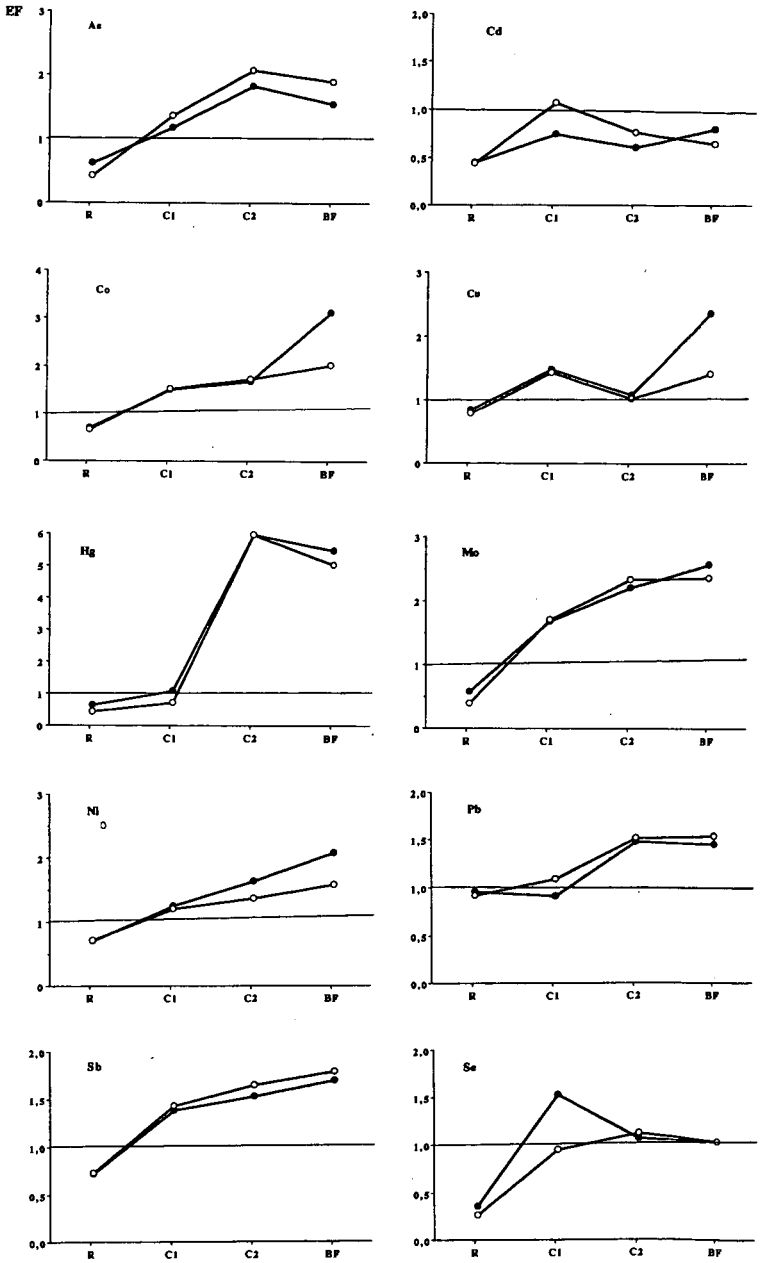

Figure 1. Enrichment factors EF for the ashes taken from the bed (R), cyclones (C1 and C2) and baghouse filter (BF), in the experiences with (●) and without limestone (O).

TRACE METAL CAPTURE BY VARIOUS SORBENTS DURING FLUIDIZED BED COAL COMBUSTION

T. C. Ho, A. N. Ghebremeskel and J. R. Hopper
Department of Chemical Engineering
Lamar University
Beaumont, TX 77710

Keywords: Coal Combustion, Fluidized Bed, Trace Metals

INTRODUCTION

Toxic trace metallic elements such as arsenic, beryllium, cadmium, chromium, cobalt, lead, manganese, mercury, nickel, and selenium are usually contained in coal in various forms and trace amounts. These metals will either stay in the ash or be vaporized during high temperature combustion. Portions of the vaporized metals may eventually be emitted from a combustion system in the form of metal fumes or particulates with diameters less than 1 micron, which are potentially hazardous to the environment (1).

Current practice of controlling trace metal emissions during coal combustion employs conventional air pollution control devices (APCDs), such as electrostatic precipitators and baghouses, to collect fly ash and metal fumes. The control may not always be effective on metal fumes due to their extremely fine sizes (2).

This study is to explore the opportunities for improved control of toxic trace metal emissions from coal-fired combustion systems. Specifically, the technology proposed is to employ suitable sorbents to (1) reduce the amount of metal volatilization and (2) capture volatilized metal vapors during fluidized bed coal combustion. The objective of the study was to investigate experimentally and theoretically the metal capture process.

POTENTIAL METAL-SORBENT REACTIONS

The following reactions between metals and sorbent constituents have been confirmed both theoretically and experimentally (3,4,5):

$$2\ PbO + SiO_2 \text{ ----> } Pb_2SiO_4(s) \quad (A)$$
$$CdO + SiO_2 \text{ ----> } CdSiO_3(s) \quad (B)$$
$$CdO + Al_2O_3 \text{ ----> } CdAl_2O_4(s) \quad (C)$$
$$PbCl_2 + Al_2O_3{:}2SiO_2 + H_2O \text{ ----> } PbO{:}Al_2O_3{:}2SiO_2(s) + 2\ HCl(g) \quad (F)$$
$$CdCl_2 + Al_2O_3 + H_2O \text{ ----> } CdAl_2O_4(s) + 2\ HCl(g) \quad (G)$$

EQUILIBRIUM CALCULATION

In this study, combustion equilibrium was calculated using a PC-based computer software package (6) especially developed for predicting equilibrium compositions during fuel or waste combustion. The simulation would reveal potential metal-sorbent reactions for the proposed metal capture process.

EXPERIMENTAL

Metal capture experiments were carried out semi-batchwise in a 25.4 mm (1") OD quartz fluidized bed coal combustor enclosed in an electric furnace. The metals involved in the study were cadmium, chromium and lead. Three coal samples from the Illinois Basin Coal Sample Bank (IBCSB) and an artificially prepared metal-containing wood sample were tested in the experiments. The corresponding concentration of chlorine, sulfur, and the target metals in each sample is summarized in Table 1. The sorbents tested included bauxite, zeolite and lime. The chemical composition and fluidization properties of the sorbents are listed in Table 2.

For an experimental run, a bed of sorbent was preheated to the desired temperature under the designed operating conditions. A predetermined amount of coal or wood pellets was then charged in the bed at a constant feed rate for combustion. After the combustion was completed, the bed residue was discharged for analysis of metal concentration. The experimental parameters and operating conditions associated with the experiments are shown in Table 3. Metal concentration in the coal, wood pellets, original sorbent, and combustor residue was determined by an atomic absorption spectrophotometer. An HF modified EPA Method 3050 was used to digest metals from the sorbent, which involves the use of HNO_3, HCl and HF acids (7).

RESULTS AND DISCUSSION

Simulation Results

Equilibrium calculations were performed to identify thermodynamically preferred metal speciation in a combustion system. A typical set of simulation results indicating potential lead-sorbent reactions and the effect of sulfur on lead capture by sorbents are shown in Table 4. The corresponding elemental composition and combustion conditions used in the simulations were: carbon - 71.3 wt%, hydrogen - 5.2 wt%, nitrogen - 1.4 wt%, oxygen - 12.4 to 7.8 wt%, sulfur - 0 to 4.6 wt%, lead concentration - 50 ppm, ash - 9.3 wt%, combustion temperature - 900°C, and percent excess air - 50%.

Experimental Results

Typical experimental results indicating the effectiveness of metal capture by various sorbents are shown in Tables 5, 6 and 7 for lead, cadmium, and chromium, respectively. The combustible materials tested were three coal samples, i.e., IBC-110, IBC-111 and IBC-112, and a wood sample. The sorbents used were bauxite, zeolite and lime. It is essential to point out that, due to the non-uniformity and trace-quantity nature associated with the process, it is still difficult to discuss the effect of fuel type, coal type, and coal properties such as chlorine, sulfur, ash and metal contents on the metal capture process based on the current results. Additional experiments are being carried out to provide more statistically representative results for better understanding the metal capture process.

CONCLUSIONS

This study investigated the possibility of employing suitable sorbents to capture toxic trace metals during fluidized bed coal combustion. The observed experimental results indicated that metal capture by sorbents can be as high as 91% depending on the metal species and sorbent involved. All three sorbents tested, i.e., bauxite, zeolite and lime, were observed to be capable of capturing lead and cadmium in a various degree. Zeolite and lime were able to capture chromium. Results from equilibrium simulations suggested the formation of metal-sorbent compounds such as $Pb_2SiO_4(s)$, $CdAl_2O_4(s)$ and $CdSiO_3(s)$ under the combustion conditions.

ACKNOWLEDGEMENTS

The authors are grateful for the financial support of this study by the USDOE Pittsburgh Energy Technology Center through the 1994 University Coal Research Program (Grant No. DE-FG22-94PC94221).

REFERENCES

1. Davidson, R. L., Natush, D. F. S., Wallace, J. R., and Evans, C. A., "Trace Elements in Fly Ash Dependence of Concentration on Particle Size," Environmental Science & Technology, **8**, 1107 (1974).

2. Oppelt, E. T., "Incineration of Hazardous Waste - A Critical Review," JAPCA, **37**, 558 (1987).

3. Uberol, M. and F. Shadman, "Sorbents for Removal of Lead Compounds from Hot Flue Gases," AIChE J., **36**, 307 (1990).

4. Uberol, M. and F. Shadman, "High-Temperature Removal of Cadmium Compounds Using Solid Sorbents," Environmental Science & Technology, **25**, 1285 (1991).

5. Ho, T. C., R. Ramanarayan, J. R. Hopper, W. D. Bostick, and D. P. Hoffman, "Lead and Cadmium Capture by Various Sorbents during Fluidized Bed combustion/ Incineration," Proceedings of Fluidization VIII, p. 899, held in Tours, France May 14-19, 1995.

6. Ho, T. C., Incineration Equilibrium IECP, software listed in CEP Software Directory, 68 (1996).

7. Gao, D. and Silcox, G. D., "The Effect of Treatment temperature on Metal Recovery from a Porous Silica Sorbent by EPA Method 3050 and by An HF-Based Method," Air and Waste, **43**, 1004 (1993).

Table 1. Concentration of Chlorine, Sulfur and Target Metals in Tested Coal Samples and Wood pellets (Units: ppm for metals, % for Cl and S)

Species	IBC-110	IBC-111	IBC-112	Wood*
Cd	<0.4	<0.4	<0.3	5
Cr	11	14	14	20
Pb	10	18	27	30
Cl	0.0%	0.0%	0.2%	0.0%
S	4.6%	2.0%	2.8%	0.0%

*Spiked Metals: Metal Nitrates

Table 2. Major Composition, Trace Metal Concentration and Fluidization Properties of the Three Tested Sorbents

Composition or Property	Bauxite	Zeolite	Lime
SiO_2 (%)	9.0	66.7	0.7
Al_2O_3 (%)	78.0	12.1	0.3
CaO (%)	0.0	3.1	97.2
Cd (ppm)	3.0	1.3	2.5
Cr (ppm)	286	3.5	4.5
Pb (ppm)	51.8	22.0	25.2
d_p (mm)	0.5	0.5	0.5
U_{mf} (cm/s)	3.8	3.5	3.8

Table 3. Experimental Parameters and Operating Conditions

Parameter	Range
Fuel Type	Coal, Wood
Coal Size	2.0 - 2.8 mm
Wood Size	4.8 mm
Fuel Amount	60 g
Fuel Feed Rate	0.22 g/min
Sorbent Type	Bauxite, Zeolite, Lime
Sorbent Size	0.4-0.6 mm
Sorbent Amount	22.5-30 g
Static Sorbent Height	6 cm
Air Flow Rate	3 U_{mf} of Sorbent
Combustor Temperature	900°C
Combustion Duration	4.5 hrs

Table 4. Equilibrium Simulation Results for Lead with or without Sulfur

Sorbent Constituent	Metal	With or Without Sulfur	Sulfur-Metal-Sorbent Compound	
SiO_2	Pb	Without S	**Pb_2SiO_4(s)**	< 1000°C
			PbO(g)	> 1000°C
		With S	**$PbSO_4$(s)**	< 950°C
			Pb_2SiO_4(s)	< 1000°C
			PbO(g)	> 1000°C
Al_2O_3	Pb	Without S	PbO(s)	< 900°C
			PbO(g)	> 900°C
		With S	**$PbSO_4$(s)**	< 950°C
			PbO(g)	> 950°C
CaO	Pb	Without S	PbO(s)	< 900°C
			PbO(g)	> 900°C
		With S	**$CaSO_4$(s)**	> 500°C
			$PbSO_4$(s)	< 950°C
			PbO(g)	> 950°C

Table 5. Percentage Lead Capture by Sorbents (%)

Fuel Type	Bauxite	Zeolite	Lime
Coal (IBC-110)	68	60	27
Coal (IBC-111)	58	91	51
Coal (IBC-112)	66	51	21
Wood Pellets	48	52	53

Table 6. Percentage Cadmium Capture by Sorbents (%)

Fuel Type	Bauxite	Zeolite	Lime
Coal (IBC-110)	66	64	43
Coal (IBC-111)	74	21	57
Coal (IBC-112)	72	84	21
Wood Pellets	14	36	8

Table 7. Percentage Chromium Capture by Sorbents (%)

Fuel Type	Bauxite	Zeolite	Lime
Coal (IBC-110)	0	57	8
Coal (IBC-111)	0	19	5
Coal (IBC-112)	0	17	12
Wood Pellets	0	33	34

TRACE ELEMENTS OF PETROLEUM - FCCU FEEDSTOCK, FRESH, SPENT AND DEMETALLIZED FCCU CATALYST SOLIDS & LEACHATES; DEMETALLIZATION REDUCES LEACHABILITY, INCREASES STABILITY

S. K. Pavel and F. J. Elvin
Coastal Catalyst Technology, Inc., 9 Greenway Plaza, Houston, TX 77046.

Trace elements contaminate Fluid Catalytic Cracking Unit (FCCU) catalysts by blocking pores and catalyzing steam deactivation. Elemental analyses of catalyst solids and leachates are necessary to characterize the system. Demetallization removes a portion of contaminants by pyrometallurgical and hydrometallurgical procedures. Catalysts were leached by various methods and IAW TCLP. Demetallized catalyst TCLP leachates are below the UTS TCLP limits proposed September 14, 1994, for all fourteen elements. Immediate catalytic activity improvement and improved resistance to steam deactivation is shown micro-activity (MAT) tests before and after severe steaming.

Fluid Catalytic Cracking is a valuable refining process to upgrade heavy hydrocarbons to high valued products (Avidan, 1993). Through the cycles of cracking, fresh catalyst deactivation is caused by contaminant blockage of active sites (nickel, vanadium, iron, et al.) and by steam catalyzed by contaminants, e.g. vanadium, sodium, et al. (Pine, 1990; Pavel, 1992). To compensate for decreased FCC feedstock conversion and product selectivity, a portion of the circulating catalyst equilibrium inventory is withdrawn for spent catalyst disposal, and fresh catalyst is added to the system (Habib, 1979).

Spent FCCU catalyst disposal quantities have been published in various formats, and disposition alternatives include those "options which recover metals: 1) On-site demetallization and recycle for FCCU catalysis -- on-site source reduction [13]; 2) Off-site demetallization and recycle for FCCU catalysis -- original application recycle [14]; 3) Off-site spent catalyst (ultra-low metals) sale to others [16] for further metals loading, a limited market at equilibrium which requires disposal by others and does not affect disposal of total replacement volumes of fresh catalyst sold, and the metals deposited from feedstocks. 4) Off-site demetallization for metals recovery prior to secondary use or disposal [17]; 5) Other waste treatment technologies prior to disposal, e.g. solidification, stabilization, vitrification, cementation, etc. [18]; 6) Cement kilns, with or without pretreatment, either 6a) cement kilns permitted/licensed for hazardous wastes, or 6b) cement kilns blending wastes as alternative feed stocks[16,19]; 7) Landfills [11,12,16,19]." (Pavel, 1995)

Trace elements enter the FCCU system from feedstocks, fresh catalysts, feedstock and/or catalyst additives. Analyses of petroleum by Filby, Yen, Shah, et al. (Yen, 1975), showed a wide range of elements in petroleum. The feedstock to FCCUs typically includes the gas oil fraction, between diesel and asphalt, and in some cases all of the long residue with a boiling point above diesel. Refiners normally analyze FCCU feedstock for C and S and occassionally N, for Ni and V fairly often, sometimes seldom analyze for more than Ni, V, and in some cases, Na, Fe. ICP elemental analyses for several feedstocks are shown in Table 1. Elemental analyses of spent Fluid Catalytic Cracking (FCC) catalyst solids and leachates are necessary to characterize the total FCC catalyst system including yield impacts and environmental considerations.

Catalyst and leachate analyses: Elemental analyses of solids and leachates were performed using ICP and XRF, analyses of leachates were performed by ICP. Table 2 shows a representative catalyst test set which includes a fresh, spent, and demetallized spent catalyst. Toxicity Characteristic Leaching Procedures (TCLPs) were performed in accordance with EPA standard methods, and results were compared to the proposed Universal Treatment Standards, Land Disposal Restrictions -- Phase II (LDRII), published September 19, 1994. Additional leach tests were performed with deionized water flushed (DIF) through catalyst using 20 parts water to 1 part catalyst. Demetallized catalyst TCLP leachates are below the UTS for all elements including vanadium (Pavel, 1994). New pyrometallurgical and hydrometallurgical controls and procedures further improve metal removal and enhance catalytic properties. Immediate activity improvement is seen in MATs prior to steaming. Improved resistance to steam deactivation, catalyzed by vanadium and other elements, is shown after spent and demetallized spent catalyst were steamed for 4 and 16 hours at 1450°F, and then ASTM microactivity (MAT) tested.

Demetallization processing (DEMET) takes a portion of spent FCC catalyst, removes a portion of metal contaminants by pyrometallurgical (calcining, sulfiding, nitrogen stripping, chlorinating) and hydrometallurgical (leaching, washing, drying) procedures, to return the base demetallized spent catalyst to the FCC. Standard demetallization has most frequently utilized 1450°F calcining and sulfiding with 650°F chlorinating. Off-gases from reactors are scrubbed (Elvin, 1993). Contaminant metals are precipitated and filtered for disposal in the same manner used for spent catalyst, or they can be shipped to a Best Demonstrated Available Technology recycler of metals, depending on the client preference or regulatory environment. The operation of one unit for one refiner has resulted in the recycle of over 15,000 tons of spent FCC catalyst back to the FCC. Demetallized spent FCC catalyst recycle has reduced the requirements for fresh catalyst additions and reduced generation of catalyst fines. DEMET processing removes contaminants known to be detrimental to conversion, product selectivities, and mechanical performance of the FCC. With DEMET capacity sized to reduce metals levels on circulating catalyst, yields could be improved due to lower metals on circulating catalyst.

New DEMET procedures improve metal removal, initial activity and hydrothermal stability. Standard DEMET processing utilizes a series of pyrometallurgical and hydrometallurgical procedures for metal removal. By removal of contaminants, access channels to active sites are renewed. Care is taken during processing to maintain the catalyst integrity and hydrothermal stability. New advancements in sulfidization and aqueous processing have further improved metal removal and demetallized spent catalyst characteristics of high initial activity, and low hydrothermal deactivation rates.

Table 1. FCCU Feedstock Elemental Analyses (ppm) by ICP

Element	Feed1	Feed2	Feed3	Feed4	Feed5	Feed6	Feed7
Aluminum	2.9	38.7	0.4	1.6	4.8	nt	0.5
Antimony	0.2	2.1	1.1	0.2	0.2	<0.2	<0.2
Barium	nt	nr	0.9	<0.1	<0.1	nt	<0.2
Beryllium	*nt*	*nt*	*nt*	nt	nt	nt	nt
Bismuth	0.6	bdl	<0.1	0.2	0.2	<0.2	<0.2
Boron	<0.1	4.3	<0.1	0.7	<0.1	nt	<0.2
Calcium	19.9	15.3	1.6	2.7	0.5	0.4	0.5
Carbon	nr	nr	1.4	7.8	4.4	2.2	4.8
Cerium	0.2	nr	<0.1	<0.1	<0.1	nt	nt
Chromium	0.6	nr	<0.1	<0.1	<0.1	<0.2	<0.2
Copper	0.2	0.4	0.2	0.1	<0.1	<0.2	<0.2
Iron	14.3	16.6	5.2	16.0	7.6	3.4	5.3
Lanthanum	0.1	nr	<0.1	<0.1	<0.1	nt	nt
Lead	0.3	2.4	0.1	0.3	0.6	<0.2	<0.2
Magnesium	2.5	3.5	2.6	1.0	0.1	0.2	0.3
Manganese	0.2	0.1	<0.1	0.1	<0.1	<0.2	<0.2
Neodymium	<0.1	nr	<0.1	<0.1	<0.1	nt	nt
Nickel	2.2	4.8	3.4	22.0	3.9	13.0	12.1
Phosphorus	0.7	2.3	0.6	0.1	0.2	<0.2	<0.2
Potassium	0.6	5.7	0.6	0.5	0.7	nt	<0.2
Praseodymium	<0.1	nr	<0.1	<0.1	<0.1	nt	nt
Selenium	nt	bdl	<0.1	0.2	0.2	nt	<0.2
Silica	nt	nt	nt	nt	nt	nt	nt
Sodium	21.4	27.4	1.4	28.0	1.2	2.1	0.5
Strontium	0.6	nr	<0.1	<0.1	<0.1	<0.2	<0.2
Sulfur	nr	nr	1.3	1.2	0.3	0.13	0.37
Tin	0.1	0.4	0.7	0.5	0.7	<0.2	0.8
Titanium	0.1	0.7	<0.1	0.1	<0.1	<0.2	<0.2
Vanadium	3.5	4.3	2.4	40.0	6.5	0.9	8.6
Zinc	0.9	2.6	0.4	1.2	0.3	nt	<0.2
Zirconium	<0.1	nr	0.1	<0.1	<0.1	nt	<0.2

note: "nt" indicates "not tested" at the time of that sample; "nr" indicates "not reported"

Improved metals removals are accomplished primarily during the pyrometallurgical steps of processing. Special DEMET procedures were developed by rigorous thermodynamic modeling of the sulfidizationenvironment to ensure the reaction mix and temperature appropriate to convert available contaminant oxides to sulfides (Pavel, 1993). Accurate analyses of all contaminant elements (not just nickel and vanadium) are required for accurate modeling. Improved metals removal enables more efficient utilization of hardware and provides the ability to lower metals on circulating catalyst. Improved metals removal shows that more sites have been uncovered, and micropore channels leading to active catalytic sites restored.

Elements not tested and/or reported in the following tables, but often found on catalysts include three groups. Elements most typical, but not tested and/or reported: Carbon, Chlorine, Hafnium, Hydrogen, Nitrogen, Oxygen, Scandium. The second group accounts for he rare earth mix supplied fresh catalyst manufacturers which includes the four reported plus Samarium, Europium, Gadolinium, Terbium, Dysprosium, Holmium, Erbium, Terbium, Ytterbium, Lutetium. The third group includes elements found in crude and on occassion various catalysts: Fluorine, Iridium, Osmium, Palladium, Platinium, Rhenium, Rhodium, Ruthenium. All tests have been performed by third party laboratories. The demetallization procedure used was for recycle of spent demetallized catalyst, alternative procedures would be utilized if processing for any other purposes. When some elements are removed, the elements remaining might appear to increase as a portion of the total remaining material. The list of elements is extensive, but not complete, as elemental testing includes over 70 elements.

Every FCCU feedstock, hardware, and catalyst system are unique. Some systems have more elements than in the following table (Table 2).

Improvements in hydrothermal stability and additional activity for recycle to the FCC are achieved through the hydrometallurgical processing steps. Special DEMET procedures were developed by rigorous modeling of solution properties during the wash step (Pavel, 1993). Additional proprietary steps are incorporated in the washing prior to drying on the belt filter. Aqueous processing modifications resulted in a number of attractive alternatives which can be selected through regulating variables in a single flexible design DEMET unit. For simplicity of graphic and tabular presentation, only one of the alternative advanced procedures is shown, it is labeled "special". Spent FCC catalyst was demetallized in the laboratory pilot plant. Microactivity and XRD testing were performed in accordance with ASTM standards. Steaming was performed at 1450°F 100% steam for 4 hours and 16 hours. The results prior to steaming and after 4 and 16 hours of steaming are shown in the Table 3 in comparison of the fresh, spent, standard demetallized, and special demetallized sample performance demonstrated by MAT testing.

Table 2. Fresh, Spent, and Demetallized Spent FCC Catalyst Solid and Leachate Analyses (ppm)

Elements Analyses by ICP	UTS LDRII TCLP	Fresh Catalyst Solid	Fresh Catalyst Leachates TCLP	Fresh Catalyst Leachates DIF	Spent Catalyst Solid	Spent Catalyst Leachates TCLP	Spent Catalyst Leachates DIF	Demetallized Spent Solid	Demetallized Spent Leachates TCLP	Demetallized Spent Leachates DIF	Element removal wt%spent
Aluminum	.....	142110	87.469	0.549	141190	114.813	2.961	175200	34.010	4.720	+24%
Antimony	2.1	246	bdl	bdl	1526	1.766	9.491	310	bdl	bdl	80%
Arsenic	5.0	215	0.223	bdl	250	1.495	bdl	96	0.113	0.205	62%
Barium	7.6	118	0.018	bdl	77	0.667	0.014	52	0.329	0.060	32%
Beryllium	0.014	3	0.006	0.002	38	0.368	0.509	10	bdl	0.014	74%
Bismuth	.....	bdl	bdl	bdl	7	0.319	0.015	bdl	bdl	bdl	bdl
Boron	.....	20	0.029	0.021	20	0.109	0.094	14	0.067	0.037	30%
Cadmium	0.19	4	bdl	bdl	20	bdl	bdl	30	bdl	bdl	-55%
Calcium	.....	1372	7.059	0.278	1819	1.889	0.283	961	4.061	1.084	47%
Cerium	.....	4682	13.183	0.085	1171	14.915	0.065	1264	26.627	3.481	+ 8%
Chromium	0.86	675	0.043	0.011	586	bdl	bdl	579	bdl	bdl	-16%
Cobalt	.....	8	bdl	bdl	193	0.013	0.013	12	0.142	0.052	93%
Copper	.....	9	0.013	0.009	29	0.103	0.002	9	0.012	0.001	69%
Iron	.....	3053	0.219	0.016	4292	0.328	0.301	902	2.320	0.053	79%
Lanthanum	.....	3518	8.401	0.017	2757	46.975	0.246	2782	57.195	8.928	+1%
Lead	0.37	27	bdl	bdl	38	bdl	bdl	bdl	bdl	bdl	~99%
Lithium	.....	42	0.054	0.007	56	0.431	0.314	32	0.385	0.285	43%
Magnesium	.....	316	2.041	0.106	62	0.827	0.094	33	0.844	0.333	47%
Manganese	.....	12	0.055	0.001	12	0.052	0.001	8	0.036	0.012	33%
Mercury	0.020	bdl	bdl	bdl	bdl	bdl	bdl	bdl	bdl	bdl	bdl
Molybdenum	.....	8	0.016	0.011	14	0.227	0.474	4	0.058	bdl	71%
Neodymium	.....	2303	8.914	0.036	1703	20.987	0.192	1182	31.298	3.293	31%
Nickel	5.0	33	0.049	0.006	3432	1.868	0.269	153	1.745	0.547	96%
Potassium	.....	890	2.801	0.348	281	1.205	0.224	242	0.097	0.012	16%
Presodymium	.....	587	1.991	bdl	432	6.347	bdl	381	9.512	1.071	11%
Selenium	0.16	11	0.046	bdl	10	0.040	bdl	bdl	bdl	bdl	~99%
Silicon	.....	310010	68.917	8.428	310485	50.384	32.506	282500	55.571	8.440	9%
Silver	0.3	bdl	bdl	bdl	bdl	bdl	bdl	bdl	bdl	bdl	bdl
Sodium	.....	3178	62.518	12.795	2283	26.993	16.473	2211	16.367	12.147	3%
Sulfur	.....	2973	84.625	61.931	446	1.134	0.882	2357	86.837	13.326	+428%
Thallium	0.078	92	0.047	0.032	60	0.867	0.353	bdl	bdl	bdl	~99%
Tin	.....	bdl	bdl	bdl	bdl	bdl	bdl	bdl	bdl	bdl	bdl
Titanium	.....	4170	0.064	0.029	7550	0.016	0.165	3800	0.264	0.016	50%
Vanadium	0.23	63	0.137	0.160	4967	48.437	68.500	1176	0.123	0.187	76%
Zinc	5.3	91	0.537	nt	136	0.162	bdl	95	1.360	0.098	30%
Analyses by XRF		solids only			solids only			solids only			
Bromine	.....	< 0.4			< 0.4			< 0.4			NoChange
Cesium	.....	< 7.5			22.3< 7.5			22.3< 7.5			NoChange
Gallium	.....	28.6+/- 1.0			53.2+/- 2.0			29.7+/- 2.0			44%
Germanium	.....	< 0.7			2.1+/- 0.5			< 1.0			~99%
Indium	.....	< 0.6			< 1.8			< 1.8			NoChange
Iodine	.....	9.4+/- 2.8			22.5+/- 4.0			10.3+/- 3.0			54%
Niobium	.....	13.7+/- 1.0			25.3+/- 1.0			9.9+/- 0.8			61%
Phosphorus	.....	653.0+/-38.0			666.0+/-37.0			604.0+/-31.0			9%
Rubidium	.....	3.6+/- 0.5			2.9+/- 0.6			1.7+/- 0.6			41%
Strontium	.....	60.5+/- 1.0			67.5+/- 1.0			60.6< 1.4			10%
Tantalum	.....	< 4.9			< 8.0			< 8.0			NoChange
Tellurium	.....	< 1.4			< 2.5			< 2.5			NoChange
Thorium	.....	6.7+/- 1.0			18.7 < 1.0			16.8+/- 1.0			10%
Tungsten	.....	<3.1			< 18.9			< 18.9			NoChange
Uranium	.....	2.7+/-1.0			4.1+/- 1.1			3.2+/- 1.1			22%
Yttrium	.....	59.8+/-1.0			32.6+/- 1.0			27.4+/-1.0			15%
Zirconium	.....	103.0+/-1.0			125.0+/- 2.0			125.0+/- 2.0			NoChange

Note: bdl = below detection limit; nt=not tested; ~99%=removal to below detection limits.

Table 3. Fresh, Spent, Standard Demetallized, and Special Demetallized Spent Catalyst

	Fresh without DEMET	ECAT without DEMET	DCAT after Standard DEMET	DCAT after Special DEMET
MAT yields prior steaming, wt%				
Conversion	94.29	55.55	67.74	70.78
2nd Order Conversion	16.50	1.25	2.10	2.42
Gasoline/Conversion	0.27	0.63	0.56	0.54
2ndOrderConversion/Coke	0.79	0.15	0.24	0.21
Dry Gas/2ndOrderConversion	0.38	1.55	1.23	1.03
LCO/LCO+Slurry	0.47	0.52	0.60	0.63
Hydrogen	0.29	0.46	0.26	0.46
Dry Gas (C1+C2s)	6.22	1.93	2.57	2.50
Propane	17.06	0.85	2.30	1.74
Propylene	2.17	2.74	4.34	4.84
Isobutane	14.36	2.28	6.17	5.60
Normal_Butane	6.65	0.56	1.35	1.22
Isobutene	0.39	0.93	0.96	1.17
Total Butenes	1.21	3.24	3.91	4.51
Gasoline (C5-430F)	25.41	34.98	38.10	38.34
LCO (430-650F)	2.66	22.94	19.36	18.55
Slurry (650F+)	3.05	21.51	12.91	10.68
Coke	20.91	8.51	8.74	11.56
MAT yields after 16 hours steaming, wt%				
Conversion	62.91	35.86	40.38	56.56
2nd Order Conversion	1.70	0.56	0.68	1.30
Gasoline/Conversion	0.66	0.56	0.65	0.68
2ndOrderConversion/Coke	0.37	0.07	0.14	0.45
DryGas/2ndOrderConversion	1.11	2.98	2.55	1.37
LCO/LCO+Slurry	0.68	0.33	0.37	0.52
Hydrogen	0.07	0.64	0.34	0.21
DryGas (C1+C2s)	1.88	1.67	1.72	1.78
Propane	1.19	1.01	0.66	0.79
Propylene	4.22	1.73	2.21	3.97
Isobutane	3.94	0.54	0.95	2.54
Normal_Butane	0.82	0.19	0.28	0.51
Isobutene	1.17	0.63	1.19	1.99
Total Butenes	4.77	1.63	3.17	5.70
Gasoline (C5-430F)	41.47	20.18	26.22	38.20
LCO (430-650F)	21.36	20.89	21.92	22.47
Slurry (650F+)	15.73	43.25	37.70	20.98
Coke	4.56	8.28	4.83	2.87

Demetallized spent FCCU catalyst TCLP leachate is below the proposed LDR-II UTS for all 14 elements. Demetallization for primary recycling to FCCUs can reduce fresh catalyst additions, reduce circulating inventory metals (or hold a metals level with increasing feed stock metals), and reduce leachable metals for a portion of spent catalyst withdrawn. Contaminant metals are controlled in FCCUs due to their deleterious affects on conversion, selectivity, and deactivation of fresh catalyst. Similarly, cement kiln blends are limited to a kiln blend of 83 ppm vanadium due to potential problems with refractories (Petrovsky, 1994). For those kilns not already at a vanadium limit due to vanadium content of the local quarry supply, the dilution of vanadium sets the limit of spent FCCU catalyst processed to 1-2% of kiln feed stock. The mobility of vanadium is well known in refining, and it appears the conditions of cement kiln processing do not limit vanadium mobility. Demetallization could be used to reduce the leachable metals prior to secondary recycling (cement kilns, etc.) or disposal. Using DEMET to remove vanadium from feed stocks to cement kilns would increase capability to substitute spent FCCU catalyst in the kiln blend." (Pavel, 1995)

Conclusion. Demetallization reduces the leachability of contaminant elements measured by TCLP and de-ionized water flushes. After demetallization of spent FCCU catalyst all fourteen TCLP leachate elements are below the proposed LDR-II Universal Treatment Standard levels. For every indicator of catalyst performance after severe steaming, standard demetallization appears superior to equilibrium catalyst without demetallization, and special demetallization appears superior to standard demetallization and far superior to equilibrium catalyst without demetallization. Graphs show higher conversion, and higher gasoline yields with lower coke for special demetallized catalyst compared to equilibrium catalyst. The graphs also show the special demetallized catalyst performance ratios are also superior with lower dry gas/kinetic conversion ratios, higher gasoline/coke ratios, higher gasoline/conversion selectivities, higher light cycle oil selectivities, higher dynamic activities, as well as increased C3 and C4 olefins and isobutylene. DEMETallization appears very well suited for the marketplace of new gasolines and higher middle distillate demands. The special DEMET process significantly increases the activity, selectivity and hydrothermal stability of the catalyst and minimizes the fresh catalyst required to maintain FCCU activity.

References:

Avidan, A. A. (1993). Origin, development and scope of FCC catalysis, J. S. Magee and M. M. Mitchell, Jr., Eds., Fluid Catalytic Cracking: Science and Technology, Studies in Surface Science and Catalysis, Vol. 76, (Amsterdam, Elsevier) 1.

Elvin, F. J. and Pavel, S. K. (1993). Commercial Operations of a DEMET Unit, NPRA Annual Meeting #AM-93-54.

Federal Register (1994), 40 CFR Parts 148, et al. Land Disposal Restrictions Phase II -- Universal Treatment Standards, and Treatment Standards for Organic Toxicity Characteristic wastes and Newly Listed Wastes; Final Rule, Sep. 19, 1994.

Habib, T. H. and Venuto, P. B. (1979). Fluid Catalytic Cracking with Zeolite Catalysts, (NY, NY: Marcel Dekker).

Pavel, S. K. (1992). The deactivating effects of vanadium and steam are compared for fresh, equilibrium, and demetallized catalyst. AIChE Annual Meeting, Miami, FL.

Pavel, S. K., and Elvin, F. J. (1993). Minimization of Petroleum Refinery Waste by Demetallization and Recycling of Spent FCCU Catalyst, Hager, J., Hansen, B., Imrie, W., Pusatori, J., and Ramachandran, V., eds., Extraction and Processing for the Treatment and Minimization of Wastes, The Minerals, Metals & Materials Society, WDC, 1015.

Pavel, S. K. and Elvin, F. J. (1994). Elemental Analysis of FCCU catalysts: Fresh, Equilibrium, and Demetallized, Symposium on Recent Advances in FCC Technology, AIChE Spring National Meeting, Atlanta, GA.

Pavel, S. K. and Elvin, F. J. (1995). Fresh, Spent and Demetallized Spent FCCU Catalysts Characterized by Detailed Elemental Analysis of Powder and Leachate", Symposium on New Techniques in Materials and Catalyst Characterization Preprints, ACS, Division of Petroleum Chemistry, Washington, DC. 198.

Pavel, S. K. and Elvin, F. J. (1996). New New FCCU DEMET® Process to produce demetallized spent catalyst with high activity and low hydrothermal deactivation rates. NPRA Annual Meeting, #AM-96-45.

Petrovsky, J. (1994). Question & Answer Session on Waste Issues", 1994 NPRA Refinery & Petrochemical Plant Environmental Conference (Washington, D. C., National Petroleum Refiners Association).

Pine, L. (1990). Vanadium-Catalyzed Destruction of USY Zeolites, J. Catal., 125, 514.

Yen, T. F., ed., (1975). The Role of Trace Metals in Petroleum, (Ann Arbor, MI: Ann Arbor Science Publishers, Inc.).

DETERMINATION OF TOTAL MERCURY IN COAL

Lori J. Blanchard and J. David Robertson
Department of Chemistry
University of Kentucky
Lexington, KY 40506-0055

Keywords: Mercury, radiochemical neutron activation analysis

INTRODUCTION

The determination of mercury in coal is of interest due to its extreme volatility during coal combustion and its potential to be toxic if released into the environment. However, the low concentration of mercury in coal, frequently at the low ng/g level, makes analysis extremely difficult. In addition, mercury's volatility makes sample cross-contamination more likely. Despite the emphasis placed on mercury analysis, the analytical method of choice to give accurate, reproducible results for coal samples remains debatable. In 1988, 18 independent laboratories participated in an interlaboratory comparison of EPA Method 245.5 (sample digestion/dissolution followed by amalgamation/CVAA) for the analysis of mercury in NIST-SRM 1633a coal fly ash which has a certified value of 0.16 ± 0.01 µg/g. The results gave a mean that was 230% of the true value with an overall standard deviation of 200%.[1] More recently, an extensive round robin experiment on Hg analysis was carried out in which 11 laboratories were supplied with three different coals for analysis. The analytical methods employed were cold vapor atomic absorption spectroscopy (CVAAS), cold vapor atomic fluorescence spectroscopy (CVAFS), and instrumental neutron activation analysis (INAA). The study showed that there was approximately a 50% inter-laboratory variability corresponding to a reproducibility of 0.04 µg/g for a coal with an approximate Hg concentration of 0.08 µg/g.[2]

INAA is one method that has commonly been used for mercury analysis in coal. NAA has the advantage over other analytical methods in that once the sample is sealed in the irradiation vial sample cross-contamination is prevented. However, the ^{75}Se ($t_{\frac{1}{2}}$=120 d) 279.5 keV γ-ray is a direct spectral interferant for the ^{203}Hg ($t_{\frac{1}{2}}$=47 d) 279.2 keV γ-ray. The interference can be mathematically corrected for using the ^{75}Se 264.7 keV γ-ray, but this can result in large uncertainties associated with the mercury values, particularly in coal samples where the selenium concentration is many times larger than the mercury concentration.

Our laboratory has developed a new radiochemical neutron activation analysis (RNAA) method based on pyrolysis followed by double gold amalgamation. During pyrolysis the more volatile elements, such as mercury and selenium, are liberated from the coal sample, and the mercury is preferentially collected by amalgamation with gold. While this procedure does not completely separate the mercury from the selenium it does greatly increase the Hg-to-Se ratio in the 279 keV peak, thereby reducing the measurement's uncertainty. Furthermore, since other elements in the sample are not amalgamated with the gold, the spectrum background is drastically reduced which results in a greater sensitivity for mercury.

EXPERIMENTAL

Sample Preparation

Samples of NIST SRM 1632a were dried at 105°C overnight and cooled. 10.00 µg/mL and 50.00 µg/mL Hg solutions were prepared from a 1000 ± 3 µg/mL Hg in 2% HNO_3 certified standard (High Purity Standards). Appropriate amounts were added to

known quantities of dry SRM 1632a to obtain spike concentrations of approximately 200, 400, 650, and 1000 ng/g. The spiked samples were dried at 35-45°C overnight. After cooling, the samples were shaken on a mixer mill for twenty, 2-3 minute intervals.

Irradiation

Approximately 70-100 mg of the spiked standards were placed in acid washed quartz vials (4 mm i.d, 6 mm o.d.) and sealed. Samples were irradiated at the University of Missouri Research Reactor (MURR) for 48 hours at a thermal flux of 5.150 x 10^{13} n/cm^2/sec. One to two weeks after irradiation the vials were washed with aqua regia.

Radiochemical Separations

Apparatus. The experimental setup is shown in Figure 1. All glassware was constructed of quartz and was soaked overnight in 10% HNO_3 prior to analysis. Quartz wool was placed in the tube furnace downstream from the sample to trap coal particulates and ensure complete pyrolysis.

Gold traps were prepared by folding a 10 cm x 10 cm gold mesh in half and rolling lengthwise. These gold mesh "cylinders" were blanked by heating to 800°C for 1 hour. After cooling, each mesh was placed inside a 6 mm i.d. quartz tube with quartz wool plugs at each end to keep the mesh in place.

Procedure. Sample vials were cooled in liquid nitrogen for several minutes, wrapped in a thin layer of quartz wool, and rolled in aluminum foil. The vials were crushed and the foil was partially unwrapped before being placed inside the tube furnace. Samples were then heated to 550°C for 1 hour. After the furnace had cooled to <90°C, the heating tape wrapped around the first gold mesh was heated to 400°C for 30 minutes. Throughout the procedure the nitrogen flow rate was kept constant at about 250 mL/min.

Counting

Activated samples were counted prior to being opened (as in INAA) for 6 hours with a HPGe detector. After radiochemical separation the second amalgamated gold mesh was counted for 4 hours with a larger, higher efficiency HPGe detector.

RESULTS & DISCUSSION

Typical γ-ray spectra obtain before and after radiochemical separation are shown in Figures 2 & 3. The reduction in the spectral background results in a lowering of the sensitivity for mercury from about 190 ng/g for INAA to about 15 ng/g for RNAA (calculated using the $3\sigma_{bkg}$ method).

The radiochemical separation also greatly reduces the uncertainty associated with a mercury determination due to the increase in the Hg-to-Se ratio in the 279 keV peak. Prior to separation, the relative standard deviation (rsd) in the specific activities (counts in the 279 keV peak per gram of sample) ranged from 12% for the 1000 ng/g spiked sample to 75% for the 200 ng/g spike sample. After separation, the rsd of the specific activities ranged from 1-4%.

The accuracy of the method was evaluated with SRM 1632a. RNAA analysis yielded an experimental value of 114 ± 13 ng/g, well within the certified Hg concentration of 130 ± 30 ng/g. Although only one sample of the standard has been analyzed thus far the results are very promising, and repeat analyses of the SRM are planned in the future.

The linearity and reproducibility for the method are illustrated in Figure 4. The correlation coefficient for these results was calculated to be 0.916 suggesting reasonable linearity. The discrepancy seen in the reproducibility is most

likely introduced during the opening of the vials. It is possible that some sample was lost during the breaking of the vial and/or placement in the tube furnace.

SUMMARY

As increasing emphasis is placed on sensitive and accurate mercury determinations, analytical methods will be placed under more scrutiny and current methods have already been shown to yield inconsistent results. To meet future requirements, either current methods must be revised or new methods must be developed.

In the development of this analytical method the greatest obstacle encountered thus far has been devising a process that ensures quantitative sample recovery during vial opening. The focus of future research will be on refining this aspect of the procedure.

Despite this difficulty, performing radiochemical separations using pyrolysis and amalgamation on irradiated coal yielded accurate results and resulted in significant improvements in sensitivity and the relative standard deviation in mercury determinations. Both of these characteristics are critical in yielding reliable, accurate results for the analysis of mercury in coal.

ACKNOWLEDGMENTS

This work was supported by the U.S. DOE and the Kentucky EPSCOR Programs.

REFERENCES

1. Environmental Monitoring Systems Laboratory. EPA/600/S4-88/11, (1988).

2. Lengyel, J. DeVito, M. S., and Biloneck, R. A. Proceedings of the 87th Air and Waste Management Association Meeting, Cincinnati, OH, June, 1994.

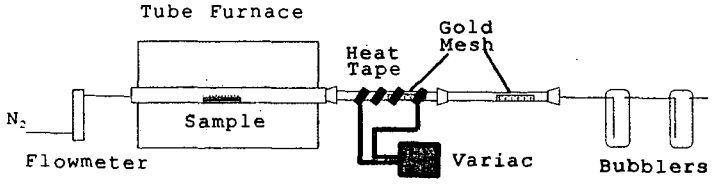

Figure 1. A schematic of the experimental setup for the radiochemical separation of mercury.

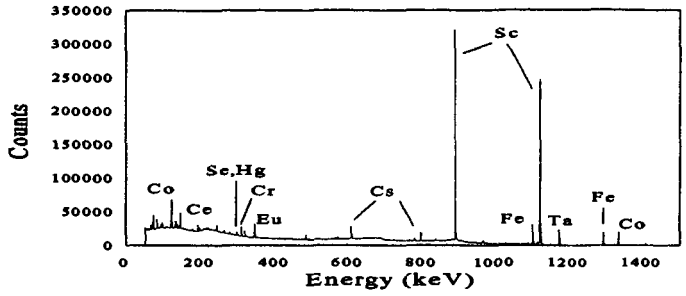

Figure 2. γ-ray spectra of irradiated coal. (48 hour irradiation, 80 day decay, 6 hour count).

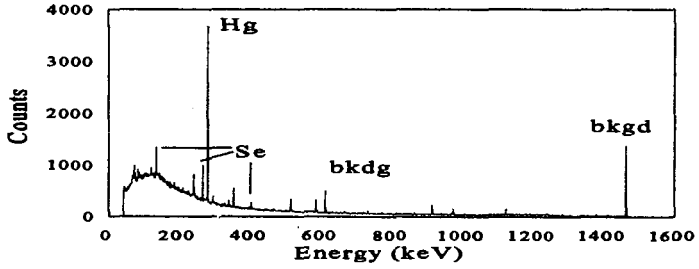

Figure 3. γ-ray spectra of amalgamated gold containing mercury from coal sample. (75 day decay, 4 hour count).

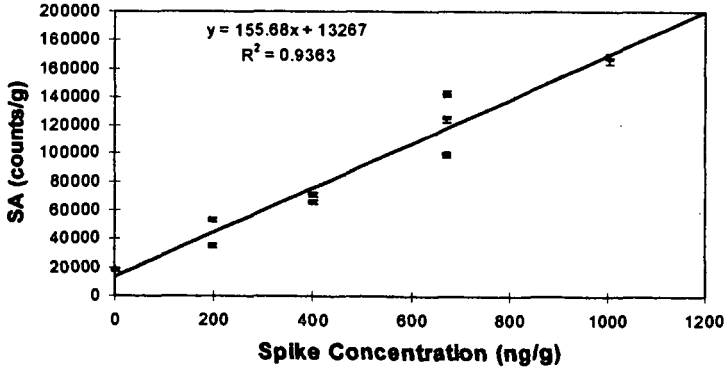

Figure 4. Graph of specific activity vs. Spike concentration.

EVALUATION OF MICROWAVE DIGESTION AS THE PREPARATION METHOD FOR MERCURY-IN-COAL MEASUREMENT

Jenny Sun and Rich Hoffman
University of North Dakota
Energy & Environmental Research Center
PO Box 9018
Grand Forks, ND 58202
(701) 777-5000

Keywords: Microwave digestion, mercury in coal, mercury analyzer

INTRODUCTION

The 1990 Clean Air Act Amendment (CAAA) empowered the U.S. Environmental Protection Agency (EPA) to set emission standards for a number of potentially hazardous air pollutants (HAPs) generated by a variety of specific combustion sources. Eleven elements (or compounds of these elements) present in coal are among the 189 pollutants identified as air toxics by the CAAA legislation. Mercury is included in this list. Generally mercury concentrations in coal are well below 1 ppm (1 μg/g). However, because such a large tonnage of coal is consumed for electric power generation, coal combustion represents a potentially significant source of mercury entering the environment (1).

Determination of the concentration of mercury in coal is becoming an increasingly important issue. Because of the relatively low concentration of mercury in coal and the relatively high detection limits of current analytical methods, information on the mercury content of coals to any degree of certainty is still unavailable. Therefore, evaluating the precision and accuracy of current analytical methods and improving existing methods are very important in estimating potential atmospheric emissions and associated risks.

Complete sample dissolution is necessary prior to instrumental analysis for most solid samples. In general, this step is the most critical in trace metal analysis and is time-consuming and labor-intensive. Several preparation methods are currently being used for mercury-in-coal measurements. A method (2) that combusts the coal sample in a tube furnace and collects the mercury vapor using a gold wire collector has shown some higher results (1) compared to other methods. Method ASTM D3684 uses an applied oxygen combustion bomb on the coal sample and subsequent rinsing of the inside of the bomb after combustion. Method SW846 is an open-beaker acid digestion method, which has been considered not suitable for mercury determination because of the volatile properties of mercury. The method presented here has proven to be reliable and rapid for the decomposition of coal samples for mercury determination, as well as for other trace metals.

EXPERIMENTAL

Instrumentation

A Model MDS-2100 microwave oven (CEM Corporation) with pressure control was used. The power range (maximum 950 W) of the oven was adjusted to 1% increments. Since the sample decomposition consists of several separate stages of control, the microwave is also equipped with a removable 12-position carousel. Teflon vessels of 100-mL volume, allowing a maximum 120 psi of pressure, were used.

A Leeman Labs, Inc., PS200 automated mercury analyzer was used as the analytical instrument to measure the mercury in digested coal acid solutions. The pump rate was 5 mL/min. The gas flow rate was 0.3 L/min.

Reagents and Standards

Concentrated sulfuric acid, concentrated nitric acid, and concentrated hydrochloric acid were all trace metal grade. $SnCl_2$ and $Mg(ClO_4)_2$ were analytical grade. Mercury standards were analytical grade.

Procedures

Microwave Digestion

Approximately 0.5 g of coal, accurately weighed to 0.0001 g, was placed in a Teflon microwave digestion vessel with 1 mL of concentrated sulfuric acid and 0.25 mL of concentrated nitric acid (added separately). Approximately 2 minutes was given for the reaction to take place. An additional 1 mL of concentrated nitric acid was then added to the vessel. The digestion vessels were capped and placed

in the microwave, and Step 1 was run (See Table 1). The vessels were removed from the microwave after the run was completed. The vessels were cooled to room temperature and the gases vented. An additional 2 mL of concentrated nitric acid was added to the vessel. The digestion vessels were put through additional heating (Steps 2 and 3) until the solution was a clear light yellow color, with cooling and venting between each step. 0.5 mL of concentrated hydrochloric acid was put in each digestion vessel, and Step 4 was run. 5 mL of concentrated hydrochloric acid was added, and the solution was diluted to 50.0 mL with distilled water in a volumetric flask. The solution was filtered and run on the cold-vapor atomic adsorbance (CVAA) mercury analyzer using matrix-matched standards.

Cold-Vapor Atomic Absorption Mercury Analyzer

After about 1 hour equilibrating the instrument, a five-point calibration was performed. A quality control standard was analyzed immediately after the instrument was standardized to verify calibration accuracy. Samples were run in duplicate, with the mean reported. A calibration check standard was analyzed every ten samples. If the check standards did not read within 10% of the expected value; the instrument was recalibrated. A sample spike was performed every ten samples as well as for each different matrix to verify analyte recovery. A digestion blank and one standard reference material was run along with the samples for quality assurance.

RESULTS AND DISCUSSION

Effect of Acids in Combination

Hot concentrated perchloric acid is a strong oxidizing agent that attacks metals that are unresponsive to other acids. However, hot concentrated perchloric acid is potentially explosive when in contact with organic material (3). Because of this potential hazard, alternative acids to complete dissolution were investigated, and perchloric acid was not used.

Sulfuric acid is a highly effective solvent for many organic samples. Hot concentrated sulfuric acid can completely destroy almost all organic compounds. In this study, sulfuric acid was added as the first step to convert the organic compounds in the coal to inorganic carbon. Because sulfuric acid absorbs the water generated during the reaction, the equilibrium is pushed to the right, helping to maintain the reaction.

Nitric acid is a strong oxidizing reagent widely used for liberating trace metals from various types of matrices as highly soluble nitrate salts. Nitric acid added after the sulfuric acid will convert inorganic carbon to carbon dioxide and produce soluble salts. But only a small amount (0.25–0.5 mL) of nitric acid should be added at first to allow the reaction to start at ambient temperature. If 3 mL of total nitric acid was added at one time, the reaction between the coal and acids would actually slow down as a result of the large amount of water in the concentrated nitric acid (more than 30%) absorbing the heat.

Hydrochloric acid is used for dissolution of coal and, more importantly, for preserving mercury in solution.

Bloom (4) and other researchers (5) reported that most trace metals, including mercury, are completely leached from silicate and sulfide minerals by hot acids; thus there is no need for complete hydrofluoric acid breakdown. Trials using hydrofluoric acid at the end of the digestion stage were carried out in this investigation. The analysis results showed no difference. Therefore, hydrofluoric acid was not used in the digestions.

A comparison was made of digestions with and without sulfuric acid. The results showed a 50% longer digestion time for complete dissolution without sulfuric acid. Adding a mixture of the acids to the coal sample instead of adding them separately was tested. Longer digestion times and incomplete digestions resulted in poor precision and accuracy.

Efficiency of Digestion

Although many studies have been devoted to evaluate recoveries of trace metals from coal matrices, little has been done to establish how completely the coal was digested. If a clear and colorless solution resulted, it has been assumed that digestion was complete. A visible residue of silicate material (a grayish color) often remained. In the case of high-ash coals, the presence of this residue made confirmation of complete digestion even harder. Matusiewicz et al. (5) used total residual carbon to evaluate the degree of completion of digestion. This digestion method was used in several interlaboratory proficiency studies and round-robin studies for mercury and other trace metals, and the overall results indicate that this digestion method is precise and accurate.

Pressure Evaluation

The pressure of the first stage was set at 40 psi, and the power was set with slow ramp. The running time should be adequate to allow the sulfuric acid to react with the coal completely. The maximum pressure in the second stage was raised to 70 psi, because after additional nitric acid is added, the reaction between inorganic carbon and nitric acid can be very violent and large amounts of gases can be generated, resulting in a rapid pressure increase and membrane blowout. The pressure control was connected to the vessel containing the largest and, presumably, the most reactive sample when different types of samples were digested at the same time. Different types (i.e., different ranks) of coal have different responses to microwave pressure. Low-rank coal tends to be digested fairly easily because of its loose organic structure and low carbon content. High pressure is generated in the first couple of steps as a result of the rapid chemical reaction. A low percentage of microwave power should be applied to such samples.

Potential Sources of Interference and Contamination

Organic matrices cause interference on inorganic instrumentation. Some researchers used postdigestion methods such as a potassium persulfate digestion after the microwave digestion to reduce the organic matrices. But we found the method presented here provides a good, complete digestion with good precision and accuracy without any postdigestion. Also, postdigestion can potentially become a source for contamination.

Matrix-matched standards were used to compensate for any contamination from the trace-metal-grade acids used.

The mineral content in coal gave very small or no interference on instrument readings because of the very small amount of mineral content left after the complete digestion.

A digestion blank is very important for accurate analyses of the trace level of analytes in most fossil fuel samples. As impurities in the acids used are compensated for using matrix-matched standards, the digestion blank will verify other potential sources of contamination occurring during the digestion period.

Precision and Accuracy

Without any other laboratory's involvement for testing the method, we cannot verify this method's precision and accuracy, but we can discuss the data we generated from the perspective of precision and accuracy. Tables 2 and 3 show the instrumental precision and digestion precision and accuracy for the three standard reference materials used in this investigation.

A relatively large sample size, about 0.5 g compared with most other methods using 0.1–0.2 g, gives more analyte in the solution provided, resulting in a more accurate reading, since mercury in most of the coals are at trace levels and are barely above the instrument detection limit after the dissolution.

Instrument Detection Limit

The instrument detection limit for coal matrices was calculated based on the seven readings of several different low-level mercury matrix-matched standard concentrations (between 0.1 and 0.5 ppb). The method used for calculation was Code of Federal Regulations 40. The detection limit for coal on the instrument used in this study is 0.1 μg/L in digestion solution or 0.01 μg/g in solid, based on 0.5 g of coal digested and brought to a final volume of 50 mL.

CONCLUSION

Sample digestion in pressurized Teflon vessels using microwave heating proved to be a very rapid method for the complete digestion of fossil fuel samples. Results obtained from this study for trace mercury in coal are in good agreement with certified values. The use of $HClO_4$ at high temperature and high pressure should be avoided because of the potentially explosive nature of the acid. Multiple digestions and analysis for other important trace metals in a certified standard reference material (National Institute of Standards and Technology) [NIST] 1635 and South Africa Reference Material [SARM] 19) were carried out by the Analytical Research Laboratory investigators at the Energy & Environmental Research Center. Data showed that this digestion method is a good coal dissolution method for other trace metals (As, Cd, Ni, Se, Cr, Be, etc.) in coal.

REFERENCES

1. Lengyel, J. "Round Robin Study of Mercury in Coal," final report; 1993.

2. Handbook for SRM Users; NBS Publication 260–100, U.S. Department of Commerce.

3. Kingston, H.M.; Jassie, L.B.; *Introduction to Microwave Sample Preparation: Theory and Practice*; 1988.

4. Bloom, N.S.; Miklavcic, V.L.; Prestbo, E.M. "Determination of Mercury in Fossil Fuels at the ppb Level by Cold Vapor Atomic Fluorescence Spectrometry, after Total Wet Oxidation with Perchloric Acid in Teflon Microwave Digestion Bombs," Presented at the Conference on Managing Air Toxics: State of the Art, Washington, DC, July 13–15, 1993.

5. Matusiewicz, H.; Sturgeon, R.E.; Berman, S.S. "Trace Element Analysis of Biological Material Following Pressure Digestion with Nitric Acid–Hydrogen Peroxide and Microwave Heating," *Journal of Analytical Atomic Spectrometry* **1989**, *4*.

TABLE 1

The Microwave Setup

Coal Digestion Step 1					Coal Digestion Step 2			
Stage	1	2	3	4	Stage	1	2	3
Power	25	35	40	40	Power	40	45	50
PSI	30	40	45	50	PSI	30	40	60
Time (min)	10	10	60	60	Time (min)	10	10	30
TAP (min)	1	1	60	60	TAP (min)	1	1	30
Fan	100	100	100	100	Fan	100	100	100

Coal Digestion Step 3				Coal Digestion Step 4			
Stage	1	2	3	Stage	1	2	3
Power	30	50	60	Power	35	50	60
PSI	60	85	100	PSI	80	90	100
Time (min)	10	10	20	Time (min)	10	10	20
TAP (min)	1	1	20	TAP (min)	1	1	20
Fan	100	100	100	Fan	100	100	100

TABLE 2

Instrumental Precision

	1635	SARM 19	SARM 18
% RSD *	2.40	2.45	2.43

* % relative standard deviation (RSD) was from seven readings.

TABLE 3

Digestion Precision and Accuracy

	SARM	NIST	SARM 18	Commanche	Absaloka	Blacksville
Uncertified Value	0.2	0.02	0.04	NA*	NA	NA
EERC Result	0.207	0.0186	0.024	0.071	0.049	0.084
% RSD**	11.9	32.8	2.56	8.2	19.0	23.9
Number of Digestions	14	12	8	NA	NA	NA
% Recovery	104	93	60	NA	NA	NA

* Not applicable.

** % RSD was calculated from number of digestions.

PRECOMBUSTION REMOVAL OF MERCURY FROM COAL BY MILD PYROLYSIS

Amy C. Merdes, Tim C. Keener, Department of Civil and Environmental Engineering
and Soon-Jai Khang, Department of Chemical Engineering
University of Cincinnati
Cincinnati, OH 45221-0071

Keywords: mercury in coal, mild pyrolysis, clean coal

INTRODUCTION

Coal combustion is one of the most popular sources for energy in the United States. However, increasing environmental regulations concerning the emissions of various pollutants resulting from coal combustion are being promulgated. Title III of the 1990 Clean Air Act Amendments specifies that air toxics will be controlled to the maximum extent technically possible (maximum available control technology, MACT). A number of compounds listed as toxic are found in coal and are released into the atmosphere when coal is burned. Under Title III, a plant that emits over 10 tons/year of any one of the listed toxic compounds, or emits over 25 tons/year (or more) of any combination of these pollutants are required to comply to the control standards. Mercury is present in coal at varying ppm (μg/g) levels and is considered to pose a significant environmental health risk from coal combustion. Reviews[1] on mercury in the ambient air have suggested that the average concentration of mercury in the gaseous form in regionally polluted areas, such as the east coast, are in the range between 3 to 4 ng Hg/m^3. And in urban air the average concentrations may be as high as 10 ng Hg/m^3. Coal combustion has been estimated to account for over 8 % of the mercury emissions to the atmosphere.[2] Lindberg[3] reported that in the plume of a coal-fired power plant, gaseous mercury is present in excess of 1000 ng Hg/m^3 within a few kilometers of the source. Material balances on mercury in power plants have shown that only approximately 10% of the total mercury from the coal is found in the fly ash, and the remainder exits the stack in vapor form.[4, 5] Other studies investigating the effects of existing flue gas clean-up (FGC) technologies on mercury concentration in flue gases report that varying levels of removal can be achieved, ranging from 10% to 90% removal.[6, 7, 8, 9] This large variation is most likely due to differences in combustion reactors as well as differences in the chemical form of mercury and variations in chlorine levels in the feed coal.

The terminology of pyrolysis is used to refer to the processes in which coal is heated in the absence of oxygen. The coal partially decomposes and produces gaseous, liquid and solid residuals. Mild pyrolysis is performed using low temperatures (<600°C), low pressure (about 1 atm.) and usually low heating rates. The original coal matrix remains largely intact while the heating value of the coal is retained. Mild pyrolysis of coal has been shown to be an economically and technically viable method of desulfurization and denitrification.[10, 11] Most "organic" sulfur in Ohio #8 coal is released below 500°C in the form of H_2S which can be quickly scrubbed by solid sorbents. During pyrolysis the majority of trace elements in coal are retained in the solid residue, but volatile elements such as mercury, bromine, and antimony are released in vapor form. Elemental mercury has a low boiling point (356 °C) and has been shown to be released from coals at the lower temperatures indicative of mild pyrolysis.[12,13,14] The release of mercury from the coal structure before combustion by mild pyrolysis offers the greatest potential for the separation of mercury and its compounds from the evolved gases and vapors. The concentration of these species are at their greatest in the vapor phase during this period and may be collected by means of adsorption or chemisorption to solid sorbents. This precombustion removal represents a pollution prevention strategy. (Regulations controlling the release of mercury will most likely be promulgated in the future for coal burning power plants.)

This study investigates the influences of temperature and residence time on the evolution of mercury from coal during mild pyrolysis. While optimizing the temperature and residence time so as to maximize the evolution of mercury, it was also important to maintain the original heating value of the parent coal.

MILD PYROLYSIS METHODOLOGY

A Lower Freeport #6A coal mined in Harrison County, Ohio was the primary coal investigated in this study. The Lower Freeport sample was sieved to 115 x 150 mesh (~115μm) size prior to shipment. During the sieving and shipment time period the sample lost some moisture and became slightly oxidized. The condition of the sample as received was maintained by storing it with CO_2 headspace in poly-urethane containers. A Pittsburgh #8 Coal mined in Greene County, Pennsylvania was also used in this study so as to provide a comparison. This sample was also sieved to 115 x 150 mesh (~115μm) size and was maintained in an as received condition by storing it with CO_2 headspace in poly-urethane containers. The two parent coal samples examined in this study are high volatile bituminous coals. The original samples were riffled for characterization tests, and a summary of the test results is shown in Table 1.

The mild pyrolysis process was carried out in a Lindberg tube furnace with nitrogen flow. A diagram of this system is shown in Figure 1. It is a well known fact that trace values for mercury in coal vary largely even within a single coal seam. Before pyrolyzing the coal samples, it was necessary to extract a portion of the coal (~10grams), cone and separate that portion so as to produce a homogenized sample, and then determine a mean value for the mercury content of that homogenized sample. Samples to be pyrolyzed were then extracted from the homogenized sample, weighed to 0.5g ± 0.1mg, and placed in nickel alloy sample boats. The tube furnace was stabilized at a predetermined temperature, and the nitrogen flow was regulated so that the gas velocity in the hot zone of the tube was maintained at approximately 3cm/s.

Each sample was placed in the cool zone of the tube and purged of any trapped gases by the nitrogen flow. The sample was then pulled into the hot zone of the tube furnace and heated for a predetermined time. The sample was then pushed back into the cool zone of the tube where it remained in a nitrogen atmosphere until room temperature was achieved. The pyrolyzed coal was then analyzed for total mercury content using the ASTM D3684-78 procedure. The ASTM method was written specifically for fresh coal samples, but should effectively mineralize the pyrolyzed coal as well.

EXPERIMENTAL RESULTS AND DISCUSSION

Coal samples were subjected to mild pyrolysis conditions and percent removal of mercury was determined by comparing the final total mercury content of each pyrolyzed sample with an initial mercury value. The initial mercury value for each sample was calculated by multiplying the weight of the sample prior to pyrolysis with the mean mercury value which was established for the homogenized coal from which the sample was extracted.

The results are shown in Table 2, and graphical representations of the mercury removal as a function of temperature are shown in Figures 2 and 3. The data indicate a general trend within each residence time data set in which the percent removal increases with temperature rise, peaks at some temperature, and then declines. Thermomechanical analysis of both parent coals revealed that the two coals become fluid at about 400°C and remain fluid until resolidification occurs at 464°C for the Lower Freeport sample and 477°C for the Pittsburgh coal sample. When a coal is heated at temperatures in which it becomes plastic, a soft layer develops on the outside of the coal particles and internal depolymerization occurs. As the carbon becomes soft, it swells and traps gases. Once the coal becomes more plastic, the gases break through. It is possible that once the coal becomes plastic, the evolution of the mercury is greatly inhibited by this trapping action. The increased heating rate accompanying the higher temperatures increases the trapping because the devolatilization is greater than the plasticity.

Within each temperature range data set, a general trend exists in which the removal of mercury initially increases rapidly with residence time and then levels off as it seemingly approaches an asymptotic limit. This suggests that under the conditions given in the methodology, the rate of evolution of total mercury is proportional to the fraction of mercury and its compounds remaining in the char at any time multiplied by some reaction rate coefficient dependent on temperature. This can be expressed as a first order homogeneous decomposition with an asymptote dependent on temperature, time, reactor configuration, pressure, heating rate, and particle size:

$$\frac{X}{X_{max}} = 1 - e^{-kt}$$

Where: X = percent conversion
X_{max} = maximum percent available for conversion under a specified set of conditions
t = reaction time (min)
k = reaction rate coefficient (min^{-1})

By maximizing the regression coefficient when comparing the experimental data to the linear form of the equation, X_{max} can be obtained for each temperature. The slope of the linearization provides a value for k, the reaction rate coefficient. Table 3 lists the values of X_{max} with the corresponding R^2 and k for both coal samples and all temperatures. A comparison of the Lower Freeport #6A data with the above equation indicates a reasonable agreement between theory and measurements for all temperatures except 275°C and 325°C. The Lower Freeport #6A data indicates an interesting trend once a pyrolysis temperature of 325°C is achieved. Below this temperature, analysis results in a maximum possible removal of 100%, but after 325°C, X_{max} increases with temperature until it peaks at 500 °C. A comparison of the Pittsburgh #8 data with the equation, however, indicates a reasonable agreement between theory and measurements only within the temperature range of 325°C to 400°C.

By applying Arrehnius' law to the Lower Freeport #6A experimental data, a plot of ln(k) vs. 1/T results in figure 4. The plot shows two regimes for mercury removal in the Lower Freeport #6A coal. The data produces a straight line with a large slope in the 275°C to 400°C temperature range. This indicates a large activation energy, E, which can be associated with

chemical reaction control. The temperature at which the plot's slope changes dramatically, indicating a shift in controlling mechanism of the reaction, coincides with the coal's plastic zone. Application of Arrehnius' law to the Pittsburgh #8 experimental data results in figure 5. The plot indicates that the Pittsburgh #8 coal behaves similar to the Lower Freeport #6A coal under the pyrolysis conditions given in the methodology. The activation energies for the mercury removal in the lower temperature region (<400°C) are calculated using information from the equation of the straight line plotted in that temperature region. The activation energies for mercury removal from the Lower Freeport #6A coal and the Pittsburgh #8 coal are 6615 cal/gmol and 4939 cal/gmol respectively.

After treating a coal by mild pyrolysis, it is important to examine what effects the pyrolysis process has had on the overall heating value of the coal. An oxygen bomb calorimeter was used to determine the net heat of combustion of each of the Lower Freeport #6A pyrolyzed samples. These values were compared to an initial heat of combustion value which was calculated using the inital sample weight and a mean value for the net heat of combustion of the parent Lower Freeport #6A coal. Figure 6 shows a plot of this comparison. The results indicate that there is little change in the overall heating value of the Lower Freeport #6A pyrolyzed coal until pyrolysis temperatures are greater than 400°C. During the 200-400 °C temperature range, there is apparently little carbon loss although devolatilization of other components does occur. Once temperatures exceed 400 °C, there is a decrease in overall heating value which drops with temperature rise.

CONCLUSIONS

Given the conditions of the reactor used in this study, mild pyrolysis of coal can achieve up to 74% removal of mercury from the Lower Freeport #6A coal investigated and up to 80% removal of mercury from the Pittsburgh #8 coal investigated. The results show that precombustion removal of mercury from coal by mild pyrolysis can be modeled as a homogeneous reaction with a distinct maximum percent mercury available for conversion and a distinct reaction rate coefficient for each temperature range. The results also indicate that removal of mercury occurring when pyrolysis is performed at low temperatures (<400°C) on plastic or caking coals is characterized by chemical reaction control. At these low temperatures, the coal matrix suffers little destruction. The results verify that the overall heating value of the coal is essentially unaffected by mild pyrolysis at temperatures lower than 400 °C.

Table 1: Summary of Characterization Analysis on Original Coal Samples

	Lower Freeport #6A (Harrison Co., OH)		Pittsburgh #8 (Greene Co., PA)	
	As Determined	Dry Basis	As Determined	Dry Basis
%Ash	11.52	11.65	10.00	10.25
%Carbon	68.03	68.78	73.41	75.22
%Hydrogen	5.07	5.13	5.2	5.33
%Nitrogen	1.62	1.64	1.67	1.71
%Sulfur	4.24	4.29	1.09	1.12
%Oxygen (difference)	9.52	9.62	8.63	8.84
%Moisture	1.09 (residual)		2.40	
Density, g/cm^3		1.294		1.293
Hg Conc., ppm		0.57 ± 0.07		0.12 ± 0.04
Surface Area, m^2/g		1.105		1.386
Btu/lb	12,870	13,019	13,207	13,532
kJ/kg	29,933	30,280	30,717	31,473

Figure 1: Furnace with Nitrogen Flow

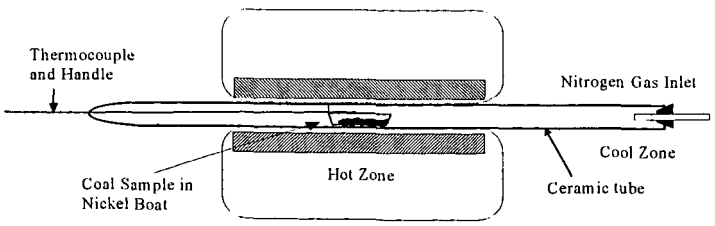

Table 2: Mild Pyrolysis Test Results

	Lower Freeport #6A %Removal of Mercury				Pittsburgh #8 %Removal of Mercury				
Temp. °C	2 Minute Residence Time	4 Minute Residence Time	8 Minute Residence Time	10 Minute Residence Time	2 Minute Residence Time	4 Minute Residence Time	6 Minute Residence Time	8 Minute Residence Time	10 Minute Residence Time
275	0	5.5	5.6	5.3	-	-	-	-	-
300	0	8.0	14.9	24.2	-	-	-	-	-
325	0	37.6	29.5	41.4	0	0	-	36.1	52.0
350	14.0	33.6	44.8	48.6	-	-	-	-	-
400	39.9	50.3	57.7	57.7	53.0	70.6	79.6	-	-
450	9.7	58.8	68.4	68.1	47.0	46.6	46.9	-	-
500	-	62.4	73.9	-	-	-	-	-	-
600	-	49.5	59.1	-	-	-	-	-	-

Figure 2: Lower Freeport #6A Mild Pyrolysis Data

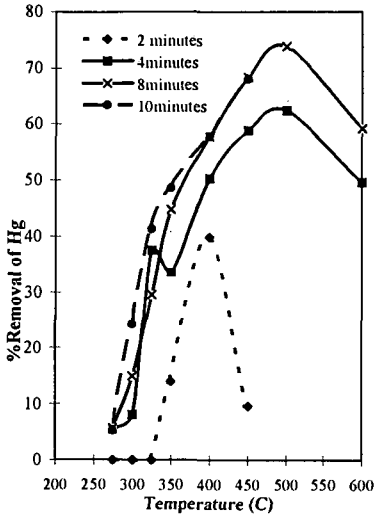

Figure 3: Pittsburgh #8 Mild Pyrolysis Data

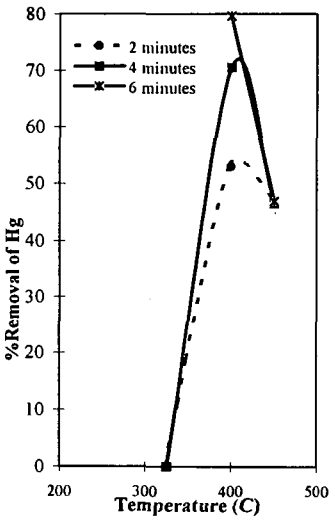

Table 3: Values of X_{max}, R^2, and k

	Lower Freeport #6A			Pittsburgh #8		
Temp.(°C)	X_{max}	R^2	$k(min^{-1})$	X_{max}	R^2	$k(min^{-1})$
275	1.00	0.683	0.006	-	-	-
300	1.00	0.939	0.028	-	-	-
325	1.00	0.657	0.044	1.00	0.850	0.071
350	0.54	0.993	0.234	-	-	-
400	0.58	0.972	0.502	0.86	0.998	0.441
450	0.70	0.931	0.449	1.00	0.598	0.097
500	0.77	0.999	0.422	-	-	-
600	0.62	0.999	0.386	-	-	-

Figure 4: Arrehnius Plot of Lower Freeport #6A Data

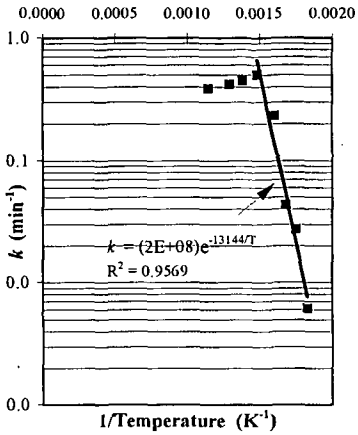

Figure 5: Arrehnius Plot of Pittsburgh #8 Data

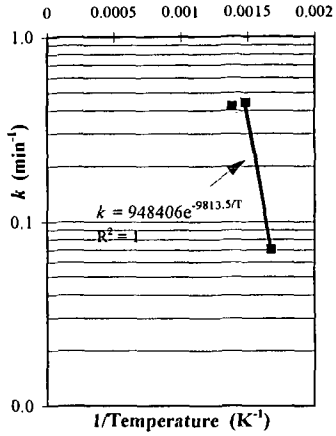

Figure 6: Comparison of Lower Freeport #6A Parent Coal and Pyrolyzed Coal Heating Values

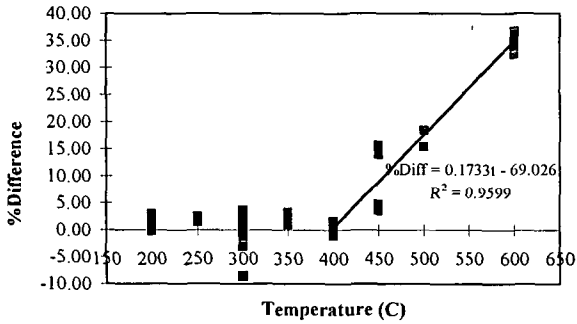

REFERENCES

1. Mercury Health Effects Update, Health Issue Assessment, U.S.E.P.A. 1984.
2. Sittig, M., Environmental Sources and Emissions Handbook, Noyes Data Corporation, Park Ridge, NJ 1975
3. Lindberg, S.E., "Mercury Partitioning in a Power Plant Plume and it Influence on Atmospheric Removal Mechanisms", ***Atmos. Environ.***, 14, 1980.
4. Schultz, H., Hattman, E.A., and Booher, W.B., *Am. Chem. Soc.*, 15 (1975), 196
5. Kalb, B.W., *Am. Chem. Soc.*, Ser. 141 (1975), 154.
6. Clarke, L. B. *Fuel*, Vol. 72 No.6 (1993), 731-735.
7. Meij, R., *Water, Air and Soil Pollution*, 56 (1991), 21-33.
8. Kumar, K. Sampath, and Feldman, Paul L., 'Fine Particulate and Trace Element Control in Wet Electrostatic Precipitators', *A&WMA 87th Annual Meeting & Exhibition*, Cincinnati, Ohio (1994)
9. Peterson, Joe, Seeger, Dave, Skarupa, Ron, Stohs, Miriam, and Hargrove, Buddy, 'Mercury Removal by Wet Limestone FGD Systems: EPRI HSTC Test Results', *A&WMA 87th Annual Meeting & Exhibition*, Cincinnati, Ohio (1994)
10. Keener, T.C. Khang, S.J., and Jenkins, R.G., *Fuel Proc. Tech.*, 33 (1993),33-48.
11. Khang, S.J., Lin, L., and Keener, T.C., *Proceedings of World Congress III on Eng. and Environ.*, Vol. 2, Beijing, China (1993),571-587.
12. Karr, C., Jr., (ed) Analytical Methods for Coal and Coal Products, 3 volumes Academic Press, 1978.
13. Ruch, R.R., Gluskoter, J.J. and Kennedy, E.J., *IL Env. Geo. Notes.*, 1971.
14. Ebdon, L., Wilkinson, J.R., and Jackson, K.W., *Analyst*, 107 (1982), 269.

REACTIONS OF GASEOUS, ELEMENTAL MERCURY WITH DILUTE HALOGEN SOLUTIONS

M. H. Mendelsohn and C. D. Livengood
Energy Systems Division, Building 362
Argonne National Laboratory
Argonne, IL 60439

Keywords: mercury, mercury oxidation, mercury reactions

ABSTRACT

Of the trace elements known to exist in fossil fuels, mercury (Hg) has emerged as one of the greatest concerns. Mercury has been found to be emitted from combustion in at least two different chemical forms: elemental Hg and oxidized Hg compounds. Precise identification of the oxidized compounds emitted has not been accomplished to date. However, most workers in this field assume that mercuric chloride should be the predominant oxidized species. Mercuric chloride should be readily removed in a wet scrubber system because of its relatively high solubility in water. However, it has been presumed, and we have shown, that elemental Hg will pass through a wet scrubber system with little or no removal being effected. Therefore, it is important, in order to obtain a high total Hg removal, to study methods that might result in a removal of gaseous, elemental Hg from a flue-gas stream. In this regard, we have been studying the effect of dilute halogen-containing solutions on elemental Hg in gas streams of various compositions. In particular, the results of passing Hg through bubblers containing solutions of iodine, chlorine, and chloric acid are described. Mercury found in the bubbler solutions is an indication of the extent of reaction (oxidation) of elemental Hg with the halogen species, since we have found very little Hg transferred to the liquid phase when only distilled water is used in the bubblers. Results using commercial iodine, sodium hypochlorite, and NOXSORB™ solutions are presented and discussed.

INTRODUCTION

The 1990 Clean Air Act Amendments designate 189 substances as hazardous air pollutants also called "air toxics." Mercury (Hg) has emerged as one of the air toxics of greatest concern. Mercury has been found in the stack emissions from U.S. power plants [1]. Coal-fired power plants account for the vast majority of the estimated total Hg emissions from all U.S. power plants. Mercury emitted from coal-fired power plants has been found in a variety of chemical forms, including elemental Hg and oxidized Hg compounds, such as mercuric chloride [1]. Highly soluble Hg compounds, such as mercuric chloride, are assumed to be readily removed in a wet scrubber system. However, elemental Hg, because of its very low solubility in water, has been shown *not* to be captured in a laboratory-scale wet scrubber system [2]. Therefore, in order to remove elemental Hg with a wet scrubber system, an additional method must be incorporated into a typical wet flue-gas scrubbing process.

We have been studying methods to oxidize gaseous elemental Hg in a typical flue-gas environment, which includes the presence of other potentially reactive gases in the gas mixture, such as oxygen (O_2), nitric oxide (NO), and sulfur dioxide (SO_2). In this paper, we summarize results of Hg removal found by bubbling various gas mixtures containing elemental Hg through solutions of iodine, chlorine, and chloric acid. Although there are some literature references to reactions of elemental Hg with these reactants, we believe that this is the first study that also includes NO and SO_2 in the gaseous reaction mixture. Results for iodine solutions showed that a very high Hg removal was obtained only when the gas phase mixture consisted of Hg and nitrogen (N_2). When other gases were included in the feed gas mixture, the amount of Hg found in the liquid phase was drastically reduced. With chlorine solutions, a more complex behavior was observed that depended on the feed gas mixture and concentration of chlorine used. Chloric acid solutions were prepared from a commercial NOXSORB™ preparation obtained from the Olin Corporation. These solutions showed a moderate amount of Hg removal (14-27%) for the concentrations studied when only O_2 and N_2 were added to the feed gas mixture. Substantially more Hg was removed (34-70%) when NO was added to the feed gas mixture. Finally, when SO_2 was added to the mixture with NO, a moderate decrease in Hg removal from that observed with NO alone was noted (23-49%). All the results are presented and discussed more fully below.

EXPERIMENTAL SETUP AND PROCEDURES

A calibrated and certified Hg permeation tube from VICI Metronics was used as a constant source of vapor-phase, elemental Hg. The permeation tube was placed in a constant temperature water bath controlled to about ± 0.5°C. Bottled, high purity (99.998%) nitrogen gas flowed around the permeation tube to produce a gas stream with a constant concentration of elemental Hg. This gas stream was then combined with another gas stream containing nitrogen and other gaseous components, including O_2, carbon dioxide (CO_2), NO, and SO_2. Carbon dioxide was used as a carrier gas for the NO. Oxygen was used from a laboratory air line without further purification. Carbon dioxide, NO, and SO_2 were used from bottled gases without further purification. Nominal purities for these gases were as follows: CO_2, 99.5%; NO, >99.0%; SO_2, >99.98%. Gases were blended and their initial composition checked with the following Beckman instruments: O_2, Model 755 Oxygen Analyzer; CO_2, Model 864 Infrared Analyzer; NO, Model 951A NO/NO_x Analyzer; SO_2, Model 865 Infrared Analyzer. Typical concentrations of the various gas components were as follows: O_2, 5%; CO_2, 15%; NO, 250 ppm; and SO_2, 1000 ppm. After the feed gas composition had stabilized, a valve was turned to admit the gas mixture to a series of three bubblers, each containing 150 mL of solution. The first bubbler contained the solution to be studied, while the

second and third bubblers usually contained distilled water. Commercial solutions of iodine, chlorine (sold as sodium hypochlorite), and chloric acid (sold as NOXSORB™ by the Olin Corporation) were used without further purification. Each test was performed by allowing the gas mixture to bubble through the bubblers for exactly 30 min. Liquid phase samples from each bubbler were saved for total Hg analysis. Mercury analyses were performed by a standard cold-vapor atomic absorption spectrophotometric method (U.S. EPA Method 7470A, SW-846). Mercury concentrations were determined to ± 0.02 μg Hg/L. Estimated accuracy for this method is ± 10%.

RESULTS AND DISCUSSION

The purpose of the tests described above was twofold. First, we wanted to study the effects on Hg removal from additions of the gases NO and SO_2 to a Hg-containing gas stream. Second, we wanted to learn about the Hg removal process in regard to gas phase versus liquid phase reaction mechanisms. We realized, after we began testing, that only minimal information on our second objective could be gained from these experiments. We could presume that Hg found in the second bubbler was due to gas phase reactions, assuming that liquid carryover from the first bubbler was negligible. However, the situation in bubbler #1 is more complex. From these tests, we cannot distinguish in bubbler #1 between gas phase reactions inside the gas bubble followed by rapid dissolution of products in the liquid phase, and gas-phase dissolution at the gas-liquid interface followed by rapid liquid-phase reaction.

Before tests were performed with various solutions in bubbler #1, initial baseline tests were carried out with only distilled water in all three bubblers. When no elemental Hg was added to the gas stream, no Hg was found in any of the bubbler solutions. This result demonstrates that our system is free of Hg contamination to the detection limit (± 0.02 μg Hg/L or ± 0.003 μg Hg in 150 mL of water) of the Hg analytical method described above. Such baseline tests were run periodically to ensure that no Hg contamination had built up during the course of testing described in this paper. A second baseline test was performed with Hg added to the feed gas stream, but again with only distilled water in all three bubblers. For this test, amounts of Hg barely above the detection limit (0.004-0.005 μg Hg in 150 mL) were found in each of the three bubblers. This amount of Hg may be compared with the calculated amount of Hg in the gas stream of 1.9 μg for the 30-minute test. This result shows that the amount of Hg removed in this experimental apparatus by using only distilled water is less than 0.3%. Therefore, any amounts of Hg found in the bubblers greater than this baseline amount must be from reactions of elemental Hg with components of the various solutions tested in bubbler #1.

Iodine Solutions

Commercial iodine solutions generally contain potassium iodide as a stabilizer, as well as dissolved iodine. A commercial preparation of 0.100 N iodine solution was diluted to make up various iodine concentrations. Previous experiments in our laboratory had shown that iodine solutions react rapidly with elemental Hg vapor [3] in gas streams containing only Hg and N_2. However, those tests had been performed by using only a gas-phase Hg analyzer to measure the elemental Hg concentration in both the feed and effluent gas streams. The analyzer used in those tests has recently been shown by us to be unreliable for measuring Hg in various complex gas mixtures. The tests reported here are the first ones where Hg in the liquid phase has been analyzed. Using a solution of about 125 ppb iodine in bubbler #1, we found that more than 90% of the gas-phase Hg was in the bubbler solutions when only N_2 and Hg were in the feed-gas stream. When O_2 and CO_2 were added to the gas mixture, Hg removal was reduced to about 6%. Only one test was performed with a higher iodine concentration in bubbler #1 (~250 ppb iodine). This test, for a gas stream containing only Hg and N_2, did not give a result substantially different from the lower concentration test (~81% Hg removal). However, when either NO or SO_2 (or both) were added to the gas mixture, the amount of Hg found in the bubbler solutions went either to zero (for NO and for NO plus SO_2) or close to zero (~1% for SO_2). Iodine solutions were not investigated further in these bubbler tests.

In earlier unpublished work in our laboratory, we found that the concentration of gaseous elemental Hg was substantially reduced simply by passing Hg vapors (mixed with nitrogen gas only) over an agitated iodine solution (~250 ppb). These tests showed that the most likely Hg removal mechanism was a rapid gas-phase reaction between iodine vapors and elemental Hg, probably yielding mercuric iodide. This gas phase reaction is probably why a considerable portion (~35%) of the total mercury found in the liquid phase was found in bubblers #2 and #3. However, as discussed above, we cannot exclude the possibility that some of the Hg found in bubbler #1 is from a liquid-phase reaction at the gas-liquid interface. Indeed, a published report on the reaction of iodine in solution with dissolved Hg stated that "the rate was too fast to measure" [4]. The product of the solution reaction was shown to be mercuric iodide by its ultraviolet spectrum [4]. Therefore, without further modeling studies and knowledge of the rate constants (no experimental data on the gas phase reaction of Hg with iodine could be found in the literature), we cannot specifically analyze how much of each reaction (gas phase versus liquid phase) is responsible for the Hg found in bubbler #1.

We conclude that the reaction of Hg with iodine is extremely rapid in the gas phase. However, the presence of other gases readily interferes with this reaction. Whether this interference is caused only by reaction of iodine with the other gaseous components, or whether another mechanism is responsible for the interference cannot be determined from these tests. In any case, iodine would

not seem to be an attractive option for oxidation of elemental Hg in the presence of gases other than nitrogen.

Chlorine Solutions

Solutions of molecular chlorine (Cl_2) are more complex than those of iodine because of the greater tendency of Cl_2 to disproportionate in aqueous solution to hypochlorous acid and chloride ions. Commercial chlorine solutions are sold as sodium hypochlorite because in alkaline solutions the equilibrium between Cl_2 and hypochlorite ions greatly favors the latter. Nonetheless, because of the various equilibria involved, detectable amounts of Cl_2 will exist both in the gas and liquid phases. Results for the removal of Hg by chlorine solutions appeared to depend both on the composition of the feed gas mixture and, in some cases, on the concentration of the chlorine solution. These results are presented in Table 1 and discussed below.

The results in Table 1 are given as a percentage of the total gas-phase mercury found in the liquid phase of all three bubblers; that is, we calculated the total amount of Hg in the gas phase that passes through the bubblers from the known rate of Hg generation by the permeation tube times the 30 min duration of each test. Then the total Hg in the bubblers is found by simple addition of the amounts found in the individual bubblers (in general, bubbler #3 was not analyzed for Hg unless a significant amount was found in bubbler #2). Finally, the total liquid-phase Hg is divided by the total gas-phase mercury and the result is multiplied by 100%. As can be seen from Table 1, removal of Hg in gas mixtures containing only O_2 and N_2 did not change much for different chlorine solution concentrations. Some literature data are available on the gas phase reaction of Hg with Cl_2. Recent modelling work has assumed the rate constant to be very small [5]. On the other hand, laboratory experiments have shown conflicting results. Some workers have found this reaction to be slow [6] while others have found it to be relatively fast [7]. Still other work has shown the reaction of Hg with Cl_2 to be surface catalyzed [8]. It appears from these conflicting results that one must be very careful in interpreting data for this reaction. Our data suggest that the rate of reaction between Hg and Cl_2 is not fast, because not much change in Hg removal was observed with increasing chlorine concentration. Our conclusion on the gas-phase reaction of Hg with Cl_2 is that it is slow unless there is an appropriate surface available to catalyze the reaction.

For the gas mixtures containing NO and NO plus SO_2, Hg removal increased with increasing chlorine concentration. However, the rate of increase differed for the two gas mixtures studied. Addition of NO to the feed-gas mixture appeared to have a definite positive effect on the amount of Hg transferred to the liquid phase, when compared to the removals obtained with only O_2 and N_2 present. An explanation for this behavior might be that NO reacts with Cl_2 to yield nitrosyl chloride (NOCl). This reaction has been described in the literature and appears to occur rapidly at room temperature [9]. Although we could not find a literature reference to the reaction of NOCl with elemental Hg, there was a paper which found that NOCl oxidizes mercurous chloride to mercuric chloride as well as oxidizing elemental zinc and copper [10]. Our conclusion for the reaction of Hg in the presence of NO is that NOCl probably reacts faster with Hg than Cl_2 does.

Also, as can be noted in Table 1, when SO_2 is added to the feed-gas mixture, Hg removal is much lower at the lower chlorine concentrations than when SO_2 is not present. However, at the highest chlorine concentration studied, the Hg removal performance with SO_2 present actually slightly exceeded performance without SO_2. It is well-known that sulfite ions will reduce molecular halogens to their corresponding halides. Because of this reaction, it is hard to understand how the presence of SO_2 could actually increase the oxidation of Hg by Cl_2. Perhaps the improvement in Hg removal with chlorine concentration can be understood as simply being caused by the presence of an excess of Cl_2 that swamps the reaction between dissolved bisulfite (from absorbed SO_2) and Cl_2 and/or hypochlorite ions in solution.

Plotted in Figure 1 is a graph of the fraction of Hg found in the liquid phase as a function of the logarithm of the initial chlorine concentration in bubbler #1. The data for the tests with NO and *no* SO_2 in the feed gas mixture are shown with a straight line fit, while the data for the tests with NO *and* SO_2 in the feed gas mixture are shown with a power curve fit. The curve fits are only a guide to show the difference in the removal dependencies with chlorine concentration for the two gas mixtures. A fuller understanding of this behavior will require more detailed testing.

Chloric Acid Solutions

Chloric acid solutions ($HClO_3$) were prepared from concentrated NOXSORB™ solutions. Concentrated NOXSORB™, sold by the Olin Corporation, has a nominal composition of 17.8% $HClO_3$ and 22.3% sodium chlorate. Tests with two different $HClO_3$ concentrations were performed: 0.71% $HClO_3$ (25:1 dilution of the concentrated stock solution) and 3.56% $HClO_3$ (5:1 dilution). The primary vapor-phase species above these solutions is thought to be chlorine dioxide (ClO_2). However, ClO_2 is very reactive and readily photolyzes to Cl_2 and O_2. Also, in the presence of moisture, ClO_2 can produce a number of different chlorine oxyacids, such as HOCl, $HClO_2$, etc. Therefore, a large number of different species may be present in the vapor above a $HClO_3$ solution. To the best of our knowledge, the reaction of Hg with either ClO_2 or chlorate anions has not been studied previously. Results of our tests with two different chloric acid concentrations are shown in Table 2.

From the results shown in Table 2, we first note that the change in Hg removal from a solution of 0.71% $HClO_3$ concentration to Hg removal from an $HClO_3$ solution with about a five times higher concentration is about the same for each of the three different feed-gas mixtures; that is, Hg

removal was about a factor of two higher with the higher concentration $HClO_3$ solution. Next, we note that gas mixtures which contained NO showed a higher Hg removal that the gas mixture without NO. This result is similar to that observed with chlorine solutions. However, in this case, a mechanism different than that proposed for Cl_2 is probably responsible. It has been postulated that reaction of NO with NOXSORB™ solutions produces hydrochloric and nitric acids among its products [11]. Because nitric acid dissolves liquid elemental Hg, we propose that this gaseous nitric acid by-product causes the improved Hg removal when NO is present in the gas stream. Contrary to the behavior observed with chlorine, we found that for both concentrations studied, the presence of SO_2 in the feed-gas stream reduced the Hg removal by about 30% from the level without SO_2 but with NO. Also in contrast to the behavior observed with Cl_2 solutions, it appears as though the mechanism that causes a reduction in Hg removal when SO_2 is present *cannot* be overcome with higher $HClO_3$ concentrations. This result again points to the possibility that a mechanism different from Cl_2 oxidation of Hg is operating for these $HClO_3$ solutions. These tests with $HClO_3$ suggest that the gas-phase reaction of Hg with nitric acid might be rapid and should be examined further.

ACKNOWLEDGMENT

This work is supported by the U.S. Department of Energy, Assistant Secretary for Fossil Energy, under contract W-31-109-ENG-38, through the Pittsburgh Energy Technology Center (PETC). We acknowledge the support provided by Perry Bergman and Tom Brown of the PETC. In addition, we express our appreciation and gratitude to Sherman Smith for his invaluable contributions on the maintenance of the experimental apparatus, as well as the performance of the tests described herein.

References

1. Chu, P., and D.B. Porcella, *Mercury Stack Emissions from U.S. Electric Utility Power Plants*, Water, Air, and Soil Pollution, **1995**, *80*, 135-144.
2. Mendelsohn, M.H., J. Wu, H. Huang, and C.D. Livengood, *Elemental Mercury Removals Observed in a Laboratory-Scale Wet FGD Scrubber System*, Clean Air '94, **1994**, Toronto, Canada.
3. Livengood, C.D., M.H. Mendelsohn, H.S. Huang, and J.M. Wu, *Development of Mercury Control Techniques for Utility Boilers*, 88th Annual Meeting Air & Waste Management Association, **1995**, San Antonio, TX.
4. Warrick, Jr., P., E.M. Wewerka, and M.M. Kreevoy, *The Reactions of Iodine in Solution with Elemental Mercury*, J. Am. Chem. Soc., **1962**, *85*, 1909-1915.
5. Pleijel, K., and J. Munthe, *Modelling the Atmospheric Mercury Cycle - Chemistry in Fog Droplets*, Atmospheric Environment, **1995**, *29*, 1441-1457.
6. Skare, I., and R. Johansson, *Reactions Between Mercury Vapor and Chlorine Gas at Occupational Exposure Levels*, Chemosphere, **1992**, *24*, 1633-1644.
7. Skripnik, V.A., L.F. Fedorovskaya, L.I. Kravetskii, and I.M. Umanskaya, *Mechanism and Kinetics of Mercury Oxidation by Chlorine-Containing Solutions*, Zh. Prikl. Khim. (Leningrad), **1979**, *52*, 1233-1237 (Engl. trans. 1169-1172).
8. Medhekar, A.K., M. Rokni, D.W. Trainor, and J.H. Jacob, *Surface Catalyzed Reaction of Hg + Cl_2*, Chem. Phys. Letters, **1979**, *65*, 600-604.
9. Stoddart, E.M., *The Kinetics of the Reaction between Chlorine and Nitric Oxide*, J. Chem. Soc., **1944**, 388-393.
10. Partington, J.R., and A.L. Whynes, *The Action of Nitrosyl Chloride on Some Metals and Their Compounds*, J. Chem. Soc., **1948**, 1952-1958.
11. Kaczur, J.J., *Oxidation Chemistry of Chloric Acid in NOx/SOx and Air Toxic Metal Removal from Gas Streams*, AIChE 1996 Spring National Meeting, **1996**, New Orleans, LA.

TABLES

Table 1. Summary of Hg removal results for tests with chlorine solutions (Cl) in bubbler #1

	Hg removal from Cl solution (%)		
Feed Gas Composition	2.5 ppm Cl	250 ppm Cl	2500 ppm Cl
$O_2 + N_2$	12	14	9
$O_2 + N_2 + NO + CO_2$	19	42	60
$O_2 + N_2 + NO + CO_2 + SO_2$	0.5	14	66

Table 2. Summary of Hg removal results for tests with $HClO_3$ solutions in bubbler #1

	Hg removal from $HClO_3$ Solution (%)	
Feed Gas Composition	0.71% $HClO_3$	3.56% $HClO_3$
$O_2 + N_2$	14	27
$O_2 + N_2 + NO + CO_2$	34	70
$O_2 + N_2 + NO + CO_2 + SO_2$	23	49

FIGURE

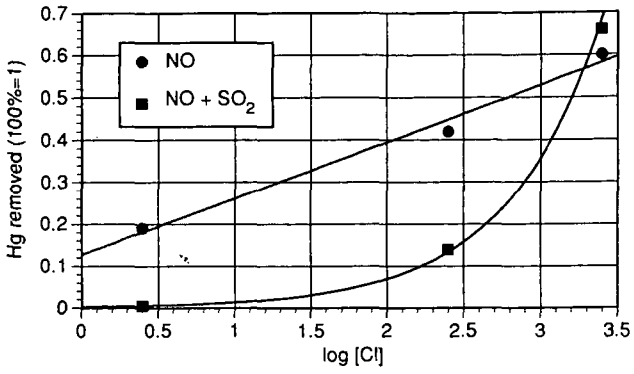

Figure 1. Dependence of Hg removal on the logarithm of the chlorine concentration for two different feed-gas mixtures

THREE WAY CONVERSION CATALYSTS FOR AUTOMOTIVE POLLUTION ABATEMENT

Patrick L. Burk*, Zhicheng Hu, Harold N. Rabinowitz, and Samuel J. Tauster, Shau-Lin F. Chen
Engelhard Corporation, 101 Wood Ave., Iselin, New Jersey 08830

Keywords: Three Way Conversion Catalysts, Palladium, Sulfur

INTRODUCTION

The revisions to the Clean Air Act of 1990 and recent regulatory actions taken by the California Air Resources Board mandate the development of automobiles with much lower tailpipe emissions. For the original equipment manufacturers (OEM's) to meet the target fleet emissions numbers for automobiles defined in California's Low Emission Vehicle program, the OEM's must qualify each model into one of the emissions categories defined in Table 1. The emissions are calculated using the Federal Test Procedure (FTP) protocol wherein a test vehicle fitted with a catalytic converter is driven on a chassis rolls over a tightly defined driving cycle. A key feature of the evaluation is that the FTP is conducted after the catalyst has dealt with 50,000 - 100,000 miles of raw engine exhaust. During the FTP, 50 - 80% of the total pollutants emitted to the atmosphere by the vehicle occurs immediately following the startup of the engine when the engine block and manifold are cold, and the catalytic converter has not reached high conversion efficiencies, and are known as "cold start" emissions. The stringency of the regulations becomes evident when to qualify for either Low Emission Vehicle (LEV) or Ultra Low Emission Vehicle (ULEV) status, the hydrocarbon engine out emissions of 2.0 g/mile, typical for a six cylinder vehicle, must be reduced over the entire FTP by 97% and 99%, respectively. These regulations spurred a variety of new technology thrusts aimed at attacking the cold start hydrocarbons including electrically heated catalysts, hydrocarbon traps, exhaust gas burners, and close coupled catalysts (1).

The FTP test poses a unique catalytic challenge. After tens of thousands of startups and shutdowns, the three way conversion (TWC) catalyst must respond excellently, and rapidly to a wide range of operating conditions: Gas hourly space velocities and exhaust gas temperatures can both quickly jump two orders of magnitude in either direction, and the reactant species present in the exhaust gas vary moment-by-moment in composition, concentration, and relative ratio of oxidants to reductants. To meet these stringent emission levels three way conversion catalyst technologies have undergone a fundamental shift in composition and structure to address the needs for lower light-off temperatures, higher thermal durability, and better tolerance to sulfur poisoning. Much of the research effort has been devoted to mediating the primary deactivation mode for TWC catalysts, thermal sintering of both the precious metals and the base metal oxides. This talk will discuss the base metal and precious metal chemistries that have been blended into these durable heterogeneous catalysts for the efficient conversion of auto exhaust gases.

RESULTS AND DISCUSSION

Palladium has a well documented reputation for both hydrocarbon and CO oxidation (2). When our research began on palladium, this metal was known to damage rhodium's NOx efficiencies via the formation a palladium/rhodium alloy and by itself would give only moderate to low NOx conversion efficiencies. Since the functionality of the precious metal is strongly influenced by the surface upon which it sits, rare earth oxides were examined for their NOx promotional effects on palladium. The palladium-only catalysts were formulated utilizing washcoated cordierite (400 cpsi) substrates prepared from slurries containing mixtures of catalyst powders impregnated with palladium nitrate solutions and other oxide additives. All catalysts were aged to simulate in-use catalyst performance in a laboratory honeycomb reactor kept at 1223 K for 12 hr using a simulated auto exhaust gas stream or as full size pieces aged on engine test beds for 75 - 95 hr with a maximum bed temperature of 1193 K. Figures 1(a) and 1(b) summarize laboratory reactor data showing the promotional effects of the rare earth oxides on palladium for NOx reduction and CO oxidation respectively. In the absence of sulfur, the oxides of lanthanum, neodymium, and cerium improved NOx performance, whereas CO performance was only improved by the ceria. Interestingly, only ceria caused both the CO and NOx performances to increase as the temperature was raised. Apparently in the low temperature regime, the catalysis occurs on the palladium, whereas at higher temperatures the catalytic functionality of the ceria is activated and moves the palladium CO/NOx catalysis to a new performance level. However, the benefits of an intimate palladium-ceria interaction for CO/NOx proved a detriment for hydrocarbon activity, especially at elevated temperatures.

With lead levels in the U.S. fuel supply now well below 1 ppm, the most influential fuel component on catalyst performance is sulfur. Sulfur poses a number of challenges to the functioning of TWC catalysts via its interference with both precious metal and base metal function. The sulfur effect on the rare earth oxide promoters for the palladium-only catalysts was examined in the laboratory reactor. Figure 2 demonstrates how lean aging in the presence of sulfur lowered NOx activity via formation on an intermediate surface oxysulfate on the rare earth oxide. The loss in high temperature ceria performance was particularly notable, but fortunately the oxygen storage function can be restored by subsequent stoichiometric operation.

These findings were then used to create a new palladium-only catalyst architecture wherein the NOx and HC activities were segregated into separate catalytic layers. For best NOx performance the topcoat was formulated to contain the oxides of lanthanum, neodymium, and cerium so that their NOx promoting activity would have first access to the CO for NOx conversion. The bottom coat was kept ceria-free so as to maintain palladium's hydrocarbon and CO oxidation activity. A 0.69 liter palladium-only honeycomb catalyst, at 3.5 g/l palladium, was aged on an engine test bed using 300 ppm sulfur containing gasoline for 75 hr along with a production 5/1 platinum/rhodium catalyst at 1.41g/l of precious metal. The total FTP hydrocarbon/CO/NOx conversions efficiencies for the palladium-only catalyst on a 4.6 l vehicle was 95.1%/84.4%/84.1% versus the platinum-rhodium catalyst performance of 89.8%/80.5%/81.9%. The palladium catalyst gave the best hydrocarbon and NOx efficiencies and proved the catalyst formulation strategy of keeping the NOx reduction function separate from the hydrocarbon oxidation components..

The palladium-only catalyst showed sensitivity to the sulfur concentration in the exhaust gas in the low temperature regimes. In seeking to maintain the excellent hydrocarbon activity of palladium, but instill better sulfur tolerance into TWC catalysts, we investigated augmenting the best features of the palladium-only catalyst with platinum and rhodium. A Box-Behnken experimental design was employed with the metal loadings of 0 to 0.47 g/l for platinum, 1.41 to 5.65 g/l for palladium, and 0.09 to 0.37 g/l for rhodium. The catalysts were aged in 10% H_2O/ 90% air at 677 K for four hours. The catalysts were then evaluated on an engine test stand and the results of sweep test evaluations carried out at 673 K under stoichiometric conditions are summarized as contour performance plots for each pollutant in Figure 3. The contour plots show the metals work together synergistically to deal with the pollutants. Palladium makes the greatest contribution to the performance of the trimetal catalysts leading to improved performance for all three pollutants as the palladium content in the catalysts increases. The roles of platinum and rhodium can also be discerned from the contour plots where rhodium contributes to NOx conversion and the platinum, especially at high palladium levels contributes significantly to CO and NOx activity. The trimetal formulations also showed an improvement in sulfur tolerance. Experiments were conducted with a produetion 5/1 platinum/rhodium TWC eatalyst at 1.41 g/l of precious metal versus a trimetal catalyst designated ETM II with a precious metal loading of 3.71 g/l with a platinum/palladium/rhodium ratio of 1/14/1. Both catalysts were aged on a fuel cut aging cycle with an inlet temperature of 1173 K. FTP tests were conducted at various fuel content levels on a 2.0 liter vehicle fitted with multiport injectors. The catalyst volumes used in these experiments were approximately one-half what would be used in serial production to accentuate the impact of sulfur on TWC performance. At 300 ppm fuel sulfur, ETM II outperformed the platinum/rhodium catalyst for all three pollutants giving FTP g/mile emissions for hydrocarbons/CO/NOx of 0.79/3.4/1.05, whereas the platinum/rhodium catalyst gave 0.76/4.5/1.4. Sulfur had little impact on either catalyst for hydrocarbon conversion between sulfur concentrations of 50 - 300 ppm. However, when the sulfur content in the fuel was raised from 50 and 150 ppm both catalysts showed deterioration in CO and NOx conversion efficienecies. The platinum/rhodium catalyst allowing tailpipe CO and NOx emissions to increase from 3.4 to 4.4 g/mile and 1.15 to 1.45 g/mile, respectively. ETM II showed the same trends with CO increasing from 3.1 to 3.4 g/mile and NOx from 0.80 to 1.05 g/mile. Although ETM II proved more resilient to sulfur and the deactivation is reversible by high temperature exposure, continued research is required to develop strategies that mediate sulfur's impact on both the precious metal and oxygen storage components.

SUMMARY

The NOx performance of palladium-only TWC catalysts were substantially improved by bringing oxides of lanthanum, neodymium, and ceria into intimate contact with the palladium in the topcoat of a two coat catalyst formulation. The concepts used to improve the palladium-only catalyst were successfully applied to trimetal formulations which in turn proved to be more sulfur tolerant than corresponding platinum/rhodium catalyst.

REFERENCES
1. Burk, P.L., Hochmuth, J.K., Anderson, D.R., Sung, S., Punke, A., Dahle, U., Tauster, S.J., Tolentino, C.O., Rogalo, J., Miles, G., Mignano, M., and Niejako, M., Catalysis and Automotive Pollution Control III, eds. Frennet, A., Bastin, J.-M., Elsevier Science Publishers, 919 (1995).

2. Taylor, K.C., Automobile Catalytic Converters in Catalysis Catal. Rev., 35(4) 457-481, 1993.

Table 1.
California's Low Emission Vehicle Program Certification Standards

	Federal Test Procedure (grams/mile)[a]		
Low Emission Vehicle Category	Nonmethane Organic Gases	CO	NOx
Transition	0.125	3.4	0.4
Low	0.075	3.4	0.2
Ultra Low	0.040	1.7	0.2
Zero	0.000	0.0	0.0

[a] Emissions after 50,000 miles

Figure 1 (a & b). Laboratory reactor data on aged Pd cores containing 1.75 g/l Pd and 12.2 g/l rare earth oxides

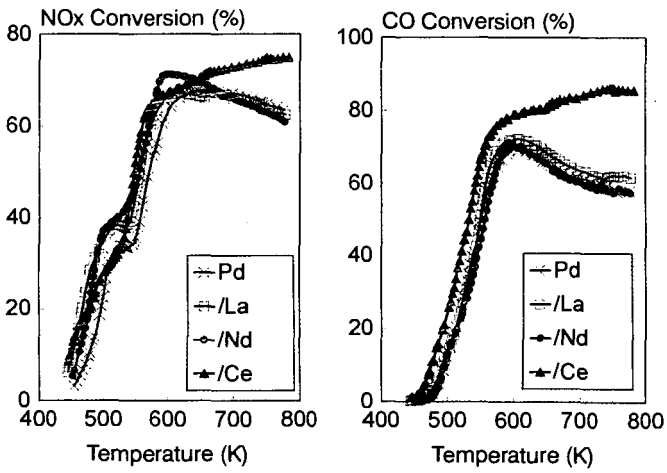

evaluated in a simulated exhaust gas of 0.75% CO, 0.25% H_2, 0.6% O_2, 1600 ppm NO, 280 ppm propene, 16.3% CO_2, 10% H_2O and N_2 balance at 50,000hr^{-1}.

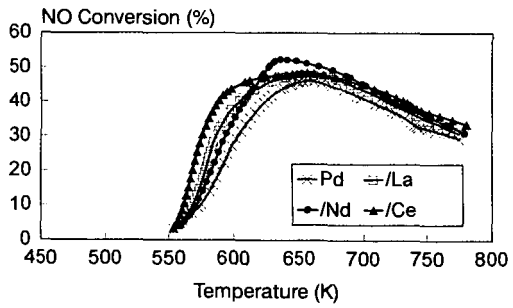

Figure 2. Laboratory reactor data on Pd cores containing 1.75 g/l Pd and 12.2 g/l rare earth oxides after aging in 10%H_2O/90% air and 40 ppm SO_2.

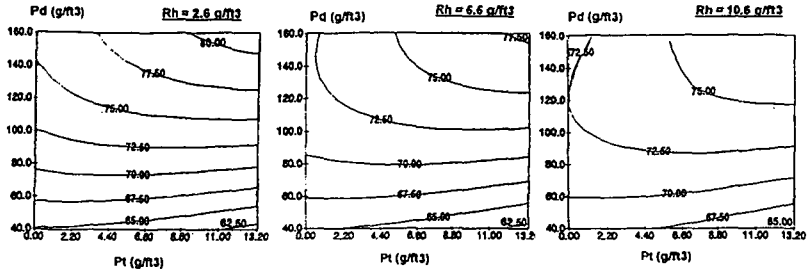

Figure 3(a). Hydrocarbon conversion activities.

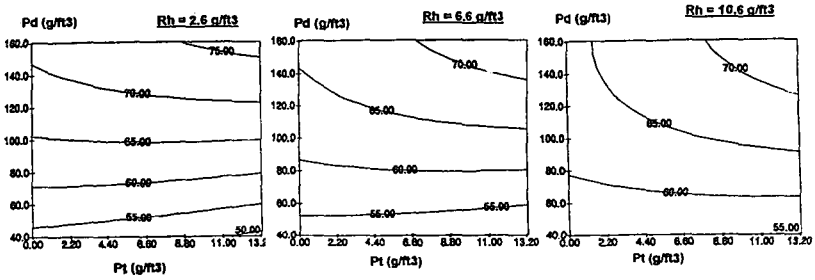

Figure 3(b). CO conversion activities.

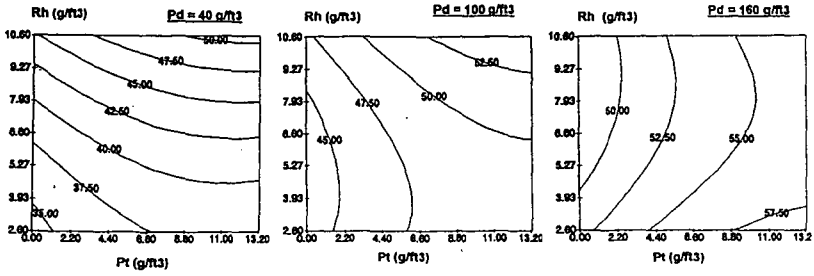

Figure 3(c). NO conversion activities.

THE CLEAN AIR ACT. IMPACT ON THE FUELS INDUSTRY. BACKGROUND . . . AND FUTURE?

James M. Kulakowski
Texaco Refining and Marketing Inc.
10 Universal City Plaza
Universal City, CA 91608

Key words: clean air act, air quality, fuels

The Clean Air Act - Presentation Topics (Slide 1)

Environmental regulations, including the Clean Air Act have a profound impact on the petroleum industry. For example, a recent study by the National Petroleum Council found that compliance with environment, health and safety regulations would cost the US refining and marketing industry some 37 billion dollars in the 1990s. This is greater than the entire 31 billion dollar asset base in 1990.

The federal Clean Air Act is arguably the most comprehensive single piece of legislation ever passed by Congress. The act was originally passed in 1963 and has had several revisions, the most recent being in 1990. The act has provisions that cover many pollutants and different sources of pollution.

This paper will only discuss limited portions of the clean air act that impact "mobile sources", that is fuels and vehicles. In addition to a discussion of the background for several of these issues, the paper provides a report of the current status. Finally, some recommendations are made to improve the flexibility in the act and the regulations it requires.

Setting Air Quality Goals (Slide 2)

The clean air act requires that the EPA set standards for air quality. The "criteria" pollutants include sulfur dioxide (SO_2), particulate matter, nitrogen dioxide (NOx), carbon monoxide (CO), ozone and lead. Areas that meet a standard for a pollutant are in "attainment", while those that do not are in "non-attainment". The clean air act specifies attainment dates for areas based on the level of a pollutant in a base year. For example, an area with ozone between 138 and 160 ppb ozone is classified as "moderate" and must attain the standard by 1996 while an area with greater than 280 ppb ozone is classified as "extreme" and must attain the standard by 2010. These ambient air quality standards also indicate how often an area can exceed the standard and remain in attainment. For example, the fourth 1 hour measurement over the 120 ppb ozone standard in 3 years puts an area in non-attainment. Stated another way, an area may exceed the standard 0.011% of the time and remain in attainment. The EPA has set standards for many pollutants but those that most impact mobile sources are ozone, carbon monoxide and particulate matter. It should be noted that EPA is considering a revision to the ozone standard. One revision being considered would increase the number of ozone non-attainment areas by 60%, from 79 to 119 based on estimates by the American Petroleum Institute.

Tropospheric (low level) ozone, or "summer smog" is a secondary pollutant, that is a pollutant which is formed in the atmosphere as opposed to being directly emitted from a source. The primary reactants are hydrocarbons and oxides of nitrogen, or NOx. Under certain conditions, these reactants, in the presence of sunlight which acts as a catalyst, react to form ozone. The atmospheric chemistry is very complex and is dependent on the ratio of hydrocarbon and NOx. In some areas, reducing one reactant can actually increase ozone. Tropospheric ozone should not be confused with stratospheric ozone, the subject of global warming concerns.

Carbon monoxide (CO) pollution is typically a winter time problem. CO is directly emitted, primarily from gasoline powered vehicles (as opposed to diesels).

Particulate matter is the fine particles suspended in the air. The current standard only covers particles less than 10 microns in diameter (PM10). This would include windblown dust as well as man made particulates. EPA is considering a new standard that would cover smaller particles and would focus more attention on man made particulate emissions.

State Implementation Plans (Slide 3)

States have the primary responsibility for meeting the federal air quality standards. They are required by the Clean Air Act to submit a plan to the EPA detailing how they will meet these standards. This plan is called the State Implementation Plan or SIP. Failure to submit a SIP can result in sanctions against an area in the form of lost federal highway funds. Actual demonstration of attainment is determined by monitoring ambient air quality.

Once a SIP is accepted by EPA, the regulations contained therein are federally enforceable.

Clean Air Act - Specific Control Measures (Slide 4)

The Clean Air Act includes mandated measures for certain areas. For example, the 9 areas with the highest ozone levels are required to include federal reformulated gasoline in their SIPs. Areas in non-attainment for CO are required to implement an oxygenated gasoline program. States with higher levels of ozone or CO are required to implement an enhanced vehicle inspection and maintenance program. The EPA-designed inspection and maintenance program is very specific as to type of test equipment, testing frequency and repair cost limits to earn a waver from the program.

Clean Air Act - Reformulated Gasoline (Slide 5)

The reformulated gasoline (RFG) program is contained in the clean air act. The act specifies several elements of the program, while leaving other key elements to the discretion of EPA. The statutory provisions for the RFG program contain both performance and prescriptive standards. For example, RFG must attain certain emission reductions, which are performance based, for toxic compounds, hydrocarbons and NOx. In addition, RFG is mandated to contain a minimum of 2.0 wt% oxygen and less than 1 volume % benzene. These are prescriptive standards that must be met irrespective of the emissions performance of the fuel.

As was noted earlier the 9 worst ozone areas are mandated to have RFG. The act also provides the opportunity for other non-attainment areas to "opt-in" to the program. Several areas did this, and subsequently desired to opt-out of the program. EPA allowed these "opt-outs", changing the overall volume of RFG demand. This change in RFG volume had the potential to drastically reduce the value of investments made for RFG compliance.

The enforcement program for RFG is very complex. In essence, it requires tracking of every molecule of gasoline from cradle to grave. Some of the elements include independent sampling and testing, year-end audits of production, and periodic reporting. Several of these provisions also apply to non-reformulated, or conventional, gasoline.

The RFG program includes two phases. The first phase, which was effective in 1995, includes statutorily developed targets for toxic and hydrocarbon emission reductions as well as a requirement that there be no increase in NOx emissions. In the second phase, EPA was given discretion over the level of the more stringent standards required by the act. EPA included a requirement for NOx reduction not originally conceived of in the act, in addition to further reductions in hydrocarbon and toxic emissions. This second phase is effective in 2000.

Clean Air Act - Regional Air Quality Organizations (Slide 6)

The Clean Air Act provides for several regional air quality organizations. This was done in recognition that some pollutants may be transported from one air basin to another and impact

air quality in these "downwind" areas. An example is the Ozone Transport Assessment Group which consists of representatives of the 37 states east of the Rocky Mountains. These states are evaluating a host of measures that could assist downwind ozone non-attainment areas to reach the standard. The analysis of transported pollutants and their impact on ozone is exceedingly complex and is only now beginning.

These organizations face an implicit political problem. Namely, it will be difficult for an elected official to pass a regulation which will cost his constituents when the benefits will be realized by others, perhaps in another state.

What's Going On Now? (Slide 7)

Several initiatives are underway which could further impact the fuel and automotive industries.

As mentioned above, the OTAG is looking at options, some of which include further fuel reformulation to address the issues related to pollutants transported from attainment to non-attainment areas.

EPA is considering revisions to the air quality standards for ozone and particulate matter. These standards are expected to be more stringent than the current standard and will put pressure on states to find more emission reductions.

EPA is considering revisions to allow attainment areas to opt-in to federal RFG. This could drastically increase the volume of RFG requirements. There are significant legal questions regarding whether the Clean Air Act grants EPA the authority to allow attainment area opt-ins.

California has included in its ozone SIP a measure that calls on EPA to adopt more stringent emissions standards nationwide for diesel trucks. This is driven by the fact that a significant portion of the Los Angeles NOx emissions inventory is sourced in out-of-state trucks visiting the area. EPA is working with California regulators and the engine manufacturers to determine whether these standards are attainable. At this point, it appears that changes to diesel fuel will not be immediately considered as a part of this strategy.

Finally, the auto makers are calling for a "nationwide fuel" that would have tighter specifications than those of the American Society for Testing Materials (ASTM) whose specifications are enforced by most states. The environmental necessity of such a fuel is questionable, as many areas of the country in which the fuel would be sold already attain federal air quality standards. Such a requirement would provide a fuel with less variability and assist the auto makers in the design of their vehicles, but would also represent a costly reformulation of gasoline for most refiners.

None of these initiatives were considered in the 37 billion dollar investment cited earlier. Needless to say, there will be continued pressure on the petroleum industry to deliver cleaner products to market.

What Needs to Happen? (Slide 8)

There are several areas where the Clean Air Act and the regulations it spawns can be improved. The items detailed below are but a few ideas.

Use of performance based standards will allow greater compliance flexibility and result in lower compliance cost. However, recent regulations that are advertised as performance based, are overlaid with elements of the command and control regulatory mind set. For example, if a party were to develop an additive that was demonstrated to reduce vehicle emissions to the same level as RFG, that party would have several regulatory hurdles to clear to certify that additive as a part of the RFG program. Hopefully, as more experience is gained in implementing performance based regulations, this will change.

The practice of air quality management needs better tools with which to do the job. An example is the Urban Airshed Model for predicting ozone. These models are tremendously complex, needing super computers to run efficiently. However, even with this complexity, their predictive capabilities are only marginal. Another area which needs improvement is the type of test used to characterize vehicle emissions. There are recognized shortfalls in the "federal test procedure". For example, it does not adequately test all driving modes (e. g. high acceleration) and is capped at 55 miles per hour. Finally, there needs to be testing of reformulated fuels on prototype advanced vehicles. Questions regarding the need for, and performance of these fuels of the future in the vehicles of the future have not been addressed.

There needs to be a consideration of risk-based air quality standards. Can our society afford to guarantee pristine air in all air basins regardless of the levels of population and economic activity? Risk-based, rather than health-based air quality standards will allow EPA to consider these types of questions.

Finally, there needs to be an explicit requirement that major regulations be subjected to some type of cost effectiveness test. To their credit, EPA generally has attempted to apply this type of analysis to fuels regulations. The California Clean Air Act contains such an explicit requirement. This has impacted the decisions of California regulators. It is time for all parties to recognize the need for air quality regulations to provide the necessary emissions reductions at the lowest possible cost.

The Clean Air Act.
Impact on the Fuels Industry.
Background . . . and Future?

Mike Kulakowski
Texaco Refining and Marketing
ACS Meeting - Orlando Florida
August 1996

Clean Air Act Presentation Topics

- **The Clean Air Act:**
  - Sets air quality goals
  - Outlines process by which states develop clean air programs
  - Outlines specific measures
    - Reformulated gasoline
    - Vehicle inspection and maintenance
  - Establishes regional air quality organizations

Air Quality Goals

- **Health-based standards set by EPA**
  - Ozone (formed by hydrocarbons and NOx)
  - Carbon monoxide
  - Particulate matter
- **Attainment deadlines set by initial air quality levels**
  - Higher levels of pollutant results in more time to attain standard
  - Example: Moderate ozone 1996. Extreme ozone 2010

State Implementation Plans (SIPs)

- **SIP details how an area will meet federal air quality standards**
  - Quantifiable
  - Enforceable
- **Regulations in SIP are federally enforceable**
- **Very specific guidance to states by EPA**
- **State maintains autonomy**

Clean Air Act. Specific Control Measures

- **Reformulated Gasoline (RFG)**
  - 9 mandatory areas specified in Act
  - Opt-in of ozone non-attainment areas allowed
- **Oxygenated Gasoline**
  - Winter carbon monoxide strategy
- **Vehicle inspection and maintenance**
  - Goal - On road vehicles' emission performance maintained at or near design levels

Clean Air Act Reformulated Gasoline

- **Performance standards**
  - Hydrocarbon/NOx/Toxic emissions
- **Prescriptive standards**
  - Oxygen/benzene fuel content
- **2 Phases to program**
  - Phase I - 1995
  - Phase II - 2000
- **"Anti-dumping" controls**
- **Very complex enforcement scheme**

Clean Air Act - Regional Air Quality Organizations

- **Examples**
  - Ozone Transport Commission (OTC)
  - Ozone Transport Assessment Group (OTAG)
  - Grand Canyon Visibility Task Force
- **Recognition of transported pollutants and precursors**
- **Allow for coordinated planning**
- **Political Issues**

What's Going on Now?

- **OTAG - Region-wide fuel standards?**
- **EPA reassessment of ozone and particulate matter standards**
- **EPA - Attainment area opt-in to RFG?**
- **EPA - Nationwide diesel engine standards?**
  - Driven by Los Angeles' ozone non-attainment
- **Automakers - desire for nationwide fuel specifications.**

Clean Air Act What Needs to Happen?

- **Better performance-based regulations**
  - More flexibility
  - Lower cost
  - Opportunities for new technologies
- **Better tools**
  - Air quality models
- **Risk-based air quality standards**
- **Explicit requirements for cost benefit tests for new regulations**

IMPACT OF FUEL CHARACTERISTICS ON IN-USE PERFORMANCE OF EXHAUST CATALYSTS

Donald. D. Beck
GM Research and Development Center
Warren, MI, 48090

William A. Short
GM Powertrain Group
Milford, MI, 48380

Keywords: in-use emissions, fuel impact, catalyst performance

ABSTRACT

In order to improve air quality, California has implemented a plan requiring low emission vehicles with advanced technology exhaust catalyst systems. These vehicles are certified and intended to operate on an advanced reformulated gasoline (California Phase 2). Other states have or intend to adopt a similar vehicle program, but although these vehicles will also be certified and designed for operation on the California Phase 2 gasoline, they will in practice be operated on a variety of gasolines, both reformulated and unreformulated. In some regions, enhanced inspection/maintenance tests will periodically be required which includes a test of the exhaust emission control system using a transient driving schedule. These tests will be performed using available commercial fuels, thus we have undertaken a study to determine the impact of several individual fuel properties on the resulting emissions produced during such a test. Properties varied individually include distillation, oxygenate content and sulfur level. In addition, the impact of each variable was measured at several different test temperatures to gain insight on the effect of ambient temperature on in-use emissions. We will discuss the result of these impacts and possible explanations based on additional insight gained from modal (second-by-second) emissions data as well as catalyst temperatures logged during the tests.

INTRODUCTION

One of the requirements for improving air quality called for by the Clean Air Act Amendments of 1990 involves the improvement of current programs in which vehicles are inspected in-use for emissions compliance. The enhancement as proposed by the Environmental Protection Agency for many non-attainment and neighboring areas requires vehicle owners to pass an emissions test at either a centralized inspection station or a qualified repair-and-test facility station in order to obtain a permit to register their vehicle [1]. In addition to the emissions test, the fuel vapor recovery system on the vehicle must also be checked for system integrity, and the OBD-II system checked for an activated MIL and stored fault codes.

One of the enhanced inspection/maintenance tests supported by the EPA involves an exhaust emissions compliance test in which tailpipe emissions of hydrocarbon, carbon monoxide and oxides of nitrogen are measured while the vehicle is driven over a transient schedule for 239 seconds [1-3]. This test, called the IM240 (inspection/maintenance 240) requires a relatively sophisticated chassis dynamometer and emissions measurement bench and is best administered at a centralized facility. It is already being utilized in enhanced I/M programs in Arizona and Colorado, and is being implemented in states such as Wisconsin, Maryland and Connecticut. Although alternative I/M tests may be adopted by other states, we will use the IM240 as the focus of this study.

As stated earlier, we are particularly interested in varying some fuel characteristics and the ambient test temperature to determine the impact on the resulting emissions. Such tests serve to probe the variety of test conditions that can be anticipated for I/M tests performed in the 49 states outside California, and allow us to compare such tests to those that would more closely represent conditions anticipated within California, recognizing that California has adopted a strictly controlled low-sulfur reformulated fuel to be sold state-wide [4]. This may be particularly important for Low Emission Vehicles which may be held to strict emission standards, even in in-use tests. Although these vehicles were originally proposed by California as part of their state plan to achieve better air quality, member states of the Ozone Transport Region (13 Northeast states and the District of Columbia) have or are in the process of considering adoption of the California Low Emission Vehicle program to meet their state implementation plan (SIP) requirements, without also adopting the California Reformulated Fuel Program.

For this study, then, we compare IM240 tests performed using a pre-production Transitional Low Emission Vehicle under relatively moderate temperatures using low-sulfur-content California reformulated phase 2 fuel to similar tests performed under a range of

temperatures and using federal fuel surrogates with various distillation, oxygenate and sulfur content properties.

EXPERIMENTAL

The vehicle used for the enhanced inspection maintenance testing was a 2.2 L OHV Corsica equipped with a 4-speed automatic transmission and linear EGR. The vehicle was configured as a production-intent 1996 MY California TLEV and included a complete OBD-II system. The inlet of the single underfloor converter used with this vehicle is located approximately 50" from the exhaust manifold, and the converter itself is 110 cubic inches in volume, containing 2 oval cross section monoliths of the same size. The forward monolith contained a palladium technology washcoat, while the rear contained platinum and rhodium. A single converter was used for these tests and had accumulated 89,000 miles in customer service. This converter was evaluated for FTP performance using certification fuel on this vehicle with the following results: 0.089 g/mi THC, 2.28 g/mi CO and 0.32 g/mi NOx (all values comply with TLEV standards).

The vehicle was also configured with a converter inlet tap for modal engine-out emissions measurements. In addition, several locations in the exhaust stream and in the converter monolith beds were instrumented with thermocouples for monitoring the temperature at those locations. A portable laptop computer equipped with a serial port and an analog/digital conversion board was used to log selected engine operation and temperature data in real time during the IM240 test schedule.

The reference fuel used for this study conformed to the California Phase II reformulated gasoline standards, and contained sulfur at a level of 32 ppm. A relatively high vapor pressure fuel used as Wintertime surrogate contained sulfur at a higher level (485 ppm) and was used both with and without oxygenate modifications. A lower vapor pressure fuel used as a Summertime surrogate also contained sulfur at a higher level (480 ppm) and was also used with and without oxygenate modifications. MTBE was used in any oxygenate modifications. A summary of the fuel properties is listed in Table 1.

IM240 tests described in this study were conducted using a single 48" dynamometer roller which was electrically-loaded. This test site was capable of collecting both bag (integrated) and modal (second-by-second) emissions data, and is located in an environmental cell capable of test temperatures between -9°C and 36°C. Testing at low temperature with the high volatility Winter fuel simulates an IM240 test that would be encountered in much of the U.S. (outside of California) in the Wintertime. In practice the IM240 test may be run in a heated/closed bay; however, the vehicle will be exposed to cold temperatures during the urban driving phase and time at idle, and may also encounter these conditions during the exhaust test itself. Since the climate in the highly populated areas of California is moderate for the entire year, testing at ambient temperature with the strictly controlled California reformulated fuel simulates a California IM240 test for a majority of the state and for most of the year. Whenever fuels were changed in these tests, a purge procedure was followed to allow the vehicle sufficient exposure to the new fuel prior to conducting tests.

The IM240 emission tests were conducted using a procedure described in a previous publication [5] and was used to simulate typical customer driving history prior to an I/M test and to obtain highly repeatable results. This procedure generally included a soak period followed by an urban driving phase (bag II of the FTP), followed by an idle for 15 minutes, and finally the IM240 test (the 15 min waiting period for an IM test is considered to be representative of a typical wait time in the field [6]). For the purpose of this discussion we will focus on the modal emissions data generated during the IM240 portion of this study. Following the IM240 test, the vehicle was left to soak at the test temperature for at least 1 h with the fan directed into the radiator, and the entire test procedure (FTP Bag 2 + idle + IM240) could then be repeated. This entire procedure was repeated to produce two complete IM240 measurements for each fuel and time at idle matrix element.

RESULTS AND DISCUSSION

The first set of IM240 tests were run using the California Phase 2 reformulated fuel at 74°F (23°C). We found that the engine-out FTP emissions of 1.7 g/mi HC, 8.9 g/mi CO and 1.9 g/mi NOx were relatively consistent with the engine-out IM240 emissions of 1.3 g/mi HC, 9.2 g/mi CO and 2.7 g/mi NOx. The relative agreement in the engine-out emissions values provides further support for the IM240 test procedure as a relatively rapid surrogate for the FTP test. The tailpipe emissions performance on the IM240 was the following: 0.119 g/mi THC, 1.633 g/mi CO and 0.384 g/mi NOx, which also compare favorably with the FTP results at 0.089 g/mi THC, 2.28 g/mi CO and 0.32 g/mi NOx. In this case, the IM240 results were 34% greater for THC, 40% greater for CO and 20% greater for NOx when compared to an FTP test result. As will become apparent later, the IM240 results were consistently larger than the corresponding value obtained during an FTP test.

Our discussion will now turn to IM240 test conditions that can be commonly expected when Wintertime oxygenated fuel is available, typically November to March. In this study we ran IM240 tests at 20°F (-7°C), 40°F (4°C) and 60°F (16°C) to cover a wide range of ambient temperatures that can be expected for most of the country during the Winter. Although the numerical results are not reported here, the engine-out emissions obtained for these tests at the three temperatures mentioned above generally remained the same for all test temperatures and was similar to the results obtained using the California reformulated fuel, with the exception of NOx, which increased by roughly 45% as the temperature was decreased to -7°C from 16°C. The tailpipe emissions, however, are clearly impacted by both fuel property and test temperature. For example, test results obtained using the federal fuel at 16°C are between 40 and 100% greater (88% for HC, 85% for CO and 45% for NOx) when compared to test results using the California fuel at 20°C. Tailpipe emissions continue to increase dramatically with further decreases in test temperature, even with the same federal fuel being used for the tests. At -7°C, the tailpipe emissions levels are between 200% and 300% greater than the results obtained using California fuel at a test temperature of 20°C (specifically, 275% for HC, 275% for CO and 230% for NOx). Although the observed increase in the tailpipe emissions for NOx can be partly attributable to an increase in engine-out NOx levels under colder test conditions, most of the observed increase in HC, CO and NOx tailpipe emissions can be attributable to differences in the fuel properties and test conditions. As will be suggested by the following results, fuel oxygenate can influence tailpipe emissions, but not at all temperatures. At the lowest temperature used in this study (-7°C), tailpipe emissions are affected more by sulfur content and distillation.

A similar set of IM240 tests were also performed at 20°F (-7°C), 40°F (4°C) and 60°F (16°C) using the same fuel base, but with no oxygenate present. Tests using this fuel also resulted in increased tailpipe emissions when compared to tests using the California Phase 2 Reformulated fuel, and the increases were generally similar when compared with the oxygenated Wintertime fuel, except that CO was affected more and NOx was affected less with the non-oxygenated fuel at test temperatures above -7°C. Tests using this fuel at 16°C, for example, produced 0.205 g/mi HC, 4.38 g/mi CO and 0.401 g/mi NOx. This represents increases of 88% for HC, 150% for CO and ~0% for NOx when compared to the California fuel. Further decreases in test temperature to -7°C did result in further increases in tailpipe emissions, reaching 0.392 g/mi HC, 6.55 g/mi CO and 1.37 g/mi NOx, which represents increases of 260% for HC, 273% for CO and 230% for NOx. At moderate test temperatures of 16°C and 4°C, then, the addition of oxygenate to the fuel does reduce CO emissions as demonstrated in prior published studies. At -7°C, however, the presence of oxygenate in the fuel has no influence on the tailpipe emissions. A summary of the tailpipe results for both types of higher vapor pressure fuels are shown in Figure 1.

The observed IM240 tailpipe emission increases attributable to fuel and test condition effects are in good agreement with our previously reported study [5] of IM240 tests in which a similar test comparison was made between tests using commercial Winter fuel and California Phase 2 fuel using a similar TLEV. These results are in contrast to the typically cited 10-20% in-use emissions increases predicted by MOBIL5a to account for differences in the fuel properties, the latter forming the basis for the most stringent IM240 cutpoint tables. As mentioned above, although the increase in the tailpipe emissions for NOx can be partly attributable to an increase in engine-out NOx levels under colder test conditions, most of the observed increase in HC, CO and NOx tailpipe emissions can be attributable to factors which directly influence catalytic converter performance. It turns out that such factors are not related to converter temperature, since this was found to be similar regardless of the test fuel or test temperature, but rather to a combination of the influence of sulfur, operating air/fuel ratio, and HC composition and combustion characteristics of the fuel on converter efficiency as suggested by the modal data. A thorough discussion of these impacts is beyond the scope of this paper, but will be discussed more completely in a future paper.

Similar tests were conducted using a lower vapor pressure fuel to represent a summertime blend, but with an elevated sulfur (475 ppm) level. Tests were conducted both with and without oxygenate (~11% MTBE), and at test temperatures of 20°C, 16°C, and 4°C (the fuel drivability was poor at -7°C, thus tests were not run at that temperature). We found that in general, use of this fuel did not affect engine-out emissions when compared to the California Reformulated fuel (except that NOx was increased by 20% at 4°C, similar to the Wintertime fuel), but increases in the tailpipe emissions were observed. These increases, however, were not as significant as with the Wintertime fuel for the same test temperature. For example, tests at 16°C resulted in increases of ~30% for HC, 55% for CO, and 25% for NOx when compared to similar tests at 20° using the California fuel. Further decreases in test temperature did result in further increases in tailpipe emissions, but these increases

were not as significant as with the Wintertime fuel. When a similar set of tests were run with the oxygenated version of this fuel, a similar trend was observed in that the tailpipe emissions increased with decreasing test temperature. However, the magnitude of the increase was smaller than observed for the non-oxygenated version of this fuel for a given test temperature. In summary, then, of the four federal fuel surrogates used in these tests, the highest tailpipe emissions were generally observed for vehicle operation at relatively low temperature (-7°C) using the high vapor pressure (or Wintertime) fuel blend with oxygenate present. The lowest tailpipe emissions were observed for vehicle operation at relatively moderate (~20°C) temperature using a lower vapor pressure fuel (Summertime) with oxygenate present. For comparison, the California phase 2 reformulated fuel produced even lower tailpipe emissions when tested under a moderate temperature condition. As we have mentioned previously, modal data indicates that the large observed difference in the tailpipe emissions (particularly hydrocarbon) when comparing low vapor pressure fuel tested at moderate temperature with high vapor pressure fuel tested at relatively low temperature can be attributed primarily to effects of the operating air/fuel ratio and the fuel hydrocarbon composition and combustion characteristics on converter efficiency. Colder test conditions lead to poorer air/fuel control, while higher vapor pressure fuels contain a larger relative percentage of relatively unreactive short-chained saturated hydrocarbons, part of which escapes combustion in the engine and/or oxidation in the catalyst. The presence of higher sulfur levels appears to accentuate these effects.

SUMMARY

We have investigated the effects of several fuel properties and test temperatures on the IM240 tailpipe emissions performance of a 1996 Corsica TLEV. We found that in all cases, the lowest emissions were obtained using a California phase 2 reformulated gasoline in tests at 20°C, while tests using federal fuel surrogates all produced higher tailpipe emissions, and the highest emissions were produced when high vapor pressure fuels were used under relatively cold temperatures (-7°C). In the latter case, the tailpipe emissions were between 200% and 300% greater than similar tests run using the California fuel at 20°C. The large increase in the emissions observed when tests were run on the federal fuels can be attributable to a combination of higher sulfur levels, lower test temperature, and different fuel hydrocarbon makeup (indicated by high vs. low vapor pressure).

REFERENCES

1. "Inspection/Maintenance Program Requirements", Federal Register Notice, November 5, 1992; 40 CFR, Part 51, Subpart S.

2. "High-Tech I/M Test Procedures, Emission Standards, Quality Control Requirements, and Equipment Specifications: Final Technical Guidance", U.S.E.P.A. Document No. EPA-AA-EPSD-IM-93-1, April, 1994.

3. W. M. Pidgeon and N. Dobie, "The IM240 Transient I/M Dynamometer Driving Schedule and the Composite I/M Test Procedure", U.S.E.P.A. Report No. EPA-AA-TSS-91-1, January, 1991.

4. Title 13, California Code of Regulations, Sections 2262.1-2262.7.

5. D. D. Beck, W. A. Short, T. A. Angelos and R. R. Dils, "IM240 Emissions tests with a 2.2 L Corsica TLEV", SAE Paper No. 942001, 1994.

6. R. Babcock, presentation at the Tenth Annual Clean Air Act Conference, Estes Park, Colorado, September 27-29, 1994.

Table 1.
Summary of Selected Properties of Test Fuels

Fuel Description	Vapor Pressure (psi)	Oxygenate (% vol.MTBE)	Sulfur (ppm)	Saturates/Olefins/Aromatics (%)
California Phase 2 federal fuel	6.6	11.1	29	73 / 5 / 22
(high vapor pressure) federal fuel	11.8	*	480	71 / 7 / 22
(low vapor pressure)	7.9	*	475	74 / 4 / 22

* Each of these fuels were used with no MTBE added and with 11.5% vol. MTBE added.

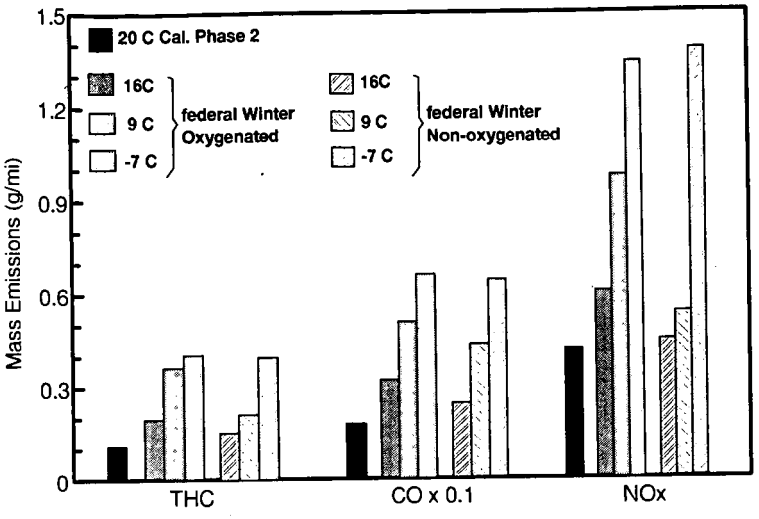

Figure 1. Comparison of IM240 tailpipe emissions at various test temperatures and for operation on different fuels.

FUEL REFORMULATION AND EMISSIONS IN EUROPE AND JAPAN

H.J.Lovink
Catalyst Consultant
Aletta Jacobslaan 17
3818 LP Amersfoort
The Netherlands

Keywords: Diesel,Gasoline,Emissions Improvements,Europe,Japan.

A. Introduction

In the drive for a cleaner environment of the transportation sector not only the vehicles,but also the fuels are studied for further improvements. Europe and Japan are no exceptions,although in motorgasolines the US is clearly leading.
While diesel is only 17% of US motor fuels,it is more important in Europe,Japan and the rest of the world with some 45%-plus,and so is its reformulation.

Recently an extensive European Oil/Auto test program,called EPEFE has been completed in order to decide on new "Europe-wide"specs. for both diesel and motorgasolines.
Later this year the European Commission and Parliament will decide on the specifics,the time schedule etc. after having heard all parties concerned.

Much earlier work and study has preceded this;but in the final judgement both any extra CO_2 and costeffectiveness will be considered,plus special local problems (big cities:Milan,Athens,etc.)

CONCAWE, the "Oil Companies' European Organization for Environment,Health and Safety",
established in 1963,has played as important role in this and earlier test programmes as well as ACEA (Auto Co's) and national institutes active in the collective interest.

The Japanese situation,on-the-ground at least as difficult as southern Europe/California,is different:
- --Tight regulations on emissions,
- --A severe testing schedule,and young vehicle population,
- --Good fuels,see later.

Their extensive statistics,reporting "road-side SOx and -NOx" demonstrate the results of their efforts.As in Holland and Germany SOx and HC are coming down, but NOx stays high. Because yes,we all are driving more and more using ever more motor fuels!

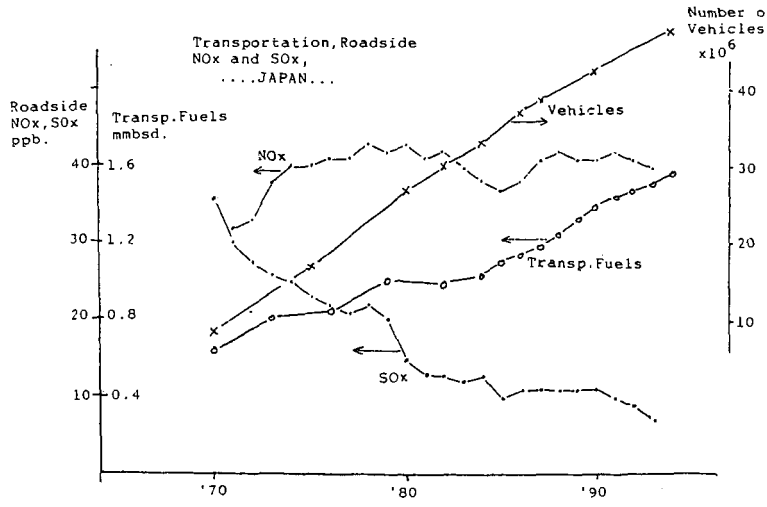

fig.1

B . Diesel Fuel Studies in Europe

During the last decade the improvement of diesel engines and fuel has been high on the agendas of both manufacturers and refiners. Like in gasoline, most progress has been made in engine design, and most recently, with catalytic soot filters.

In the recent past CONCAWE had already shown that:

a) The Cetane Number is the most important parameter for most emissions; much more than Density, Aromatics, and T90. The latter have varying effects of some 5% at best within the limits of commercial interest.
b) Catalytic filters are able to reduce CO/HC/PM by some 20-25%, moreover all fuel effects become smaller, see lit.2&3.

The European Programme on Emissions, Fuels and Engine Technology, EPEFE, described above, had selected for experiments those areas that had not been covered sufficiently earlier or elsewhere in the US and Japan.
An outstanding feature of their recent series is the use of engines with "year 2000"-technology, so not today's engines.
This choice shows clearly in the level of emissions, Table 1, in particular the low HC/CO/PM -values. They could even be comparable to California TLEV 's.

However, in these vehicles the effects of variations in diesel-properties , even over a wide range are limited, see table no 1.
When comparing the results in Light Duty and Heavy Duty vehicles table 2, the plusses and minusses do not even match always, so a "Solomon's Judgement" is needed!

Table 3 gives the principle characteristics of the average diesel fuels of the US, Japan and Europe, plus some of the "talked about" changes in specs, which now have entered the environmental-economic-political arena in Brussels.
The costs of diesel reformulation has been calculated for several scenarios by CONCAWE, lit.5; table 6 has been derived from a still "modest" scenario. A cetane spec. change to 58 min indeed looks unlikely seen the costs of widespread deep aromatics hydrogenation and the extra energy-to-CO_2!

C. Motorgasolines Studies, Europe

With all the work done in this particular area in the US and the results of actions in California, the EPEFE program has only tried to fill in some blank spaces because of the different car population, and the speedier driving habits: the European tests are now containing a 120 km/hr. section.
Here also cars with "yr-2000" engines have been used, which shows up in their low av. emissions. One car has such a good, flexible air:fuel ratio controler that its NOx is 0.07 g/km for all fuels. Its other emissions were also so low that no fuel quality effects could be detected! Table 4 has the results of this section of the recent European tests. Earlier US conclusions regarding Sulphur were confirmed; all other parameters gave "plusses & minusses"

Although the general feeling is strongly in favor of "one percent Benzene max, these and other health risk studies suggest this is not necessary now and in the nearby future.

Table 5 compares the average values of motor gasoline inspections of the US, Japan and Europe. (only some essential items)
The octanes are slightly higher in Europe, even of the lead-free grades. All new cars are designed for RON/MON=95/85.
Re-setting the specs to the values "talked about" will have enormous consequences for the refining industry.
A "reg-neg" process, as in the US, leading to Simple and Complex models is not feasible in Europe. A gradual introduction of new specifications, allowing the industry time to invest, both the auto makers and the refining side, is most likely.

Table 6 summarizes the costs of the above depicted targets of reformulation of both gasoline and diesel fuel: virtually every refinery will need new equipment, particularly hydrocrackers and hydrotreating/hydrogenation units. (from lit.5)

In Japan a further study as a result of the "1995 White Paper on the Environment" is expected to lead shortly to new legislation. However, an increasing part of acid rain seems to come from the rapidly developing neighboring countries!

D. Concluding Remarks

--Reformulation of motorfuels in Europe is now under general scrutiny; tighter specs on both diesel and gasoline are expected, rather than "complex or simple models".

--Major improvements can only be expected from new engine-and exhaust treatment technology; first indicationsare that also here some 10% reduction of emissions can be obtained from so-called cleaner fuels.

--NOx from diesel engines could be the remaining problem; a catalytic solution is highly desirable! (See lit.6)

Literature:

1--Petroleum Industry in Japan,1995, by "The Japanese Committee for World Petroleum Congresses"(fax +81-3-5395-5384)

2--Concawe Report no.92/54

3-- " " no.94/55&56

4--EPEFE report,Diesel Project, WEFA conf.'95 .M.Hublin

5--Concawe Report no.95/54

6--Motor Vehicle Pollution, Reduction Strategies beyond 2010. OECD-publication 1995. Paris.

TABLE 1
Diesel Reformulation Test results
European -EPEFE test program with
"Yr.-2000 engines and catalysts"

		grams per km.			
A Light Duty Vehicles		CO	HC	NOx	PM
-- Emissions level of testvehicles		0.45	0.10	0.55	0.06
-- Vehicle Euro-specs. '95/'96		2.1	0.25	0.62	0.12
California TLEV		2.1	0.15	0.3	0.08
-- Major Improvements by Reformulations	%	25[3]	25[3]	3.4[2]	19[1]
B Heavy Duty Vehicles		grams per KWh			
-- Test vehicle level		0.59	6.3	3.6	3.6
-- Euro-specs.		4.0	1.1	7.0	0.15
-- Calif.'94 level		11.0	1.0	6.7	0.11
-- Major Improvements by Reformulation	%	10[3]	6.3[3]	3.6[1]	3.6[2]

C. Fuels Programme:

1)Density decrease: 0.855 to 0.828
2) Poly Aromatics%: from 8 to 1%
3)Cetane Number : " 50 to 58
4) T-95,degrees C : " 370 to 325

TABLE 2
Comparison of effects of fuel properties
..Light and Heavy Duty Vehicles...

		CO	HC	NOx	PM
DENSITY	LD*	-17.1%	-18.9%	+1.4%	-19.4%
855-828 kg/m3	HD**	+5.0%	+14.3%	-3.6%	-1.6%**
poly-aromatics	LD*	+4.0%	+5.5%	-3.4%	-5.2%
8-1%	HD**	-0.1%***	-4.0%	-1.7%	-3.6%
cetane number	LD*	-25.3%	-26.3%	-0.2%***	+5.2%
50-58	HD**	-10.3%	-6.3%	-0.6%	-0.1%***
T95	LD*	-1.8%***	+3.4%***	+4.6%	-6.9%
370-325 deg C	HD**	+6.6%	+13.4%	-1.7%	0.0%***

- * ECE+EUDC cycle
- ** ECE R49 13-mode cycle
- *** Statistically non significant

TABLE 3

Average Properties of Diesel Fuels
(excl. color,cold flow,stab.etc.)

	US	JAPAN	EUROPE	Changes "Talked-about"
Density,g/ml	0.848	0.838	0.840	"down"
Aromatics %	30	23	25	25 max.
Poly- Arom.%	-	-	4-6	?
Cetanes:				
-number	46	55	51	55 min.
-index	47	57	53	-
Sulphur ppm	----------500 max---------			"down"?
T20 C	240	240	215	-
T50 C	270	260	265	-
T95 C	315	345	360	?

TABLE 4

Motor Gasoline Reformulation Europe,
Results of the recent EPEFE test programme

	CO	HC	NOx
	---------grams/km -------		
Test Vehicles used, "Yr. 2000 technology"	1.41	0.16	0.18 a)
Euro/EFTA-specs.	2.0	0.25	0.12
California TLEV	2.1	0.16	0.62
Japan '94	2.1	0.15	0.24

Maximum Improvements:

1) S from 400 to 20 ppm : all emissions down 10%!
2) Aromatics from 50% to 20% : CO/HC down 10%: NOx up 10%.
3) E100 °C 60% to 40% : no effect.
4) T90 °C 185 to 165 : CO/HC down 5%: NOx,see 2);no change.
5) Benzene 2.5%-0.95% : down from 5% to 3,5% in HC emitted.

a) One vehicle,with a new very good A-F ratio controler tested 0.07 g NOx per km!

TABLE 5

Typical Properties -Motor Gasolines '94
.....Averages,Summer.....

	US Baseline '90	US RFG-II	JAPAN	EUROPE
RVP. psi	7.8	6.7	8	7-9
Sulphur,ppm	338	140	40	300
Oxygen %	-	2.1	0.5	0.6
Aromatics %	28.6	25	30	35
Olefins %	10.8	12	16	12
Benzene %	1.6	0.95	2.5	2.1
RON/MON	-----95/84-----		94/84	96.5/86
T50 °F	207	200	204	200
T90 °F	332	313	300	320
E200°F,vol %	46	49	51	45
E300°F,vol %	83	87	91	84

"Europe" may reduce in) stages the following) items:

Sulphur to 100 ppm max.
Aromatics to 25 % max.
Olefins to 10 % max.
Benzene to 1 % max.
Oxygen to 1.5% min.

TABLE 6

Economic Impact of Reformulation
of Gasoline and Diesel-- Europe.
(Concawe Report no.95/54,yr.2000)

A) Diesel - quality,appr.table 3;200 ppm S; 100×10^6 tons/yr.

	Capital charge	All other op.costs	Total	Extra CO_2 from Refining, kg/ ton
	----------$/mTon--------			
Cetane No. =55	15	5.5	20.5	50
Cetane No. =58	20	19	39	350

Compare with the late '95 prices of av. diesel fuel:
..in bulk ,tax free: $/ton 170
..at the pump,
incl. all taxes : " 700-1200

B) Motor Gasoline -quality table 5; quantity 125×10^6 tons/yr.

Capital Charge,excl.for MTBE: $/ton.. 16
Other fixed & variables " .. 6
" 22+

Compare with:..'95 market price, excl. taxes: $/ton 200
"At-the pump" incl. taxes...: " 1200-1500!

AQIRP AND EPEFE - A COMPARISON OF THE PROGRAMS AND THEIR RESULTS

Brian H. Rippon
Ford Motor Company
The American Road, Room 255 WHQ
Dearborn, Michigan 48121-1899

Keywords: Gasoline, Emissions, AQIRP, EPEFE

ABSTRACT

Since it was established in 1989 by 14 oil companies and three domestic automakers, the U.S. Auto/Oil Air Quality Improvement Research Program (AQIRP) has made substantial progress in developing an information base of fuel and vehicle effects on emissions. This program was the largest and most comprehensive project of this nature ever attempted. More recently, the European Programme on Emissions, Fuels, and Engine Technologies (EPEFE) marked an unprecedented cooperation between the European motor and oil industries to extend the information on fuels and engine technologies for the European continent. AQIRP and EPEFE were the first large scale systematic efforts to develop extensive data on the inter-relationships among fuel composition, vehicles, emissions, and air quality. This scientifically based information will allow legislators and regulators to design cost effective methods with which to achieve their clean air goals.

INTRODUCTION

Motor vehicles have historically been viewed as one of the main sources of ozone and carbon monoxide pollution in the United States. But over the past three decades, the contribution of the automobile to urban pollution has been steadily decreasing. Nationwide, emissions of HC, CO, and NO_x from on-road vehicles have declined in absolute quantity, as well as relative to other sources of air pollution.

Even though today's new vehicles produce substantially less ozone-forming HC and NO_x emissions than the new vehicles of 25 years ago, ozone concentrations in 33 urban areas remain above the current federal air quality standard. In the same time frame, nine cities were above the carbon monoxide standard. While these numbers represent a major improvement from prior years, significant future reductions in emissions from a variety of sources – stationary and mobile – will be required to help meet the ozone standard in the remaining areas.

Similarly, many European cities are experiencing unique and significant problems caused by the use of diesel fuel by both passenger cars and trucks and the consequent increased burden of particulate matter. Reductions from many sources, including mobile, will be needed to tackle the air quality problems.

Mobile source reductions will be achieved in many ways. Future vehicle systems are being designed to achieve lower emissions. In addition, gasoline and diesel fuels are being reformulated in some areas to reduce emissions from both existing and future vehicles. Alternative fuels also may play a role in decreasing emissions.

In the past, the successful achievement of these goals has been hampered by a lack of scientific knowledge in a variety of areas. For instance, one specific need has been comprehensive data about the interrelationships among fuel composition, vehicles, emissions, and air quality. The U.S. Auto/Oil Air Quality Improvement Research Program (AQIRP) and the European Programme on Emissions, Fuels, and Engine Technologies (EPEFE) were created to develop that knowledge.

AQIRP

The Auto/Oil Air Quality Improvement Research Program (AQIRP) was established in 1989 by 14 oil companies and three domestic automakers. The program has made great progress in developing an information base on fuel and vehicle effects on emissions. The overall objective of AQIRP has been to provide this data to help legislators and regulators achieve the nation's clean air goals through a research program that included:

(1) Estimation of potential reductions in vehicle emissions from changes in fuel composition.
(2) Estimation of potential improvements in air quality - primarily ozone - and fuel reformulation.
(3) Estimation of the relative cost effectiveness of some fuel/vehicle systems.

This program was the largest and most comprehensive project of this nature ever attempted.

Over the course of the six-year program, AQIRP conducted more than 5,000 emissions tests using over 80 fuel compositions in over 100 vehicles. The tests measured engine, tailpipe, evaporative, and running-loss emissions, and quantified the concentrations of 153 different organic compounds plus oxides of nitrogen (NO_x) and carbon monoxide (CO). Using the 175 megabytes of data generated by these tests, AQIRP has developed an extensive data base of fuel composition and vehicle effects on emissions.

The emissions data were employed in air-quality modeling studies for New York City, Los Angeles, and either Chicago or Dallas-Fort Worth, using state-of-the-science models and emissions inventories. In these studies, AQIRP focused on fuel and vehicle changes that would reduce predicted ozone air pollution. Extensive refinery modeling studies were also conducted to develop cost estimates for producing various research gasoline formulations.

AQIRP found that the following changes can be effective in reducing vehicle mass emissions and/or improving ozone air quality.

- Lowering the aromatic content of gasoline lowers toxic emissions.
- Lowering the T_{90} and/or T_{50} (boiling range) of gasoline reduces ozone and exhaust HC emissions.
- Lowering the sulfur content of gasoline decreases exhaust emissions of HC, CO, NO_x, toxics, and ozone.
- Lowering the olefin content of gasoline reduces NO_x and ozone, but increases exhaust HC emissions.
- Adding oxygenates to gasoline reduces CO in older and current technology vehicles.
- Lowering the Reid vapor pressure (RVP) of gasoline reduces evaporative emissions, exhaust HC and CO emissions, and ozone.
- Identifying and repairing high-emitting vehicles reduces evaporative emissions, exhaust emissions and ozone.
- The introduction of newer vehicle technology has resulted in decreases in regulated emissions, toxics and ozone.

EPEFE

The European Programme on Emissions, Fuels, and Engine Technologies (EPEFE) began in 1994. It was an essential part of the European Auto-Oil Programme which constituted a new approach in setting environmental legislation and which harnessed the expertise of the European Commission, industry, and consultants in Europe. The intent of the Auto-Oil Programme was to identify which new measures may be required to meet rational air quality objectives in the most cost effective way, derived from scientifically sound data. The EPEFE program was designed to extend the information on the relationships between fuel properties and engine technologies and to quantify the reduction in in-use emissions that can be achieved by combining advanced fuels with the vehicle/engine technologies under development for the year 2000. Specifically, EPEFE included:

(1) Assessment of the current state of emissions relationships available from fuels/vehicles.
(2) Generation of new data for the air quality modeling program in Europe.
(3) Estimation of the cost benefit of fuel/vehicle technologies relative to the year 2000 requirements.

During its two years of activity, EPEFE examined 12 gasolines in 16 gasoline-powered vehicles, and 11 diesel fuels in 19 light duty vehicles and 5 heavy-duty engines. More than 2000 emissions tests were performed, providing over 500,000 measurements of HC, CO, and NOx exhaust emissions, and diesel-generated particulates.

The emissions data from EPEFE were used in air quality modeling studies for seven European cities including London, Cologne, Hague, Lyon, Athens, Milan, and Madrid. Additional studies are also being conducted to identify the most cost effective way to implement the findings.

The following EPEFE results confirm that both fuels and engine technologies are important determinants of motor vehicle emission levels.

* Lowering the aromatic content of gasoline decreases exhaust HC and CO.

* Reducing the aromatic level of gasoline reduces CO_2 at each E100 volatility level with no impact on fuel consumption.

* Increasing the mid-range volatility of gasoline decreases exhaust HC.

* Decreasing the T90 (boiling range) of gasoline reduces light-duty PM and heavy-duty exhaust NO_x.

* Lowering the sulfur level of gasoline reduces exhaust HC, CO, and NO_x.

* Decreasing the density of diesel fuel reduces light-duty diesel HC, CO, and PM, and reduces heavy-duty diesel NO_x.

* Decreasing the polyaromatic content of diesel fuel reduces light-duty diesel NO_x and PM, heavy-duty diesel HC, NO_x and PM.

* Increasing the cetane rating of diesel fuel reduces diesel HC and CO.

Conclusions About AQIRP and EPEFE

These landmark cooperative research programs have contributed enormously to the understanding of the relationships between fuels and vehicles.

AQIRP was a milestone in cooperatively developing a sound technical database for use by regulators. In addition to developing new test techniques for measuring and speciating emissions, the program also made significant contributions to the development of atmospheric models and the understanding of how fuels impact atmospheric pollution.

The California Air Resources Board (CARB) has adopted gasoline specifications based on program findings. CARB and the U.S. Environmental Protection Agency have both made use of AQIRP's data in developing mathematical models to predict emission changes from changes in fuel properties. AQIRP data will continue to influence decisions on air quality improvement control options for years to come.

EPEFE, which was inspired by the AQIRP, is providing similar benefits for Europe as it provides a scientific basis for the establishment of cost effective European exhaust emission standards for the year 2000. The program brought together European Union Commission, the European oil industry, and the European auto industry for the first time in a large scale cooperative research program. The program enhanced the body of data already in existence within Europe and from AQIRP to expand on the relationships between fuels and automotive emissions. The EPEFE process aided the search for a balanced set of measures which could help meet the European Union's air quality objectives.

These programs have shown that:

* Oil and automotive industries can work together effectively on important research objectives.

* Both programs have made important findings and have substantially increased the body of knowledge of vehicle/fuel effects.

* Matching fuels to vehicles is critical. They form a "system" which maximizes the potential of each.

* Controlling mobile source air pollution requires a detailed understanding of fuel/vehicle systems, inventories, atmospheric chemistry, and cost effectiveness.

Results (Gasoline)

AQIRP

- Aromatics (per vol. % decrease) FTP Cycle

HC	CO	NOx
-0.2	-0.5	NS

Note: AQIRP results are for "Current" Technology vehicles unless otherwise noted.

EPEFE

- Aromatics (per vol. % decrease)* MVEG 11-second Cycle
  - * @ E100 = 35%

HC	CO	NOx
-1.1	-0.6	+0.5

  - * @ E100 = 50%

HC	CO	NOx
-0.4	-0.6	+0.3

  - * @ E100 = 65%

HC	CO	NOx
-0.3	-0.6	+0.1

* 5% CO_2 reduction from high to low aromatics

Results (Gasoline cont.)

AQIRP

- T_{90} (per 5°F decrease)

HC	CO	NOx
-1.4	NS	+0.3

- T_{50} (per 5°F decrease)*

HC	CO	NOx
-2.1	NS	+1.3

* HC results for 180 - 240°F range
CO and NOx results for 185 - 215°F range

EPEFE

- T_{90} - held constant in EPEFE matrix for each level of E100
- E-100 (per % evaporated)
  - * E-100 @ 20% Aromatics

HC	CO	NOx
-0.8	-0.1	+0.2

  - * E100 @ 35% Aromatics

HC	CO	NOx
-1.2	-0.1	+0.4

  - * E100 @ 50% Aromatics

HC	CO	NOx
-1.4	-0.1	+0.7

Results (Gasoline cont.)

AQIRP

- Sulfur (per 50 ppm decrease - not linear) FTP Cycle

HC	CO	NOx
-2.2 to -2.9	-2.4 to -2.8	-1 to -1.5

EPEFE

- Sulfur (per 50 ppm decrease)
  - * MVEG Cycle - composite new 11 sec. idle

HC	CO	NOx
-1.2	-1.2	-1.4

  - * EUDC Portion (Sulfur results)

HC	CO	NOx
-7.1	-5.8	-2.8

  - * ECE Portion (Sulfur results)

HC	CO	NOx
NS	-0.9	NS

Results (Gasoline cont.)

AQIRP

- Olefins (per vol. % decrease)

HC	CO	NOx
+0.4	NS	-0.4

- Oxygenate (per wt. % increase)

HC	CO	NOx
-1.9	-4.1	NS

- RVP (per psi decrease)

HC	CO	NOx
-4%	-9%	NS

EPEFE

Results (Diesel)

AQIRP

- Diesel - not tested

EPEFE

- Reducing Density 0.855 - 0.828 g/l

HC	CO	NOx	PM
		LD	
-18.9	-17.7	+1.4	-19.4
		HD	
+14.3	+5	-3.6	NS

- Reducing Polyaromatics 8 to 1% m/m

		LD	
+5.5	+4	-3.4	-5.2
		HD	
-4	NS	-1.7	-3.6

Results (Diesel cont.)

AQIRP

- Diesel - not tested

EPEFE

- Increasing Cetane number 50 to 58

HC	CO	NOx	PM
		LD	
-26.3	-25.3	NS	+5.2
		HD	
-6.3	-10.3	-0.6	NS

- Reducing T_{95} from 295 - 370°C

		LD	
NS	-1.8	+4.6	-6.5
		HD	
+13.4	+6.6	-1.7	NS

CHEMICAL KINETICS OF CETANE NUMBER IMPROVING AGENTS

K.Hashimoto, Y.Akutsu, M.Arai and M.Tamura

Department of Chemical System Engineering, School of Engineering, The University of Tokyo

7-3-1 Hongo Bunkyo-ku Tokyo 113 Japan

INTRODUCTION

The increasing demand for diesel fuels has resulted in the use of greater percentage of cracked distillates having poor ignition properties. The ignition properties of diesel fuels can be rated in terms of their cetane number and diesel fuels having low cetane number may have poor ignition properties such as diesel knock, difficulties to start engines in the cold weather and so on. Such diesel fuels need cetane number improving agents. In the 1940s and 1950s alkyl nitrates, alkyl nitrites and organic peroxides were found to be effective cetane number improving additives (1). Our recent study suggests that free radicals produced from thermal decomposition just before ignition should have an important role to improve their ignition properties (2). However no studies on the reaction mechanism for improving effect of these additives have been attempted because of complex nature of spontaneous ignition reaction of hydrocarbons. In order to clarify the reaction mechanism for improving effects of cetane number improving agents. We here have attempted to simulate the spontaneous ignition of n-butane as a model compound in the presence of alkyl nitrites as cetane number improving agents.

CALCULATION METHOD

Calculations are performed using Chemkin and Senkin programs from the Sandia National Laboratories. Simulation reactions are assumed to be carried at under adiabatic condition at constant volume. Kozima's model (3) partly revised by adding thermal decomposition of cetane number improving agents was used for spontaneous ignition of n-butane in the presence of cetane number improving agents. Batt and the other's kinetic data (4) were used for simulation of the thermal decomposition of alkyl nitrites. Unknown thermochemical data were estimated by using the THERM program (5).

RESULT AND DISCUSSION

Addition effects of n-amyl nitrite addition on ignition delay period of n-butane are shown in Fig.1. Fig.1 shows that n-amyl nitrite addition to n-butane reduces ignition

delay period suggesting that this reaction model can simulate the effect of cetane number improving agents on ignition delay period.

Fig.2 shows the mechanism for thermal decomposition of n-amyl nitrite. In the thermal decomposition of n-amyl nitrite, weak N-O bond is dissociated to produce n-amyloxy radical and nitric oxide. Then beta-fission of n-amyloxy radical immediately produce n-butyl radical. Under the preignition conditions of n-butane, n-amyl nitrite may be thermally decomposed to induce complex radical reactions that enhance the n-butane ignition reactions. Thus n-amyl nitrite would reduce the ignition delay period of n-butane spontaneous ignition.

Fig.3 and Fig.4 show effects of initial pressure and temperature on ignition delay period of n-butane in the presence of n-amyl nitrite respectively.

Table I shows additive effect of n-amyl nitrite, n-propyl nitrite and t-amyl nitrite on ignition delay of n-butane. The effect of n-amyl nitrite is larger than that of n-propyl nitrite and t-amyl nitrite. Our previous experimental results (2) show that the effect of n-amyl nitrite on cetane number is larger than that of n-propyl nitrite and t-amyl nitrite. The present calculation results would be much in agreement with the experimental results.

Fig.5 shows the mechanism for thermal decomposition of n-propyl nitrite and t-amyl nitrite. Thermal decomposition of n-propyl nitrite and t-amyl nitrite can produce ethyl radical. We suggest that larger ignition delay reduction effect of n-amyl nitrite than that of n-propyl nitrite and t-amyl nitrite should be due to larger reactivity of n-butyl radicals than ethyl radicals under the preignition condition of n-butane.

CONCLUSION

In order to clarify the reaction mechanism for improving effects of cetane number improving agents, we have attempted to simulate the spontaneous ignition of n-butane in the presence of alkyl nitrites. As a result, it is shown that n-alkyl nitrite can reduce the ignition delay period of n-butane. It is known that cetane number improving agents decompose to produce alkyl radicals under operation conditions of diesel engine. We suggest that alkyl radicals produced would enhance the pre-ignition reactions of hydrocarbons to reduce ignition delay period. And it is also shown that the cetane number improving agents having higher cetane number can reduce the ignition delay period of n-butane more effectively. We also suggest that more reactive radicals should have larger effects on reduction of ignition delay period.

LITERATURE CITED

(1)Robbins, W.E., Audette, R.R. and Reynolds, N.E., SAE Quart. Trans., 5, 404 (1951)

(2)Hashimoto, K., Kawakatsu, Y., Arai, M. and Tamura, M., J. Jpn. Inst. Energy, 74, 200(1995)

(3)Kojima, S., Combust. Flame, 99, 87(1994)

(4)Batt, L. and Milne, R.T., Int. J. Chem. Kinet., 8, 59(1976)

(5)Ritter, E.R. and Bozzelli, J.W., Int. J. Chem. Kinet., 23, 767(1991)

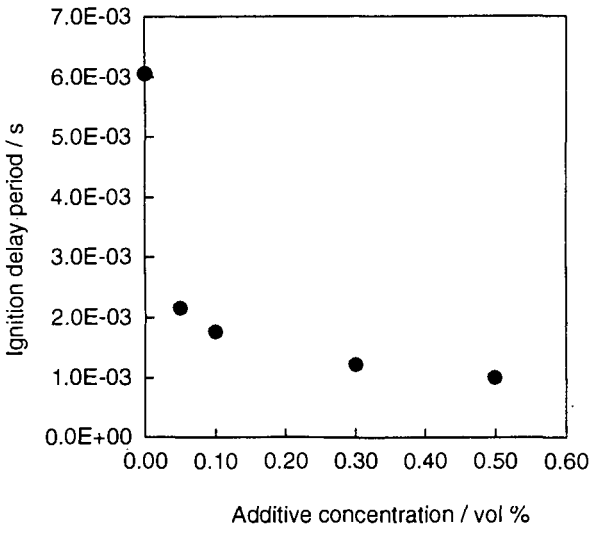

Fig.1 Ignition delay period vs additive concentration

Additive : n-Amyl nitrite

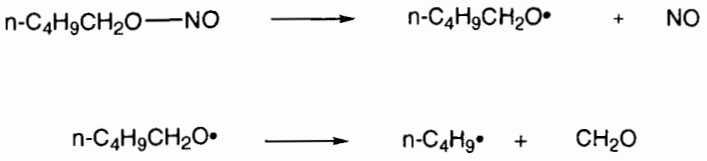

Fig.2 Mechanism for thermal decomposition n-amyl nitrite

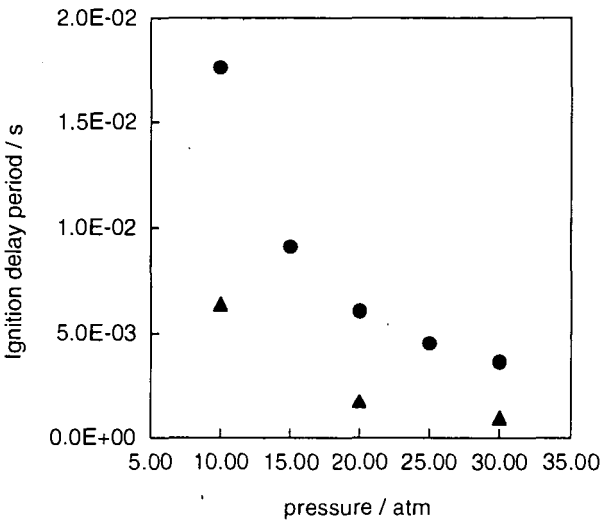

Fig.3 Ignition delay period vs initial pressure

Initial temperature : 800K

● No additive

▲ n-Amyl nitrite 0.1 vol %

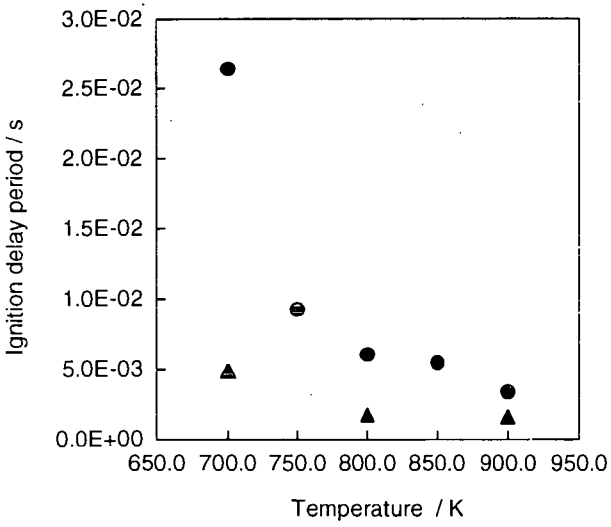

Fig.4 Ignition delay period vs initial temperature

Initial pressure : 20atm

● No additive

▲ n-Amyl nitrite 0.1 vol %

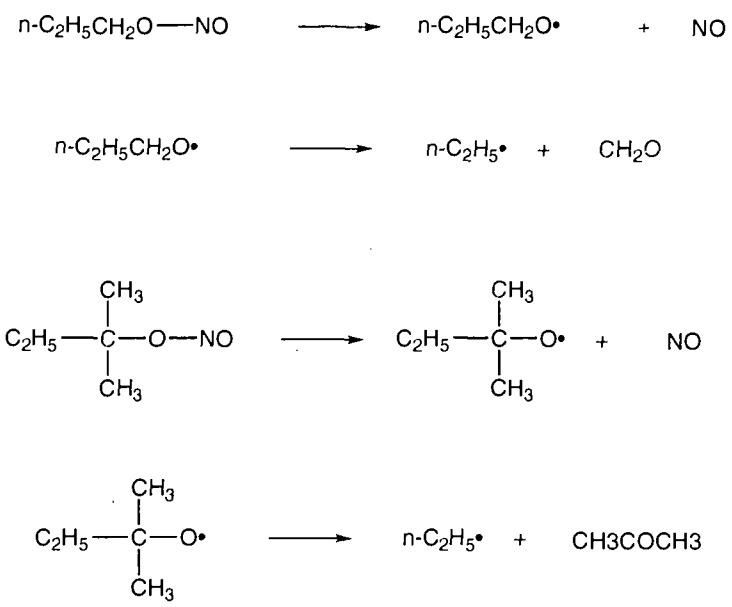

Fig.5 Mechanism for thermal decomposition of n-propyl and t-amyl nitrite

Table 1 Ignition delay period in spontaneous ignition of n-butane in the presence of additives

Additive concentration : 0.1 vol %
Initial temperature : 800K
Initial pressure : 20atm

Additives	Ignition delay period / 10^{-3}s
n-Amyl nitrite	1.76
t-Amyl nitrite	1.92
n-Propyl nitrite	1.92

THE PERFORMANCE OF DI-TERTIARY-BUTYL PEROXIDE AS CETANE IMPROVER IN DIESEL FUELS

Manish K. Nandi
ARCO Chemical Company, Newtown Square, PA 19073.

Key Words: Diesel Fuel; Cetane Improver; Heavy-duty diesel engine emissions

Abstract

Increasing the cetane number of diesel fuel, either by lowering aromatic content of the fuel through hydrotreating and/or by addition of chemical cetane improvers, is a cost-effective option to reduce diesel engine emissions. It is generally recognized that chemical cetane improvement additives represent a low cost alternative to aromatic reduction. Although both methods significantly reduce engine emissions, deep hydrotreating tends to adversely affect some fuel properties. We are evaluating the performance of a peroxide based cetane improver for diesel fuel. A comparison is made between the performance of di-t-butyl peroxide and the conventional cetane improver, 2-ethylhexyl nitrate. Correlation between the cetane response of the peroxide with the different fuel properties is discussed. Both the additives significantly reduce all regulated and unregulated emissions including NOx emissions. The NOx emissions from the peroxide treated fuels are consistently lower than those for the nitrate treated fuels at similar cetane level. The chemistry for the synthesis of di-t-butyl peroxide is discussed.

Introduction

The implementation of stringent diesel engine emissions regulations is growing worldwide. In the United States, the 1990 Clean Air Act mandates lowering oxides of nitrogen (NOx) emissions to 4.0 grams per horsepower-hour (g/hp-hr) in 1998. Future proposals by EPA call for a further reduction of a combined NOx and HC to 2.5 g/hp-hr for the year 2004 for heavy-duty trucks and buses. Such emission reduction will require a combination of new engine technology and economically viable low emission diesel fuels.

It is widely accepted that increasing the cetane number represents one option for production of cleaner burning diesel fuels. Numerous studies, including the Coordinating Research Council VE-1 and VE-10 programs, have demonstrated that increasing the cetane number of the fuel significantly reduces all the regulated emissions.[1] Increasing the cetane number of diesel fuel can be achieved by lowering aromatic content of the fuel through hydrotreating and/or by addition of chemical cetane improvers. It is generally recognized that chemical cetane improvement additives represent a low cost alternative to obtaining higher cetane number achieved through aromatic reduction. Moreover, deep hydrotreating to reduce aromatics tend to adversely affect some fuel properties, e.g., waxing and cold flow.[2]

Chemical cetane improvers are those compounds that readily decompose to form free-radicals, which in-turn promote the rate of initiation. This increased rate of chain initiation leads to improved ignition characteristics of diesel fuel. Chemicals selected from alkyl nitrates, certain peroxides, tetraazoles, and thioaldehydes can serve as cetane improvers. Due to their low costs, alkyl nitrates have played the most significant role in commercial use. 2-Ethylhexyl nitrate (EHN) has been used as a commercial cetane improver for a number of years and today is the predominant cetane improving additive in the marketplace. Di-tertiary-butyl peroxide (DTBP) was first recognized as an effective cetane improver in the 1940's.[3] Due to its higher cost, DTBP has not achieved the same wide spread usage as EHN. New technology has been developed by ARCO Chemical Company that will substantially reduce the cost of DTBP to a level comparable to that of EHN. Moreover, DTBP has a potential advantage over alkyl nitrates in reducing NOx emissions since it does not contain nitrogen.[4] DTBP is currently used in limited amounts in an after market fuel treatment package.[5] This fuel additive package containing DTBP, has been evaluated, certified and approved for use by the Department of the Navy.[6]

Synthesis

Dialkyl peroxides can be synthesized by the reaction of an alcohol and/or an olefin with an organic hydroperoxide, using an acidic catalyst. In the process developed at ARCO Chemical Company, t-butyl alcohol and/or isobutylene is reacted with t-butyl hydroperoxide in the presence of an acidic resin catalyst.[7]

Cetane Response

Cetane response, which may be defined as the relationship between the change in cetane number of the fuel and the concentration of the cetane improver, is a key factor for commercial acceptance of a cetane improver. We have studied, in details, the cetane response of DTBP in a variety of commercial diesel as well as in various diesel fuel blend stocks, worldwide.[8] The relative effectiveness of DTBP versus the commercial cetane enhancer, EHN, was determined in numerous base fuels with varying fuel properties as well as different blend stocks.

On an average, DTBP is between 85% to 90% as effective as EHN in increasing cetane number of diesel fuels.

It is also very important to understand the relation between the diesel fuel composition or properties and its cetane response for DTBP. We have developed a predictive cetane response equation for DTBP based on various fuel properties, viz., aromatics, mid-range distillation point (T_{50}), flash point, and pour point. The regression equation describing the change in cetane number due to the addition of DTBP is:

$$\Delta C = (39.8727 + 0.02335 * Z_2 - 0.0823 * Z_3 + 0.1405 * Z_4 - 0.0777 * Z_5) + (-0.1176 * Z_3 + 0.0430 * Z_5) * X + (-0.1190 * Z_4 - 0.0113 * Z_5) * X^2$$

with $R^2 = 0.889$ and RMSE = 1.6846

where ΔC = expected change in cetane number,
X = concentration of additive (wt%)
Z_2 = flash point (°F)
Z_3 = aromatics (wt%)
Z_4 = pour point (°F)
Z_5 = mid-range distillation point, T_{50} (°F)

Thus, given the values for appropriate fuel properties, the above equation can be used to predict, within their limits of uncertainty, the expected change in cetane number due to the addition of a specific amount of DTBP. However, it is recommended that this equation be used within the valid range of the experimental data used to generate it and the results not be extrapolated beyond an additive concentration of 0.75 wt%. Since this equation reduces to a simple quadratic form on substitution of the fuel properties, it can also readily be solved to determine the amount of additive required to increase the cetane number of the fuel by a desired amount.

Although the cetane response equation was generated based on several fuel properties, statistically, the two most influential fuel parameters were the aromatic content and the mid-range distillation temperature (T_{50}).

The cetane response of DTBP was inversely related to the aromatic content of the fuel. Thus, low aromatic fuels will respond well to the additive. On the contrary, fuels with high aromatic content or highly aromatic blend stocks like light cycle oil (LCO) or light cycle gas oil (LCGO) will respond very poorly to cetane improvers. Indeed, a highly aromatic (87%) LCGO blend stock did not respond at all to either of the cetane improvers, DTBP or EHN. Assuming the cetane improvers react through formation of free radicals to accelerate combustion, this low response for the aromatics may be attributed to the higher activation energy required for the nitrate or peroxide free radicals to react with an aromatic fragment compared to a aliphatic hydrocarbon fragment of the fuel. This, in fact, follows a similar trend for natural cetane for different fuel fragments, where aromatics have poor natural cetane numbers while straight chain aliphatic hydrocarbons have the highest natural cetane numbers.

The relationship between the cetane response of the two additives for the different fuels and the mid-range distillation temperature of the fuel is less clearly understood. In general, it was observed that the lighter fuels respond better to cetane improvers compared to the heavier fuels, especially at low additive levels. More work is needed to understand this effect.

It must be emphasized that although the cetane response equation, described here, use the base diesel fuels' properties to compute the expected change in its cetane number, the relationship between these changes and the fuel properties are by no means causal. Rather, the fuel properties are merely manifestations of some other more fundamental attributes of the fuel.

Engine Emissions

Numerous studies by the Coordinating Research Council and others have shown that increasing the cetane number through the use of additives reduces all regulated emissions.[1] The Coordinating Research Council's VE-10 program addressed the effect of cetane additives on diesel emissions.[9] The first part of this study, using two different 1994 heavy-duty engine technologies, demonstrated that the use of cetane improvement additives produces significant reduction in carbon monoxide and oxides of nitrogen emissions, with hydrocarbon and particulate matter being either unaffected or slightly reduced. Cetane additives including DTBP and EHN at levels up to 1.25 wt% were included in the continuation of this study using 1998 engine technology. Even using 1998 engine technology, having lower emissions than any diesel engine on the road today, increasing the cetane number with either EHN or DTBP reduced all engine emissions.

ARCO Chemical Company has conducted extensive testing on the effects of cetane additives on emissions from heavy-duty diesel engines.[10] This testing was conducted on a 1991 Detroit Diesel Series 60 heavy-duty diesel engine, typical of an engine currently in service, using the 1992 Federal Test Procedures for transient testing of heavy-duty engines. A total of four

fuels, representative of those currently commercially available, were used. The properties of the four test fuels are described in Table 1. One of these fuels, designated C, is a standard 2-D fuel, which meets the requirements for a diesel engine certification fuel as defined in CFR 86.1313-94(b)(2). The effects of both the cetane improvers, including a mixture of the two additives in fuel C, on engine emissions are summarized in Table 2.

Table 1: Test Fuels Properties

Property	Fuels			
	A	B	C	D
Cetane Number (D613)	46	41	43	38
Aromatics, vol% (D1319)	20	25	32	35
Sulfur, wt%	0.01	0.01	0.03	0.01
API Gravity, (D287)	37.9	35.4	35.7	33.4
Distillation Range (D86)				
IBP, °C	200	168	178	181
50% Point (T50), °C	243	247	259	248
EP, °C	328	333	334	344

Table 2: Effect of Cetane Improver on Regulated Emissions

Base Fuel	Additive	Additive Level (wt%)	Increase in Cetane Number	Hydrocarbon	Carbon Monoxide	NOx	Particulate Matter
A	EHN	0.40	10	- 41%	- 27%	- 1.9%	11%
	DTBP	0.50	11	- 43%	- 29%	- 2.2%	12%
B	EHN	0.70	15	- 59%	- 40%	- 2.8%	0.7%
	DTBP	0.80	16	- 58%	- 40%	- 3.9%	2.5%
C	EHN	0.60	9	- 60%	- 37%	- 1.9%	2%
	DTBP	0.65	10	- 59%	- 36%	- 5%	- 4%
	EHN/DTBP	0.31	10	- 59%	- 37%	- 2.6%	- 6.6%
D	EHN	0.65	10	- 75%	- 47%	- 2.8%	- 40%
	DTBP	0.75	10	- 77%	- 49%	- 3.3%	- 40%

As evident from the results increase in cetane number can significantly reduce hydrocarbon and carbon monoxide emissions in all the fuels. The NOx emission from the cetane improved fuels showed a small reduction compared to the base fuels, with the limited number of tests used for these study. The NOx emissions from the peroxide treated fuels, although not statistically significant, were lower than that from the nitrate treated fuels, in each of the base fuels. The peroxide produced about 0.5% to 3% lower NOx when compared to the nitrate at the same cetane level. These results indicate that when blended to comparable cetane numbers, DTBP produces lower NOx emissions than EHN. This trend is not only observed in this work but also in other works with different fuels, different engines, and using different international test protocols.

Gaseous Toxics Emissions

The use of a cetane enhancer substantially reduces the four gaseous toxic emissions of 1,3-butadiene, benzene, formaldehyde, and acetaldehyde.[10] Typical reductions in these four gaseous toxic emissions achievable by increasing the cetane number of a fuel by ten numbers, which on average required 0.65% cetane improver, vary from 30% to 70%.

Ozone Forming Potential

Complete speciation of the volatile hydrocarbons, aldehydes and ketones into C_1-C_{12} fractions was included as part the test program conducted by ARCO Chemical Company. Using standard Minimum Incremental Reactivity (MIR) values, the ozone forming potential was calculated.[10] Typical reductions in the ground level ozone forming potential achieved by a ten number increase in cetane using additives is between 50% to 75%. With ground level ozone, a major cause of smog, becoming an increasing problem in metropolitan areas, significant reductions

in ground level ozone attributed to diesel engine emissions can be obtained through the use of cetane improvers.

Soluble Organic Fraction of Particulate Matter

The use of DTBP produces substantial reductions in the soluble organic fraction of the particulate matter.[10] These reductions in the soluble organic fraction of the particulate matter are expected in-turn to reduce the emissions of both polyaromatic hydrocarbons and nitrated polyaromatic hydrocarbons.

Thermal and Oxidative Stability

A cetane improvement additive that is thermally or oxidatively unstable under actual conditions impacts on the fuel quality and could lead to poor engine performance resulting from the decrease in cetane number or fuel degradation. Thus, for commercial acceptance the peroxide based cetane improvement additives must be stable, thermally and oxidatively, at actual use temperatures.

The thermal stability of DTBP was demonstrated by determining the effects of heating on the treated fuels and also by measurement of the decomposition rates in a low sulfur diesel fuel.[8] A fuel treated with DTBP showed no statistically significant loss in cetane number after heating for 100 hours at 92°C. The half-life for DTBP at 70°C in diesel fuel is in excess of 10,000 hours, with greater than 97% of the additive remaining after nearly 700 hours. Even at 100°C, the half-life of DTBP in diesel fuel is over 300 hours. Even though the rate of thermal decomposition of the peroxide is five to ten times faster than the nitrate, the peroxide additive is very stable under typical fuel system temperatures.

Additives can cause diesel fuel degradation if they are not oxidatively stable. The oxidative stability of DTBP was demonstrated by the standard ASTM methods. Both the accelerated oxidative stability test (D274)[12] and the long term storage stability test (D4625)[13] did not show any gum formation in most of the diesel fuels tested. In some inherently unstable fuels degradation was observed. But they can be controlled easily by addition of very small amount of antioxidants.

Conclusion

Increasing the cetane number by addition of chemical cetane improvement additive is a cost effective way to produce cleaner burning diesel fuels. A peroxide based cetane improvement additive, di-t-butyl peroxide, can be very effective as a cetane improver. DTBP can be synthesized cheaply by the reacting isobutylene with t-butyl hydro peroxide. It is comparable in performance to 2-ethylhexyl nitrate, the cetane improver currently used commercially. DTBP has the potential of reducing NOx emissions more that the nitrate at comparable cetane level. The additive is thermally and oxidatively stable in diesel fuels at typical fuel systems temperatures.

Acknowledgement

The author wishes to thank Dr. Frank Liotta, Dr. Jeffrey McFarland, Dr. Daniel Pourreau, Dr. David Jacobs, Mr. Richard Englebach and Mr. Michael Camesi at ARCO Chemical Company for their contribution to the project. The author also thanks Mr. Dan M. Montalvo and Mr. Terry L. Ullman at Southwest Research Institute (SwRI) for their help in the emissions testing program.

References

1.(a) Nandi, M.; Jacobs, D. C.; Kesling, H. S.; Liotta, F. J. ; "The Performance of a Peroxide-based Cetane improvement Additive in Different Diesels Fuels"; SAE 942019, October 1994 and references there.

(b) Nandi, M. K.; Jacobs, D. C.; "Cetane Response of Different Di-tertiary-butyl Peroxide in different diesel fuels; SAE Paper 952369; October 95 and references there.

2. Stocky, T.; "Role of Cetane Improvers", Reformulated Diesel Symposium, Toronto, Canada; 1994.

Marriott, M.; "Diesel Quality and Emissions - European Experiences",. Reformulated Diesel Symposium, Toronto, Canada; 1994.

3. Wiles, Q.T.; Bishop, E.T.; Devlin, P. A.; Hopper, F. C.; Schroeder, C.W.; Vaughan, W. E.; Ind. and Eng. Chem., 1679 (1949).

4.(a) Reference1(a).

(b) Liotta, F. J.; "A Peroxide Based Cetane Improvement Additive with Favorable Fuel Blending Properties", SAE Paper 932767, October 1993.

(c) Coordinating Research Council VE-10 Project Final Report (1995).

5. U.S. Patent 4797134.

6. Department of The Navy, Office of The Assistant Deputy Under Secretary (Safety and Survivability), Justification and Approval No. 94-004, (10/14/93).

7. US Patent 5,371,298.

8. Reference 1(b).

9. Coordinating Research Council VE-10 Project Final Report (1995).

10. References 1(a) and 3(b).

11. Kesling, H. S.; Liotta, F. J.; Nandi, M. K.; "The Thermal Stability of a Peroxide-Based Cetane Improvement Additive"; SAE Paper 941017; March, 1994.

12. Reference 4(b).

13. Internal ARCO Chemical Company results.

DIMETHYL CARBONATE PRODUCTION FOR FUEL ADDITIVES.

Y.Okada, T.Kondo, S.Asaoka, Chiyoda Corporation
3-13 Kanagawa-ku, Yokohama 221, Japan

Key wards : Dimethyl carbonate, Octane enhancing oxygenates, Zeolite catalysts

Abstract

We have taken note of the transesterification reaction as a highly safe process of dimethyl carbonate (DMC) production for fuel additives. The reaction proceeds under the low corrosiveness and in the relatively mild condition. We have aimed to use an inorganic solid catalyst for this process. The inorganic solid catalyst is thermally stable and can be used in the large-scale fixed bed reactors without a catalyst separation unit.

Through the transesterification of ethylene carbonate(EC) with methanol, DMC and ethylene glycol (EG) are co-generated as the products[1].

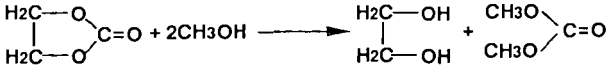

EG is one of the bulk chemicals produced in the large scale plant comparable to one for the fuel additives. The market balance is important in the co-production process. On the assumption that the amount of the co-production meets the market balance, the co-production of DMC and EG is commercially viable. If we can control the amount of the EG co-production in this process, it makes the process more flexible in the commercial production. Accordingly we have proposed a conceptual process scheme to control the amount of the EG co-production.

In this symposium, the inorganic solid catalyst system applying to the transesterification process and the conceptual process scheme how to control the amount of co-product will be discussed.

1.Introduction

Dimethyl carbonate (DMC) is very attractive as for use as an oxygenate for the fuel additives. Many routes of the DMC synthesis have been proposed. Among those routes, the DMC production process for the chemical raw material has been commercialized. The process for the fuel additives should be easy to scale up in the capacity to satisfy the large demand. Moreover, it is also required to be safe in the operation and to be stable in the supply.

2.Selection of DMC synthesis route

2-1 Probable routes of DMC synthesis

DMC is produced several ten thousands ton per year in the world as chemical raw material used in the carbonylating and methylating agent, etc. DMC had been formerly produced from phosgene. The proposed synthesis methods including commercialized routes as non-phosgene DMC production are classified generally into the following 4 routes. Fig.1 shows the relation of raw materials and intermediates of those routes. All routes start from methanol. There is the other route to produce DMC using nitrous acid ethers[2] except in Fig.1. This route has been in commercial for the chemical raw material use. Though the nitrous acid ethers are less toxic than phosgene, they are still considered as toxic materials. Accordingly, we put the process using nitrous acid ethers out of our research scope. The investigation results of the routes shown in Fig.1 are the following.

2-2 Oxidative carbonylation route

Oxidative carbonylation processes in both the liquid phase and the vapor phase have been developed. The liquid phase oxidative carbonylation is the oxidation of carbon monoxide with oxygen in methanol in the presence of copper chloride[3]. The catalyst is used in a slurry mixture. Now, DMC for the chemical use is being produced in this oxidative carbonylation process. In the vapor phase oxidative carbonylation, palladium chloride-copper chloride[4], cupric chloride on activated carbon[5], etc. is proposed as the catalyst. All of these oxidative carbonylation processes including technologies under development inevitably need the presence of both oxygen gas and chloride.

In these situation, Chiyoda Corporation has tried to investigate halogen-free solid catalysts to improve the oxidative carbonylation process in the view point of less corrosiveness and the separability of the catalyst. We have succeeded to find the zeolite fixed the cation of copper as this kind catalyst which is particularly effective as the catalyst of the following reactions.

$$2CuCl + 2CH_3OH + 1/2O_2 \longrightarrow 2Cu(OCH_3)Cl + H_2O$$

$$2Cu(OCH_3)Cl + CO \longrightarrow (CH_3O)_2CO + 2CuCl$$

2-3 Esterification route

The route from carbon dioxide and methanol into DMC through the dehydration is the simplest one. We have tried it challengingly. Since this reaction is very disadvantageous in the equilibrium, the reaction could not be successfully proceeded.

$$2CH_3OH + CO_2 \longrightarrow \begin{matrix} CH_3O \\ CH_3O \end{matrix}\!\!>\!C=O + H_2O$$

2-4 Route through urea

In this route, firstly urea is synthesized from carbon dioxide and ammonia. Subsequently, the urea reacts with methanol into DMC.

$$CO_2 + 2NH_3 \longrightarrow \begin{matrix} NH_2 \\ NH_2 \end{matrix}\!\!>\!C=O + H_2O$$

$$2CH_3OH + \begin{matrix} NH_2 \\ NH_2 \end{matrix}\!\!>\!C=O \longrightarrow \begin{matrix} CH_3O \\ CH_3O \end{matrix}\!\!>\!C=O + 2NH_3$$

Though methyl carbamate is easily generated as mono-changed intermediate in the second reaction step, the intermediate can not be transformed into DMC.

2-5 Transesterification route (glycol co-production route)

As shown in Fig.1, ethylene carbonate (EC) is used as the raw material instead of the direct reaction of carbon dioxide in the transesterification route. The EC is commercially produced from carbon dioxide and ethylene oxide. Subsequently, DMC is obtained from the EC through the transesterification with methanol. Ethylene glycol (EG) is converted from ethylene oxide as a main

co-product in this route. EG produced conventionally through the hydration of ethylene oxide is one of the bulk chemicals quantitatively comparable to fuel additives. In this transesterification route, the dried EG can be produced.

We have studied zeolite catalysts applying to the co-production of DMC and EG through the transesterification reaction. Zeolite catalysts have the excellent properties of resistance to heat and organic solvents and can be used in the large fixed bed reactors without a catalyst separation unit. We have found that some of zeolites have catalytic activity to the transesterifieation reaction. These results were presented at 207th ACS National Meeting. The catalytic activity depends on the Al_2O_3/SiO_2 ratio which represents the quantity of active sites. Since zeolite A has a maximum value of the Al_2O_3/SiO_2 ratio at 0.5 in the various type zeolites, the zeolite shows the highest activity. The cation species in the zeolite have an influence to the catalytic activity, the order of the activity is; 3A (KA) > 4A (NaA) > 5A (CaA).

2-6 Selection of the DMC synthesis route

Transesterification reaction is mild with small exotherm, and is carried out in the liquid phase without any toxic or corrosive chemicals. Therefore, it is essentially safe. Moreover, these features will be the merit in scaling up, because the large production will be able to perform with a low fixed capital.

In consideration of the above, we have selected the transesterification route as the most suitable one to large scale production of DMC for fuel additives and proceeded the further research in focus on this route.

3.The conceptual process of DMC production for fuel additives

3-1 The co-production of DMC and EG through the transesterification reaction

Fig.2 shows the conceptual process scheme of DMC production through the transesterification route. Fig.3 shows the concrete concept of the process scheme. The scheme consists of 9 units (blocks), ie. transesterification reactor, DMC-MeOH / EG-EC separation unit, MeOH separation unit, EC hydration reactor, etc. In the scheme, EG is co-produced quantitatively comparable to DMC.

3-2 The concept to control the EG co-production

If we can produce the only DMC or control the amount of the EG co-production in the selected route, it will make the process more flexible in the commercial production. This concept means that the large DMC production is possible freely from the demand of EG. Fig.4 shows the process scheme of the advanced concept. In this scheme, the co-produced EG is required to re-convert into the started EC. Accordingly, we have investigated the reaction to re-convert EG into EC.

In the first, we have conducted a test of the transesterification of EG and DMC, which is a reverse reaction of DMC and EG co-production. EC and methanol were generated with intermediate in stoichiometric proportions. It has been confirmed this transesterification is a reversible reaction. Therefore, we have considered EG would be able to re-convert into EC on the preferable catalyst. From the investigation of various reaction with the catalyst, we have confirmed that EC is generated from EG using urea instead of DMC.

3-3 The conceptual process of DMC production controlled the EG co-production

It is considered the combination of the EC regeneration reaction and urea synthesis makes the DMC production process controlled the EG co-production possible. Fig.5 shows the conceptual process scheme. In the scheme, urea is the intermediates synthesized from carbon dioxide and ammonia. Since the process of urea synthesis from carbon dioxide and ammonia had been established commercially, we can avail the process into the our proposed process complex without basic research. Fig.6 shows the total reaction scheme on which this conceptual process are based. In this reaction scheme, the DMC is synthesized from carbon dioxide and methanol through the dehydration reaction by the several steps.

4.Conclusion

we have selected the transesterification route as the most suitable one to large scale production of DMC for fuel additives. Transesterification reaction is mild with small exotherm, and is carried out in the liquid phase without any toxic or corrosive chemicals. Therefore, it is essentially safe. Moreover, these features will be the merit in scaling up. Zeolites can be used as the catalysts of this reaction. The zeolite catalysts have the excellent properties of resistance to heat and organic solvents and can be used in the fixed bed reactors without a catalyst separation unit.

EG is co-produced with DMC in the transesterification route. EG is one of the bulk chemicals quantitatively comparable to the fuel additives. On the assumption that the amount of the co-production meets the market balance, the co-production of DMC and EG is commercially viable.

As the option for this process, we have investigated the concept for the only DMC production or the control of the amount of the EG co-production. This concept means that the large DMC production is possible freely from the demand of EG. We have proposed the conceptual process scheme of the DMC production controlled the amount of the EG co-production. The conceptual process is consist of the urea synthesis and the re-conversion of EG into EC. In this conceptual process scheme, the DMC is synthesized from carbon dioxide and methanol through the dehydration reaction by the several steps. We have confirmed that EC is generated from EG using urea with the catalyst. However, the improvement of the catalyst and the investigation of the reaction conditions for the EC regeneration are required to rise the DMC yield in the total process.

5.References

1) John F.Knifton et al, J.of Molecular Catalysis, vol.67, 389-399 (1991)
2) EP 425197 (1990)
3) Ugo Romano et al., Ind. Eng. Chem. Prod. Dev., vol.19, 396-403 (1980)
4) EP 452997 (1988)
5) JP 91190846 (1991)

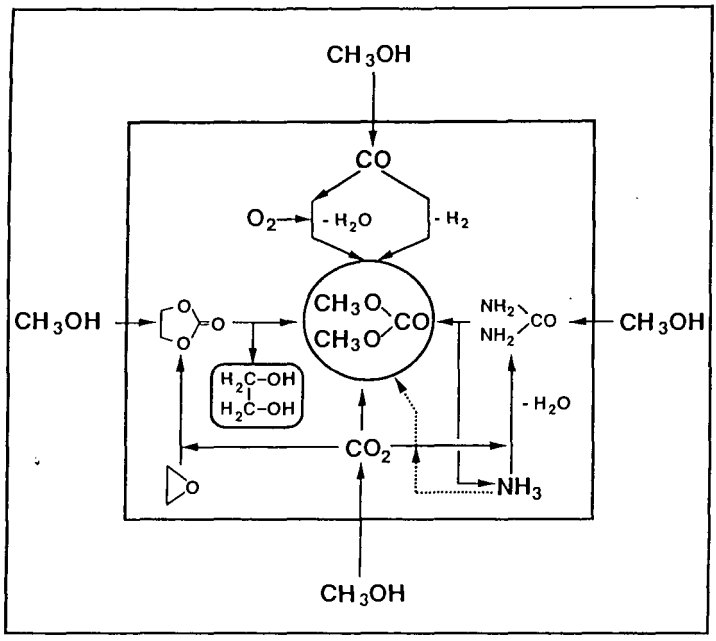

Fig.1 Routes of DMC synthesis without Cl_2CO

DMC:Dimethyl carbonate EC: Ethylene carbonate EG: Ethylene glycol

Fig.2 The conceptual process scheme of the DMC and EG co-production through the transesterification route

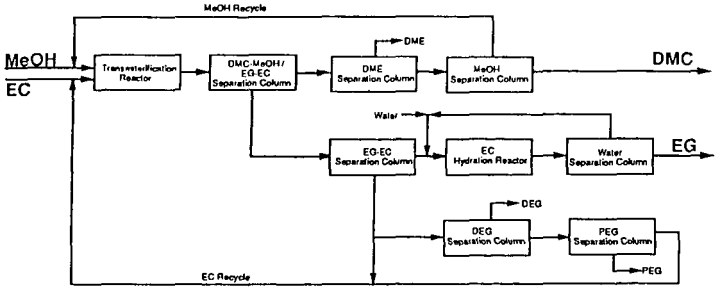

Fig.3 The concrete concept of the DMC and EG co-production process through the transesterification route

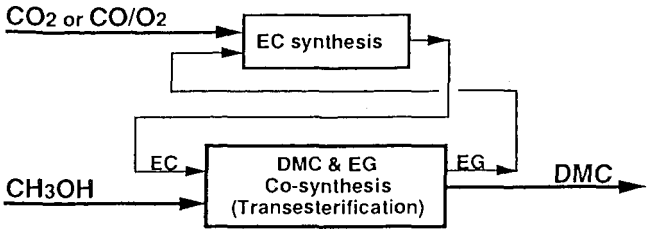

DMC:Dimethyl carbonate EC: Ethylene carbonate EG: Ethylene glycol

Fig.4 The conceptual process scheme of the DMC production without the EG co-production through the transesterification route

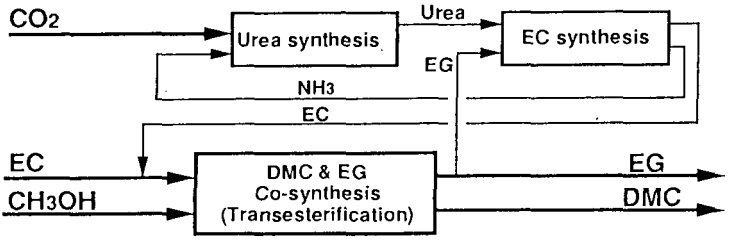

DMC:Dimethyl carbonate EC: Ethylene carbonate EG: Ethylene glycol

Fig.5 The conceptual process scheme to control the EG co-production in the DMC production through the transesterification route

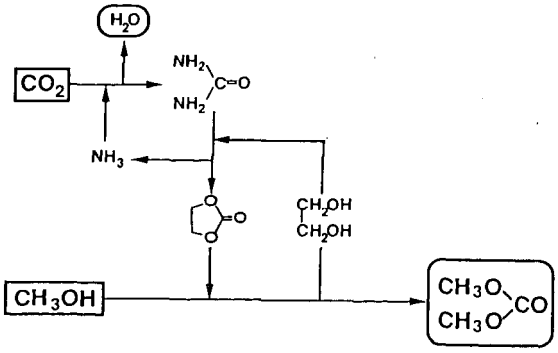

Fig.6 The reaction scheme of DMC synthesis from CH_3OH and CO_2

ISOBUTANOL SYNTHESIS FROM SYNGAS

C.-H. Finkeldei, B. Jaeger, W. Keim, K.A.N. Verkerk
Institut für Technische Chemie und Petrolchemie
RWTH Aachen, Worringerweg 1
52074 Aachen, Germany

Keywords: Isobutanol Synthesis, Synthesis Gas

INTRODUCTION

The hydrogenation of CO to oxygenates is a field of growing interest due to their properties as gasoline blends and the necessity to search for alternatives for future automotive fuels (1). While methanol synthesis from syngas is a well established process, the work on higher alcohol synthesis has been less successful. The demand for MTBE (Methyl-*tert*-butylether) is shifting the interest from higher linear alcohols towards the branched members, mainly isobutanol.

The application of slurry reactors for exothermic reactions has gained considerable interest in the industrial and academic world. For synthesis gas conversions the LPMeOH process by Air Products is a well known example (2). This prompted us to apply this technology to isobutanol synthesis which runs under more extreme reaction conditions.

Because of much easier and faster handling and the necessity to compare results from slurry reactions with the fixed bed reactions cited in literature fixed bed reactor systems are preferred for catalyst development and optimization. The main differences e.g. temperature gradients, backmixing and particle sizes will obviously have major influence on a reaction which mechanistically consists of a network from parallel and consecutive steps (3).

Due to this objective, a fixed bed reactor study has been performed running a typical isobutanol catalyst with different particle sizes and linear velocities. The catalyst developed by us consists of a potassium promoted ZrO_2/ZnO/MnO possessing high activity for isobutanol and methanol (4). These tests provide data to study the behaviour of residence time and temperature on reaction products. Furthermore mass transfer limitations which affect activity and selectivity (5) can be determined.

EXPERIMENTAL AND EQUIPMENT

The catalyst was prepared by coprecipitation of the metal nitrates with potassium hydroxide at 80 °C, keeping the pH constant at 11 ± 0.2. The precipitate was washed, pelletized and dried at 130 °C. After calcination at 450 °C for 3 hours (heating rate: 4°/min) the resulting catalyst was powdered, pressed and sieved to sizes of 0.25-0.50 mm and 1.60-2.0 mm.

For catalytic testing a continuous lab scale unit was set up which can be operated at temperatures up to 500°C and pressures up to 40 MPa. The unit was constructed to switch directly from fixed bed to slurry reactor. A Process management system and on line GC analysis with gas partitioner as well as an automatic product sampler for off line analysis allows continuous operation.

Catalyst activations and reactions have been carried out in a fixed bed reactor from stainless steel with an inner diameter of 9 mm. Catalyst particles have been mixed with an equal amount of copper particles of the same size. Glass particles were added on top as a preheating zone.

The catalyst was activated in situ by pressurizing with hydrogen (30 $Nl \cdot h^{-1}$, 3 MPa) and heated to 225 °C with a rate of 4°/min keeping this temperature constant for 120 min. Subsequently the reactor was pressurized with H_2/CO (1/:1) to 25 MPa while temperature was increased up to reaction conditions with 4°/min.

All reactions were conducted at 25 MPa varying temperature from 430 °C to 370 °C in steps of 30°. Afterwards the measurements at 430 °C were repeated to test reproducibility. At each temperature linear gas velocity was changed in six steps from 24 to 227 $Nl \cdot h^{-1}$. All setpoints were allowed to come to steady state for 75 min. Then the first on line measurement was started followed by collecting one off line sample. A second on line measurement 75 minutes later ended each analysis.

Using this procedure, four test runs have been performed changing bed volume from 2 ml to 4 ml of catalyst and particle sizes from 0.25-0.50 mm to 1.60-2.00 mm.

RESULTS AND DISCUSSION

Typical reaction conditions of the potassium promoted ZrO_2/ZnO/MnO catalysts are above 400 °C. Data to show yields of typical products from fixed bed reactions are given in Table 1. Runs up to 415 °C using a 300 ml CSTR with decalin as inert liquid proved the possibility to perform the isobutanol synthesis under slurry conditions. The advantage of removal of exothermic heat by an inert liquid is diminished by approaching the critical temperature. The differences in heat removal between decalin and the syngas itself become very small in high temperature reactions (6).

The fixed bed reactor study resulted that the CO conversion towards alcohols shows a clear dependence upon variation of particle size. All measurements show that activity increases with decreasing particle size which can be interpreted as mass transfer limitation by porous diffusion.
As presented in Figure 1, CO conversion to isobutanol is showing this behaviour in a typical way. Activity increases with increasing temperature following Arrhenius' law. The smaller particle sizes show higher conversions than the larger ones which is an effect of mass transfer limitation. The difference in activity between the two particle sizes grows with temperature due to the temperature dependence which is smaller for mass transfer than for chemical reaction kinetics.
The opposite behaviour can be observed in for the CO conversion to methanol (Figure 2). The activity decreases with temperature which can be explained through an approach to chemical equilibrium. At higher temperatures the values are close to equilibrium and no dependence on residence time can be seen. The measurement at 370 °C shows the characteristics discussed above reaching a steady state value at long residence times in the catalyst bed.
Film diffusion might be an additional limiting step in heterogeneously catalyzed reactions. The influence of film diffusion increases with temperature in the same way as porous diffusion and decreases with linear velocity by reducing laminary films covering the catalyst pellets. Figure 3 exhibits that film diffusion has no influence on CO conversion to isobutanol at 370 °C and only little effect at 430 °C.
The most accepted reaction network for higher alcohol synthesis given by Klier at al. for cesium promoted Cu/Zn-oxide catalysts describes the mechanistic differences between the reaction paths to methanol and isobutanol (3). The first step in higher alcohol synthesis is hydrogenation of CO to a surface intermediate which is very similar to methanol. Linear primary alcohols are built by linear chain growth including CO insertion steps. Isobutanol and 2-methylbutanol-1 origin from β-addition including aldolic condensation. Formation of 1-propanol can be reached via both pathways (Scheme 1).
Isobutanol and 2-methylbutanol-1 do not undergo consecutive reactions following this network. They cannot react further in aldolic condensations and the probability of linear chain growth is low. On the other hand the linear alcohols are able to undergo linear chain growth as well as β-addition.
The CO conversions to the afore mentioned alcohols ethanol, 1-propanol and 2-methylbutanol-1 are plotted in Figures 4, 5 and 6. The branched alcohol 2-methylbutanol-1 shows similarities to the conversion to isobutanol with an increasing activity with temperature (Figure 4). The conversions to ethanol (Figure 5) and 1-propanol (Figure 6) show a similar behaviour as described for methanol. They exhibit a lower activity at higher temperature and seem to be independent from linear gas velocity at 430 °C.

CONCLUSIONS

The fixed bed reactor study with the potassium promoted ZrO_2/ZnO/MnO catalyst proved that mass transfer limitations occur at high temperatures even with lab scale particle sizes of 1.60-2.0 mm. Further it could be shown that CO conversion to methanol follows an equilibrium behaviour at higher temperatures, whereas isobutanol does not. For the conversion towards linear alcohols a similar behaviour as observed for methanol was found, where 2-methylbutanol-1 follows the characteristics as pointed out for the other branched member isobutanol.
Future studies adress a further optimization of the ZrO_2/ZnO/MnO system in order to achieve milder reaction conditions which will benefit slurry reactor operations.

ACKNOWLEDGMENT

We thank the US Department of Energy and Air Products and Chemicals, Inc. for the support of this work.

LITERATURE

(1) R.R. Chianelli, J.E. Lyons, G.A. Mills, Catal.Today, 22, 361-396 (1994).
(2) G.W. Roberts, D.M. Brown, T.H. Huisung, J.J. Lewnard, Chem. Eng. Sci., 45(8), 2713-2720 (1990).
(3) K.J. Smith, C.-W. Young, R.G. Herman, K. Klier, Ind. Eng. Chem. Res., 30, 61-71 (1991).
(4) W. Falter, W. Keim, Catal. Lett., 3, 59-64 (1989).
(5) H. Berndt, V. Briehn, S. Evert, D. Gutschick, W. Kotowski, Catal. Lett., 14, 185-195 (1992).
(6) C.-H. Finkeldei, PhD Thesis (submitted), RWTH Aachen (1996).

T [°C]	370		430	
GHSV [h^{-1}]	12000	23250	12000	23250
STY [g/(l·h)]				
Methanol	478	748	242	516
Ethanol	37	43	17	30
1-Propanol	34	38	15	29
Isobutanol	34	35	176	265
2-Methylbutanol-1	11	12	19	29
U_{CO} [%]	25	16	48	42
S_{CO2} [%]	50	39	56	49

Table 1. Space time yields to alcohols with ZrO_2/ZnO/MnO/K catalyst in fixed bed reactor (V_{Cat} = 4 ml, Particle size: 0.25-0.50 mm)

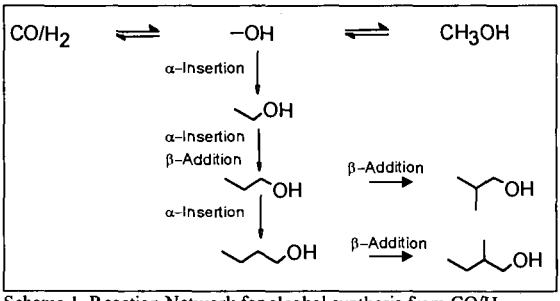

Scheme 1. Reaction Network for alcohol synthesis from CO/H_2

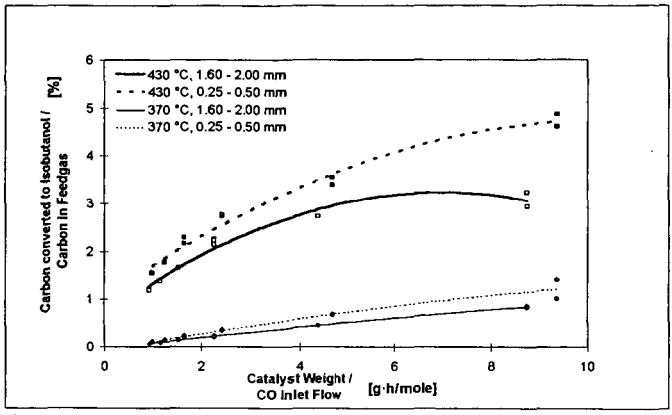

Figure 1. Effect of particle size on CO conversion to isobutanol (V_{Cat} = 4 ml)

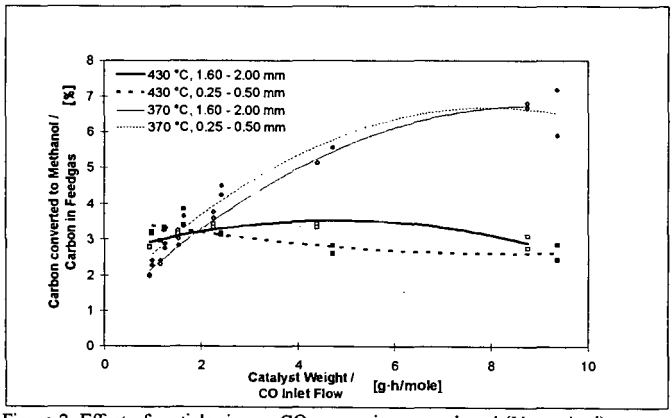

Figure 2. Effect of particle size on CO conversion to methanol (V_{Cat} = 4 ml)

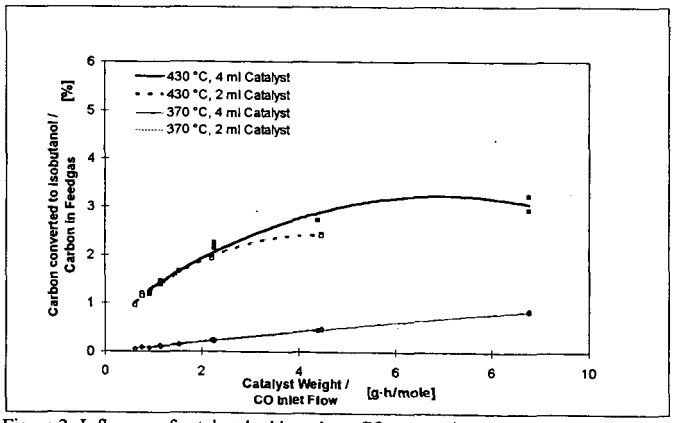

Figure 3. Influence of catalyst bed length on CO conversion to isobutanol (Particle Size: 1.60-2.00 mm)

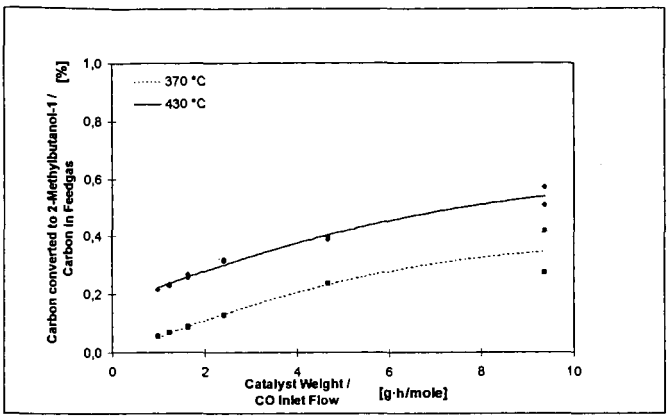

Figure 4. CO conversion to 2-methylbutanol-1 (V_{Cat} = 4 ml, Particle Size: 0.25-0.50 mm)

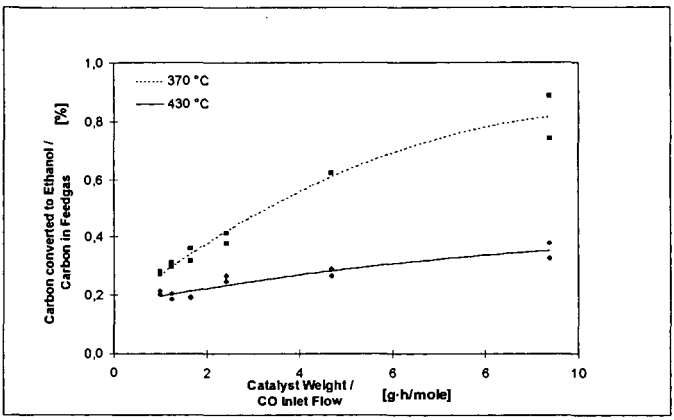

Figure 5. CO conversion to ethanol (V_{Cat} = 4 ml, Particle Size: 0.25-0.50 mm)

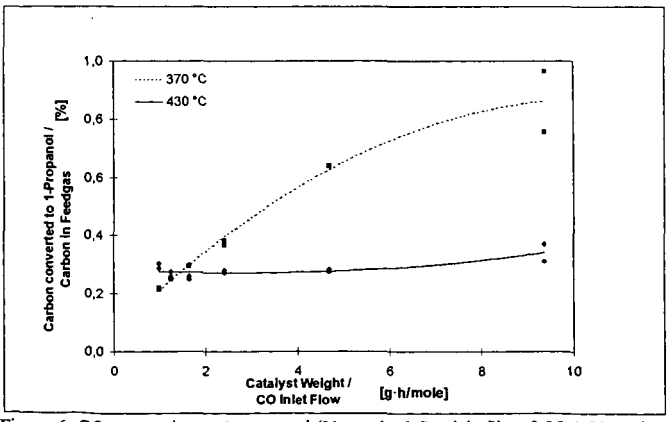

Figure 6. CO conversion to 1-propanol (V_{Cat} = 4 ml, Particle Size: 0.25-0.50 mm)

METHANOL vs ETHANOL -- '96

G. R. James, Paul T. Richards,
William E. Schaefer and Steven A. Wilmes
James Chemical Engineering, Inc.
110 South Road, Groton, Connecticut 06340

Keywords: Methanol, Ethanol, Manufacture

The objects of this paper are:

- To review the manufacture of ethanol and methanol.
- To compare current costs of manufacture.
- To look at current use situation.
- To comment on the current government subsidies for methanol and ethanol produced from renewable resources.
- To consider the possibilities of making methanol and ethanol from various renewable resources.

METHANOL

Methanol, known as "Wood Alcohol" for generations, was initially produced as a by-product from the destructive distillation of wood. Pyroligneous liquor, from heating wood in the absence of air, contains some 4 percent methanol and 7 percent acetic acid. Thus, wood produced the majority of methanol (and other by-products such as charcoal and fuel gas) until the mid 1920's.

Synthesis of methanol directly from H2 and CO appeared in the 1920's (in some cases methanol was a step in the purification of H2/N2 mixtures on route to ammonia synthesis). Methanol is still made directly from H2 and CO, which can be made from any hydrocarbon source. At present, natural gas is the major source, however, coal, oil, solid waste, and wood can and are being used to make methanol.

Methanol use (and price) have climbed, particularly in the past few years as shown in Figure #1. Figure #1 also illustrates that MTBE has been the significant driver of methanol demand in recent years.

The overall methanol market in the U.S. is expected to continue increasing by perhaps 10% in the next four years. At the same time, because of gas limitation in the U.S., imports are projected to increase from low priced gas locations with relatively low shipping costs to the U.S.

MTBE, the major driver in the past few years, has recently suffered some setback but is expected to continue growing at a moderate rate instead of the explosive rate of 1990 through 1995. The ETBE/Ethanol situation, briefly discussed below, has and will have considerable effect on the MTBE and methanol demand.

Federal Tax Credits in the past years for so-called renewable feed based fuel and gasoline additives (currently 54¢/gal. for ethanol and 60¢ for methanol) from 1978 raised production of ethanol from 800,000 short tons to 3,500,000 short tons by 1984. The credits or subsidies boosted the uneconomic use of corn based ethanol (food to fuel) but, unfortunately, did nothing for the biomass to methanol industry which makes considerable sense in the U.S. for several reasons:

1. Biomass* is available up to a large percent of our fuel use.
2. Methanol produces the most economical fuel oxygenate, MTBE.
3. Methanol itself is an efficient, clean burning fuel. As the biomass to fuel industry develops, it will compete with gasoline with no subsidy.

*Biomass includes:
- Solid waste
- Wood
- Agricultural residues (see Table 5)

ETHANOL

Known as "Grain Alcohol" for the millennia, ethanol has been the basis of recreational beverages forever. It can be made from fruit or sugar containing materials such as

molasses. For fuel use in the USA, it is made from starchy materials such as corn, barley and sorghum. These are all renewable resources and require, for example, about 0.38 bushel of corn per gallon of 100% ethanol. There are various by-products depending upon which system is used.

The "Wet Mill" system produces by-products such as germ, gluten and a small amount of CO2. The "Dry Mill" process produces DDGS (an animal feed supplement) and a small amount of CO2. There are disagreements in the industry as to which process is most economical. Apparently, it depends largely on the return from by-products at any particular time in the overall economy.

Ethanol is also made from petroleum sources by reaction of ethylene to ethyl sulfates and then hydrolysis to crude ethyl alcohol and dilute sulfuric acid (which is then concentrated for re-use). Another process produces ethanol directly from ethylene via hydration over a catalyst.

Subsidies to the ethanol industry have resulted in rapid changes in the past 15 years. Plant capacity in 1979 of only 20 MM gallons PA became 750 MM gallons PA in 1986 and in 1994 was some 1,400 MM gallons (renewable resource based). At the same time, because of variations in the cost of grain, raw materials (approximately 45% in 1994) and apparent reduction in demand (July 1994 data show 8% reduction in demand over 1993), many U.S. Government loan guaranteed ethanol plants have had difficulty.

The dramatic changes in ethanol demand in the USA over the last 30 years are illustrated in Figure #2.

In the recent pase two things have happened to the ethanol/fuel industry:

1. The corn price has gone up from $2.75 in August 1995 to a current price of $3.90/bushel. At .38 bushels per gallon, this equals some 38¢ per gallon net increase (see Figure 9).
2. The public is at last becoming aware of the give-away of public funds by both political parties to corporations using corn uneconomically to make ethanol.

PRODUCTION COSTS

Methanol

Although methanol can be produced from various raw materials, natural gas remains the major raw material for production of methanol as illustrated in Figure #3.

This, of course, is the result of lower capital and operating costs for natural gas based methanol production versus methanol produced from other feedstocks as shown in Figure #4.

The result is that locations with low cost natural gas are able to make methanol and ship it to markets. This provides a means of using remote natural gas and shipping it to market as methanol for low polluting direct fuel use or as a raw material for MTBE (36% methanol), the leading current gasoline additive.

If it were decided to make methanol from wood, then costs might be some $200/Ton or $80.00/Ton above the cost from natural gas (approximately 25¢ per gallon above natural gas cost). Given the government tax credit of 60¢ per gallon for methanol made from sources other than petroleum, natural gas or coal, production from wood may be a very attractive option.

Ethanol

Assume corn as the feed stock and other utilities as follows:

Steam	$6.00/2000 lb. ton
Power	$0.05/KWH
Corn	$2.25/bushel [now $3.90]
By-product Sales	65% of corn cost (Wet Mill)*
	50% of corn cost (Dry Mill)*

Depreciation, Taxes, Insurance and Maintenance = 18% PA

*Assume 50% increase in by-product return with $3.90/bushel corn.

Capital costs versus plant capacity are as given in Figure #5 for methanol plants based upon conventional reforming of natural gas, wet mill ethanol process plants, and dry mill ethanol process plants. Then production costs versus plant capacity are as given in Figure #6.

Thus, methanol can be made from natural gas ($2.00 /MM BTU Gas) versus ethanol from corn ($2.25/bushel) [$3.90/bushel] for approximate prices shown in Table 1.

However, if corn based ethanol receives 54¢ per gallon credit, in the $2.25/bushel corn it is somewhat less expensive than methanol per gallon. Also, since methanol has only 73% of the heating value of ethanol, ethanol should then win hands down as a direct fuel.

On the other hand, if renewable resourced methanol were used at 78¢ per gallon with a 60¢ per gallon credit, it would compete well with 98¢ ethanol (i.e. 78 - 60 = 18¢ methanol versus 98 - 54 = 44¢ ethanol). Also, methanol is 50% oxygen versus ethanol at 34.7%. Thus, if the water separation problem with direct methanol addition is solved with other additives, oxygen addition is easier with methanol.

Both the above paragraphs are considerably changed by the current $3.90 per bushel corn price. Thus, methanol without the tax credit is clearly ahead of ethanol on price at $3.90/bushel for corn with the tax credit (see Table 1 and Figure 9).

MTBE and ETBE

Major gasoline additives containing methanol and ethanol are MTBE (Methyl Tertiary Butyl Ether) and ETBE (Ethyl Tertiary Butyl Ether).

Table 2 shows the cost of production for MTBE based on:
1. approximate cost of methanol production at 50¢ per gallon
2. current methanol market price of $.45 per gallon
3. subsidized methanol price of $.78* - .60 (tax credit) = 18¢ per gallon

*Methanol from renewable resources (biomass)

The same table also shows the production cost of ETBE based on:
1. approximate cost of ethanol production at $1.10 per gallon [1.35]*
2. subsidized price of $1.10 [1.35] - .54 (tax credit) = 56¢ per gallon [81¢]

*[ ] = based on corn at $3.90/bushel

Figure #7 is a plot of estimated production costs of MTBE and ETBE versus plant capacity showing the variation of production costs with ethanol / methanol feedstock prices. It shows relative per ton costs of MTBE (36% Methanol) and ETBE (45% ethanol). It does not show the effect of oxygen content on RFG mixtures. Oxygen contents are as follows:

Ethanol	- 34.7%
MTBE	- 18.2%
ETBE	- 15.7%

Thus, for 2.0% and 2.7% oxygen mixtures the costs per gallon of RFG are shown in Table 3 for Ethanol, ETBE and MTBE.

In spite of the above figures, which show that ethanol is by far the most economical oxygenate of these three, particularly with the U.S. Government subsidy and other State benefits, and that ETBE (with the Tax Break) and MTBE are quite competitive, the published information to date shows that marketers are choosing MTBE by some 80% to 10% with another 10% undecided. There is some indication that ethanol may be in short supply, however, prices do not show as much variation in ethanol price as has occurred in methanol, for example. Thus, a more important consideration for ethanol may be the vapor pressure effects in summer and the problems with switching from one oxygenate to another as well as the question of who makes which material and whether blenders are concerned with cost of production or market price.

US Gulf Coast market prices for MTBE and Ethanol are illustrated in Figure #8.

ENERGY USE

A brief review of the cost of energy use in the manufacture of ethanol and methanol (see Table 4) indicates that per gallon of either energy costs are similar neglecting the energy required to make corn fed into the ethanol process.

While manufacture of methanol from natural gas seems to use the least energy, methanol from wood (including the wood), costs only 40% more for energy than the dry mill ethanol system (excluding the cost of corn).

Figures prepared by the U.S. Dept. of Energy indicate that some 40 quadrillion BTU/year can be available through wood utilization in our forests. Another 4.2 quads is available from forest residues. Of this, the Department of Energy estimates that 6 quads can be captured. Other agricultural residues and municipal solid waste add up to some 4 quads for a total of some 10 quads that can be converted to ethanol or methanol.

Table 5 shows the estimated production of ethanol or methanol from these materials. The projected amounts are 54 x 10^9 gallons of ETOH in the year 2000 or 154.7 x 10^9 gallons of MEOH in the year 2000 - (equals 8.7 quads of energy). Total energy use in the U.S. in 1992 has been estimated at 82 quads.

CONCLUSIONS

1. Methanol can be made for about half the cost of ethanol per gallon.
2. More methanol than ethanol (about 3 times as much) can be made from renewable raw materials available.
3. Subsidies and loan guarantees to ethanol producers have benefited a few but by and large they have not brought about a strong ethanol based fuel sector. (Note the upset in ethanol caused by the high price of corn this year.)
4. It appears that encouraging ethanol production from corn over methanol from natural gas actually results in use of more fossil fuel for energy than if the energy were used directly. Further, it appears that methanol from wood using 16¢ worth of power per gallon will consume less fossil fuel energy than ethanol from corn (20¢/gal., excluding the energy used in growing the corn).
5. The current tax subsidy for renewable resource based methanol and MTBE, the use of wood as a feedstock may be an attractive option.
6. Use of corn to make fuel seems to be a waste. Corn is a food. It could be used to feed people in areas of the world suffering from lack of basic food.

LITERATURE CITED

1. Wood, P.R., "New ETOH Process Technology Reduces Capital and Operating Costs for Ethanol Producing Facilities", PSI, Memphis TN, *Fuel Reformulation*, July/August 1993.
2. James, G.R., P.T. Richards and W.E. Schaefer, "MEOH From Gas, Coal or Residual Oil", presented at the Asian Methanol Conference, Singapore, (1993).
3. James, G.R., B.L. Huson and P.T. Richards, "MEOH and MTBE - Their Relationships in Manufacturing and Marketing", presented at The Fertilizer Association of Indonesia Conference (APPI) (1991).
4. "21st Century Fuel News", Hart Publications, November 1994 and "Oxy Fuel News", Hart Publications, October 1994.
5. "21st Century Fuels", Hart Publications, May & June 1994, February & April 1996.
6. Kane, S. and J. Reilly, "Economics of ETOH Production in the U.S.", U.S. Dept. of Agriculture Economic Report #607, March 1989.
7. Candella, J.P., "Fuel Ethanol: Profit Margins and Product Flexibility for the Gasoline Marketer", presented at the National Conference on Fuel Ethanol, Washington, D.C. (1988).
8. U.S. Department of Energy Fact Book, 1980.
9. "Corn Fertilizer Information", Fertilizer Round Table, Atlanta, GA, 1982.
10. Unzelman, George, "U.S. Gasoline Composition: '90 Decade and Horizons", *Fuel Reformulation*, May/June 1994.
11. Singh, Margaret and Barry McNutt, "Energy and Oil Input for Producing Reformulated Gasolines", *Fuel Reformulation*, Sept./Oct. 1993.
12. Haigwood, Burl, "September/October Fuel Reformulation MTBE Survey", *Fuel Reformulation*, Sept/Oct. 1993.

13.Office of Highway Information Management; Highway Funding and Motor Fuels Division "Highway Taxes and Fees", May 1995.
14.Federal Register Vol. 60 No. 151 Rules and Regulations, August 1995.
15.Chas. A. Stokes, Sc.D, P.E., "The Methanol Industries Missed Opportunities", 1995 World MEOH Conference, Phoenix, Arizona
16.Albert J. Smith, III, Chas. A. Stokes and Peter Wilkes, "The Rebirth of Methanol From Biomas", World MEOH Conference, Atlanta, GA, November 29 - December 1, 1993.
17.Refining Economics Report, February 1996.
18.Hart's "Octane Week", April 29, 1996, Vol. XI, No. 18.

TABLE 1 CORN AT $2.25 / BUSHEL				
CAPACITY	METHANOL ¢/GAL.	ETHANOL ¢/GAL.		AVERAGE DELTA ¢
		WET MILL	DRY MILL	
500 STD	64.50	[135.00] 100.00	[140.00] 99.00	[73.00] 35.00
1000 STD	53.25	[126.00] 91.00	[133.00] 92.00	[76.20] 38.30
1500 STD	48.61	[122.00] 87.00	[130.00] 89.00	[77.40] 43.40
[@ $3.90/bushel. Includes 50% increase in by-product sales price]				

TABLE 2 MTBE and ETBE PRODUCTION COST					
				MTBE	ETBE
	PLANT CAPACITY (STD)			607	704
	Units	Unit Price	Unit Cons.	Annual Cost (1000's)	Annual Cost (1000's)
RAW MATERIALS					
Isobutylene for MTBE	Ton	$200	0.64	$25,640	
Isobutylene for ETBE	Ton	$200	0.55		$25,555
Methanol	Ton		0.364	see below	
Ethanol	Ton		0.45		see below
Catalyst	Ton	$4,550	0.00018	$164	$190
UTILITIES					
Steam	Lb	$0.006	1,000	$1,202	$1,394
Power	kwh	$0.05		$80	$93
Cooling Water	1000 gal	$0.113		$97	$113
LABOR					
Operating	MH	20.00	24,000	$480	$480
Overhead (150%)				$720	$720
REPAIR & MAINTENANCE				$698	$768
LABORATORY, SUPPLIES, & MISC.				$175	$175
TOTAL OPERATING COST				$29,256	$29,488
INTEREST (10% Debt)				$1,396	$1,536
TAXES & INSUR. (2%)				$465	$512
DEPRECIATION				$2,327	$2,560
NET PRODUCTION COST WITHOUT MEOH/ETOH				$33,445	$34,095
PRODUCTION COST / ST MTBE WITHOUT MEOH				$166.96	
PRODUCTION COST / ST ETBE WITHOUT ETOH					$146.76
PROD. COST / ST MTBE - MEOH AT $0.50 / GAL.				$221.56	
PROD. COST / ST MTBE - MEOH AT $0.45 / GAL.				$216.10	
PROD. COST / ST MTBE - MEOH AT $0.18 / GAL. (.78-.60)				$186.62	
PROD. COST / ST ETBE - ETOH AT $0.95 / GAL. [at 1.35/gal]					$276.11 [330.57]
PROD. COST / ST ETBE - ETOH AT $0.39 / GAL. (with $0.54/gal Tax Subsidy) [$0.81/gal.]					$199.86 [257.05]

TABLE 3 CORN AT $2.25/BUSHEL		
	2% ¢/Gal.	2.7% ¢/Gal.
Ethanol - Wet Milled	[7.25] 5.24	7.08
(TB)	[4.15] (3.23)	(4.36)
Dry Milled	[7.66] 5.30	7.16
(TB)	[4.55] (3.28)	(4.44)
ETBE - (ETOH Cost)	[14.04] 11.75	15.86
(ETOH, TB)	[10.92] (8.49)	(11.46)
MTBE - (MEOH Cost)	8.12	10.95
(MEOH/TB)	(6.84)	(9.23)
TB = With Tax Break [ ] = Corn at $3.90/bushel		

TABLE 4 ENERGY COST PER GALLON OF PRODUCT			
	$/GAL.		NET CORN COSTS
Ethanol Wet Mill Steam & Power Dry Mill Steam & Power	 0.24* 0.20*	*Neglects corn use and energy required to produce it.	 30¢/gal. [52] 45.5¢/gal. [79]
Methanol From Natural Gas Natural Gas & Power From Wood	 0.186** (.178 from gas) 0.28** (.12 from wood)	**Includes Natural Gas at $2.00/MM BTU and wood at $20.00/ Ton	
[ ] = corn at $3.90/bushel			

TABLE 5 Projected Maximum Alcohol Production from U.S. Biomass Resources (Source: U.S. Department of Energy)								
	(Billions of Gallons/Year)							
	1980		1985		1990		2000	
	ETOH	MEOH	ETOH	MEOH	ETOH	MEOH	ETOH	MEOH
Wood	23.5	86.3	21.8	80.2	20.2	74.2	25.8	95.0
Agricultural residues	9.1	33.4	10.3	38.1	11.3	41.5	13.1	48.1
Grains								
Corn	2.3		2.1		0.9			
Wheat	1.2		1.4		1.6		2.0	
Grain Sorghum	0.4		0.3		0.3		0.3	
Total Grains	3.9		3.8		2.8		2.3	
Sugars								
Cane			0.2		0.7		0.7	
Sweet Sorghum			0.2		3.0		8.3	
Total Sugars			0.4		3.7		9.0	
MSW	2.2	8.6	2.3	9.2	2.5	9.9	2.9	11.6
Food Processing Waste								
Citrus	0.2		0.2		0.3		0.4	
Cheese	0.1		0.1		0.1		0.2	
All Other	0.2		0.3		0.3		0.3	
Total Processing Waste	0.5		0.6		0.7		0.9	
TOTAL	39.2	128.3	39.2	127.5	41.2	125.6	54.0	154.7
Based on following biomass-alcohol conversion factors: Wood and agric. residues-173 gal methanol per dry ton, 47 gal ethanol per dry ton. Corn-2.6gal ethanol per bushel. Wheat-2.7 gal ethanol per bushel. Grain sorghum-2.6 gal ethanol per bushel. Sugars-136 gal ethanol per ton fermentable sugars. MSW-100 gal methanol per dry ton, 25 gal ethanol per dry ton. Citrus waste-107 gal ethanol per dry ton. Cheese waste-95 gal ethanol per dry ton. Other food processing waste-90 gal ethanol per dry ton.								

Figure #1: US METHANOL CONSUMPTION

By End Products

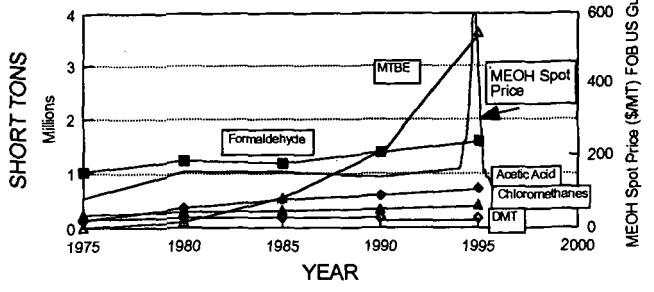

Methanol consumption from other markets range from 0.82 - 1.35 MM short tons Per Year
Total methanol consumption in the US in 1995 approximately 8 MM short tons

Figure #2: US ETHANOL CONSUMPTION

By End Product

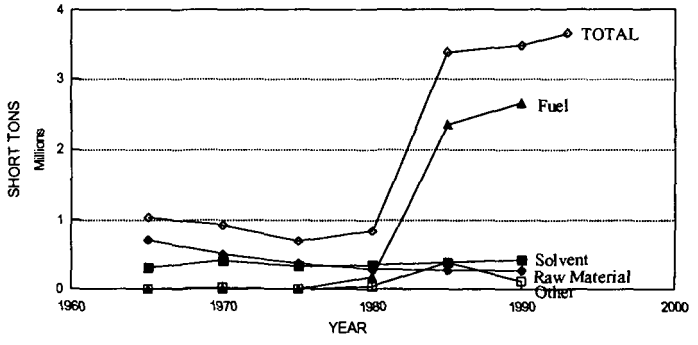

Figure 3: WORLD METHANOL PRODUCTION

BREAKDOWN BY FEEDSTOCK

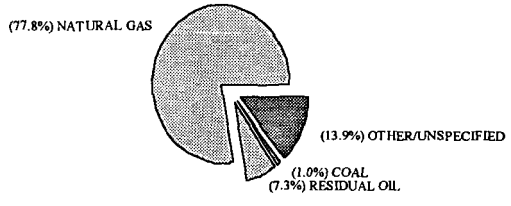

Source: Various

Figure #4: MEOH PRODUCTION COST VS. FEEDSTOCK COST

NATURAL GAS, COAL, WOOD, & RESIDUAL OIL

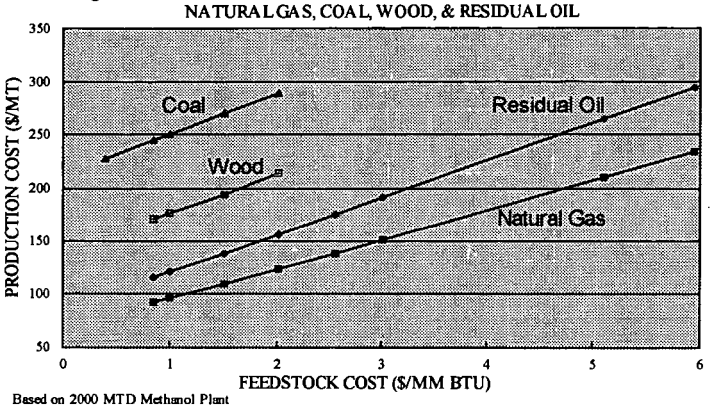

Based on 2000 MTD Methanol Plant
Coal - $10 to $51/MT : Oil - $5 to 35/BBL

Figure #5: PLANT CAPITAL COSTS VERSUS CAPACITY

METHANOL & ETHANOL

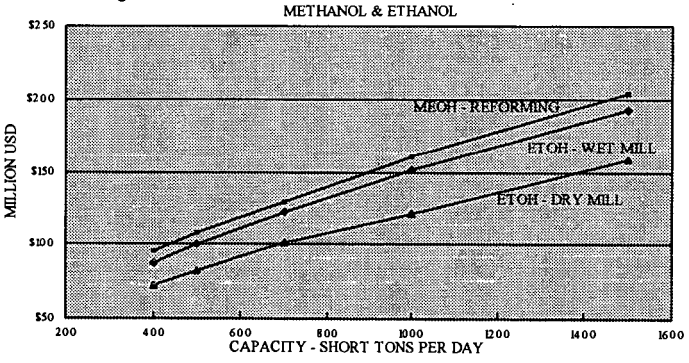

Figure #6: PRODUCTION COSTS VS PLANT CAPACITY

METHANOL & ETHANOL

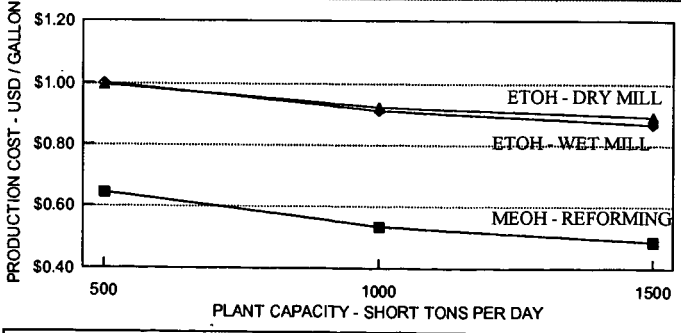

Ethanol production cost based upon $2.25 per bushel corn price
See table 1 for $3.90 per bushel corn

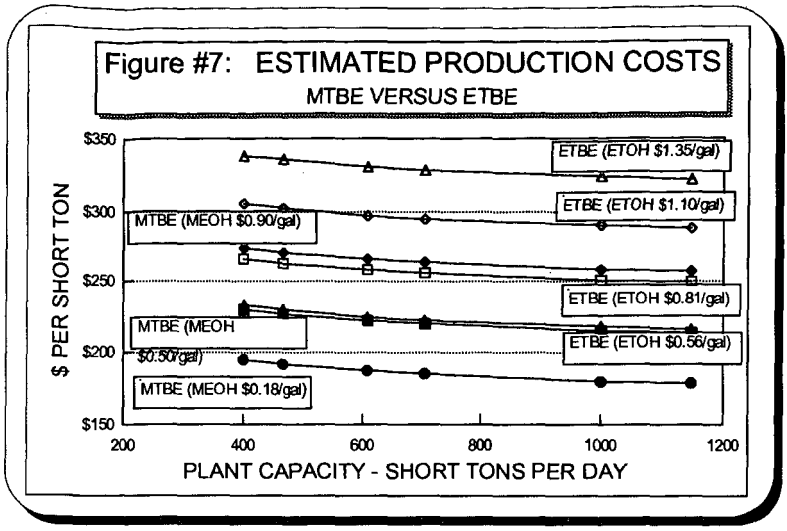
Figure #7: ESTIMATED PRODUCTION COSTS
MTBE VERSUS ETBE
$ PER SHORT TON
$350
$300
$250
$200
$150
200
400
600
800
1000
1200
PLANT CAPACITY - SHORT TONS PER DAY
ETBE (ETOH $1.35/gal)
ETBE (ETOH $1.10/gal)
MTBE (MEOH $0.90/gal)
ETBE (ETOH $0.81/gal)
MTBE (MEOH
$0.50/gal)
ETBE (ETOH $0.56/gal)
MTBE (MEOH $0.18/gal)

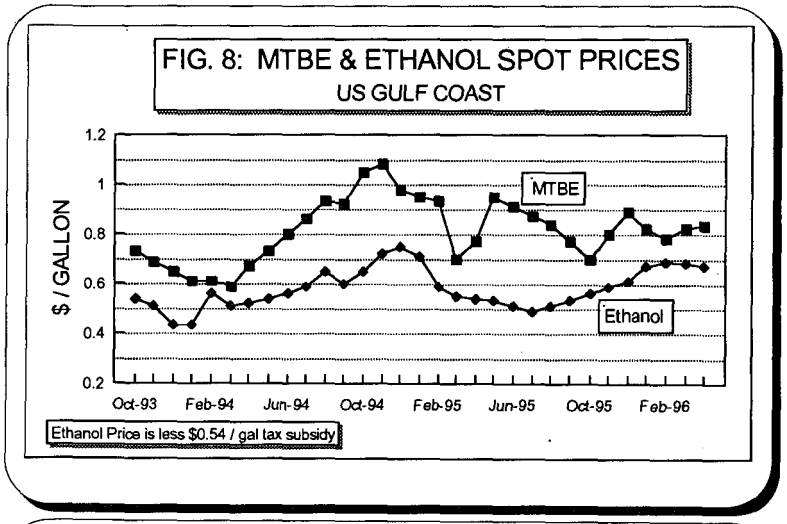
FIG. 8: MTBE & ETHANOL SPOT PRICES
US GULF COAST
$ / GALLON
1.2
1
0.8
0.6
0.4
0.2
Oct-93
Feb-94
Jun-94
Oct-94
Feb-95
Jun-95
Oct-95
Feb-96
MTBE
Ethanol
Ethanol Price is less $0.54 / gal tax subsidy

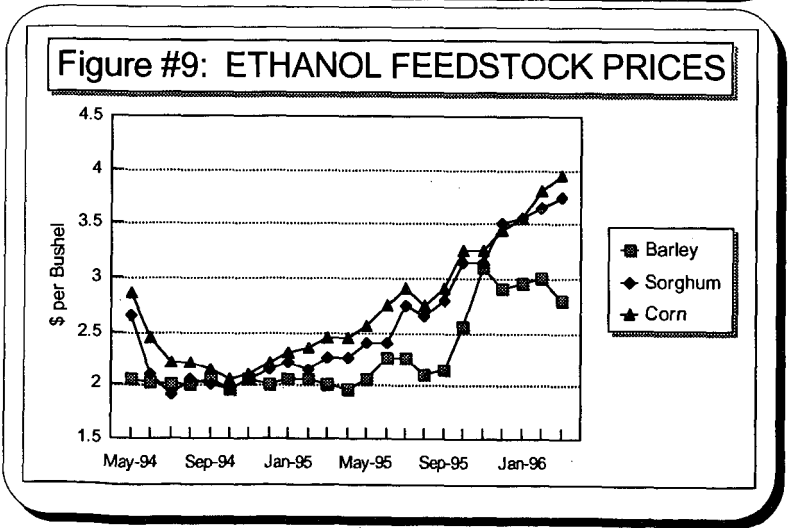
Figure #9: ETHANOL FEEDSTOCK PRICES
$ per Bushel
4.5
4
3.5
3
2.5
2
1.5
May-94
Sep-94
Jan-95
May-95
Sep-95
Jan-96
Barley
Sorghum
Corn

Maximizing the FCC's Potential for RFG Production

Lark E. Chapin
Stone & Webster Engineering Corporation
1430 Enclave Parkway
Houston, TX 77077

Keywords: Propylene, Catalytic Cracking , RFG

INTRODUCTION

The Fluidized Catalytic Cracking (FCC) unit has traditionally been the dominant conversion process in U.S. refineries. It has served as a major source of high octane naphtha for blending into the gasoline pool. With the passage of the Clean Air Act, U.S. refiners are reformulating their gasoline blends utilizing increasing volumes of "clean burning" alkylate and ethers. Both of these premium products use light olefins including propylene as feedstocks. Environmental trends in other major world markets will force much of the world FCC operating capacity to follow the same path.

Concurrently, the petrochemical demand for light olefins, in particular propylene, has outpaced conventional supply routes (ie., steam crackers). Propylene production from steam cracking is highly dependent on the overall economics for ethylene production. Given the current and anticipated demand for propylene relative to ethylene and the fact that the Steam Cracker can not offer the necessary flexibility to modify yields, it is likely that refinery sourced propylene will grow in importance. Obviously, a need for an economical light olefin generating process is required to meet the demand of these light olefins. New catalytic cracking technologies, such as Deep Catalytic Cracking(DCC), appear to be very promising for this application.

DCC is a new commercially proven fluidized catalytic cracking process for selectively cracking a wide variety of feedstocks to light olefins. The technology was originally developed by the Research Institute of Petroleum Processing (RIPP) and Sinopec both located in the Peoples Republic of China. Stone & Webster is the exclusive licensor of this technology outside of China. Currently three units are operating in China and another three are under construction. One of the units under construction is part of a Stone & Webster grassroots DCC complex in Thailand for Thai Petrochemical Industry Co. Ltd.

Although DCC can readily be integrated into either a refinery or petrochemical facility, the intent of this paper is to quantify its impact on the gasoline pool and overall profitability of a U.S. Gulf Coast refinery dedicated to making reformulated gasoline (RFG).

PROCESS DESCRIPTION

DCC is a fluidized catalytic process for selectively cracking a wide variety of feedstocks to light olefins. Propylene yields over 20 wt% are achievable with paraffinic VGO feeds. A traditional reactor/regenerator unit design is employed using a catalyst with physical properties similar to traditional FCC catalyst. The DCC unit may be operated in one of two operational modes: Maximum Propylene (TYPE I) or Maximum Iso-Olefins (TYPE II). Each operational mode utilizes an unique catalyst as well as reaction conditions. DCC Maximum Propylene (Type I) uses both riser and bed cracking at severe reactor conditions while Type II utilizes only riser cracking like a modern FCC unit at milder conditions.

The overall flow scheme of DCC is very similar to that of a conventional FCC. However, innovations in the areas of catalyst development, process variable selection, and severtiy enables the DCC to produce significantly more olefins than FCC. A detailed process description has been published previously[1] and is not included in this paper.

DCC PRODUCT YIELDS

DCC reaction products are light olefins, high octane gasoline, light cycle oil, dry gas and coke. Typical Type I and II DCC yields are shown in the Table 1. Yields for FCC in a maximum olefin operating mode with a low rare earth , high mesopore activity, and high ZSM-5 catalyst are shown for comparison.

Table I
DCC vs. FCC Yield Comparison, wt%

Products	DCC Type I	DCC Type II	FCC
Dry Gas	10.9	5.6	3.2
LPG	41.0	34.2	31.8
Naphtha	26.6	39.2	34.6
LCO/HCO	12.7	15.9	25.2
Coke	8.8	4.6	5.2
Total	100.0	100.0	100.0
Ethylene	6.1	2.3	0.9
Propylene	20.5	14.3	11.4
Butylene	14.3	14.6	11.2
in which $IC_4^=$	5.4	6.1	4.2
Amylene	--	9.8	8.5
in which $IC_5^=$	--	6.5	4.3

Although large amounts of dry gas are produced in the DCC Type I operation it is rich in ethylene and may be desirable for petrochemical enduse. Propylene is abundant in the DCC LPG stream and considerably higher than FCC. The DCC LPG is also rich in butylenes making it an ideal MTBE and/or alkylation feedstock. Of particular interest is the selectivity of both Type I and II towards $IC_4^=$. The ratio of isobutylene to total butylene is much higher for DCC than FCC(38-42 vs. 17-33 wt%). The same result is true for the isoamylene to total amylene ratio. Obviously , this can have a significant impact on downstream MTBE and TAME production capabilities. The high olefin yields are achieved by seleetively overcracking naphtha.

Because of the high conversion, all of the DCC C_5+ liquid products are highly aromatic. Consequently the octane values of the naphtha are quite high: 84.7 MON and 99.3 RON . The BTX content of the naphtha is over 25 wt % making it suitable for extraction. The naphtha will need to be selectively hydrotreated to improve its stability due to the di-olefin content. This is easily accomplished without octane loss.

The LCO will need further upgrading before it can be included in the diesel pool or it can be used as an excellent cutter stock due to its low viscosity and pour point. The HCO and small amounts of slurry oil can go directly to fuel oil blending or be used as hydrocracker feedstock.

CASE STUDY BASIS

In order to illustrate the overall economic impact of adding either DCC Type I or II versus an FCC in a U.S. Gulf Coast refinery dedicated to the production of reformulated gasoline three possible processing options were examined. Each case was analyzed with regard to the disposition of propylene (ie., alkylation or petrochemical sales). An overall onstream factor of 94 % was used for the 100,000 BPD refinery. The production rate was optimized based on producing prime fuels and fuel grade coke from an Arabian Light Crude source. Wright-Killen's 'Refine" model was used to evaluate the different processing scenarios. A simplified overall Block Flow Diagram is shown above.

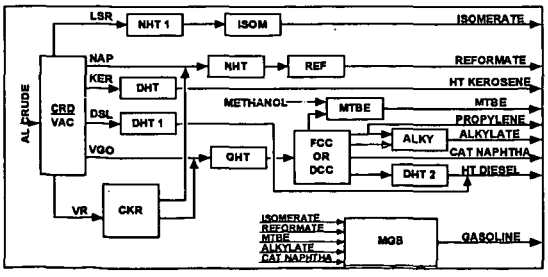

Purchased feedstocks included butanes, methanol and MTBE. The primary products were:

- LPG(C_3/ C_4's)
- Reformulated Gasoline
- Jet/ Low Sulfur Diesel
- Fuel Grade Coke
- Sulfur

The feedstock and product prices are reported in Table 5 which can be found at the end of the paper. These prices represent typical current U.S. Gulf Coast Basis. Product specifications used to constrain the model are reported in Table 6. Key gasoline blending parameters were set so that the resulting reformulated gasoline pool would :

- Not exceed 1 LV% Benzene
- Contain 2 Wt% Oxygen, and
  Meet EPA mandated reductions in emissions

A simple economic evaluation was performed utilizing the following assumptions:

Delta Capital Cost:	Estimated for U.S. Gulf Coast
Project Life:	20 years from completion
Depreciation:	10 years straight line
Salvage Value:	20% of original investment
Tax Rate:	35% starting in year 1
Inflation Rate:	0 %
Feedstock Prices:	Constant based on current U.S. Gulf Coast prices
Product Prices:	Constant based on current U.S. Gulf Coast prices
Delta Utility Cost:	Constant current average prices
Operating Capital:	0
Investment Timing:	All in year 0

The price of propylene was varied from +/- 30% of the base cost to determine the sensitivity to propylene cost.

RESULTS

The following tables summarize the gasoline pool quality, operating severities, revenues,and overall economics for each case. As previously mentioned the price of propylene was varied to determine its impact for the cases where propylene is routed to sales and is shown in Figure 1 later in the paper.

The impact of switching propylene from petrochemical sales to alkylation and ultimately to the gasoline pool is readily apparent in each case. as shown in Table 2. The DCC operation magnifies this effect over the FCC operation. DCC Type I produces the largest amount of propylene and the least amount of gasoline. The isobutane requirment for the cases where the propylene goes to alkylation is quite substantial for the DCC options. In addition, the increased isobutylene yield with both DCC Type I & II significantly reduces the purchased

Table 2
Feedstocks and Products

Feedstocks, BPD	**Base Case FCC**		**Case 1 DCC I**		**Case 2 DCC II**	
C3= Disposition	**Alky**	**Sales**	**Alky**	**Sales**	**Alky**	**Sales**
Crude	100,000 BPD		100,000 BPD		100,000 BPD	
Isobutane	4684	1174	14433	1705	11831	2162
Methanol	342	342	914	914	1042	1042
Purchased MTBE	6105	5533	5041	2972	4755	3184
Products, BPD						
Propylene		2722		9860		7491
LPG (C3 & C4)	4345	4345	5603	5603	6190	6190
Gasoline (RFG)	63716	58240	70462	50625	70940	55869
Low Sulfur Diesel	24712	24712	21615	21615	21220	21220
Jet Fuel	14621	14621	14621	14621	14621	14621
Coke (Ton /day)	820	820	817	817	815	815
Sulfur (Lton/day)	203	203	203	203	203	203
Refinery Fuel (FOEB)	1985	1985	4846	4846	2532	2532

MTBE requirement.. The LPG make also increases significantly with both types of DCC operation. The middle distillate production is relatively constant for each case.

The operating severities for each unit are shown in Table 3. The reformer severity was kept constant for all cases at 97 RON. Although a future case might be warranted where the severity is lowered. The reformer feed was prefractionated to an IBP of 190°F to minimize the benezene precursors. The DCC has a much higher C5+ liquid conversion than the FCC.

Table 3
Operating Severities

Qualities	Base Case FCC		Case 1 DCC I		Case 2 DCC II	
C3= Disposition	Alky	Sales	Alky	Sales	Alky	Sales
FCC/DCC Conversion, vol%	75.8	75.8	85.3	85.3	86.8	86.8
Reformate, RON	97	97	97	97	97	97
Captive MTBE, BPD	1004	1004	2679	2679	3056	3056
Purchased MTBE, BPD	6105	5533	5041	2972	4755	3184

The gasoline pool was constrained to meet Federal Phase 1 RFG specifications and if possible CARB specifications. The purchase of MTBE was limited to a maximum of 2.0 wt% for all cases. The Rvp requirement of 7.1 applies only in the summer months and can be quite difficult to meet. Although pulling all of the normal butane from the pool may seem like the obvious first step it is often not desirable as addition of this blendstock permits the refiner an easy control of his pool Rvp. Alkylating the propylene versus selling it satisfies the more stringent summer Rvp requirement in all cases. The alkylate dilutes the overall pool with its low Rvp. The dilution effect of the alkylate is also evidenced by the reduction in aromatics, olefin and sulfur content of the pool as compared to the cases where the propylene is sold.

Table 4
Gasoline Pool Quality

Qualities	Base Case FCC		Case 1 DCC I		Case 2 DCC 2	
C3= Disposition	Alky	Sales	Alky	Sales	Alky	Sales
RON	95.7	95.7	96.7	97.4	96.3	96.6
MON	86.9	86.4	89.0	87.8	88.5	87.5
FON	91.3	91.1	92.9	92.6	92.4	92.1
RVP	7.1	7.2	6.8	7.2	6.8	7.2
Olefin, vol%	7.9	8.7	6.6	9.2	7.4	9.3
Aromatics, vol%	24.2	26.5	21.9	30.6	22.5	28.6
Benzene, vol%	0.86	0.95	0.63	0.87	0.69	0.88
Oxygen, wt%	2.0	2.0	2.0	2.0	2.0	2.0
Sulfur, ppmw	32	35	34	46	46	57

Does not meet one of the following Federal Phase 1 specifications : 7.1 RVP max 9.1 vol% olefins or 27 vol% aromatics.

Although the aromatic, olefin and Rvp Phase 1 RFG specifications are not met in Cases 1 and 2 where the propylene is sold the reformer severity can be lowered bringing these specifications easily into compliance. For example, when the reformer severity is lowered to 89 and 92 for Cases 1 & 2 respectively the pool specifications are met. The FON drops to 89.5 and 90.0 for Case 1 and Case 2 at these severities.

The T50 and T90 specifications were not evaluated for this study as the 'Refine" model does not accurately account for changes in product distillations. Typically, the T90 specification is one of the most difficult and costly specifications to meet. Complying with this specification will also have a great impact on reducing the T50. FCC gasoline and reformate typically do

not meet the T90 specification and will require further fractionation or processing. This evaluation is outside the scope of this study basis.

ECONOMIC ANALYSIS

The gross profit for each case is shown in the following bar chart. For the cases where propylene is routed to alkylation, both DCC type I and II generate more gross profit than the FCC case. DCC type II is the most favorable option. The gross profit for the cases where propylene is routed to petrochemical sales shows that both DCC Type I and II are more profitable than the base FCC operation. Of the DCC operations, DCC type II again generates the greatest gross profit.

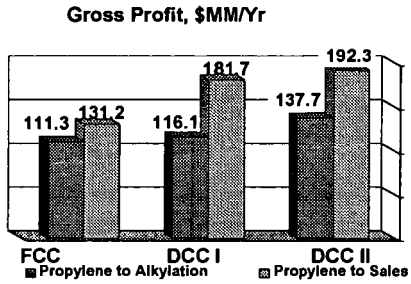

The Internal Rate of Return (IRR), Payout and Net Present Value figures were calculated for the cases where propylene was routed to alkylation or to sales for each type of operation. The analysis showed that for the cases where propylene was routed to alkylation the DCC Type II operation was the most profitable with an IRR of 20.3%. The cases where propylene was routed to petrochemical sales showed that the installation of an DCC unit in place of a conventional FCC was very profitable. The incremental IRR for DCC Type I was 31.1% and 55.6% for DCC Type II. The payout was 2.2 years after tax for DCC Type II and 3.6 years for DCC Type II.

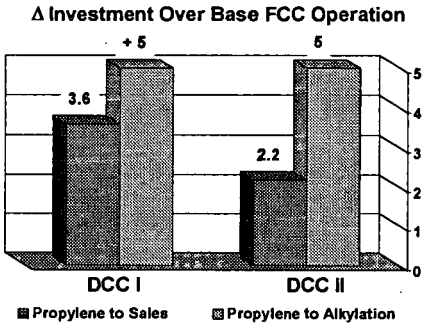

PROPYLENE SENSITIVITY

The price of propylene was varied from +/- 30% of the base price and its impact on the IRR is shown in Figure 1. Even at a propylene price 30% lower than the base value the IRR for DCC Type II is still attractive. The sensitivity to the propylene value is more pronounced for DCC Type I. Although it still appears favorable at propylene values up to 10 % less than the base value.

Figure 1

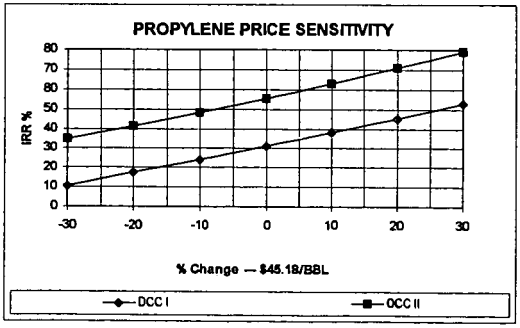

REVAMP ECONOMICS

Work recently completed in Stone & Websters' Milton Keynes office indicates that a revamp of an existing FCC to an equivalent DCC type I operation (most extreme revamp) can be quite attractive. The majority of the revamp costs were found to be in the regenerator and flue gas system to handle the

additional coke burning capacity. Polymer grade propylene was produced for petrochemical sales. A very attractive pretax payback of 1.5 years was found

CONCLUSION

As the price of propylene remains high there will be continued interest in refinery sourced propylene for petrochemical sales. Based on average prices during the last two years, a new DCC plant for production of propylene provides an attractive return on investment. The sensitivity of the project economics to fluctuations in propylene prices is relatively low.

The integration of DCC technology into a refinery offers an atractive opportunity to produce large quantities of light olefins by the conversion of heavy vacuum gas oils. Thus, providing the refiner with the flexibility to produce either polymer grade propylene or premium gasoline blending components (ie. ethers and alkylate).

Acknowledgement

The author would like to thank Mike Dent and Glenn Johnson for their invaluable assistance in the preparation of this paper.

References

1. 'Deep Catalytic Cracking, Maximize Olefin Production", L.Chapin, W.Letzsch. 1994 NPRA meeting AM-94-43.
2. "A New Propylene Production Process from Heavy Gas Oil", J. Fukang, L. Zaiting, W. Xieqing, M.Enze. 1990 NPRA meeting AM-90-40.
3. 'Propylene from Heavy Gas Oils", J. Bonilla, A. Batachari . Stone & Webster 7th Annual Refining Seminar 1995.
4. 'Propylene in West Europe-An Outlook", Andrew Pettman, CMAI Europe. Dec. 1995.
5. 'Catalytic Cracking to Maximize Light Olefins", D. Hutchinson, R. Hood. Association Francaise Des Techniciens et Professionnels Du Petrole, IFP Dec. 1996.

Table 5
Feedstock and Product Pricing*

Feedstocks	$/BBL
Arabian Light	18.47
Isobutane	17.64
Methanol	18.90
MTBE	42.84
Products	
Sulfur (LT)	75.00
Propane	14.35
N-Butane	16.80
Petroleum Coke	25.00
Fuel Gas (FOEB)	9.30
Low Sulfur Diesel	20.89
Kerosine/Jet Fuel	23.12
RFG Gasoline Blend	30.86
Propylene to Sales	45.18

US Gulf Coast Pricing Basis
Sources: The Oil Daily, 28 June 95 & Octane Week, 29 May 95

Table 6
Product Specifications

Propylene	Polymer Grade	
Reformulated Gasoline*	CARB Phase 2 March 1996	Phase 1 Federal Jan 1 1995
• RVP (max)***	7.0	8.0(N) / 7.1(S)**
• FON (min)	91.0	91.0
• Olefins (vol%, max)	6.0	9.2
• Aromatics (vol%, max)	25.0	27.0
• Benzene (vol%, max)	1.0	1.0
• Oxygen (wt%, min)	2.0	2.0
• Sulfur (ppm,wt%)	40	339
Diesel		
• Sulfur (wt%, max)	0.05	
• Aromatics (vol%, max)		
• Cetane No. (min)	40.0	
Jet Fuel		
• Sulfur (wt%, max)	0.3	
• Aromatics (vol%, max)	24.0	

* T50 and T90 specs beyond scope of this evaluation
** (N) Northern States, (S) Southern States
*** Summer Season only

CONTROL AND ORIGIN OF NOx IN THE FCCU REGENERATOR
THE PERFORMANCE OF XNOx-2, A COMMERCIAL NOx REDUCTION CATALYST

A. W. Peters, W. Suárez, Manoj Koranne, Carmo Pereira,
G. D. Weatherbee, Xinjin Zhao, S. Davey, and B. Lakhanpal

Grace Davison, Columbia, MD 21044

Keywords: fluid catalytic cracking unit (FCCU) regenerator, carbon monoxide (CO) oxidation, nitrogen oxide (NOx) reduction

Introduction

In this paper we describe the performance of a NOx control additive for the FCCU regenerator. This formulation reduces NOx and at the same time functions as a CO oxidation promoter. The NOx reduction catalyst is added to the total FCC inventory at levels similar to combustion promoter. This promoter has been pilot unit tested in the Davison circulating riser, and the results have been confirmed in commercial testing. Laboratory results suggest that these catalysts decrease NO emissions by chemically reducing the NO with CO in the regenerator to form N_2 and CO_2. While this reaction also occurs to a certain extent in commercial regenerator operation, it is not catalyzed by conventional platinum based CO oxidation promoters.

The Chemistry of NOx in the FCCU Regenerator

The major environmental pollutants from burning coke in the FCCU regenerator include CO (carbon monoxide) and nitrogen and sulfur oxides. Both CO and SOx emissions can be controlled to a low level using relatively small amounts of commercial additives. NO_X emissions are also regulated, but are not so easily controlled. NOx emissions, including NO, NO_2 and N_2O, are typically in the range of 100 ppm to 500 ppm. Since regulations based on regional considerations vary from state to state and even from refinery to refinery, emissions in this range may be outside allowable limits. The NO_2 is formed only after the NO is emitted to the atmosphere, while N_2O is formed in small quantities if at all. Since most of the nitrogen oxides in the regenerator are in the form of NO, the formation and control of NO in the regenerator is the major issue.

The chemistry of NO in the regenerator has recently been described in two independent studies (1,2). Both studies agree in essentials. About half of the nitrogen in the feed appears as coke on the catalyst. The NO in the regenerator derives entirely from burning the nitrogen in the coke during regeneration. At the relatively low temperature in the regenerator, $\leq 800°C$, thermodynamic considerations show that NO is not formed from oxidation of the nitrogen in the air introduced into the regenerator.

The surprise is that only a small percentage of the coke nitrogen is converted to NO during regeneration. Under normal unpromoted regenerator operation most of the nitrogen is converted to N_2. These results were obtained by nitrogen balancing a pilot plant scale FCCU (3) using a relatively high nitrogen feed stock, 0.32% N at relatively high conversions. The catalyst was regenerated using an argon oxygen mixture in place of air, eliminating all sources of molecular nitrogen in the regenerator except from the coke, Table 1.

Table 1. Nitrogen Balance in a pilot plant FCCU. Regeneration with an Ar/O_2 mixture.

Feedstock:	Moderate Nitrogen	High Nitrogen
N, Wt%	0.13	0.32
Wt. % Conversion	73.9	59.8
Coke, Wt. % of Feed	3.68	4.26
Flue Gas NO,	62 ppm	211 ppm
Flue Gas N_2,	450 ppm	1250 ppm
Recovery of Feed N, %		
in Total liquid product	47.4	50.1
in Coke	35	-
% of Feed N recovered as NO	2.6	2.7
as N_2	38	32.7
Recovery of Regenerator N, %	**5**	**7**
as N_2	**95**	**93**
as NO	**5**	7
Total N Recovery, Wt. %	**88.0**	**85.6**

In this experiment the molecular nitrogen formed in the regenerator was directly measured by gas chromatography. The results show that more than 90% of the nitrogen in the coke forms N_2 rather than NO in an unpromoted regenerator. This means that the nitrogen in the coke is either converted directly to N_2 during regeneration, or is converted to NO and then reduced in the regenerator to N_2. The regenerator contains a variety of reductants including carbon monoxide (CO) and unburned coke on catalyst that has just entered the regenerator as well as residual coke on regenerated or partially regenerated catalyst. CO is present in relatively high concentrations, especially in an unpromoted operation. Although the NO can react with both the coke and the CO, the reaction with the CO to form N_2 and CO_2 is probably the most important. These events explain the observed increase in NO emissions with the addition of CO combustion promoter (less CO in the regenerator), and the decrease in NO_X levels observed with operation in partial burn conditions due to increased amounts of CO as well as coke. A number of NO_X reduction strategies including regenerator design changes based on this chemistry have been described in the patent literature. Some are based on placing more reductant in the regenerator, and in other cases the regenerator flue gas contacts reductant in the form of CO or spent catalyst (4-8).

The Reduction of NO with CO or with Coke on Spent Catalyst.

Previous work has shown that the reaction of NO with coke to form N2 is nearly as rapid as the reaction of oxygen with coke (9). We were able to directly observe the reaction of NO with coke on a spent FCCU catalyst under approximate regenerator conditions, Figure 1.

Figure 1: Reaction Between NO and Coke on Spent Catalyst to form Molecular Nitrogen and CO.

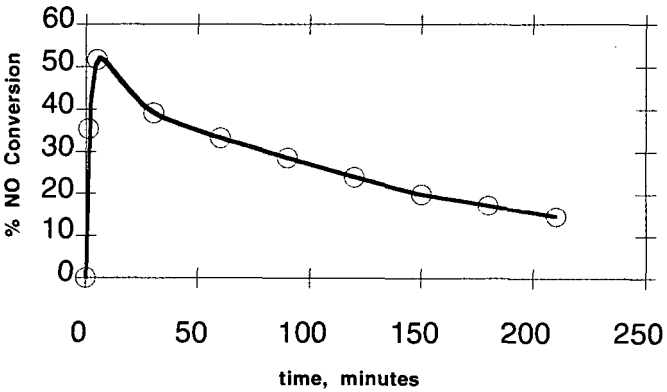

The result of this experiment shows a stiochiometry of approximately 1:1 consistent with the reaction

$$2\,C + 2\,NO = 2\,CO + N_2.$$

Another possibility is the reduction of NO with CO in the regenerator. Reactor studies show that while NO and CO do not react at regenerator temperatures in an empty reactor or over a low surface area inert, the reaction will occur over equilibrium catalyst, especially with nickel, vanadium and possibly other contaminants. Previous work has shown that high nickel equilibrium catalysts can function as CO oxidation promoters (10). Vanadium on titania is a well known commercial SCR catalyst. This result shows that equilibrium catalysts containing metal can also function as a promoter for the reaction of CO with NO, Table 2.

Table 2. Activity for NO conversion by reduction with CO. Reaction conditions 9,000 GHSV, 1700 ppm NO, CO/NO = 3/1.

Equilibrium Catalyst	A	B
Ni, ppm	378	1598
V, ppm	471	2298
Reactor Temperature, °C	**% Conversion**	
550	0.0	0.0
673	9	24
711	9	45
732	9	56

NO emissions can be reduced by reaction with CO in the regenerator or coke on the catalyst. These reactions form the basis for commercial strategies for NO control such as operation in partial burn, operation with low levels of promotion and higher levels of CO, and a variety of patented processes. However, it is not generally desirable to sacrifice CO conversion or to increase coke on regenerated catalyst for the sake of NOx reduction. Since NOx emissions increase with the addition of CO oxidation promoter, it is important to develop a promoter which catalyzes both the oxidation of CO to CO_2 as well as the reduction of NO to N_2 with CO. The operation of such a promoter, XNOx-2, in a FCC pilot unit is shown in Figure 2. The pilot unit operation is the Davison Circulation Riser (DCR) described elsewhere (11) running a feed stock previously described (1) containing 0.13 wt. % nitrogen.

Figure 2: Comparison of NO emissions in the DCR (Davison Circulating Riser)with a circulating catalyst inventory containing 0.5% of 500 ppm Pt on alumina (x) and 0.5% of XNOx-2 (o).

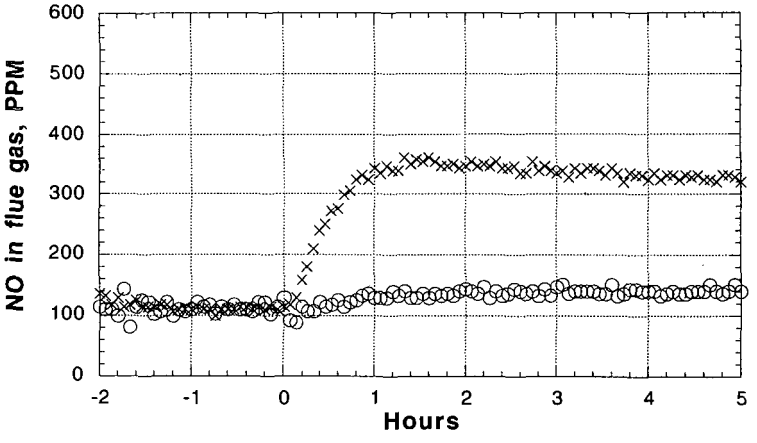

XNOx-2 and Pt/Alumina Activity for NO Reduction by CO

XNOx-2 works by providing a balanced bifunctional catalytic activity for both the oxidation of CO to CO_2 and for the reaction of CO with NO to produce CO_2 and N_2, controlling both CO and NO emissions. To demonstrate the catalytic basis for this effect we passed CO and NO over XNOx-2 and over a conventional CO combustion promoter containing 500 ppm Pt impregnated on alumina with the results shown in Figures 3 and 4. The activity for CO conversion in the presence of NO over platinum flattens and drops off over 400 °C, while the activity for this reaction over XNOx-2 increases rapidly up to at least 600°C, the highest temperature tested, Figure 3a. The NO conversion plot with temperature shows the same trend, Figure 3b. In this experiment the platinum promoter cannot convert more than 50% of the NO, while the XNOx-2 converts essentially all of the NO. By comparison conversion over Ecat is an order of magnitude or more lower, Table 2.

A plot of CO conversion on one axis and NO conversion on the other axis, Figure 4, is especially interesting. In the case of XNOx-2 we obtain a 45° plot showing one to one conversion. This agrees with the proposed stoichiometry. For every molecule of NO converted, one molecule of CO is converted, the stoichiometry for the desired reaction

$$2CO + 2NO \longrightarrow 2CO_2 + N_2.$$

Over the platinum promoter more NO is converted than CO. This indicates the conversion of NO to nitrogen species other than N_2. The platinum based CO promoters do not promote the reaction between NO and CO very effectively at regenerator temperatures, and the product is not the desired N_2. XNOx-2, on the other hand, is selective for the conversion of NO to N_2 in the presence of CO and at regenerator temperatures.

Figure 3: CO and NO conversion over 500 ppm Pt on gamma alumina (x) and over XNOx-2 (o) at 25,000 GHSV, 1375 ppm NO, and 3000 ppm CO.

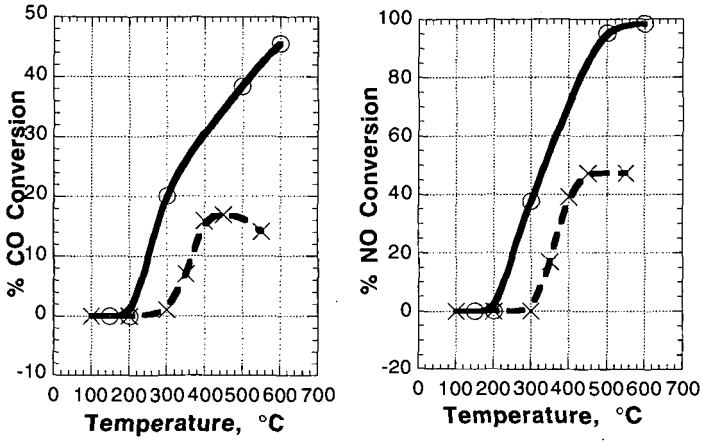

Figure 4: CO and NO stiochiometry for the results in Figure 3.

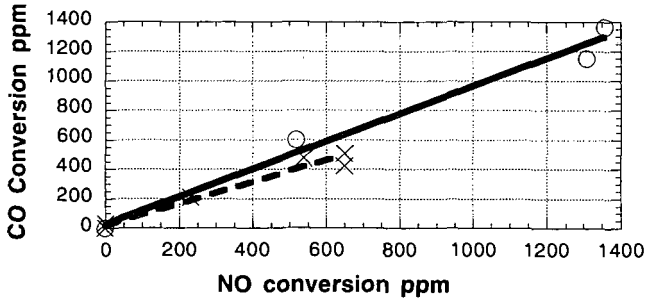

Commercial Testing

XNOx-2 has been tested in a commercial application currently using a conventional Pt on alumina CO combustion promoter. The conventional combustion promoter was discontinued and XNOx-2 begun at day zero shown in Figure 5. NOx emissions decreased slowly over a period of thirty days from a level of 500 units to a level of about 150 units, a drop of about 70%. During this period of time the afterburn, a measure of CO promotion efficiency, remained within normal limits. The commercial NOx reduction is somewhat greater than observed in DCR testing. The reason for this is probably the poorer mixing and higher localized CO concentrations in the commercial regenerator. In regions of high CO concentration the XNOx-2 will be especially effective.

Figure 5: Commercial test of the combustion promoter XNOx-2 compared to a conventional Pt on alumina promoter.

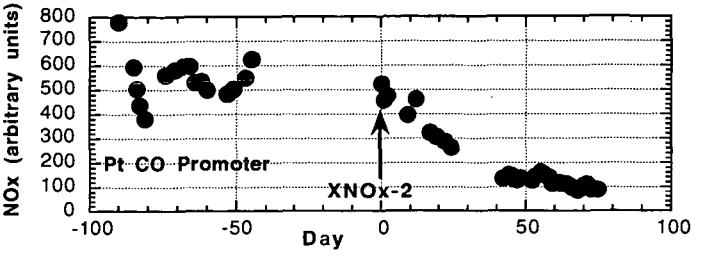

Acknowledgment

We would like to acknowledge the valuable laboratory work and the useful suggestions of Kevin Kreipl and Cathy Smith in the execution of the work described in this paper.

References

(1) A. W. Peters, G. D. Weatherbee, and Xinjin Zhao, Fuel Reformulation, Volume 5, No. 3, May/June 1995, p.45-50.
(2) S. Tamhankar, R. Menon, T. Chou, R. Ramachandran, R. Hull, and R. Watson, Oil and Gas Journal, March 4, 1996, p. 60-68.
(3) G. W. Young, in Fluid Catalytic Cracking: Science and Technology, Studies in Surface Science and Technology, J. S. Magee and M. M. Mitchell, Jr., eds., Elsevier, 1993, p.257.
(4) An example is a counter-current regenerator design by Kellogg claimed to reduce NOx by 50% or more. Spent catalyst is distributed over the top of the regenerator bed. NO reacts with the coke on the spent catalyst.
(5) A. R. Hansen, M. N. Harandi, D. L. Johnson, P. H. Schipper, S. A. Stevenson, Conversion of NOx in FCC Bubbling Bed Regenerator, US 5382352, 1995.
(6) J. S. Buchanan and D. L. Johnson, FCC Regeneration Process with Low NOx CO Boiler, US 5372706 (1994).
(7) P. H. Terry, Fluid Catalytic Cracking System, US 5360598, (1994).
(8) H. Owen and P. H. Schipper, Regeneration with Partial CO Combustion, US 5077252.
(9) Xi Chu and L. D. Schmidt, Ind. Eng. Chem. Res., 1993, **32**, 1359-1366.
(10) P. K. Doolin, J. F. Hoffman, and M. M. Mitchell Jr., Appl. Catal., 71 (1991) 233.

FCCU Regenerator Lab-Scale Simulator for Testing New Catalytic Additives for Reduction of Emissions from the FCC Regenerator

George Yaluris, Xinjin Zhao, Alan W. Peters
W. R. Grace & Co.-Conn.
Washington Research Center
7500 Grace Dr., Columbia, MD 21044

Keywords: Fluid catalytic cracking unit (FCCU) regenerator lab-scale simulator, combustion promoter, NO_x reduction

Introduction

Catalyst additives are commonly used in the FCC regenerator to control CO, SO_x and NO_x emissions (1). For example, Pt based combustion promoters are typically used to reduce CO emissions. The development of DESOX® technology has provided refiners with catalyst additives that can reduce the SO_x emissions (2-4). Recent environmental regulations have increased the importance of such catalyst additives in the FCC process and the need to develop new FCCU regenerator additives (5). Due to the lack of a realistic lab-scale simulator of the FCCU regenerator, most of the work in developing catalyst additives for the regenerator has been conducted using either refinery FCC units or pilot plants (e.g., Davison Circulating Riser (DCR), an adiabatic riser with continuous catalyst regeneration) (6,7). The efforts to develop new catalyst additives can be facilitated by the development of a lab-scale unit that simulates the FCCU regenerator. This simulator would allow us to examine the regenerator chemistry and the mechanisms through which additives affect gas emissions, as well as routinely test new additives. In this paper we present the development of such a lab-scale simulator of the FCCU regenerator and its use in testing combustion promoter additives.

Lab-Scale Simulator Unit of FCCU Regenerator

Attempting to simulate all of the operational characteristics of refinery-scale regenerators, which vary significantly in design, in a small lab-scale unit is not practical. For example, it is difficult to simulate the catalyst and gas flow patterns of a large regenerator in an idealized lab-scale reactor, and to simulate the true condition of the catalyst and additives entering the regenerator from the stripper. Thus, we have designed a one-pass system that utilizes pre-coked catalyst, operates as close as possible to the operation conditions of refinery regenerators, captures the chemical phenomena occurring in a true regenerator, and predicts the performance of catalyst additives.

The main characteristics of the lab-scale simulator unit of the FCCU regenerator (FCCU-RSU) are:

1. Fluidization of the FCC catalyst and additives
2. Continuous coked catalyst flow through the reactor and ability to control the catalyst residence time in the reactor
3. Control of the excess oxygen in the reactor effluent
4. Control of the temperature of the exothermic coke burning reaction
5. Ability to conduct mechanistic and kinetic experiments to probe the regenerator chemistry (formation of CO, SO_x and NO_x) and the mechanism through which catalyst additives work

In Figure 1 we show a schematic diagram of the FCCU-RSU we have built. The system consists of a quartz glass tube reactor (2.54 cm diameter) with a gas-catalyst particles disengagement section at the top. Further, separation of catalyst fines is achieved in the cyclone that follows the reactor. A custom designed oven allows control of the reactor temperature during the fast exothermic coke burning reaction. Air, oxygen, nitrogen, CO, NO, SO_2, and evaporated liquid feed can be fed in the reactor. Typically, nitrogen is used to fluidize the catalyst bed. Emission gases, like CO, NO and SO_2, are used in kinetic and mechanistic experiments to study the interactions between these gases, the catalyst, and the additives. A

Figure 1: Schematic diagram of FCCU regenerator lab-scale simulation.

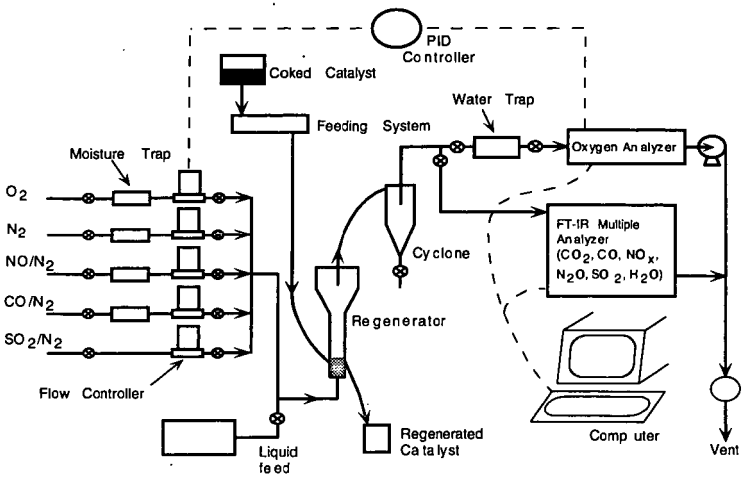

portion of the reactor effluent is sent to a Horiba oxygen analyzer (MPA-510), and through a feedback loop a PID controller controls the amount of air or oxygen needed to maintain the desired excess oxygen in the effluent. All other reactor gas products are analyzed by an On-Line Technologies 2002 FTIR Multigas analyzer which can measure CO_2, CO, NO, N_2O, NO_2, SO_2, H_2O and other FTIR-active gases. The catalyst flows continuously through the reactor using a custom-designed catalyst flow system purged with nitrogen to avoid contamination of reaction products with atmospheric gases. The catalyst residence time in the reactor depends on the catalyst flow rate, and can be controlled from about 5 min to more than 2 h. Detailed mixing experiments showed that mixing in the reactor is close to that of a CSTR.

Experimental

Using the FCCU-RSU we studied the performance of conventional Pt-based CO combustion promoters as well as that of new non-conventional additives that combine the CO combustion promotion functionality with reduction of NO_x from the regenerator (XNOx™ additives). The additives were used in our studies as synthesized both after calcination in air at 773 K and after reduction at 773 K in flowing 4% H_2 in N_2. Commercial FCC catalysts were coked in our pilot plant (DCR) using a resid FCC feed (API @ 60 °F: 20.6) that contains 0.41% sulfur, 0.18% total nitrogen, 0.06% basic nitrogen, and 5.1% Conradson carbon. The coked catalysts contained *ca.* 0.9 - 2.5% coke. The additives were added to the catalyst at the level of 0.5 wt%. Before charging the catalyst to the catalyst feed system, the catalyst was dried overnight at 373 K.

Typically the catalyst residence time in the reactor was about 16 min, and the excess oxygen was controlled at 1.1%. Unless otherwise noted, the reaction temperature was varied from 973 K to 1003 K. Data was collected for 30 - 60 min after steady state had been achieved.

Results

The results of coked catalyst regeneration in the FCCU-RSU show that the unit simulates well the catalyst regeneration process in the refinery regenerator. The CO/CO_2 ratio is a strong function of temperature and excess oxygen and decreases with increasing temperature and increasing excess oxygen. In Figure 2 we show that the amounts of CO detected in the flue gas follow inversely the amount of excess oxygen. At 1043 K, CO_2 increases from 1.6% to 3.0% to 4.4% as the catalyst flow increases from 0.47 to 1.07 to 1.67 g/min. Figure 2 shows that as the catalyst flow increases (catalyst residence time decreases) the amount of SO_2 increases roughly proportional to the increase in catalyst flow. These results are an

Figure 2: Composition of reactor effluent gas during regeneration of an FCC catalyst containing about 2.5% coke. CO, NO, SO_2 in ppm. Excess O_2 in %. Reactor temperature 1043 K.

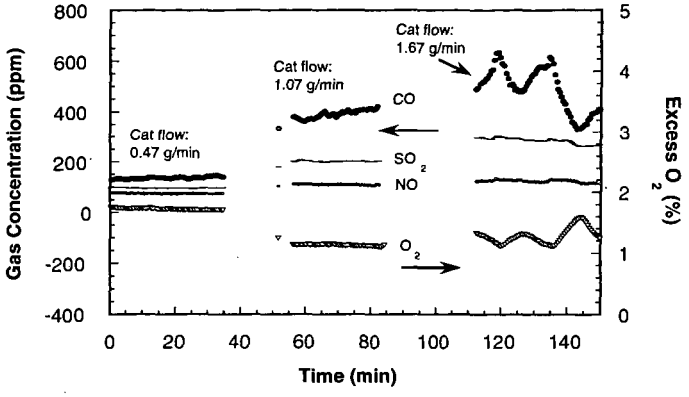

Figure 3: NO emissions from the pilot plant (DCR) regenerator when Pt-based and XNOx™-based combustion promoters are added in the catalyst (at 0 h)at 0.5 wt% additive level. Typical DCR regenerator temperature is 977 K.

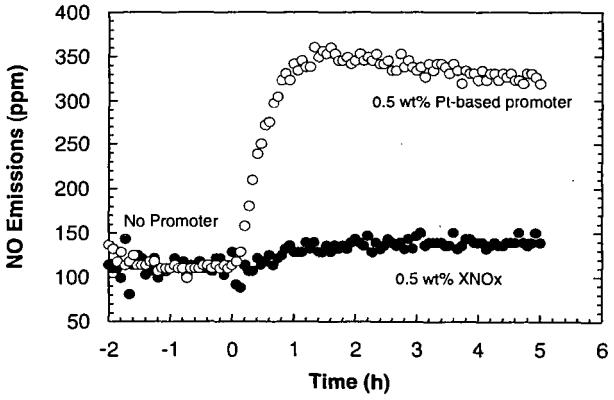

indication that at the temperature of this experiment most combustion of coke occurs during the first few minutes of the catalyst residence time in the regenerator. CO also increases with decreasing catalyst residence time, but its concentration in the flue gas depends on oxygen flow as well. NO increases as more coked catalyst is fed to the reactor. However, because of its reaction with CO, it does not increase in proportion to the catalyst flow increase.

According to refinery as well as our pilot plant experience (8), when Pt-based combustion promoters are added in the regenerator to reduce CO emissions, NO_x emissions increase. In DCR testing (Figure 3), the addition of Pt-based promoter in the regenerator increased NO formation during the cracking of a light paraffinic feed by about 3 times. In agreement with these results, the FCCU-RSU also shows a dramatic increase of NO_x in the reactor effluent when a Pt-based combustion promoter is added to the coked catalyst at the level of 0.5 wt%. The magnitude of the increase in the amount of nitrogen oxides produced depends on the reactor temperature and can be as high as five fold (Table 1)

Recently we developed new combustion promoter technology (8) that can achieve similar reduction of CO emissions from the FCCU regenerator as can be

Table 1: Average amounts of gas formation during FCC coked catalyst regeneration (1.2 wt% coke) with or without combustion promoter additives. Values shown are in cc/g catalyst passed through the reactor, averaged over 30 - 60 min after the unit has achieved steady state.

Promoter	Nominal Bed Temp (K)	CO_2	CO	N_2O	NO	SO_2	Nitrogen Oxides (%) Change	Effect on CO (%) Change
None	973	11.7	9.74	0.008	0.039	0.080	0	0
Pt-based oxid.	973	18.9	1.59	0.003	0.251	0.061	435	84
Pt-based red.	973	18.0	1.36	0.002	0.245	0.056	420	86
XNOx™ oxid.	973	17.2	2.45	0.004	0.169	0.021	264	75
XNOx™ red.	973	18.0	2.52	0.003	0.173	0.020	270	74
None	988	18.2	3.75	0.031	0.065	0.086	0	0
Pt-based oxid.	988	19.7	1.51	0.005	0.255	0.066	171	60
Pt-based red.	988	20.7	1.41	0	0.260	0.067	172	62
XNOx™ oxid.	988	19.5	1.83	0.008	0.188	0.027	105	51
XNOx™ red.	988	19.9	1.95	0.008	0.186	0.025	103	48

achieved with Pt-based promoters, while it produces a significantly smaller increase in NO_x emissions. We tested in the DCR a non-conventional combustion promoter based on XNOx™ technology (Figure 3). With the new combustion promoter in the DCR regenerator, NO emissions increased only 20%. The lab-scale simulator of the FCC regenerator qualitatively gives the same performance results. When XNOx™ is added to the coked catalyst at 0.5 wt%, nitrogen oxides in the flue gas increase about 40% less than the increase measured for the Pt-based additive (Table 1).

The observed reduction in nitrogen oxide emissions is achieved at only a slight cost in CO combustion promotion (Table 1). When the formulation of the XNOx™ combustion promoter is adjusted to achieve the same combustion promotion as the Pt-based additive, the FCCU-RSU still shows that, compared to the Pt-based additive, the XNOx™ additive achieves similar decreases in the concentration of nitrogen oxides in the reactor effluent to those shown in Table 1. Thus, the reduced NO_x achieved with the use of XNOx™ combustion promoters is a result of the additive's unique chemistry and not due to an increase of the CO reaction with NO that may result from the small increase of CO in the reactor. It is worth noting that according to the data in Table 1, significant amounts of N_2O are formed only in the absence of combustion promoters. Apparently, when these additives are present in the reactor, N_2O is rapidly oxidized to NO.

In an FCCU, the combustion promoters enter the regenerator after being reduced in the riser. To determine if the oxidation state of the additive affect its performance, we tested both oxidized and reduced additives. Our results (Table 1), indicate that, at least in the FCCU-RSU, the oxidation state of the additive does not have a significant impact on either the CO combustion promotion or the observed increase in NO_x. This result does not imply that the redox properties of the additive do not impact the flue gas composition. We speculate that upon entering the reactor, at the conditions of these experiments (>973 K, >1% O_2, and CO present), the additive rapidly reaches its equilibrium oxidation state. The presence of redox catalytic cycles involving surface sites and O_2, CO, NO and other nitrogen species may then play a role in determining the amount of nitrogen oxides produced during catalyst regeneration.

Conclusions

We have developed a lab-scale simulator of the FCCU regenerator that can be used to study the performance of FCC regenerator catalyst additives, and investigate the mechanism (e.g., role of additive's oxidation state) and kinetics through which these additives affect the formation of carbon, nitrogen and sulfur oxides. The lab-scale system includes a custom-designed fluidized bed reactor and catalyst flow system, and allows control of the important operation parameters (catalyst residence time, excess oxygen, reactor temperature). Coked catalyst

regeneration experiments and performance tests of conventional and non-conventional combustion promoters show that the FCCU-RSU can simulate the operation and capture the chemistry of the FCCU regenerator.

References:

1. Bhattacharyya, A.A., and Yoo, J.S. *in* "Fluid Catalytic Cracking: Science and Technology" (Magee, J.S. and Mitchell, M.M., Jr. Eds.), *Stud. Surf. Sci. Catal.* Vol. 76, p. 531 . Elsevier Science Publishers B. V., Amsterdam, 1993.
2. Lane, P.A., and Latimer, J.A. *in* "Advanced Fluid Catalytic Cracking Technology" (Chuang, K.C., Young, G.W. and Benslay, R.M. Eds.), *AIChE Symp. Ser., No. 291* Vol. 88, p. 76. American Institute of Chemical Engineers, New York, 1992.
3. Yoo, J.S.,Karch, J.A.,Radlowski, C.A., and Bhattacharyya, A.A. *in* "Catal. Sci. Technol., Proc.," Tokyo, 1990, (Yoshida, S., Takezawa, N. and Ono, T. Eds.), , p. 183. Kodansha , Tokyo, 1991.
4. Yoo, J.S.,Bhattacharyya, A.A.,Radlowski, C.A., and Karch, J.A., *Appl. Catal., B* **1(3),** 169 (1992).
5. Evans, R.E., and Quinn, G.P. *in* "Fluid Catalytic Cracking: Science and Technology" (Magee, J.S. and Mitchell, M.M., Jr. Eds.), *Stud. Surf. Sci. Catal.* Vol. 76, p. 563. Elsevier Science Publishers B. V., Amsterdam, 1993.
6. Peters, A.W.,Weatherbee, G.D., and Zhao, X., *Fuel Reformulation* **5(3),** 45 (1995).
7. Young, G.W. *in* "Fluid Catalytic Cracking: Science and Technology" (Magee, J.S. and Mitchell, M.M., Jr. Eds.), *Stud. Surf. Sci. Catal.* Vol. 76, p. 257 . Elsevier Science Publishers B. V., Amsterdam, 1993.
8. Davey, S.W., and Haley, J.T. *in* "Oil & Gas Journal International Catalyst Conference and Exhibition," Houston, Texas, February 1-2, 1996.

Mesoporous Zeolite-Supported Noble Metal Catalysts for Low-Temperature Hydrogenation of Aromatics in Distillate Fuels

Kondam Madhusudan REDDY and Chunshan SONG*

Fuel Science Program, Department of Materials Science and Engineering
209 Academic Projects Building, The Pennsylvania State University
University Park, PA 16802, USA

Keywords: Mesoporous zeolite, Catalyst, Noble Metals, Hydrogenation, Fuels

Introduction

The present work is concerned with deep hydrogenation of aromatics in distillate fuels at low temperatures using mesoporous zeolite-supported noble metal catalysts. This work is a part of our on-going effort to develop advanced thermally stable jet fuels from coal-derived liquids and petroleum. Saturation of naphthalene and its derivatives not only reduces aromatics contents of jet fuels, but also generates decalins which show much higher thermal stability than long-chain alkanes in jet fuels at high temperature (Song et al., 1994). This work also has a bearing on developing new catalytic processes for low-temperature hydrogenation of distillate fuels.

The Clean Air Act Amendments of 1990 and new regulations call for the production and use of more environmentally friendly transportation fuels with lower contents of sulfur and aromatics (Lee et al., 1993; Unzelman, 1993). High aromatic content in distillate fuels lowers the fuel quality and contributes significantly to the formation of environmentally harmful emissions (Stanislaus and Cooper, 1994). California Air Resources Board (CARB) has passed legislative measures to limit the sulfur and aromatic contents of diesel fuel to 0.05 wt% and 10 vol%, respectively, effective October 1993 (Lee et al., 1993). Currently, conventional hydrotreating technology is adapted for aromatics saturation. Some studies have shown that complete hydrogenation of aromatics is not possible owing to equilibrium limitations under typical hydrotreating conditions, and existing middle distillate hydrotreaters designed to reduce sulfur and nitrogen levels would lower the diesel aromatics only marginally (Stanislaus and Cooper, 1994).

Deep hydrogenation may become necessary in the near future for reducing aromatic contents of distillate fuels to meet increasingly more stringent regulations. One of the significant findings by The US Auto/Oil Air Quality Improvement Research Program (which involved Ford, General Motors, Chrysler, and 14 largest US petroleum companies) is that lowering aromatic content lowers toxic emissions (Kreucher, 1995; Unzelman, 1993). The significant findings of the European Program on Emissions, Fuels, and Engine Technologies (EPEFE) also include the following related to aromatics: 1) decreasing aromatics reduces catalytic converter light-off time, improves the converter efficiency and decreases exhaust hydrocarbons; and 2) decreasing fuel polyaromatics reduces light-duty diesel exhaust nitrogen oxides and particulate material and heavy-duty exhaust hydrocarbons, nitrogen oxides, and particulate material (Kreucher, 1995).

Typical conventional catalysts for fuel hydroprocessing are sulfided Co-Mo and Ni-Mo supported on alumina. However, such catalysts are active only at relatively high temperatures (e.g., >300°C). Because hydrogenation is exothermic, deep hydrogenation is favored at lower temperature. It is therefore natural to consider deep hydrogenation at low temperatures (e.g., ≤300°C), and the potential candidate catalysts for low-temperature hydrotreating include noble metals. Since it is known that noble metal catalysts are easily deactivated by sulfur compounds, a two-stage processing strategy may be adopted. The first stage would involve deep desulfurization of the fuels using metal sulfide catalysts, and the second stage deals with deep hydrogenation over noble metal catalysts. Such a two-stage processing scheme may become practically applicable, since deep desulfurization is likely to be required by regulations to further reduce sulfur contents of transportation fuels in the near future.

The objective of this work is to explore the potential of mesoporous zeolite as support of noble metal catalysts for deep hydrogenation of aromatics in jet fuel and diesel fuel. Recently, Mobil researchers have invented MCM-41 type mesoporous molecular sieves possessing a hexagonal array of uniform mesopores (Beck et al., 1992; Kresge et al., 1993). We have synthesized mesoporous zeolites with MCM-41 type structure using three different aluminum sources (Reddy and Song, 1996a, 1996b). We are currently exploring their applications for catalytic fuel processing (Reddy and Song, 1996b; Song and Reddy, 1996). In our preliminary work, Pt/MCM-41 catalysts containing 3 wt% Pt were prepared with the mesoporous zeolites synthesized using pseudo boehmite, Al isopropoxide, and Al sulfate, and applied for hydrogenation of naphthalene at 200°C and that of phenanthrene at 300°C. The results showed that the sample made by using Al isopropoxide gives the best catalyst (Reddy and Song, 1996b). In the present work, supported catalysts containing 2 wt% Pt or 2 wt% Pd were prepared using proton-form MCM-41

* Corresponding author. E-mail: csong@psu.edu; Tel: 814-863-4466; Fax: 814-865-3075

(synthesized using Al isopropoxide) as well as Al_2O_3 and TiO_2 as the support materials. This paper reports on their performance for hydrogenation of naphthalene in n-tridecane at 200°C.

Experimental

Catalyst Preparation

The mesoporous zeolite with MCM-41 type structure was synthesized using aluminum isopropoxide as the Al source according to the procedure described elsewhere (Reddy and Song, 1996). Supported catalysts containing 2 wt% Pt or 2 wt% Pd were prepared using proton-form mesoporous MCM-41 zeolite as well as Al_2O_3 and TiO_2 as the support materials. Table 1 gives their properties. The Pt catalysts were prepared by impregnation from aqueous solution of hydrogen hexacholoro platinate (IV) hydrate, $H_2PtCl_6xH_2O$ (Aldrich, 99.995% Pt, metal basis). The Pd catalysts were prepared by impregnation of $PdCl_2$ (Aldrich, 99.999% Pd, metal basis) dissolved in dilute hydrochloric acid (sufficient to form soluble $PdCl_4^{2-}$). In both cases, water was removed by rotary evaporation at about 60°C. The catalyst precursors were dried in an oven at 60°C over night, and then calcined in an electric furnace at 450°C for 4 h. The nominal metal concentration was kept at 2 wt% for both Pt and Pd catalysts. Metal reduction was done in situ during naphthalene hydrogenation tests.

Catalyst Evaluation

All the catalysts were tested at 200 °C for a given residence time in 25-mL stainless-steel microautoclaves. The total volume of the system including the connecting tube between reactor and pressure gauge is about 30 mL. Typically, the reactor was charged with 1.0 g naphthalene (Aldrich, 99%), 4.0 g n-tridecane solvent, and 0.1 g catalyst. The charged reactor was flushed with H_2, then pressurized to 1000 psig (cold) to start the test. The reactor was mounted on a holder, immersed in a fluidized sand bath preheated to 200°C, and shaken vertically at 240 cycles/min with a 1 cm stroke.

At the end of the test, the reactor was taken out of the sandbath, quenched in cold water, and then allowed to cool down in air to room temperature. The gaseous products were collected for analysis and then the reactor was opened. The contents of the reactor were washed with acetone onto a filter. Solution products were analyzed by GC-MS and GC-FID. The capillary columns were 30mx0.25mm DB-5 (J&W Scientific) for GC-MS and 30mx0.25mm DB-5 (Hewlett-Packard), for GC-FID and the oven temperature program for both GC instruments was 60-280 °C at 10 °C/min. GC and GC-MS indicate that cracking or isomerization of n-tridecane, if any, were negligible. The yields of products were determined by quantitative GC analysis using n-nonane as internal standard, and the conversion was determined by the amount of naphthalene recovered after the reaction.

Selected tests were conducted to examine the effect of pre-reduction. Pre-reduction was carried out at 200°C for 1 h under reaction conditions except that naphthalene was not present during the reduction stage. After the reduction, the reactor was cooled down to ambient temperature, vented and opened. The reactor was re-sealed after the addition of 1 g naphthalene, and re-pressurized to 1000 psig H_2 at room temperature. Hydrogenation over the pre-reduced catalysts was also conducted at 200°C for 0.5 h.

Table 1. Properties of the Mesoporous MCM-41 Zeolite, Titania and Alumina Supports

Support ID	Material Type	Surface Area, m^2/g	Pore Vol cc/g	SiO_2/Al_2O_3 mol ratio	Source
MCM-41	Mesoporous zeolite	1206	1.77	40.7	PSU Fuel Science, Synthesized with Al
TiO_2	Titania	53	---	---	Degussa, Titania P25
Al_2O_3	γ-Alumina	113	---	<0.001	Degussa, Aluminum Oxide C

Results and Discussion

Table 2 shows the distribution of products from naphthalene hydrogenation over Pd and Pt catalysts at 200°C for 60 min. The main products from naphthalene hydrogenation were tetrahydronaphthalene (tetralin or THN), and cis- and trans-decahydronaphthalene (decalin or DeHN). Δ9,10-octalin was also detected as a minor product in many tests, which is an intermediate from tetralin to decalin. The selectivity to tetralin+decalin+octalin approaches to unity in all the runs, indicating that there were essentially no side reactions such as ring-opening cracking

and ring-contraction isomerization under the conditions. Based on the present and previous results (Lai and Song, 1996; Schmitz et al., 1996), the reaction pathways can be represented by Scheme I.

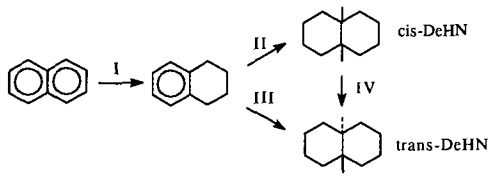

Scheme I

Effect of Supports

For Pt catalysts on different supports, the yield of tetralin decreased in the order of alumina > titania > MCM-41, whereas the yields of trans- and cis-decalins increased in the order of alumina < titania < MCM-41. In the case of Pt/MCM-41, the intermediate product tetralin was almost completely hydrogenated, whereas tetralin still remains as a major product with Pt/Al_2O_3 and Pt/TiO_2.

Table 2 Hydrogenation of Naphthalene at 200°C for 60 min over Pt and Pd Catalysts

Expt ID	79	115	81	82	83	84
Catalyst	Pt/Al_2O_3	Pt/TiO_2	Pt/MCM-41	Pd/Al_2O_3	Pd/TiO_2	Pd/MCM-41
Conversion (%)	98.3	99.9	100.0	99.9	99.9	100.0
Selectivity (wt%)						
Tetralin	57.0	35.8	0.0	42.5	30.5	0.0
9,10-Octalin	0.8	1.0	0.0	0.7	0.3	0.0
trans-Decalin	10.6	14.9	50.2	34.6	43.9	64.4
cis-Decalin	31.1	47.9	49.4	22.0	25.1	35.4
Others	0.5	0.4	0.4	0.2	0.2	0.2
trans-/cis-DeHN	0.3	0.3	1.0	1.6	1.7	1.8
DeHN+Tetralin	98.7	98.6	99.6	99.1	99.5	99.8
DeHN/Tetralin	0.7	1.7	2444.3	1.3	2.3	1235.3

For Pd catalysts, we observed essentially the same trends in terms of catalytic activity reflected by the increasing yields of decalins or decreasing yields of tetralin. Moreover, both Pd/MCM-41 and Pt/MCM-41 catalysts promoted the hydrogenation to completion such that the dominant products are trans- and cis-decalin, whereas tetralin is still one of the major products with both Al_2O_3- and TiO_2-supported Pd and Pt catalysts. These results indicate MCM-41 supported Pt and Pd catalysts are more active than titania and alumina supported catalysts.

The higher activity of the mesoporous zeolite-supported Pt and Pd may be due to better dispersion of the noble metals on MCM-41, since it has much larger surface than that of Al_2O_3 and TiO_2 supports (Table 1). According to a recent report (Koussathana et al., 1991), hydrogenation of naphthalene and benzene is insensitive to the geometric structure of the Pt species. The mild acidity of MCM-41 may also be a contributing factor, since it contributes to the electron deficiency of the metal on zeolite surface. It is known that noble metals on Y-zeolite and mordenite are often better dispersed and electron deficient as compared to those on alumina (Stanislaus and Cooper, 1994). The zeolitic protons can act as chemical anchors for reduced noble metal particles (Satchler and Zhang, 1993).

The selectivity to decalin isomers depends on the support and metal type. Compared to Pd/Al_2O_3 and Pd/TiO_2 catalysts, Pd/MCM-41 catalyst afforded higher trans/cis ratio, indicating a higher selectivity to trans-decalin. There appears to be one major difference between Pt and Pd catalysts in selectivity: Pd shows higher selectivity to trans-decalin. Therefore, among the three supports, MCM-41 corresponds to higher trans/cis ratios. Among the two metals, Pd catalysts always afford higher trans/cis ratios. Overall, MCM-41 supported Pd catalyst display highest selectivity to trans-decalin.

Effect of Reaction Time

Since complete naphthalene conversion was reached in 1 h, we reduced the residence time and conducted 30 min runs at 200°C. Table 3 shows the results. Although unreduced catalysts were used, nearly complete naphthalene conversion was achieved in all the runs within 30 min. However, the product distribution changed with residence time. Yields of tetralin increased and decalin yields decreased with decreasing residence time. It is also clear that the absolute yields of tetralin and decalins strongly depended on the type of support and metal.

Even with reduced residence time, the MCM-41 supported Pt and Pd catalysts are substantially more active than the corresponding catalysts supported on alumina and titania (Table 3). In general, the activity of both Pt and Pd catalysts for complete hydrogenation of naphthalene to decalin decreased in the following order with respect to the support type: MCM-41 > TiO_2 > Al_2O_3.

Table 3 Hydrogenation of Naphthalene at 200°C for 30 min over Pt and Pd Catalysts

Expt ID	109r	110	92	93	94	111r
Catalyst	Pt/Al_2O_3	Pt/TiO_2	Pt/MCM-41	Pd/Al_2O_3	Pd/TiO_2	Pd/MCM-41
Conversion (%)	97.2	99.9	100.0	99.9	100.0	99.9
Selectivity (wt%)						
Tetralin	68.9	51.9	0.1	81.3	62.6	17.1
9,10-Octalin	1.1	0.2	0.00	0.9	1.0	0.3
trans-Decalin	6.5	8.2	45.2	10.3	21.1	52.8
cis-Decalin	23.3	39.0	54.3	7.4	15.1	29.7
Others	0.2	0.7	0.6	0.1	0.2	0.1
trans-/cis-DeHN	0.3	0.2	0.8	1.4	1.4	1.8
DeHN+Tetralin	98.7	99.1	99.4	99.0	98.8	99.6
DeHN/Tetralin	0.4	0.9	2160.2	0.2	0.6	4.8

When compared to the 60 min-runs, the yields of tetralin were generally higher and decalin yields lower in 30 min-runs, particularly when Pt or Pd was supported on alumina or titania. The trans/cis ratios of the decalin isomers are lower in the 30 min runs than in 60 min runs, even in the case of Pt/MCM-41 where tetralin was completely converted to decalin within 30 min. These results are consistent with Scheme I and indicate that cis-decalin isomerizes into trans-decalin during the hydrogenation reaction over MCM-41 supported catalysts, being consistent with the previous results from this laboratory (Lai and Song, 1996; Schmitz et al., 1996). TPD of n-butylamine indicates that hydrogen MCM-41 is acidic, but its acidity is lower than that of hydrogen Y zeolite. It appears from comparative examination that the presence of Pd metal and acid sites facilitates both tetralin hydrogenation and cis-decalin isomerization into trans-decalin.

Effect of Pre-Reduction

The above results clearly indicate that both Pd and Pt catalysts supported on the mesoporous MCM-41 are superior over those supported on Al_2O_3 and TiO_2. It should be noted that there may be two contributing factors, since the calcined catalysts were applied without reduction pretreatment. First, the in situ generation of active metal particles by H_2 reduction may be slower in Al_2O_3- and TiO_2-supported Pt and Pd than in MCM-41 supported metals. Second, the reduced metal species on MCM-41 are more active than those on Al_2O_3 and TiO_2. To see if this is the case, we examined the effect of pre-reduction under reaction conditions (hydrogenation over the pre-reduced catalysts at 200°C for 0.5 h).

The results showed that even after pre-reduction, the MCM-41 supported Pt and Pd catalysts are considerably more active than the corresponding Al_2O_3- and TiO_2-supported Pt and Pd catalysts. The differences between the MCM-41 supported catalysts are that pre-reduced Pd/MCM-41 displayed higher activity for tetralin hydrogenation than pre-reduced Pt/MCM-41, whereas the in-situ reduced Pd/MCM-41 was less active than the in-situ reduced Pt/MCM-41. Our previous results of XRD suggested that the zeolite-supported Pt and Pd catalysts were completely reduced after 60 min or 30 min under comparable conditions (Reddy and Song, 1996; Schmitz et al., 1996). Therefore, it is considered that essentially all the noble metal species would have been reduced to metallic particles by a pre-reduction treatment at 200°C for 60 min under an initial H_2 pressure of 1000 psig using n-tridecane solvent. Another puzzling observation was that the pre-reduced catalysts are not always as active as the in-situ reduced catalysts under the reaction conditions employed in this work. Further study is in progress.

Conclusions

Mesoporous MCM-41 zeolite that was synthesized by a proper method may be used as a very effective support for noble metal catalysts. For hydrogenation of naphthalene in n-tridecane at 200°C, both the Pt and Pd catalysts supported on MCM-41 zeolite are substantially more active than the corresponding catalysts supported on Al_2O_3 and TiO_2. In general, the activity of both Pt and Pd catalysts for complete hydrogenation of naphthalene to decalin decreased in the following order with respect to the support type: MCM-41 > TiO_2 > Al_2O_3.

Both Pd/MCM-41 and Pt/MCM-41 catalysts promoted the hydrogenation to completion such that the dominant products are trans- and cis-decalin, whereas tetralin is still one of the major products with both Al_2O_3- and TiO_2-supported Pd and Pt catalysts. In general, Pd catalysts showed higher selectivity to trans-DeHN, whereas higher selectivity to cis-DeHN was displayed by Pt catalysts.

The selectivity to decalin isomers also depends on the support and metal type. Among the three supports, MCM-41 gives higher trans/cis ratio. Among the two metals, Pd affords higher trans/cis ratio. In other words, Pd catalysts showed higher selectivity to trans-decalin, whereas higher selectivity to cis-decalin was displayed by Pt catalysts.

Acknowledgments

We are very grateful to Prof. H. H. Schobert for his encouragement and support. Financial support was provided by US Department of Energy, Pittsburgh Energy Technology Center, and US Air Force, Wright Laboratories. We wish to thank Mr. W. E. Harrison III of USAF and Dr. S. Rogers of DOE for their support, Drs. W.-C. Lai, A. Schmitz and S.-D. Lin for helpful discussions, and Degussa Corporation for providing alumina and titania supports.

References

Beck, J. S., J. C. Vartuli, W. J. Roth, M. E. Leonowicz, C. T. Kresge, K. D. Schmitt, C. T. W. Chu, D. H. Olson, E. W. Sheppard, S. B. McCullen, J. B. Higgins, and J. C. Schlenker. J. Am. Chem. Soc., 1992, 114, 10834.

Koussathana, M., D. Vamvouka, H. Economou and X. Verykios. Appl. Catal., 1991, 77, 283.

Kresge, C. T., M. E. Leonowicz, W. J. Roth, J. C. Vartuli, and J. S. Beck, Nature, 1992, 359, 710-712.

Kreucher, W. M. Chem. Ind., 1995, Aug 7, 601.

Lai, W.-C. and Song, C. Catalysis Today, 1996, in press.

Lee, S. L., Wind, M. De, Desai, P. H., Johnson, C. C., and Mehmet, Y. Asim. Fuel Reformulation, 1993, May/June, 26.

Lin, S.D., and Song, C. Catalysis Today, 1996, in press.

Reddy, K. M. and Song, C. Catalysis Letters, 1996a, 36, 103.

Reddy, K. M. and Song, C. Catalysis Today, 1996b, in press.

Satchtler, W. M. H. and Z. Zhang, Adv. Catal., 1993, 39, 129.

Schmitz, A., Bowers, G. and Song, C. Catalysis Today, 1996, in press.

Song, C., Lai, W.-C. and Schobert H. H. Ind. Eng. Chem. Res., 1994, 33, 548.

Song, C., Lai, W. -C., Schmitz, A. D., Reddy, K. M., Am. Chem. Soc. Div. Fuel Chem. Prepr., 1996, 41 (1), 71.

Song, C. and Schmitz, A. Am. Chem. Soc. Div. Petrol Chem. Prepr., 1996, 41 (3-4), in press.

Song, C. and Reddy, K. M. Am. Chem. Soc. Div. Petrol Chem. Prepr., 1996, 41 (3-4), in press.

Stanislaus, A. and Cooper, B. H. Catal. Rev. - Sci. Eng., 1994, 36, 75.

Unzelman, G. H. Fuel Reformulation, 1993, May/June, 38.

BENZENE REDUCTION USING OCTGAIN®
- A NEW WAY TO MEET RFG SPECIFICATIONS

P. P. Durand, N. A. Collins, R. Hu, J. C. Trewella and T. L. Hilbert
Mobil Technology Company, PO Box 480, Paulsboro NJ 08066-0480

Keywords: benzene reduction, octane, low sulfur

Introduction

Phase II reformulated gasoline specifications in the U.S. requires refiners to reduce the sulfur, olefins and benzene content of gasoline. Conventional solutions for sulfur reduction such as FCC feed hydrotreating or gasoline hydrofinishing require a large capital investment or lead to a large loss in octane. Mobil's OCTGAIN® process lowers FCC gasoline sulfur and olefin content without a high capital investment and without a loss in octane[1]. This same process can also be used for benzene reduction. Cofeeding a benzene rich reformate fraction to the OCTGAIN process leads to benzene conversions of up to 47%. Depending on the feedstock, there may also be an octane boost of 1.5 numbers for processing heart-cut reformate.

Experimental - feeds

The feedstocks for the study were four different FCC naphthas with different boiling ranges and two heart-cut reformates. The properties are given in Table 1. The octane of the reformates are low despite their high benzene content (39 and 24 wt%) because they also contain significant amounts of low octane n-hexane (24.8 research octane number, 26 motor octane number) and isohexanes (73.4 RON, 73.5 MON). The properties of the different blends were also measured, and these are reported in Table 2.

Experimental - Pilot plant setup

The experiments were conducted in a continuous, fixed-bed pilot plant. Hydrogen flow was once through and liquid feeds were downflow. Pressure was maintained on the system by a high pressure separator with a back-pressure regulator on the gas side and a liquid level control valve. Gases were metered using a wet-test flowmeter, and then sampled by on-line GC. The liquid product was weighed, chilled and sent for octane and composition analysis. All octanes reported in this work are based on full engine tests. Octanes were corrected by subtracting on a volumetric basis the octane of C4- material in the liquid sample, and adding in the contributions of any C5+ material that was found in the offgas. Similarly the C5+ yields are corrected to include any C5+ material in the offgas. Mass closures were typically in the range 97-103 wt%.

Experiments were conducted at typical OCTGAIN process conditions with the OCT-100 catalyst system. The next generation of the catalyst system [2] is expected to show similar benzene reduction performance. Benzene content was measured by GC FTIR or PIONA.

Results - Benzene content

As shown in Figure 1, up to 47% benzene conversion was obtained depending on the feedstock and the temperature of the catalyst system. Benzene is removed by alkylation, but there is also benzene formation by dealkylation of alkylbenzenes. As the temperature of the catalyst system increases, both of these rates increase. When reformate is present benzene alkylation dominates. At sufficiently severe conditions there is also some dehydrogenation of naphthenes, providing an additional route for benzene formation. This is particularly true as pressure is reduced, shifting the equilibrium towards the aromatic species.

The compositional changes that are occurring are shown in Figure 2 as a function of benzene conversion for the two lightest FCC blends. The separation between the curves gives the relative amounts of the different components. As benzene conversion increases, there is initially a reduction in C_7-C_{10} aromatics due to hydrogenation. As severity is increased, aromatics in this boiling range increase due to the desired alkylation of benzene. The technology also gives a dramatic reduction in olefin content. Sulfur removal is not shown in this plot, but is also essentially complete (i.e. > 95 wt%), even at modest benzene conversion levels. At the highest benzene conversion levels there is a yield loss caused by formation of light hydrocarbons, labeled offgas HC in Figure 2. The composition by weight of the light hydrocarbons is typically 2-7% C_1 and C_2, 30-40% C_3, 5-15% mixed C_3 and C_4 olefins, 25-30% iC_4, 25-30% nC_4. Without the presence of reformate, dealkylation of heavy aromatics causes an increase in feed benzene content, the extent of the increase being feed dependent.

The feed benzene content is an important variable affecting overall benzene conversions. The higher the feed benzene content, the higher the conversion. Figure 3 shows the benzene conversion as a function of catalyst temperature for the 215°F+ FCC naphtha feed on its own and in the two blends with reformate. Clearly there is benzene formation for the 215°F+ FCC feed when processed on its own. Note that we have also observed benzene formation in hydroprocessing of FCC gasoline[3]. The feed with 4 wt% benzene shows little benzene

conversion, while there is appreciable conversion for the feed with 6.9 wt% benzene. These results suggest that an equilibrium is established between benzene formation by dealkylation of heavy aromatics and benzene removal, which occurs primarily by alkylation of benzene. Higher feed alkylaromatics will thus be more detrimental to high benzene conversions. This is a function of FCC operation and naphtha end point.

Reducing pressure from 600 to 300 psig causes increased benzene formation by aromatization of cycloparaffins, and so benzene conversion is lower. Consider Table 3 below:

Table 3: Effect of pressure on benzene conversion in OCTGAIN™

Pressure	300 psig	600 psig
C5+ Road Octane	91.2	89.6
Cycloparaffins in product, wt% of total feed	8.9	11.2
Benzene Conversion, wt%	26.1 %	33.1 %

Feed: 215°F+ FCC naphtha, with 2.14:1 v/v FCC naphtha, reformate 2
The same temperature was used for each experiment

The shifts in benzene and other aromatics are driven by thermodynamic equilibrium. Reducing pressure and increasing temperature shifts the hydrogenation / dehydrogenation equilibrium towards aromatics formation. The higher aromatics level at lower pressure also contributes to the improved octane. Note that in each case the product octane is significantly greater than 85.6 which is the feed road octane.

Results - Yield and Octane

By cofeeding reformate, a substantial yield-octane improvement over conventional OCTGAIN was obtained. Figure 4 shows the C5+ yield plotted versus road octane (product - feed). The solid line is the yield versus octane curve for the blend of FCC naphtha and reformate. The yield at 86 octane is slightly above 100% due to a volume expansion over the OCTGAIN catalyst system. A similar yield-octane curve was measured for the FCC naphtha on its own. The dashed line represents what would be achieved if the refiner chose to blend reformate with the OCTGAIN product from processing FCC naphtha on its own. The curve is calculated from volumetrically blending reformate yield and octane (100%, 76.2 road) and FCC naphtha yield and octane (measured in a pilot plant run) in a 1:2 v/v proportion. The data in Figure 4 show a clear improvement when reformate is cofed to the OCTGAIN unit with the FCC naphtha. In particular, at 98 vol% C5+ yield, there is an octane benefit of 1.5 road numbers. We believe that the benefit is due to improved octane uplift for the heart-cut reformate cofeed.

Conclusions/Summary

Benzene conversions as high as 47% were obtained when coprocessing heart-cut reformate with FCC naphthas over the OCTGAIN catalyst system. A road octane benefit of about 1 number at 99 vol% C5+ yield was also observed from cofeeding reformate. This octane benefit may result in an even higher defacto benzene reduction via reoptimization of reformer severity. These results highlight the versatility of the OCTGAIN process in helping refiners meet their RFG needs.

The process with reformate cofeed retains all the other advantages of OCTGAIN. We continue to exploit the unique chemistry of the process, which allows us to have deep desulfurization of the gasoline and a high level of saturation of olefins while retaining a high product octane. This is in contrast to conventional hydrotreating or mild hydrofinishing of FCC gasoline at high LHSV. The economic evaluation of the OCTGAIN process [4] looks attractive, even when the benzene reduction capabilities of the process are not comprehended. With this additional benefit, the technology offers refiners a powerful new tool for manufacture of RFG.

References:

1 Sarli, M. S., Fletcher, D. L., Hilbert, T. L., Karsner, G. G., Shih, S. S. and P. Xayariboun, "OCTGAIN™ A unique Gasoline Desulfurization Process", NPRA 1994 Annual Meeting, March 20-22, 1994

2 Hilbert, T. L., Kirker, G. W., Shih, S., Riedinger, S. L., Timken, H. C., Mazzone, D. N., Holtan, T. P. and M. Schrauben, "OCTGAIN™, A new Desulfurization Process", Hydrofinishing 1 Symposium, AIChE Meeting, March 21 1995, Houston, Texas.

3 Del Rossi, K. J., Riedinger, S. L, and T. L. Hilbert, "Hydrofinishing Olefinic Gasoline", Paper 40C, AIChE Spring National Meeting, Hydroprocessing 1 Symposium, March 21st, 1995

4 Podar, S. K., Chum, K., Ragsdale, R., Hilbert, T. L. and M. S. Sarli, "Octgain™ Evaluation for the Manufacture of Reformulated Gasoline via LP Modeling", National Petroleum Refiners Association (NPRA) 1995 Annual Meeting, Paper AM.95.73, March 19-21, 1995.

Table 1 : Feed Properties

Feed	Heavy FCC Naphtha	215+ FCC Naphtha	230+ FCC Naphtha	Full-Range FCC naphtha	Reformate 1	Reformate 2
Research Octane	96.4	95.5	93.0	93.3	78.5	74.8
Motor Octane	84.0	83.8	81.5	81.1	73.8	71.8
API	22.8	34.6	41.1	46.3	61.0	67.9
Bromine Number	10.4	17.8	37.1	59.9	5.2	4.9
Sulfur, wt%	1.90	1.00	0.2	0.11		
Nitrogen, ppmw	180	76	98	52		
Distillation (D86), F						
IBP	194	215	232	107		
5 %	382		256	134	150	
10%	394	267	261	146	151	
20%	408		269	165		
40%	427		289	209		
50%	435	319	303	237	157	
60%	443		318	265		
80%	462		352	325		
90%	476	443	373	357	172	
95%	488		387	377	179	
EP	511	491	401	395		
Composition, wt%						
Isopentane					1	0.5
n-Pentane					1.6	1.7
Cyclopentane					1.8	2.4
Benzene	0.1	0.2	0.2	0.9	39.3	24.0
C6 Isoparaffins					28.6	39.9
n-Hexane					14.4	16.6
C6 Naphthenes					1.4	1.3
Toluene					2.3	0.7
C7 Isoparaffins					8.5	9.8
n-Heptane					0.9	1.1
C7 Naphthenes					0.3	0

Table 2: Properties of the blends (Measured, not calculated)

FCC Feed Reformate Feed FCC/Reformate ratio, vol/vol	Heavy Naphtha Ref 1 2/1	230+ Naphtha Ref 1 3/1	Full Range Ref 1 5/1	215+ Naph Ref 2 2.14/1	215+ Naph Ref 2 4.28/1
Research Octane	91.2	90.9	91.9	90.8	93.4
Motor Octane	80.8	80.6	80.5	80.3	81.5
API	32.9	45.7	56.4	43.9	40.0
Bromine Number	12.7	36.3	56.1		
Sulfur, wt%	1.5	0.14	0.11	0.72	0.84
Nitrogen, ppmw	130	71	47	55	64
Distillation (D86), F					
IBP	141	156	106		
5 %	166	190	135		
10%	177	199	143		
20%	197	212	154		
40%	386	253	180		
50%	418	276	197		
60%	425	298	221		
80%	452	338	303		
90%	469	366	345		
95%	494	382	368		
EP	510	398	411		
Benzene, wt%	10.4	9.2	8.3	6.9	4.1

Figure 1

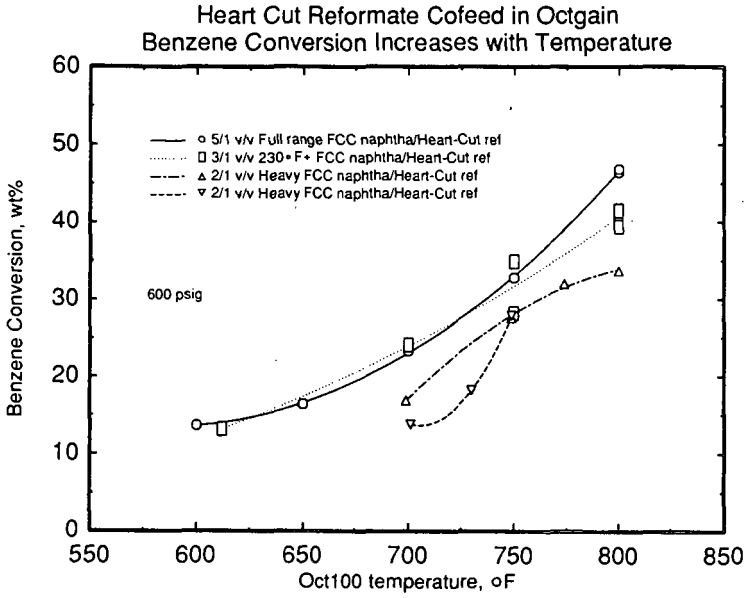

PPD/NAC 3:35pm 5/22/1995 benz_redn

Figure 2

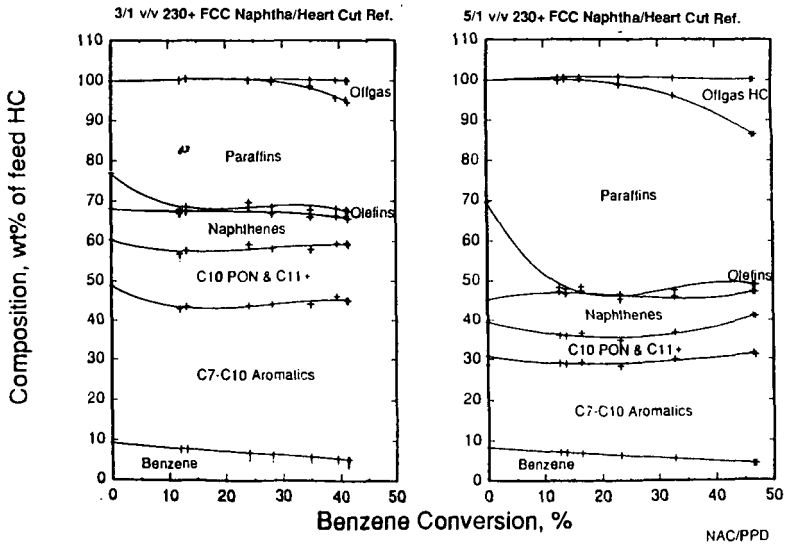

Figure 3

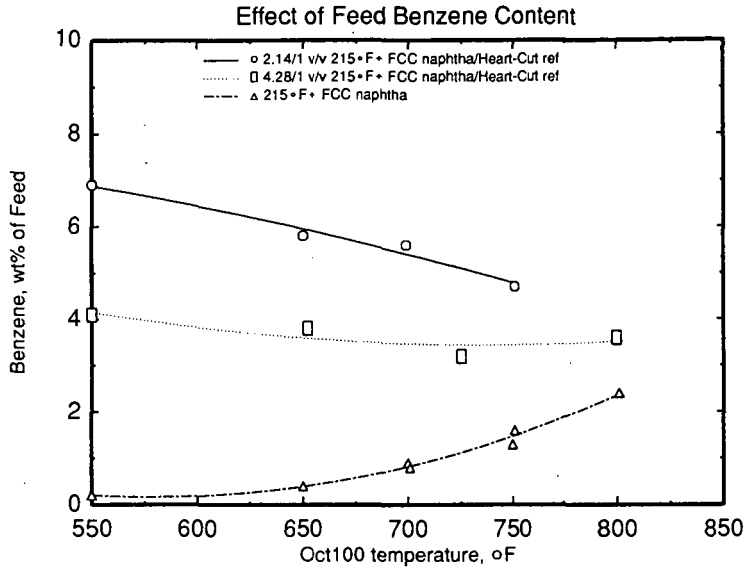

PPD/NAC/RH 3:34pm 5/22/1995 benz_redn

Figure 4

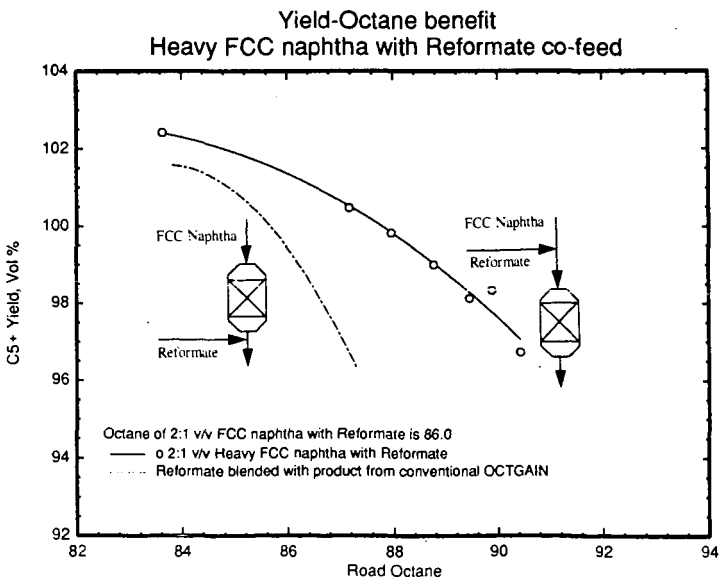

ALKYLATE IS KEY
FOR CLEANER BURNING GASOLINE

J. Randall Peterson
STRATCO, Inc.
4601 College Boulevard, Suite 300
Leawood, KS 66211

KEYWORDS: STRATCO, ALKYLATION, RFG

ABSTRACT
Alkylate is a key component in cleaner burning gasoline. The alkylation process reacts light olefins (propylene, butylenes, and amylenes) with isobutane in the presence of a strong acid catalyst. The alkylate that is produced consists of branched paraffins having a low Reid vapor pressure (Rvp), high research and motor octane numbers (RON & MON), low sulfur content, and a good driveability index (DI). Therefore, alkylation removes olefinic, high Rvp components from the gasoline pool and converts them to an ideal, high octane blendstock for cleaner burning gasoline.

INTRODUCTION
The intent of cleaner burning or "reformulated" gasoline is to reduce ground-level ozone formation by reducing the amount of volatile organic compounds (VOCs) emitted from automobiles during the high ozone season (primarily summer). Reformulated gasoline also strives to reduce toxic air pollutants throughout the year. These toxics include benzene, polycyclic aromatics, butadiene, formaldehyde, and acetaldehyde. The primary emission precursors are thought to be high Rvp gasoline components along with olefins, benzene, aromatics, and sulfur.

Alkylate from a modern STRATCO Alkylation Unit adds zero or negligible amounts of these emission precursors and toxics and reduces the Rvp of the gasoline pool. In addition, alkylate lowers the levels of benzene, aromatics, and sulfur through dilution and helps replace some of the octane lost when lead or aromatics are taken out of gasoline. For these reasons, an increase in the demand for alkylate is seen due to the increased worldwide requirements for cleaner burning gasoline.

Figure 1
Worldwide Alkylation Capacity

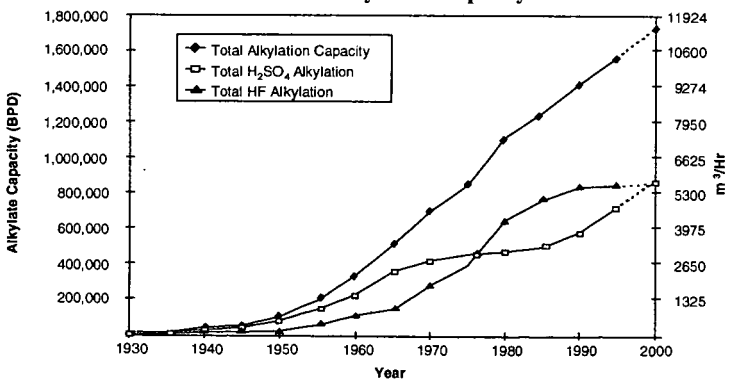

Source: Oil and Gas Journal, 1938-1994

In the United States, government legislation in the form of the 1990 Clean Air Act Amendments attempts to address the issue of excessive levels of ground-level ozone in the more populated areas of the country. As recently as 1987, approximately 100 metropolitan areas in the U.S. failed to meet the mandated ground-level ozone standard of 120 ppb. Ozone is of concern because even in very low concentrations it can cause damage to the lungs. It forms in the lower atmosphere as a result of reactions between hydrocarbons, nitrous oxides and sunlight.

Many other countries have watched the United States enact this legislation and are considering similar requirements. It is hoped that by producing cleaner burning gasoline, that some of the air quality problems surrounding the larger cities may be alleviated. While many countries are moving toward cleaner burning gasolines, no one other than the United States has passed a piece of legislation with the broad coverage of the Clean Air Act.

TRENDS

Legislation that requires reduced Rvp and benzene drives refiners to include more alkylate and ethers in the gasoline pool. In the U.S., alkylate is already being used as much for Rvp control as for octane. This trend will only increase in coming years. Significant increases in alkylate capacity may be required, especially with the larger emissions reductions of 29% in VOCs, 22% in toxics, plus a 6.8% reduction in NO_x required in the year 2000.

In California, the low olefin and Rvp specifications are driving several refiners to alkylate their amylenes. This has required an increase in their alkylation unit capacities. Furthermore, some refiners are considering changes in FCC catalyst to increase the amount of light olefins available for use as feedstock to the alkylation and etherification units.

Properties of alkylate that are exceptionally attractive to refiners are shown in Table 1. For comparison purposes, other common blending components are shown as well.

Table 1
Gasoline Blendstocks and Their Typical Properties

	Alkylate	FCC Naphtha	Reformate	Poly Gasoline
Aromatics, LV%	0	29	63	0
Olefins, LV%	0	29	1	95
Sulfur, ppmw	26*	756	55	125
T_{50}, °F (°C)	216 (102)	220 (104)	256 (124)	236 (113)
T_{90}, °F (°C)	289 (143)	366 (186)	334 (168)	346 (174)
Driveability Index**	1134	1223	1299	1251
RON	93.2	92.1	97.7	94.4
MON	91.I	80.7	87.4	81.9

Source: NPRA Survey of U.S. Gasoline Quality, January 1991

* Alkylate sulfur values of less than 10 ppmw are typically reported for STRATCO Units.

** $DI=(1.5 \times T_{10}) + (3.0 \times T_{50}) + T_{90}$ (D86 T values are in °F). Since the T_{10} value is highly dependent on the Rvp of the finished gasoline product, a value of 131°F (55°C) was assumed for all blendstocks.

As Table 1 shows, alkylate is an ideal blendstock. It has negligible amounts of toxics and ozone precursors. It has high RON and MON values. And its DI is consistently below the limit of 1200 currently proposed by the American Automobile Manufacturers Association (AAMA).

ALKYLATION CATALYSTS

Alkylation catalyst options for refiners today consist of hydrofluoric (HF) and sulfuric (H_2SO_4) acids. H_2SO_4 represents 45% of the world's installed capacity and HF represents 55%.

There is a significant amount of research being conducted on alternate alkylation catalyst technologies, primarily solid catalysts, but as of this date there are no commercially proven processes. Additional information on each of the research efforts in this area is supplied at the end of this paper.

STRATCO has been instrumental in developing options for refiners with HF alkylation units to convert to H_2SO_4 catalyst. STRATCO's ConvEx™ low cost HF to H_2SO_4 Conversion/Expansion Revamp Process reuses both the reaction and distillation sections of the existing HF alkylation unit. Both Phillips and UOP-designed HF alkylation units can be converted to H_2SO_4 alkylation units for about the same cost as installing mitigation facilities ($20 - 30 million U.S.). This revamp eliminates the safety hazards associated with HF, typically allows for a significant capacity increase, and often improves the octane of the alkylate product.

Feed Availability and Product Requirements

Historically, butylenes from the FCC were the traditional olefins fed to the alkylation unit. Today, alkylation units are using a broader range of light olefins including propylene, butylenes and amylenes. Alkylate composition and octane from pure olefins and mixed olefins are quite different for each catalyst as shown in Table 2:

Table 2
Alkylate Octanes

	H_2SO_4		HF	
	RON	MON	RON	MON
Propylene	89-92	88-90	91-93	89-91
Butene-1	97-98	93-94	90-91	88-89
Butene-2	97-98	93-94	96-97	92-93
Isobutene	90-91	88-89	94-95	91-92
Amylenes	90-92	88-90	90-92	88-89

Propylene

Alkylation of propylene in an HF unit is advantageous due to a significant hydrogen transfer side reaction that occurs:

Primary Alkylation in HF: $C_3^= + iC_4 \rightarrow C_7$ Alkylate

Hydrogen Transfer Reaction: $C_3^= + 2iC_4 \rightarrow C_3 + C_8$ Alkylate

This reaction will cause an increase in alkylate octane resulting from equimolar production of more C_8 alkylate (from the $iC_4^=$ formed) and less C_7 alkylate (since $C_3^=$ has disappeared). Reaction extent varies greatly, with 15-20% being common, while the reaction is favored by process conditions (such as high isobutane/olefin ratios) which produce high quality alkylate. Refiners must carefully analyze isobutane and propane price projections and the value of incremental octane to determine the impact of this reaction on unit economics.

Butylenes

Composition and quality of alkylates produced from butene-1 and butene-2 are very similar for H_2SO_4 alkylate but not for HF alkylate. When butene-1 is used, HF alkylate contains a lower amount of trimethylpentanes (TMP's) and a greater amount of dimethylhexanes (DMH's) than H_2SO_4 alkylate. This composition difference results in a several octane number advantage for H_2SO_4 alkylate. Conversely, alkylate produced from butene-2 is similar whether produced from the H_2SO_4 or HF process. Although not shown, distribution of TMP's varies significantly, with HF alkylates having a higher concentration of 2,2,4-TMP (100.0 RON) but a lower concentration of the other TMP isomers.

The 2,3,3- and 2,3,4-TMP's (109.6 and 106.1 RON, respectively) are more predominant in H_2SO_4 alkylate, accounting for the slight octane advantage. HF alkylation with isobutene yields a product that has a higher concentration of TMP's resulting in a several octane number advantage over the corresponding H_2SO_4 alkylate. Addition of an MTBE unit ahead of an alkylation unit improves H_2SO_4 alkylate quality and reduces HF alkylate quality.

Amylenes

Amylenes have traditionally been left in the FCC gasoline pool due to their relatively high octanes. However, these constituents also have high Rvp values. As refiners continue to look for means of reducing the Rvp of the gasoline pool, STRATCO is seeing continued interest in alkylation of these components. For comparison purposes, the octanes and Rvp of amylene alkylate are also provided in Table 3.

Table 3
C_5 Octanes and Vapor Pressures

	RONc	MONc	Rvp (Psi / Bar)
1-Pentene	90.9	77.1	19.1 / 1.32
2-Pentene*	~94	~80	15.3 / 1.06
2-Methyl-1-Butene**	102.5	81.9	18.4 / 1.27
2-Methyl-2-Butene	97.3	84.7	14.3 / 0.99
3-Methyl-1-Butene***	?	?	26.4 / 1.82
Cyclopentene	93.3	69.7	? / ?
Isopentane	92.3	90.3	20.4 / 1.41
Pentane	61.7	62.6	15.6 / 1.08
C_5 Alkylate	**91.5**	**90.0**	**3.0 / 0.21**

* 2-Pentene octane values not found in literature. Values are estimated.

** Literature specifies 2-Methyl-1-Butene RONc equal to 0.2 gm of lead per gallon of 2,2,4-trimethylpentane. 102.5 value is estimated.

*** 3-Methyl-1-Butene octane values are not found in literature.

Amylene alkylate octanes from either a H_2SO_4 or HF alkylation unit have lower octanes than those produced with other feedstocks. In H_2SO_4 alkylation of amylenes, acid consumption increases about 30 to 50% above that for butenes. In an HF unit, acid soluble oil production increases when amylenes are alkylated.

Safety & Environmental Considerations

Safety and environmental concerns are extremely important when choosing an alkylation technology. A huge concern is the large volume of LPG present within the unit. Refineries must protect against conditions that could lead to LPG releases and potential fire hazards. All of the alkylation technologies being evaluated have similar volumes of hydrocarbon within the unit. In addition, neither acid catalyst impacts the flammability of LPG, therefore, no one technology has an advantage over another in this regard.

Another major safety concern is the acid catalyst used to promote the reaction. Both HF and H_2SO_4 acids are hazardous materials, however, HF is considerably more dangerous. In the United States, HF has been identified as a hazardous air pollutant in current federal and state legislation. Sulfuric acid has not.

HF and H_2SO_4 represent a potential danger to personnel working on alkylation units. Contact with either HF or H_2SO_4 can result in chemical burns. However, HF burns tend to be more severe since the fluoride ion penetrates the skin and destroys deeper layers of tissue. If not treated, it may even cause dissolution of the bone. In addition, inhalation of HF vapors may cause pulmonary edema and, in severe cases, may result in death.

The volatility of the acid at ambient conditions is a chief concern. HF is a toxic, volatile gas at these conditions while H_2SO_4 is a toxic liquid. Therefore, H_2SO_4 is much easier to contain in the event of an accidental release. In more densely populated areas of the world, safety and environmental concerns of HF usage have given H_2SO_4 alkylation a notable advantage.

In 1986, tests were conducted in the Nevada desert to determine the dangers of a possible HF liquid release. Under conditions similar to those that exist in an alkylation unit, lethal concentrations of an HF aerosol were present up to 5 miles from the release points. During these tests, HF releases were observed to be much more dangerous than previously thought.

Although HF alkylation plants have, for many years, had good safety records, several accidents that have occurred in the past ten years have raised questions about potential dangers. The most serious accident occurred in October, 1987, in Texas City, Texas. A piece of equipment was dropped on an overhead line from a partially filled HF tank. The line ruptured and allowed HF to vaporize and form a toxic aerosol cloud. As a result, 3,000 people were evacuated from the nearby community and several hundred people were hospitalized. Another accidental release of HF at a different refinery in the late 1980s killed one refinery worker and critically injured another. An incident in the early 1990s killed two pump maintenance workers.

Due to these risks, many refiners are implementing water mitigation and detection devices in an effort to remove any HF that would vaporize in the event of a release. With water/HF ratios of 40:1, nearly 90% of the HF can be removed. However, these systems are expensive and there is the concern that the water sprays could become inoperative as a result of an accident. In addition, details have not yet been obtained, or at least reported, on the fate of the HF that is not removed by the water sprays. Many refiners with HF units are also considering HF modifiers to reduce the vapor pressure and thus the aerosol-forming tendencies of HF. These HF modifiers are still in the development stage and are expected to be used in combination with mitigation systems. Recent tests of two of these additives have indicated substantial reductions in HF aerosol and vapor cloud formation. Figures quoted are in the range of 63-80% reduction of airborne HF due to the additive. When coupled with an effective mitigation system, reduction in the quantity of airborne HF would be in the range of 95-97% compared to an unmitigated release from an alkylation unit without additive.

Tests conducted in 1991 by Quest Consultants, Inc. showed that the potential for a H_2SO_4 aerosol formation from an alkylation unit release is highly unlikely. Several tests were performed under a variety of conditions resembling those observed in an alkylation unit. The tests provided conditions favorable to the formation of airborne particles. However, the released acid did not remain airborne and an aerosol was not formed. It is apparent, based on these tests, that a sulfuric acid aerosol will not form under conditions similar to those present in a STRATCO Effluent Refrigerated Alkylation Unit.

SOLID CATALYST DEVELOPMENTS

Research in the area of a solid catalyst for alkylation has been ongoing for many years. Numerous patents exist for different catalysts, catalyst supports, and processes. It is well known that Lewis acids will catalyze the alkylation reaction (alkylation of isobutane with olefins was discovered using aluminum chloride promoted with HCl). Several of the current preferred solid catalysts use a salt of HF: either boron trifluoride (BF_3) or antimony pentafluoride (SbF_5). Since every alkylation process produces heavy polymers, solid catalysts have the tendency to foul quickly. Therefore, the solid catalyst process has two major hurdles to overcome: catalyst life and catalyst regeneration. Several companies are engaged in active research in this area, but no one has yet commercialized a new alkylation technology.

Catalytica

A joint venture of Neste Oy, Conoco, and Catalytica started up a 7 BPD (0.05 m^3/hr) pilot plant in January, 1993 at Neste's Technology Center adjacent to their refinery in Porvoo, Finland. It has been operating on MTBE raffinate. According to the patent literature, the research group is testing boron trifluoride on an alumina support.

The technology requires a feed preparation section to reduce water and impurities such as sulfur and oxygenates. A CSTR reactor configuration using a dilute slurry of catalyst is currently being used although other reactor designs are being considered. Catalyst is continually removed from the reactor and continually regenerated. Spent catalyst exits the regeneration section and is disposed as non-hazardous waste. With MTBE raffinate, the research group reports that they have been able to produce good quality alkylate with high octane at reasonable I/O ratios (5-12).

However, it has been stated that additional funding for the project from Neste Oy and Conoco has been discontinued. As a result, the pilot plant is no longer operational. It appears that these partners feel that this process does not have a significant economic advantage over the existing alkylation technologies. Catalytica continues to promote the technology, although they will need an additional funding source to continue their research, development and commercialization efforts.

Haldor Topsoe

Haldor Topsoe's technology utilizes triflic (trifluoromethanesulfonic acid) on a bed of silica. The triflic is supported on the silica in a plug flow, packed bed reactor. Haldor Topsoe claims that since their technology is not a true solid catalyst but rather a liquid catalyst on a solid support, that less deactivation of the catalyst occurs. They have been operating a 0.5 BPD (0.003 m^3/hr) pilot plant since 1991.

With time, the triflic migrates from one end of the bed to the other. As the acid catalyst breaks through, it is sent to an acid recovery unit for separation of ASO and acid. An alkylate wash unit is used to remove the catalyst from the alkylate product. The reaction's optimal temperature has not been made clear; they have stated that this technology may or may not require refrigeration. However, if octane is valuable, refrigeration is recommended. Haldor Topsoe is working with the M.W. Kellogg Company on the engineering for this process. They are currently looking for a refining partner to participate in scaling up this technology.

IFP

IFP has done some work with a fluorine modified zeolite, but they report that the prospects for zeolites in alkylation are not good due to poor selectivity and stability. Recent work appears to be centered around "promoted H_2SO_4" on silica. Not much information has been released about their research.

Kerr McGee

Kerr McGee has done some preliminary, laboratory scale work using aluminum chloride at levels of less than 1% as a promoter for the alkylation reaction. With this scheme, the catalyst is actually soluble in the hydrocarbon phase. As the catalyst ages, it will precipitate out of the hydrocarbon and then can be gravity separated for recovery and regeneration.

In order to proceed in the research and development of this technology, Kerr McGee will require a partner for funding. The Kerr McGee Corporation is currently engaged in exiting from the refining business.

Mobil

Mobil has been granted many patents on solid catalysts for alkylation. Most of these involve boron trifluoride plus zeolites as the catalyst.

CR&L

CR&L (a partner with ABB Lummus in the CD Tech joint venture) is doing research with a salt of antimony pentafluoride on a silica support. Their scheme uses a fluidized bed at a relatively cold temperature, similar to that of the H_2SO_4 alkylation process. The 10 BPSD (0.07 m^3/hr) pilot plant that they were operating at Clark's Port Arthur, TX refinery since December of 1993, was shut down in 1995. The company cited wide feedstock fluctuations and their negative impact on the catalyst as the primary reason for shutting down the pilot plant. CR&L has subsequently been operating a bench scale pilot plant at their office in Pasadena, TX with a capacity of 1 BPSD (0.01 m^3/hr). They are refocusing their efforts in an attempt to improve catalyst regeneration requirements.

UOP

UOP is also working on solid catalyst alkylation technology, referred to as SCA, although little technical data is available on the process. They have been granted patents utilizing carbon supported HF and zeolites. We believe that in order to minimize catalyst regeneration, a rather extensive feed pretreatment system would be required to reduce feed contaminants down to very low levels.

Very few details are available on the specifics of the reactor employed by UOP for this process. Olefin conversion is said to be nearly 100% depending upon the frequency of internal catalyst regeneration. UOP claims the alkylate product is comparable to that produced in either an H_2SO_4 or HF alkylation unit. We understand that this comparison has only been made for one particular butylene isomer and the same comparison has not been made for a standard refinery alkylation feed.

From a utility and capital standpoint, UOP has stated that they expect SCA expenses to be somewhat higher than existing HF technology expenses and to be comparable with existing H_2SO_4 technologies. Until this technology is used commercially, these claims cannot be challenged.

SUMMARY

International demand for alkylation technology will continue to increase as countries look to their refining industries to produce cleaner burning fuels. Due to heightened concerns over the safety of HF, the majority of alkylation technology implemented in the last five years has been H_2SO_4 technology. During this time, over 90% of the H_2SO_4 alkylation unit revamps & expansions as well as grassroots units built throughout the world have been designed by STRATCO (shown in Figure 2).

Figure 2
Installed Alkylation Capacity (1990-1995)

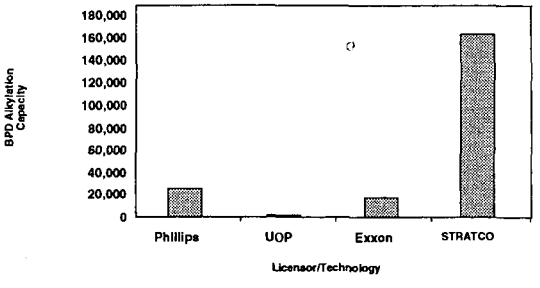

While the search for a commercially proven solid catalyst technology continues, STRATCO is committed to finding ways to improve our technology as well. We currently have an extensive alkylation R&D program underway with a goal of minimizing catalyst requirements and improving equipment efficiencies for our technology. We are also committed to providing cost-effective methods to convert HF alkylation units to use H_2SO_4 catalyst. For about the same cost as mitigation, STRATCO's ConvEx™ conversion revamp eliminates the liability of HF permanently, typically allows for a significant capacity increase, and usually improves the octane of the alkylate product.

STRATCO will continue in our efforts to provide the utmost in customer service and maintain our position as the leading licensor of alkylation technology well into the 21st century.

PREPRINT EXTENDED ABSTRACT
Presented Before The Division Of Environmental Chemistry
American Chemical Society
Orlando, FD August 18-23, 1996

The Analysis of Reformulated Gasolines Using Fast Gas Chromatography / Mass Spectrometry

Vincent P. Nero and Donald E. Drinkwater,
Texaco FLTD, Beacon, NY 12508

The requirement that all reformulated gasoline (RFG) sold in the United States be analyzed by gas chromatography / mass spectrometry (GC/MS) for aromatic content presents a unique challenge and opportunity for petroleum analytical analyses. A fast GC/MS method was developed which encompasses or surpasses not only the basic EPA performance requirements for analysis of total aromatics, but will simultaneously measure individual aromatics and oxygenates in reformulated gasolines. Furthermore, the combined procedure requires only 10 minutes of instrument and computational time. In contrast, ASTM Method D 5769 generally takes 90 minutes just to measure total aromatic content. The measurements of oxygenates, benzene, and toluene also compare favorably to the standard ASTM methods. The method matches the precision and accuracy of ASTM Method D3606, a GC/GC method, which is the only current acceptable method for individual aromatics in RFG. Furthermore, it can measure methyl *t*-butyl ether (MTBE) and *t*-amyl methyl ether (TAME) as accurately as ASTM D5599, the approved OFID method for oxygenates.

The fast chromatography method meets of all of the requirements of the EPA and ASTM methods. The EPA primarily list performance objectives requiring GC/MS and 2% overall accuracy. The ASTM Method does not restrict the chromatography or types of internal standards. The Texaco Method has procedural enhancements which enable it to expand the basic scope of these methods beyond total aromatics and to surpass their precision and accuracy while maintaining performance requirements of both the EPA and ASTM methods. These enhancements are:

- The additional use of deuterated surrogate, toluene, which is not required, but allowed by the ASTM method.
- The use of micro-bore capillary gas chromatography, which reduces greatly processing time, and prevents ion saturation of the mass spectrometer source.
- More appropriate selection of quantitation ions, which enhances precision and accuracy without changing any operating procedures.

Since toluene is generally the most abundant individual aromatic hydrocarbon component in gasoline, its accurate measurement is critical. (The EPA requires that total aromatics in RFG be measured to the within 2% of the theoretical value.) Benzene is a poor choice as an internal standard for toluene for two reasons. First, benzene is found in commercial gasolines at a much lower level than toluene. (~0.1-.5% vs. ~10%) Second, benzene has a very different mass spectral fragmentation pathway. It lacks a benzylic carbon-carbon bond. The addition of a deuterated toluene surrogate at an appropriate concentration ensures its accurate measurement.

Typical calibration curves illustrating benzene and toluene are shown in *Figures 1 and 2.* Both curves are essentially linear over the entire concentration range with correlation coefficients approaching 1.0.

The use of micro-bore and mini-bore capillary GC columns for quantitative analysis provides a number of advantages over conventional capillary columns. In addition to the decreased elution time provided by the more efficient separation, the decreased capacity of these columns may be used to increase the dynamic range of the mass spectrometer, thus improving calibration linearity and accuracy. The smaller inside surface area and shorter length of these columns leads to a much reduced phase bleed level in the ion source, lengthening the time between ion source cleanings and, therefore, instrument recalibration. The decreased gas flow through the narrow-bore columns greatly improves the gas load into the ion source, as well as simplifying the running of these columns at high split ratios for neat samples such as gasolines.

Figure 3 shows the comparison of the chromatography using a conventional capillary column and a micro-bore capillary column in the region of C_3-benzenes (trimethyl benzenes, ethyl methyl benzenes, and propyl benzenes). Note that there is no loss of chromatographic resolution or change in the relative ion abundances, but the GC retention time has been reduced from 38 minutes to 6 minutes.

Ten full mass range scans across each GC peak are necessary for adequate precision. The mass spectrometry should be capable of scanning from 45 to 250 amu every 0.1 seconds. Most modern commercial instruments can achieve this rate. The Texaco method has been implemented on four different mass spectrometers from three different vendors.

Table 1 shows typical repeatability for this method (generally the standard deviations are less than 0.5). The EPA requires accuracy within 2.0% of the actual value. *Figure 4* shows a comparison of benzene data using this method, which was collected on four different GC/MS systems.

Comparison to other standard methods.

Figure 4 also compares the analysis of benzene in gasoline using ASTM Method D3606 (a GC/GC column switching method, which is the only current acceptable method for individual aromatics in RFG) and the Texaco GC/MS Method. The results of both methods is essentially identical. (However, the Texaco Method also simultaneously measured all the individual aromatics, their total sum, and oxygenates.)

Table 2 compares the analysis of total aromatics in gasoline using the Texaco fast GC/MS method with the ASTM Method D1319, using fluorescent indicator adsorption open column liquid chromatography (FIA), ASTM Method D5769 (the routine total aromatic method using GC/MS), and ASTM D5580 Method (a GC/GC column switching method being adopted by CARB). The FIA method is not precise, but it is on average accurate. The average of 65 different laboratories produced results essentially the same as the Texaco fast GC/MS Method. The routine ASTM D5780 generally will result in somewhat lower total aromatics, since the method does not currently consider the differences in mass spectral response factors between carbon and hydrogen benzylic losses in the heavier alkyl aromatic region. For example pentamethyl benzene molecular ion has a very different relative response factor to that of the pentyl benzene.

Figure 5 compares the analysis of MTBE and TAME using the fast GC/MS method and the ASTM Method D5599 (OFID). Again, the Texaco Method results are essentially the same as the OFID results. Again, it must be noted that these results were obtained simultaneously with the measurements of benzene, toluene, and total aromatics.

figure 1

Benzene Calibration

Benzene m/z 78 (0.1 to 5 wt%) vs. Benzene-d6 m/z 83,84 (2 wt%)

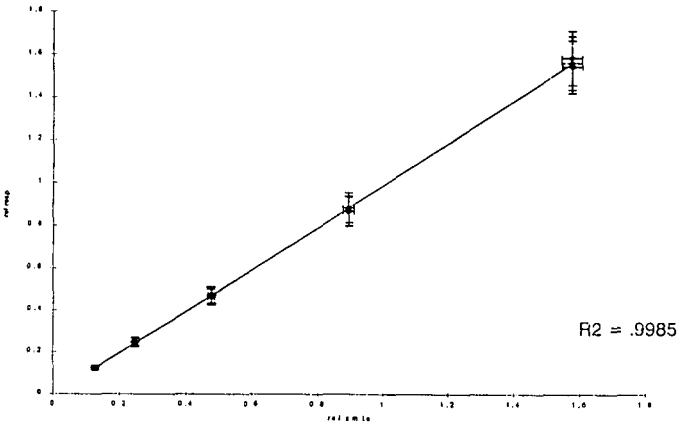

figure 2

Toluene Calibration

Toluene m/z 92 (2 to 20 wt%) vs. Toluene-d8 m/z 99,100 (7 wt%)

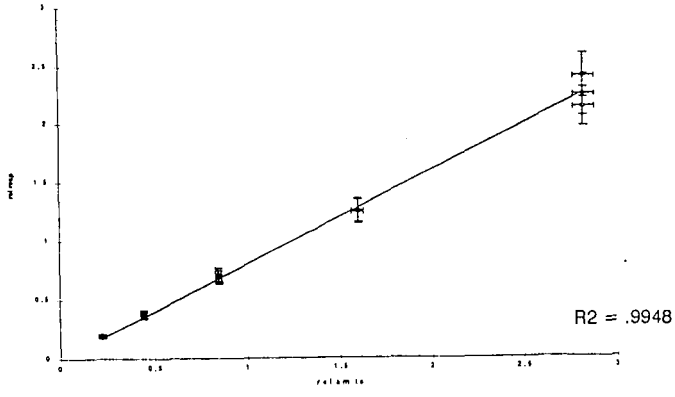

Generally used version of ASTM Method
SIR Chromatogram

figure

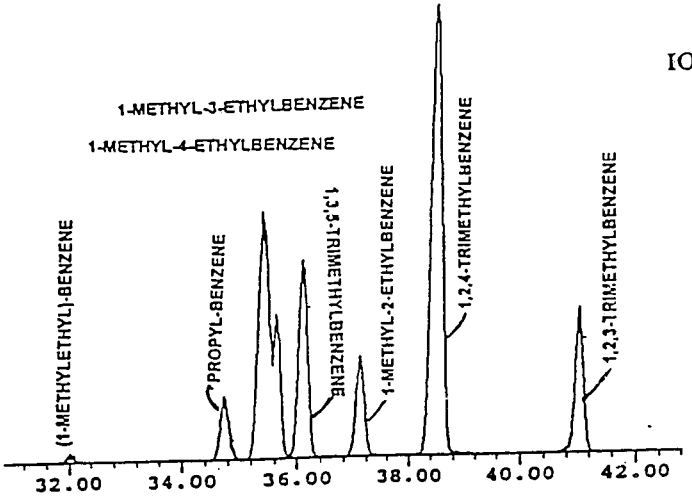

Texaco Version SIR Chromatogram
(still meets all EPA and ASTM requirements)

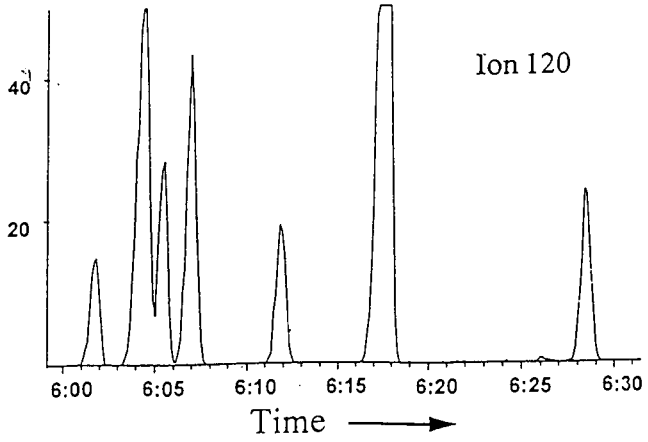

figure 4

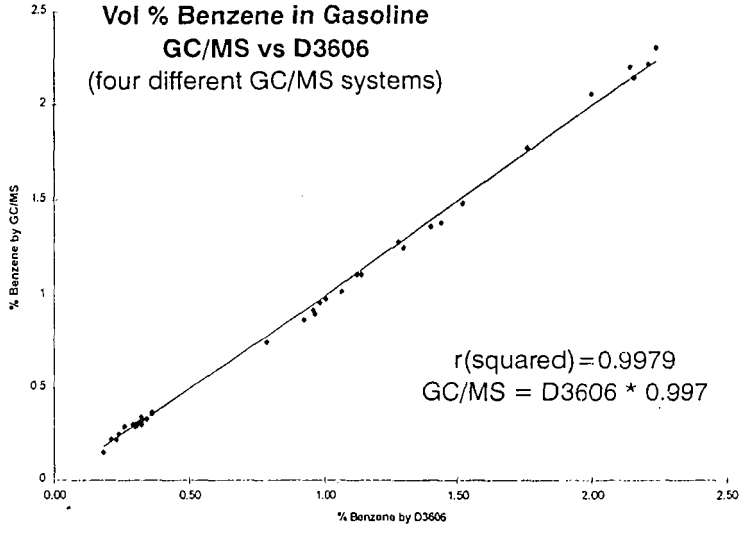

figure 5

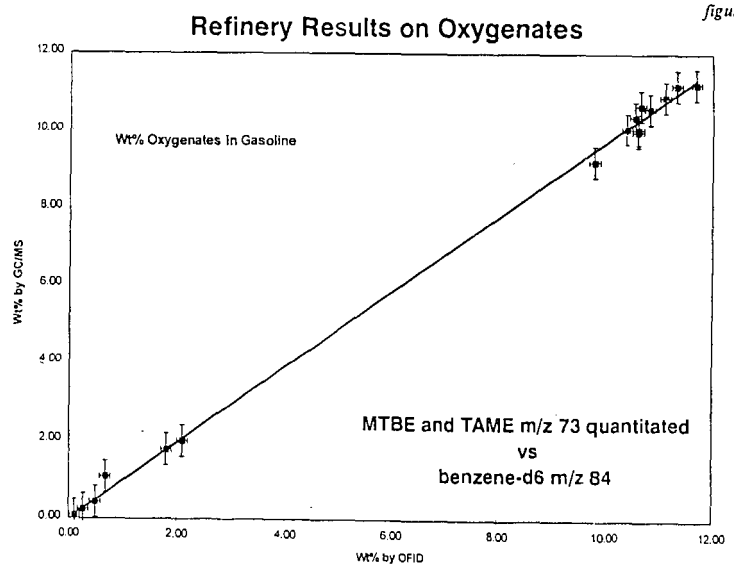

Sample Precision (wt %)

table 1

Compound	#1	#2	#3	#4	Average	Std Dev
Benzene	**1.13**	**1.16**	**1.20**	**1.15**	**1.16**	**0.03**
Toluene	8.80	8.45	8.66	8.28	8.55	0.23
ethyl benzene	2.30	2.30	2.34	2.18	2.28	0.07
m,p xylene	5.04	5.09	5.23	5.04	5.10	0.09
o-xylene	1.73	1.71	1.77	1.64	1.71	0.05
cumene	0.07	0.09	0.08	0.07	0.08	0.01
propyl benzene	0.36	0.39	0.36	0.37	0.37	0.01
m-ethyl toluene	1.15	1.18	1.20	1.20	1.18	0.02
p-ethyl toluene	0.70	0.72	0.68	0.70	0.70	0.02
1,3,5-trimethyl benzene	0.59	0.60	0.59	0.58	0.59	0.01
o-ethyl toluene	0.38	0.36	0.36	0.38	0.37	0.01
1,2,4-trimethyl benzene	1.73	1.72	1.71	1.73	1.72	0.01
1,2,3-trimethyl benzene	0.32	0.33	0.34	0.32	0.33	0.01
indan	0.55	0.56	0.55	0.59	0.56	0.02
C4 benzenes (cymenes)	0.11	0.08	0.11	0.12	0.10	0.01
C4 benzenes (straight chain)	1.49	1.46	1.50	1.47	1.48	0.02
C4 benzenes (tetramethyl)	0.29	0.29	0.27	0.26	0.28	0.01
C6 benzenes	0.08	0.09	0.08	0.08	0.08	0.01
naphthalene	0.19	0.20	0.20	0.20	0.20	0.01
C5 benzenes	0.22	0.22	0.20	0.22	0.21	0.01
2-methyl naphthalene	0.18	0.18	0.18	0.18	0.18	0.00
1-methyl naphthalene	0.07	0.08	0.08	0.06	0.07	0.01
TAME	0.0	0.0	0.0	0.0	0.0	0.0
MTBE	11.5	11.2	11.5	11.4	11.4	0.1
Total Aromatics	**27.46**	**27.25**	**27.69**	**26.82**	**27.30**	**0.37**

table 2

	Jul-95			
Aromatics			2SD	N
ASTM FIA (Corrected)	25.46	+/-	3.76	65
Texaco fast GC/MS	25.60			
routine ASTM D5769 GC/MS	20.94	+/-	2.00	27
ASTM 5580	27.20	+/-		2
Benzene				
ASTM 3606	0.63	+/-	0.12	50
Texaco fast GC/MS	0.65			
routine ASTM D5769 GC/MS	0.63	+/-	0.10	20
ASTM 5580	0.59			2

	Aug-95			
Aromatics			2SD	N
ASTM FIA (Corrected)	21.09	+/-	4.06	49
Texaco fast GC/MS	19.32			
routine ASTM D5769 GC/MS	17.47	+/-	3.12	33
ASTM 5580	19.73	+/-	1.96	3
Benzene				
ASTM 3606	0.29	+/-	0.04	56
Texaco fast GC/MS	0.29			
routine ASTM D5769 GC/MS	0.30	+/-	0.02	25
ASTM 5580	0.26	+/-	0.02	3

	Sep-95			
Aromatics			2SD	N
ASTM FIA (Corrected)	13.59	+/-	2.08	54
Texaco fast GC/MS	13.88			
routine ASTM D5769 GC/MS	12.79	+/-	1.58	34
ASTM 5580	14.41	+/-	2.14	3
Benzene				
ASTM 3606	0.26	+/-	0.08	58
Texaco fast GC/MS	0.27			
routine ASTM D5769 GC/MS	0.28	+/-	0.06	28
ASTM 5580	0.23			2

A LIQUEFACTION KINETIC RESEARCH NEEDS ASSESSMENT

J. Ferrance, and R. P. Warzinski
U. S. Department of Energy
Pittsburgh Energy Technology Center
Pittsburgh, Pennsylvania 15236

Keywords: Direct liquefaction, kinetic modeling assessment, processing variable effects

INTRODUCTION In February 1989, the Department of Energy released its assessment of the research needs for coal liquefaction.[1] Under direct liquefaction, 4 of the 12 recommendations focused on developing models and determining kinetics. Reasons accompanying these recommendations stressed the need to understand the retrograde reactions, the reactions taking place as the coal is heated to the reaction temperature, and the effects of coal types and solvent on liquefaction reactions. By understanding the liquefaction process better, suggestions for improving the process may be made. A good kinetic model would provide a basis for testing suggestions which would attempt to control reactions or effects in the development of improved liquefaction technologies. Brandes et al. suggests that a kinetic model could also possibly have a large impact on the economics of coal liquefaction.[2] Cost factors which could be studied using a kinetic model include: coal preparations, reactor throughput, hydrogen usage, catalyst usage, product yields and selectivity, and process control.

The purpose then of a kinetic model is to have a tool for evaluating the liquefaction process as the inputs and the processing conditions are changed. The model has to be able to account for the effects of these changes and provide valuable results to someone using the model. As a starting point for the development of this type of kinetic model, the assessment described in this work was carried out. The assessment included an intense review of earlier kinetic models found in the literature, along with reviews of the current work being carried out in this area. It was meant to discover the strengths, weaknesses, and limitations of available models and provide guidelines for future models. At the same time, the assessment looked at questions of who uses liquefaction models, why they use them, and what they expect the model to do.

SMALL-SCALE MODELS At the level of small-scale processes, most kinetic models for batch reactors use a variation on the simplified reaction scheme shown in Figure 1. Reaction rate constants are determined in each of these studies by fitting liquefaction results obtained in that particular set of experiments. Because of this, no consistent set of rate constants or activation energies has been found for these reactions. Even within a single study, changing coal or solvents required new rate constants to be determined. More complicated reaction schemes, based more on the actual chemistry taking place during the liquefaction process, have also been developed. A scheme by Suzuki, shown in Figure 2, includes a free radical pool as the first product of coal dissolution.[3] This allows retrograde reactions to be included as one of the important reactions taking place during liquefaction.

Weller found four problems with these types of kinetic models.[4] First, the reactions listed are not elementary and therefore cannot be described by simple rate laws. Second, the liquefaction system is not a single phase. Third, the quantities used in rate laws must be described in terms of liquid-phase concentration, not just masses in the reactor. Fourth, the reactivity of the intermediate products change with time. This assessment has revealed three additional problems with these models. One, they do not include hydrogen as a reactant but assume hydrogen is present in excess and does not affect the rates. Two, reactions during heat-up times are usually ignored, but even for fast heat-ups (1-2 min) significant amounts of the coal will break down during this period. Three, these models do not fulfill the basic purpose of a model because they have little predictive value for determining results of liquefactions run under different processing conditions.

This situation has been partially corrected in a current model containing additional retrograde reactions and calculations during the heat-up time.[5] The reaction scheme for this model is shown in Figure 3. The kinetic expressions derived from this scheme are based not on mass, but on liquid-phase concentrations. This can be done because thermodynamic calculations are also included in the model to account for the three-phase nature of the liquefaction process. Hydrogen is included directly in the necessary expressions, and the gas-phase contribution to this concentration is determined through the mass transport calculations which are also part of the model. Processing variables are incorporated directly into these calculations in one or more ways. An example is the type of solvent, which affects mass transport through its viscosity, thermodynamics through its partition coefficient, and kinetics through its hydrogen donating ability. The effects of changing some processing variables can be predicted, but some important variables, such as the type of catalyst used, have not yet been incorporated into this model.

Like most of the earlier models, this model also suffers from the fact that the reactions are not truly elementary and the reactivity of the intermediate products change. Lack of

elementary reactions in the scheme is inherent in any model dealing with coal. Because of the large number of reactions actually taking place within the coal, there is no real way to include and write kinetic expressions for all of these reactions (see Current Models below). In models which lump the products as preasphaltenes, asphaltenes, and oils, these simple product definitions give no indication of the internal nature of each product. Reactions within a single product, which change the quality and reactivity of that product, cannot be included in the model. Inclusion of more product fractions in the model would be one way of handling this problem. The small amounts of material recovered in small-scale batch reactors, however, often prevent further fractionation of the products.

In continuous reactors, sufficient product can be recovered for separation into additional fractions, but this is not always done. Many of the models for continuous reactors therefore also use solubility-defined products and suffer from the same problems as the batch models. Studies which have fractionated the oil into more species by boiling point ranges usually then lump the widely different preasphaltene, asphaltene, and nondistillable oil fractions as a single fraction. This single product is usually called resid or solvent refined coal (SRC). Though reactions and reactivities of the distillate fractions can be defined in models using such products, the major changes which take place within the resid product are now lost.

One of the better continuous models was given by Singh et al.[6] This model defined three distillate products based on boiling point ranges along with a SRC product. The kinetic expressions developed in the model included terms for both the hydrogen pressure and the mineral matter content of the slurry. Inclusion of these terms made the model applicable to more situations, but no justification was given as to the final form of these terms which were based on empirical fitting of experimental data. In addition, the kinetic parameters were still limited by a simplified reaction scheme, containing an instantaneous initial reaction and no retrograde reactions and experimental data from only a single coal.

LARGER SCALE MODELS Kinetic modeling of large-scale liquefaction processes was carried out using both Wilsonville and HTI pilot plant data. The Wilsonville model was developed in two parts using data from both the actual plant and a specially designed batch reactor.[7] For the thermal liquefaction unit, the reaction scheme, shown in Figure 4, considered light and heavy hydrocarbon gas products along with a resid fraction, but lumped all of the liquid product into a single distillate fraction. Heteroatom gases were also included as products since much of the hydrogen used in the liquefaction process goes into these products. In setting up the actual kinetic expressions, the Wilsonville model developers used the results of tracer studies which showed that the thermal liquefaction unit could be modeled as a CSTR. However, two different residence time definitions were used in the various kinetic expressions. The actual residence time above 370°C, including both the reactor and part of the preheater, was used in the hydrocarbon gas formation expressions, but the nominal residence time, just over the reactor, was used in the heteroatom expressions. These choices came purely from data fitting and had no theoretical basis.

The hydrotreating unit part of the Wilsonville model included a set of secondary reactions considered to be purely catalytic. These reactions, shown in Figure 5, included hydrotreated resid and hydrotreated distillate products. Internal reactions within these two products are included in the model to account for changes in their reactivity and composition. No indication was given, however, on how these hydrotreated products could be separated or identified, and kinetic expressions were not developed for these reactions. Catalyst deactivation terms were included in the kinetic expressions which were determined from this reaction scheme.

The overall Wilsonville model was thus not only specific for the processing condition being used, but suffered from the same problems as the small-scale models. Two-phase effects were accounted for in some of the expressions by using actual residence times, but not for all of the reactions, and the choice of residence time definition for a reaction was not justified. The reaction scheme was also too simplified with product lumps which were too encompassing.

The model developed at HTI, shown in Figure 6, is significantly different from the Wilsonville model.[8] Two distillate products, a high boiling gas-oil, and a low boiling naphtha, were defined, along with resid and gaseous products. High, low, and unreactive coal fractions were defined, and the reactions scheme included both parallel and implied sequential reaction pathways leading from coal to all of the products. This represents a move towards a reaction scheme based more on the underlying liquefaction mechanisms. Two problems remain, however. First, there are no retrograde reactions specified, and, second, no secondary reaction scheme is established.

Coal type was taken into account in the model by the amounts of high, low, and unreactive fractions (a, b, and c), and by the distribution of products formed in the initial parallel reactions during coal dissolution (f-j). One would then expect that if a-c and f-j could be determined independent of the model, then liquefaction using any coal type could be predicted by this model. Unfortunately, the rate constants (k_1 and k_2) used in the coal breakdown reactions were also made coal dependent. Catalyst deactivation rates, included for reactions which were

found to be catalyst dependent, were made coal dependent as well.

Additional problems with the HTI model included inconsistencies in both the reaction scheme and the rate constants which required changes in the model when it was applied to batch autoclave liquefactions. The model developers suggest that their product lumps are too large and that significant changes occur within the individual product fractions during liquefaction. No reactions describing this process are included in the model, however. There are no kinetic expressions for heteroatom removal or hydrogen consumption, and gas-oil kinetics are only found by difference in the model rather than through a direct expression.

CURRENT WORK In addition to the current model for small-scale batch processes described above,[5] work is also being conducted on statistical models. These models represent coal by a large number of random chain molecules which have the same statistical characteristics (carbon content, aromatic content, etc,) as the original coal. Rules for breaking bonds within the chains are specified and a Monte Carlo simulation is run to follow the breakdown of the coal molecules with time. By defining products based on specific chain characteristics, the production of individual products with time can also be followed. To be comparable to experimental data, the products defined in the model must be characterizable by methods currently available for analyzing coal liquefaction products.

Monte Carlo simulations require significant amounts of computer time to carry out. This time increases greatly as the number of initial molecules in the simulation increases, as the number of possible reactions increase, or as simulation time is increased. This limits the starting point to a small representative sample of all possible coal chain molecules. Reactions which take place within a single product fraction, such as naphtha, can be included, but will not really be detectable at the actual experimental level. In addition, these simulations usually represent purely kinetic descriptions of the process and do not account for transport or thermodynamic considerations of the reaction system.

MODEL USERS Two groups of researchers are expected to be the predominant users of coal liquefaction kinetic models: those who use them for economic analysis, and those who use them for scientific or engineering analysis. For economic analysis of large-scale processes, the structure or organization of the model itself is not usually important. What is needed is for the model to accept specific characteristics of input streams and predict the expected compositions of the output streams. If the type of reactor and separation units to be used are known, cost analysis will focus mainly on changes in the amounts of useful product in the exit stream as processing conditions are changed. Catalyst cost is a major factor, however, so both economic and scientific users are interested in the rate at which catalyst must be replaced in the reactor.

Scientific users are more interested in what is going on inside the reactor and how various conditions affect the process. The model must be able to show what happens as the space velocity is changed, as the reactor temperature is changed, or as the hydrogen treat rate is changed. It would be beneficial to separate the kinetics of the reactions from the physical effects of the reactor, such that the model is applicable to any reactor system design. By having an accurate description of what is going on inside the reactor, it may also be possible to adjust conditions to control the particular reactions taking place.

RESULTS This assessment has helped to identify a number of specific areas important to the development of future kinetic models. Decoupling of the processing variables from the kinetic parameters is needed to make the model applicable over a wider range of experimental conditions. To do this, intrinsic rate constants must be determined for the various reaction steps which are independent of the coal, solvent, reactor, and all other processing conditions. Since the model must still be able to predict the effects of changing these processing conditions, other ways must be found to incorporate these variables.

Some of the models described above have begun to take these variables into account, but this is only a start. In the model of Ferrance and Holder, literature correlations based on coal characteristics are used to determine ultimate conversions and hydrogen availability.[5] These correlations, however, were developed using data from a limited range of coals. More basic research is needed to extend the applicability of such correlations to the entire range of coal types. Similar correlations, independent of the model itself, will also be needed to determine initial product distributions and the hydrogen donating ability of both coals and solvents.

Decoupling the reaction rates from the design of the reactor will make the kinetics applicable to all reactor setups. This means that the model will have to be able to handle and incorporate the mixing and mass transport characteristics within the reactor. Mass transport calculations will require accurate predictions of the viscosity and hydrogen gas solubility of the slurry, two areas in which further work needs to be carried out. In addition to solubilities, other areas of the thermodynamics of liquefaction systems also need work. In particular, studies are needed on partitioning of the solvent and light products into the vapor-phase since these may represent the hydrogen donating or hydrogen shuttling species in the reactor.

While modeling of both small-scale and large-scale reactors would be possible, much more work is needed for development of a large-scale model which can be used for both economic and engineering purposes on a commercial level. For work at this scale, inclusion of the preheater in the model was determined to be of great importance. Simulation of pilot plant preheaters have shown that up to 90% of the total coal conversion may be complete by the time the slurry exits the preheater.[9] The rates of the coal dissolution reactions are very fast and produce large changes in the characteristics of the slurry. Free radical and retrograde reactions which occur as the slurry is heated may have an influence on the final product yields. The possible presence now of dispersed catalyst in the preheater, fed or recycled with the slurry, adds to the complexity of the reactions occurring in this unit.

Product definitions have also been found to be an important area in which improvements are needed, because the reaction scheme and kinetic expressions depend on the products. What is needed, is standardization of a choice of product fractions which can be analytically defined and experimentally characterized. For the distillate products, definition of fractions by boiling point ranges will allow use of the various correlations developed by the petroleum industry. For the nondistillable products, additional solubility separations might be possible, or molecular weight separations might be used to give additional fractions. CONSOL has directed a study to evaluate the usefulness of various analytical methods for characterizing coal liquefaction process streams.[10] Though applicable methods have been determined, no set of products which could be defined by these methods has been established.

Enough product fractions must be defined so that each fraction has stable and consistent physical and thermodynamic properties which can be used for engineering analyses. Inclusion of too many product fractions, however, will lead to a large number of reactions and an unwieldy model. A reaction scheme will have to be set up relating how each of these products, plus any additional intermediates are formed and reacted. The scheme must include a set of initial reactions, giving the products formed directly from the coal, as well as a set of secondary reactions describing the further breakdown into low molecular weight products. As this reaction scheme is setup, it is also important to distinguish between those reactions which are purely thermal, those which have both thermal and catalytic components, and those which are only catalytic. The assessment has found that this is the best way to explicitly include the impact of catalysts in the model. Rate constants for the catalytic reactions will always be catalyst dependent and will have to be determined independently for each catalyst. However, incorporation of catalyst variables, such as the amount of catalyst or the catalyst particle size, must be independent of these rate constants for the model to be valuable.

EXPERIMENTAL Experimental work has begun at the Pittsburgh Energy Technology Center in conjunction with the assessment to study some of these areas. Determining a workable reaction scheme was felt to be the most important contribution at this stage. To do this, specific product cuts from a bench-scale continuous facility are being reacted in microautoclave reactors under different conditions. Both the initial and reacted products are being analyzed to determine how fractions can be defined using readily available techniques. How the amounts and types of fractions change during the process will help to elucidate the secondary reactions which take place during liquefaction to convert or produce each fraction.

A second set of experiments has been designed to investigate the initial reactions which take place. In these experiments, coal will be reacted in microautoclave reactors under conditions typically found in a coal liquefaction preheater. Time/temperature profiles determined for pilot-plant preheaters are shown in Figure 7.[11-12] By simulating heating of the coal to different temperatures along this curve in a tubing bomb, the initial reactions which occur as coal is converted to a liquid will be observed. The prevalence of secondary reactions taking place before the slurry exits the preheater will also be determined through these experiments. A true scheme for the formation of light products from coal both directly and through sequential reactions will be developed. This determination of the early reactions taking place in the preheater should help in the design of better preheaters for large-scale processes.

FUTURE WORK The assessment is not complete. Discussions with investigators working at both the bench-scale and larger scale continue to provide additional input on what should be incorporated into future models to make them useful and valuable. This input is solicited through distribution of preliminary reports and on-line through a coal liquefaction kinetic modeling home page (http://www.petc.doe.gov/kinetics.html).

What has become evident already is that kinetic modeling has developed independent of mass transport and thermodynamic considerations which affect the liquefaction process. Future efforts will require assessing the studies carried out in these areas to determine what additional work will be needed to incorporate these results into liquefaction models. Monitoring of current external experimental work relevant to all areas listed will continue. Continuing adjustments of the PETC internal experimental program as data is collected, and as additional input arrives will also be carried out.

REFERENCES

1. "Coal Liquefaction - A Research Needs Assessment," DOE/ER-0400, 1989.

2. Brandes, S.D., Robbins, G.A., Winschel, R.A., Burke, F.P., "Coal Liquefaction Process Streams Characterization and Evaluation, Volume II," DOE/PC/89883-93, 1994.

3. Suzuki, T., "Development of Highly Dispersed Coal Liquefaction Catalysts," Energy & Fuels, 1994, 8, 341.

4. Weller, S.W., "Kinetics of Coal Liquefaction: Interpretation of Data," Energy & Fuels, 1995, 9, 384.

5. Ferrance, J.P., Holder, G.D., "Development of a General Model for Coal Liquefaction," This volume, 1996

6. Singh, C.P.P., Shah, Y.T., Carr, N.L., Prudich, M.E., "Liquefaction of Coal by SRC-II Process, Part I: A New Kinetic Model," Can. J. Chem. Eng., 1982, 60, 248.

7. Catalytic, Inc., "Development of a Simulation Model for Bituminous Coal Liquefaction in the Integrated Process at Wilsonville," DOE/PC/50041-89, 1987.

8. Comolli, A.G., Johanson, E.S., Lee, L.K., Popper, G.A., Smith, T.O., "Final Report," DE-88818-TOP-03, 1993.

9. Brandes, S.D., Lancet, M.S., Robbins, G.A., Winschel, R.A., Burke, F.P., "Coal Liquefaction Process Streams Characterization and Evaluation," DOE/PC/89883-53, 1992.

10. Robbins, G.A., Brandes, S.D., Winschel, R.A., Burke, F.P., "Coal Liquefaction Process Streams Characterization and Evaluation, Volume I," DOE/PC/89883-93, 1994.

11. Catalytic, Inc., "Operation of the Wilsonville Advanced Coal Liquefaction R & D Facility," DOE/ET/10154-122, 1982.

12. Gulf Science & Technology Co., "Slurry Preheater Design: SRC-II Process," Report No. 560RM149, 1981.

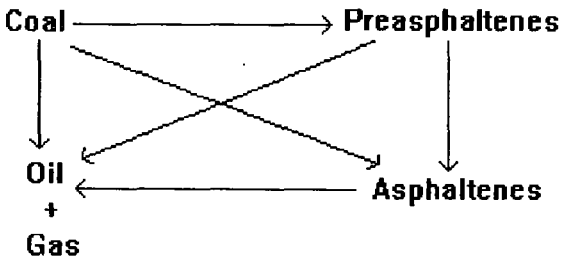

Figure 1 Reaction scheme used in most earlier simple models

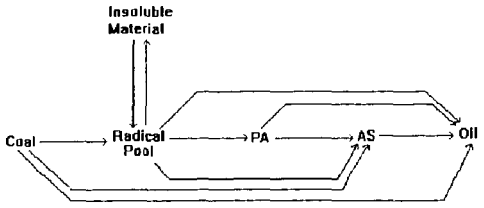

Figure 2 Reaction scheme of a recent model by Suzuki.

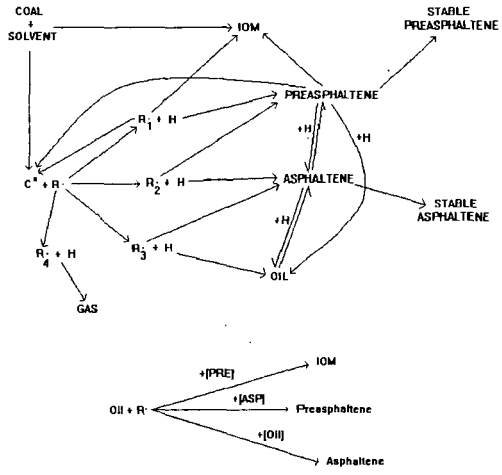

Figure 3 Reaction scheme of Ferrance and Holder

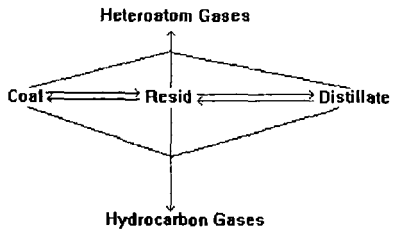

Figure 4 Wilsonville reaction scheme for the thermal liquefaction unit

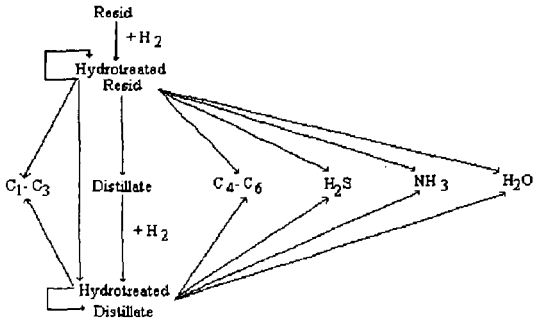

Figure 5 Wilsonville reaction scheme for the hydrotreater unit

$$Coal \xrightarrow{\qquad\qquad} a\,C_1 + b\,C_2 + c\,Unreactive\ Coal$$

$$C_1 \xrightarrow{k_1} f Resid + g Gas\ oil + h Naphtha + i Hydrocarbon\ gases + j Byproduct\ gases$$

$$C_2 \xrightarrow{k_2} f Resid + g Gas\ oil + h Naphtha + i Hydrocarbon\ gases + j Byproduct\ gases$$

$$Resid + H_2 \xrightarrow{catalyst} Products$$

Figure 6 Reactions used in the HTI coal liquefaction model

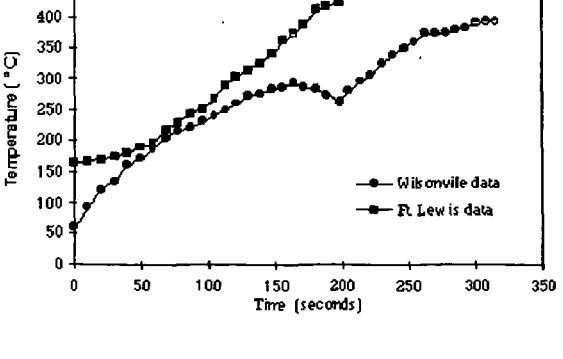

Figure 7 Time/temperature profiles for two pilot-plant preheaters

COAL LIQUEFACTION KINETICS

Shaojie Wang, Keyu Wang, He Huang, Michael T.Klein and William H. Calkins*
Department of Chemical Engineering
University of Delaware, Newark, Delaware 19716

Key words: kinetics, coal liquefaction, modelling

Introduction

Understanding the mechanisms of uncatalyzed direct coal liquefaction by means of reaction kinetics has been a long sought goal. Curran et al. in 1967 (1) and Wiser in 1968 (2) and Neavel in 1976 (3) measured the rates of liquefaction of various coals and postulated a free radical mechanism to explain the data obtained. The kinetics as determined by these and other workers is described in detail by Gorin in Chapter 27 of Elliott's Second Supplementary Volume to the Chemistry of Coal Series (4). However, it has been well known that most coals contain some material extractable by organic solvents. The solvents used in direct coal liquefaction would of course be expected to also extract soluble material as well as effect the liquefaction reaction. If the extractable material were a significant quantity in the coal, it would seriously affect the kinetics. Cassidy et al. (5,6) used a stirred autoclave with a sampling port at the bottom in their kinetic studies. They observed that hot charging the coal rapidly formed an oil which they considered to originate predominantly from the "guest component", i.e., extractables, in the lignite they studied. Also, the free radical nature of the liquefaction process would be expected to produce secondary reaction products which would complicate the kinetics as well as lead to retrograde products.

With this background, it seemed important to measure the kinetics of direct liquefaction at very short contact times where the extractables would be quickly removed and secondary reactions due to the free radical nature of the liquefaction would be minimized. By the use of a special Short Contact Time Batch Reactor (SCTBR), we have been able to show that direct coal liquefaction occurs both thermally and catalytically in at least two separate and distinct stages: an extraction stage and a slower breakdown and liquefaction of the coal macromolecules themselves (7,8). With this equipment, it is possible to study the kinetics of each stage and to measure the kinetic parameters of each. The kinetics of two coals (Illinois #6 bituminous and Wyodak-Anderson subbituminous coals) investigated at reaction times from 10 s to 60 min are reported in this paper.

Experimental

Apparatus. The Short Contact Time Batch Reactor was used to carry out the liquefactions. The design and operation of the reactor system including a schematic diagram have been described elsewhere (9,10). In brief, a 30 cm^3 reactor is constructed of 3/4" o.d. stainless steel tubing of approximately 12" length with wall thickness of approximately 0.433". The 21 ft lengths of coiled stainless tubing used for both the preheater and precooler are 1/4" o.d. with wall thickness of 0.035". The reactor system is capable of containing up to 17 MPa (2500 psi) pressure at temperatures of up to 500°C.

In operation, both the empty preheater and the reactor are immersed in a Techne IFB-52 fluidized sand bath. They are brought up to the reaction temperature prior to the start of the reaction. High pressure hydrogen or nitrogen gas provided the driving force to deliver the slurry mixture of coal-solvent or coal-solvent-catalyst under study from a small blow case at ambient temperature into the empty reactor through the hot preheater tubing. Hydrogen or nitrogen gas was then bubbled through the reactor from the bottom to provide the agitation needed in the liquefaction reaction. The degree of agitation was controlled by the exit gas flow rate from the top of the reactor. In the case of running under hydrogen pressure, the gas bubbles were also used to supply the hydrogen for the liquefaction reaction.

The temperature of the reactants (ca.30 g) initially at ambient temperature, approach the desired reaction temperature to within 5-8°C during the transport process (approximately 0.3 seconds) and reaches the predetermined reaction temperature within 30 seconds. At a preselected time, the high pressure gas is again used to drive the reactor contents from the reactor into a cold receiver through the precooler. Both receiver and precooler are immersed in a water bath. Quenching of the product mixture to about 25°C is achieved during the transport time of about 0.3 seconds.

Coal Studied. Illinois #6 bituminous and Wyodak-Anderson subbituminous coals from the Argonne Premium Coal Sample program were investigated in this study. Proximate and elemental analyses, together with other analytical data, of these coals are available in the User's Handbook for the Argonne Premium Coal Sample program (11).

Workup Procedures of the Reaction Products. The product mixtures were filtered and the solid residues washed with cold fresh tetralin thoroughly and dried in a vacuum oven with a nitrogen purge at 105°C for 48 hours. The filter cake was then rinsed with methylene

chloride and dried in a vacuum oven with a nitrogen purge at 105°C for 12 hours. The solid residue and the liquid filtrate were analyzed separately by various procedures.

Thermogravimetric Analysis. The thermogravimetric analyzer was a Model 51 TGA (TA Instruments, New Castle, Delaware). The TGA which was run on liquefaction residues provided a measure of the amount of volatile matter (VM), fixed carbon (FC) and ash. The mineral matter of the coal was shown to accumulate in the coal residue and not in the coal liquids. Ash in the residue was therefore used to calculate the conversion using the formula:

$$Conversion\ (wt\%) = (1 - \frac{A_0}{A_s}) \times 100\% \qquad (1)$$

where A_0 and A_s are the weight fractions of ash (derived from the coal mineral matter) in a control sample and in the liquefaction residue, respectively.

The volatile matter (VM) in the residue turned out to be only a function of the reaction time and temperature. The fixed carbon (FC), however, is a measure of the retrograde processes occurring during the liquefaction and the kinetics of the FC formation could be followed by TGA.

Results and Discussion

Liquefaction Conversion vs Time. Figure 1 shows conversion vs time curves for Illinois #6 coal without added catalyst in tetralin (8 to 1 tetralin to coal weight ratio) at four temperatures and 1000 psig nitrogen atmosphere. There are several stages in the liquefaction as shown by these curves. There is an initial rapid conversion which is due to the extraction of soluble matter into the tetralin. This is followed by a pseudo-induction period during which little conversion appears to occur. This is not due to the build up of any intermediates such as free radicals as shown by ESR spectroscopy (12). Actually it is due to the simultaneous ending of the extraction stage and the slow conversion of the coal structure to liquid products. As the temperature increases, the extent of the extraction process increases and the pseudo-induction period becomes shorter. At still higher temperatures, particularly in the presence of a strong hydrogenation catalyst, the induction period becomes almost undetectable.

In nitrogen, there is little increase in conversion to liquid products above 408°C, although the reaction mixture is changing rapidly. We have shown that the volatile matter (VM) content decreases steadily as the time and temperature increases. However, the fixed carbon (FC) values increase dramatically at higher temperature, resulting in decreased yield of tetralin soluble materials (8).

Similar conversion curves are obtained for the liquefaction of the Wyodak-Anderson subbituminous coal in tetralin (8 to one tetralin to coal by weight)(8). These curves show the characteristic stages of extraction, induction period and coal liquefaction similar to the Illinois #6 coal.

Conversion vs time curves for both Illinois #6 and Wyodak Anderson coals in tetralin in the presence of hydrogen and added catalysts will be presented with a kinetic analysis in a future paper.

Kinetic Analysis of Coal Liquefaction. As shown in the previous section, three distinct phases in the coal liquefaction process in the absence of hydrogen and a catalyst are observed. The initial rapid conversion (in the first 30 to 60 s) is due to the extraction of a soluble fraction of the coal into the processing solvent. This is followed by a pseudo-induction period and then the slow conversion of the coal structure to liquid products. This pseudo-induction period is a transition interval which is due to the simultaneous occurrence of these two processes, a very rapid extraction which is ending and a relatively slower liquefaction of the coal matrix which is becoming dominant. Based on this hypothesis, the liquefaction conversion observed in experiments, therefore, is the sum of the conversions of these two processes:

$$X = X_s + X_r \qquad (2)$$

where X is the liquefaction conversion determined in the experiments; X_s is the solubilizing conversion which is due to the extraction of the soluble materials in the coal; and X_r is the liquefaction reaction conversion which is due to the chemical breakdown of the coal structure. From Eq. 2, the liquefaction rate is the sum of the derivatives of these conversions, i.e.,

$$\frac{dX}{dt} = \frac{dX_s}{dt} + \frac{dX_r}{dt} \qquad (3)$$

The extraction rate could be expressed by

$$\frac{dX_s}{dt} = k_s(X_{s0} - X_s) \qquad (4)$$

where k_s is the extraction rate constant; X_{s0} is the equilibrium level of extraction of coal under liquefaction conditions; and X_s is the soluble fraction at time t. The breakdown rate for the coal matrix is given by

$$\frac{dX_r}{dt} = k_r' ((1-X_{s0}) - X_r)^{\alpha} C_t^{\beta} P_{gas}^{\gamma} \quad (5)$$

where k_r' is the reaction rate constant; X_r is the liquefaction reaction conversion at time t; C_t is the tetralin concentration; and P_{gas} is the nitrogen or hydrogen pressure. When a large amount of tetralin is used in the liquefaction (for example, 8 to 1 of tetralin to coal ratio was used in this study), C_t is approximately equal to a constant. P_{gas} is held a constant during the liquefaction run in this study. Assuming $\alpha = 1$, Eq. 5 is simplified to

$$\frac{dX_r}{dt} = k_r((1 - X_{s0}) - X_r) \quad (6)$$

Integrating with boundary conditions of $X_s = 0$ and $X_r = 0$ at $t = 0$ and substituting $(1 - X_{s0})$ by X_{r0} which is defined to be the maximum conversion due to liquefaction reactions, Eqs. 4 and 6 become

$$\ln(1 - \frac{X_s}{X_{s0}}) = -k_s t \quad (7)$$

and

$$\ln(1 - \frac{X_r}{X_{r0}}) = -k_r t \quad (8)$$

respectively.

Kinetics of Illinois #6 and Wyodak-Anderson Coal Liquefactions. The plot of $\ln(1-X_s/X_{s0})$ against t for the Illinois #6 coal liquefaction in tetralin under 1000 psig N_2 at 390 °C is shown in Figure 2. The slope gives a measured rate constant for extraction of $k_s = 2.81$ with an r^2 of 0.97. The plot of $\ln(1-X_r/X_{r0})$ against t for the Illinois #6 coal liquefaction reaction process is illustrated in Figure 3. It shows two distinct reaction stages: a rapid one with a rate constant of 0.027 for the first 5 minutes, and a slower one of 0.0054 for times greater than 5 minutes. The kinetic parameters of the Illinois #6 and Wyodak-Anderson coal liquefactions evaluated by the proposed model are summarized in Table 1. As an example, Figure 4 shows experimental data and modelling curve at the reaction times up to 10 min for Wyodak-Anderson coal liquefaction in tetralin at 390 °C under 1000 psig N_2. It shows that the model fits the experimental data very well.

Rate constants of k_s and k_r at three temperatures (358, 390, and 408 °C) were used to estimate activation energies of extraction and liquefaction reaction processes. The plot of $\ln k_s$ against 1/T and $\ln k_r$ vs 1/T shown in Figures 5 and 6 give activation energies of 14 and 22 kcal/mol for the solubilization and liquefaction reaction processes, respectively.

It is of interest to compare these results with those obtained by others at higher conversion. Wiser (2) obtained an activation energy value of 28.8 kcal/mol for Utah bituminous coal liquefaction at 63 to 94% conversion. Curran et al. (1) obtained two values for a rapid and a slow rate with mean values of 30 and 38 kcal/mol on Pittsburgh Seam bituminous coal at 2.5 minutes and 2 hours, respectively. They used a process-derived solvent from 325 to 435°C. While the 22 kcal/mole value seems rather low, coal has obviously both weak and strong bonds which will be broken in order of their bond strength. The process derived solvent may strongly affect the relative amounts of the extraction and liquefaction stages in the Curran work. All of these values are low compared to the strength of carbon-carbon bonds and obviously the activation energies observed by us and others reflects the reaction complexity as well as the particular bonds being broken.

The Retrograde Reactions Occurring during liquefaction. As reported above, increasing temperature results in a levelling off of liquefaction yields due to the production of fixed carbon (FC) which results in lower liquefaction yields and production of tars and coke. Understanding this onset of retrograde reactions is of great importance for improvement of the direct coal liquefaction process. Analysis of these residues show decreasing hydrogen to carbon ratios as the coal residues are exposed to higher temperatures and longer reaction times (see Figure 7). It is not surprising therefore that introduction of a hydrogenation catalyst in the liquefaction process has a profound effect limiting the rate of formation of fixed carbon FC and therefore increasing the liquefaction yields. Interestingly, however, when a good hydrogenation catalyst is used, increasing reaction temperature up to a point actually increases yield and decreases FC formation (8).

Summary and Conclusions

The direct liquefaction of coal shows distinct stages: an extraction stage and multiple slower stages representing the breakdown of various components of the coal structure. These only become apparent with a reactor system capable of accurately distinguishing conversions at reaction times as low as 10 seconds.

The liquefaction conversion observed in the experiments is the sum of the two simultaneous liquefaction processes of extraction and liquefaction of the coal structure. Based on this model, the liquefaction kinetics in each stage of the entire process can be adequately described.

The extraction stages in the bituminous and subbituminous coals studied to date are about two orders of magnitude faster than the structure breakdown stages and have correspondingly lower activation energies. The liquefaction of the coal structure itself also consists of multiple steps of different rate constants and activation energies.

The retrograde reactions can be followed by thermogravimetric analysis of the coal liquefaction residues. They are suppressed by catalytic hydrogenation during the liquefaction process.

Acknowledgements

The support of this work under DOE Contract DE-PS22-93PC93201 is gratefully acknowledged.

References

1. G.P. Curran, R.T. Struck, and E. Gorin *I&EC Process Design and Development* **6**, 1, pp. 166-173 (1967).
2. W.H. Wiser *Fuel* **47** pp. 475-485 (1968).
3. R.C. Neavel *Fuel* **55** pp. 237-242 (1976).
4. E. Gorin *Chemistry of Coal Utilization Second Supplementary Volume* Elliott, M.A. Editor, Chapter 27, pp. 1845-1918, Wiley Interscience (1981).
5. P.J. Cassidy, W.R. Jackson, F.P. Larkins, M.B. Louey, D. Rash and I.D. Watkins *Fuel* **68**, pp. 32-39 (1989).
6. P.J. Cassidy, W.R. Jackson, F.P. Larkins, M.B. Louey and I. Watkins *Fuel* **68** pp. 40-44 (1989).
7. H. Huang, K. Wang, S. Wang, M.T. Klein, and W.H. Calkins *Coal Science and Technology 24: Coal Science*, Proceedings of the 1995 International Conference on Coal Science, Eds J.A. Pajares and J.M.D. Tascon, Vol. II, p. 1207 (1995).
8. H. Huang, K. Wang, S. Wang, M.T. Klein and W.H. Calkins *Energy and Fuels* 1996, in press.
9. H. Huang, W.H. Calkins, M.T. Klein *Energy and Fuels* **8** pp. 1304-1309 (1994).
10. H. Huang, D.M. Fake, W.H. Calkins, and M.T. Klein *Energy and Fuels* **8** pp. 1310-1315 (1994).
11. K.S. Vorres 'User's Handbook for the Argonne Premium Coal Sample Program' *ANL/PCSP-93/1.*
12. W.D. Provine, B. Jung, M.A. Jacintha, D.G. Rethwisch, H. Huang, W.H. Calkins, M.T. Klein, C.G. Scouten, C.R. Dybowski *Catalysis Today* **19**, 3, 409 (1994).

Table 1 The rate constants of the Illinois #6 and Wyodak coal liquefactions

Coal	T,℃	time	Liquefaction stage	Rate constant k	r^2
Illinois #6	358	0 - 2 min	Extraction	0.848	0.996
		0 - 60 min	Reaction	0.00275	0.999
	390	0 - 1.5 min	Extraction	2.81	0.997
		0-5 min	Reaction (R1, fast)	0.0276	0.999
		> 5 min	Reaction (R2, slow)	0.00541	0.998
	408	0 - 1 min	Extraction	6.05	0.998
		0-10 min	Reaction (R1, fast)	0.0458	0.972
		> 10 min	Reaction (R2, slow)	0.00301	0.987
Wyodak-Anderson	390	0 - 0.5 min	Extraction	11.8	0.996
		0-15 min	Reaction (R1, fast)	0.0195	0.995
		> 15 min	Reaction (R2, slow)	0.0161	0.999

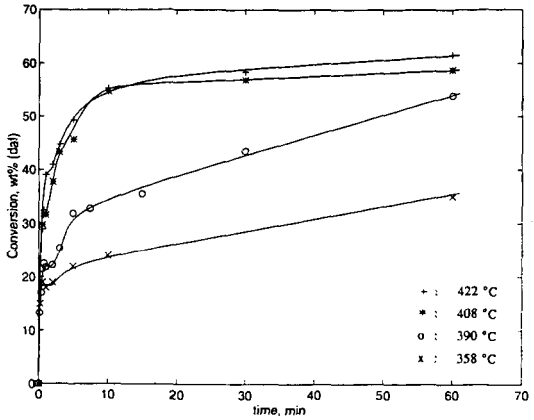

Figure 1 Conversion vs time for Illinois #6 coal liquefaction without added catalyst in tetralin (tetralin:coal = 8:1 mass ratio) under 1000 psig N_2

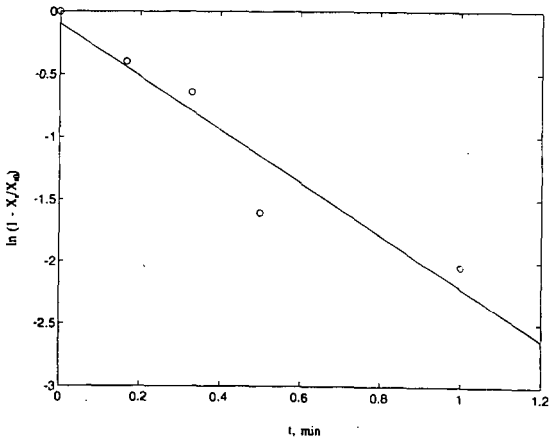

Figure 2 $\ln(1-X_r/X_{r0})$ vs t for the Illinois #6 coal liquefaction in tetralin under 1000 psig N_2 at 390 °C

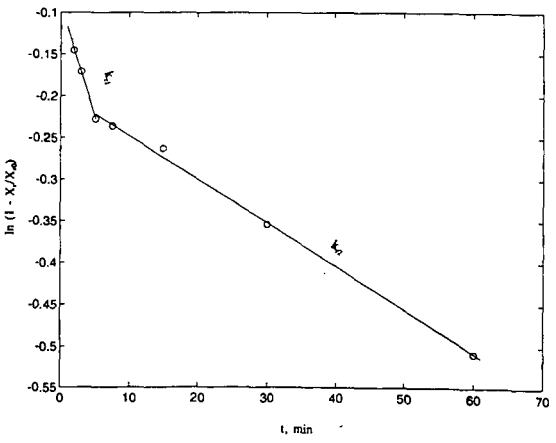

Figure 3 $\ln(1-X_r/X_{r0})$ vs t for the Illinois #6 coal liquefaction in tetralin under 1000 psig N_2 at 390 °C

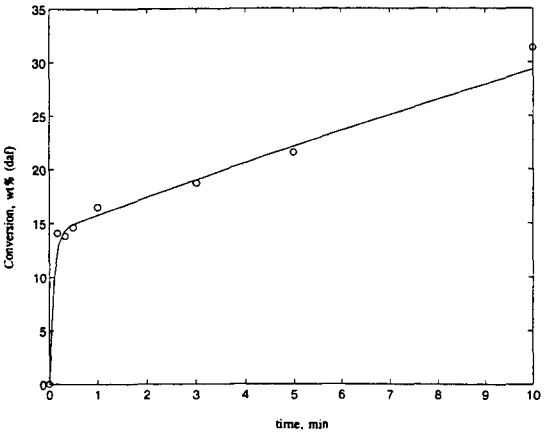

Figure 4 Plot of the experimental data and modelling curve at the reaction times up to 10 min for Wyodak-Anderson coal liquefaction in tetralin at 390 °C under 1000 psig N_2.

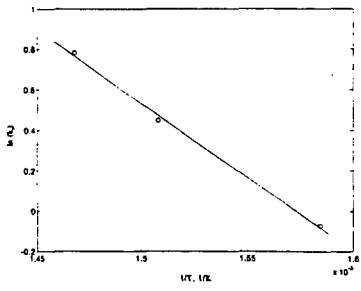

Figure 5 $\ln k_e$ vs 1/T for the thermal liquefaction of Illinois #6 coal (Extraction stage)

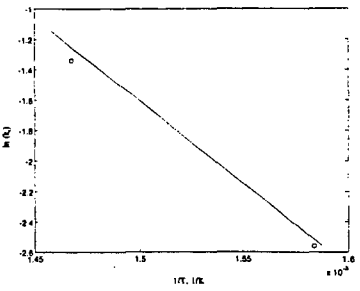

Figure 6 $\ln k_r$ vs 1/T for the thermal liquefaction of Illinois #6 coal (Reaction stage)

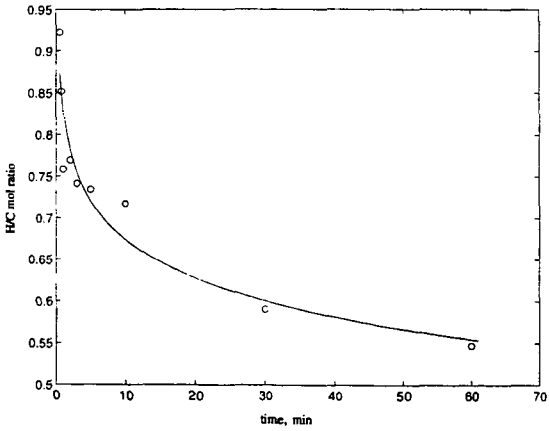

Figure 7 H/C mol ratio of the liquefaction residues of Illinois #6 coal without added catalyst in tetralin (tetralin:coal = 8:1 mass ratio) under 1000 psig N_2 at 422 °C

DEVELOPMENT OF A GENERAL MODEL FOR COAL LIQUEFACTION

Jerome P. Ferrance and Gerald D. Holder
Department of Chemical Engineering
University of Pittsburgh
Pittsburgh, PA 15261

Keywords: Kinetic modeling, coal liquefaction simulation, processing condition effects

INTRODUCTION One goal of coal liquefaction kinetic models is to be able to predict the results of coal liquefaction experiments in order to identify optimal processing conditions. A second goal is to be able to define experimental conditions that provide the greatest amount of information per experiment. This is especially important in comparing catalysts. A third goal is simply to be able to identify those processing variables which will have the greatest effects in a given system. This will reduce the number of actual experiments needed to investigate new systems by focusing on only the most important variables.

Previous investigators have taken into account the effects of a number of variables in development of their kinetic models.[1] These effects include temperature, coal type, solvent type, and hydrogen pressure. Temperature is readily taken into account through determination of activation energies from rate constants found at different temperatures. Coal type and solvent type were sometimes taken into account through ultimate conversions, but most often were included by adjusting the rate constants for each coal or solvent. Hydrogen pressure was included as a separate term in the rate equations in some models.

These models could not fulfill the three goals listed above, because the rate constants determined in each of these models was specific for the conditions of the experiment. Changing conditions in these models meant redetermining the kinetic parameters in the rate expressions. These new parameters could only be obtained by first doing actual experiments under the new conditions. Figure 1 shows the model and rate constants determined by Giralt et al. for a system in which only the solvent was changed.[2] The widely different reaction rate constants for some of the reactions indicate that no predictions of how the system would have performed when the solvent was changed would have been possible.

A model which is to fulfill the above goals must be able to account for the effects which take place when processing conditions are changed without resorting to redetermining the kinetic constants from experimental data. One approach has been to include additional terms directly in the kinetic equations used in the calculations. For example, basing ultimate conversion on coal type provides a way to include the type of coal directly into the models predictions. The ultimate conversion is related to characteristics of the coal being used. Such advances provide a partial answer, but coal type affects more than just the ultimate conversion, as different coals have different solubilities, amounts of mobile phase, numbers of free radicals, and donatable hydrogen. Solvent, solvent/coal ratio, reactor type, heat-up time, mixing speed, coal treatment, and gas phase pressure and composition must also be included in the model. As shown in Table 1, all of these variables have been included in this general model which has been developed.

GENERAL MODEL

NEW CALCULATIONS Two things included in the kinetics of this model, which had not been included in previous models, are the basing of reaction rates on the *concentration* of reactants in the liquid phase and inclusion of an explicit hydrogen concentration. Earlier models used masses of reactants in the reactor, and ignored variable phase volumes and distribution of components between phases. Earlier models also assumed that hydrogen was not limiting in their systems and the hydrogen supply was considered constant. That prevents these models from being applied to systems in which the amount of hydrogen does influence the results of the reactions.

To include the effects of concentration and hydrogen pressure into the kinetic calculations required two additional sets of calculations to be simultaneously carried out. To determine reactant concentrations, both the volume of the liquid phase and the amount of each component in the liquid phase has to be determined. This required that the thermodynamic state of the system be continuously determined in conjunction with the kinetics, as changes in the reactor contents take place. Mass transfer calculations are also required to determine the rate at which solid coal particles dissolve into the liquid phase, and the rate at which hydrogen gas dissolves into the liquid phase. Mass transfer calculations require the thermodynamics calculations to set the maximum solubilities of coal and hydrogen gas in the liquid phase. Mass transfer also depends on kinetic calculations, through the viscosity of the liquid phase which changes as the liquefaction reactions take place. Thus the mass transfer, thermodynamic, and kinetic calculations are completely dependent on each other.

The model was set-up to be as accurate as possible in terms of mass transport and thermodynamic calculations. Figure 2 shows partition coefficients calculated by the model for

the hydrogen/tetralin system along with experimental data.[3] Figure 3 shows calculated and experimental viscosities for a coal liquid at three pressures for a range of temperatures.[4] These figures reflect the different kinds of experimental data which were incorporated into the development of this model. By including thermodynamics and mass transport, the properties of the solvent being used, such as its solubility parameter, vapor pressure, and viscosity became intimately connected with the calculations. The processing variables, solvent/coal ratio and mixing speed, are also directly taken into account through these calculations.

NEW REACTION SCHEME As mentioned above, hydrogen concentration was used in the reaction rate equations. To do this, a new scheme had to be developed for the liquefaction mechanism in which hydrogen directly participated in some of the reactions. The reactions were based more on the underlying chemistry which has been determined to take place, through both model compound and liquefaction studies. One of the major improvements in this model was the inclusion of free radical reactions as a significant part of the coal breakdown mechanism. The free radical intermediates could be either capped in reactions in which hydrogen participated, or recombined in retrograde reactions. The numbers of free radicals present was determined from both the coal type and the temperature in the reactor using correlations developed from literature data.

As in some earlier models, we assume a fixed fraction of the coal is unreactive. This amount is based on the coal type, but it does not have to be experimentally determined in this new model. Instead, a literature correlation of maximum conversions based on coal characteristics has been adapted to provide this value for any coal used in the model. In addition to the unreactive coal, the retrograde reactions form some material which will be unreactive; some fraction of the preasphaltenes and asphaltenes produced in the liquefaction are also considered to be stable. Empirical correlations were developed to determine the stable fractions also based on the coal characteristics. Data from a large number of liquefactions run under different conditions was used to determine the final coefficients in these correlations.

Both parallel and serial reactions were included in the scheme to allow for the production of asphaltenes and oils directly from the coal. Two separate coal breakdown reactions were specified, representing the two types of bonds which are normally broken in the coal structure, ether bonds and alkyl linkages between aromatic structures. The amounts of each fraction formed by these initial reactions was also set up to be dependent on the type of coal used in the model. The series reactions, including preasphaltenes to asphaltenes to oils and preasphaltenes to oils, were also made hydrogen dependent since hydrogen addition is a big part of the conversion to lower molecular weight products. In the model, hydrogen for these reactions comes from three sources: the coal, the solvent if it has donatable hydrogen, and hydrogen gas if present. The amount of hydrogen available from the coal is also determined from a literature derived correlation.

COMPUTER PROGRAM To make the model useable, a computer program was written to carry out all of the simultaneous kinetic, mass transport, and thermodynamic calculations. Including all of the various correlations for stable fractions, free radicals, coal solubility parameter, and the amount of donatable hydrogen from coal, allows the user to specify only the type of coal without having to first do all of these calculations to use the model. This required storing default values of the coal characteristics for each type of coal within the program. Solvent characteristics were also stored within the program for use in both the thermodynamic and transport calculations.

The final computer program which was produced is designed such that the user does not have to understand the inner workings of the model or the calculations included in the model. The user interacts with the program answering questions about the processing conditions which are to be used. Variables which must be input to the program include the reaction temperature, the type and amount of coal, the coal particle size and if the coal has been dried, the type and size of the reactor, the mixing speed and heat-up time, the type and mass of solvent, and the type of and pressure of the gas phase. The computer program calculates all necessary parameters which are dependent on the users input, then simulates the experiment using the model's calculations. Results of the simulation are given as preasphaltene, asphaltene, oil, gas, and THF insoluble material.

PARAMETER FITTING As with other kinetic models, the activation energies and frequency factors for each of the reactions had to be determined from experimental data. This model had a number of additional parameters which also had to be fitted. What is unique about this model is that data from experiments run under widely varying conditions was combined to carry out this parameter fitting. The data covered temperatures from 300 to 480°C, 6 different types of coal, 4 different solvents, in both stirred autoclave and microautoclave reactors; short and long heat-up time experiments were included. Both hydrogen and inert gas phases were represented at pressures from 0 to 2000 psi, and solvent to coal ratios from 1/1 to 8/1 were covered.

Figure 4 shows a parity plot of experimental versus predicted coal conversions for 100 data points. Figure 5 shows a parity plot of the oil yields for those same data points. Because these points were used in fitting the model parameters, it is not surprising that the model predicts these results well. The diversity of conditions under which these simulations were run using the same set of kinetic constants, however, shows that the model has been able to incorporate a wide variety of processing conditions.

RESULTS The real test for this model was to show that the effects reported in the literature for changes in processing conditions could be reproduced by the model. A simulation was run using a set of conditions selected as the base case. The processing variables were then varied one at a time and the simulation results compared with experimental results for similar changes. The effects of temperature and solvent to coal ratio are predicted by this model. An effect of solvent is predicted, but comparison with experimental data shows that all properties of the solvent have not been fully incorporated into the model. Changes in product yields due to changes in coal type are predicted by the model, but do not follow the exact pattern seen in experimental studies. This was not completely unexpected, as the literature correlations used for taking coal characteristics into account in the model were determined over limited ranges of coal types. The effects of changing hydrogen pressure are predicted by the model, with less of a hydrogen effect seen in good hydrogen donating solvents as expected.

CONCLUSIONS A first generation general model for coal liquefaction has been developed in which the model parameters are not dependent on the liquefaction conditions. This allows the effects of changes in processing variables to be modelled without having to first run experiments to get the necessary kinetic parameters. Inclusion of both mass transport and thermodynamic calculations, along with the kinetic calculations, was needed to incorporate these processing variables into the model predictions. Development of a computer program proved to be the best way to carry out all of the simultaneous calculations which are needed in the model. The interactive nature of the computer program makes the model accessible for use by those unfamiliar with the underlying concepts on which the model was designed.

REFERENCES

1. Ferrance, J. P.,Ph.D. Thesis, University of Pittsburgh, 1996

2. Giralt, J., Fabregat, A., Giralt, F., Ind. Eng. Chem. Res., 1988, 27, 1110.

3. Simnick, J.J., Lawson, C.C., Lin, H.M., Chao, K.C., AIChE J, 1977, 23, 469.

4. Hwang, S.C., Tsonopoulos, C., Cunningham, J.R., Wilson, G.M., Ind. Eng. Chem. Process. Des. Dev., 1982, 21 127.

Table 1 Processing variables included in the model

Variable	Incorporated into model through:
Temperature	Influence on reaction rates Influence on ultimate conversion Influence on hydrogen availability from the coal and solvent Influence on the thermodynamics of the system
Coal type	Influence on ultimate conversion Influence on hydrogen available from coal Influence on initial production fractions Influence on the number of free radicals Influence on coal solubility
Solvent (type and amount)	Influence on the amount of available solvent hydrogen Influence on the system thermodynamics Influence on the coal and hydrogen gas solubilities Influence on the concentrations of reactants Influence on the viscosity
Pressure and gas phase composition	Influence on the system thermodynamics Influence on the amount of hydrogen available from the gas phase Influence on the hydrogen solubility
Reactor (type, size, and mixing speed)	Influence on the thermodynamics of the system Influence on the cold volume in the reactor Influence on the coal and hydrogen dissolution rates
Heat-up time	Reaction rates change during non-isothermal operation Amount of available hydrogen changes with temperature

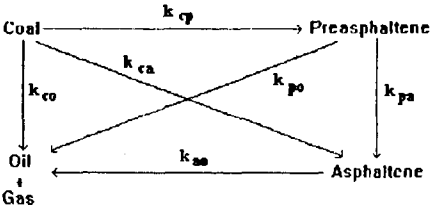

	400°C		350°C	
	Tetralin	Anthracene oil	Tetralin	Anthracene oil
k_{cp}	.0964	.0978	.0575	.0766
k_{ca}	.0540	.0044	.0283	.0022
k_{co}	.0241	.0235	.0191	.0195
k_{pa}	6.2E-6	.0066	2.7E-6	.0039
k_{po}	1.8E-4	0	7.4E-5	0
k_{ao}	.0080	.0125	.0027	.0054

Figure 1 Reaction scheme and rate constants in two different solvents for a kinetic model by Giralt et al.

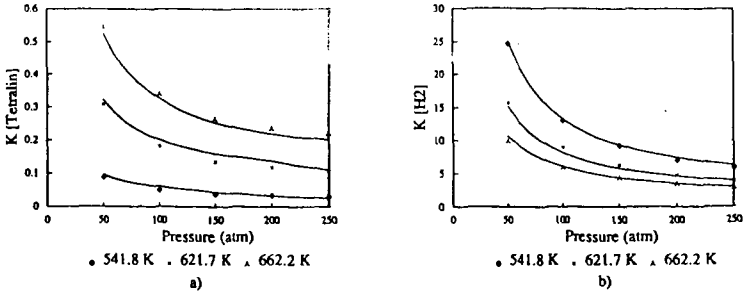

Figure 2 Predicted and experimental partition coefficients for hydrogen/tetralin system: a) tetralin, b) hydrogen.

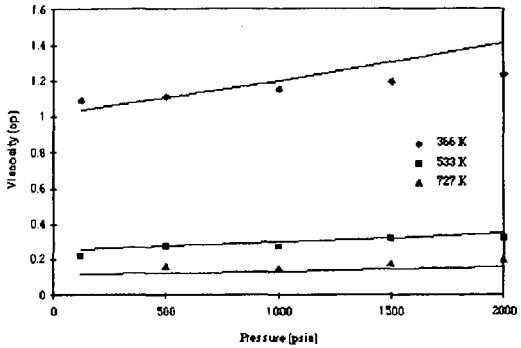

Figure 3 Viscosity of a coal liquid versus pressure at three different temperatures.

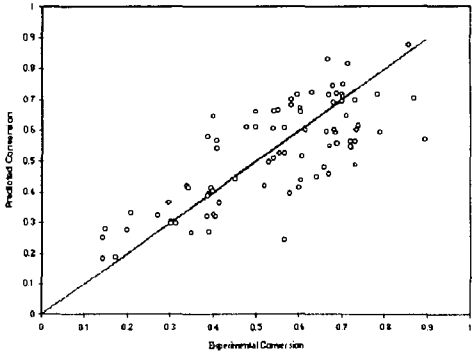

Figure 4 Parity plot of experimental and predicted coal conversions.

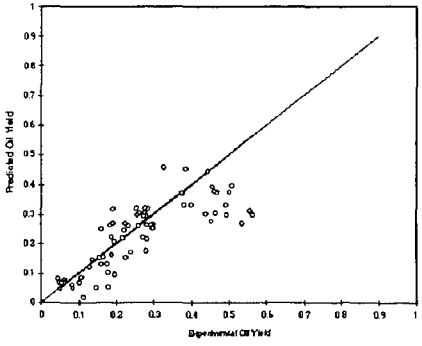

Figure 5 Parity plot of experimental versus predicted oil yields.

DISPERSED SLURRY CATALYSTS FOR HYDROCONVERSION OF CARBONACEOUS MATERIALS

L.K. Lee, V.R. Pradhan, G. Popper, and A.G. Comolli
Hydrocarbon Technologies, Inc.
Lawrenceville, NJ 08648

Keywords: Dispersed Catalysts, Coal Liquefaction, Coal/Waste Coprocessing

ABSTRACT

Dispersed slurry catalysts, based upon the *in situ* sulfided forms of transition metals such as iron and molybdenum, have been developed and successfully employed in the multi-stage hydroconversion of various carbonaceous materials including coal, heavy petroleum resid, waste plastics, and different combinations of these feedstocks. For example, using HTI's proprietary iron-based catalyst and commercial Molyvan-A additive, over 95 % maf coal conversion has been obtained accompanied by over 90 % maf conversion of 524°C+ residuum and over 65 % maf yield of C_4-524°C distillate yield in a fully back-mixed high pressure reaction system. The use of an in-line fixed-bed hydrotreater in such a hydroconversion process that relies only on dispersed slurry catalysts for conversion allows to selectively upgrade the light distillate products (IBP-400°C) from the process resulting in premium quality naphtha and mid-distillate products with less than 10 ppm nitrogen, an H/C ratio of 1.9, and about 20 ppm sulfur. The use of dispersed catalyst for such hydroconversion processes has a significant positive impact (as much as 20 % cost potential reduction) on the process economics because the reactor throughput can be increased by as much as 70 % while maintaining the equivalent residence time and the cost associated with the expensive high pressure catalyst addition/withdrawal system, used for supported extrudate catalyst, and that associated with expensive ebullating pumps can be reduced or eliminated completely.

INTRODUCTION

Two-stage catalytic conversion of coal and other carbonaceous feedstocks have been studied extensively using Ni/Mo or Co/Mo supported catalysts. The low/high temperature mode of operations was demonstrated in 3 ton/day scale at both the Wilsonville advanced Coal Liquefaction facility and Hydrocarbon Research, Inc. This mode of operations in combination with an in-line hydrotreater yields liquids of premium quality containing less than 20 ppm of nitrogen. The high conversion was achieved at the expense of high replacement rate of the supported catalysts which became deactivated with carbon and heavy metal depositions. The deactivation rate of supported catalysts for feedstocks, that contain high degree of heavy metals, such as vanadium and nickel and materials that have high tendency to form coke, is one of the key factor affecting the design and cost of the conversion facility.

Dispersed slurry catalysts, which offer better contact with the reactants than the supported extrudate catalysts, have drawn much attention in recent years. Hydrocarbon Technologies, Inc. has been studied the use of anion modified iron based catalyst at its bench scale (30 Kg/day) multi-stage unit located at Lawrenceville, New Jersey. It is observed that the use of dispersed catalyst, with or without supported catalyst, in conjunction with an in-line hydrotreater increase the throughput of a system significantly without compromising much in the product qualities. This paper discusses the use of HTI's proprietary dispersed catalysts in processing coal and other carbonaceous feedstocks, such as heavy oil and waste plastics. Due to the high activity of these dispersed iron-based catalysts, they can be used in small concentrations of 0.1-1.0 wt% iron relative to weight of feed for the various hydrogenation and hydroconversion reactions mentioned above, and are preferably recycled with the unconverted or partially converted high boiling fraction (454°C+) back to the reactor for further reaction. Because these dispersed fine-sized iron catalysts are produced based on use of available relatively inexpensive materials and since the principal component is cheap and environmentally friendly iron, they are usually disposable for large scale processes and do not require recovery and regeneration. HTI's proprietary dispersed catalyst can be used either as a wet cake consisting of a gel of precipitate particles in water containing 50-80 wt% water or as a dry powder obtained after drying and/or calcination of the oxyhydroxide precipitates. In the gel mode of usage, the precipitates from hydrolysis are not filtered or dried, but are used as is. The catalyst gel form reduces the catalyst cost significantly and also does not compromise at all on its activity for relevant hydroprocessing reactions. These catalysts, either in the dry powder form or in the wet-cake form, have been successfully tested (in the presence of a sulfiding source) both at a 20 cc microautoclave reactor scale and at a 30 kg/day continuous two-stage bench-scale operation, under hydrogen pressures of 5-20 MPa and operating temperatures of between 400 to 460°C. The key to the higher activity of these HTI's catalysts as compared with some other iron-based catalysts disclosed in literature, is believed to be their initial fine size, high surface area, a high extent of catalytic dispersion, and their ability to preserve the state of high dispersion under reaction conditions due to presence of anionic modifiers which are known to prevent sintering or agglomeration of fine-sized particles at high temperatures.

EXPERIMENTAL

The activity of catalyst was tested in a 20 cc vertically shaken microautoclave unit and in a two-stage bench scale continuous flow system of nominal capacity of 30 Kg/day. The bench-scale operations, employing dispersed catalysts, were conducted in HTI's fully back-mixed reaction system employing off-line pressure filtration for solids separation; a simplified schematic of the hydroconversion process used during this work is shown in *Figure 1*. As shown in *Figure 1*, the hydroconversion process, followed here, is based upon a catalytic multi-stage reactor system supported by an independent feed preparation/handling section, high pressure product fractionation section, light distillate refining and solids separation/heavy distillate recovery sections. The hydroconversion reactors could be operated in a close-coupled mode or an interstage product fractionator could be used for taking the lights off the feed going to the second stage hydroconversion reactor. The light product fraction (400°C- material) from the hydroconversion reactors was selectively processed through an in-line fixed-bed hydrotreating unit. This step achieves a significant function of improving the quality of distillable products from the process. The heavier product fraction (400°C+ material) is substantially recycled and unreacted feed (including solids in case of coal) is either partly recycled or rejected from the process completely with minimal loss of organics. The HTI iron based catalyst is an anion modified oxyhydroxide catalyst prepared in either a dry or a gel form which contains about 50-80 w% water. Molybdenum catalyst was added in form of Molyvan A at the desired concentration levels. Coal used in this study is from Wyoming Black Thunder Mine. The coal was prepared by Empire Coke Company of Alabama and was used in the last run of the DOE Proof of Concept program. The heavy oil is a California Hondo vacuum tower bottom, while the waste plastic was a curb side plastic waste containing mostly high density polyethylene, polystyrene and polypropylene.

RESULTS AND DISCUSSION

The activity screening of dispersed slurry catalysts, performed using shaken microautoclaves, is summarized in *Table 1*. From the *Table 1* results, it is seen that the HTI's dispersed slurry catalysts, used in either a wet cake (gel) form or a dried particulate form, provided hydroconversion results superior to those obtained using the two known iron oxide catalysts. Specifically, the percent coal conversion based on tetrahydrofuran (THF) solubility and percent conversion of 524°C+ resid fraction were both significantly greater than for the commercial iron oxide catalysts. The addition of about 100 ppm of molybdenum to HTI's iron catalyst improved both the coal and the resid conversions; the gel form of iron catalyst appeared slightly better than the dry powder form. The best performance of HTI's dispersed catalyst was almost equivalent to that obtained using a more active supported NiMo catalyst, Akzo AO-60, with which a shade better performance was obtained at same temperature but for a longer reaction time (60 minutes).

The dispersed iron-based catalysts described in this paper have been used extensively in continuous bench-scale two-stage operations with throughput up to 30 kg/day of moisture and ash-free (maf) coal feed for direct catalytic two-stage liquefaction of coal. As shown in *Table 2*, under the prevailing operating conditions, for the direct liquefaction of a sub-bituminous Wyoming Black Thunder Mine coal, dispersed catalyst containing 615-10000 ppmw of iron and 50-200 ppmw of molybdenum was used, relative to maf coal feed, in the form of HTI's iron-based dispersed catalysts. The dispersed catalysts were used either in an all-dispersed slurry catalyst mode, or in a hybrid system utilizing dispersed catalyst in one of two close-coupled hydroconversion reactors and the extrudate supported catalyst in the other reactor. The use of iron and molybdenum containing dispersed catalysts has resulted in a coal conversion range of 93-96 wt%, a 524°C+ residuum conversion range of 83-92 wt%, and C_4-524°C distillate liquid yields of 60-66 wt% (all on maf coal basis). When evaluated on the basis of the maf coal feed, this performance provides up to 4 barrels of C_4-524°C distillate liquid products per ton of the maf coal feed. Specifically, the direct comparison between the data from Bench Run 83 Condition 4 and Run 91 Condition 1B shows that in an hybrid catalytic mode of operation, higher molybdenum loading (100 vs. 50 ppm) results in better liquid distillate yields (66.3 vs. 63.4) and higher conversions of coal (94.7 vs. 92.8) and resid (90.0 vs. 87.4). The performance of HTI's dispersed slurry catalysts has been compared with some other dispersed and supported type catalysts for direct coal liquefaction as shown in *Figure 2*. The process performance has been compared on the basis of total coal conversion (based on quinoline solubility of the products), 524°C+ residuum conversion, and C_4-524°C distillate yield. The first bar (None-Cat) in *Figure 2* represents process performance with a thermal first stage reactor and an expanded supported catalyst bed in the second stage reactor; the second bar (Cat-Cat) represents process performance with supported catalysts in both the reactor stages; the third bar (Mo-Cat) represents molybdenum dispersed catalyst in first stage reactor and an expanded supported catalyst bed in the second stage reactor; the fourth bar (HTI-Cat) represents performance with HTI's iron-based dispersed catalyst in the first stage reactor and an expanded supported catalyst in the second stage reactor; the fifth bar (HTI-HTI) represents the performance of an all-dispersed slurry catalyst two-stage reactor system utilizing the HTI's dispersed catalyst It can be clearly seen from *Figure 2* that the reactor configurations utilizing HTI's dispersed catalysts alone result in the highest extent of total coal and 524°C+ residuum conversion, and C_4-524 C distillate

yields. The result obtained with the 'all dispersed catalyst' mode of operation were also better than those obtained with 'Supported catalyst-catalyst' or 'hybrid mode'of operations. At 5000 ppm of iron and 50 ppm of molybdenum, 2 % higher coal conversion, higher light distillate products were obtained; the yield of light gases was also higher in an 'all dispersed' catalyst mode. The use of dispersed catalyst allows the higher volume of reactor for thermal cracking.

Bench-scale continuous multi-stage operations were also conducted to evaluate the performance of HTI's dispersed iron-based catalysts for hydroconversion of (a) heavy petroleum oil (California Hondo resid vacuum tower bottoms), (b) mixtures of heavy petroleum resid oil and mixed plastics (containing high density polyethylene, polypropylene, polystyrene, and other organic/inorganic impurities) from municipal solid waste streams, © mixtures of Wyoming Black Thunder Mine coal and Hondo resid, and (d) combinations of coal, Hondo resid, and the mixed plastics feeds. Significant process performance was obtained with all of these varied feedstocks with dispersed catalysts in each stage reactor, under conditions similar to those employed for direct coal liquefaction. The prevailing operating conditions, feed type and composition, dispersed catalyst metal loadings, and process performance and yields are summarized in *Table 3*. As shown in *Table 3*, consistently high feed conversions and light distillate oil yields have been realized in the bench-scale operations. With the bench-scale operations involving either heavy petroleum resid, Hondo resid alone or in a mixed feed with coal, as high as 99 wt% feed conversion to quinoline soluble products was obtained, with as high as 75 wt% C_4-524°C distillate liquid yields. During the operations, involving mixed plastics from a municipal solid waste stream, either with coal or with heavy resid or mixtures of coal and heavy resid, over 93 wt% total feed conversions were realized with about 75 wt% distillate liquid yields.

CONCLUSION

Based upon the data presented in this paper, it is evident that the sulfate-modified iron-based dispersed catalysts, HTI has developed, are very effective in achieving the levels of performance that is tantamount to or better than that obtained using the conventional supported extrudate catalysts. The iron-based dispersed slurry catalysts were also very effective for the hydroconversion of organic wastes such as heavy petroleum resids and MSW plastics, in combination with coal, into the value-added distillate products.The higher activity of these HTI's catalysts as compared with some other iron-based catalysts disclosed in literature, is believed to be due to their initial fine size, high surface area, a high extent of catalytic dispersion, and their ability to preserve the state of high dispersion under reaction conditions due to presence of anionic modifiers which are known to prevent sintering or agglomeration of fine-sized particles at high temperatures. The overall high levels of yields and conversions are obtained with HTI's proprietary dispersed catalyst, especially at the metal loadings that potentially make the use of these catalysts possible on a disposable basis. The replacement of supported extrudate catalysts by fine-sized dispersed slurry catalysts also allows for operations at significantly higher throughput under similar overall reaction severity. It is anticipated that the use of dispersed catalysts would lower the overall cost of hydroconversion of coal and other organic feeds discussed in this paper.

ACKNOWLEDGMENT

The financial support provided for this work by the U.S. Department of Energy under the Contract Nos. DE-AC22-93PC92147 and DE-AC22-92PC92148 is gratefully acknowledged.

Table 1. Activity of Dispersed Catalyst in Microautoclave Testing*

Coal: 2 g, Solvent: 6g, DMDS: 0.2 g 427°C @ 14 MPa for 30 min. Fe: 5000 wppm

Catalyst Type	THF Conversion [%]	524°C+ Conversion [%]
Fe_2O_3 (Aldrich)	76.1	34.1
Fe_2O_3 (Mach I)	80.6	42.8
Fe/SO_4^{2-} (dry)	83.3	53.3
Fe/SO_4^{2-} (gel)	86.2	55.1
$Mo.Fe/SO_4^{2-}$ (dry)	86.8	59.6
$Mo.Fe/SO_4^{2-}$ (gel)	89.9	63.3

***The THF Conversion under similar reaction conditions (but 60 minute long reaction time) for a supported extrudate $NiMo/Al_2O_3$ catalyst (fresh Akzo AO-60) was 92.1 w% and the 524°C+ residuum conversion was 64.4 w%.**

Table 2 Process Performance using Dispersed and Supported Catalysts
Wyoming Black Thunder Mine Coal
Dispersed Catalyst: HTI sulfated Iron; Supported Catalyst: Shell S-317

Run I.D. Condition	CMSL-6 4	PB-02 1B	CMSL-11 1	PB-1 1
Process Conditions				
Mode	Thm/Cat	Thm/Cat	All Disp.	All Disp.
Recycle/Coal ratio	1.3	1.0	1.0	1.0
Space Velocity, Kg mf coalh/M³	640	665	703	694
1st Stage Temperature, °C	449	447	441	433
2nd Stage Temperature, °C	429	427	449	449
Catalyst Concentration				
Iron, w%	0.0615	0.500	0.500	0.500
Molybdenum, wppm	100	50	50	50
Process Performance W% maf Coal				
C_1-C_3	11.3	10.3	15.7	12.4
C_4-177°C	18.2	20.8	19.7	21.2
177°-343°C	33.5	26.4	32.1	28.0
343°-524°C	14.9	16.2	9.0	12.7
524°C+	4.5	5.4	3.7	6.6
C_4-524°C Distillate	66.6	63.4	64.6	61.9
Coal Conversion	94.5	92.8	95.5	94.7
524°C+ Conversion	90.0	87.4	91.5	88.0
H_2 Consumption	7.0	7.3	6.9	6.4

Note: Thm/Cat = Thermal/Catalytic two-stage mode; All Disp. = All Dispersed Catalyst two-stage mode

Table 3 Hydroprocessing of Mixed Feeds using HTI's Iron Based Dispersed Catalyst

Run I.D. Condition	CMSL-9 9	CMSL-11 3A	CMSL-11 4B	PB-1 4	PB-1 9	PB-1 7
Feed Composition,w%						
Black Thunder	50	67	75	0	0	33.3
Waste Plastics	50	33	25	0	50	33.3
Hondo VTB	0	0	0	100	50	33.4
Process Conditions						
Space Velocity, Kg mf coalh/M³	669	687	662	1059	1250	1033
1st Stage Temperature, °C	449	450	447	441	451	450
2nd Stage Temperature, °C	462	459	461	451	460	461
Catalyst Concentration						
Iron, w%	1.00	0.500	0.500	0.500	0.500	0.500
Molybdenum, wppm	300	100	100	50	50	50
Process Performance W% maf Coal						
C_1-C_3	7.5	8.6	7.4	5.0	4.3	7.6
C_4-177°C	30.0	16.8	13.4	16.2	21.4	26.2
177°-343°C	26.2	24.9	26.1	27.7	24.3	24.6
343°-524°C	18.1	25.3	28.1	32.2	30.5	22.0
524°C+	8.9	11.4	11.2	16.5	15.7	10.9
C_4-524°C Distillate	74.3	67.0	67.6	76.1	76.2	72.8
Coal Conversion	97.0	95.3	94.7	N.A.	N.A.	96.3
524°C+ Conversion	88.1	83.9	83.5	83.3	84.0	85.4
H_2 Consumption	3.5	4.1	4.9	1.7	1.8	3.4

Figure 1. Simplified Schematic of HTI's Catalytic Multi-Stage Hydroconversion Process

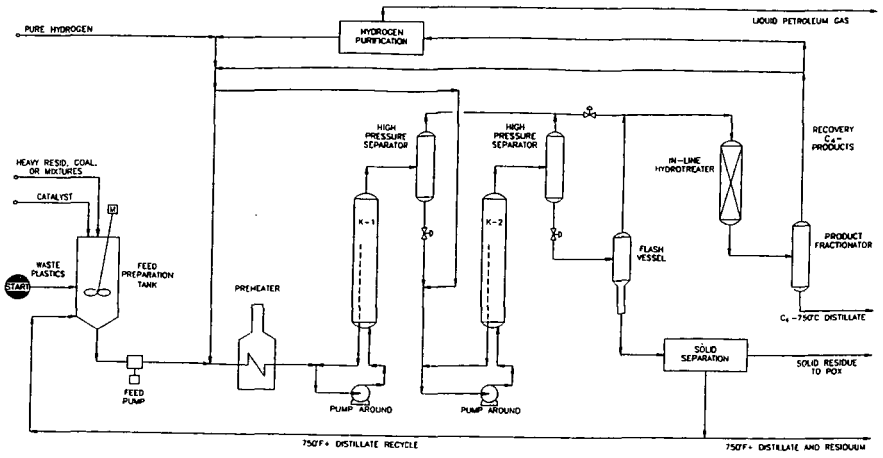

Figure 2. Comparison of Catalyst Performance in Bench-Scale Direct Coal Liquefaction

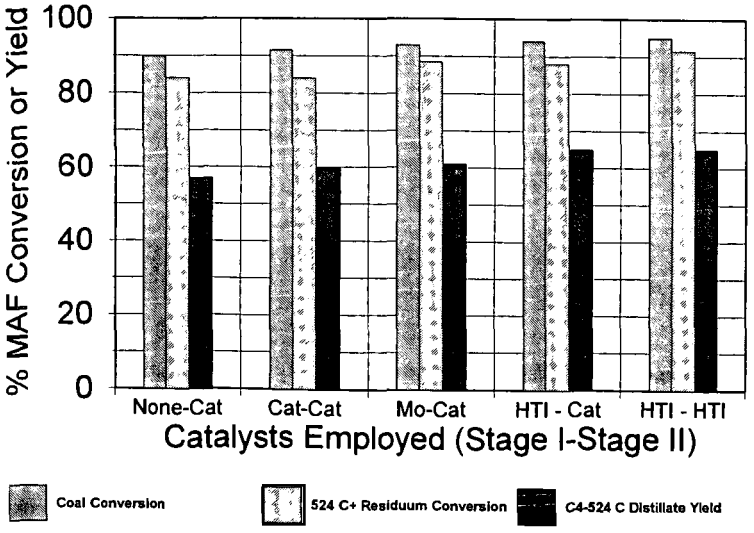

RESULTS OF HYDROTREATING THE KEROSENE FRACTION OF HTI'S FIRST PROOF OF CONCEPT RUN

Frances V. Stohl, Stephen E. Lott, Kathleen V. Diegert, David C. Goodnow
Process Research Dept. 6212
Sandia National Laboratories
P.O. Box 5800
Albuquerque, NM 87185-0709

Keywords: Hydrotreating coal liquids; Factorial experimental design; Continuous reactor studies

ABSTRACT

The objective of Sandia's hydrotreating study is to determine the relationships between hydrotreating conditions and product characteristics for coal liquids produced using current technologies. The coal-derived liquid used in the current work is the kerosene fraction of the product from Hydrocarbon Technologies Inc.'s first proof-of-concept run for it's Catalytic Two-Stage Liquefaction Technology. Sandia's hydrotreating experiments were performed in a continuous operation, microflow reactor system using aged HDN-60 catalyst. A factorial experimental design with three variables (temperature, pressure, liquid hourly space velocity) was used in this work. Nitrogen and sulfur contents of the feed and hydrotreated products were determined using an Antek 7000 Sulfur and Nitrogen Analyzer. Multiple samples were collected at each set of reaction conditions to ensure that each condition was lined out. Hydrotreating at each set of reaction conditions was repeated so that results could be normalized for catalyst deactivation. The normalized results were statistically analyzed. Increases in temperature and pressure had the greatest effects on nitrogen removal. The highest severity condition (388°C, 1500 psig H_2, 1.5g/h/g(cat)) gave a measured nitrogen value of <5 ppm.

INTRODUCTION

DOE/PETC's refining of coal liquids program is aimed at determining the most cost effective combination of existing refinery processes and blending options necessary to upgrade direct and indirect coal liquids into transportation fuels that meet year 2000 specifications. A main reason for this program is that coal liquefaction processing has improved significantly since the last refining evaluation was done by Sullivan and Frumkin[1] at Chevron in the early 1980s. In addition, a recent publication by Zhou, Marano and Winschel[2] indicates that blending coal liquids with petroleum may allow refiners to produce specification products with less refining than if each fraction was processed separately.

The objective of Sandia's refining of coal-derived liquids project is to experimentally evaluate options for hydrotreating coal liquids and various distillate cuts of coal liquids, and to develop a database relating hydrotreating parameters to feed and product quality. The hydrotreating effort is being conducted using a bench-scale, continuous flow, trickle-bed reactor that enables us to evaluate many hydrotreating options in a rapid and cost effective manner. The coal-derived liquid used in this work was produced in Hydrocarbon Technologies Inc.'s (HTI) first proof-of-concept run (POC #1) in their 3 ton/day Process Development Unit using their Catalytic Two-Stage Liquefaction Technology. This 57 day run used Illinois #6 coal and produced up to 5 barrels of distillate liquid product/ton moisture-ash-free coal. After completion of this run, HTI shipped 2500 gallons of coal liquids to Southwest Research Inc. (SwRI) for characterization, fractionation, and evaluation. The kerosene fraction that Sandia hydrotreated was obtained from SwRI as was the aged Criterion HDN-60 catalyst used in Sandia's hydrotreating study. This work is being done in conjunction with DOE/PETC's Refining and End-Use Study of Coal Liquids project (Bechtel, SwRI, Amoco, M. W. Kellogg). Results from Sandia's hydrotreating work will be analyzed by Bechtel using the PIMS refinery model as part of their effort to determine the best way to incorporate coal liquids into an existing refinery.

EXPERIMENTAL SECTION

Sandia's experimental procedures included using a factorial experimental design, hydrotreating the kerosene fraction of the POC #1 whole coal liquid, characterizing the feed and products, and reporting results to other program participants.

Reactor Feeds and Catalyst. The POC #1 kerosene fraction that was hydrotreated at Sandia was collected when HTI's in-line hydrotreater was not in operation. The nitrogen and sulfur contents of this fraction were 645 ppm and 239 ppm respectively. The initial boiling point was 385°F and the final boiling point was 489°F. The nitrogen and sulfur values are Sandia's values and the boiling points are from SwRI. The hydrotreating experiments used aged HDN-60 catalyst that was obtained from SwRI.

Continuous Operation Hydrotreating System. Sandia's hydrotreating experiments are being conducted using a bench-scale, continuous flow, trickle-bed reactor. The system has all required safety features to enable it to be operated unattended. Ranges of operating conditions for this system are as follows: liquid flow from 0.05 to 4 cm^3/min; gas flows up to 2 L/min for N_2 and H_2 and up to 0.5 L/min for H_2S; maximum temperature of 620°C; maximum pressure of 1800 psig; reactor volume of 59 cm^3; and

maximum catalyst loading of 25 cm^3. For this kerosene hydrotreating run, 10g of aged HDN-60 catalyst was used as received from SwRI, and the actual hydrogen flow rate was 4600 ft^3/bbl. Four samples can be collected automatically during unattended operation. With a 45 minute sample collection time and liquid hourly space velocities (LHSV) of 1.5 and 3 g/h/g(cat), the amounts of sample collected would weigh about 11 g and 22 g respectively.

Factorial Experimental Design. Based on experience, three parameters were chosen for the factorial experimental design used for hydrotreating the kerosene fraction (Figure 1): temperature ranging from 327°C to 388°C, pressure from 500 to 1500 psig H_2, and LHSV from 1.5 to 3 g/h/g(cat)). Nitrogen and sulfur contents of the hydrotreated products were monitored during the hydrotreating experiments to ensure that activity was lined out at each set of reaction conditions. After line-out was attained, multiple samples were collected over a 24 hour period. All reaction conditions were tested at least twice so the effects of catalyst deactivation could be determined for each condition and appropriate corrections could be made. An Analysis of Variance (ANOVA) was used to model the results, which had been normalized for differences in catalyst deactivation and extrapolated to a total of 28,000 g of feed processed. The controlled variables used in the ANOVA are the measured temperature, pressure, and LHSV. In addition, SwRI requested that we test the center points of the cube edges parallel to the temperature axis. These points were also included in the ANOVA.

Nitrogen and Sulfur Analyses. Small samples were collected either manually or automatically throughout the run. Nitrogen analyses were used to determine when line-out was achieved at each reaction condition. These analyses were performed using an Antek 7000 Sulfur & Nitrogen Analyzer with an automatic sampler. Standards were prepared using phenanthridine for nitrogen, thianthrene for sulfur, and toluene for the solvent. Six standards prepared by serial dilution were used in the analysis. Standards were measured at least twice. A polynomial fit of the intensity versus concentration data was used for analysis of nitrogen, and a linear fit of the intensity versus concentration data was used for sulfur. Results will only be shown for nitrogen because sulfur values are very low with only one sample having a measured value >20 ppm.

RESULTS AND DISCUSSION

This run was very successful. There was one unplanned shutdown on the second day of the run due to an operator error. The reactor was restarted and operated continuously for 55 days until the end of the run. The letters at each data point in Figure 2 show the order in which the various conditions were evaluated. The first number after the letter is the average ppm nitrogen at that condition. The number in parentheses is the total amount of feed in grams that had been processed through the reactor from the start of the evaluation of the experimental design to the time the samples were collected. All eight corners and the center point of the cubic design were run at least twice so that the rate of catalyst deactivation could be determined for each condition. The four points at the center points of the cube edges parallel to the temperature axis were only tested once because of lack of feed.

Catalyst Deactivation Correction. Results for each condition (Figure 2) show that the measured nitrogen contents get higher as the amount of feed processed increases, thus indicating catalyst deactivation. The first step in the analysis of the results was to normalize the results for catalyst deactivation so that all results could be compared based on an equal amount of feed processed. This was accomplished by plotting nitrogen values for each lined-out sample collected at a given condition versus the total amount of feed processed from the start of the run until that sample was collected. For example, the numbers of lined-out samples collected at 388°C, 500 psig H_2, and 1.5 g/h/g(cat), were 8 for point A, 3 for point J, and 6 for point R. The equation for the straight line calculated for these 17 samples was $Y = 0.00705X + 49.3$ with $r^2 = 0.97$. The slope of this equation (0.00705 ppm/g of feed processed) was then used to extrapolate the nitrogen content of each individual sample obtained at this condition out to 28,000 g of total feed. This was approximately the total amount of feed processed in this hydrotreating run. This analysis was performed for each reaction condition. These normalized nitrogen values for all conditions were then used in the ANOVA to give a model for the remaining nitrogen at 28,000 g total feed processed. The slopes of the lines for the various conditions are shown in Figure 3. The slopes used to correct the values at the center points of the cube edges parallel to the temperature axis were the averages of the high temperature and low temperature slopes at the same LHSV and pressure. The negative deactivation slope at 327°C, 500 psig H_2, 3 g/h/g(cat) is due to the collection of only two samples, which gave poor reproducibility in the nitrogen analysis, at the second repeat of this test condition.

Model for Nitrogen Remaining at 28,000 g Total Feed Processed. The ANOVA model for nitrogen contents of samples at 28,000 g of total feed processed is shown in Table 1. Results show a good fit of the model to the data as indicated by an r^2 value of 0.95. Calculated nitrogen values vary from 7.9 ppm at the highest severity condition (388°C, 1500 psig H_2, 1.5 g/h/g(cat)) to 599.7 ppm at the lowest severity condition (327°C, 500 psig H_2, 3.0 g/h/g(cat)). The greatest impacts on the nitrogen content are due to the individual effects of temperature and pressure. Changing LHSV by itself has the least effect on nitrogen content. Figure 4 gives a comparison of the calculated and measured results for all reaction conditions. The biggest difference between the calculated and measured results is at the lowest severity condition 327°C, 500 psig H_2, 3 g/h/g(cat). The calculated value for nitrogen at this condition is 675.6 ppm, whereas the amount of nitrogen in the feed is 645 ppm. This discrepancy is probably due to higher variability in

analytical results as nitrogen contents get higher. Efforts are currently underway to quantify and decrease the sources of variability in the nitrogen analysis procedure.

CONCLUSIONS

Results of hydrotreating a coal liquid produced using HTI's Catalytic Two-Stage Liquefaction process show that good denitrogenation and good desulfurization can be obtained under relatively mild conditions. Processing at the highest severity condition (388°C, 1500 psig H_2, 1.5 g/h/g(cat)) decreases nitrogen from 645 ppm in the feed to 7.9 ppm in the hydrotreated product. Sulfur contents were very low for all hydrotreated products. The feed had 239 ppm sulfur whereas all hydrotreating conditions gave <20 ppm sulfur. The results of this work will be used by Bechtel in their Refining and End-Use Study of Coal Liquids project to determine the best way to introduce direct coal liquids into an existing refinery.

Acknowledgment: This work was supported by the U.S. Department of Energy at Sandia National Laboratories under contract DE-AC04-94-AL85000.

REFERENCES

1. Sullivan, R. F., Frumkin, H. A., ACS Div. of Fuel Chem. Preprints 31(2), 325, 1986.
2. Zhou, P.-Z., Marano, J. J., Winschel, R. A. ACS Div. Fuel Chem. Preprints 37(4), 1847, 1992.
3. Comolli, A. G., Lee, L. K., Pradhan, V. R., Stalzer, R. H., Proceedings of Coal Liquefaction and Gas Conversion Contractors' Review Conference, Pittsburgh, PA, August 29-31, 1995.

Table 1. Model for Nitrogen Content of Reaction Products (Normalized to 28,000g of Feed Processed)

	NITROGEN (ppm)		
Parameter	**Model Estimate**	**Meas'd. Average**	**Std. Error**
Constant*	599.3		9.3
Temperature	-330.7		14.4
Pressure	-331.0		16.9
LHSV	0.4		0.2
Temp. x Press Int.	70.3		24.9
Temp. x LHSV Int.	169.5		17.3
Press. x LHSV Int.	87.3		19.6
Temp. x LHSV x Press. Int.	-192.1		33.3
Experimental Error	46.5		
327°C, 500 psig, 1.5**	599.3	520.0	13.0
388°C, 500 psig, 1.5	268.6	246.8	3.1
327°C, 1500 psig, 1.5	268.3	254.6	4.6
388°C, 1500 psig, 1.5	7.9	1.4	0.9
358°C, 1000 psig, 2.25	326.4	360.4	2.5
327°C, 500 psig, 3.0	599.7	675.6	6.3
388°C, 500 psig, 3.0	438.5	412.6	20.1
327°C, 1500 psig, 3.0	356.0	361.8	5.2
388°C, 1500 psig, 3.0	72.9	73.9	3.2
358°C, 500 psig, 1.5	434.0	439.8	8.3
358°C, 1500 psig, 1.5	138.1	139.0	2.7
358°C, 500 psig, 3.0	519.1	565.1	10.7
358°C, 1500 psig, 3.0	214.4	181.0	4.3
R^2	0.95		

* Value calculated for 327°C, 1.5 g/h/g(cat), 500 psig H_2

** g/h/g(cat)

Figure 1: Factorial Experimental Design (Temperature = °C, Pressure = psig H_2, LHSV = g/h/g(cat))

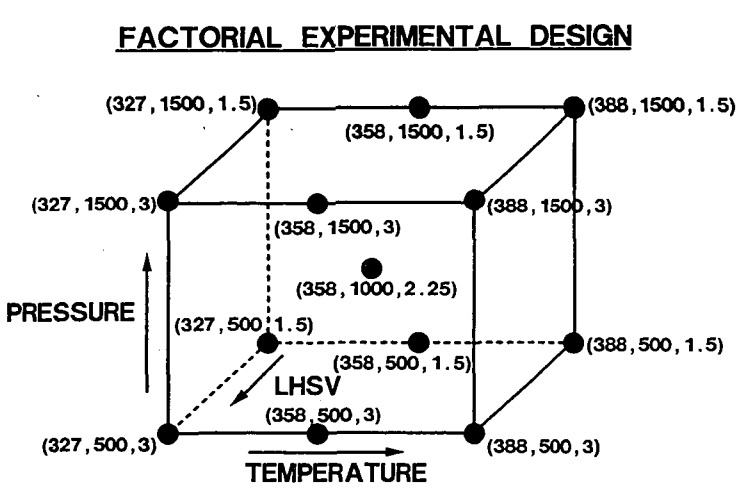

Figure 2: Testing Sequence, Measured Average Nitrogen Values, and Total Amount of Feed Processed From Start of Run Until Sample Collected

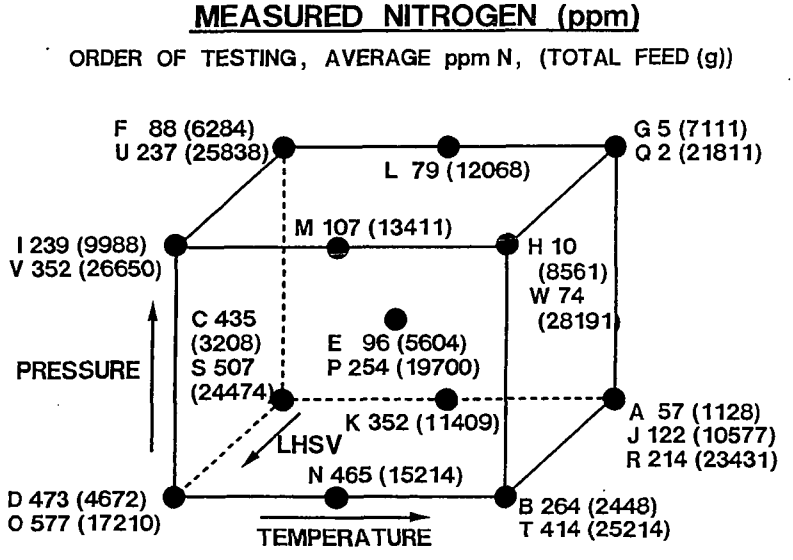

Figure 3: Deactivation Rates for Each Experimental Condition
(ppm N/1000 g Feed)

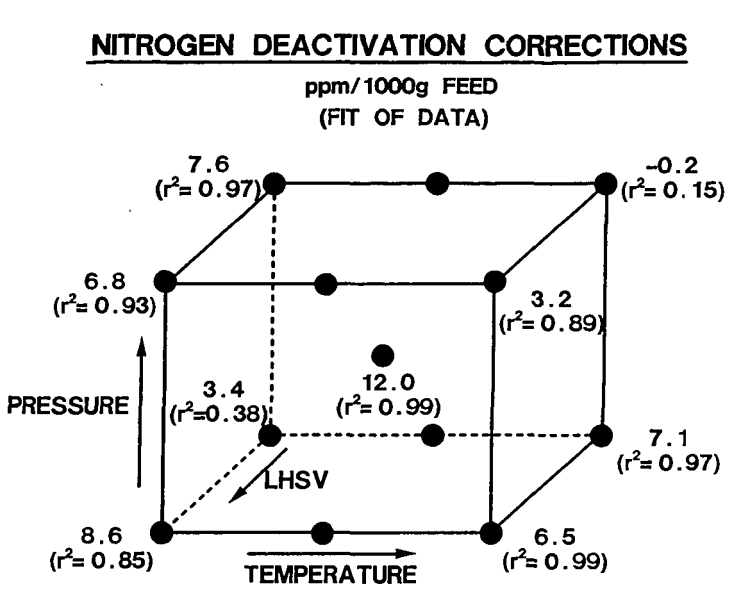

Figure 4: Measured and Calculated Nitrogen Values
(At 28,000g Total Feed Processed)

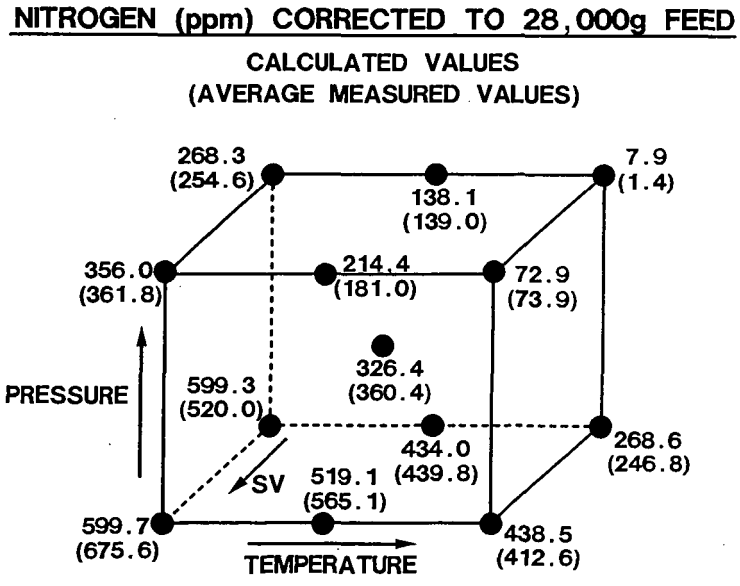

THE EFFECT OF H_2 PARTIAL PRESSURE AND COAL CONCENTRATION ON *CATALYTIC COAL LIQUEFACTION AND COPROCESSING*

Anthony Cugini, Kurt Rothenberger, Donald Krastman, Robert Thompson, and Ray Bernarding
U.S. Department of Energy, Pittsburgh Energy Technology Center
Pittsburgh, PA 15236

KEYWORDS: Liquefaction, Hydrogenation, Coprocessing

INTRODUCTION

An effort is under way at PETC to study the potential of reducing pressure in coal liquefaction. The objective of this effort is to reduce pressure and maintain overall coal conversions, yields and product quality. Several observations have been made during this study and have been reported. [1,2,3] The potential for reducing pressure appears to be tied to a combination of solvent quality and catalyst concentration. Other observations were made concerning the hydrogenation of products from reactors containing coal. These include suppression of two-ring aromatic hydrogenation in the presence of coal and the large consumption of hydrogen observed in the earliest stages of coal liquefaction.

Cugini et al.[1] and Rothenberger et al. [2] reported that catalytic hydrogenation of naphthalenes is suppressed in the presence of coal (using supported or unsupported catalysts). This effect was also observed in several other studies.[4,5,6] The efforts of Cugini et al[3] also indicated the need for a combination of catalyst and donor solvent system to reduce pressure. They found that the donor solvent/low pressure/no catalyst system resulted in consistently lower coal conversions than the non-donor solvent/high pressure/catalyst system. Also, high hydrogen consumption was observed during the early stages of catalytic coal liquefaction. Approximately 50% of the hydrogen consumption during a 30-minute test occurred during the heat-up (~ 2 minutes) and subsequent 2 minutes of the test.

The current effort attempts to provide more information regarding the suppression of catalytic hydrogenation of aromatic compounds by coal and the high initial consumption of hydrogen in catalytic liquefaction. The observation of suppression of catalytic hydrogenation of two-ring aromatic compounds is extended to other multi-ring aromatic compounds. These include phenanthrene and pyrene. Also, short-time liquefaction tests are being studied to determine the differences between donor/non-catalytic and non-donor/catalytic systems.

The remainder of the study was directed toward the investigation of coal/oil coprocessing. The effect of coal concentration, catalyst concentration and pressure were investigated as part of this study. The earlier results from coal liquefaction studies had indicated that pressure and catalyst concentration were interrelated. This phase of the effort attempts to extend the results from the coal liquefaction efforts to coal/oil coprocessing. Essentially, it is hoped that catalyst could (to some extent) be used to compensate for pressure reduction as was observed in coal liquefaction applications. Lower coal concentrations were also investigated because of earlier results that had indicated that a synergism to distillate product was observed at low concentration and that coal could be used to effectively remove the metals from the liquid products even at relatively low coal concentrations.[7]

EXPERIMENTAL

Materials. Purified grade 1-methylnaphthalene (1-MN), phenanthrene, pyrene, and tetralin from Fisher Scientific Company were used in these studies. Hondo residual oil, vacuum tower bottoms obtained from Paramount Petroleum Corporation, was used. Blind Canyon coal, DECS-6, from the U.S. Department of Energy's Coal Sample Program and Illinois No. 6 coal were used. A supported molybdenum catalyst, Akzo AO-60, obtained from HTI, Inc. was used in the microautoclave catalytic tests. An unsupported MoS_2 catalyst prepared at PETC[2] was also used in the microautoclave tests. Aqueous ammonium heptamolybdate (AHM) was used as the precursor for MoS_2 in the 1-L semi-batch tests.

Reactions. Microautoclave reactions were completed in a stainless steel batch microautoclave reactor system (42 mL) constructed at PETC. Semi-batch 1-L reactions were completed in a stainless steel 1-L autoclave. A 97% H_2 / 3% H_2S gas mixture was used in the 1-L tests to sulfide the catalyst. Sample work-up and coal conversions for both the microautoclave and 1-L autoclave tests were calculated by a procedure described previously.[8]

Gas and Pressure Analyses. At the completion of each run, product gases were collected and analyzed at PETC by a previously published method.[3] Hydrogen consumption was determined by a method developed at PETC.[4]

GC-Mass Spectrometry (GC-MS). The THF soluble material from the autoclave runs was analyzed by GC-MS to determine the amount of solvent which had been hydrogenated. The samples were run as 1% solutions (w/w) in methylene chloride on a HP 5890A gas chromatograph equipped with a 50 m capillary column of 50% phenylmethylsilicone and a HP 5970 mass selective detector. The integrated areas of hydrogenated solvent peaks were compared against those of unconverted solvent peaks.

RESULTS

The initial studies were directed toward the effect of solvent type. As indicated, coal was found to suppress the catalytic hydrogenation of 1-MN. Two other aromatic solvents, pyrene and phenanthrene, were tested to evaluate the effect of coal addition on aromatic hydrogenation. The results from testing the two solvents as well as the earlier data with 1-MN are shown in Table 1. The data indicate that catalytic hydrogenation of pyrene and phenanthrene is suppressed by the presence of coal as shown by comparing tests B and C for the two cases. Further, exposure to coal continues to suppress the catalytic hydrogenation of phenanthrene even after coal is removed from the system, as shown by a comparison of tests B and D for phenanthrene. However, the results from the pyrene system are not as straightforward, because the tests using fresh catalyst and catalyst recovered after exposure to coal (tests B and D for pyrene) both appear to reach equilibrium[9] within the reaction time. Figure 1 shows the pressure as a function of time for the two tests with pyrene, fresh catalyst and catalyst exposed to coal. In the case with fresh catalyst, the pressure drops rapidly to 1,470 psig before the pressure levels off for the remainder of the test. This indicates that equilibrium is rapidly achieved during the test. On the other hand, with the catalyst that had been exposed to coal, the pressure drops continuously over the course of the test. This indicates that equilibrium was achieved only after the full reaction time. The net result is that the rate of catalytic hydrogenation of pyrene was also suppressed by exposure of the catalyst to coal just as in the other two examples.

Table 1. Effect of Blind Canyon Coal Addition on Catalytic Hydrogenation of Aromatic Solvents

	Percentage of Product					
Microautoclave Sample	0-H	2-H	4-H	6-H	other	% Hydrog.
Pyrene:						
(A) pyrene only	96	4	0	0	0	4
(B) with catalyst	68	21	2	8	1	32
(C) with coal + catalyst	85	14	0	0	1	15
(D) with THF insols from (C)	66	23	2	6	2	34
Phenanthrene:						
(A) phenanthrene only	97	2	0	1	0	4
(B) with catalyst	47	12	10	24	7	53
(C) with coal + catalyst	80	13	5	1	1	20
(D) with THF insols from (C)	67	16	13	0	4	33
1-Methylnaphthalene:						
(A) 1-MN only	100	----	0	----	0	0
(B) with catalyst	47	----	52	----	1	53
(C) with coal + catalyst	92	----	7	----	1	8
(D) with THF insols from (C)	86	----	12	----	2	14

425°C, 0.5 h, 1000 psig H_2 (cold), and 1000 ppm Mo

Short-time tests were made to compare the effects of catalyst and tetralin on coal conversion. Fast heat-up rates and 2-minute and 30-minute duration tests were conducted. The results of these tests are shown in Table 2. These results indicate that, in this time interval, coal conversion was enhanced in the catalytic case over the tetralin case. Detailed analyses of the insoluble products are being conducted to determine if more coke or hydrogen-deficient species are observed in the tetralin case.

Table 2

Effect of Solvent Quality, Pressure, and Catalyst on Blind Canyon Coal Conversion

					Coal Conversion
A	Tetralin	400 psig (cold)	No Catalyst	2 minutes	70%
B	Tetralin	1000 psig (cold)	No Catalyst	2 minutes	73%
C	Tetralin	400 psig (cold)	No Catalyst	30 minutes	85%
D	Tetralin	1000 psig (cold)	No Catalyst	30 minutes	86%
E	1-MN	1000 psig (cold)	AO-60	2 minutes	79%
F	1-MN	1000 psig (cold)	AO-60	30 minutes	89%
G	1-MN	1000 psig (cold)	MoS_2	30 minutes	93%

The effects of pressure and coal concentration in coal/oil coprocessing were studied in batch autoclave tests. The results are shown in Figure 2. The results indicate that there does appear to be an area at low coal concentration (between 0 and 10% coal) where the distillate conversion is higher than with no coal. Above 10% coal, the distillate conversion falls with increasing coal concentration. This trend was observed at two pressures, 1,000 and 2,500 psig. As catalyst concentration was increased from 100 ppm Mo to 300 ppm Mo, conversion increased. It appeared that, like in the coal liquefaction system, catalyst concentration could be used to compensate for the effect of pressure reduction.

SUMMARY

The results obtained indicate that the catalytic hydrogenation of two-ring aromatic compounds and several types of multi-ring compounds are suppressed in the presence of coal. It appears that the suppression is the result of a combination of competition and poisoning of specific catalytic sites. This is due to the fact that catalytic hydrogenation of aromatics remains suppressed even after coal is removed from the system.

In the case of tetralin as a donor solvent for coal liquefaction, it seems that that there is insufficient hydrogen donated during the early stages of coal liquefaction to prevent the formation of hydrogen deficient species. This results in lower coal conversion compared to catalytic cases. This may contribute to the consistently lower conversions observed in tetralin tests compared to catalytic tests.

Coal/oil coprocessing may be most effective at lower coal concentrations. The distillate yields are higher at coal concentrations between 0 and 10%. At higher coal concentrations the distillate conversion drops with increasing coal concentration. The potential for reducing pressure in coal/oil coprocessing is enhanced by increasing catalyst concentration. At lower pressures, increasing catalyst concentration increases conversions and distillate yield.

DISCLAIMER

Reference in this manuscript to any specific commercial product or service is to facilitate understanding and does not necessarily imply its endorsement or favoring by the United States Department of Energy.

REFERENCES

1. Cugini, A.V., Rothenberger, K.S., Ciocco, M.V., McCreary, C. In *Coal Science, Proceedings of the Eighth International Conference on Coal Science, Volume II*; Pajares, J.A.; Tascon, J.M.D. Eds.; Coal Science and Technology Series, Volume 24; Elsevier: Amsterdam; 1995; pp 1299-1302.
2. Rothenberger, K.S., Cugini, A.V., Schroeder, K.T., Ciocco, M.V., Veloski, G.A., Am. Chem. Soc., Fuel Chem. Div., Prepr. Pap. **39**(3), 688-694 (1994).
3. Cugini, A.V., Rothenberger, K.S., Ciocco, M.V., Veloski, G.A., Martello, D.M.,, Am. Chem. Soc., Fuel Chem. Div., Prepr. Pap. **39**(3), 695-701 (1994).
4. Suzuki, T., *Energy & Fuels*, **8**(2), pp. 341-347 (1994).
5. Ikenaga, N., Kobayashi, Y., Saeki, S., Sakota, T., Watanabe, Y., Yamada, H., Suzuki, T., *Energy & Fuels*, **8**(2), pp. 947-952 (1994).
6. Schroeder, K.T., Bockrath, B., Miller, R., Davis, H., AIChE Summer Meeting, 1991.
7. Cugini, A.V., Lett, R.G., and Wender, I., *Energy & Fuels*, **3**(2), pp. 120-126 (1989).
8. Cugini, A.V., Krastman, D., Lett, R.G., and Balsone, V.D., *Catalysis Today*, **19**, pp. 395-408 (1994).
9. Stephens, H.P. and Kottenstette, R.J., Am. Chem. Soc., Fuel Chem. Div., Prepr. Pap. **30**(2), 345-353 (1985).

Figure 1

Effect of AO-60 Exposure to Coal on Pyrene Hydrogenation

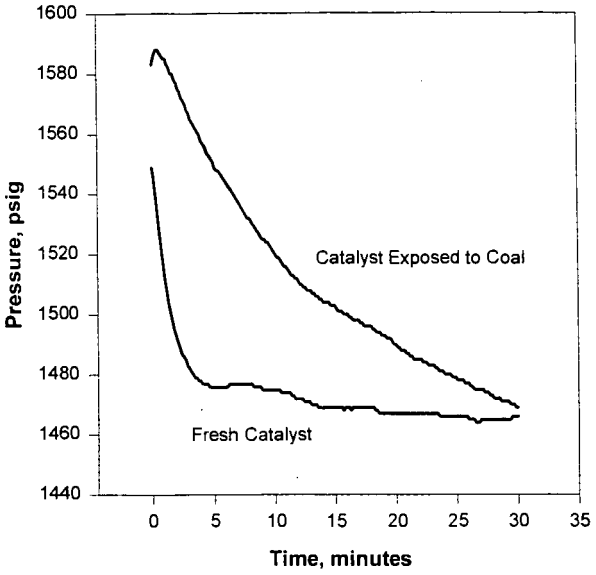

Microautoclave 425°C, 30 minutes, and 1000 psig H_2 (cold)

Figure 2

Effect of Coal Concentration and Pressure in Coprocessing

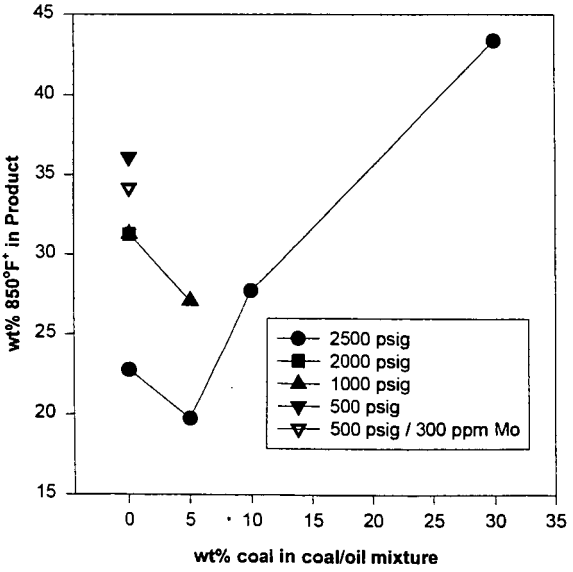

Semi-Batch 1-L Autoclave 425°C, 1 h, 100 ppm Mo (added as AHM), 2:1 Hondo Resid to Illinois No. 6 Coal

EFFECT OF SOLVENT CHARACTERISTICS ON COAL LIQUEFACTION

He Huang, Shaojie Wang, Keyu Wang, Michael T. Klein and William H. Calkins*
Department of Chemical Engineering
University of Delaware, Newark, Delaware 19716

Key words: liquefaction solvent, hydrogen donor, solubility parameter

Introduction

It has been known for a long time that the characteristics of the liquefaction solvent has a profound effect on direct coal liquefaction. The amount of hydrogen consumed during the liquefaction process, the degree and quantity of retrograde reactions that occur, and the quality of the liquid products are all influenced by the process solvent (1). A number of analytical approaches have been developed to determine the important characteristics of the solvent for coal liquefaction (1). The hydrogen donor ability has clearly been important (2). However, such other characteristics of a liquefaction solvent as solubility parameter (1), content and type of higher aromatic hydrocarbons (3), and phenolic content have also been found to be significant (1). Finseth et al. (4) have shown that the bulk of the hydrogen consumed from an uncatalyzed donor solvent liquefaction above 400 °C is consumed in gas generation, heteroatom removal and hydrogenolysis of the coal matrix. Wilson et al. (5) have also shown that the major role of hydrogen in uncatalyzed liquefaction is consumed by alkyl fission and hydrogenolysis reactions and not with hydrogenating aromatic rings. McMillan et al. (6) have postulated that a radical hydrogen transfer process along with donor solvent capping of thermally produced radicals from the coal as possible processes involved with the hydroaromatic donor solvents in coal liquefaction.

With the development of a short contact time batch reactor (SCTBR) (7), determining the influence of the processing solvent on the liquefaction rates, conversion profiles and the quality of the liquid product at a particular time became possible. The influence of type of solvent, combined with other effects, such as gas atmosphere (i.e., in hydrogen and in nitrogen) and catalyst, on the coal liquefaction is reported in this paper.

Experimental

Apparatus. A Short-Contact-Time Batch Reactor (SCTBR) was devised to carry out the coal liquefaction. It allows the heat up of the process stream to reaction temperature in about 0.3 seconds. The removal and quenching of the reaction products occurs in a similar time period. The design and operation of such a SCTBR reactor system have been described in detail elsewhere (7,8).

Solvents Used. Four solvents: 1,2,3,4-tetrahydroquinoline (98%), tetralin (99%), 1-methylnaphthalene (98%), and decahydronaphthalene (99+%) from Aldrich with different hydrogen donor abilities and solubility parameters have been used in the coal liquefaction experiments.

Catalyst Used. Molybdenum naphthenate (6.8 wt% molybdenum from Shepherd Chemical Co.) was the liquefaction catalyst used in this study. The catalyst was prepared by dissolving about 0.5 g molybdenum naphthenate (equivalent to about 0.9 wt% Mo based on the amount of the coal charged) in the processing solvent. The catalyst was then sulfided by reacting the solution with about 1 g of methyl disulfide during the transport into the reactor and liquefaction.

Coal Liquefaction. Illinois #6 bituminous and Wyodak-Anderson subbituminous coals from the Argonne Premium Coal Sample program were used in this study. Proximate and elemental analyses, together with other analytical data, of these coals are available in the User's Handbook for the Argonne Premium Coal Sample program (9). All liquefactions were run as mixtures of processing solvent (S) and coal (C) at a mass ratio of S/C ≈ 8 to minimize the effect of changing processing solvent concentration during the reaction. About 4 grams of coal were used for each reactor run, together with the added processing solvent to make up the reactant slurry.

Workup Procedures of Reaction Products. After a liquefaction run, the product mixture was filtered and the solid residue washed with cold fresh tetralin thoroughly and dried in a vacuum oven with a nitrogen purge at about 105 °C for 48 hours. The filter cake was then rinsed with methylene chloride and dried in a vacuum oven with a nitrogen purge at 105°C for 12 hours. The solid residue and the liquid filtrate were analyzed separately (10). The mineral matter of the coal was shown to accumulate in the coal residue and not in the coal liquids. Therefore, ash in the residue determined by thermogravimetric analysis was used to calculate the conversion (10).

Results and Discussion

Coal Liquefaction Processes. The conversions of Illinois #6 liquefaction in tetralin

without added catalyst under 1000 psig nitrogen at four temperatures (358 °C, 390 °C, 408 °C and 422 °C) for short reaction times (10 s to 10 min) are shown in Figure 1. Three distinct phases in the process were observed: a very rapid conversion followed by an induction period and then a slower liquefaction of the coal structure. The initial rapid conversion in the first 30 to 60 s is due to the extraction of a soluble fraction of the coal into the hot tetralin. The slow conversion after 1 or 2 min is caused by the chemical breakdown of the coal structure to liquid products. The induction period observed is actually a transition interval which is due to the simultaneous occurrence of two processes: a very rapid extraction and a relatively slower liquefaction of the coal structure itself. The amount of extraction increases as the liquefaction temperature increases. The equilibrium extraction of the Illinois #6 coal at 358 °C, 390 °C, 408 °C and 422 °C were about 18.4 wt%, 22.0 wt%, 31.9, and 39.8 wt%, respectively. Similar behavior was also observed in Wyodak-Anderson subbituminous coal liquefaction. The equilibrium extraction of the Wyodak-Anderson coal in tetralin at 390 °C under 1000 psig nitrogen is about 14.1 wt%.

From these observations, a hypothesis of two processes of coal liquefaction was postulated (10). Based on this hypothesis, Wang et al. (11) have developed a model to evaluate the kinetic parameters for each stage. They have reported that the extraction stage is about two orders of magnitude faster than the structure breakdown stages and have correspondingly lower activation energies. The liquefaction of the coal structure itself also consists of multiple steps of different rate constants and activation energies. The rate constant of the extraction stage and the equilibrium extraction fraction are dependent on the solvent characteristics and coal structures as well as liquefaction conditions.

It is important to point out that the coal liquefaction kinetic studies reported in the literature are largely based on liquefaction to high conversions (2,12,13). Therefore, the kinetic measurements are actually combinations of the rapid extraction with the much slower liquefaction of the coal structure.

Effect of Gas Atmosphere on the Coal Liquefaction. Conversions of the liquefaction of Illinois #6 and Wyodak-Anderson coals in tetralin at 390 °C for 30 min under 1000 psig N_2 or 1000 psig H_2 is shown in Figure 2. For the Illinois #6 coal, the liquefaction conversion in hydrogen was higher than in nitrogen. However, there was no difference for the Wyodak-Anderson coal liquefied in hydrogen or in nitrogen. The contents of pyritic sulfur in Illinois #6 and Wyodak-Anderson are 2.81 wt% and 0.17 wt%, respectively. This is a strong indication that pyrite in the Illinois #6 provides some catalysis for the liquefaction in the presence of hydrogen.

Catalysis of Molybdenum Naphthenate. Conversion of the Illinois #6 coal with molybdenum naphthenate (equivalent to 0.9 wt% Mo) was studied in an effort to understand the role of a hydrogenation catalyst relative to the liquefaction solvent in coal liquefaction. Figure 3 summarizes the results of a series of experiments aimed at determining the active species when the molybdenum naphthenate is the added catalyst. The sulfiding agent used was methyl disulfide. Comparison of the conversions in different liquefaction conditions shown in Figure 3 indicates that: 1). sulfided molybdenum naphthenate in the absence of hydrogen is not active; 2). the sulfiding agent itself plays no direct role in coal liquefaction; and 3). only sulfided molybdenum naphthenate (presumable as Mo_2S_3 or MoS_2) in the presence of hydrogen is the active catalyst for coal liquefaction.

Effects of Solvent, Catalyst, and Gas Atmosphere on the Coal Liquefaction. Conversion vs. time curves of the thermal (without added catalyst) liquefaction of Illinois #6 coal in 1,2,3,4-tetrahydroquinoline (THQ), tetralin, and 1-methylnaphthalene, in decreasing order of hydrogen-donor ability, run under 1000 psig nitrogen at 408 °C are shown in Figures 4a and 4b for two different time intervals. The liquefaction conversions using 1-methylnaphthalene as a processing solvent shows distinct stages of liquefaction kinetics: a very rapid extraction and followed by an extremely slow liquefaction of the coal structure. The equilibrium extraction of the Illinois #6 coal using 1-methylnaphthalene was 30.7 wt%. This value is very close to that using tetralin as a processing solvent. The solubility parameters of 1-methylnaphthalene and tetralin are 20.3 and 19.4, respectively. This suggests that the extraction stage in the coal liquefaction is dominated by the solubility characteristics of the processing solvent used. However, the rates of coal structure breakdown in tetralin and in 1-methylnaphthalene were 0.0458 wt%/min and 0.00168 wt%/min, about 27 times difference. For the very strong hydrogen donor solvent of 1,2,3,4-tetrahydroquinoline, the extraction stage becomes indistinguishable from the liquefaction of the coal structure. This is because the rate of coal structure breakdown in the very strong hydrogen donor solvent is close to the rate of extraction. The rate of coal structure breakdown measured in this solvent was 1.41 wt%/min. Comparison of the rates of the coal structure breakdown in 1,2,3,4-tetrahydroquinoline, tetralin, and 1-methylnaphthalene suggests that hydrogen transfer from the solvent is the rate-determining step in uncatalyzed coal liquefaction. This is consistent with the observations that the activation energies for coal structure breakdown is much less than carbon-carbon bond strength (2,11-13).

Effects of solvent on the thermal liquefaction of the Illinois #6 coal in nitrogen and in

hydrogen are illustrated in Figure 5. These data show that the very strong hydrogen donor solvent, such as 1,2,3,4-tetrahydroquinoline, gives much higher conversion than tetralin. More interestingly, the liquefaction conversion in this very strong donor solvent shows no sensitivity to gas atmosphere (i.e., in nitrogen or in hydrogen), indicating little if any hydrogen is derived from the molecular hydrogen in the case of a very strong hydrogen donor solvent used. On the other hand, the liquefaction in the poor hydrogen donor solvents, such as decahydronaphthalene and 1-methylnaphthalene, shows much lower conversion than in tetralin under nitrogen pressure. However, for these very poor hydrogen donor solvents, the liquefaction conversions of the Illinois #6 coal in hydrogen is much higher than that in nitrogen, showing strong sensitivity to gas atmosphere. These results suggest that, in a poor hydrogen donor solvent, the hydrogen needed in the liquefaction process must be mostly derived from molecular hydrogen when a hydrogenation catalyst is present in the parent coal (for example, the pyrite in the Illinois #6 coal) and/or is added (such as sulfided molybdenum naphthenate).

Effect of molybdenum naphthenate catalyst in different solvents on the Illinois #6 coal liquefaction is shown in Figure 6. Liquefaction conversions are always higher in tetralin than in 1-methylnaphthalene for both of the thermal and catalyzed liquefactions. However, with the added catalyst, the conversions in tetralin increased only by a factor of 53%, 31%, and 29% for 30 min liquefaction at 390 °C, 403 °C, and 420 °C, respectively, compared to those in 1-methylnaphthalene by a factor of 123% and 97% for 10 min at 397 °C and 30 min at 410 °C, respectively. These results indicate that the catalysis by an added hydrogenation catalyst in coal liquefaction is more responsive when a poor hydrogen donor solvent is used. It also suggested that a hydrogenation catalyst could be used to compensate for the lack of hydrogen donor ability of a processing solvent.

To quantitatively evaluate the effects of solvent, catalyst, and gas atmosphere for the coal liquefaction, specific liquefaction conversion ratios of α, β, and γ are defined using the coal liquefaction conversion in nitrogen as a reference, i.e.,

$$\alpha = \frac{X_{H_2}}{X_{N_2}}$$

$$\beta = \frac{X_{catalyst}}{X_{N_2}} \qquad (1)$$

$$\gamma = \frac{X_{catalyst}}{X_{H_2}}$$

where X_{N2} is the liquefaction conversion in nitrogen; X_{H2} is the liquefaction conversion in hydrogen; and $X_{catalyst}$ is the catalyzed liquefaction conversion in hydrogen. The α is selected to evaluate the hydrogen gas effect. The larger the α, the stronger the hydrogen gas effect. When $\alpha = 1$, it means there is no hydrogen gas effect in the coal liquefaction. The β is calculated to evaluate the catalyst reactivity and the γ is used to evaluate the net reactivity of the added catalyst. The data to show the combination of the effects of solvent, catalyst, and gas atmosphere on the Illinois #6 and Wyodak-Anderson coal liquefactions, together with the calculated specific ratios of α, β, and γ, are summarized in Table 1. Based on the α values, the order of the hydrogen gas effect on the Illinois #6 coal liquefaction for different solvents was decahydronaphthalene ~ 1-methylnaphthalene > tetralin > 1,2,3,4-tetrahydroquinoline. The stronger the hydrogen donor solvent, the less will be the hydrogen gas effect. In fact, there is no hydrogen gas effect on the Illinois #6 coal liquefaction for the very strong donor solvent of 1,2,3,4-tetrahydroquinoline for which $\alpha = 1$. The Wyodak-Anderson coal shows no hydrogen gas effect ($\alpha = 1$) during the liquefaction in tetralin. Based on the β values, the order of the catalyst influence on coal liquefaction in different hydrogen donor solvents was 1-methylnaphthalene > tetralin. Furthermore, the higher the liquefaction temperature, the lower the catalyst influence on liquefaction conversion. This may be because, as temperature increases, the selectivity to liquid products during the liquefaction decreases. This is also supported by the γ values for the liquefaction of the Illinois #6 in 1-methylnaphthalene.

Summary and Conclusions

The extraction stage in the coal liquefaction is dominated by the solubility characteristics of the processing solvent. The liquefaction of Illinois #6 using 1-methylnaphthalene shows distinct stages of liquefaction kinetics similar to tetralin. However, compared to tetralin, it has an extremely slow breakdown rate of the coal structure. The equilibrium extraction for 1-methylnaphthalene was 30.7 wt% at 408 °C, which is very close to that (31.9 wt%) in tetralin. The extraction and coal structure breakdown stages of the Illinois #6 coal liquefaction in 1,2,3,4-tetrahydroquinoline, however, were indistinguishable.

A hydrogen atmosphere increases the thermal (uncatalyzed) conversion of Illinois #6, but had no effect on Wyodak-Anderson subbituminous coal. This is apparently due to the catalytic

effect of pyrite (or pyrrhotite derived from the pyrite) in the Illinois #6 coal, since this coal contains substantial amounts of pyrite whereas the Wyodak-Anderson coal contains only trace amount of pyrite.

Liquefaction yields and rates of coal structure breakdown are greatly increased by the use of a strong hydrogen donor solvent in which most of the hydrogen is contributed by the solvent rather than molecular hydrogen, suggesting that hydrogen transfer from the solvent is the rate-determining step in uncatalyzed coal liquefaction.

The order of the hydrogen gas effect on the Illinois #6 coal liquefaction for different solvents was decahydronaphthalene ~ 1-methylnaphthalene > tetralin > 1,2,3,4-tetrahydroquinoline. The stronger the hydrogen donor solvent, the less the hydrogen gas effect. When a poor hydrogen donor solvent was used and a hydrogenation catalyst either was present in the coal itself (for example, pyrite in the Illinois #6 coal) or was added (such as sulfided molybdenum naphthenate catalyst), hydrogen is predominantly contributed by molecular hydrogen.

Acknowledgments

The support of this work by the Department of Energy under DE22-93PC93205 is gratefully acknowledged.

References

1. D.D. Whitehurst, T.O. Mitchell and M. Farcasiu in Chapter 9 of *Coal Liquefaction - The Chemistry and Technology of Thermal Processes*, Academic Press (1980).
2. R.C. Neavel *Fuel* **55**, 237 (1976).
3. A. Grint, W.R. Jackson, F.P. Larkins, M.B. Louey, M. Marshall, M.J. Trewhella and I.D. Watkins *Fuel* **73**, 381 (1994).
4. D.H. Finseth, D.L. Cillo, R.F. Sprecher, H.L. Retcofsky and R.G. Lett *Fuel* **64**, 1718 (1985).
5. M.A. Wilson, R.J. Pugmire, A.M. Vassallo, D.M. Grant, P.J.Collin and K.W. Zilm *Ind. Eng. Chem. Prod. Res. Dev.* **21**, 477 (1982).
6. D.F. McMillen, R. Malhotra, S.-J. Chang, W.C. Ogier, S.E. Nigenda and R.H. Fleming *Fuel* **66**, 1611 (1987).
7. H. Huang, W.H. Calkins and M.T. Klein *Energy & Fuels* **8**, 1304 (1994).
8. H. Huang, D.M. Fake, W.H. Calkins and M.T.Klein *Energy & Fuels* **8**, 1310 (1994).
9. K.S. Vorres 'User's Handbook for the Argonne Premium Coal Sample Program' *ANL/PCSP-93/1*.
10. H. Huang, K.-Y. Wang, S.-J., Wang, M.T. Klein and W.H. Calkins *Energy & Fuels* in press (1996).
11. S.-J. Wang, K.-Y. Wang, H. Huang, M.T. Klein and W.H. Calkins see preprints of this symposium.
12. G.P. Curran, R.T. Struck, and E. Gorin *I&EC Prod. Des. & Dev.* **6**, 155 (1967).
13. W.H. Wiser *Fuel* **47**, 475 (1968).

Table 1 Effect of solvent on the thermal and catalytic liquefactions of the Illinois #6 and Wyodak-Anderson coals in 1000 psig N2 or H2

Sample	Coal	Solvent	T C	t min	Gas	Catalyst [Note 1]	X wt% [Note 2]	α	β	γ
DOE00	Illinois #6	Tetralin	390	30	N2	No	42.6	1.09	1.53	1.41
DOE07	Illinois #6	Tetralin	390	30	H2	No	46.3			
DOE14	Illinois #6	Tetralin	392	30	H2	Yes	65.3			
DOE09	Illinois #6	Tetralin	404	30	N2	No	54.4	N.A.	1.31	N.A.
DOE16	Illinois #6	Tetralin	402	30	H2	Yes	71.2			
DOE10	Illinois #6	Tetralin	422	30	N2	No	59.9	N.A.	1.29	N.A.
DOE17	Illinois #6	Tetralin	418	30	H2	Yes	77.1			
DOE14	Illinois #6	1-methylnaphthalene	398	10	N2	No	24.7	1.41	2.23	1.58
DOE15	Illinois #6	1-methylnaphthalene	396	10	H2	No	34.9			
DOE15	Illinois #6	1-methylnaphthalene	395	10	H2	Yes	55.1			
DOE18	Illinois #6	1-methylnaphthalene	409	30	N2	No	33.7	1.63	1.97	1.20
DOE18	Illinois #6	1-methylnaphthalene	412	30	H2	No	55.1			
DOE18	Illinois #6	1-methylnaphthalene	412	30	H2	Yes	66.4			
DOE18	Illinois #6	THQ [Note 3]	412	30	N2	No	85.6	1.00	N.A.	N.A.
DOE18	Illinois #6	THQ	415	30	H2	No	85.5			
DOE23	Illinois #6	Decahydronaphthalene	400	30	N2	No	22.2	1.49	N.A.	N.A.
DOE23	Illinois #6	Decahydronaphthalene	400	30	H2	No	33.0			
DOE08	Wyodak-Anderson	Tetralin	392	30	N2	No	39.6	1.01	N.A.	N.A.
DOE08	Wyodak-Anderson	Tetralin	390	30	H2	No	39.8			

Notes:

1. Catalyst: Molybdenum naphthenate (equivalent to 0.9 wt% Mo) sulfided in-situ by methyl disulfide.
2. X: Liquefaction conversion on the daf (dry-ash-free) basis.
3. THQ: 1,2,3,4 - Tetrahydroquinoline

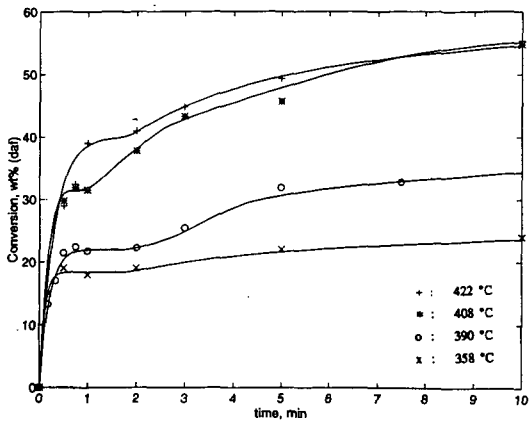

Figure 1 Conversion vs time for Illinois #6 coal liquefaction without added catalyst in tetralin (tetralin:coal = 8:1 mass ratio) under 1000 psig N_2 (for short contact times up to 10 min)

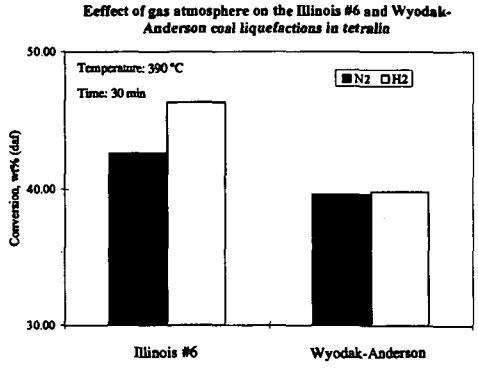

Figure 2

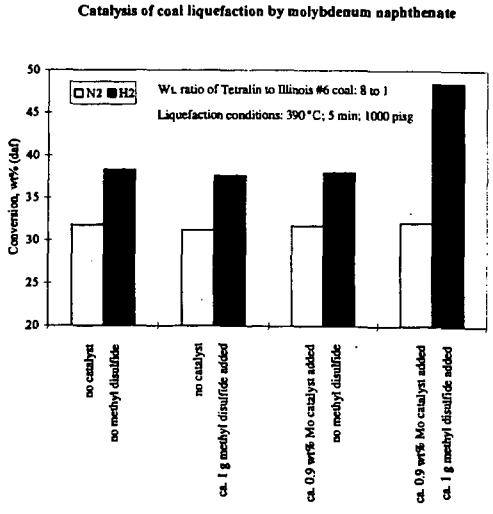

Figure 3

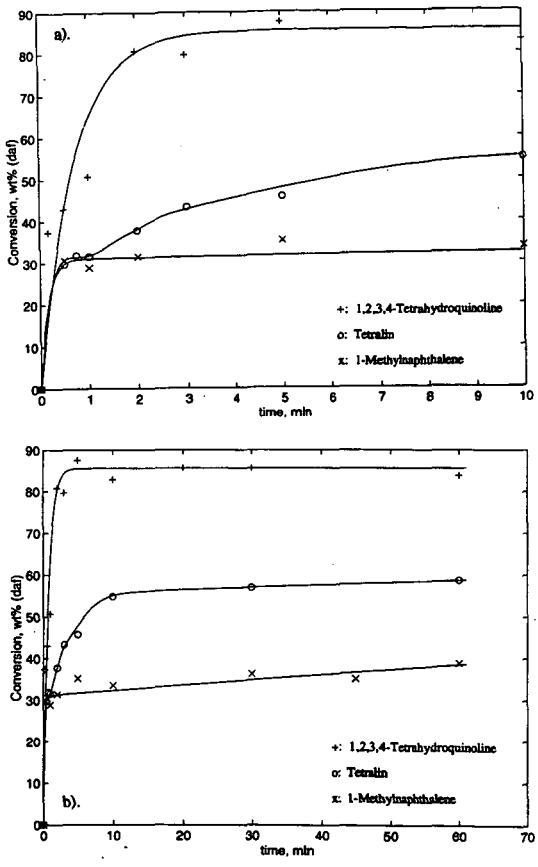

Figure 4 Conversion vs. time curves of the thermal liquefaction of Illinois #6 coal in 1,2,3,4-tetrahydroquinoline (THQ), tetralin, and 1-methylnaphthalene under 1000 psig nitrogen at 408 °C (Solvent:Coal = 8:1): a). for short contact times; b). for up to 60 min

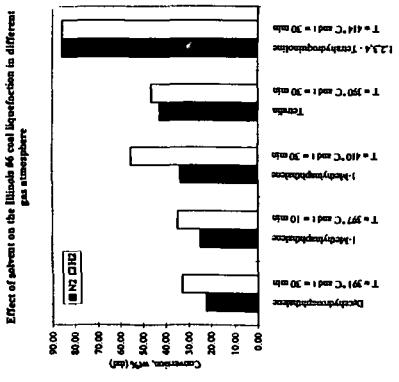

Figure 5

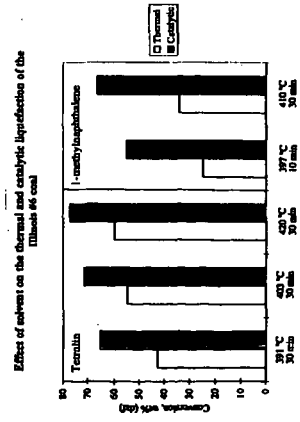

Figure 6

CONTRIBUTION OF MINERAL MATTER TO LOW TEMPERATURE LIQUEFACTION MECHANISMS.

Shona C. Martin, Harold H. Schobert

Fuel Science Program, The Pennsylvania State University, University Park, PA 16802

Keywords: Low rank coals, mineral matter, low temperature liquefaction.

Introduction

The pathways by which coal macromolecules can be depolymerised to give lighter products have long been sought by coal scientists and the precise roles of individual functional groups in the reactions which occur during liquefaction are still not clear. Generally, radical reactions for hydrogen incorporation are dominant at temperatures ≥ 350 °C. However, reactions of coals are not necessarily limited to free radical processes. Recently, the existence of non-radical pathways has been proposed, upon the observation of a higher gas-phase H_2 consumption observed in comparative non-catalytic runs with raw and dried low rank coals at 350 °C [1]. However, the preliminary data largely ruled out the possibility that, under the conditions employed, there was non-radical incorporation of molecular H_2 into coal. It was therefore proposed that the reaction of H_2 may be mineral matter catalysed.

To date, the exact role of much of the mineral matter in coals remains unclear [2-4]. These mineral and inorganic species can act as catalysts or poisons during liquefaction depending on reaction conditions. The physical role of minerals could be to block access to pores or reaction sites. Conversely, the chemical roles of inorganics include: clays which can act as cracking catalysts and the hydrogenation catalyst, pyrite. Catalytic activity, mainly attributed to pyrite, is well documented [2, 5]. Conversely, removal of naturally occurring anions such as Na^+, Ca^{2+} and K^+ has been shown to enhance liquefaction conversions [4,6] and several authors have observed a favorable influence of demineralization on coal depolymerization. Shams et al. [7] reported that the treatment of coals with methanol and HCL removes virtually all of the calcium species, leading to retardation of the retrogressive reactions Ca was proposed to catalyse.

The aim of the work reported here was to evaluate the nature and distribution of coal mineral matter in both untreated and treated (demineralized) samples of Wyodak coal, and consider the influence of these compounds by assessing their possible catalytic effect. To date, a series of experiments has been undertaken to compare the effect of demineralization on coal conversion at low temperatures (*ca* 300-350 °C), where preliminary results indicated that conversions were comparable upon pretreatment.

Experimental

Demineralization Wyodak coal (DECS-8) , ≤60 mesh, was obtained from the Penn State Coal Sample Bank; proximate and ultimate analyses are listed in Table 1[8]. Demineralisation was facilitated by successive acid treatments. The first stage was an HCl wash (10 ml per gram of coal) to remove any alkaline earths which would form insoluble fluorides at the HF wash stage. This was stirred at 60 °C for 1 hour, filtered and washed. In the second stage, a 40% HF solution (10 ml per gram of coal) was digested at 60 °C for 1 hour. The final sample was thoroughly washed with distilled water to ensure removal of residual HF. The filtrate was tested with $AgNO_3$ to indicate the presence of any residual chloride ions.

ICP-AAS Both the untreated and demineralised samples were analysed by ICP-AAS to more clearly identify the mineralogical distribution changes upon acid treatments. Samples were ashed at 950 °C and the ash dissolved using a lithium metaborate fusion technique. Solutions were then analysed using a Leeman Labs PS3000UV inductively coupled plasma spectrophotometer (ICP).

Liquefaction The demineralised coal samples were dried in a vacuum oven at 110 °C for 2 hours prior to use. Liquefaction was carried out in a 25 ml tubing bomb with *ca* 4g coal, at 300 and 350 °C, 1000 psi H_2 or N_2 for 30 min. When solvent was present, the coal:solvent ratio was 1:1 w/w; both H-donor (tetralin) and non-donor solvents (1-methyl naphthalene) were utilised. The gaseous products were collected and analyzed by GC; the liquid and solid products were recovered and separated by sequential Soxhlet extraction into *n*-hexane solubles (oils), toluene solubles (asphaltenes) and THF solubles (preasphaltenes). The THF-insoluble residue was washed with acetone followed by *n*-pentane to remove any residual THF. All recovered products were finally dried under vacuum at 110 °C for *ca* 10 hours. The conversion of coal into soluble products and gases was calculated on the basis of recovered THF-insoluble residue and reported on a dmmf basis. Residues were further analysed by FTIR and ^{13}C NMR.

FTIR Fourier transform infrared (FTIR) spectra of the demineralised coal and liquefaction residues were recorded on a Digilab FTS-60 spectrometer by co-adding 400 scans at a resolution of 2 cm^{-1}. The samples were prepared as KBr discs; predried sample (3 mg) was mixed with KBr (300 mg). All spectra were baseline corrected.

^{13}C NMR Solid state ^{13}C NMR spectra were recorded on a Chemagnetics M-100 NMR spectrometer using the cross polarization magic angle spinning (CP-MAS) technique. The measurements were carried out at a carbon frequency of 25.1 MHz.

Results and Discussion

ICP-AAS

As summarised in Table 2, metal concentration was determined by ICP-AAS in the normal and demineralised Wyodak coal samples. Ash was determined as 8.94 wt%. Upon demineralisation, ash concentration fell to *ca* 0.37 wt%, with the corresponding metal concentrations as indicated. All values are expressed in weight percent on an ash basis with the exception of HTA, which is on an as-received basis.

Liquefaction Data

Results for the reactions conducted at 350 °C, both in the presence and absence of solvent, are reported in Table 3. For purposes of initial comparison, these will be discussed with respect to data with untreated Wyodak coal [1]. It is clearly demonstrated that demineralization imparts no seriously detrimental effects on liquefaction under such conditions.

The overall conversions and liquid product distribution indicates that the most significant changes occur in the presence of solvent, both H-donor and non-donor. In the absence of solvent, conversion can be considered to be solely due to pyrolysis, i.e. there are no solvent dissolution or H donation contributions. Higher conversion is the result of increased gas yield rather than liquid yield and quality. This may be derived from two contributions. If the reduction in Fe concentration, as highlighted by ICP, also comprises pyrite, this would account for the decrease in liquid yield. Moreover, if the increased gas make is due to CO_2, removal of the mineral matter may be considered to promote more facile pyrolysis of -COOH versus -COO$^-$M$^+$.

Reaction in the presence of the non-donor solvent, 1-methyl naphthalene, results in increases in both gas and liquid yield relative to the no-solvent situation. With "normal" coal and 1-MN, the increase in liquid yield for the raw coal is 5.1%. Presumably this increase is the "extra" liquid dissolved out by the solvent. With demineralised coal and 1-MN, the increased liquid yield is 12.4%. Therefore, the solvent is undoubtedly better able to dissolve material from the demineralised coal. This suggests that there is improved access of the solvent to the coal interior upon removal of mineral species.

The best liquid conversion, defined by oil concentration as a fraction of the total liquid yield, occurs upon reaction with tetralin. This is not surprising because tetralin is an H donor, thus any enhancement in tetralin conversion relative to 1-MN can be attributed to H donation. The increase in liquid yield for normal coal in tetralin, relative to 1-MN, is 7.4%; the increase for demineralised coal is 8.6%. The difference in these numbers is within experimental error, ±3%, hence demineralisation has no effect on H transfer from tetralin and there is no mineral matter catalysis of H donation.

Table 4 summarises the results of liquefaction conducted under an inert N_2 atmosphere and those facilitated in H_2. No significant deviation in overall conversion or product distribution was observed, even in the presence of solvent.

There are similarities between the results presented here and those of other studies, not necessarily limited to demineralised samples. Tomic and Schobert [9] also observed solvent effects under mild liquefaction conditions of subbituminous coals; the addition of a solvent was observed to enhance conversion relative to the reaction with no solvent, similar to the results in Table 3. And if, indeed, pyrite concentration has been reduced, the results in Table 4 confirm those reported by Tomic and Schobert [9], Artok [10] and Huang [11] who similarly reported that utilization of H_2(g) is ineffective without a good hydrogenation catalyst, as illustrated by the similarities in the comparitive H_2 and N_2 runs. Serio et al. [4], also reported enhanced conversion for low rank coals following demineralization. This raises questions as to possible contribution of mineral species to low temperature liquefaction mechanisms. Joseph [6] ascribed this phenomenon to cations inhibiting hydrogen transfer from donor solvent/gaseous hydrogen to free radicals, in effect promoting retrogressive reactions. Therefore, it could be that the absence of these species allows for better access to reactive sites in the coal interior.

FTIR Comparative FTIR spectra of the normal and demineralised coal and associated residues are shown in Figures 1 and 2. The spectrum of the whole demineralised coal indicates the presence of most of the groups of interest in this study.

Hydroxyl groups at	3300-3600 cm^{-1}
Aromatics	3030 cm^{-1} and associated bands at 1450-1600 cm^{-1}
Aliphatics	2920, 2850 cm^{-1}
Carboxylic acids	1710-1760 cm-1
Conjugated Ketones	1715 cm-1
Esters	1712-1735 cm^{-1} (present as a shoulder on the C=O band)

After reaction under H_2 at 350 °C, the most notable feature of the whole product spectrum is a decrease in hydroxyl concentration, in part attributed to a loss of H_2O. Further examination of the THF-insoluble residue from this experiment confirms the loss of OH functionality coupled with the disappearance of the ester shoulder. The FTIR spectrum of the THF-insoluble residue from the reaction conducted with tetralin displays somewhat contrasting features. The carboxyl stretching region is much broader; moreover, the ester shoulder is more pronounced and the carbonyl region is much more defined.

The FTIR spectra of the THF-extracted raw coal and the residues from the runs conducted at 350 °C under N_2 demonstrated that under all conditions, i.e. both in the presence and absence of solvent, no marked changes were observed. The residue from these sets of experiments is currently undergoing further analysis by Py-GC-MS, to evaluate in more detail the fundamental differences in speciation resulting from non-catalytic treatment under different regimes.

Solid State ^{13}C NMR The ^{13}C CP-MAS spectra of the normal and demineralised coal is shown in Figure 3. The ^{13}C CP-MAS spectrum of the demineralised Wyodak displays many similarities to that of the untreated coal. The region between 0 and 80 ppm consists primarily of aliphatic carbons, e.g. methoxy groups and the symmetry of this band should be noted. The second region of interest between 90 and 170 ppm is due to the presence of aromatic carbon. The shoulders present on the side of the aromatic band may be attributed to specific functionalities, e.g. catechol groups (at 142 ppm) and phenolic groups (at 152 ppm). The carboxylic functionality is prominent at 180 ppm, similarly for the carbonyl at *ca* 210 ppm. In the aliphatic band, the symmetry observed for the parent coal is lost, and the appearance of a shoulder at ~25 ppm is observed. This may be attributed to a number of groups, including CH_3-Ar side chains (20-21 ppm). Furthermore, the distinct shoulders observed in the aromatic region have virtually disappeared, indicating a loss of oxygen functionalities.

Conclusions

As anticipated, relative to runs at 350 °C with untreated coal, demineralisation affords higher overall conversions; this trend becomes more apparent when either an H-donor (tetralin) or non-donor (1-mn) solvent are used. Specifically, there is no evident mineral matter effect on solvent H donation. Thus, initial results between the two sets of data suggests that the reactions undergone at 350 °C are not mineral matter catalyzed.

With respect to mineral matter identification, further ICP-AAS studies have been conducted, in association with CC-SEM and XRD determinations to identify the mineral phases and species contributing to possible low temperature hydrogenation mechanisms.

References

1. C. Song, A.K. Saini, H.H. Schobert Energy and Fuels **8**, 301 (1994)
2. Maldonado-Hodar, F.J., Rivera-Utrilla, J., Mastral-Lamarca, A.M., Ferro-Garcia, M.A. Fuel **74**(6), 818 (1995) and references therein.
3. Mochida, I., Yufu, A., Sakanishi, K., Korai, Y. Fual **67**, 114 (1988)
4. Serio, M.A., Solomon, P.R., Kroo, E., Bassilakis, R., Malhotra, R., McMillen, D. Am. Chem. Soc., Div, Fuel Chem., Prep. **35**(1), 61 (1990)
5. Garcia, A.B., Schobert, H.H. Fuel **68**, 1613 (1989) and references therein.
6. Joseph, J.T., Forrai, T.R. Fuel **71**, 75 (1992)
7. Shams, K., Miller, R.L., Baldwin, R.M. Fuel **71**, 1015 (1992)
8. Penn State Coal Sample Bank and Database
9. Tomic, J., Schobert, H.H. Energy and Fuels **10** 1996 (in press)
10. Artok, L., Schobert, H.H., Erbatur, O Fuel Proc. Tech. **37**, 221 (1994)
11. Huang, L. PhD. Dissertation Thesis, The Pennsylvania State University, 1995

Table 1. Analysis of Wyodak Subbituminous Coal (DECS-8).

Proximate Analysis (as received)				Ultimate Analysis (wt%, dmmf basis)				
Vol. Matter	Fixed Carbon	Ash	Moisture	C	H	N	S	O
32.4	29.3	9.9	28.4	75.8	5.2	1.0	0.5	17.5

Table 2. Spectrochemical Analysis of Normal and Demineralised Wyodak Coal Samples by ICP-AAS.

Sample	Ash	Metal Concentration (wt%) Fe	Ca	Mg	Na	K
Normal	8.94	5.53	13.2	3.02	1.12	0.78
Demineralised	0.37	56.8	9.23	1.51	0.20	0.24

Table 3. Results of Non-Catalytic Liquefaction of Normal and Demineralised Wyodak Coal at 350 °C for 30 min. Under 6.9 MPa H_2.

Pretreatment	Solvent	Product Distribution (% dmmf basis) Gas	Oil	Asph	Preasph	% Conv.
-	-	3.3	2.1	2.6	4.5	12.5
demineralised	-	10.0	0.8	0.4	5.3	16.6
-	Tetralin	4.2	4.1	7.6	10.0	25.9
demineralised	"	12.0	7.1	6.3	14.4	40.3
-	1-MN	4.0	1.1	5.8	7.4	18.3
demineralised	"	7.7	5.6	3.3	10.3	26.9

Table 4. Results of Non-Catalytic Liquefaction of Demineralised Wyodak Coal at 350 °C for 30 min. Under 6.9 MPa H_2 and N_2.

Gas	Solvent	Product Distribution (% dmmf basis) Gas	Oil	Asph	Preasph	% Conv.
H_2	-	10.0	0.8	0.4	5.3	16.6
N_2	-	10.7	1.2	0.7	5.2	17.8
H_2	Tetralin	12.0	7.1	6.3	14.4	40.3
N_2	"	10.4	10.3	3.6	17.8	42.1
H_2	1-MN	7.7	5.6	3.3	10.3	26.9
N_2	"	8.7	5.8	1.4	8.4	24.4

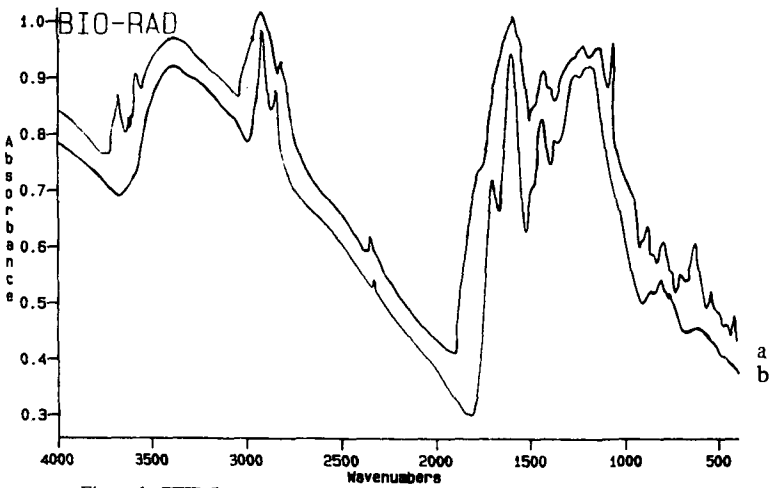

Figure 1. FTIR Spectra of (a) normal and (b) demineralised Wyodak Coal.

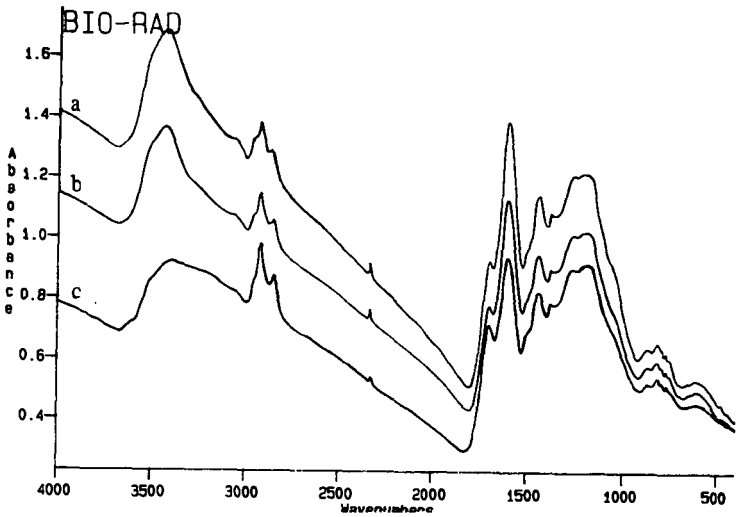

Figure 2. FTIR Spectra of THF-Insoluble Residue from Reaction of Demineralised Wyodak Coal in (a) Absence of Solvent, (b) Presence of Tetralin and (c) Presence of 1-MN.

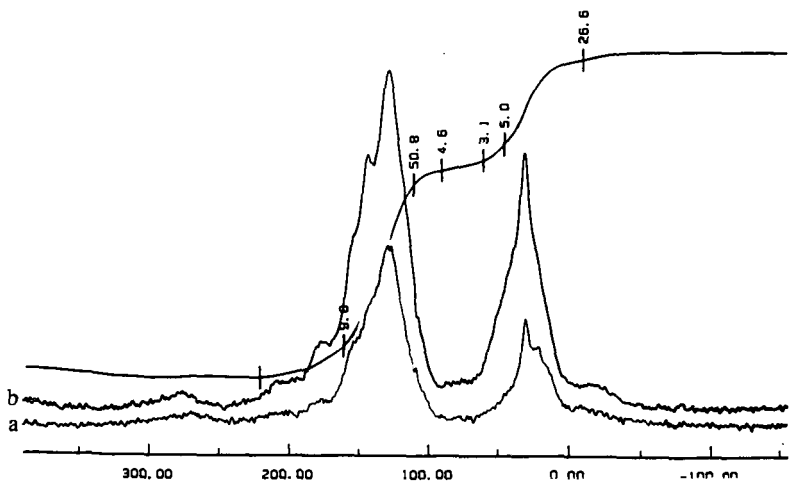

Figure 3. ^{13}C CP-MAS Spectra of (a) Normal and (b) Demineralised Wyodak Coal.

SOLVENT RECYCLABILITY AND HYDROTREATMENT SEVERITY IN DIRECT LIQUEFACTION OF LOW-RANK COAL

Melanie D. Hetland and John R. Rindt
University of North Dakota
Energy & Environmental Research Center
PO Box 9018
Grand Forks, ND 58202-9018
(701) 777-5000

Keywords: Direct liquefaction; solvent recyclability; hydrotreatment severity

INTRODUCTION

A multistep direct liquefaction process specifically aimed at low-rank coals (LRCs) has been developed at the Energy & Environmental Research Center (EERC). The process consists of a preconversion treatment to prepare the coal for solubilization, solubilization of the coal in the solvent, and polishing using a phenolic solvent or solvent blend to complete solubilization of the remaining material. The product of these three steps can then be upgraded during a traditional hydrogenation step.

Research was performed to address two questions necessary for the further development and scaleup of this process: 1) determination of the recyclability of the solvent used during solubilization and 2) determination of the minimum severity required for effective hydrotreatment of the liquid product. The research was performed during two tasks, the first consisting of ten recycle tests and the second consisting of hydrotreatment tests performed at various conditions.

EQUIPMENT

The EERC's time-sampled, batch autoclave system was used during these studies. The system is capable of close-coupled multistage operation. It can be configured to multiple designs with reactor sizes ranging from 1–8 L. Maximum operating conditions are 7500 psig and 510°C. System control and data acquisition are computerized, with the operators and computers located at a control panel separated from the high-pressure, high-temperature system by a steel barricade.

COMPOSITE SOLVENT

Different solvents have proven to be more effective in different steps during the multistep process. It is important that the solvent(s) chosen for the Task 1 testing 1) have the hydrogen donor characteristics needed during the pretreatment and solubilization steps, 2) have the characteristics of the phenolic solvent during the polishing step, and 3) be easily separable from heavier streams for recycling purposes. To meet these criteria, a composite feed solvent was prepared for the recycle tests using equal quantities of phenolic solvent (cresylic acid) and a light fraction of hydrogenated coal-derived anthracene oil (HAO61).

The solvent recycling scheme is summarized in Figure 1. The solubilization solvent initially consisted of equal parts of phenolic solvent and HAO61 light fraction. Heavy fraction HAO61 was added to the product slurry of the polishing step to serve as the vehicle solvent for the hydrotreatment step. The entire mixture was distilled to remove the phenolic solvent, HAO61 light fraction, and light coal-derived liquids (CDLs). The light materials were then recycled to the pretreatment and polishing steps.

SOLVENT RECYCLABILITY TESTS

Ten solvent recyclability tests were performed. In the first test, feed coal and composite solvent were pretreated at 175°C under 1000 psig (cold-charge pressure) CO in the presence of H_2S for 60 min. The pretreated slurry was solubilized at 375°C under 1000 psig (cold-charge pressure) CO and H_2S for 60 min. The product of the solubilization step was polished with additional phenolic solvent under 1000 psig (cold-charge pressure) H_2 for 20 min at 435°C. The polished product slurry was combined with a vehicle solvent and distilled to remove water, solubilization solvent equal to the amount added in the polishing step, and oxygenated light CDLs. If hydrotreatment were part of this task, the bottoms from this distillation would go to the hydrotreatment step. The solubilization solvent was recycled to the pretreatment step for the next test. This scheme was repeated for all ten multistep tests.

Material balances were calculated for all of the processing steps during the solvent recyclability tests. The recoveries for each of the steps were similar. The liquid balance for the pretreatment/solubilization step ranged from 90.4% to 91.7% and from 95.9% to 97.7% for the

polishing step. The overall mass balances for the pretreatment/solubilization step ranged from 96.0% 100.4%, for the polishing step from 98.2% to 99.2%, and for the distillation step from 96.3% to 99.6%. The consistency of the mass balances is indicative of the operational stability of the system. Overall mass balances of at least 96.0% indicate that significant leaks or spills that might have skewed the data did not occur. The data appear to reliably describe the process.

Table 1 shows the distillate yields and solvent balances for each of the solvent recyclability tests. During the original distillation, some of the distillable material from the third test was not collected because of a pressure transducer problem caused by an unexpected power outage. The distillation bottoms were redistilled, and the additional material collected was added to the recycle solvent stream used in the sixth test feed slurry. The table shows that as a result of the lower fraction of light distillate present in the fourth and fifth tests, solvent recovery dropped from approximately 15% excess solvent to about 5% excess solvent. Excess solvent was produced in each of the tests, with an average excess solvent production for all tests of 16.8 wt%. Excluding the low solvent balances for the fourth and fifth tests, the average excess solvent produced was 19.48 wt%.

Detailed analyses were performed to determine the changes in composition of the light solvent as it was recycled during the recyclability tests. Two types of analyses were performed. The first determined the relative aromatic concentration in the recycle solvent, providing an indication of the ability of the solvent to maintain its hydrogen donor characteristics during processing. Fourier transform infrared spectroscopy (FT-IR) was used for this analysis. Table 2 shows that the number of aromatic C-H bonds did not change significantly during the test sequence, indicating that the solvent maintained its hydrogen donor capabilities. The second analysis determined the cresol (or equivalent) concentration in the solvent. The results of this analysis are plotted in Figure 2. As is easily seen from the plot, the cresol concentration appears to be approaching a constant value of approximately 32%-34% wt% of the recycle solvent stream. This concentration agrees with that attained during direct liquefaction research performed in 1983 at the EERC, which indicated that solvent lineout occurred at about 32 wt% phenolics after 40 passes through the system.

Several conclusions can be drawn from the solvent recyclability test results:

- The system is operationally stable. Even when some solvent was not removed for recycle (as in Test 3) or was added back as additional solvent (as in Test 6), little change in product quality was observed.
- Excess solvent was produced for each multistep test.
- Product yield structures were fairly constant for all tests.
- The process produces recycle solvent consisting of approximately 32%-34 wt% cresol (or equivalent).
- The recycle solvent maintains its hydrogen donor capability.

In general, the tests showed that it is possible to produce a consistent, viable recycle solvent stream using the EERC multistep direct liquefaction process.

HYDROTREATMENT SEVERITY TESTS

The purpose of the hydrotreatment severity study was to determine the lowest-severity hydrotreatment conditions that produce high-quality liquid product. A statistical approach to data collection was used so as to predict the lowest-severity conditions in a relatively small number of tests. The results of this type of experimental matrix can be statistically analyzed to develop mathematical equations describing the process. A factorial design consisting of ten tests was employed to test the effects of temperature, pressure, and residence time on product quality. Maximum or minimum conditions of each factor were tested for eight of the tests; tests were performed at temperatures of either 405° or 445°C, at pressures of either 1920 or 3080 psig, and at reaction times of either 34 or 112 min. Two tests were performed at center point conditions (425°C, 2500 psig, and 73 min) to determine lack of fit of the equations. The matrix was randomized to minimize skewing of data that can occur when one variable is held constant for several tests in a row. The liquid product from solvent recyclability Tests 1, 2, 4, and 6 were combined into a single sample to be used as the feedstock for the hydrotreatment severity tests. For each test, composite feed and sulfided Shell 424 catalyst were hydrotreated at experimental matrix-specified conditions.

The analytical and mass balance data from the hydrotreatment severity tests were used to calculate various product quality indicators, including the saturated molar H-to-C ratio of the hydrotreated product; the percent improvement in saturated molar H-to-C ratio of the product over that of the solubilized feed slurry; the distribution of product as pot residue, middle oil, light oil, and cold

trap liquids; the hydrogen consumption of the hydrotreatment step; the yield of hydrocarbon gases from the hydrotreatment step; and the ratio of hydrocarbon gas yield to hydrogen consumption.

The product quality indicators were analyzed using regression analysis. The effect on product quality of each operating parameter or combination of parameters was determined for each indicator by using both backwards elimination and stepwise regression analyses. During a regression analysis, the degree of effect of all independent variables and their combinations on the dependent variable is determined. When the backwards elimination procedure is employed, the independent variable having the least (statistically) significant effect on the dependent variable is dropped. The procedure is repeated until the remaining independent variables are all considered to significantly affect the dependent variable. The stepwise procedure is the reverse of the backwards elimination procedure, in that independent variables are added until one is found not to be statistically significant. The mathematical equation indicated by both regression procedures describes the combined effect of the independent variables on a given dependent variable. Each equation was checked for statistical lack of fit to the data. All of the equations were found to fit the data at a 90% confidence interval.

Spreadsheets were constructed for each product quality indicator by inputting values of the operating parameters over their ranges and calculating the value of a given product quality indicator using the mathematical equation derived during statistical analysis. Nonsignificant operating parameters were held constant at their center point values during these calculations. The calculated product quality indicators were plotted to show what their values would be at various operating conditions that were not actually tested.

The plots showed that a high hydrotreatment temperature (about 440°C) results in the production of hydrocarbon gases at the expense of the production of desirable liquid products, especially when reaction time exceeds 100 min. The plots also showed that an increase in pressure improves total liquid yield.

The various plots were compared to determine the lowest-severity set of conditions that would result in the optimum values for the majority of the product quality indicators. The lowest-severity conditions were determined to be: 405°C temperature, 3000 psig pressure, and 60 min reaction time. A test was performed at these conditions to verify the accuracy of the predictions. The predicted values for each of the product quality indicators are compared with the actual values calculated for the test in Table 3. The data show that the equations predicted the product quality indicator values fairly accurately.

The hydrotreatment temperature at which the verification test was performed was at the lower end of the valid range of the predictive equations. The effect of lowering the temperature below 405°C cannot be determined. Therefore, it is possible that an even lower temperature might effectively hydrotreat the liquid product from the multistep process.

Interpretation of the hydrotreatment severity data led to the following conclusions:

- The mathematical equations derived during statistical analysis of the data effectively predicted the effects of changing the hydrotreatment operating parameters on product quality.
- The composite solvent used during the solvent recyclability test sequence produced solubilized material that could be as effectively hydrotreated as the product of batch tests using optimal solvents for each test.
- Because the production of appropriate distillate material is crucial to a favorable yield structure, it is doubtful that hydrotreatment reaction severity can be reduced by reducing operating pressure. Reductions in hydrotreatment severity must therefore come from reductions in either temperature or reaction time or both.
- Reaction time can probably be reduced to approximately 30 minutes without a substantial reduction in product quality.
- It may be possible to reduce hydrotreatment temperature to less than 400°C while maintaining desired product quality and yield.

It appears that the EERC multistep direct liquefaction process produces a liquid that requires less severe hydrotreatment conditions than are employed during traditional direct liquefaction processing.

ACKNOWLEDGMENT

This research was performed under the U.S. Department of Energy Grant No. DE-FG22-94PC94050.

TABLE 1

Distillate Yields and Solvent Balances for Task 1 Tests

Test No.	Hydrotreatable Solubles, wt% maf[a]		Solvent Yield, wt% maf	Solvent Balance, %
	Liquid Basis[b]	Gas Basis[c]		
1	79.52	87.02	42.01	116.42
2	71.23	86.49	68.17	127.75
3	86.00	86.08	46.27	118.57
4	86.02	85.00	13.67	105.47
5	82.61	83.08	17.12	106.80
6	83.35	79.63	49.53	120.00
7	79.57	83.83	39.52	115.84
8	72.86	79.86	44.88	118.07
9	75.90	79.44	45.03	117.96
10	81.60	81.69	47.20	121.22
Average	79.87	83.21	41.34	116.81

[a] Weight percentage of moisture- and ash-free coal fed to the system.
[b] Yield calculated from liquid stream mass balance data.
[c] Yield calculated by subtracting the gas yield from unity.

TABLE 2

Relative Aromatic Concentrations in Recycle Solvent

Test Number	C-H Absorbance
1	0.35
4	0.34
7	0.36
10	0.35

TABLE 3

Predicted and Actual Product Quality Indicator Values for the Verification Test

Product Quality Indicator	Predicted Value	Actual Value
Saturated Molar H:C	0.3252	0.3306
H:C Improvement, %	48.33	50.82
Pot Residue, wt% of product slurry	10.78	7.72
Middle Oil, wt% of product slurry	80.42	86.16
Light Oil, wt% of product slurry	5.23	1.43
Cold-Trap Liquids, wt% of product slurry	2.91	4.69
Hydrogen Consumption, %	2.97	1.96
Hydrocarbon Gas Yield, %	0.41	0.36
HC Gas Yield:H_2 Consumption	0.1268	0.1822

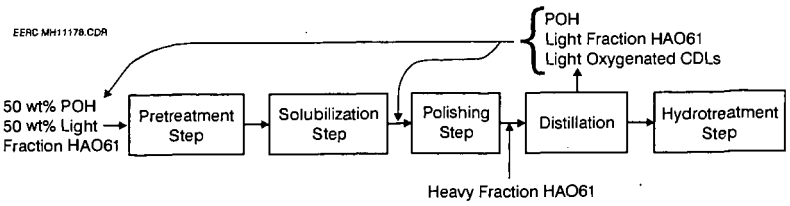

Figure 1. Block diagram summarizing the composite solvent scheme.

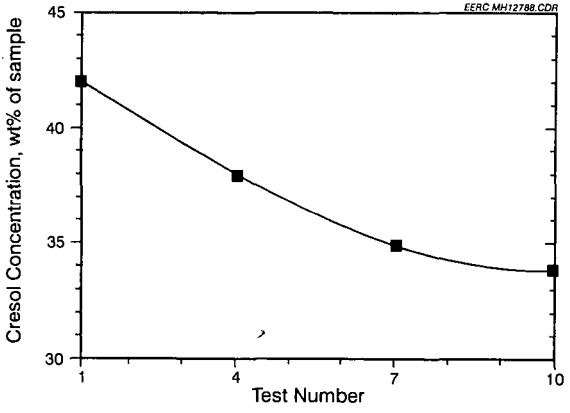

Figure 2. Cresol concentration in recycle solvent as a function of test number.

MDH/djs

EFFECT OF A CATALYST ON THE SOLVENT-FREE LIQUEFACTION OF DECS-17 COAL

R.P. Warzinski, B.C. Bockrath, G.A. Irdi, H.B. Booher, and A.W. Wells
U.S. Department of Energy
Pittsburgh Energy Technology Center
P.O. Box 10940
Pittsburgh, PA 15236.

Keywords: Coal liquefaction, molybdenum sulfide catalysts, reaction mechanism

INTRODUCTION

Dispersed catalysts are important factors in efforts to improve the first stage of direct coal liquefaction processes. Understanding the role of these catalysts is vital to improving their performance. Prior work at the Pittsburgh Energy Technology Center has been devoted to studying the role of a dispersed catalyst, apart from that of added solvent or vehicle, in the first stage of liquefaction (1). In that work, $Mo(CO)_6$ was found to be an excellent precursor for generating dispersed MoS_2-containing catalyst for the solvent-free liquefaction of coal

In the work reported here, solvent-free thermal and catalytic microautoclave experiments with DECS-17 coal were performed at various residence times to investigate the role of the MoS_2-containing catalyst formed from $Mo(CO)_6$ in the initial stages of the liquefaction process. A temperature slightly above that where pronounced catalyst-induced hydrogen uptake was previously observed (375°C) was used in this study. The focus of this paper is on the characterization of the THF-insoluble products. These products were characterized by organic petrology, oxygen speciation analysis, solid-state ^{13}C NMR, and elemental analysis. A more complete account of this work and of similar experiments conducted at 350°C and 400°C is not possible here but will be reported at a later time.

EXPERIMENTAL

All experiments were performed with DECS-17 (Blind Canyon) coal from the Penn State Coal Sample Bank. The elemental analysis (on a dry basis) provided with the coal was as follows: 76.3% carbon, 5.8% hydrogen, 1.3% nitrogen, 0.4% sulfur (0.02% pyritic sulfur), 6.6% ash, and 9.7% oxygen (by difference). The moisture content of the as-received coal was 3.7%. Because this coal contains low levels of pyrite, the influence of native catalyst precursors is minimized.

Microautoclave liquefaction experiments were performed according to previously described procedures in 316-stainless-steel microautoclaves of approximately 46 cm^3 internal volume (1). Separate microautoclaves were used for thermal and catalytic experiments to avoid residual catalytic effects. In the experiments reported here, 6.6 g of coal was used along with a hydrogen/3% hydrogen sulfide gas mixture at 7.2 MPa (1030 psig) cold pressure. In catalytic experiments, $Mo(CO)_6$ was used as the catalyst precursor and was simply added to the microautoclave along with the coal at a level of 1000 ppm Mo based on daf coal. Slow heat-up to a reaction temperature of 375°C and a rapid cool-down were employed. The heat-up time was approximately 55 min. Residence times at temperature of 0, 30, and 60 min were used. All experiments were performed at least in duplicate and the respective products combined to prepare sufficient quantities for subsequent characterization. The products were recovered according to the referenced procedures (1).

Elemental analyses of the liquefaction products were performed at Huffman Laboratories in Golden, Colorado. Extensive characterization of the unreacted coal and the THF-insoluble liquefaction products was performed. This included solid-state ^{13}C NMR spectra, obtained at Western Research Institute in Laramie, Wyoming, following published procedures (2). Oxygen speciation analyses were also performed at PETC. The total hydroxyl contents of the coal and THF-insoluble products were determined by potentiometric titration following reaction with tetrabutylammonium hydroxide. Carboxylic acid contents were determined by exchange with barium ions under nitrogen and in a precisely calibrated buffer solution. The barium was then reacted with standard perchloric acid which was back-titrated to determine the extent of ion exchange. Petrographic analyses were also performed at PETC. The vitrinite reflectance measurements were performed on the vitrinite particles in the raw coal and 0-min residence time samples and on vitroplast (particles derived from heated vitrinite) in the 30-min and 60-min residence time samples according to ASTM procedure D 2798-91.

RESULTS AND DISCUSSION

In prior work with $Mo(CO)_6$ and the DECS-17 coal, the onset of a catalytic effect on hydrogen uptake was detectable at 325°C. The rate of hydrogen uptake due to the catalyst became more pronounced near 370°C (1). In 1-h residence time experiments, the presence of the catalyst promoted conversion of the coal to THF- and cyclohexane-soluble products at temperatures above 325°C and 375°C, respectively. To further define the role of the catalyst, experiments have been conducted at 375°C at residence times of 0, 30, and 60 minutes. This temperature is slightly above that where the pronounced hydrogen uptake caused by the catalyst was observed. To prepare sufficient quantities of material for characterization, twice the usual amount of coal was used. The catalyst loading and initial hydrogen pressure remained the same.

Figure 1 contains the conversion results obtained for the recent experiments with 6.6 g of coal, as well as respective conversions from the previous 1-h experiments at 375°C in which 3.3 g of coal was used. Part A contains the thermal conversions, Part B the catalytic conversions, and Part C the data obtained after subtraction of the thermal conversions from the catalytic data at each residence time. All thermal and catalytic experiments were performed at least in duplicate. The bars on the data in parts A and B represent the range of values obtained and are shown if they are larger than the size of the symbol.

No improvements in the conversions attributable to the catalyst are observed in Figure 1 (part C) after the heat-up to reaction temperature (0 residence time). At the longer times, the catalyst is effective in promoting conversion to THF-soluble products; however, a definite catalytic effect is only observed at the longest reaction time with respect to cyclohexane conversion. With the smaller coal charge, no significant improvement in cyclohexane conversions was noted at 60 minutes. However, at a longer residence time of 8 h (not shown here), a catalytic effect was observed (1). A smaller but significantly lower catalyst-promoted THF conversion was also noted for the liquefaction of the smaller coal charge (part C of Figure 1). This latter observation appears to be due to the lower thermal conversion for the larger coal sample (part A of Figure 1), indicating that in the absence of catalyst, more retrogressive reactions occurred in the larger coal mass. However, with catalyst, the THF conversions were nearly the same for both coal amounts. This highlights the efficacy of the $Mo(CO)_6$ precursor in forming a highly dispersed, active coal liquefaction catalyst.

A procedure has been developed that uses the pressure and temperature data recorded throughout the experiment to monitor the change in gas content of the reactor during solvent-free liquefaction experiments. A description of the procedure used to obtain this representation of the data has been published (1). Figure 2 contains these data for the current 1-h work and for the prior work with 3.3 g of coal. The prior work also showed that the catalyst had little effect on the gases liberated. Therefore, the thermal components, mainly liberation of CO, CO_2, and hydrocarbon gases, have been subtracted from catalytic data to obtain the curves shown in Figure 2 which therefore primarily reflect the hydrogen uptake as a function of time and temperature. The only other major influence on the data in this figure that is unaccounted for is the liberation of water vapor from reactions associated with the catalyst.

Table 1 compares temperatures of the onset of gas uptake, both initial and rapid, and the initial rates of rapid gas uptake obtained from the data in Figure 1.

Table 1. Onset of catalytic activity and rates of gas uptake due to the catalyst for experiments at 375°C with various amounts of DECS-17 coal.

	Amount of Coal	
	3.3 g	**6.6 g**
Onset of Catalyst Activity, °C	345	335
Onset of Rapid Gas Uptake, °C	360	365
Initial Rate of Rapid Gas Uptake, mmol g^{-1}(daf coal) min^{-1}	0.084	0.106

The conversion data and the data in Table 1 show that doubling the loading of the coal had little effect on reactivity. The total pressure in the microautoclave upon reaching reaction temperature with 6.6 g coal charged was about 11.9 MPa (1710 psig) and the total reduction in pressure after

1 h was 1.2 MPa (170 psi). Thus, a pseudo first-order condition with a nearly constant hydrogen partial pressure was maintained even in the case of greatest hydrogen demand.

The change in the slope of the curves shown in Figure 2 during the reaction at 375°C suggests that two major catalytic events are occurring during the course of the liquefaction reaction. This is most evident in the data for the reaction using 6.6 g of coal. Near the end of the heat-up period and for about 15 minutes into the reaction at 375°C, the rate of gas uptake is rapid. After this, the rate of gas uptake drops by about one-third to 0.31 mmol g^{-1}(daf coal) min^{-1}. The change in the apparent rate of hydrogen consumption could be due to different time constants for the various reactions occurring in the liquefaction process. It was observed in thermal experiments that the generation of gas, primarily CO_2 at this temperature, was confined mainly to the early part of the reaction. The release of this gas has been associated with the onset of thermal reactions in the coal which can lead to a more refractory product in the absence of catalyst (3). The high hydrogen demand in the early part of the reaction may be due to the capping of the radicals generated by these thermal reactions. After this event, the lower hydrogen demand could be due to capping of radicals formed from the thermal reactions which occur in parallel with those responsible for the initial burst of activity. This hypothesis is in accord with the idea of an equilibrium between a radical pool and a reactive insoluble product recently used by Suzuki to model the liquefaction of a low-rank coal (4). The catalyst undoubtedly has other roles, especially in the later parts of the liquefaction process. These include heteroatom removal, hydrogenation of aromatic systems, and hydrocracking reactions; all of which would lead to the increase in the lighter, cyclohexane-soluble products observed after 60 minutes (part C of Figure 1).

To obtain additional information on the role of the catalyst, a detailed characterization of the THF-insoluble products from the reactions at 0, 30, and 60 min was performed. The following analytical techniques were used: organic petrography, ^{13}C solid-state NMR, an oxygen speciation technique developed at PETC, and elemental analysis.

Figure 3 shows the change in the H/C ratio and the vitrinite reflectance as a function of conversion of the coal to THF-soluble products. The THF conversion increased with residence time (see Figure 1); however, little change occurred after 30 min in the thermal experiments. The vitrinite reflectance values were determined as part of the petrographic examination of the vitrinite in the raw coal and the vitrinite or vitroplast in the THF-insoluble products. H/C data were also obtained for the same samples and for a sample of the raw coal that had been extracted with THF using the same procedure as for recovering the insoluble residue. The data show that hydrogen is added to the residue in the presence of the catalyst and that the H/C ratio is maintained at a level near that observed for the THF-extracted coal even up to a reaction time of 30 minutes (part A of Figure 3). Without catalyst, the H/C ratio drops even for the 0-residence time sample. The vitrinite reflectance measurements shown in part B of Figure 3 indicate that using catalyst results in a product that is less aromatic and therefore more reactive than in the thermal cases. Even for the 0-residence time sample, the presence of the catalyst resulted in a reflectance value at or even less than that of the starting coal. As with the H/C data, most of the changes in the thermal samples occur within the first 30 minutes at reaction temperature.

The THF-insoluble products obtained from the 0-min residence time experiments still consisted of identifiable macerals. The catalytic samples contained vitrinite particles that exhibited rounding of the edges which may indicate that the catalyst was promoting the initiation of coal softening. Catalytic hydrogenation has been observed to lower the initial softening temperature of coal and extend its plastic range (3). Vitrinite reflectance measurements were also recorded at the centers and edges of the vitrinite particles. In the thermal samples, the reflectance measurements were nearly constant across the particles (0.70% center, 0.69% edge). The values for the catalytic samples were substantially lower and there was a slight increase in vitrinite reflectance from the edge areas (0.58%) to the center (0.61%). Similar observations have been reported in the literature for coal liquefied using naphthalene as a solvent (5). The petrographic and elemental analyses show that, even though the catalyst had not affected the yields of THF-soluble products at 0-min residence time, significant changes had already been induced in the coal by its presence.

The inferences drawn from petrographic and elemental analyses were strengthened by additional information provided by solid-state ^{13}C NMR, summarized in Figure 4. At the onset of liquefaction, the presence of the catalyst limited the increase in the fraction of aromatic carbons in the THF-insoluble product (part A of Figure 4) as compared to the thermal product. This

corroborates the vitrinite reflectance measurements shown in part B of Figure 3. With time, this effect became more pronounced. At the longer reaction times, the catalyst exerted a definite effect on limiting the growth of aromatic clusters in the insoluble product (part B of Figure 4). The presence of the catalyst also resulted in lower attachments per average cluster (part C of Figure 4) and lower molecular weights of the clusters with respect to the amount of conversion that occurred. Liquefaction creates a hydrogen demand that is partially satisfied in the thermal case by condensation and aromatization reactions in the residue. The catalyst provides an alternate source of hydrogen from the gas phase, thus resulting in less condensation and aromatization in the residue.

The effect of catalyst on the oxygen-containing species present in the THF-insoluble products is made evident by the data assembled in Figure 5 from elemental, NMR, and oxygen speciation analyses. Part A contains the atomic O/C ratios as a function of conversion. Only small overall changes are noted and no overall concentration of oxygen-containing species was apparent as more of the coal liquefied. The NMR data in part B and the results of oxygen speciation analyses in part C show that initially the amounts of hydroxyl or phenolic substituted carbon in the THF-insoluble products were similar to that in the starting material. Also, based on data from the potentiometric titrations (not shown), the relative proportion of strong acids in the THF-insoluble products from reactions with catalyst increased. Without catalyst little change was noted.

After 30-min reaction time in the absence of catalyst, the unconverted material does not change in regard to oxygen content or speciation. This is in marked contrast to the extensive increase in aromaticity seen in Figure 4. Catalyst does not seem to have a profound effect on oxygen distribution with the exception that the number of hydroxyl and phenolic substituted carbons becomes somewhat more concentrated in the small fraction of coal left unconverted.

Part D of Figure 5 contains additional information derived from the oxygen speciation analysis and shows that the presence of the catalyst resulted in a small but definite increase in the amount of carboxyl groups in the THF-insoluble products. Virtually no change was observed in the products from the thermal experiments. The carboxyl groups are not formed during the liquefaction reaction but rather through aerial oxidation of the residues during the workup procedure. Catalytic liquefaction apparently renders the remaining residues more susceptible to such oxidation.

CONCLUSIONS

Solvent-free liquefaction with a well-dispersed catalyst provides an excellent opportunity to study its effects on coal without the complications generated by excess extraneous material. The results presented here show that a low level of catalyst addition significantly promotes conversion and the uptake of hydrogen from the gas phase even in the early stages of the liquefaction process. Even before the yields of THF-soluble products are affected, the catalyst causes significant changes in the coal. Petrographic analysis of the liquefaction residues indicates the catalyst promotes hydrogenation and softening. Solid-state ^{13}C NMR analysis reveals pronounced differences between thermal and catalytic residues. The former are more aromatic, contain more aromatic carbons per cluster, and more attachments per cluster. A net effect of catalyst is to protect the unconverted material from thermal reactions leading to the formation of a highly aromatic char. At the conditions of these experiments, reactions involving oxygen functionalities did not seem to be greatly affected by the presence of the catalyst.

ACKNOWLEDGMENTS AND DISCLAIMER

The authors would like to thank Richard Hlasnik and Jerry Foster for performing the microautoclave work. The NMR analyses were performed by Dr. Francis Miknis and Dr. Daniel Netzel of the Western Research Institute in Laramie, Wyoming. Reference in this report to any specific product, process, or service is to facilitate understanding and does not imply its endorsement or favoring by the United States Department of Energy.

REFERENCES

1. R.P. Warzinski; B.C. Bockrath Energy & Fuels **1996**, 10, 612-622.
2. M.S. Solum; R.J. Pugmire; D.M. Grant Energy & Fuels **1989**, 3, 187-193.
3. F.J. Derbyshire; A. Davis; R. Lin Energy & Fuels **1989**, 3, 431-437.
4. T. Suzuki Energy & Fuels **1994**, 8, 341-347.
5. F.J. Derbyshire; A. Davis; M. Epstein; P. Stansberry Fuel **1986**, 65, 1233-1239.

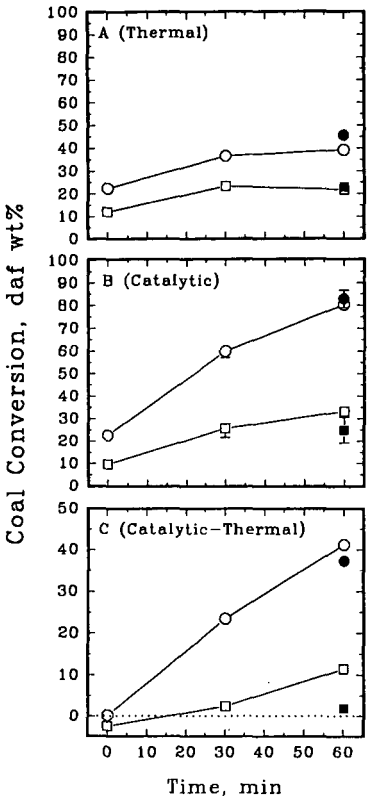

Figure 1. Conversion results for 375°C experiments with DECS–17 coal. (○ , ●) THF conversion; (□ , ■) cyclohexane conversion. Open symbols – 6.6 g coal; closed symbols – 3.3 g coal.

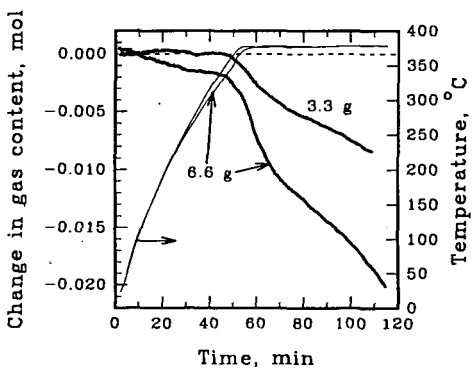

Figure 2. Effect of coal loading on changes in gas content in the microautoclave due to the catalysts for 1–h experiments with DECS–17 coal.

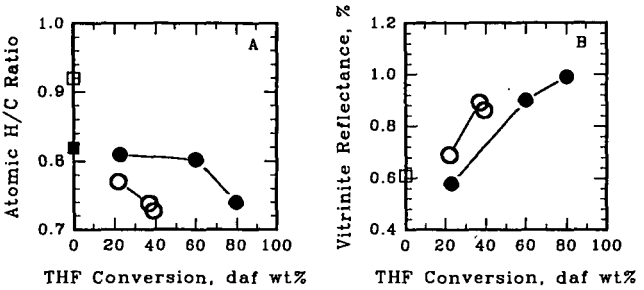

Figure 3. Vitrinite reflectance data and atomic H/C ratios for THF insols from experiments at 375°C with DECS-17 coal. (○ thermal; ● catalytic; □ untreated coal; ■ untreated, THF-extracted coal.)

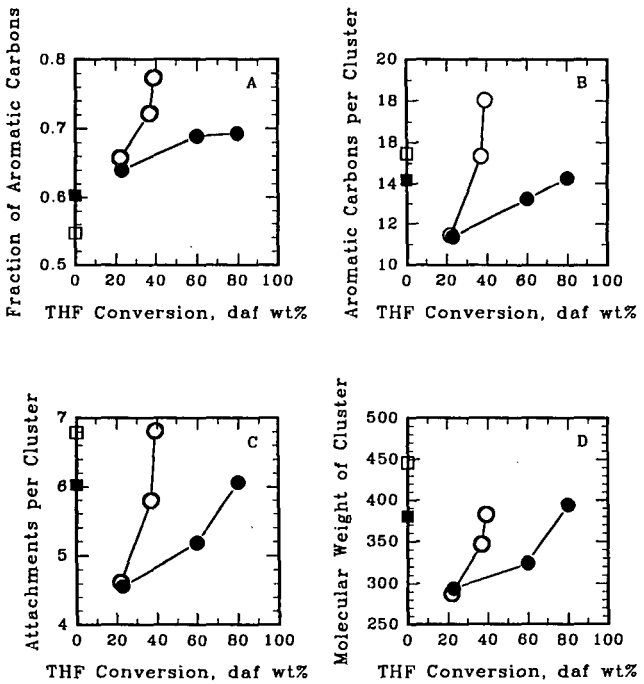

Figure 4. Solid-state ^{13}C NMR data for THF insols from experiments at 375°C with DECS-17 coal. (Symbol definitions are the same as in Figure 3.)

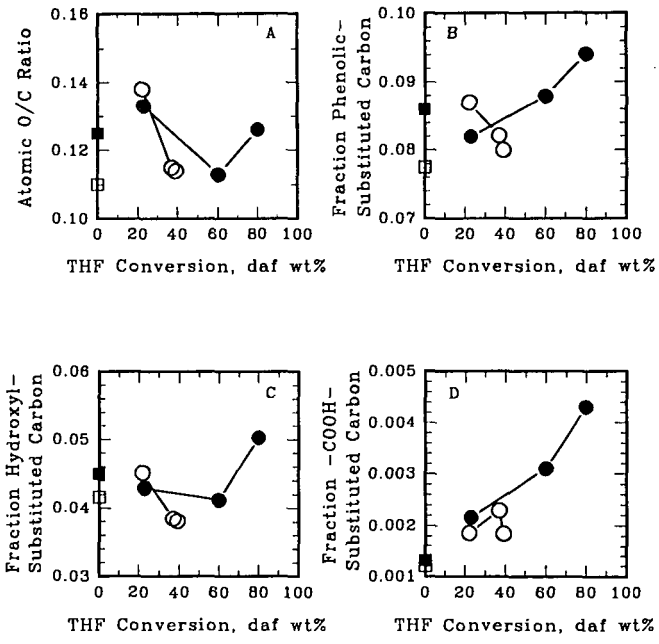

Figure 5. *Oxygen species data for THF insols from* experiments at 375°C with DECS-17 coal. (Symbol definitions are the same as in Figure 3.)

EFFECTS OF SURFACE-ACTIVE AGENTS ON MOLYBDENUM ADSORPTION ONTO COAL FOR LIQUEFACTION

Godfried M. K. Abotsi, Kofi B. Bota, Gautam Saha and Stacey Mayes
Department of Engineering
Clark Atlanta University
Atlanta, GA 30314

Keywords: Surfactants, adsorption, molybdenum catalysts.

INTRODUCTION

The aim of this work is to enhance catalyst loading and dispersion in coal for improved liquefaction by preadsorption of surfactants onto coal. The use of surfactants to increase the dispersion and stability of coal-water slurries and to enhance coal beneficiation is well known. However, the effects of surfactants on catalyst loading and dispersion prior to coal liquefaction have not been investigated. This paper discusses the influence of the cationic surfactant dodecyl dimethyl ethyl ammonium bromide (DDAB) and sodium dodecyl sulfate (SDS, anionic) on the surface properties of Illinois No. 6 coal and its molybdenum uptake from solution.

Extensive investigations on molybdenum and other metals as coal liquefaction catalyst precursors have shown that more effective catalyst loading techniques are required to attain sufficiently high levels of catalyst dispersion in coal for liquefaction on a commercial scale. Studies (1-3) in our laboratory have shown that the surface charge properties of coal exert significant influence on the uptake, dispersion and activities of aqueous soluble calcium and potassium catalysts that were applied to coal char gasification. In general, the surfaces of the three types of coal investigated were negatively charged. The surface charge density was linked to the dissociation of coal surface phenolic and carboxylic groups which promoted the adsorption and dispersion of calcium and potassium ions (1, 2).

Coal surface contains both hydrophobic and hydrophilic sites. The hydrophilic regions consist of inorganic or polar organic surface groups; the hydrophobic surface regions are primarily non-polar organic moieties. When added from aqueous solution, the catalyst will be attracted to the hydrophilic sites on the coal but it will be repelled by the hydrophobic sites. The opposite effect will occur when a catalyst is loaded from organic solution. In either case, a low catalyst dispersion will result, unless the coal surface sites are controlled to optimize the distribution of the catalyst in the coal. The current work examines the application of surface-active agents (surfactants) for controlling coal surface properties with the goal of enhancing molybdenum loading and dispersion prior to liquefaction.

EXPERIMENTAL

The Illinois No.6 coal (DECS-24) used in this study was supplied by the Penn State Coal Sample Bank. Its moisture, ash, volatile matter, and fixed carbon contents were 13.2, 11.6, 35.4, and 39.7 %wt., respectively, on as-received basis. It has an ultimate analysis of 11.6 % ash, 57.3% carbon, 4.0% hydrogen, 1.0% nitrogen, 4.8% sulfur, and 8.1%wt. oxygen (by difference). Coal-water slurries for the study were prepared by adding 2.0g of coal to 25 mL of 0.01M aqueous solution of molybdenum and 25 mL of 0.02M DDAB or 0.02M SDS. A set of six samples were

prepared for each surfactant and the pHs of the slurries ranged from about 2 to 12. Ammonium molybdate (VI) tetrahydrate (AMT) was used as the molybdenum source. After recording the original pHs of the coal dispersions, about 0.5mL of 1M HCl or 0.5M NaOH solution was added to all, except one sample, to adjust the pHs to the desired values. The samples were then shaken on a mechanical agitator for 24h, followed by redetermination of the final equilibrium pHs. The samples were then filtered and the filtrates were analyzed for molybdenum using atomic absorption spectrophotometry. The molybdenum content of the coal residues was measured by Galbraith Laboratories, Knoxville, TN, using inductively coupled argon plasma spectroscopy. Mass balance calculations showed good agreement between the two analytical techniques.

To determine the effects of the coal surface charge on the adsorption of the surfactants and molybdenum, the zeta potentials of coal slurries containing 5g of coal per liter and deionized water were measured. The measurements were conducted on 25 mL samples to which 25 mL of 0.2M, 0.02M, or 0.002M DDAB or SDS solution had been added and the pHs adjusted as described above. The samples were equilibrated for 4h by mechanical agitation, after which the pH values were recorded. The zeta potentials were measured at room temperature using a Pen Kem Model 501 zeta meter.

The interaction of the surfactants with the coal surface was studied using diffuse reflectance FTIR. The coal samples were dispersed in infrared grade KBr that had been dried overnight at 300°C and sieved through a 90 micron sieve. The FTIR spectra were recorded on 10% coal in KBr using a Nicolet Magna IR Spec 750 and 500 scans.

RESULTS AND DISCUSSION

The zeta potential results in Figure 1 show that the parent coal is negatively charged within the pH range investigated and that the charge density increased with increase in the slurry pH. This behavior is attributed to the dissociation of the surface carboxlylic and phenolic acid groups (1, 2). Figure 1 also shows that the coal particles generally produced positive zeta potentials in the presence of DDAB. In solution, SDS ($CH_3(CH_2)_{11}OSO_3^-Na^+$) and DDAB ($CH_3(CH_2)_{11}N(C_2H_5)(CH_3)_2^+Br^-$) will dissociate to produce anionic and cationic surfactants, respectively, which can be denoted as $ROSO_3^-$ and $R'N^+$. Since DDAB is cationic, the positive charge density on the coal can be explained by the coulombic attraction of the surfactant, and its subsequent adsorption, to the negatively charged sites on the coal surface. In contrast to the effect of DDAB, the zeta potentials of the coal particles became more negative than those of the parent coal in the presence of SDS, as shown in Figure 2. The negative charge density increased with increase in pH and in the concentration of SDS. Since the surface of the raw coal is negative, the adsorption of SDS must occur through the hydrocarbon chain of the molecule, with the anionic head oriented towards the aqueous solution.

The effects of the surfactants and pH on molybdenum loading onto the coal are shown in Figure 3. A remarkable dependence of catalyst loading on both parameters was observed. The minimum catalyst loading occurred on the parent, untreated coal in contrast to the DDAB-treated coal which contained the highest molybdenum content. Around pH 2.5, the molybdenum loadings of these samples were about 5 and 15

mg/g of coal, respectively. An intermediate molybdenum loading (~9 mg/g coal) occurred on the SDS-treated sample.

The observed molybdenum adsorption patterns can be explained by the electronic charges on the coal surface and on the molybdenum species. In aqueous solution, AMT will dissociate to form various molybdenum oxyanions which are pH dependent (4). It is reported that $Mo_8O_{26}^{4-}$ predominates below pH 2 whereas $Mo_7O_{24}^{6-}$ exists as the dominant species between pH 2 and 6. MoO_4^{2-} and $Mo_7O_{24}^{6-}$ occur in the pH 6 to 8 range; MoO_4^{2-} predominates above pH 8. Thus, the adsorption of the molybdenum species should be promoted by the positively charged DDAB sites on the coal. It is observed from Figure 1 that at 10^{-3} M DDAB, the zeta potentials are positive and become negative above ~pH 9. At 10^{-2} M DDAB, the zeta potentials are positive within the entire range of pH studied and they increased almost exponentially with increase in pH. This implies progressively stronger adsorption of DDAB onto the coal surface. When the DDAB concentration was raised to 10^{-1} M, the zeta potential increased steadily, passed through a maximum around pH 6-8, and then decreased thereafter. This phenomenon is attributed to strong DDAB adsorption and micelle formation. When the DDAB concentration on the surface exceeded the critical micelle concentration around pH 6-8, the molecules formed aggregates with the polar head of the surfactant oriented towards the interior of the micelle (5). This should decrease the positive charge density on the coal, as was indicated by the decline in the zeta potential values.

The FTIR spectra of the original, untreated coal and those onto which molybdenum and DDAB or SDS were adsorbed are shown in Figure 4. The FTIR spectrum for the original coal after loading with molybdenum is provided in Figure 4A. Significant differences can be seen in the C-H bands at 2800-3000 cm^{-1}. The intensities of these bands are higher for the surfactant-treated samples than for the raw coal (Figure 4B). It is also noted that the intensity of the DDAB-treated coal (Figure 4C) is stronger than for the SDS-treated specimen (Figure 4D). The FTIR spectra confirmed the adsorption of the surfactants onto the coal surface.

In conclusion, it has been shown that the adsorption of molybdenum onto Illinois No. 6 coal (DECS-24) is significantly promoted by preadsorption of dodecyl dimethyl ammonium bromide (DDAB) and sodium dodecyl sulfate (SDS). The former surfactant effected higher catalyst loading since its cationic character favored its adsorption onto the negatively charged coal surface and promoted the uptake of molybdenum oxyanions. This study has shown that the surface properties of coal can be modified for effective catalyst loading onto coal. The influence of the catalyst addition technique on catalyst dispersion and on coal liquefaction activities will be discussed in subsequent papers.

REFERENCES

(1) Abotsi, G. M. K., Bota, K. B., G. Saha, *Energy &Fuels* , 1992, 6, 779.
(2) Abotsi, G. M. K., Bota, K. B., G. Saha, *Fuel Sc. Tech. Intl.*, 1993, 11, 327.
(3) Bota, K. B., Abotsi, G. M. K., L. L. Sims, *Energy & Fuels* , 1994, 8, 937.
(4) Honig, D. S., Kustin, K., *Inorg. Chem.*, 1972, 11, 65.
(5) Rosen, M. J., "Surfactants and Interfacial Phenomena," 2nd Edn., John Wiley, 1989, p. 108.

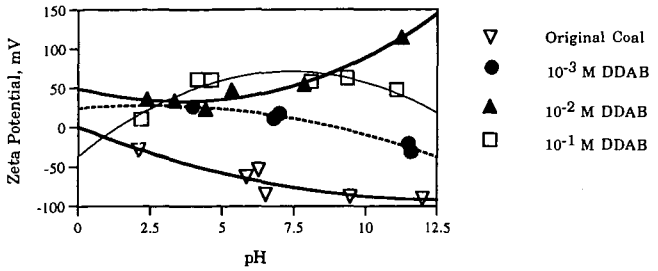

Figure 1. Zeta Potential of DECS-24 Coal as a Function of DDAB Concentration and pH.

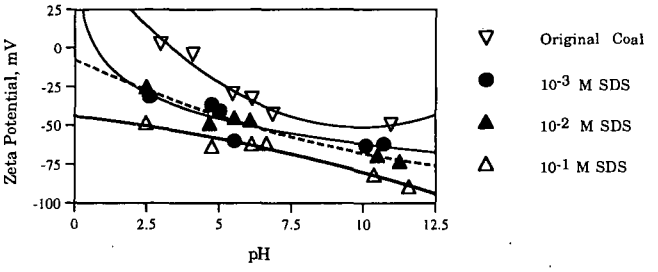

Figure 2. Zeta Potential of the Coal as a Function of SDS Concentration and pH.

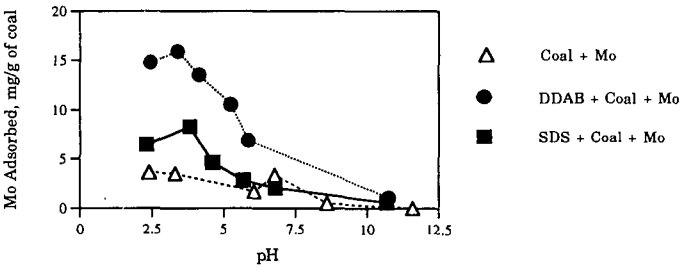

Figure 3. Effect of Surfactant and pH on Molybdenum Adsorption by the Coal.

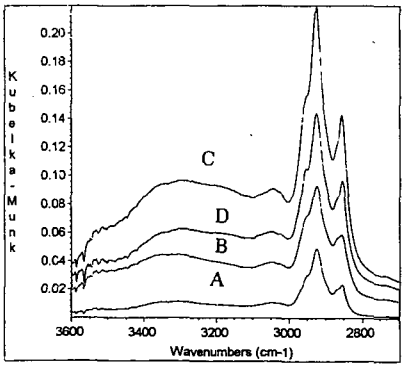

Figure 4. FTIR spectra of the Original and the Surfactant-Treated Coals after Molybdenum Adsorption.
A: Coal + Mo; B: Original Coal only;
C: Coal + DDAB + Mo; D: Coal + SDS + Mo

USE OF DISPERSED CATALYSTS FOR DIRECT COAL LIQUEFACTION

A. S. Hirschon, S. Kim, and R. B. Wilson
SRI International, Menlo Park, CA 94025

and O. Ghaly
Bechtel Corporation, San Francisco, CA 94115

Keywords: Coal liquefaction, syngas, dispersed catalysts

INTRODUCTION

With dwindling supplies of petroleum products, efforts to utilize alternative energy feedstocks such as coal, is essential. Several areas in coal conversion technology have been identified that, if improved, could make coal liquefaction more cost competitive with petroleum.[1-4] The objectives of this project are to address possible improvements in the economics by utilizing low-rank coals, new precursors to dispersed catalysts, and processing variations such as using syngas atmospheres. The purpose of the dispersed catalysts is to better control retrogressive reactions and avoid char formation, while the purpose of the carbon monoxide atmosphere is to improve the economics by simplifying or totally eliminating a separate water-gas-shift step, and perhaps help remove oxygen in the product slate. These possible improvements are being examined and evaluated for potential use in a 2-stage liquefaction process with the goal of converting coal to distillable liquids at a cost competitive to petroleum of $25/bbl.

To evaluate our catalysts and process conditions, we used three types of laboratory-scale operations. In the first operation, we compared the reaction chemistry of various ranks of coals and catalysts in synthetic solvents such as hexadecane. This method allowed us to better compare our catalysts without the complications of solvent initiated chemistry. Once the catalysts were tested in this manner, they were examined for the conversions of a Black Thunder subbituminous coal using a recycle vehicle derived from the same coal as the solvent. Finally, we upgraded selected first-stage conversion products using a conventional hydrotreating catalyst to compare with recent results in two-stage coal liquefaction development. The results were evaluated for economic feasibility through a subcontract with Bechtel Corp.

EXPERIMENTAL

Catalysts: MolyVanL and iron oxide were received from the Wilsonville liquefaction facility. Pentacarbonyl iron was obtained from Aldrich, and the sulfur-containing iron cluster, $(\mu\text{-}S_2)Fe_2(CO)_6$, referred to as Fe_2S_2, was prepared by the method of Bogan et al.[5] Ammonium tetrathiomolybdate, (MoS_4), was obtained from Alfa Chemicals. The organometallic molybdenum catalyst was $(C_5H_5)_2Mo_2(\mu\text{-}SH)_2(\mu\text{-}S)_2$, referred to as Mo(OM), and was prepared by modification of the method of Dubois et al.[6] Nickel biscyclooctadiene [$Ni(COD)_2$] was obtained from Strem Inc. The hydrotreating catalyst Shell 317, obtained courtesy of Criterion Chemical Company, was presulfided under flowing 10% H_2S/H_2 before use.

Coal conversions in synthetic solvents: The model coal liquefaction experiments were conducted in a 300 mL Autoclave Engineers (AE) stirred reactor using 5.0 g of coal, 3 mmol of catalyst, 30 g of solvent, and 500 psig (cold) hydrogen. Reaction temperatures were held at either 400°C or 425°C for 20 minutes.

Black thunder studies: The screening experiments were conducted in a 300 mL autoclave with conversions being run at 425°C for 1 hour. Two autoclaves were used, referred to as autoclave A and B. The properties of autoclave B are such that for a high viscosity medium the conversions are lower in autoclave B than in A. The molybdenum based catalysts were first screened in autoclave B, and then selected reactions were repeated in autoclave A for comparison. The feedstock consisted of 2.5 parts by weight of recycle vehicle (50g) from Wilsonville run #263 to 1 part Black Thunder coal (20g). The total gas charge was up to 1000 psi (cold), and contained 3% H_2S. Carbon monoxide concentrations ranged from 20% to 50%. The simulated 2-stage liquefaction experiments were conducted in a 1 liter autoclave (AE) equipped with an injection port.

RESULTS AND DISCUSSION

Coal conversions using synthetic solvents: The comparison of model coal conversions using various catalysts for a hexadecane solvent system is presented in Table 1. The first three liquefaction experiments listed in Table 1, were conducted at 400°C. They include a noncatalyzed conversion, and conversions using molybdenum (MoS_4 and Mo(OM)) catalysts on an Illinois #6 coal. The fourth liquefaction experiment was conducted in tetralin, for comparison. Most of the conversions are quite low, as expected. For instance, in the absence of catalyst, the Illinois #6 coal was converted to 25% toluene-soluble material.

However, in the presence of the molybdenum catalysts, the conversions were greatly enhanced. For instance, the coal impregnated with $(NH_4)_2MoS_4$ gave a conversion of 41% toluene-soluble material, compared to 54% for the organometallic molybdenum-impregnation [Mo(OM)].

The remaining five experiments, conducted at 425°C using an Argonne lignite coal, compare various soluble iron-, molybdenum-, and nickel-based catalysts. Both the soluble organometallic iron complexes, $Fe(CO)_5$ and $Fe_2S_2(CO)_6$, are effective for the low rank coals, giving toluene-soluble conversions in the range of 40% (carbon-based yields). In previous work we found that these catalysts gave only nominal conversions for the Illinois #6 coal. X-ray analyses of the residues show that both catalysts were converted into pyrrhotite; however, the iron carbonyl also appeared to have been converted into elemental iron and other iron-based products. The Mo(OM) catalyzed reaction gave a higher conversion of 49% for this lignite, consistent with the better efficacy of Mo catalysts over Fe catalysts. Considering the organic chemistry of carboxylates, we also decided to investigate nickel as a potential catalyst for low rank coals. Since iron has a tendency to form dimers during decarboxylation of organic acids,[7,8] and nickel tends to promote decarboxylation without dimerization we speculated that nickel may be a better catalyst for oxygenated coals.[8] Consistent with this premise, the conversion using a Ni-based catalyst [$Ni(COD)_2$] shows that the lignite conversion increased from 40% with the iron catalyst to 60% with the nickel catalyst.

Black Thunder screening tests. The iron oxide catalysts were found to give poorer liquefaction yields than either the iron carbonyl and thiolato iron carbonyl. For instance, under hydrogen atmospheres, the iron oxides gave THF-soluble conversions in the range of 75% compared to over 90% for the iron carbonyl and thiolato iron carbonyl. However, in the presence of syngas, the iron carbonyl gave significantly lower yields than the thiolato iron carbonyl catalyst. Thus the latter catalyst appears to be superior for concepts that take advantage of the carbon monoxide chemistry, and no evidence of methanation was observed.

In a similar manner, Figure 1 illustrates the relative abilities of the MolyVanL and the thiolato Mo catalyst for conversions of the Black Thunder coal. In this case the conversions were conducted in Reactor B, which gives lower conversions than in Reactor A. The molybdenum content in all cases was 500 ppm of Mo. As seen in Figure 2, the MolyVanL gave relatively low conversions in Reactor B, but they were about the same (50%) whether in hydrogen atmospheres or syngas atmospheres. Thus the molybdenum catalyst appears to be able to use the carbon monoxide atmospheres. In the presence of the thiolato molybdenum catalyst, however, the conversion increased from 50% with the MolyVanL catalyst to over 75% conversion showing that the organometallic molybdenum catalyst is a far superior catalyst.

Table 2 compares the conversions using various catalysts in Reactor A. This table lists the best iron-catalyzed conversions described above as well as results from a series of MolyVanL conversions that were repeated in Reactor A for comparison. Prompted by the high conversions obtained for the $Ni(COD)_2$-catalyzed lignite conversions, we also conducted conversions on Black Thunder coal with this catalyst. We investigated both hydrogen atmospheres and syngas atmospheres containing 50% CO; these results are also included in Table 2. The last column of Table 2 lists the coal conversions based on conversions to THF-soluble materials and allows for contributions from the recycle solvent. The nickel-catalyzed reactions both under hydrogen and under 50% carbon monoxide gave very high conversions to THF-soluble material, with overall coal conversions in excess of 90%.

Simulated Two-Stage Conversion. A base-line run was also conducted to simulate a two-stage liquefaction conversion process. For this simulated conversion we used the MolyVanL catalyst in hydrogen atmospheres, and for comparison, in syngas atmospheres. We decided to use this catalyst as a baseline case for comparison with other work that has recently used this commercially available oil-soluble molybdenum compound. Note, however, we have identified other catalysts that are more active than MolyVanL. For instance our thiolato molybdenum catalyst was found to give coal conversions of over 25% greater than that found for the MolyVanL catalyst under mild coal conversion conditions (reactor B). Thus we expect a significant improvement using this catalyst over these base-line conditions.

Tables 3 and 4 list the distillation yields and elemental analyses for the hydrogen atmosphere and syngas atmosphere conversions, respectively. The conversions using the two systems were similar, with the syngas conversion giving a slightly lighter product (C5-650°F product contents were 47.6%) than the hydrogen conversion products (C5-650°F product contents were 40.8%). Furthermore, the amounts of the 1000°F+ fractions were similar, at 25% for the hydrogen conversion and 28% for the syngas conversion. Although there was not enough data using the batch results to obtain a complete economic analysis without a significant amount of approximations, we were able to deduce some effects of the use of syngas in the first stage of the coal conversion. For instance, we found that more value-added products are produced (mainly phenols), the CO shift requirement is reduced, and there is an added effort in the purification of hydrogen for the second stage reactor. The preliminary results suggest that the benefits of syngas in the first stage slightly outweigh the disadvantages.

FUTURE WORK

These preliminary results are encouraging, but economics need to be conducted on the best catalysts. Additionally, we have only used hydrogen in the second stage upgrading step, and thus not achieved the full economic benefits of syngas atmospheres. However, we feel that with proper catalyst and process development, our methods may significantly improve the final product quality and economics during coal liquefaction.

ACKNOWLEDGMENTS

The authors gratefully acknowledge the support of this work by the Department of Energy under Contract DE-AC22-91PC91039.

REFERENCES

1. S. N. Rao, H. D. Schindler, and G. V. McGurl, ACS Fuel Preprints, (1988) 33(3), 145-156.
2. J. M. Lee, O. L. Davies, T. E. Pinkston, and J. R. Gough, ACS Fuel Reprints, (1988) 33(3), 157-171.
3. D. Gray and G. Tomlinson, ACS Fuel Preprints (1988) 33(3), 172-179.
4. S. V. Gollakota, J. M. Lee, O. L. Davies, and T. E. Pinkston, DOE Direct Liquefaction Contractors' Review Meeting, Pittsburgh, Pennsylvania, October 1988.
5. Bogan, L. E. Jr., Lesch, D. A., and Rauchfuss, T. B., J. Organometallic Chem. (1983) 250, 429-438.
6. Cowens, B. A., Haltiwanger, R. C., and DuBois, M. R., Organometallics (1987) 6, 995-1004.
7. J. March, *Advanced Organic Chemistry*, second edition (McGraw-Hill Book Company, NY, 1977), p. 514.
8. S. Patai, "The Chemistry of Carboxylic Acids and Esters" (Interscience-Publishers, NY, 1969), pp. 362-371.

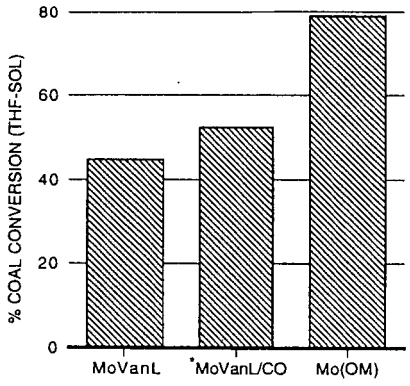

Figure 1. Effect of molybdenum catalysts for Black Thunder coal conversions in Reactor B.

Table 1

CONVERSION TO TOLUENE-SOLUBLE PRODUCTS IN HEXADECANE[a]

Catalyst	Coal	T(°C)	% TS[b]
None	Illinois # 6	400	25
MoS_4	Illinois #6	400	41
Mo(OM)	Illinois #6	400	54
Mo(OM)[c]	Illinois #6	400	61
None	Lignite	425	24
$Fe(CO)_5$	Lignite	425	41
Fe_2S_2	Lignite	425	39
Mo(OM)	Lignite	425	49
$Ni(COD)_2$	Lignite	425	60

[a]Reaction conducted in a 300-mL autoclave with 5 g coal, 3 mmol catalyst, 30 g solvent and 500 psi H_2 for 20 min at temperature.
[b]Yields calculated on daf basis for Illinois #6 coal and on carbon basis for the lignite.
[c]Reaction run in tetralin under identical conditions.

Table 2

DAF YIELDS OF USING VARIOUS METAL CATALYSTS IN REACTOR A[a]

Catalyst	Atmosphere[c]	THF Insol	Preasphaltene	Asphaltene	Oils	% Conv
Recycle	As received	8.7	7.5	60.9	23.2	–
Recycle	1000 psi H_2	6.7	4.4	51.3	29.7	–
$Fe(CO)_5$	1000 psi H_2	5.8	7.5	54.9	21.7	96.5
$Fe(CO)_5$	50% CO	14.9	18.7	34.8	25.4	64.7
$Fe_2S_2(CO)_6$	1000 psi H_2	7.6	11.8	37.5	24.4	90.2
$Fe_2S_2(CO)_6$	50% CO	10.7	11.2	35.4	23.9	79.4
MolyVanL[b]	1000 psi H_2	5.1	10.0	40.2	28.8	98.9
$Ni(COD)_2$[b]	1000 psi H_2	7.2	11.6	41.8	20.7	91.6
$Ni(COD)_2$[b]	50% CO	7.4	11.8	46.3	23.3	90.9

[a]Reaction conducted in a 300-mL autoclave for 1 hr with 20 g Black Thunder Wyodak coal, 2% iron metal in catalyst, 50 g recycle solvent and at 425°C. Atmosphere contained 3% H_2S in H_2.
[b]500 ppm metal added.
[c]Total pressure 1000 psi.

Table 3

ANALYSES OF DISTILLATION PRODUCTS FOR H_2/H_2 TWO-STAGE COAL CONVERSION[a]

Fraction °F	Wt. %	C	H	N	S	H/C
C5-350	4.3	83.63	16.37	b	b	2.332
350-650	21.6	86.24	10.13	0.68	0.17	1.398
650-850	14.9	87.91	9.91	0.64	0.30	1.344
850-1000	15.9	88.48	9.02	0.70	0.49	1.215
1000+	25.0	89.60[c]	6.12[c]	0.97[c]	ND	0.812
Ash	8.5					
H_2O	5.5					

[a]425°C, 30 minutes first-stage, 400°C, 30 minutes second-stage.
[b]Too low for accurate N and S determination.
[c]Calculated on an ash-free basis.

Table 4

ANALYSES OF DISTILLATION PRODUCTS FOR CO/H_2 1ST STAGE, H_2 2ND STAGE TWO-STAGE COAL CONVERSION[a]

Fraction °F	Wt %	C	H	N	S	H/C
C5-350	3.5	85.10	14.34	0.5	0.07	2.008
350-650	20.9	85.05	10.61	0.52	0.05	1.449
650-850	23.2	88.55	9.06	0.60	0.14	1.219
850-1000	8.9	89.87	7.92	0.71	0.24	1.049
1000+	28.3	68.33[a]	4.46[a]	0.87[a]	ND	0.778
Ash	9.6[b]					

[a]425°C, 30 minutes first-stage, 400°C, 30 minutes second-stage.
[b]Calculated on an ash-free basis.

DEVELOPMENT OF AN ALL-SLURRY LIQUEFACTION TEST FOR SCREENING DISPERSED CATALYSTS

Terry Rantell, Richard K. Anderson and Edwin N. Givens
University of Kentucky, Center for Applied Energy Research
3572 Iron Works Pike, Lexington, KY 40511-8433

Keywords: Coal liquefaction, catalysis, molybdenum

ABSTRACT

Exceptionally high distillate yields have previously been achieved in the direct liquefaction of subbituminous coal using dispersed catalysts. As part of a program sponsored by the U. S. Department of Energy, selected dispersed catalysts are being evaluated in continuous bench-scale runs. In consequence, a laboratory test has been developed to screen candidate dispersed catalysts and determine the optimum range of operating conditions to maximize coal conversion and distillate yield. The objectives of the test are to simulate operation in an all-slurry mode with coal conversion and product selectivity at least as good as that achieved in 2-stage operation at the Wilsonville Advanced Coal Liquefaction Facility. Tests are conducted in microautoclaves using pilot plant derived solvents and a Wyodak coal in the ratio of 1.85/1. An Fe-Mo catalyst contained in a Wilsonville process solvent has been used as a reference. The influence of residence time at 440 °C on 524 °C+ resid conversion has been determined and evaluations of various Mo formulations will be discussed.

INTRODUCTION

A DOE sponsored program is currently being conducted, in part, at the CAER to develop viable slurry catalysts for producing a distillate product equivalent to that obtained in a run made at the Wilsonville Advanced Coal Liquefaction R&D Facility in 1992. In the Wilsonville study, Runs 262E and 263J, Wyodak coal from the Black Thunder mine was used as feed. Unlike those runs, which were made in a 2-stage configuration in which the 1st-stage was operated as a thermal reactor, with a Mo-Fe dispersed catalyst, and the 2nd-stage as an ebullated bed reactor, with a Ni-Mo extrudate catalyst,[1] the objective tahe current work[2] is to develop a process involving an all-slurry reactor configuration using only dispersed catalyst. By eliminating the 2nd-stage catalyst, considerable cost reduction can be achieved if a dispersed catalyst can be found that can provide the same level of coal conversion and product selectivity that was obtained in the 2-stage Wilsonville operation.

Various methods for introducing dispersed catalyst precursors into the reaction system is being investigated in this project. One approach is to impregnate the catalytic metal precursors onto coal and activate these metals *in situ*. Such catalysts require that several interrelated process parameters be optimized in order to generate active catalysts. Although Mo is an active component in all these catalysts, the co-metals and their particular salt precursors must be defined as well as the concentration of metal on the coal substrate. In addition, limitations on the amount of the feed coal that must be impregnated, the conditions and reactants necessary to activate the catalyst as well as maintain its activity in the process, and the concentration of the catalyst in the recycle stream must be specified. The effect of each catalyst on product yields and quality must also be determined.

A catalyst screening test is being developed to facilitate the selection of catalysts and their concentration in the reaction system. The test simulates the liquefaction performance in an all-slurry liquefaction mode and expands upon the a catalyst screening test that was recently reported that simulates the first-stage reactor.[3] The active catalyst, which is contained in the ashy resid portion of the recycle solvent from Wilsonville Run 262E, has been used as a reference catalyst. The performance of various test catalysts will be compared to the performance of the Run 262E catalyst, which appears to be far more active than any others that have been tested in our laboratory. Distillate yield and coal conversion are used as a measure of catalyst activity.

EXPERIMENTAL

Wyodak coal, obtained from the Black Thunder Mine in Wright, Wyoming, was ground to -200 mesh, riffled and stored under nitrogen at 4 °C. Proximate and ultimate analyses of the coal are presented in Table 1. Samples of the various components of the recycle solvents from Runs 258 and 262 were obtained from the Advanced Coal Liquefaction R&D Facility at Wilsonville, AL. All of these materials were produced at Wilsonville when the plant was operating in a close-coupled configuration and feeding Black Thunder coal. Run 262E recycle solvent contains sizable concentrations of iron and molybdenum resulting from addition of iron oxide and Molyvan L to the feed slurries. This solvent had previously been described in detail.[4] Molyvan L is an organic-based Mo containing material supplied by R. I. Vanderbilt Co.

Based on previous Mössbauer studies on solids obtained from liquefaction of Black

Thunder coal in Run 262 solvent, the iron in the THF IOM was present in combination with sulfur as pyrrhotite. The molybdenum was presumed to be present as MoS_2. A sample of THF insoluble material in the Run 262 563 °C+ ashy resid was isolated by exhaustively extracting with THF for 2 days.[5] Another sample of catalyst-enriched solids from Run 262 solvent was obtained by filtering a THF slurry at ambient temperature. In both cases the samples were dried overnight at 40 °C at 125 torr.

The catalyst screening tests are run in 50 mL microautoclaves in 2-3% H_2S in H_2 at a nominal total pressure at ambient temperature of 1350 psig which provides a hydrogen to feed coal ratio of about 18 wt % on dry coal. Total pressure at operating temperature is approximately 2500 psig. In the test, approximately 2.4 g dry coal is slurried in a solids-free solvent mixture comprising 33 wt % Run 258B heavy distillate (Wilsonville Vessel Number V-1074) and 67 wt % Run 258 ROSE deashed resid (Wilsonville Vessel Number V-130). Although the deashed resid is a bottoms cut from a 565 °C (1050 °F) vacuum tower, it still contains 8.3% 524 °C- (975 °F-) distillate and 16.0% of the 524-565 °C fraction, as determined in our laboratory. The various distillate cuts and feed coal concentrations in the starting mix are shown in Table 2. The ash contents of the deashed resid and distillate materials were determined to be quite small, i.e., 0.13 wt% and 0.12 wt%, respectively.

Reactions were conducted in 50 cc microautoclaves pressurized with hydrogen at ambient temperature. After pressurization, the reactor was placed in a fluidized sandbath set at the specified temperature and continuously agitated at a rate of 300 cycles per minute. At the end of the reaction period, the reactor was quenched to ambient temperature and the gaseous products collected and analyzed by gas chromatography. The solid and liquid products were scraped from the reactor using THF and the mixture was extracted in a Soxhlet apparatus for 18 hours. The THF insoluble material, which included IOM and ash, was dried (80 °C at 125 torr) and weighed. The THF solubles were concentrated by removing excess THF in a rotary evaporator and subjected to vacuum distillation using a modified D-1160 procedure, which is described elsewhere.[6] The methods for calculating material balances are included in the previous descriptions. In the following discussion, coal conversion equals 100 minus the yield of THF-insoluble organic material (IOM). Resid conversions are calculated as shown below, while coal conversion is derived from the net yield of IOM.

$$Resid\ Conv = 100\ [\ 1 - \frac{[IOM + 524°C^{+}\ Resid\ (maf)]_{Products}}{[Coal\ (maf) + IOM + 524°C^{+}\ Resid\ (maf)]_{Feed}}]$$

RESULTS AND DISCUSSION

The objective of our program is to identify catalysts that warrant further testing in a continuous recycle bench-scale operation. The criteria for a screening test are to simulate, as closely as possible, actual process conditions that would exist under recycle operation. For that reason, solvents were used in the test that were actually generated from Wyodak Black Thunder coal in the Wilsonville plant. In our previous laboratory studies, the Mo catalyst contained in the Run 262E recycle solvent was found to be the most active of any catalyst we had tested. In our microautoclave reactors, we reported that the 565 °C+ (1050 °F+) resid conversion of Black Thunder Wyodak coal after 22 min at 440 °C was 32%.[5] This essentially replicated the conversion observed in the 1st-stage reactor in both Wilsonville Runs 262E and 263J, which were essentially identical. The purpose for the catalyst screening test that is being developed in this program is to identify catalysts that can match the resid conversion that was obtained after the 2nd-stage of the Wilsonville operation with the Mo catalyst contained in the Run 262E recycle solvent.

Because of the complications associated with solids contained in the recycle solvents used in the Wilsonville plant, our intention was to devise a reformulated solids-free solvent containing a significant residual fraction but free of either mineral matter or accumulated catalysts. A solvent composition was chosen comprising a 565 °C- (1050 °F-) distillate material and a 565 °C+ (1050 °F+) solids-free resid, both taken from Wilsonville Run 258. The resid component was a solids-free 565 °C+ (1050 °F+) material produced by the ROSE-SR unit, which made up only about 7% of the total plant recycle solvent. The other major component in the Wilsonville recycle solvent was an ashy resid recycled from the vacuum distillation tower. In the screening test, the distillate and deashed resid components are blended with feed coal in a way to give a resid/maf coal ratio of approximately 1.1, which is similar to that contained in the feed in Run 263J. The composition of the reaction mixture in the catalyst screening test, as determined from distillations on the feed solvent in our laboratory, is shown in Table 2.

The reaction temperature of the catalyst screening test of 440 °C is the same as used in the Phase I test, however, the sulfiding agent was changed from dimethyl disulfide to 2% H_2S in H_2

with an initial starting pressure of 1350 psig. This provides a hydrogen to feed coal ratio of about 18 wt % on dry coal. Total pressure at operating temperature was approximately 2500 psig. The reaction time was selected from a series of experiments that were used to determine the time necessary to provide the same 565 °C+ resid conversion of Wyodak coal as observed in Run 263J. The microautoclave runs in our laboratory were made by adding 30 wt% dry Wyodak BT coal to Run 262E Mo-containing solvent, at a Mo concentration of 300 ppm on dry coal. The 565 °C+ resid conversion after 22, 30, 60 and 90 min were determined to be 32, 44, 47 and 52%, respectively (see Table 3). The source of the 22 min data was above. The corresponding resid conversions on an maf coal basis in these tests were quite high indicating a conversion even higher than observed at Wilsonville. In a plot of log unconverted resid versus reaction time, the 60 and 90 min conversions depart significantly from a plot of the 22 and 30 min reaction results, as shown in Figure 1. Since the resid conversions observed in Run 263J at Wilsonville was about 38%, a 30 min residence time was chosen for the test, since it most closely replicated those results.

To verify the validity of the catalyst test procedure for identifying active catalysts, samples of the catalyst dispersed in the Run 262E recycle solvent were isolated and evaluated in the screening test. This entailed isolating the catalyst-rich solids from the ashy resid portion of the solvent. One sample was prepared using a Soxhlet extraction technique with THF as the extracting solvent. Another sample was prepared by separating the solids from a THF-ashy resid slurry by filtration at ambient temperature. Both materials were dried overnight at 40 °C at 125 mm Hg. The filter cake obtained from the THF slurry was found to contain 740 mg Mo/kg, which provides a Mo/dry coal ratio of 300 ppmw in the test mixture.

In the catalyst screening test, both of these materials added to the reaction mixture at a Mo level of 300 ppmw on dry coal gave 524 °C+ resid conversions of 23-24%, which were significantly lower than the 40+% expected. Although the activities were less than expected, both samples showed activity that was well above the resid conversion activity of coal in the absence of any catalyst, i.e., 19%. By contrast, the coal conversion to THF solubles for the Mo-catalyst runs were much more in line with expected values, i.e., 99-101%.

As a check to determine if the unusually high 565 °C- distillate fraction in the Run 258 deashed resid or the composition of this fraction could be causing an unexpected result, a full range recycle solvent from Run 258, i.e., Wilsonville designation V-131B, was filtered and used as solvent in the screening test. Distillation indicated this material contained 50.2% 524 °C- distillate, 44.3% 524 °C+ resid, and 5.5% THF insolubles. The 524 °C+ resid conversion for Wyodak coal in this solvent, to which was added filter cake to a level of 300 ppm Mo on dry coal, was 26%, as shown in Table 4. This result is comparable to the result when using the deashed resid. For comparison, the 18% resid conversion in the absence of any added catalyst was essentially the same as when deashed resid was used as solvent.

Progress in developing this catalyst screening test will be discussed as well as possible reasons for this difference in activity for catalyst that was isolated from the reaction slurry versus catalyst that remained suspended in the solvent. In addition, results for various dispersed catalysts in this screening tests will be presented.

REFERENCES

1. Technical Progress Report, "Run 263 with Black Thunder Mine Subbituminous Coal and Dispersed Molybdenum Catalyst", DOE/PC/90033-23, Dec. 1992.
2. Final Technical Report for "Advanced Coal Liquefaction Concepts for PETC Generic Units", DOE/PC/91040-55, March 1995.
3. Anderson, R. K.; Derbyshire, F. J.; Givens, E. N. Prep. Pap.-Am. Chem. Soc., Div. Fuel Chem. 1994, 39(4), 1108.
4. Quarterly Technical Report for "Advanced Coal Liquefaction Concepts for PETC Generic Units", DOE/PC/91040-21, February 1993, p.74ff.
5. Anderson, R. K.; Lim, S. C.; Ni, H.; Derbyshire, F. J.; Givens, E. N. Fuel Process. Tech. 1995, 45, 109-122.
6. See Reference 1, p. 1-1.

Table 1. Black Thunder Coal Analysis					
Proximate Analysis	wt%	Ultimate Analysis	wt%	Sulfur Types	wt%
Moisture	21.2	Carbon	68.68	Total	0.39
Ash	5.15	Hydrogen	4.76	Pyritic	0.07
Volatile Matter	34.4	Nitrogen	1.21	Sulfate	0.09
Fixed Carbon	39.3	Sulfur	0.56	Organic	0.23
		Oxygen (diff)	18.25		
		Ash	6.54		
		Ash, SO_3-free	5.42		

Table 2. Composition of Feed in Catalyst Screening Test		
	Dry coal basis, wt %	
Cut point, °C	565	524
Dry coal	35	35
Distillate, wt% at cut point	21.5	26.6
Deashed Resid, wt% at cut point	43.5	38.4

Table 3. Liquefaction of Wyodak Black Thunder Coal in Wilsonville Run 262 Recycle Solvent 440 °C, 30 min, 1350 psig, 2 vol% H_2S/H_2			
Run No.	I	II	III
Feed Composition			
Coal, mf, wt%	30.0		
565 °C- Heavy Distillate, wt%	30.5		
565 °C+ Ashy Resid, wt%	39.5		
Added Catalyst, wt%	none		
Mo Concentration, mg/kg mf coal	380		
Reaction Results			
THF Coal Conv	106	106	107
Gas Yield	22	32	32
565 °C+ Resid Conv	44	47	52
565 °C+ Resid Conv (on maf coal)	92	98	110
H_2 consumption, wt%	4.6	5.4	5.9

Table 4. Catalyst Screening Test Results with Added Wilsonville Run 262E Mo-Containing Solids 440 °C, 30 min, 1350 psig, 2 vol% H_2S/H_2					
Run No.	IV	V	VI	VII	VIII
Source of Run 262E extract	none	filtered	Soxhlet	none	filtered
Feed Composition					
Run 262E extract, wt%	none	12.4	12.6	none	12.4
Mo Concentration, mg/kg mf coal	none	295	300	none	300
Coal, mf, wt%	35	31	31	35	30
Run 258 565 °C- Distillate, wt%	21.5	18.8	22.4	-	-
Run 258 565 °C+ Deashed Resid, wt%	43.6	38.1	35.3	-	-
Run 258 Filtered Recycle Solvent, wt%	-	-	-	65	57.6
Reaction Results					
THF Coal Conv	68	99	101	77	111
Gas Yield	21	21	19	20	20
524 °C+ Resid Conv	19	23	24	18	26
524 °C+ Resid Conv (on maf coal)	41	57	59	35	58
H_2 consumption, wt%	1.7	4.2	3.9	1.9	4.3

Figure 1

Resid Conversion in 262E Recycle Solvent

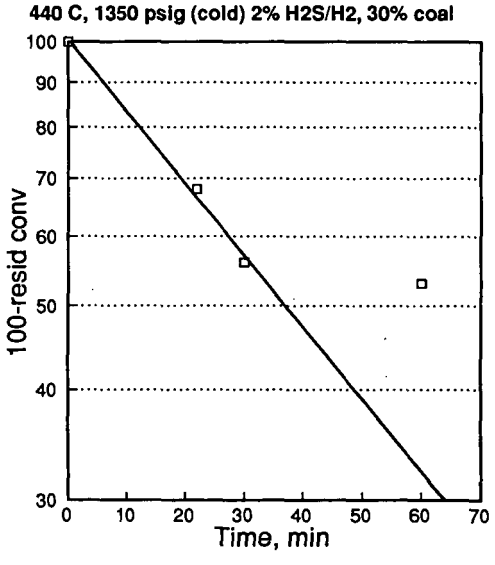

EVALUATION OF FINE-PARTICLE SIZE CATALYSTS USING BITUMINOUS AND SUBBITUMINOUS COALS

Frances V. Stohl, Kathleen V. Diegert, David C. Goodnow
Process Research Dept. 6212
Sandia National Laboratories
P.O. Box 5800
Albuquerque, NM 87185-0709

Keywords: Coal liquefaction; Fine-particle size catalysts; Catalyst test procedures

ABSTRACT

The objectives of Sandia's fine-particle size catalyst testing project are to evaluate and compare the activities of fine-particle size catalysts being developed in DOE/PETC's Advanced Research Coal Liquefaction Program by using Sandia's standard coal liquefaction test procedures. The first test procedure uses bituminous coal (DECS-17 Blind Canyon coal), phenanthrene as the reaction solvent, and a factorial experimental design that is used to evaluate catalysts over ranges of temperature, time, and catalyst loading. The best catalyst evaluated to date is West Virginia University's iron catalyst that was impregnated onto the coal. Current work is aimed at developing a standard test procedure using subbituminous Wyodak coal. This test is being developed using Pacific Northwest Laboratories' 6-line ferrihydrite catalyst and coal samples impregnated with either molybdenum or iron at Argonne National Laboratories. Results of testing catalysts with bituminous coal will be summarized and the development of the subbituminous coal test procedure will be presented.

INTRODUCTION

There are several potential advantages of using cheap, unsupported, fine-particle size (<40 nm) catalysts in direct coal liquefaction. Among these are improved coal/catalyst contact due to good dispersion[1] of the catalyst, and the potential for using low quantities of catalyst (<0.5% based on the weight of coal) because of their very high surface areas. These catalysts could be combined with the coal as either active catalysts or catalyst precursors that would be activated in situ. Research efforts to develop fine-particle size, unsupported catalysts for direct coal liquefaction[2,3] indicate that the use of these catalysts could result in significant process improvements, such as enhanced yields of desired products, less usage of supported catalyst, and possibly lower reaction severities. Realization of these improvements would result in decreased costs for coal liquefaction products.

The goal of Sandia's project is to evaluate and compare the activities/selectivities of fine-particle size catalysts being developed in the DOE/PETC Advanced Research (AR) Liquefaction Program by using standard coal liquefaction activity test procedures. Since bituminous and subbituminous coals have significantly different properties, it is feasible that catalysts may perform differently with these coal types. Because all previous testing has been done with the DECS-17 Blind Canyon bituminous coal, it is important to develop the capability of evaluating catalysts using a subbituminous coal. Wyodak coal from the Argonne Premium Coal Sample Program[4] was chosen for development of this test primarily because there has been significant research work done with Argonne's premium coals and because using existing well characterized samples eliminates the need to collect, prepare, and characterize another coal. The purpose of the current work is to develop a test using the Wyodak subbituminous coal.

EXPERIMENTAL SECTION

Materials. Two coals are being used in this project. DECS-17 Blind Canyon bituminous coal was obtained from The Penn State Coal Sample Bank[5]. It's a high volatile A bituminous coal with 3.74% moisture, 0.36% iron, 0.02% pyritic sulfur, and 7.34% mineral matter (on a dry basis). The particle size is -60 mesh. Subbituminous Wyodak coal was obtained from the Argonne Premium Coal Sample Program. It has 28.09% moisture, 0.17% dry pyritic sulfur, and 9.82% mineral matter (on a dry basis using the Parr formula). Phenanthrene is used as the reaction solvent. Elemental sulfur was added to the reactors to sulfide catalyst precursors.

Microautoclave Reactors. Testing is performed using batch microautoclaves made of type 316 stainless steel components. The total volume of a reactor is 43 cm^3 with a liquid capacity of 8 cm^3. The reactors are loaded with 1.67g coal and 3.34g phenanthrene. If the reaction is catalytic, the catalyst loading is either 0.5 wt% or 1.0 wt% of the amount of coal loaded into the reactor. The amount of sulfur addition (if needed) is specified by the catalyst developer. Reactors are charged to 800 psig H_2 (cold charge) and heated to reaction temperatures in fluidized-sand baths. Temperatures, pressures and times are recorded with a digital data acquisition system every 30 seconds during the course of the reactions. Following the heating period, the reactors are rapidly cooled to ambient temperature in a water bath and a gas sample is collected. The reaction data is analyzed to determine the actual reaction time and the averages and standard deviations for reaction temperature and pressure. Heat-up times and cooling times are also determined.

Product Workup Procedures. The reaction products are rinsed out of the reactors with tetrahydrofuran (THF). THF and heptane solvent solubilities are measured using a Millipore 142 mm diameter pressure filtration device with air pressurization and Duropore (0.45 micron) filter paper. The filter cakes are rinsed twice with THF or heptane as appropriate. After the filtrations are complete, the filter papers are dried under vacuum at 70°C, cooled to room temperature, and weighed to determine the insoluble portions. The THF soluble material is quantitatively sampled for gas chromatographic (GC) analysis, which is used to determine the reaction solvent recovery and final composition. THF is removed from the solubles by rotary evaporation prior to determining heptane conversion. The quantity of gases (CO, CO_2, CH_4, C_2H_6) produced in a reaction is calculated using the post-reaction vessel temperature and pressure with the ideal gas law and the mole percents in the gas sample as determined using a Carle GC and standard gas mixtures.

Factorial Experimental Design and Analysis. The factorial experimental design (Figure 1) evaluates the effects of three variables at two levels: temperature (350 and 400°C), time (20 and 60 minutes), and catalyst loading of either 0.0 wt% or 1.0 wt% of the amount of coal loaded into the reactor. With this full factorial experimental design, the experimental results are evaluated for all combinations of levels of the three variables so that 2^3 evaluations are required. Additional reactions are performed at the center point of this cubic design. An Analysis of Variance (ANOVA) is performed to estimate the effects of the experimental variables and to statistically test their significance. Replication of the experiments is used to estimate measurement error and to reduce its effect on the estimated effects of the variables. Models are constructed using the estimates of the effects of the variables to calculate the expected experimental results for specified sets of reaction conditions[6]. The controlled faetors used in the ANOVA are the measured average reaction temperature, measured reaction time, and the actual weight of catalyst used.

Catalyst. The catalyst chosen for development of the subbituminous coal test was a 6-line ferrihydrite catalyst precursor supplied by J. Linehan of Pacific Northwest National Laboratories (PNNL). This catalyst had been evaluated previously using Sandia's standard test procedure with Blind Canyon coal. It was the best catalyst in the form of a powder found to date. No pretreatment is required. Testing of this material used a 1:1 sulfur to catalyst precursor ratio on a weight basis. All reactions including thermal reactions had the same amount of added sulfur.

RESULTS AND DISCUSSION

Procedure for Comparing the Wyodak Coal with the DECS-17 Blind Canyon Coal

Testing of fine-particle size catalysts at Sandia has been based on a test using DECS-17 Blind Canyon coal, a bituminous coal. Since bituminous and subbituminous coals have significantly different properties, it is feasible that some catalysts may perform better with one coal type than with the other coal type. Therefore, it is important to have the capability of evaluating catalysts using a subbituminous coal. Wyodak coal from the Argonne Premium Coal Sample Program was chosen for development of this test primarily because there has been significant researeh work done with Argonne's premium coals and because using available samples eliminates the need to collect, prepare and store another coal.

One aspect of developing a test with Wyodak coal entails determining how results will be compared to those obtained with Blind Canyon coal. To do this comparison, we decided to evaluate Wyodak coal with PNL's 6-line ferrihydrite catalyst that had been evaluated previously at Sandia using the Blind Canyon coal. This is the best catalyst in the form of a powder evaluated to date at Sandia. The same factorial experimental design that is being used in the Blind Canyon coal test will be used with Wyodak coal. This decision was made because it was felt that the ranges of the three variables were broad cnough to also apply to the Wyodak coal. One of the many significant differences between Blind Canyon coal and Wyodak coal is the moisture content: Blind Canyon coal has 3.74% water and Wyodak has 28.09% water. To ensure that good comparisons could be made, the Wyodak coal was dried to about 6% water. This amount was chosen because it was close to the value for Blind Canyon coal and was also close to the water contents of several coal samples that had been impregnated with either Mo or Fe by Karl Vorres at Argonne National Laboratory. The Fe impregnated sample had 6.79% water and the Mo impregnated sample had 6.19% water. These impregnated coals will be evaluated after the subbituminous coal test is finalized. The dry sulfur contents of the Wyodak coal and the DECS-17 Blind Canyon coal are 0.63% and 0.44% respectively. The dry mineral matter is 10.01% for Wyodak coal (based on the modified Parr formula) and 7.49% for the DECS-17 coal.

Experimental Test Procedure

The testing used 1.67g Wyodak coal, 3.34g phenanthrene, and 1 wt % sulfur for all reactions. Catalyst loadings were either 0%, 0.5%, or 1.0 wt % based on thc experimental design. Sulfur was added to all reactions because previous studies with Blind Canyon coal showed that Fe in the mineral ankerite was converted to pyrrhotite during reaction thus yielding a catalytic effect. The impact of sulfur addition on Wyodak coal conversion will be quantified by comparing results to reactions of Wyodak coal without sulfur addition. Figure 1 shows the factorial experimental design used in the testing.

Testing Results for PNL's 6-Line Ferrihydrite Catalyst with Wyodak Coal

Results for THF conversion (%), heptane conversion (%), 9,10-dihydrophenanthrene (DHP (%)) in the reaction product, and gas yield (mol%) from this testing are shown in Figures 2-5. The values in

parentheses for each reaction condition are the average measured values obtained using PNL's catalyst with the Blind Canyon coal. The following discussion is based on these measured results. A statistical analysis of this data is currently being performed and will include a comparison of the Blind Canyon coal results and the Wyodak coal results.

Results for THF conversion (Figure 2) suggest that at low severity conditions (350°C, no catalyst), THF conversions are about 7.5% (absolute) lower for Blind Canyon coal. However, for all other conditions THF conversions are higher for Blind Canyon coal. At the most severe reaction condition (400°C, 60 minutes, 1% catalyst), Blind Canyon coal yielded 89.6 % conversion whereas Wyodak coal gave about 75.5%.

Results for heptane conversion (Figure 3) suggest that Wyodak coal may give higher heptane conversions for most if not all reaction conditions. Results at the lowest severity condition (350°C, 20 minutes, 0% catalyst) show a small negative conversion (-3.0%) for Blind Canyon coal, but an average conversion of 9.9% was obtained for Wyodak coal. Results at the highest severity condition (400°C, 60 minutes, 1% catalyst), gave an average 34.3% conversion for Wyodak coal but only 26.8% for Blind Canyon coal. Results at 400°C without catalyst show some overlap of results from the two coals. The statistical analysis will determine what differences are statistically significant.

Figure 4 shows the weight % of DHP (based on GC analyses of phenanthrene and DHP in the reaction product) after completion of the run. Results suggest that the Blind Canyon coal yields more DHP at all reaction conditions. At 400°C, 60 minutes, 1% catalyst, there is almost double the amount of DHP in the reaction product with Blind Canyon coal. The lower DHP in the product of the Wyodak reactions may be due to several causes. One possibility is that some of the hydrogen in the DHP is transferred to additional light reaction products as evidenced by higher heptane conversions with Wyodak coal. This could be due to Wyodak's lower coal rank. Another possibility is that Blind Canyon coal may yield higher DHP because some of the ankerite in the coal may get converted to pyrrhotite during the reaction and thus yield extra hydrogenation catalyst.

Figure 5 shows the total amount of gases (CO, CO_2, CH_4, C_2H_4) produced at each reaction condition. Results suggest that there are significantly more gases present with the Wyodak coal. For Blind Canyon coal, the total amount of gases ranges from about 0.30 to 1.86 mol% whereas for Wyodak coal the total amount ranges from about 1.90 to 4.35 mol%. In all cases, CO_2 is by far the biggest contributer to the gas yield, which was also observed with Blind Canyon coal.

CONCLUSIONS

Initial efforts towards developing a subbituminous coal test are aimed at comparing the reactivities of the Wyodak subbituminous coal and the Blind Canyon bituminous coal. Therefore, the same factorial experimental design was used with the Wyodak coal as was used previously with the Blind Canyon coal. In addition, PNL's 6-line ferrihydrite catalyst precursor was used in the development of the Wyodak coal test procedure because this catalyst is the best powder catalyst found to date in Sandia's tests with Blind Canyon coal. Results show that Blind Canyon coal yields higher DHP amounts in the reaction products and higher tetrahydrofuran (THF) conversions at the higher severity conditions. Wyodak coal gives higher heptane conversions and higher gas yields for all conditions tested.

FUTURE WORK

Future work on developing the catalyst test with Wyodak coal will include performing the statistical analyses of the results obtained from the experiments with PNL's 6-line ferrihydrite catalyst. Results from this study with Wyodak coal will be statistically compared to previous results obtained from Blind Canyon coal with PNL's catalyst.

Acknowledgment: This work was supported by the U.S. Department of Energy at Sandia National Laboratories under contract DE-AC04-94-AL85000.

REFERENCES

1. Huffman, G. P.; Ganguly, B.; Zhao, J.; Rao, K. R. P. M.; Shah, N.; Feng, Z.; Huggins, F. E.; Taghiei, M. M.; Lu, F.; Wender, I.; Pradhan, V. R.; Tierney, J. W.; Seehra, M. S.; Ibrahim, M. M.; Shabtai, J.; Eyring, E. M., Energy Fuels 1993, 7, 285-296.
2. Pradhan, V. R.; Tierney, J. W.; Wender, I. Energy Fuels 1991, 5, 497-507.
3. Stohl, F. V.; Diegert, K. V. Energy & Fuels 1994, 8, 117-123.
4. Users Handbook for the Argonne Premium Coal Sample Program, K. S. Vorres, Argonne National Laboratory, Argonne, Illinois, October 1993.
5. The Department of Energy Coal Sample Bank, DECS-Series Data Printouts, The Pennsylvania State University, August 1995.
6. John, P. W. M., Statistical Design and Analyses of Experiments; MacMillan Co., 1971.

FIGURE 1.

FACTORIAL EXPERIMENTAL DESIGN

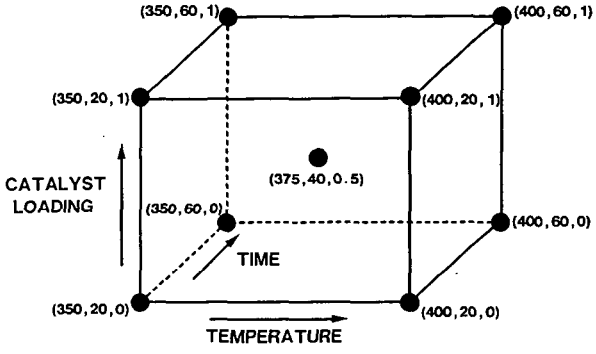

(TEMPERATURE = °C; TIME = MINUTES; CATALYST LOADING = WT % AR COAL)

FIGURE 2.

MEASURED THF CONVERSIONS
(PNL'S 6-LINE FERRIHYDRITE + WYODAK COAL)

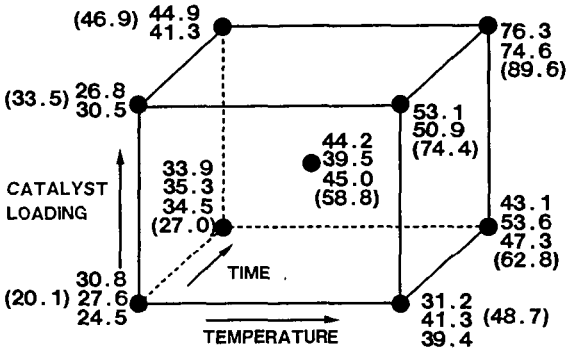

PARENTHESES = AVERAGE MEASURED VALUES FROM BLIND CANYON COAL

FIGURE 3.

MEASURED HEPTANE CONVERSIONS
(PNL'S 6-LINE FERRIHYDRITE + WYODAK COAL)

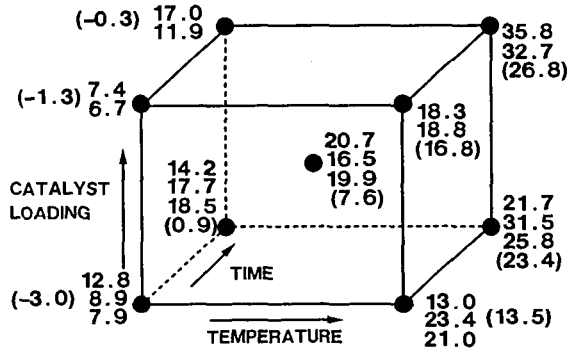

PARENTHESES = AVERAGE MEASURED VALUES FROM BLIND CANYON COAL

FIGURE 4.

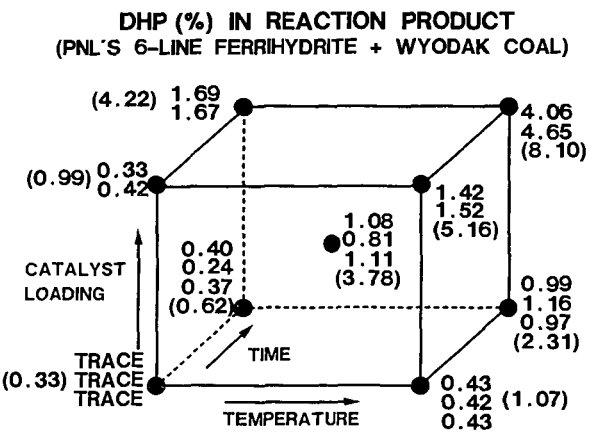

FIGURE 5.

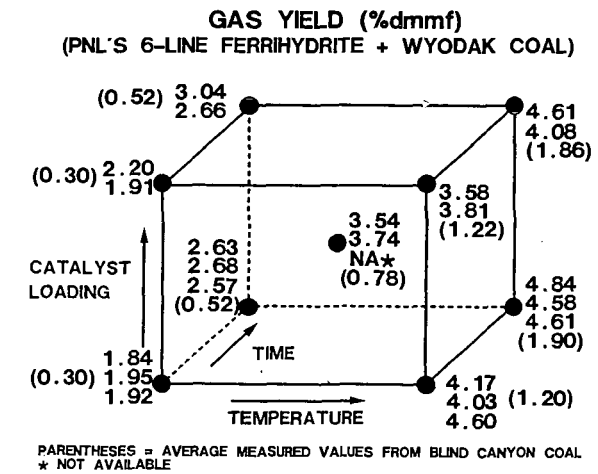

MÖSSBAUER INVESTIGATION OF MATERIALS USED IN SANDIA'S DCL CATALYST TESTING PROGRAM

K. R. P. M. Rao, Frank E. Huggins, G. P. Huffman
CFFLS, University of Kentucky, Lexington KY 40506-0043

and Frances V. Stohl
Sandia National Laboratories, Albuquerque, NM 87185

Keywords: Mössbauer spectroscopy, DCL catalysts, pyrrhotite

ABSTRACT

Mössbauer spectroscopy has been used to determine the iron-bearing phases in the coal, catalysts, and IOM products used and generated in the Direct Coal Liquefaction (DCL) catalyst testing program at Sandia National Laboratories, New Mexico. DCL experiments were conducted with a Blind Canyon, Utah, coal both thermally and with three different iron-based catalysts: (i) a sulfated hematite catalyst (Fe_2O_3/SO_4^{2-}), (ii) a 6-line ferrihydrite catalyst, and (iii) iron-oxide impregnated directly into coal. The catalysts were added to the coal at both a 0.5 and a 1.0 wt% level and sufficient sulfur was added to ensure complete sulfidation of the iron. The Mössbauer spectrum of the Blind Canyon coal revealed that the major iron-bearing mineral present was ankerite, $Ca(Fe,Mg)(CO_3)_2$, which converts first to γ-Fe (austenitic iron) before undergoing partial sulfidation to pyrrhotite in the thermal runs. The percentages of pyrrhotite formed in the catalytic runs were higher than those in the thermal runs indicating that sulfidation of the added iron occurs more rapidly than with the ankerite. Mössbauer data on the amount of pyrrhotite present does not correlate well with THF and heptane conversion percentages, indicating that other parameters like catalyst dispersion must also be considered.

INTRODUCTION

It is well recognized that iron-based materials represent the best option for development of a low-cost, disposable catalyst for direct coal liquefaction (DCL) [1]. As a result, much effort has been recently directed towards the development of iron-oxide-based catalysts for DCL by many groups [2]. However, owing to differences in DCL testing procedures at different laboratories, it has not always been possible to compare directly the conversion and cost effectiveness of different catalyst formulations. The DCL catalyst testing program at Sandia National Laboratories was designed to resolve such uncertainties by providing a facility for the DCL research community where the effectiveness of different catalysts could be directly compared [3]. Each catalyst would be subjected to the same matrix of tests on the same coal (Blind Canyon, UT, DECS-17) under identical conditions and the analysis of the DCL products would also be standardized.

In the current study, Mössbauer spectroscopy has been used to characterize the iron in various starting materials and products from the Sandia DCL program in order to provide additional baseline information for the program. Mössbauer investigations have been carried out on the following materials:

A. (1) Blind Canyon Coal (DECS-17)

(2) A sulfated hematite catalyst, Fe_2O_3/SO_4^{2-}, from the University of Pittsburgh

(3) A 6-line ferrihydrite catalyst from Pacific Northwest Laboratories

(4) An iron-oxide based catalyst impregnated into Blind Canyon Coal from West Virginia University

B. THF-insoluble residues generated in thermal liquefaction runs at 350°C for 20 min and at 400°C for 60 min.

C. THF-insoluble residues generated in liquefaction runs with the sulfated hematite catalyst at:

350°C	20 min	1.0 wt% catalyst loading and 1 wt% sulfur
375°C	40 min	0.5 wt% catalyst loading and 1 wt% sulfur
400°C	60 min	1.0 wt% catalyst loading and 1 wt% sulfur

D. THF-insoluble residues generated in liquefaction runs with the ferrihydrite catalyst at:

350°C	20 min	1.0 wt% catalyst loading and 1 wt% sulfur
375°C	40 min	0.5 wt% catalyst loading and 1 wt% sulfur
400°C	60 min	1.0 wt% catalyst loading and 1 wt% sulfur
400°C	60 min	1.0 wt% catalyst loading and 2 wt% sulfur

E. THF-insoluble residues generated in liquefaction runs with the iron-oxide catalyst impregnated in Blind Canyon Coal at:

350°C	20 min	1.0 wt% catalyst loading and 1 wt% sulfur
400°C	60 min	1.0 wt% catalyst loading and 1 wt% sulfur

EXPERIMENTAL

The thermal and catalytic DCL experiments were carried out under 800 psig H_2 in microreactors at Sandia National Laboratories with the above catalysts and sufficient sulfur to ensure complete sulfidation of the iron [3]. Oil and total conversions, defined as the percentages of the sample after DCL that were soluble in heptane and tetrahydrofuran, respectively, were also determined at Sandia [3]. Samples of the residues and starting materials were shipped to the University of Kentucky for Mössbauer analysis. Mössbauer analysis was carried out using a Halder, GmbH, Mössbauer drive operating in the symmetric saw-tooth mode. A calibration spectrum of metallic iron was obtained at the opposite end of the drive at the same time as the unknown spectrum was being acquired. Each spectrum was acquired over 512 channels representing a velocity range of between ±8 and ±12 mm/s using Canberra/Nuclear Data multichannel scaling units located in 286DX personal computer. Spectra were obtained from all samples at room temperature and from a few samples at cryogenic temperatures as low as 13 K. Analysis of the Mössbauer spectra was conducted in the manner described previously [4,5]. Spectra were fit by means of a least-squares fitting routine as a combination of 6-line magnetic spectra, 2-line quadrupole doublets and single lorentzian-shaped peaks. Identification of the iron-bearing phases present in the samples was based solely on the values obtained for the isomer shift, quadrupole splitting, and magnetic hyperfine splitting of the individual components in the fits. The relative percentages of iron present in the different phases were derived from the areas under the individual components. Mössbauer results for the thermal and catalytic residues from the DCL tests are summarized in Tables I - III for the three different catalysts.

RESULTS AND DISCUSSION

The Mössbauer spectrum of Blind Canyon (DECS-17) coal is shown as Figure 1. The spectrum consists of one major doublet from which the principal iron-bearing mineral in the coal is identified as ankerite, $Ca(Fe,Mg)(CO_3)_2$. It has the same isomer shift (1.23±0.01 mm/s), but a significantly smaller quadrupole splitting (1.67±0.02 mm/s) than that reported [4] for siderite (1.80±0.02 mm/s). Although no positive evidence was established for the presence of pyrite in this coal, it is possible that as much as 5% of the iron could be present as FeS_2. This minor contribution cannot be resolved owing to the overlap of the low-velocity ankerite peak with the pyrite peaks coupled with the relatively poor signal/noise ratio as a result of the low iron content of this particular coal.

Essentially the same results were obtained with the three thermal runs at the two different temperatures. In the thermal residues prepared at 350°C, ankerite, and austenitic or γ-iron were observed; at 400°C (q.v. Figure 2), significant pyrrhotite ($Fe_{1-x}S$), in addition to ankerite (with a smaller quadrupole splitting, 1.52 mm/s, than was found at 350°C) and γ-Fe, was also observed. These observations imply that ankerite in the coal reduces partially to γ-Fe, which then reacts with sulfur to form pyrrhotite.

The Mössbauer spectra of the sulfated hematite consisted of a magnetic component attributed to hematite and a poorly resolved doublet that represents the sulfated surface of the hematite particles and/or superparamagnetic (spm) iron oxide particles of small size (less than about 10 nm [5]). The other two catalysts exhibited only a broad doublet in their Mössbauer spectra; such spectra are consistent with ferrihydrite, either as a separate phase [6,7] or formed by impregnation directly on the coal [7].

The Mössbauer spectra of the catalytic residues (e.g. Figure 3) were similar to each other for the most part. However, the residues from the ferrihydrite and impregnated catalysts did show the persistence of a doublet attributed to unreacted spm iron oxides that was not apparent with the sulfated hematite catalyst. The relative amount of pyrrhotite

Table I

Mössbauer analysis of iron-bearing phases in
THF insolubles from thermal and catalytic reactions
with a sulfated hematite catalyst and Blind Canyon Coal

Sample	Gamma-Fe	Ankerite	Pyrrhotite
350, 20 min, thermal	14	86	
350, 20 min, 1 wt%	26	33	41
375, 40 min, 0.5 wt%	16	33	51
400, 60min, thermal	20	37	43
400, 60 min, 1 wt%	10	21	69

Table II

Mössbauer analysis of iron-bearing phases in
THF insolubles from thermal and catalytic reactions of
with a 6-line ferrihydrite catalyst and Blind Canyon Coal

Sample	γ-Fe	Ankerite	Pyrrhotite	FeOOH/Oxide
As received 6-line ferrihydrite				100 FeOOH
350, 20 min, thermal	13	87		
350, 20 min, 1 wt%	6	28	42	24
375, 40 min, 0.5 wt%	8	25	57	10
400, 60 min, thermal	18	36	46	
400, 60 min, 1 wt%	1	13	68	18
400, 60 min, 1 wt% 2 wt% added sulfur	10	18	67	5

Table III

Mössbauer analysis of iron-bearing phases in
THF insolubles from thermal and catalytic reactions
with iron-oxide impregnated Blind Canyon Coal

Sample	γ-Fe	Ankerite	Pyrrhotite	FeOOH/Oxide
Coal impregnated with iron and sulfur compounds		31		69
350, 20 min, thermal	23	77		
350, 20 min, 1 wt% catalyst in coal	25	25	31	19
400, 60 min, thermal	15	36	49	
400, 60 min, 1 wt% catalyst in coal	5	16	51	28

formation in all three catalytic runs was greater than that in the corresponding thermal run at the same temperature indicating that the iron-based catalyst undergoes sulfidation much more rapidly than the ankerite in the original coal.

The THF conversions for the catalytic runs at 400°C, 60 min, with 1% loading for the sulfated hematite, 6-line ferrihydrite, and impregnated iron-oxide catalysts were 82.3%, 89.4% and 93.2%, respectively. These values do not show a direct correlation with %Fe as pyrrhotite listed in Tables I - III, but do correlate with %Fe remaining as spm oxide.

CONCLUSIONS

Iron in Blind Canyon coal (DECS-17) is present principally in the form of ankerite, $Ca(Fe,Mg)(CO_3)_2$, which is converted during thermal tests, first to γ-Fe and then to pyrrhotite. The conversion is not complete even after 60 mins at 400°C. In contrast, sulfidation of the catalyst materials is more rapid and is essentially complete in the case of the sulfated hematite catalyst at 350°C and nearly so in the case of the 6-line ferrihydrite and impregnated iron-oxide catalysts. With the latter two catalyst materials, a small fraction (up to 25%) of the catalyst persists as spm iron-oxide even to the most severe conditions employed for DCL (400°C, 60 min). It is this fraction of iron present as remnant spm iron-oxide, and not as pyrrhotite, that appears to show a direct correlation with the total DCL conversion percentages. This observation implies that there are significant differences in the ease of sulfidation of the iron-oxides to form pyrrhotite among the three catalysts that are also reflected in the dispersion and size of the pyrrhotite particles. It is these parameters that may have the most influence on the activity of the sulfided iron catalyst during the DCL process.

REFERENCES

1. Huffman, G. P., et al. *Energy & Fuels*, **1993**, *7(2)*, 285-296.
2. Proceedings of an ACS Division of Fuel Chemistry Symposium on Iron-based Catalysts for Coal Liquefaction, (M. Farcasiu, G. P. Huffman, and I. Wender, Eds.) *Energy & Fuels*, **1994**, *8(1)*, 2-123.
3. Stohl, F. V., and Diegert, K. V., *Energy & Fuels*, **1994**, *8(1)*, 117-123.
4. Huggins, F. E., and Huffman, G. P. in *Analytical Methods for Coal and Coal Products*, (C. Karr, Jr., Ed.), Volume III, Academic Press, NY, 1979, 371-423.
5. Ganguly, B., Huggins, F. E., Rao, K. R. P. M., and Huffman, G. P. *J. Catalysis*, **1993**, *142*, 552-560.
6. Schwertmann, U., and Cornell, R. M. *Iron Oxides in the Laboratory*, VCH, Weinheim, Germany, 1991.
7. Zhao., J., Feng, Z., Huggins, F. E., and Huffman, G. P. *Energy & Fuels*, **1996**, *10(1)*, 250-253.

ACKNOWLEDGEMENTS

This work was supported by the research program of the Consortium for Fossil Fuel Liquefaction Science (CFFLS) under contract with the U.S. Department of Energy and the Commonwealth of Kentucky. We also express our gratitude to Drs. Malvina Farcasiu and V.U.S. Rao of the Pittsburgh Energy Technology Center for their interest in and initiation of the work described here.

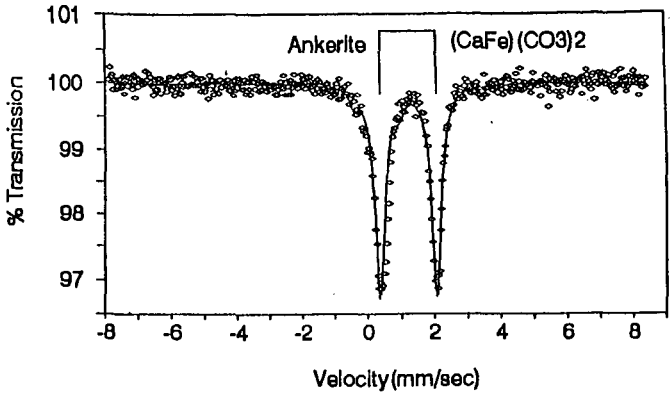

Fig.1 Mossbauer spectrum of Blind Canyon Coal

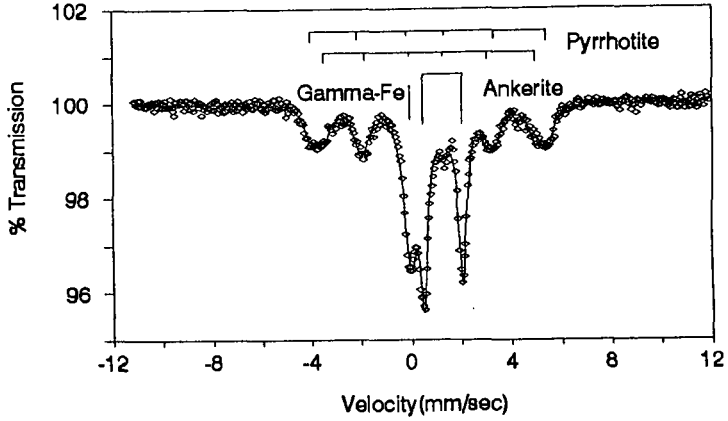

Fig.2 Mossbauer spectrum of THF insoluble from the run at 400C, 60min, without any catalyst (thermal)

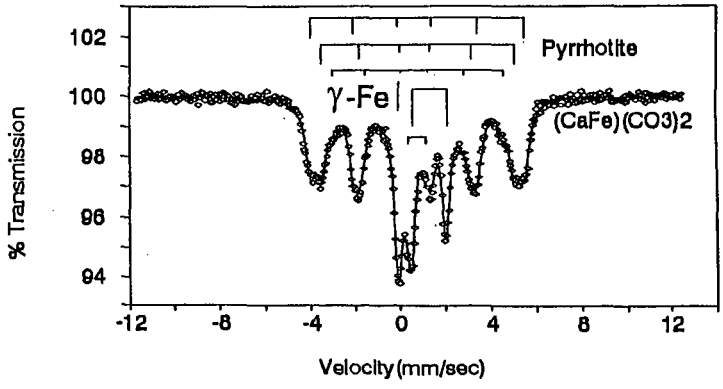

Fig.3 Mossbauer spectrum of THF insoluble from the run at 400C, 60min with Wender's 1% catalyst

SUPPORT CHEMISTRY, SURFACE AREA, AND PREPARATION EFFECTS ON SULFIDED NiMo CATALYST ACTIVITY

Timothy J. Gardner, Linda I. McLaughlin, and Ronald S. Sandoval
Sandia National Laboratories
Process Research Department, Mail Stop 0709
P.O. Box 5800
Albuquerque, NM 87185-0709

Keywords: oxide supports, hydrotreating catalysts, hydrous titanium oxide

INTRODUCTION

Hydrous Metal Oxides (HMOs) are chemically synthesized materials which contain a homogeneous distribution of ion exchangeable alkali cations that provide charge compensation to the metal-oxygen framework. In terms of the major types of inorganic ion exchangers defined by Clearfield,[1] these amorphous HMO materials are similar to both hydrous oxides and layered oxide ion exchangers (e.g., alkali metal titanates). For catalyst applications, the HMO material serves as an ion exchangeable support which facilitates the uniform incorporation of catalyst precursor species. Following catalyst precursor incorporation, an activation step is required to convert the catalyst precursor to the desired active phase.

Considerable process development activities at Sandia National Laboratories related to HMO materials have resulted in bulk hydrous titanium oxide (HTO)- and silica-doped hydrous titanium oxide (HTO:Si)-supported NiMo catalysts that are more active in model reactions which simulate direct coal liquefaction (e.g., pyrene hydrogenation) than commercial γ-Al_2O_3-supported NiMo catalysts.[2-7] However, a fundamental explanation does not exist for the enhanced activity of these novel catalyst materials; possible reasons include fundamental differences in support chemistry relative to commercial oxides, high surface area, or catalyst preparation effects (ion exchange vs. incipient wetness impregnation techniques). The goals of this paper are to identify the key factors which control sulfided NiMo catalyst activity, including those characteristics of HTO- and HTO:Si-supported NiMo catalysts which uniquely set them apart from conventional oxide supports.

EXPERIMENTAL PROCEDURE

Support chemistry effects were examined using both commercially-available oxide supports and HTO/HTO:Si supports. Commercial oxide supports studied included γ-Al_2O_3 (in extrudate form, 1/16 in. diameter) and various commercial forms of TiO_2. In order to fairly evaluate the effect of support chemistry between the commercial oxide and HTO/HTO:Si supports, it was necessary to normalize the Mo loadings per unit surface area. This approach has been previously used with success to differentiate support chemistry effects for hydrodesulfurization reactions.[8] Because it is well known that the surface area of oxide support materials can change significantly with processing (Mo loading, calcination, etc.), it was necessary to select a specific processing state to use as a reference point for catalyst support surface area. We used the support surface area after a standard calcination treatment in air at 500°C for 1 h as a reference point, since this would effectively represent the amount of support surface area available to disperse the molybdenum oxide phase which formed during the calcination procedure.

Table 1 shows the differences between the various supports evaluated in this study in terms of the method of preparation and their surface area, both as-received and after a standard calcination procedure. The surface area of the γ-Al_2O_3 extrudate is fairly typical of γ-Al_2O_3 catalyst supports, and was relatively unchanged after the calcination treatment. The titania supports exhibited different thermal stabilities depending on the preparation method, with the calcined surface area values correlating well with the crystallographic phase evolution of TiO_2. The Degussa P25 TiO_2, prepared by a high temperature flame hydrolysis procedure, showed only a slight decrease in surface area as a result of the calcination procedure. This moderate surface area material consisted of a mixture of anatase and rutile phases of TiO_2. The Tioxide TiO_2 material is prepared via a precipitation process using sulfate precursors followed by low temperature heat treatment to produce a high surface area anatase material. Further heat treatment of this material via calcination

resulted in significant surface area reduction and partial conversion of anatase to rutile. The HTO and HTO:Si supports were evaluated in acidified form following complete H^+/Na^+ exchange. In their as-prepared forms, these materials exhibit very high surface areas (~400 m^2/g). These acidified forms are generally representative of the final HTO or HTO:Si support material which remains following ion exchange (IE) processing. Calcination of these as-prepared materials results in significant surface area reduction. However, SiO_2 additions to HTO materials act to stabilize support surface area at high temperature ($\geq$ 500°C) without significantly altering ion exchange properties.[6,7,9] The improved thermal stability of the HTO:Si supports is due to the retardation of the anatase to rutile phase transformation by the SiO_2 dopant, which has been extensively documented in the literature.[10-13]

Table 1
Oxide Support Characteristics

Support Material	Preparation Technique	As-Received Surface Area (m^2/g)	Calcined Surface Area (m^2/g)*
Degussa P25 TiO_2	Flame Hydrolysis	52	47
Tioxide TiO_2	Precipitation	183	120
H^+/HTO	Sol-Gel + IE	417	63
H^+/HTO:Si	Sol-Gel + IE	390	184
γ-Al_2O_3 Extrudate	Precipitation + Extrusion	235	227

* Calcination procedure: 500°C/1h/air. Surface area was measured by the BET method.

HTO and HTO:Si ion exchangeable supports (Na:Ti and Si:Ti molar ratios = 0.5 and 0.2, respectively) were fabricated using the standard multiple step sol-gel chemistry procedure which has been described in detail elsewhere.[3,6,7,14] HTO- and HTO:Si-supported NiMo catalyst preparation was performed using a two step procedure featuring Mo anion ($[Mo_7O_{24}]^{-6}$) exchange/adsorption followed by incipient wetness impregnation using $Ni(NO_3)_2{\cdot}6H_2O$. For the commercial oxide-supported NiMo catalysts, only incipient wetness impregnation techniques were used; two separate impregnation steps were used, first with ammonium heptamolybdate ($(NH_4)_6Mo_7O_{24}{\cdot}4H_2O$), and next with nickel nitrate ($Ni(NO_3)_2{\cdot}6H_2O$) precursors. Supported Mo and NiMo catalysts with Mo loadings ranging from 0.6 to 25 Mo atoms/nm^2 support surface area were fabricated as part of this study. This range of Mo loadings corresponded to a wide overall range of Mo weight loadings, 0.1 to 25 wt.% (calcined basis), on the various supports. Regardless of the Mo loading level in the catalyst, a constant ratio of moles Ni/(moles Ni + moles Mo) = 0.35 was used to determine the Ni loading for each supported NiMo catalyst.

The final catalyst precursors were activated by first calcining in air at 500°C for 1 h and then sulfiding in 10% H_2S in H_2 at 420°C for 2 h. All TiO_2 (including HTO and HTO:Si)-supported catalysts were pelletized and granulated to -10/+20 mesh prior to activation, and all catalysts were ground and sieved to -200 mesh prior to testing. Catalyst activity was evaluated using two different model reactions representative of hydrotreating reactions: pyrene hydrogenation and dibenzothiophene hydrodesulfurization. For the pyrene hydrogenation tests, pyrene (0.1 g), hexadecane (1 g), and catalyst (0.010 g) were loaded into a batch microautoclave reactor and tested at 300°C under 500 psig H_2 for 10 min. For the dibenzothiophene hydrodesulfurization tests, dibenzothiophene (0.1 g), hexadecane (1 g), and catalyst (0.050 g) were loaded into a batch microautoclave reactor and tested at 350°C under 1200 psig H_2 for 10 min. Reversible first-order kinetics were used to model the pyrene hydrogenation test results,[15] while irreversible first-order kinetics were used to model the dibenzothiophene hydrodesulfurization test results.[16]

RESULTS AND DISCUSSION

Figure 1 summarizes the catalyst activity trends observed for the pyrene hydrogenation testing of the sulfided NiMo catalysts. This type of figure, plotting the intrinsic pyrene hydrogenation activity (rate per g total active metal [Ni+Mo]) vs. specific Mo loading (in Mo atoms/nm^2 calcined support surface area) is used to

normalize surface area differences among the various supports examined in this study. For NiMo/γ-Al_2O_3 catalysts, the intrinsic pyrene hydrogenation activity is stable at low specific Mo loadings, but decreases with increasing specific Mo loading. This behavior is in contrast to that observed for TiO_2-supported catalysts (including HTO and HTO:Si supports), where we find that a maximum in intrinsic pyrene hydrogenation activity is observed as specific Mo loading is increased. Very similar trends, including the location and value of the maximum in the intrinsic pyrene hydrogenation activity, were observed for all of the commercial TiO_2 materials evaluated: Degussa P25 TiO_2, Tioxide TiO_2, and a low surface area (10 m^2/g) rutile form of TiO_2. The characteristic behavior of sulfided NiMo catalysts supported on these commercial TiO_2 support materials is illustrated in Figure 1 by the data shown for the Degussa P25 TiO_2-supported NiMo catalysts.

However, as shown in Figure 1, the location of the maximum in the intrinsic pyrene hydrogenation activity is different for the commercial TiO_2 supports with respect to the HTO or HTO:Si supports. Since the data shown in Figure 1 has been normalized to remove support surface area effects, the differences in behavior for the HTO and HTO:Si supports must be attributable to other fundamental differences in support chemistry or catalyst preparation effects. The HTO-supported NiMo catalysts show a broad range of relatively high activity with the maximum in activity shifted to higher specific Mo loadings. This behavior shows a distinct advantage over typical commercial catalysts since it accommodates higher overall catalyst activities at high weight loading. The controlled addition of SiO_2 to the HTO support produces significant changes in this behavior. The peak intrinsic pyrene hydrogenation activity shifts to very low specific Mo loadings (lower than those observed for the commercial titanias) and is significantly increased in magnitude. This result indicates an important role of the SiO_2 dopant, which might be well dispersed on the surface of small anatase crystallites, therefore affecting the dispersion of the catalytic doped MoS_2 phase.

Similar trends to those shown in Figure 1 were also observed for Mo only catalysts, although intrinsic pyrene hydrogenation activities were consistently lower. It should be noted that due to the limited number of data points for some of the curves in Figure 1 (e.g., Degussa P25 TiO_2 and γ-Al_2O_3 supports), we can only speculate on the presence and/or location of the maximum in catalyst activity. Obviously, more data is necessary to make firm conclusions with respect to these trends.

Similar studies have been performed using the dibenzothiophene hydrodesulfurization model reaction. Very different trends are observed for this model compound reaction in terms of the intrinsic catalyst activity vs. specific Mo loading. Thus far, a valid comparison has been made only with the γ-Al_2O_3-, TiO_2-, and HTO-supported Mo catalysts. These results are shown in Figure 2. In one case (P25 TiO_2 support), both Mo- and NiMo-supported catalysts have been tested. As shown in Figure 2, and consistent with a vast quantity of published literature, the addition of Ni results in a significant promotional effect for the dibenzothiophene hydrodesulfurization reaction.[17,18] However, the trends for TiO_2-supported catalysts are very different for dibenzothiophene hydrodesulfurization compared to pyrene hydrogenation (see Figure 1). All TiO_2-supported catalysts examined to date (including HTO supports) exhibit very high intrinsic activity for dibenzothiophene hydrodesulfurization at low specific Mo loadings, with activity sharply decreasing as Mo loading is increased. In contrast to this behavior, γ-Al_2O_3-supported catalysts exhibit behavior very similar to that observed for pyrene hydrogenation. These trends observed for dibenzothiophene hydrodesulfurization with the TiO_2 (including HTO)- and γ-Al_2O_3-supported Mo catalysts are consistent with those observed previously for thiophene hydrodesulfurization.[8] The fact that the intrinsic activity for all of the TiO_2-supported catalysts is higher than that observed for the γ-Al_2O_3-supported catalysts is also consistent with previous work.[8]

These early results indicate that different types of catalysts, in terms of Mo loading, are optimum for hydrogenation vs. hydrodesulfurization reactions. This is consistent with evidence published in the literature suggesting that hydrogenation and hydrodesulfurization reactions take place on different types of active sites.[19,20] These results also show that the HTO-or HTO:Si-based supports may offer more significant advantages for hydrogenation rather than hydrodesulfurization applications.

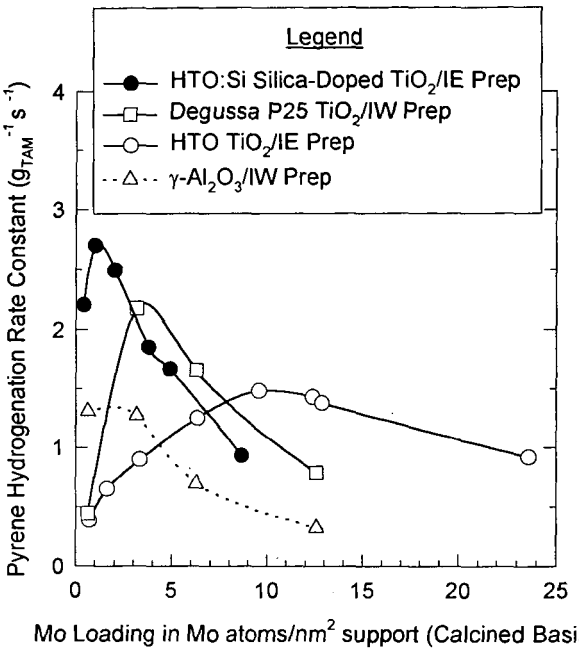

Figure 1. Intrinsic pyrene hydrogenation activity (rate per g total active metal) vs. specific Mo loading (in Mo/nm^2 support) for sulfided NiMo catalysts supported on various oxide supports. The acronyms IW and IE in the legend correspond to incipient wetness impregnation and ion exchange preparation techniques, respectively.

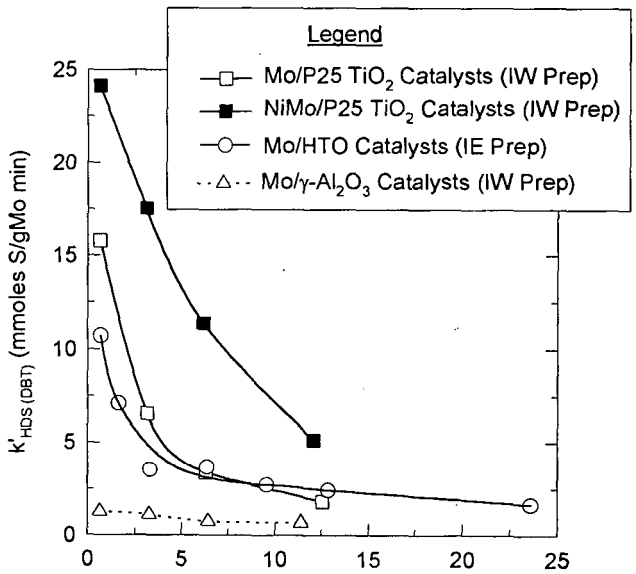

Figure 2. Intrinsic dibenzothiophene hydrodesulfurization activity results vs. specific Mo loading (in Mo atoms/nm^2 support) for selected sulfided Mo- and NiMo-based catalysts. Note that the acronyms shown in the legend were previously defined in the caption for Figure 1.

Additional work is necessary to further investigate the interesting behavior and potential benefits of the HTO- and HTO:Si-based supports. This work will include assessments of changes in MoS_2 dispersion as a function of Mo loading and support chemistry.

SUMMARY

This work has evaluated various catalyst support chemistries with a range of Mo loadings (normalized with respect to surface area) for both pyrene hydrogenation and dibenzothiophene hydrodesulfurization reactions. γ-Al_2O_3-supported Mo and NiMo catalysts were found to behave similarly with respect to both model reactions; intrinsic catalyst activity was relatively constant at low Mo loadings, but slightly decreased with increasing Mo loading. Significant differences were observed for the TiO_2 supports evaluated in this study, both with respect to the γ-Al_2O_3-supported catalyst results and for the different types of TiO_2 supports (including the HTO and HTO:Si materials). For pyrene hydrogenation, all TiO_2-supported catalysts showed a maximum in intrinsic catalyst activity, with the position of the maximum varying with changes in support chemistry and catalyst preparation procedures. In contrast to the pyrene hydrogenation results, all TiO_2-supported Mo catalysts showed a similar trend of significantly decreasing intrinsic catalyst activity with increasing Mo loading for the dibenzothiophene hydrodesulfurization model reaction. These results therefore indicate that HTO-based supports may offer more significant advantages for hydrogenation rather than hydrodesulfurization applications. Experiments are in progress to evaluate changes in MoS_2 dispersion as a function of support chemistry and Mo loading.

This work was performed at Sandia National Laboratories and was supported by the U.S. Department of Energy under contract DE-AC04-94AL85000.

REFERENCES

1. A. Clearfield, Ind. Eng. Chem. Res. **34**, 2865 (1995).
2. H. P. Stephens, R. G. Dosch, and F. V. Stohl, Ind. Eng. Chem. Res. Devel. **24**, 15 (1985).
3. H. P. Stephens and R. G. Dosch, Stud. Surf. Sci. Catal. **31**, 271 (1987).
4. S. E. Lott, T. J. Gardner, L. I. McLaughlin, and J. B. Oelfke, Submitted to Fuel.
5. S. E. Lott, T. J. Gardner, L. I. McLaughlin, and J. B. Oelfke, Prep. of Papers, Fuel Div., Amer. Chem. Soc. **39** 1073 (1994).
6. R. G. Dosch, H. P. Stephens, and F. V. Stohl, Sandia Report, SAND89-2400, Sandia National Laboratories, Albuquerque, NM, 1990.
7. R. G. Dosch and L. I. McLaughlin, Sandia Report, SAND92-0388, Sandia National Laboratories, Albuquerque, NM, 1992.
8. K. C. Pratt, J. V. Sanders, and V. Christov, J. Catal. **124**, 416 (1990).
9. T. J. Gardner and L. I. McLaughlin, Submitted to Mater. Res. Soc. Symp. Proc.
10. Y. Suyama and A. Kato, Yogyo-Kyokai-Shi **86**(3), 119 (1978).
11. C. U. I. Odenbrand, S. L. T. Andersson, L. A. H. Andersson, J. G. M. Brandin, and G. Busca, J. Catal. **125**, 541 (1990)
12. J. R. Sohn, H. J. Jang, M. Y. Park, E. H. Park, and S. E. Park, J. Mol. Catal. **93**, 149 (1994)
13. P. K. Doolin, S. Alerasool, D. J. Zalewski, and J. F. Hoffman, Catal. Lett. **25**, 209 (1994).
14. R. G. Dosch, H. P. Stephens, F. V. Stohl, B. C. Bunker, and C. H. F. Peden, Sandia Report, SAND89-2399, Sandia National Laboratories, Albuquerque, NM, 1990.
15. H. P. Stephens and R. J. Kottenstette, Prep. of Papers, Fuel Div., Amer. Chem. Soc. **30**, 345 (1985).
16. O. Weisser and S. Landa, Sulfide Catalysts, Their Properties and Applications, Pergamon Press, Oxford, 1973.
17. R. R. Chianelli, M. Daage, and M. J. Ledoux, Adv. Catal. **40**, 177 (1994).
18. M. J. Ledoux, S. Hantzer, and J. Guille, Bull. Soc. Chim. Belg. **96**(11-12), 855 (1987).
19. A. Stanislaus and B. H. Cooper, Catal. Rev.-Sci. Eng. **36**(1), 75 (1994).
20. M. Daage and R. R. Chianelli, J. Catal. **149**, 414 (1994).

HINDERED DIFFUSION OF COAL AND PETROLEUM ASPHALTENES IN A SUPPORTED HYDROTREATING CATALYST

Xiaofeng Yang and James A. Guin
Chemical Engineering Department, Auburn University, Auburn, AL 36849

Keywords: Diffusion, Mathematical Model, Asphaltenes

ABSTRACT

In this work, hindered diffusion of one coal and two petroleum asphaltenes was studied by adsorptive uptake in THF from a bath surrounding a commercial $NiMo/Al_2O_3$ catalyst. A mathematical model for the adsorption-diffusion of asphaltenes was developed. The model parameters were obtained by simulating the experimental data with the model solution. Several asphaltene fractions were defined via SEC (size exclusion chromatography), with the molecular weight of each fraction being determined by its elution characteristics using polystyrene standards. It was found that both the coal and petroleum asphaltenes have very broad molecular weight distributions; however, the molecular weights of the coal asphaltenes (50-1000) were much smaller than those of the two petroleum asphaltenes (300-10000 and 300-20000 respectively). The uptake rates for asphaltene fractions with different molecular weights were different, depending on their diffusion rates and adsorption capacities. Simulation results showed that even though the properties of coal and petroleum asphaltenes were quite different, the values of model parameters for the fractions of the three asphaltenes had the same trend; with increasing molecular weight of the fraction, the adsorption constant monotonically increases, and the effective diffusivity decreases. The experimental diffusion data of the three asphaltenes were well represented by similar mathematical models.

INTRODUCTION

Due to comparable sizes of reactant molecules and catalyst pores, hindered diffusion has been widely observed in the hydrotreatment of asphaltenes, heavy oils, coal derived liquids, and other macromolecular feeds. Direct measurements of asphaltene intrapore diffusion in porous catalysts are recent and very few in number. Baltus and Anderson (1983) studied hindered diffusion of petroleum asphaltenes through membranes, in which several fractions were defined by SEC according to their elution characteristics. Mieville et al. (1989) measured the diffusion of petroleum asphaltenes through porous materials by uptake experiments, in which the asphaltenes were treated as monodispersed and a linear adsorption isotherm was obtained.

In this work, hindered diffusion of coal and petroleum asphaltenes in THF was studied by adsorptive uptake experiments from a bath surrounding a commercial $NiMo/Al_2O_3$ catalyst. The asphaltenes were grouped into several fractions via SEC. An adsorption-diffusion model was developed for the uptake process. The objective of this work was to see if the diffusion uptake could be represented by a single mathematical model using reasonable parameter values.

EXPERIMENTAL

Materials. One coal and two petroleum asphaltenes, denoted as C-97500, P-AAK and P-AAG, respectively, were used in the diffusion study. The coal and petroleum asphaltenes, defined as THF(tetrahydrofuran) solubles and n-pentane insolubles, were extracted from a coal resid and petroleum asphalts, respectively. HPLC grade THF was used as solvent in the uptake experiments. Toluene and polystyrenes with narrow molecular weight distributions were used as calibration standards for analysis of asphaltenes on SEC. A commercial unimodal catalyst, Criterion 324, with an average pore diameter of 125 Å, was used in this study. Catalyst samples were crushed to -12+16 mesh size (-1.0+1.4 mm in diameter) and calcined at 673 K for 12 hours prior to use in uptake experiments.

Apparatus and Procedures. Diffusion experiments were performed in a magnetically stirred glass diffusion cell containing a screen wire basket for holding catalyst particles at 308 K. Catalysts were presaturated with THF before diffusion runs, during which the uptake of asphaltenes was monitored periodically by analyzing the concentration of asphaltenes in the bath solution using SEC.

SEC with a UV detector at 262 nm wavelength was used to analyze the concentration of asphaltenes in THF. Four μ-styragel columns, with nominal pore sizes of 1000, 1000, 500 and 500 Å respectively, were used in series for the SEC. A computer data acquisition system was employed to record the UV absorbance vs. elution time of the effluents. HPLC grade THF was used as mobile phase at 1 cm^3/min.

HINDERED DIFFUSION MODEL FOR ASPHALTENES

A mathematical model was utilized to describe the behavior of hindered diffusion of asphaltenes in porous catalyst particles. The asphaltenes are grouped into different fractions according to their molecular weights ascertained from SEC analysis. The porous catalyst particles were immersed in a well-stirred bath containing asphaltenes and solvent. The asphaltene molecules diffuse into the porous particle where they are adsorbed onto the solid catalyst surface. As a result of this diffusion-adsorption process, the concentration of asphaltenes in the surrounding bath is depleted. However, due to the difference in adsorption capacity and diffusion rate of each asphaltene fraction, the depletion rates for different asphaltene fractions will be different.

The hindered diffusion model developed here assumes negligible solute transport by surface diffusion, spherical catalyst particle geometry, uniform pore size distribution along the particle radius, negligible external fluid solid mass transfer resistance, and local adsorption equilibrium inside the particle pores (Yang and Guin, 1996a, 1996b). It is also assumed that the adsorption isotherm is linear for each fraction, and the properties of each fraction, e.g., molecular size, diffusivity, and adsorption capacity, are independent of every other fraction during the adsorption-diffusion process. With the above assumptions, the adsorption-diffusion mathematical model can be developed and solved analytically (Bird et al., 1960), with the dimensionless bath concentration of asphaltene fraction j being expressed as a function of dimensionless time by,

$$\theta_{bj} = \frac{B_j}{1+B_j} + 6B_j \sum_{k=1}^{\infty} \frac{\exp(-b_k^2 t_j^*)}{B_j^2 b_k^2 + 9(1+B_j)} \tag{1}$$

where, the b_k's are the non-zero roots of

$$\tan(b_k) = \frac{3b_k}{3+B_j b_k^2} \tag{2}$$

and

$$\theta_{bj} = \frac{C_{bj}}{C_{bj0}}, \qquad B_j = \frac{V_b}{V_p} \frac{1}{K_{pj}\epsilon + \rho_p K_j}, \qquad t_j^* = \frac{D_{ej}}{R^2} \frac{1}{K_{pj}\epsilon + \rho_b K_j} t \tag{3}$$

In the above equations, D_{ej} is the effective diffusivity expressed as,

$$D_{ej} = \frac{K_{pj} K_{rj} \epsilon}{\tau} D_{\infty j} \tag{4}$$

in which K_{pj} and K_{rj} factors are hindered diffusion parameters due to stearic and hydrodynamic effects, respectively, being estimated by,

$$K_{pj} = (1-\lambda_j)^2 \tag{5}$$

$$K_{rj} = 1 - 2.104\lambda_j + 2.089\lambda_j^3 - 0.948\lambda_j^5 \tag{6}$$

For a hydrodynamic diffusion solute, the molecular diffusivity $D_{\infty j}$ is related to the solute size by the Stokes-Einstein equation,

$$D_{\infty j} = \frac{kT}{6\pi\eta_0 r_{mj}} \tag{7}$$

For a typical adsorptive diffusion system, the values for most parameters in the model are known except those for K_j (or B_j) and D_{ej}. The values of these two parameters can be obtained by fitting the mathematical model to the experimental asphaltene uptake data.

RESULTS AND DISCUSSION

1. Asphaltene Molecular Weights

SEC analysis of asphaltenes requires the use of calibration standards to determine the average molecular weights of the fractions from elution volumes. Several investigators have used polystyrenes as calibration standards to obtain the equivalent molecular weight distributions of heavy oils and asphaltenes (Song et al., 1991; Baltus and Anderson, 1983; Sanchez et al., 1984; Dark and McGough, 1978). By comparing the molecular weights of prefractionated heavy oil fractions obtained from VPO

(vapor pressure osmometry) and polystyrene calibrated SEC, some studies showed that both measurements agreed well at least in some range (Brule, 1981; Bartle et al., 1984; Baltisberger et al., 1984;). However, others stated that there were differences between these two methods (Kiet et al., 1977; Wong and Gladstone, 1983). It might appear that the VPO method would give more accurate molecular weights; however, Nali and Manclossi (1995) stated that VPO molecular weight measurement failed when strong interactions among single molecules, e.g., highly aromatic compounds, were present. Mieville et al. (1989) showed that different asphaltenes with the same VPO molecular weights could elute at different volumes on SEC, inferring the absence of a universal relationship between SEC and VPO molecular weights for different asphaltenes. In the absence of any clear correlation between VPO and SEC molecular wights, we have used polystyrenes as SEC standards to calibrate the molecular weight distribution of our coal and petroleum asphaltenes.

Toluene and polystyrene standards with weight average molecular weights ranging from 92 to 14000 were first dissolved in THF. These solutions were analyzed via SEC, and the logarithm of molecular weights of the standards vs. elution volumes is shown in Figure 1, resulting a good linear fit being expressed as,

$$\log(M_W) = -0.125V_R + 7.261 \qquad (8)$$

Figure 2 shows SEC chromatograms of the coal and petroleum asphaltenes in THF. There are two x-axes in this figure, one is the elution volume, the other is the equivalent polystyrene/toluene molecular weight calculated from equation (8). It is observed that the equivalent molecular weights of the coal asphaltenes, 50-1000, are much smaller than those of the petroleum asphaltenes (300-20000 for P-AAK and 300-10000 for P-AAG). In the simulation of experimental asphaltene diffusion data, several fractions of the asphaltenes will be defined in terms of the equivalent eluted polystyrene/toluene molecular weights.

2. Effective Diffusivities and Adsorption Constants of Asphaltene Fractions

As seen in the model development section, to perform the model simulation for uptake of each asphaltene fraction, the effective diffusivity De_j and the adsorption parameter K_j are required. One method for determination of the molecular diffusivities of asphaltene fractions is to assume that they are the same as those of the polystyrene standards with same elution volumes. However, Baltus and Anderson (1983) showed that these two values are different, with the molecular diffusivities of polystyrenes being roughly two times of those of petroleum asphaltene fractions. Viewed in another way, if we know the size r_{mj} of each asphaltene fraction, the molecular diffusivity can be calculated from equation (7). Nortz et al. (1990) measured hydrodynamic properties of prefractionated heavy oils in THF and obtained the following relationship between the molecular radius in Å and VPO molecular weight,

$$r_m = 0.36\, M_W^{0.50} \qquad (9)$$

In equation (9) the molecule radius was calculated from the Stokes-Einstein equation using the molecular diffusivity experimentally determined by Taylor dispersion measurements. We have assumed that the above equation is applicable to our coal and petroleum asphaltenes, and that the molecular weights from VPO can be represented by those from SEC. With these assumptions, the molecular diffusivity of any asphaltene fraction eluted in SEC can be estimated through equation (7). The results for some asphaltene fractions are shown in Table 1. Comparison of the molecular weight ranges in Figure 2 with Table 1 shows that the effective diffusivities for the coal asphaltenes are in the range of 3-30 x 10^{-7}; while the ranges for the two petroleum asphaltenes P-AAK and P-AAG are 5-10000 x 10^{-10} and 6-1000 x 10^{-9} cm^2/s, respectively.

Due to the instability of asphaltenes in THF solvent, it is difficult to obtain the adsorption constants K_j from equilibrium experiments; however, this value can be ascertained by fitting the experimental diffusional uptake data with the model solution given by equation (1).

3. Simulation of Asphaltene Diffusion into Porous Catalyst

In our diffusion study, one coal and two petroleum asphaltenes were used as solutes. Figures 3, 4 and 5 (points) show the uptake data for the three asphaltenes in THF on Criterion 324 catalyst, respectively. It is seen from these figures that as diffusion time increases, the UV absorbances or concentrations of the coal asphaltenes fractions and most petroleum asphaltene fractions in the bath solution decrease. However, the rates of decrease for asphaltene fractions with different molecular weights are different, depending on their diffusion rates and adsorption capacities. It is interesting that for the two petroleum asphaltenes, as shown in Figures 4 and 5, respectively, some cross-overs of the SEC data were observed at higher molecular weights (approximately greater than 10000). In other words, the molecular weight distribution shifted to higher molecular weights during the uptake process, resulting in increasing bath concentrations for these fractions. A possible reason for this unusual phenomena might be the agglomeration of smaller molecules into larger ones. This aspect of the work needs further investigation.

For the numerical simulation of the experimental uptake results for the three asphaltenes, we first group the SEC data into several fractions, each with an elution volume of 0.5 cm^3. Some of the estimated effective diffusivities for these fractions are shown in Table 1. For each fraction, the dimensionless bath concentration θ_{bj} can be obtained by the ratio of the area under SEC curve at time t to that at time t=0. The adsorption constant K_j can be obtained by fitting the experimental (θ_{bj}, t) data with the model solution for each fraction. Figure 6 shows the values of adsorption constant K_j for different asphaltene fractions. It is seen that even though the properties of the three asphaltenes are quite different, as shown in Figure 2, the values of adsorption parameters for the fractions of these asphaltenes have the same trend; with increasing the molecular weight, the adsorption constant monotonically increases. It has also been observed (Takahashi et al., 1980; Dimino, 1994) that adsorption of polymers in porous materials increased as the molecular weights increased. Best fits of adsorption constant vs. molecular weight for the fractions of the three asphaltenes can be obtained with power regression from the data points in Figure 6, being expressed as,

$$\begin{aligned} C\text{-}97500: &\quad K_j = 3.352\ M_{wj}^{0.530} \\ P\text{-}AAK: &\quad K_j = 0.0239\ M_{wj}^{1.246} \\ P\text{-}AAG: &\quad K_j = 0.105\ M_{wj}^{1.151} \end{aligned} \tag{10}$$

It should be pointed out that for the two petroleum asphaltenes P-AAK and P-AAG in the above equations, we used fractions of molecular weights less than 10000. Beyond this value some of the experimental bath concentrations increased as discussed above and could not be fitted by the uptake model. In the simulation of the experimental uptake data with the model solution, adsorption constants K_j for fractions of molecular weights larger than 10000 were instead obtained by extrapolation of the above equations.

As long as the relationship between the adsorption constant K_j and the molecular weight is determined, the diffusion equation (1) can be solved for any asphaltene fraction eluted from SEC. The simulated model solution for the three asphaltenes are also shown in Figures 3, 4 and 5 (lines), respectively. It is observed that for the coal asphaltenes, the model fits experimental data quite well, as seen from Figure 3. For the two petroleum asphaltenes, the model fits the experimental data fairly well in smaller molecular weight regions, as shown in Figures 4 and 5 respectively; however, in the larger molecular weight regions, some departures were observed due to the cross-overs of the experimental uptake data, particularly at longer diffusion times.

CONCLUSION

Both the coal and petroleum asphaltenes used in this study have very broad molecular weight distributions, with the molecular weights of the coal asphaltenes (50-1000) being much smaller than those of the petroleum asphaltenes (300-20000 for P-AAK and 300-10000 for P-AAG). The coal asphaltene fractions have estimated effective diffusivities which span 1 order of magnitude, whereas these spans are more than 2 orders for the fractions of the two petroleum asphaltenes. The uptake rates for asphaltene fractions with different molecular weights are different, depending on their diffusion rates and adsorption capacities. Even though the properties of the asphaltenes used are quite different, the values of model parameters for the fractions of the three asphaltenes have the same trend; with increasing molecular weight of the fraction, the adsorption constant increases and the effective diffusivity decreases monotonically. The experimental diffusion data for the three asphaltenes can be represented fairly well in most molecular weight regions by the same mathematical model using appropriate parameter values.

Acknowledgment

This work was supported by the US Department of Energy under Grant No. DE-FG22-91PC1311.

Nomenclatures

B	dimensionless model constant
C_b	bath concentration
C_{b0}	initial bath concentration
D_m	molecular diffusivity, cm^2/s
D_e	effective diffusivity, cm^2/s
k	Boltzmann's constant, 1.38×10^{-6} erg/ °K
K	linear adsorption constant, cm^3-solution/g-catalyst
K_p	partition factor
K_r	restriction factor

M_w molecular weight, g/mol
r_m molecule radius, Å
R radius of catalyst particle, cm
t time, h
t^* dimensionless time
T temperature, °K
V_b bath volume, cm^3
V_p catalyst pore volume, cm^3
V_R elution volume on SEC
ϵ catalyst porosity
η_o solvent viscosity, g/cm-s
θ_b dimensionless concentration in bath
λ ratio of solute molecule diameter to catalyst pore diameter
ρ_p catalyst particle density, g/cm^3
τ catalyst tortuosity factor

Subscript

j jth asphaltene fraction defined on SEC

References

Baltisberger, R. J., S. E. Wagner, S. P. Rao, J. F. Schwan, and M. B. Jones, ACS Preprints, Fuel Chem, Div., 29(1), 186(1984).

Baltus, R. E., and J. L. Anderson, Chem. Eng. Sci., 38, 1959(1983).

Bartle, K. D., M. J. Mulligan, N. Taylor, T. G. Martin, and C. E. Snape, Fuel, 63, 1556(1984).

Bird, R. B., W. E. Stewart, and E. N. Lightfoot, "Transport Phenomena", John Wiley & Sons, Inc., p357, 1960.

Brule, B., ACS Preprints, 26(2), 28(1981).

Dark, W. A., and R. R. McGough, J Chrom. Science, 16, 610(1978).

Dimino, S. P., M. S. Thesis, Auburn University, 1994.

Kiet, H. H., L. Ph. Blanchard, and S. L. Malhotra, Separation Sci., 12(6), 607(1977).

Mieville, R. L., D. M. Trauth, and K. K. Robinson, ACS Preprints, Div. Petr. Chem., 34, 635(1989).

Nali, M., and A. Manclossi, Fuel Sci. And Technl. Int'l., 13(10), 1251(1995).

Nortz, R. L., R. E. Baltus, and P. Rahimi, Ind. Eng. Chem. Res., 29, 1968(1990).

Reid, R. C, J. M. Prausnitz, and B. E. Poling, Properties of Gases and Liquids, 4th ed., McGraw-Hill, New York, 599(1987).

Sanchez, V., E. Murgia, and J. A. Lubkowitz, Fuel, 63, 12(1984).

Sane, R. C., T. T. Tsotsis, I. A. Webster and V. S. Ravi-Kumar, Chem. Eng. Sci., 47, 2683(1992).

Song, C., T. Nihonmatsu, and M. Nomura, Ind. Eng. Chem. Res., 30, 1726(1991).

Takahashi, A., M. Kawaguchi, H. Hirota, and T. Kato, Macromolecules, 13, 884(1980).

Wong, J. L., and C. M. Gladstone, Fuel, 62, 871(1983).

Yang, X., and J. A. Guin, Applied Catalysis, in press, 1996a.

Yang, X., and J. A. Guin, Chem. Eng. Comm., in press, 1996b.

Table 1. Estimated effective diffusivities and other parameters at 35 °C

elution vol., cm^3	M_w[a] g/mol	r_m[b] Å	D_∞[c] cm^2/s	D_e[d] cm^2/s
23	24322.0	56.1	7.9E-07	1.3E-10
25	13677.3	42.1	1.1E-06	2.2E-09
27	7691.3	31.6	1.4E-06	1.3E-08
29	4325.1	23.7	1.9E-06	4.9E-08
31	2432.2	17.8	2.5E-06	1.3E-07
33	1367.7	13.3	3.3E-06	2.6E-07
35	769.1	10.0	4.5E-06	4.6E-07
37	432.5	7.5	5.9E-06	7.6E-07
39	243.2	5.6	7.9E-06	1.2E-06
41	136.8	4.2	1.1E-05	1.7E-06
43	76.9	3.2	1.4E-05	2.5E-06
45	43.3	2.4	1.9E-05	3.5E-06
47	24.3	1.8	2.5E-05	4.9E-06

a. Determined by equation (8).

b. Estimated from equation (9).

c. Calculated from equation (7) with THF viscosity of $4.42*10^{-3}$ g/cm-s (Reid et al., 1987).

d. Determined by equation (4) with ϵ=0.66 and τ=3.0.

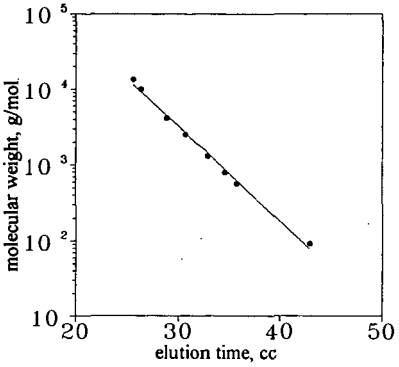

Figure 1. Calibration of SEC columns by toluene and polystyrenes.

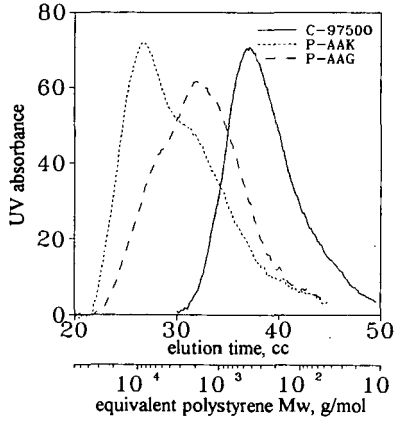

Figure 2. Comparison of SEC Mw distributions in THF for coal and petroleum asphaltenes.

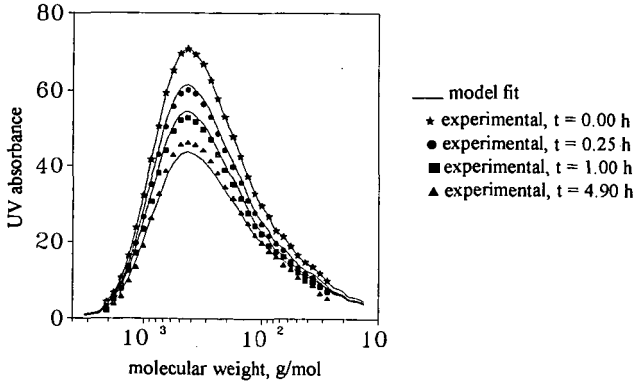

Figure 3. Simulation of experimental uptake data with math model for diffusion of coal asphaltenes in THF into Criterion 324 catalyst at 35 °C.

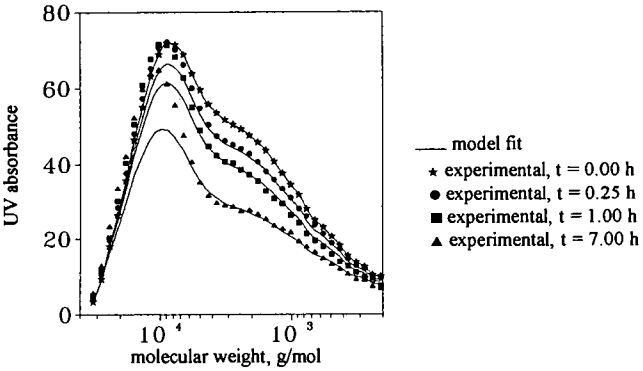

Figure 4. Simulation of experimental uptake data with math model for diffusion of P-AAK asphaltenes in THF into Criterion 324 catalyst at 35 °C.

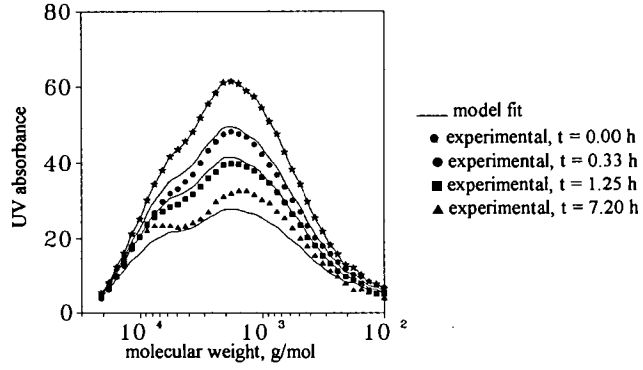

Figure 5. Simulation of experimental uptake data with math model for diffusion of P-AAG asphaltenes in THF into Criterion 324 catalyst at 35 °C.

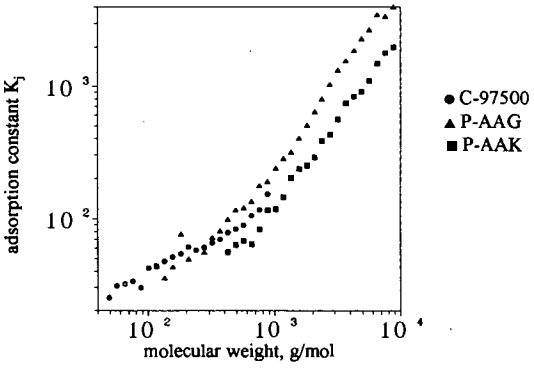

Figure 6. Relationship between molecular weight and adsorption constant for coal and petroleum asphaltenes.

Paper Presented before the ACS Division of Fuel Chemistry
212th American Chemical Society National Meeting, Orlando, FL, August 25-29, 1996

Shape-Selective Catalysis for Synthesis of High-Value Chemicals from Aromatics in Coal Liquids

Chunshan Song and Harold H. Schobert

Department of Material Science & Engineering and Laboratory for Hydrocarbon Process Chemistry
209 Academic Projects Building, Pennsylvania State University, University Park, PA 16802

Keywords: Catalysis, Chemicals, Aromatics, Coal, Coal Liquids, Anthracites, Graphites

INTRODUCTION

Liquids derived from coals contain numerous aromatic compounds. Many of the one- to four-ring aromatic and polar compounds can be converted into valuable chemicals. Economic analysis of the viability of liquefaction (and related conversion processes) may well produce a different result if some of the aromatics and phenolics are used for making high-value chemicals and some of the liquids for making high-quality fuels such as thermally stable aviation fuels. To make effective use of aromatics in coal liquids, we are studying shape-selective catalytic conversion of multi-ring compounds. The products of such reactions are intermediates for making value-added chemicals, monomers of advanced polymer materials, or components of advanced jet fuels (Song and Schobert, 1993, 1995).

Two broad strategic approaches can be used for making chemicals and materials from coals (Schobert, 1984, 1990, 1995). The first is the indirect approach: conversion of coals to liquids, followed by transformation of compounds in the liquids into value-added products. The second is direct conversion of coals to materials and chemicals. Both approaches are being explored in this laboratory (Song and Schobert, 1993, 1996).

In this paper, we will give an account of our recent work on 1) shape-selective catalysis which demonstrates that high-value chemicals can be obtained from aromatic compounds by catalytic conversion over certain zeolites; and 2) catalytic graphitization of anthracites, which reveals that using some metal compounds promotes graphitization at lower temperatures and may lead to a more efficient process for making graphites from coals.

POLYMER MATERIALS FROM AROMATIC MONOMERS

Recent years have witnessed significant growth of existing aromatic polymer materials and rapid development of advanced aromatic polymer materials such as engineering plastics, polyester fibers, polyimides, and liquid crystalline polymers (LCPs) (Beland, 1991, Song and Schobert, 1993). Consequently, there is greater demand for monomers based on aromatic and phenolic compounds. Such compounds can be made from coal-derived liquids and some refinery streams such as light cycle oils.

Scheme 1 shows the structures of some polyester materials, including thermoplastic polyethylene terephthalate (PET), polyethylene naphthalate (PEN), polybutylene terephthalate (PBT), polybutylene naphthalate (PBN), polycarbonate (PC), polyphenylene oxide (PPO), and thermotropic LCPs. PET has found widespread applications in bottles, films, and tapes. PET consumption in the United States reached 1.4 Mt in 1994, with over half being used for soft-drink or custom bottles (MP-News, 1995). Compared to PET, PEN provides five times better oxygen barrier and four times better moisture barrier, as well as 50% greater modulus and 29°C higher thermal resistance temperature. PBT is one of the major engineering plastics. PBN outperforms PBT in chemical and thermal resistance as well as tensile strength (Teijin, 1992). PEN and PBN show great commercial potential. Their markets are expected to grow rapidly. Polycarbonates have found wide-spread applications and are the second most widely used engineering plastics. PPO has an exceptionally high softening point (210°C) and is used for automotive parts, appliance, business machines, computer and electrical equipments. Of all the resins, thermoplastic polyesters grew fastest in 1994 (C&EN-News, 1993, 1994, 1995a).

Among the LCPs, Celanese's Vectra is made from three monomers: 6-hydroxy-2-naphthoic acid, 4-hydroxybenzoic acid, and terephthalic acid. Vectra's tensile strength is about ten-fold greater than regular engineering plastics such as PC. Its heat deflection temperature is also fairly high, up to 240°C. Moreover, Vectra's linear expansion is similar to that of metal. Amoco's Xydar is synthesized from *p,p´*-biphenol (or 4,4´-biphenol), *p*-hydroxybenzoic acid, and terephthalic acid (NRC, 1990). Xydar's heat deflection temperature is the highest among all the thermoplastic engineering plastics, about 350°C. Its heat-resistance is comparable to high-temperature heat-resistant polyimides. Xydar was originally developed for use in cookware; it can be used at 240°C for one hundred thousand hours (LCP-News, 1988). The global market for LCPs is about 4,500 t, about half in the Asia-Pacific market, 40% in the U.S., and 10% in Europe (MP-News, 1995). Despite their cost, LCPs are enjoying 25% annual growth worldwide and are forecast to maintain that level through the decade. Growth is 20% in the U.S. and Europe, 30% in Asia. Most LCPs are made from naphthalene-based and biphenyl-based monomers, as shown in Scheme 1. More information on these materials may be found elsewhere (Seymour, 1987; Beland, 1991; Allcock and Lampe, 1990; NRC, 1990; Song and Schobert, 1993; Relles, 1994).

Scheme 1. **Structures of Some Important Aromatic Polymer Materials**

Thermoplastic Polyesters

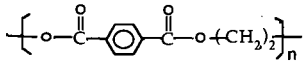

Polyethylene Terephthalate (PET) / Dacron, Mylar

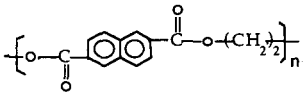

Polyethylene Naphthalate (PEN) / Teijin, Amoco

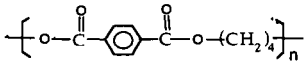

Polybutylene Terephthalate (PBT) / Valox, Celanex

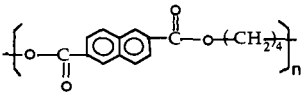

Polybutylene Naphthalate (PBN) / Teijin's PBN Resin

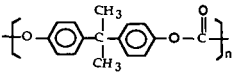

Polycarbonate (PC) /GE's Lexan, Dow's Calibre

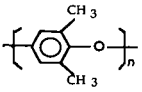

Polyphenylene Oxide (PPO) / GE's PPO, Noryl

Thermotropic Polyester LCPs

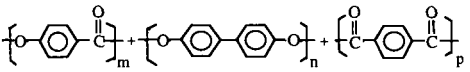

LCP / Amoco's Xydar; Sumitomo's Ekonc

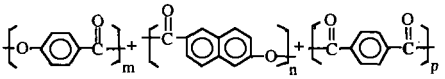

LCP / Hoechst Celanese's Vectra

High-Temp Heat-Resistant Polymers

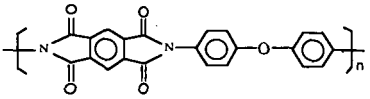

Polyimide / Du Pont's Kapton

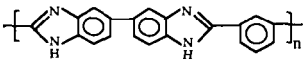

Polybenzimidazole / Celanese's Celazole

AROMATIC AND PHENOLIC CHEMICALS FROM COAL LIQUIDS

Detailed analysis of liquids from several pilot plants of coal liquefaction has clearly shown that phenol, naphthalene, phenanthrene, pyrene, biphenyl, BTX (benzene, toluene, xylene) and their derivatives are present in relatively high concentrations in various fractions (Wright et al., 1986; Lai et al., 1992). Analysis of liquefaction and pyrolysis products in the laboratory indicates the same trends (Caroline et al., 1993; Huang et al., 1993; Song et al., 1993) Many of the one- to four-ring aromatic and polar compounds in coal-derived liquids can be converted into valuable chemicals.

Phenolic Compounds from Coal Liquids. Phenol can be separated from coal liquids by liquid-phase extraction. Phenol is one of the top twenty organic chemicals and is commercially produced in a multi-step process involving benzene isopropylation, oxidation of isopropylbenzene, and separation of phenol. Phenol can be used as-is for making phenol resins or converted to monomers such as bisphenol A and 2,6-xylenol for making aromatic polymers and engineering plastics. Phenol can also be converted to ε-caprolactam, which ranks third in phenol utilization in USA and Western Europe (Weissermel and Arpe, 1993). Production of synthetic phenol has increased significantly in the past decade in USA, from 1311 to 1838 kt during 1984-1994 (C&EN-News, 1995a). The amounts of phenol produced from coal tar and waste water in USA were 20 and 21 kt in 1972 and 1989, respectively, and they are much smaller compared to synthetic phenol. Synthetic phenol production in Japan is also increasing rapidly, from 308 to 670 kt during 1987–94 (Weissermel and Arpe, 1993; C&EN-News, 1995b). Western Europe produced 1488 kt in 1991, with 98.1% synthetic phenol and 1.9% phenol from coal tar and waste water (Weissermel and Arpe, 1993). It appears that the market for phenol is large enough for considering the phenolic compounds from coal liquefaction.

Naptha fractions of coal liquefaction products generally contain 1.5–3.5 wt% oxygen, due to the presence of mainly phenolic compounds (Yoshida et al., 1991). Phenols are more abundant in the oils from coal hydrogenation using dispersed Mo catalyst and water (Saini and Song, 1994; Song and Saini, 1995). Separation of phenolics from coal-derived oils can not only produce useful chemicals, but also eliminate the need for down-stream hydrodeoxygenation which consumes the costly hydrogen to produce useless water byproduct. Therefore, such an operation also contributes to improving the economics of coal liquefaction. According to the recent reports by Yoshida and co-workers at Hokkaido National Industrial Research Institute in Japan and by Kodera and Ukegawa of National Institute for Resources and Environment in Japan, phenolic compounds (mainly phenol and cresols) can be obtained from naphtha distillates of coal liquefaction products by surfactant-mediated (Yoshida et al., 1991) or methanol-mediated (Kodera et al., 1990, 1993) aqueous extraction.

Catechol from Coal Liquids. Catechol (1,2-dihydroxybenzene) has some industrial applications such as therapeutic agent, tanning agent, anticorrosion agent, anti-UV agent, antioxidant for rubber, polyolefins and polyurethanes, intermediate for synthesis of agrochemicals, and intermediate for perfumes, cosmetics, and aromas (Phone-Poulenc, 1991). A new synthetic process developed in Italy produces 10,000 t/y of catechol and hydroquinone by hydroxylation of phenol with H_2O_2 using titanium silicate catalyst (Notari, 1991). On the other hand, catechol is one of the major products detected in flash pyrolysis-GC-MS of subbituminous coals and lignites (Song et al., 1992; 1993; Saini et al., 1992). It may be possible to obtain catechol-rich liquids from low-rank coals through some new processing methods.

Aromatic Compounds from Coal Liquids. The use of aromatics in coal liquids for making value-added chemicals requires the starting material to be reasonably pure. This requirement adds a challenge for chemists and engineers, since coal liquids contain dozens or even hundreds of components. Dealkylation or dehydrogenation of oils from coal can significantly simplify the composition, leading to simple separation of individual components by distillation.

Nomura and co-workers at Osaka University in Japan have reported making aromatic chemicals from coal through catalytic dehydrogenation and dealkylation of liquefaction products (Ida et al., 1991; Nomura et al., 1995). In particular, dehydrogenation can simplify the liquid composition, because two or more isomers (e.g., 2- and 6-methyltetralin) become one compound (e.g., 2-methylnaphthalene) upon dehydrogenation In the presence of a carbon-supported palladium catalyst, dehydrogenation of heavy naphtha (bp ca. 200-220°C) and light oil (bp ca. 220-240°C) from several coal-derived liquids is effective for producing naphthalene and methylnaphthalene, respectively (Nomura et al., 1995). Sato and co-workers at National Institute for Resources and Environment reported that non-catalytic hydrodealkylation of middle distillates (bp 180-450°C) from coal liquefaction produces mainly unsubstituted and methylsubstituted 1- to 3-ring aromatic chemicals including benzene, toluene, indene, naphthalene, methylnaphthalene, biphenyl, acenaphthylene, fluorene, and phenanthrene (Sato et al., 1992, 1994). They have also shown that catalytic cracking of the middle distillates (bp 200-260°C) from coal liquefaction produces the oils that consist mainly of alkylnaphthalenes; hydrodealkylation of such oils can produce high-purity naphthalene and methylnaphthalene as chemicals (Sato et al., 1994).

SHAPE-SELECTIVE SYNTHESIS OF HIGH-VALUE CHEMICALS

Our attention on chemicals has focused on shape-selective catalytic synthesis of value-added chemicals from polycyclic aromatic compounds that are rich in coal liquids (and in some refinery streams such as LCO). We are studying ring-shift isomerization of phenanthrene derivatives to anthracene derivatives, shape-selective alkylation of naphthalene, conformational

isomerization of *cis*-decahydronaphthalene, shape-selective hydrogenation of naphthalene, and shape-selective isopropylation of biphenyl, as described below.

Ring-Shift Isomerization. Phenanthrene and its derivatives are rich in various coal-derived liquids, but their industrial use is still very limited (Kurata, 1986, Song and Schobert, 1992). On the other hand, anthracene and its derivatives have found wide industrial applications (Song and Schobert, 1993). Some catalysts selectively promote the transformation of *sym*-octahydrophenanthrene (*sym*-OHP) to *sym*-octahydroanthracene (*sym*-OHAn), which we call ring-shift isomerization (Song and Moffatt, 1993, 1994). This reaction is in distinct contrast to, and mechanistically different from, the well-known ring-contraction isomerization of tetralin (Hooper et al., 1979; Franz and Camaioni, 1980), *sym*-OHP (Cronauer et al., 1979), and *sym*-OHAn (Collin et al., 1985); ring-contraction results in methylindane-type products.

Under mild conditions, some zeolites can afford over 90% selectivity to *sym*-OHAn with high conversion of *sym*-OHP (Song and Moffatt, 1994; Lai et al., 1995). This could provide a cheap route to anthracene and its derivatives, which are valuable chemicals in demand, from phenanthrene, which is rich in liquids from coal. Possible applications of *sym*-OHAn include the manufacturing of anthracene (for dyestuffs), anthraquinone (pulping agent), and pyromellitic dianhydride (the monomer for polyimides such as Du Pont's Kapton) (Song and Schobert, 1993).

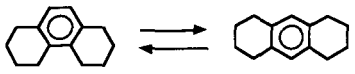

1)

sym-OHP sym-OHAn

Shape-Selective Alkylation of Naphthalene. Naphthalene and its derivatives are rich in oils from bituminous coals. Shape-selective alkylation over some molecular sieve catalysts can produce 2,6-dialkyl substituted naphthalene (2,6-DAN). 2,6-DAN is needed now as the feedstock for monomers for making advanced polyester materials such as polyethylene naphthalate (PEN, Scheme I), polybutylene naphthalate (PBN), and liquid crystalline polymers (LCP). By using some shape-selective catalysts, regioselective alkylation of naphthalene can be achieved with over 65% selectivity to 2,6-DAN by using isopropanol (Song and Kirby, 1993, 1994) or propylene as the alkylating agent (Schmitz and Song, 1994, 1995). Partially dealuminated proton-form mordenite can be used as shape-selective catalyst for isopropylation of naphthalene (Katayama et al., 1991; Schmitz and Song, 1994, 1995). We also found some simple and effective methods for enhancing the shape selectivity (Schmitz and Song, 1994, 1996b).

Shape-selective Alkylation of Biphenyl. Biphenyl and its derivatives are present in coal-derived liquids, although at concentrations lower than those of naphthalene derivatives. Shape-selective alkylation of biphenyl can produce 4,4'-dialkyl substituted biphenyl (4,4-DAB), the starting material for monomer of some LCP materials represented by Xydar (Scheme I). Partially dealuminated proton-form mordenite can be used as shape-selective catalyst for isopropylation of biphenyl (Lee et al., 1989; Sugi et al., 1991, 1994; Schmitz and Song, 1995). Dealumination of some commercial mordenites by acid treatment first increases then decreases their activity, but increases their selectivity toward 4,4-DAB in isopropylation with propylene (Schmitz and Song, 1995). More recently, we have found a simple method using an additive to inhibit deactivation of the partially dealuminated mordenite catalysts without losing activity and selectivity (Schmitz and Song, 1996c).

Conformational Isomerization. Commercial decalins obtained from naphthalene hydrogenation are almost equimolar mixtures of *cis*-decalin and *trans*-decalin. Recently we have found that *cis*-decalin isomerizes to *trans*-decalin, as shown in equation 1, at low temperatures (250°C) over some catalysts (Song and Moffatt, 1993, 1994). This reaction would require a temperature of about 450°C in the absence of a catalyst (Song et al., 1992). It is possible to achieve over 90% conversion with 95% selectivity with some zeolites at 200°C (Lai and Song, 1995). *trans*-Decalin has substantially higher thermal stability at temperatures above 400 °C (Song et al., 1992). Possible applications are high-temperature heat-transfer fluids and advanced thermally stable jet fuels, which can be used both as heat sinks and as fuels for high-Mach aircraft (Coleman et al., 1993; Song et al., 1993, 1994).

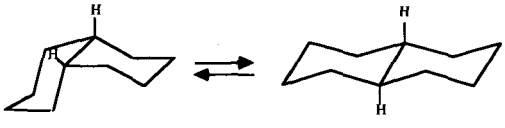

3)

cis-DeHN trans-DeHN

Shape-selective Naphthalene Hydrogenation. Complete hydrogenation of naphthalene in conventional processes produces mixtures of *cis*- and *trans*-decalin. The motivation for selective naphthalene hydrogenation comes from our accidental finding on zeolite-catalyzed isomerization of *cis*-decalin and from the need to tailor the formation of desired isomers from two-ring compounds (Song and Moffatt, 1994). In our previous studies on naphthalene hydrogenation, certain catalysts show higher selectivity towards *cis*-decalin or *trans*-decalin (Song and Grainne, 1993; Lin and Song, 1995; Schmitz et al., 1995; Reddy and Song, 1995). More recently, we found that zeolite-supported catalysts selectively promote the formation of *cis*-decalin or *trans*-decalin (Schmitz et al., 1995, 1996), as shown below.

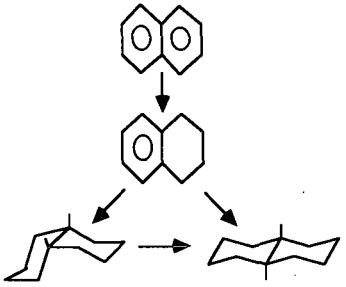

Now we can produce *cis*-decalin, with over 80% selectivity (or over 80% trans-decalin) at 100% conversion by using some zeolite-supported catalysts at 200°C (Schmitz et al., 1995, 1996). *cis*-Decalin may have potential industrial application as the starting material for making sebacic acid. Sebacic acid can be used for manufacturing Nylon 6,10 and softeners (Weissermel and Arpe, 1993).

There is also an industrial need for selective production of tetralin, a hydrogen-donor solvent, from naphthalene. Partial passivation of some zeolite-supported noble metal catalysts by sulfur can make them highly selective for the production of tetralin during metal-catalyzed hydrogenation of naphthalene at low temperatures (Song and Schmitz, 1996).

CATALYTIC GRAPHITIZATION OF ANTHRACITES

We are also exploring the direct synthesis of high-value carbon materials—graphites—from coals. Both non-catalytic and catalytic graphitization of anthracites has been studied. The main objectives of catalytic graphitization are to further improve the quality of the graphitic product, and to reduce the temperature of graphitization. A reduction in graphitization temperature from typical present-day practice (≈2900°C) to, say, 2000°C could translate into enormous energy savings for the graphite industry. The product quality parameter of interest is the apparent crystalline height, L_c, which is the thickness of the "stack" of aromatic planes.

Four Pennsylvania anthracites are being evaluated as feedstocks. The catalysts under investigation are iron, cobalt, and nickel naphthenates, used at various loadings. Preliminary results demonstrate that using some metal compounds significantly promotes the graphitization at lower temperatures. For example, West Cameron anthracite graphitized at 2000°C with added nickel naphthenate shows an interlayer spacing (d-spacing) of 0.3365 nm, approaching the value of 0.3354 nm characteristic of perfectly crystalline graphite. An unanticipated finding is that, for most anthracites and graphitization reaction conditions, the nature of the metal in the naphthenate salt is relatively unimportant in terms of improved d-spacings or L_c values. Often when a family of compounds is evaluated for catalytic activity there is a progressive change in activity among the family, depending on the metallic element in the catalyst. The metal naphthenate catalyzed graphitization of anthracites is unusual in this respect. We have not yet elucidated the reasons, but it appears that metal carbides may be intermediates. The carbides decompose at the extreme temperatures of graphitization. We hypothesize that the thermal decomposition of the carbides liberates carbon in a highly reactive form, this reactive carbon then interacting with non-graphitic carbon or with heteroatoms in the anthracite to facilitate the graphitization.

Catalytic graphitization is presently being tested by standard industrial procedures for the production of molded graphite articles. Two anthracites, one which graphitizes well without added catalyst and a second which shows significant benefit of catalyst, are being tested. Control experiments with sponge coke are being run in parallel. Nickel naphthenate is the catalyst; experiments without added catalyst will also be run. The anthracites and the petroleum coke were mixed with coal tar pitch and isostatically molded into test billets, using standard industrial mixing and molding methods. At the time of writing, the molded billets are in the baking cycle in an industrial car bottom furnace. Upon completion of baking, half the samples will be graphitized in an induction furnace at a standard industrial temperature (2850–2900°) and the other half will be graphitized at ≈2500°C. The full range of industrial characterization tests, such as density, electrical resistivity, and coefficient of thermal expansion, will be run on all graphitized samples, and the results will be compared with standard commercial products.

CONCLUDING REMARKS

Shape-selective catalysis is an effective approach for making high-value chemicals from aromatic components in coal liquids and some refinery streams such as light cycle oils (LCO). Catalytic graphitization is promising for producing graphites from anthracites at substantially lower temperatures compared to current practice. Expansion of the non-fuel uses of hydrocarbon resources, particularly coals, is desirable, because coal will also become more important as source of both energy and chemical feedstocks in the next century. From the viewpoints of the resource conservation and effective utilization, many of the components in coals as well as in petroleum should be converted to, or used as value-added chemicals, polymers, and carbon materials.

ACKNOWLEDGMENTS

Helpful discussions with Drs. F. Rusinko, W.-C. Lai, A. Schmitz, and S. Zeng of PSU, and D. Struble and W. Nystrom of Carbone of America are gratefully acknowledged. Various portions of our research were supported through funding or donations of special samples from the U.S. Department of Energy, Pittsburgh Energy Technology Center, the Pennsylvania Energy Development Authority, Air Products and Chemicals Inc., PQ Co, and Duracell Co.

REFERENCES

Allcock, H. R. and Lampe, F. W., Contemporary Polymer Chemistry. Prentice Hall, Englewood Cliffs, NJ., 1990.

NRC. Liquid Crystalline Polymers. National Academy Press, 1990, 106 pp.

Beland, S. High Performance Thermoplastic Resins and Their Composites. Noyes Data Corporation: Park Ridge, New Jersey, 1991, 177 pp.

Burgess, C. E., K. Wenzel, C. Song, P. G. Hatcher, and H. H. Schobert. Structural Correlation of Coal Liquefaction Oils with Flash Pyrolysis Products. Proc. 7th Internat. Conf. Coal Sci., Banff, Canada, Sept. 12-17, 1993, Vol. I, pp.311-314.

C&EN-News. *Chem. Eng. News*, 1993, June 28.

C&EN-News. *Chem. Eng. News*, 1994, July 4.

C&EN-News. Chem. Eng. News, 1995a, June 26.

C&EN-News. Chem. Eng. News, 1995b, December 11.

Coleman, M. M., H. H. Schobert and C. Song. Chemistry in Britain, 1993, 29 (9), 760-763.

Collin, P. J., and H. Rottendorf. Proc. 1985 Int. Coal Sci. Conf., Sydney, Oct. 28-31, 1985, pp..710-713.

Cronauer, D. C., D. M. Jewell, Y. T. Shah, R. J. Modi and K. S. Seshadri. Ind. Eng. Chem. Fundam., 1979, 18, 368-376.

Franz, J. A. and D. M. Camaioni. Fuel, 1980, 59, 803-805.

Hirota, T., M. Nomura, and C. Song. A Method for Manufacture of Aromatic Chemicals from Coals. Japan Patent, 1-279990 (Assigned to Osaka Gas Company, Japan), November 10, 1989 (in Japanese).

Hooper, R. J., H. A. J. Battaerd, and D. G. Evans. Fuel, 1979, 58, 132-1348.

Huang, L., C. Song, and H. H. Schobert. Liquefaction of Low-Rank Coals as a Potential Source of Specialty Chemicals. Am. Chem. Soc. Div. Fuel Chem. Prepr., 1994, 39 (2), 591-595.

Ida, T., Kikukawa, T., Matsubayashi, K., Miyake, M, and Nomura, M. Catalytic Hydrodealkylation of SRC Fractions. Sekkiyu Gakkaishi, 1991, 34 (1), 44-51.

Kurata, N. Kagaku To Kogyo, 1986, 60 (7). 274-280.

Lai, W.-C., C. Song, H. H. Schobert., and R. Arumugam. Pyrolytic Degradation of Coal- and Petroleum-Derived Aviation Jet Fuels and Middle Distillates. Am. Chem. Soc. Div. Fuel Chem. Prepr., 1992, 37 (4), 1671-1680.

Lai W.-C. and C. Song. Am. Chem. Soc. Div. Fuel Chem. Prepr., 1995, 40 (4), 1018-1023.

Lai W.-C., C. Song, A. van Duin, and J. W. de Leeuw. Am. Chem. Soc. Div. Fuel Chem. Prepr., 1995, 40 (4), 1007-1012.

Lai, W.-C. and C. Song. Temperature-Programmed Retention Indices for GC and GC-MS Analysis of Coal- and Petroleum-derived Liquid Fuels. Fuel, 1995, 74, 1436-1451.

LCP-News. Speciality Chemicals, 1988, 12 (8), 17-22.

Lee, G.S., J.J. Maj, S.C. Rocke, and J.M. Garces, Shape Selective Alkylation of Polynuclear Aromatics with Mordenite-Type Catalysts: A High Yield Synthesis of 4,4'-Diisopropylbiphenyl. Catal. Lett., 1989, 2, 243-248.

Lin, S.-D. and Song, C. Am. Chem. Soc. Div. Fuel Chem. Prepr., 1995, 40 (4), 962-967.

MP-News Modern Plastics, 1995, January, p.54-66.

Nomura, M.; Moritaka, S.; Miura, M. Catalytic Dehydrogenation of Coal Liquefied Products: An Alternative Route to Produce Naphthalenes from Coal. Energy & Fuels, 1995, 9 (5), 936-937.

Relles, H. H. Engineering Plastics. Technomic Publishing Company: Lancaster, PA, 1994.

Saini, A.K., C. Song, P.G. Hatcher, and H.H. Schobert. Prepr. Pap.-Am. Chem. Soc., Div. Fuel Chem., 1992, 37 (3), 1235-1242.

Sato, Y., Yamamoto, Y., and Miki, K. Thermal Hydrodealkylation of Coal Liquids and Related Model Compounds. Sekkiyu Gakkaishi, 1992, 35 (3), 274-281.

Sato, Y., Yamamoto, Y., Kamo, T., and Miki, K. Fluid Catalytic Cracking of Coal Liquids (Part 4). Production of Fuel and Chemicals from Coal Liquids. Sekkiyu Gakkaishi, 1994, 37 (1), 58-63.

Schmitz, A., G. Bowers, and C. Song. Am. Chem. Soc. Div. Fuel Chem. Prepr., 1995, 40 (4), 930-934.
Schmitz, A., and C. Song. Shape-Selective Isopropylation of Naphthalene over Dealuminated Mordenite. Am. Chem. Soc. Div. Fuel Chem. Prepr., 1994, 39 (4), 986-991.
Schmitz, A., and C. Song. Am. Chem. Soc. Div. Fuel Chem. Prepr., 1995, 40 (4), 918-924.
Schmitz, A., and C. Song. Catalysis Today, 1996a, in press.
Schmitz, A., and C. Song. Catalysis Letters, 1996b, in press.
Schmitz, A., and C. Song. 1996c, unpublished results.
Schobert, H.H., In: W.R. Kube, E.A. Sondreal, and C.D. Rao (Eds.), Technology and Utilization of Low-rank Coals. U.S. Dept. of Energy Report DOE/METC/84-13; 1984, pp. 83-103.
Schobert, H.H. The Chemistry of Hydrocarbon Fuels. Butterworths, London, 1990, Chapter 14.
Schobert, H.H. Lignites of North America. Elsevier, Amsterdam, 1995, Chapter 12.
Seymour, R. B. Polymers for Engineering Applications. ASM Int., Metals Park, OH, 1987, 198pp.
Song, C. and Bowers, G., 1993, unpublished results.
Song, C., K. Hanaoka, and M. Nomura. Short-Contact-Time Pyrolytic Liquefaction of Wandoan Subbituminous Coal and Catalytic Upgrading of SCT-SRC. Fuel, 1989, 68 (3), 287-292.
Song, C., L. Hou, A. K. Saini, P.G. Hatcher, and H. H. Schobert. CPMAS ^{13}C NMR and Pyrolysis-GC-MS Studies of Structure and Liquefaction Reactions of Montana Subbituminous Coal. Fuel Processing Technol., 1993, 34 (3), 249-276.
Song, C. and S. Kirby. Shape-Selective Alkylation of Naphthalene over Molecular Sieve Catalysts. Am. Chem. Soc. Div. Petrol. Chem. Prepr., 1993, 38 (4), 784-787.
Song, C. and S. Kirby. Shape-Selective Alkylation of Naphthalene with Isopropanol over Mordenite Catalysts. Microporous Materials, Elsevier, 1994, 2 (5), 467-476.
Song, C., W.-C. Lai, and H. H. Schobert. Hydrogen-Transferring Pyrolysis of Long-Chain Alkanes and Thermal Stability Improvement of Jet Fuels by Hydrogen Donors. Ind. Eng. Chem. Res., 1994, 33 (3), 548-557.
Song, C. and K. Moffatt. Zeolite-Catalyzed Ring-Shift and Conformational Isomerization Reactions of Polycyclic Hydrocarbons. Am. Chem. Soc. Div. Petrol. Chem. Prepr., 1993, 38 (4), 779-783.
Song, C. and K. Moffatt. Zeolite-Catalyzed Ring-Shift Isomerization of sym-Octahydrophenanthrene and Conformational Isomerization of cis-Decahydronaphthalene. Microporous Materials, Elsevier, 1994, 2 (5), 459-466.
Song, C., and A. K. Saini. Using Water and Dispersed MoS_2 Catalyst for Coal Conversion into Fuels and Chemicals. Am. Chem. Soc. Div. Fuel Chem. Prepr., 1994, 39 (4), 1103-1107.
Song, C., and A. K. Saini. Strong Synergistic Effect between Dispersed Mo Catalyst and H_2O for Low-Severity Coal Hydroliquefaction. Energy & Fuels, 1995, 9 (1), 188-189.
Song, C. and H. H. Schobert. Specialty Chemicals and Advanced Materials from Coals: Research Needs and Opportunities. Am. Chem. Soc. Div. Fuel Chem. Prepr., 1992, 37 (2), 524-532.
Song, C. and H. H. Schobert. Opportunities for Developing Specialty Chemicals and Advanced Materials from Coals. Fuel Processing Technol., 1993, 34 (2), 157-196.
Song, C. and H. H. Schobert. Aromatic Polymer Precursors from Coals: A New Direction in Coal Chemistry. Proc. 10th Ann. Internat. Pittsburgh Coal Conf., University of Pittsburgh, Pittsburgh, Sept. 20-24, pp.384-389, 1993.
Song, C. and H. H. Schobert. Non-fuel Uses of Coals and Synthesis of Chemicals and Materials. Fuel, 1996, 75, in press.
Song, C., H. H. Schobert and P.G. Hatcher. Energy & Fuels, 1992, 6, 326-328.
Song, C., H.H. Schobert, and A.W. Scaroni. Current Status of U.S. Coal Utilization Technologies and Prospects. Energy & Resources (Japanese), 1994, 15 (2), 142-153.
Sugi, Y., Matsuzaki, T., Hanaoka, T., Takeuchi, K., Tokoro, T., and Takeuchi, G. Alkylation of Biphenyl Catalyzed by Zeolites. Proc. of International Symposium on Chemistry of Microporous Crystals, Tokyo, June 26-29, 1990, 303-340.
Sugi, Y., Matsuzaki, T., Hanaoka, T., Kubota, Y., Kim, J.-H. Shape-Selective Alkylation of Biphenyl over Mordenites: Effects of Dealumination on Shape-Selectivity and Coke Deposition. Catal. Lett., 1994, 26, 181-187.
Teijin. Teijin PBN Resins-Introduction, 1992.
Weiss, R.A. and C. K. Ober (Eds.), Liquid-Crystalline Polymers. Am. Chem. Sym. Ser., 1990, No. 435, 32 chapters, ACS: Washington, D.C., 510 pp.
Weissermel, K. and H.-J. Arpe. Industrial Organic Chemistry. VCH: Weinheim, 1993, 457 pp.
Wright, C. W., D. L. Stewart, D. D. Mahlum, E. K. Chess, and B. W. Wilson. Am. Chem. Soc. Div. Fuel Chem., 1986, 31 (4), 233-239.

THEORETICAL MODELING OF COLIQUEFACTION REACTIONS OF COAL AND POLYMERS

H.F. Ades and K.R. Subbaswamy,
Department of Physics and Astronomy,
University of Kentucky, Lexington KY 40506-0055

Keywords: coliquefaction, quantum chemical modeling

Differences in the behavior of coliquefaction reactions involving polyethylene/coal and polypropylene/coal have been reported. For instance, conversion and oil yields are higher with the polypropylene/coal system while preasphaltene and asphaltene products are higher in the presence of polyethylene. Also, differences have been observed in the coliquefaction of polystyrene and polyisoprene with coal in the absence of a catalyst, with coal conversion increasing from 38% to 60% with polystyrene and to 80% with polyisoprene. Synergism was observed in the polyisoprene/coal system. In an attempt to explain the differences in coliquefaction behavior of these polymers we have begun quantum chemical studies of these systems, using the Gaussian, MOPAC and TBMD suite of programs, to investigate possible differences in cracking of the polymers, in hydrogen transfer behavior and in addition reactions between polymer fragments and coal. Reaction barrier heights for the possible reaction pathways are being calculated and will be compared in order to build a kinetic model.

I. Introduction

Coliquefaction studies of coal with waste products has focused on certain basic questions: (1) what waste products and in what combinations are the best ones to use in coliquefaction processes; (2) what catalysts are good for coliquefaction and how do they act; and (3) is there synergism involved in coliquefaction? Given the complexity of the systems involved, answering these questions will require a combination of empirical and analytical approaches.

In this report on our preliminary modeling studies pertinent to the coliquefaction of coal and waste polymers we specifically address some of the available experimental results of Huffman, et al. [1] and Curtis, et al. [2]

II. Calculations

A. Polyethylene and Polypropylene

Huffman and coworkers[1] found large differences in the coliquefaction behavior of polyethylene (PE) and polypropylene (PPE) with Black Thunder (BT) coal in the presence of a zeolite catalyst (HZSM-5) and tetralin solvent. The oil yields of PPE with BT coal are higher (71%) than with PE and BT coal (41%). The preasphaltene and asphaltene yields are higher with PE and BT coal (28%) than with PPE and BT (18%). The total conversion for PPE and BT is 93%, while for PE and BT it is 72%. In the presence of the HZSM-5 catalyst and in the absence of the coal, PE and PPE essentially undergo 100% conversion at 430°C. However, with no catalyst present PE undergoes a 65% conversion at 430°C and PPE 88% at 420°C.

In an earlier study we[3] addressed the experimental results of Huffman, et al.[1] by considering several factors that might explain the differences in the coliquefaction of the two polymers with coal, namely: (i) the ease of cracking of PE vs. PPE, (ii) hydrogen transfer reactions from coal fragments to PE+ and PPE+ fragments , and (iii) addition reactions similar to the methylation of benzene found by He et al.[4]

Zeolites are known to be cracking catalysts of hydrocarbons and these cracking reactions are thought to proceed through carbocation ion intermediates.[5]

Therefore, our starting point was to assume that the zeolite catalyst reacted with the neutral polymer to generate carbocation ions. We then looked at reactions of toluene with PE+ and with PPE+ in order to try to address the factors listed above. We used the MOPAC 5.0 program of Stewart[6] and the Tight Binding Molecular Dynamics (TBMD) program developed by Menon and Subbaswamy.[7] The TBMD method is based on parametrized Hamiltonian band structure methods of solid state physics and ideas from the extended Hückel method. Orbitals are not explicitly introduced at all, and no integrals need be computed. Hence, the method can be used for computing forces for performing molecular dynamics simulations on large systems. Results for structure are at least comparable to the commonly used semi-empirical methods such as MNDO. [6]

We calculated the bond dissociation energies (BDE) for the process

Long [PE+ or PPE+] fragment → Short [PE+ or PPE+] fragment + neutral alkene

using the MOPAC suite of programs and found the BDE for the break up of PE+ to be 2.10 eV, while that for PPE+ is 1.52 eV. The difference in BDE, indicating that PPE+ should be easier to crack than PE+ is an intrinsic factor that could contribute to the higher coliquefaction yield with PPE than with PE. Our finding is consistent with the observation of Feng, et al.,[1] who find that PPE is more easily liquefied than PE at lower temperatures, with or without a catalyst.

To investigate possible reactions with coal-derived fragments, we considered the interaction of PE and PPE carbocation ion fragments with toluene and with Model I, 4-(1-naphthylmethyl)bibenzyl, using the tight-binding molecular dynamics (TBMD) method. The method gives results similar to MOPAC, but can be used to study the "real time" dynamics of processes involving large numbers of atoms. We investigated potential H transfer from the methyl group of toluene to the carbocation ion site of the polymer and found that the H transfer occurs much more readily to PE+ than to PPE+, suggesting a higher barrier in the latter. In fact, we never observed a complete transfer of the methyl H of toluene to PPE+. Such hydrogen transfer processes might provide another pathway for subsequent break-up of the coal fragment. We also investigated the possible transfer of the ring hydrogen from the para position in toluene, since it is known that the methyl group activates the para hydrogen in electrophilic reactions. However, we found no transfer in either PE+ or PPE+.

Within the TBMD calculation we also investigated the possibility of an electrophilic addition reaction in which the PE+ or PPE+ carbocation ion fragment adds to the toluene molecule (leading to carbon-carbon bond formation). This addition reaction was found to occur from an initial C-C distance of 2.5 Å with both PE+ and PPE+. The hydrogen transfer reaction should compete with this addition reaction in the case of PE+. However, we find the addition reaction to be lower in energy than the hydrogen transfer reaction and so the addition reaction should be favored. This latter reaction would lead to higher molecular weight products, *i.e.*, a retrograde process.

In trying to explain why in the PPE coliquefaction scheme there are fewer preasphaltenes and asphaltenes than with PE, we noted the following qualitative differences in the reactions and reaction products in our simulations.

1. We find that with TBMD the C-C bond of the addition product is longer in PPE+ than in PE+. In general the longer the bond, the smaller the overlap between the orbitals of the atoms in the bond, which thus leads to weaker bonds. Therefore, the addition product formed with PPE+ should have a weaker bond compared to the PE+ addition product and the reaction could be relatively more reversible under liquefaction conditions.

2. Primary carbocation ions are much higher in energy than secondary, which are higher in energy than tertiary. Therefore, the primary carbocation should

be much more reactive and undergo faster reactions. Using the MOPAC 5.0/PM3 computational scheme, we find with PE+ that the addition products are more stable than the starting reactants by 2.2 eV; for PPE+ the corresponding stabilization energy is only 1.2 eV. Therefore, the PE+ addition is more exothermic than PPE+. In an attempt to quantify the energy differences between PE+and PPE+ for the addition reaction we compared the MOPAC calculated energies of the starting MOPAC minimized toluene and PE+ or PPE+ to the configuration that the toluene, PE+ and PPE+ took after addition but with removing the other species (a 1-SCF calculation) and found it takes 1.4 eV for PE+ to move to the configuration after addition and 1.65 eV for PPE+ to move. Including the rearrangement of the toluene, a first approximation to the "barrier" for molecular adjustment is 3.28 eV for PE+ and 3.43 eV for PPE+. Therefore, it appears that the PPE+ reaction has a higher activation energy for addition and is, therefore, slower than the PE+ addition reaction.

In our latest series of calculations we have been investigating possible hydrogen transfer reactions from solvent to the two polymeric cation fragments. It has also been found that good hydrogen donor solvents, such as tetralin, the solvent used by Huffman, et al.[1], act as chain terminators in the chain depolymerization schemes of polymers. This, in turn, will lead to lower conversion.[8] Therefore, we investigated potential hydrogen transfer from tetralin to PE+ and PPE+ using the TBMD method. (See Figure 1.) We have found that hydrogen transfer readily occurs from tetralin to PE+ at PE+— (H-tetralin) distances up to 2.5 Å . The transfer from tetralin to PPE+ was found to occur only when the PPE+ — (H-tetralin) distance was 1.9 Å . Therefore, the depolymerization of PE+ is much more readily terminated in the tetralin solvent than the depolymerization of PPE+., which would lead to lower conversions for PE. We are now quantifying the barriers for the H transfer from tetralin and for H transfer from the aliphatic carbon atoms of Model I to the two polymers, as well as the barrier for C bond formation in order to construction an overall kinetic scheme.

B. Polystyrene and Polyisoprene

Curtis, et al.,[2] have observed differences in the coliquefaction behavior of polystyrene (PS) and polyisoprene(PI) with Illinois No.6 coal. When liquefied alone, polystyrene and polyisoprene liquefied readily, while coal underwent a 38% conversion. No solvent or catalyst was used. In coliquefaction with coal, and in the absence of either catalyst or solvent, conversion increased to 60% with coal/polystyrene and 80% with coal/polyisoprene. A synergistic effect was observed in the coal/isoprene system. The experiments were carried out at 400°C.

Synergism was also observed for the PI/coal system when a Mo naphthenate plus sulfur or Fe naphthenate plus sulfur catalyst was used. However, for the PS/coal system a slight synergism was observed with the Mo naphthenate plus sulfur catalyst but not with the Fe naphthenate plus sulfur catalyst.

We have begun our modeling of the PI /coal and PS /coal systems by considering the experiments in which there were no catalysts or solvents present. We are using the PM3 option in the MOPAC computational scheme and, in the absence of any catalyst, we are assuming that free radical decomposition of the two polymers would occur. By comparing the energies of the two free radicals formed on bond cleavage to the energy of the whole polymer fragment, we calculate the BDE of PS to be 2.54 eV while that of PI is 2.42 eV. For comparison, the PM3 BDE of the bibenzyl bond of Model I is 2.96 eV. Therefore, PI should be slightly easier to liquefy than PS and both decompose more readily than Model I .

We are now investigating hydrogen transfer barriers for transfer of hydrogen between toluene (our initial model for coal derived fragments) and the two free radical fragments formed in the thermal decomposition of PI and PS.(See Figure 2.) A lower hydrogen transfer barrier in the PI/coal system, which would aid in the decomposition of coal, than in the PS/coal system might explain the synergism observed in one system and not the other. We will also consider radical hydrogen

transfer reactions and hope to extend our studies to the catalyst systems in the future.

Acknowledgements: This research was supported by USDOE contract DE-FC22-93PC93053 to the Consortium on Fossil Fuel Liquefaction Science.

References

1. Feng, Z.; Zhao, J.; Rockwell, J.; Bailey, D.; Huffman, G. *Prepr., Div. Fuel Chem., Am. Chem. Soc.*, **1995**, *40*, 34.;*Fuel Proc Tech*, **1996**, in press.
2. Curtis,C.; Tang, Y.; Luo,M. Presented at 8th Annual Technical Meeting, CFFLS, **1994**.
3. Ades, H.F.; Subbaswamy. K.R. *Fuel Proc Tech*, **1996**, in press.
4. He, S.J.X.; Long, M.A.; Wilson, M.A.; Gorbaty, M.L.; Maa, P.S. *Energy Fuels*, **1995**, 9, 616.
5. Bhatia, S. *Zeolite Catalysis: Principles and Applications*; CRC Press, **1990**.
6. Dewar, M.J.S.; Stewart, J.J.P. *Quantum Chemistry Program Exchange No. 58 vers. 5.0*, Indiana University (Bloomington).
7. Menon, M.; Subbaswamy, K.R. *Phys. Rev. Lett.*, **1991**, *67*, 3487; Menon.M.; Richter. E.; Subbaswamy, K.R. *J.Chem.Phys.* **1996**,*104*, 5875.
8. Sato,S.; Murakata, T.; Baba, S.; Saito, Y.; Watanabe, S. *J. Appl. Polym. Sci.*, **1990**, *40*, 2065.

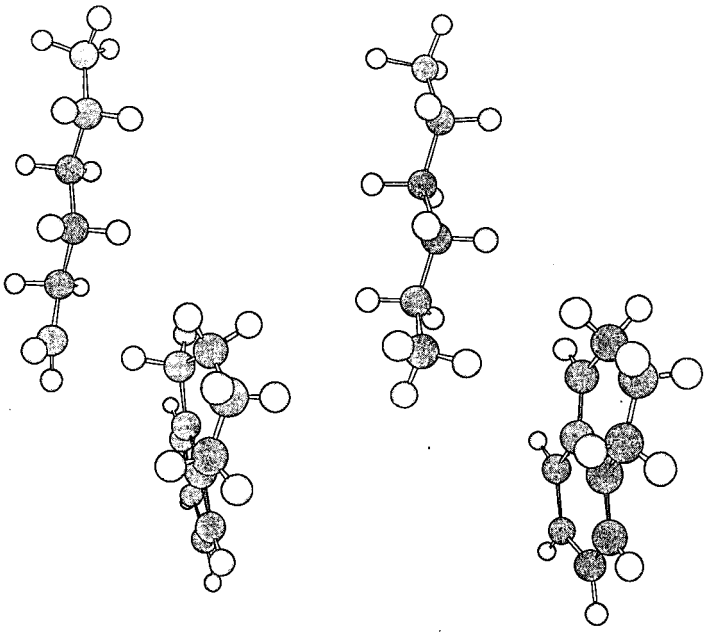

Fig. 1. Tetralin-PE^{+} before and after H transfer from tetralin to PE^{+}.

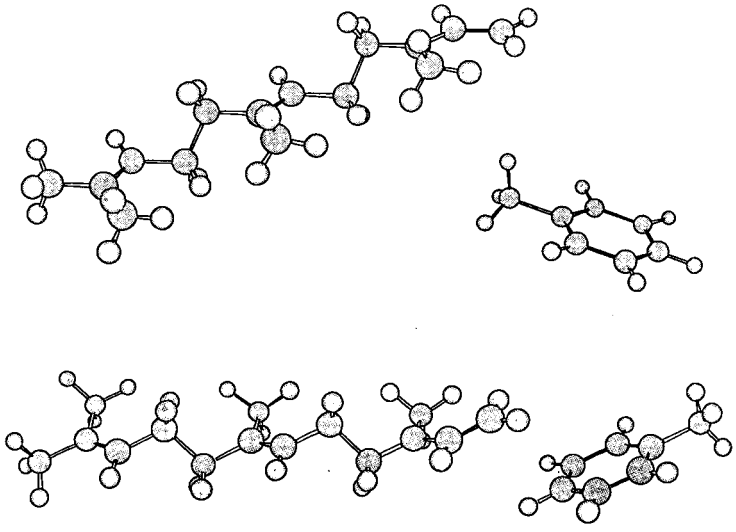

Fig. 2. Typical initial configurations considered for H atom transfer from toluene to a PI free radical fragment.

CATALYTIC TWO STAGE COPROCESSING OF WASTE PLASTICS AND COAL

Mingsheng Luo and Christine W. Curtis
Chemical Engineering Department
Auburn University, Al 36849-5127

Keywords: two stage, coprocessing, waste plastics, coal

INTRODUCTION

The disposal of post-consumer plastics has become an increasingly serious environmental problem throughout the world as well as in the United States. Because of its ever increasing volume, disposal of waste plastics by landfilling is an undesirable option, particularly in densely populated areas. Recycling of plastics is a direct way of reusing the hydrocarbon content in the plastics. (Leaversuch, 1991). However, primary recycling of plastics into the monomer is only accomplished in approximately 2% of the cases (Smith, 1995) and requires that the recycled plastic be separated from the mixed waste. Recycling the mixed plastics wastes to liquid or gases provides a means for reutilizing the hydrocarbons as fuels or chemical feedstock and abstracting the energy or chemical value from the waste material. Pyrolysis and liquefaction of waste plastics as well as liquefaction of waste plastics with coal have been explored by a number of researchers. (Taghiei et al., 1994; Anderson and Tuntawiroon, 1993; Ng, 1995a; Ng, 1995b; Palmer et al., 1995; Huffman et al., 1995)

The supply of waste plastics is limited; even if all of the waste plastics were recycled to transportation fuels, only one month's supply of would be available on annual basis (DOE, 1995). The feasibility of tertiary waste plastics recycling is limited by the availability of waste plastics and the constancy of the supply. Hence, waste plastics liquefaction can provide a valuable addition to our energy supply but will not substantially affect self-sufficiency. Utilization of a native natural resource such as coal in conjunction with waste plastics will not only provide sufficient hydrocarbon resources and a constant feedstock supply but will also provide more self-sufficiency in our energy supply.

In a previous research study, waste plastics were coprocessed directly with coal using commercial hydrotreating catalysts, slurry phase catalysts, zeolite catalysts, and fluid catalytic cracking (FCC) catalysts (Luo and Curtis, 1996 a and b). Since the reactants are composed of chemically different materials, coal being aromatic and most common plastics in the waste stream being polyolefins and aliphatic, these two materials are basically chemically incompatible. The efficacy of the conversion of coprocessed coal and waste plastics to THF soluble material depended upon the plastics composition, efficacy of the catalyst used for the reactant composition, and use of a solvent as well as type of solvent. Coliquefaction reactions of mixtures of waste plastics as well as coprocessing reactions of those mixtures with coal evinced that reaction parameters must be tailored to the waste plastics stream to achieve maximal plastics conversion to liquids. Those reaction parameters were often in conflict with the most efficacious reaction conditions for coal. Typical coal liquefaction catalysts were not sufficiently active to hydrocrack the polyolefins while hydrocracking catalysts were easily and rapidly deactivated in the presence of liquefying coal because of the heavy hydrocarbons and heteroatoms present. Hence, simultaneously coprocessing coal and waste plastics when they are initially both solid reactants does not usually produce an optimal product from either material.

To circumvent the problems associated with simultaneously reacting materials that are inherently so different, two stage processing was investigated. The two stage process was composed of a first stage in which the waste plastics mixture was liquefied and of a second stage where coal was liquefied with the hexane soluble product from the first stage. The reaction conditions and catalysts for each stage were optimized to yield the highest conversion of the reactants to THF soluble and hexane soluble materials in each stage.

EXPERIMENTAL

Materials. The model plastics used in this research were high density polyethylene (HDPE), polyethylene terephthalate (PET), and polystyrene (PS), all of which were obtained from Aldrich. A mixture consisting of 50% HDPE, 30% PET, and 20% PS was used as a base plastics mixture in single and two stage reactions. The solvents used in this study were tetralin and hexadecane, obtained from Aldrich and Fisher Scientific, respectively. The plastics and the solvents were used as received. Illinois No. 6 coal, obtained from the Argonne Premium Coal Sample Bank, was used as received. The catalysts used in this study were fluid catalytic cracking catalysts, Low Alumina and Super Nova-D, which were supplied by Davison Chemical Division of W. R. Grace and Company. A zeolite HZSM-5, obtained from United Catalysts, was also used. The catalysts used for the second stage coal reactions included the slurry phase hydrogenation catalyst precursors, molybdenum naphthenate (6% Mo; MoNaph) and iron naphthenate (6% Fe; FeNaph), obtained from Shepherd Chemical. Both of the slurry phase catalysts were reacted in the presence of excess elemental sulfur, which was obtained from Aldrich.

First Stage Reaction. In the first stage reaction, a waste plastics mixture was liquefied in order to obtain a liquid solvent to be used as the solvent in the second stage coprocessing reaction. The plastics mixture was liquefied in ~50 cm^2 stainless steel microtubular reactors at 713 K (440 °C)

for 60 min under an initial H_2 pressure of 2.8 MPa introduced at ambient temperature. The reactors were agitated vertically at 450 rpm. Ten grams of plastics mixture were charged to the reactor. The loading for the catalytic reactions using FCC and HZSM-5 catalysts was 10 wt % on a plastics charge basis. Both HZSM-5 and the FCC catalysts were pretreated prior to being used in the reaction by heating the catalysts for 2 hr at 477 K (400 °F) followed by 2 additional hours at 811 K (1000 °F). After the reaction was completed, the reactor was quenched in ambient water. The amount of gaseous products was weighed and the gaseous products were removed. The liquid products were extracted with hexane and the soluble amount determined. The hexane solvent was evaporated from the liquid product which was then used as a coal liquefaction solvent in the second stage reaction.

Second Stage Reaction. The second stage coprocessing reaction was performed with 2 g of coal and 2 g of first stage solvent in 20 cm^2 stainless steel microtubular reactors at 713 K (440 °C) for 30 min. The reactors were charged with 5.6 MPa of H_2 introduced at ambient temperature and were agitated at 435 rpm during the reaction. Slurry phase MoNaph and FeNaph catalysts at 1000 ppm of active metal and elemental sulfur at 6000 ppm were charged on a total reactant basis. In some reactions, a loading of 500 ppm of MoNaph and 500 ppm of FeNaph was used.

Product Analysis. The liquid products for the second stage reaction were analyzed by solvent fractionation using hexane as the initial solvent followed by THF. Any solid residue left in the reactor after extraction was carefully scraped from the reactor walls. The amount of hexane and THF soluble materials was determined as well as the amount of THF insoluble material or IOM (insoluble organic matter which is ash free). The hexane soluble fraction produced in the first stage was used as the solvent in the second stage reaction.

The recoveries obtained in the reactions were calculated by

$$\text{Recovery} = (\text{g Recovered} / \text{g Charged}) \times 100\%$$

as are given in the tables. The conversion of the solid reactants to THF soluble material was determined on a solvent, moisture, and ash free basis using the equation

$$\text{Solid Conversion} = 100\% - \text{IOM}\%$$

where IOM is produced from reactions of either coal or plastics or both.

RESULTS AND DISCUSSION

Two stage coprocessing of coal and waste plastics was investigated to determine if higher conversion to THF soluble material and higher production of hexane soluble material could be obtained than with single stage coprocessing. Two sets of experiments were performed. The first set of reactions consisted a first stage catalytic reaction using the base plastic mixture. Then coal was placed in the reactor and reacted with the liquefied plastics as well as the unconverted material. The second set of reactions consisted also of two stage processing, but in these reactions the hexane soluble material produced in the first reaction of the base plastics mixture was used as the solvent for second stage coal reaction. The reaction products from each stage were analyzed using solvent fractionation and a determination of the conversion of the solids to THF soluble products.

Two Stage Coprocessing. The first set of the two stage reactions is presented in Table 1. The first stage reaction involved the base plastics mixture consisting of 50% HDPE, 30% PET, and 20% PS that was reacted at 440 °C and 30 min using Low Alumina and HZSM-5 catalysts. Both catalysts promoted plastics conversion to THF solubles of more than 85% and hexane soluble yields 69.8% and 61.5%, respectively. The second stage reaction was performed with coal at 400 °C for 30 min and 5.5 MPa of initial H_2 pressure. The coal was placed in the reactor with the entire reacted base plastics mixture as well as the first stage catalyst. The products obtained from the second stage reaction were similar regardless of the first stage reaction. These second stage reactions produced high levels of gas make of 32.5 and 29.7%, respectively, for the first stage Low Alumina and HZSM-5 catalysts. The conversions from the second stage reactor were similar and low, 57.5 and 54.9%, respectively, for Low Alumina and HZSM-5 first stage catalysts. The second stage hexane solubles were also similar and low, yielding 22.8 and 23.5%, respectively.

Two Stage Coprocessing using First Stage Hexane Solubles as Solvent. The disadvantage of the first set of two stage reactions was the presence of unconverted and difficult to convert plastics in the second stage reaction. In addition, the catalyst from the first stage was present during the coal reaction. These hydrocracking catalysts promoted high gas production during the second stage. Consequently, the reaction sequence was changed to eliminate the presence of both the unconverted material and the hydrocracking catalyst in the second stage. In both stages the reaction conditions were tailored so as to promote the desired reactions during that stage and to minimize the undesirable reactions.

The first stage reaction was performed at 440 °C and 60 min with each of the three hydrocracking catalysts, Low Alumina, HZSM-5, and Super Nova-D, and the base plastics mixture. High conversions to THF soluble materials were obtained with all three reactions yielding 88.4 , 94.5, and 95.1, respectively, as shown in Table 2. The majority of the product produced was hexane

soluble material that was extracted for use as the solvent in the second stage. Although gas yields ranged from 14.9 to 17.9%, these products did not affect the second stage reaction and could presumably be used as a fuel.

The second stage reaction employed coal at reaction conditions of 400 °C and 30 min with 5.6 MPa H_2 introduced at ambient temperature (Table 3). Two reactions were performed at a higher temperature of 440 °C. The slurry phase catalysts, MoNaph and FeNaph with excess sulfur, were used individually and as a mixture. Three different solvents, each produced with one of the three different first stage catalysts, were employed in the second stage reaction.

Catalyst type strongly affected the conversion and product distribution of the second stage reaction. The reactions that contained only MoNaph as the catalyst resulted in higher conversions than the reactions with either FeNaph or the combination of the two catalysts. The highest conversions were achieved with the HZSM-5 produced solvent and MoNaph, yielding 93.7%. The next highest conversion, 88.2%, occurred using the Low Alumina produced solvent and with MoNaph. The MoNaph catalyst also gave the highest production of hexane soluble materials, yielding 42.5% in the HZSM-5 produced solvent and 39.9% in Low Alumina produced solvent. Since half of the material that was introduced into the reactor was the hexane soluble fraction of the plastics mixture and since the hexane soluble materials present after reaction was less than half of the material that was charged, the plastics mixture converted to other fractions during reaction. The most likely products produced from the reaction of these plastics oils was gas; however, in the case of Low Alumina produced solvent, the sum of gas produced and the hexane solubles was greater than 50% of the product, indicating that some of these products were produced from coal.

Comparison of the two second stage catalysts showed that regardless of the first stage solvent used, less conversion of coal to THF soluble material was achieved with FeNaph and excess S than with MoNaph and excess S. The largest difference was observed with the solvent produced with HZSM-5 which produced a conversion of 66.6% compared to 93.7% with MoNaph. The hexane soluble yields were also less with FeNaph with all of the first stage solvents than with MoNaph. Combining MoNaph and FeNaph in the second stage resulted in nearly equivalent conversion to MoNaph with the Low Alumina solvent and somewhat less conversion with the HZSM-5 solvent. The most notable difference observed between the combined and single catalysts was the product distribution. The combined catalyst produced an extremely high yield of THF soluble materials indicating that although the reactants were converted from solids to THF soluble material, little upgrading to hexane solubles occurred. In fact, both the hexane solubles yield and the gas make were low with the combined catalyst compared to either individual catalyst.

Comparison of One-Step and Two Step Coprocessing. Comparisons of one stage and two stage coprocessing of coal and base plastics mixture are given in Figures 1 to 3. In each of these figures a comparison of the product distributions, in terms of gas, hexane solubles, THF solubles and IOM, are given for four reactions. The reactions are (1) a single stage reaction of waste plastics and coal without a solvent; (2) a single stage reaction of waste plastics and coal with 30% tetralin in hexadecane solvent; (3) a two stage reaction using first stage solvent with coal and FeNaph in the second stage; and (4) a two stage reaction using first stage solvent with coal and MoNaph in the second stage. The product distributions from the two stage reactions given in the figures are the combined product distributions from both stages.

The two stage reactions produced an improved overall product slate for the coprocessing reactions than the single stage reactions reacted with or without solvent. The two stage reaction with either FeNaph or MoNaph as the catalyst produced more hexane soluble and THF soluble yields and less IOM for two of the first stage solvents (HZSM-5 and Low Alumina) than the single stage reactions. For the Super Nova-D solvent, more hexane solubles and less IOM were produced with the two stage reactions while more gas and THF solubles were produced with the single stage reaction.

CONCLUSIONS

Increased conversion and hexane soluble yields with the two stage reactions clearly point to the advantage of two stage processing of coal and waste plastics. The predissolution of the waste plastic prior to contacting coal and the ability to tailor the catalysts and the reaction conditions specifically to the materials being reacted enhanced the reactivity of the system and promoted the desired end products.

REFERENCES

1. Anderson, L.; Tuntawiroon, W. *ACS Fuel Chem. Div. Prepr. 30(4),* 816, 1993.
2. Huffman, G.P.; Feng, Z.; Mahajan, V.; Sivakumar, P.; Jung, H.; Tierney, J.W.; Wender, I. *ACS Fuel Chem Div. Prepr. 40(1),* 35, 1995.
3. Leaversuch, R. *Modern Plastics,* July, 40, 1991.
4. Luo, M.; Curtis, C. W. *Fuel Process. Techno.* in press, 1996 a.
5. Luo, M.; Curtis, C. W. *Fuel Process. Techno.* in press, 1996 b.
6. Ng, S.H. *Energy Fuels, 9,* 216, 1995.
7. Ng, S.H. *Energy Fuels, 9,* 735, 1995.

8. Palmer, S.R.; Hippo, E.J.; Tardon, D.; Blankenship, M. *ACS Fuel Chem. Div. Prepr. 40(1),* 29, 1995.
9. Department of Energy, Technical News Release on Coprocessing of Coal with Waste Plastics, 1995
10. Smith, R. Presentation at the Consortium for Fossil Fuel Liquefaction Science, Ninth Annual Meeting, Pipestem, WV August, 1995.
11. Taghiei, M.M.; Feng, Z.; Huggins, F.E.; Huffman, G.P. *Energy Fuels, 8,* 1228, 1994.

Table 1. Product Distribution from Two-Stage Plastics and Coal Liquefaction Reactions

Stage Number and Conditions	Product Distribution (%)		
	Catalyst	HZSM-5	Low Alumin
Stage 1[a,b] Base Plastic Mixture	Gas	15.4±0.7	17.9±0.1
	Hexane Solubles	75.3±0.2	66.4±0.3
	THF Solubles	4.4±0.5	4.1±0.0
	IOM[c]	4.9±0.1	11.6±0.2
	Conversion (%)	95.1±0.1	88.4±0.2
Stage 2[d] Coal Added to reacted Base Plastic Mixture	Gas	32.5±0.5	29.7±0.2
	Hexane Solubles	22.8±0.2	23.5±1.0
	THF Solubles	2.2±0.7	1.1±1.7
	IOM	42.5±0.4	45.1±1.4
	Conversion (%)	57.5±0.4	54.9±1.4
	Recovery (%)	71.4	74.8

a. Stage 1 reaction conditions and charge: 440°C, 2.8 MPa of H_2 and 30 min, 2 g of base plastic mixture and 10% catalyst based on plastic charge.
b. *Base plastic mixture:* 50% HDPE, 30% PET and 20% PS.
c. IOM: insoluble organic matter, that is ash- and moisture-free
d. Second stage reaction conditions and charge: 2 g of coal at 400°C, 5.6 MPa initial H_2 pressure for 30 min.

Table 2. Product Distribution from Catalytic Liquefaction of Base Plastics Mixture[a,b]

Catalyst	Catalyst		
	Low Alumina	Super Nova-D	HZSM-5
Gas	17.9±0.1	14.9±0.1	15.2±0.7
Hexane Solubles	66.4±0.3	75.1±0.4	75.5±0.2
THF Solubles	4.1±0.0	4.5±0.5	4.4±0.5
IOM[c]	11.6±0.2	5.5±0.8	4.9±0.1
Conversion (%)	88.4±0.2	94.5±0.8	95.1±0.1
Recovery (%)	73.9	70.8	71.8

a. Reaction Conditions: 440°C, 60 min and 2.8 MPa of H_2 introduced at ambient. 2 g of base plastic mixture and 10% catalyst based on plastic charge; no additional solvent was added.
b. *Base plastic mixture:* 50% HDPE, 30% PET and 20% PS.
c. IOM: insoluble organic matter.

Table 3. Product Distribution from Second Stage Coal Liquefaction Reactions using Hexane Soluble Plastic Oil as Solvent[a,b]

Reaction Temperature	First Stage Catalyst and Charge	Second Stage Catalyst[c]	Product Distribution, %				Conversion (%)	Recovery (%)
			Gas	Hexane Solubles	THF Solubles	IOM		
400°C	HZSM-5+Base Plastics	1000 ppm Mo	8.0±0.3	42.5±0.5	43.2±1.0	6.3±0.2	93.7±0.2	81.7±3.7
400°C	HZSM-5+Base Plastics	1000 ppm Fe	9.5±0.8	32.8±0.4	24.3±3.2	33.4±2.8	66.6±2.8	81.4±2.2
400°C	HZSM-5+Base Plastics	500 ppm+Mo 500 ppm Fe	3.8±0.1	29.2±1.1	54.2±2.4	12.9±3.6	87.1±3.6	88.7±1.3
400°C	Low Alumina+ Base Plastics	1000 ppm Mo	19.9±0.6	39.9±1.1	28.3±0.6	11.8±0.0	88.2±0.0	72.2±1.5
400°C	Low Alumina+Base Plastics	1000 ppm Fe	23.0±0.0	29.6±0.9	19.3±0.1	28.1±0.7	71.9±0.7	74.6±2.4
400°C	Low Alumina+Base Plastics	500 ppm+Mo 500 ppm Fe	3.6±0.7	19.2±2.6	64.6±0.1	12.6±1.9	87.4±1.9	92.6±2.0
440°C	Low Alumina+Base Plastics	1000 ppm Mo	49.7±1.2	8.4±5.2	6.1±1.2	35.9±2.7	64.1±2.7	75.9±1.2
440°C	Low Alumina+Base Plastics	1000 ppm Fe	46.9±0.1	0.5±1.4	4.0±0.8	48.7±0.7	51.3±0.7	81.8±1.3
400°C	Super Nova-D+ BasePlastics	1000 ppm Mo	35.7±0.1	27.2±0.0	10.0±0.1	27.1±0.3	72.9±0.3	67.5±0.6
400°C	Super Nova-D+Base Plastics	1000 ppm Fe	33.5±0.1	18.5±0.5	5.3±0.5	42.8±0.9	57.2±0.9	69.1±0.3

a. Reaction Conditions: 400 °C, 30 min, 5.6 MPa H_2 introduced at ambient temperature, and 2 g of coal and 2 g of plastic oil were added to the reactor.
b. Solvent was from base plastic mixture (HDPE:PET:PS=50:30:20), which was liquefied at 440 °C, 2.8 MPa of H_2 for 60 min.
c. Catalyst contained 1000 ppm Mo or Fe naphthenate plus 6000 ppm S. When combined catalysts were used, 500 ppm Fe and 500 ppm Mo plus 6000 ppm S were added to the reactor.

Figure 1. Comparison of One-Stage and Two-Stage Coprocessing of Coal and Base Plastic Mixture Using HZSM-5

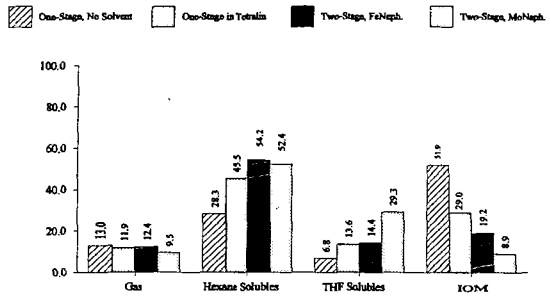

a. One-stage coprocessing: coal + base plastic mixture at 440°C.
b. Two-stage coprocessing: coal + base plastic oil at 400°C.

Figure 2. Comparison of One-Stage and Two-Stage Coprocessing of Coal and Base Plastic Mixture Using Low Alumina

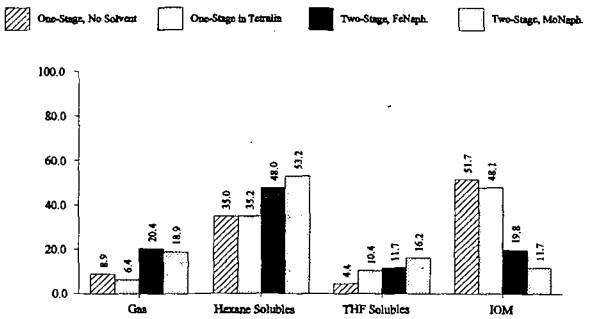

a. One-stage coprocessing: coal + base plastic mixture at 440°C.
b. Two-stage coprocessing: coal + base plastic oil at 400°C.

Figure 3. Comparison of One-Stage and Two-Stage Coprocessing of Coal and Base Plastic Mixture Using Super Nova-D

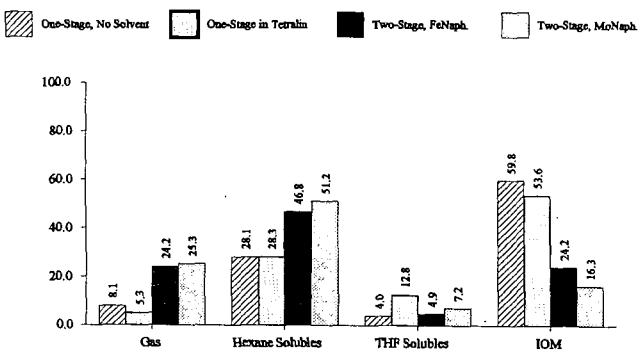

a. One-step coprocessing: coal + base plastic mixture at 440°C.
b. Two-step coprocessing: coal + base plastic oil at 400°C.

TWO-STAGE COPROCESSING OF WASTE PLASTICS WITH COAL

Weibing Ding, Jing Liang and Larry L. Anderson
3290 MEB
Department of Chemical and Fuels Engineering
University of Utah
Salt Lake City, UT 84112

Keywords: two-stage coprocessing, waste plastics, synthetic fuel

INTRODUCTION

Commingled post-consumer plastic waste (CP#2) or high density polyethylene (HDPE) was found to be thermally degraded only at temperatures higher than 430°C, while typical coal liquefaction temperatures are about 400°C. This causes difficulty for coprocessing coal with waste plastic in single stage at appropriate reaction conditions. Moreover, it is hard to find a catalyst which is effective for depolymerization of both coal and HDPE or CP#2. In this study, two-stage coprocessing was developed to produce liquid fuels. In the first stage, CP#2 or HDPE was liquefied in an 150-cm^3 autoclave reactor at 435°C, 1 hr, with stirring speed of 800 rpm, under N_2 or H_2 with and without catalyst (HZSM-5). The resulting liquid products (yields of 78-88 wt%) were utilized as solvents for liquefaction of DECS-6 coal or Fe loaded DECS-6 coal in tubing reactors at 400°C, 1 hr, 160 rpm, ~2000 psig H_2.

The conversion of coal to liquids is generally perceived to proceed via free-radical mechanisms. Reactive radical fragments are formed by thermally rupturing scissile bonds and by hydrogenolysis [1]. Once formed, fragments are either stabilized by hydrogen addition or recombined to form regressive, polymeric products. Two external sources of hydrogen are available to meet these demands. These are donor hydrogen in the solvent and gaseous molecular hydrogen. Therefore, solvent quality plays a significant role in determining which reaction path is taken during coal liquefaction. The solvents investigated were mostly hydroaromatics (tetralin, isotetralin), aromatics (naphthalene, anthracene oil, phenathrene, pyrene), naphthenics (decalin), and their combinations [2-6]. Recently, phenolic compounds (phenol, cresol) were also used as coal liquefaction solvents [7]. These solvents are relatively expensive, therefore we chose Plastic-Derived-Liquids (PDL) as a solvent for coal liquefaction.

For coal liquefaction, iron-based catalysts, because of obvious economic and environmental benefits, have been widely studied recently [8-13]. Yuen [8] investigated the effects of various iron precursors on liquefaction of DECS-6 and DECS-17 coals in absence of solvent. As an iron precursor, ammonium iron (III) sulfate dodecahydrate was found to be very effective in increasing the liquid yields of catalytic hydroliquefaction of Blind Canyon coal. Derbyshire [14] also reported that in the presence of solvent, there are the advantages of adding the precursor by impregnation over its addition in the form of particulates. Thus, a DECS-6 coal, impregnated with Fe catalyst, was selected for liquefaction studies in the second stage. Noncatalytic reactions were also examined for comparison.

EXPERIMENTAL

High-volatile bituminous Blind Canyon DECS-6 coal, obtained from the Penn. State Coal Sample Bank, was ground to pass through a 100 mesh Tyler series screen using a ball mill grinder under nitrogen. Ground coals were dried under vacuum at 100°C for six hours, kept overnight at room temperature, stored in glass bottles sealed with nitrogen, and then put in a refrigerator for future use. Iron loaded DECS-6 coal was prepared by incipient wetness impregnation. Ammonium iron (III) sulfate dodecahydrate (AFS(III)), obtained from Aldrich Chemical Company, was used as precursor of iron. After impregnation, the resulting coal was dried at the same conditions as mentioned above. The weight ratio of iron to moisture-free coal was 1.12:100.

HDPE (M.W.=125,000) in bead form was purchased from Aldrich Chemical Company. Commingled post-consumer plastic (CP#2), obtained from the American Plastics Council, was ground to -25 mesh. Detailed analyses of DECS-6 coal and CP#2 are listed elsewhere [15]. Synthesized according to U.S. Patent 4,250,345 [16], HZSM-5 catalyst contains 35 wt% Al_2O_3 binder. HZSM-5, with a Si/Al mole ratio of 35, was pulverized to -100 mesh and calcined in air at 500°C for 3 hours before use.

Depolymerization of HDPE or CP#2 was carried out in a 150-cm^3 stainless steel autoclave (Autoclave Engineers). A mixture of HDPE or CP#2 (20.0000 g) and catalyst (0.4000 g HZSM-5) were charged into the reactor. For reaction under N_2, the reactor was purged with N_2 5 times

and then closed with a zero pressure gauge value. For reactions with H_2, the reactor was pressurized with 1000 psig H_2 after being purged with N_2 at room temperature. The fixed reaction conditions were: 435°C, 60 minutes, 800 rpm. When the reaction was finished and the reactor cooled to room temperature, the gases were collected. The detailed procedure is described elsewhere [15]. Liquid and solid products were separated by filtration at room temperature. The solid portion was washed with excess pentane and then dried at 60°C under vacuum overnight. The solid yield is defined as (weight of solid)x100/(weight of feed), while oil yield is defined as {100 - gas yield - solid yield}. This oil (Plastic-Derived-Liquids) was utilized as solvent in the next stage. The weight of feed refers to weight of HDPE or CP#2. All experiments were performed in duplicate; repeatability of the results was $\pm$1.5% for oil yield.

In the 2nd stage, solvent (Plastic-Derived-Liquids , tetralin, or waste oil) and dried or iron loaded DECS-6 coal were fed into the 27-cm^3 tubing reactors with a ratio of 2:1 (solvent : dry coal, by weight). The reaction parameters were 400°C, ~2000 psig H_2, 60 minutes, 160 rpm. The reaction procedure was identical to that described in reference 15. As gaseous products came from both coal and solvent, it was difficult to determine how much gas was from coal depolymerization. Therefore, the reaction products were lumped as oil+gas, asphaltenes+preasphaltenes, and THF insolubles. The total conversion is defined as {100x[1-(weight of THF insoluble)/(weight of maf coal)]} and the asphaltenes+preasphaltenes yield as {(weight of THF soluble but pentane insoluble)x100/(weight of maf coal)}. The oil+gas yield is {100x[1-(weight of pentane insoluble)/(weight of maf coal)]}.

The gases obtained from the first stage were analyzed by a flame ionization detector on gas chromatography (HP-5890II) using a column packed with HayeSep Q. The liquid products were analyzed by GC/MS using a 30-m long DB-5 capillary column. The boiling point distribution of the liquid products from the second stage of two-stage processing were determined by modified simulated distillation according to ASTM D 2887-89 and D5307-92. The analysis was performed on HP-5890 series II gas chromatograph, using a Petrocol B column (6 inches long and 0.125 inches outside diameter).

RESULTS AND DISCUSSION

Degradation of HDPE and CP#2 to Obtain Plastic-Derived-Liquids. For degradation of HDPE, the maximum oil yield, 87.2%, was obtained under N_2 without catalyst, while the maximum gas yield, 21.2%, was produced over HZSM-5 under hydrogen (Table 1). For non-catalytic decomposition of HDPE, the solid yield obtained by reaction under nitrogen was 5.5%, while the same yield obtained under hydrogen it was 15.1%. Thermal depolymerization of HDPE was favored in N_2. Since hydrogen is a kinetic chain transfer agent; it might saturate the thermally cracked radicals and prevent them from cracking further. Catalytic reaction over HZSM-5 with hydrogen (Table 1) gave the highest gas yield (21.2%) and lowest solid yield (1.1%). The hydrogenation ability of HZSM-5 was also demonstrated by conversion of ethene [17].

Thermal degradation of CP#2 under N_2 gave the highest oil yield, 86.2%, while catalytic reaction over HZSM-5 under H_2 led to the highest gas yield, 17.6%. The cracking or hydrocracking ability of HZSM-5 is reflected in the resulting lower solid yields and higher gas yields, compared with those from thermal reactions (Table 1). Compared with degradation of CP#2 under nitrogen, the non-catalytic reaction under hydrogen gave higher solid yield and less gas and oil yields (Table 1). This means that hydrogen also inhibited thermal decomposition of CP#2 to some extent.

Upon detailed GC/MS analyses, the oil products were categorized into five groups: 1-olefins, n-paraffins, aromatics, naphthenes, and others (Figure 1), where "others" included mainly iso-paraffins, cyclic-olefins, branched and normal internal olefins. For HDPE, compared with oil products from the thermal reaction under N_2, the oil obtained from non-catalytic reaction under H_2 contained higher n-paraffins and 1-olefins, with lower naphthenes, aromatics and others. Compared with the thermal runs, catalytic reactions over HZSM-5 under both N_2 and H_2 produced oil products with large amounts of aromatics, naphthenes, and others at the expense of 1-olefins and n-paraffins (Figure 1). This is consistent with a similar observation reported previously [18]. Therefore, shape selective zeolite, HZSM-5, had not only high cracking (or hydrocracking) ability, but also had cyclization and aromatization functions.

For degradation of CP#2 under nitrogen, like HDPE degradation under N_2, the same change in oil composition was observed when HZSM-5 was added, i.e., more aromatics and naphthenes, less 1-olefins and n-paraffins. Obviously, HZSM-5 had a stronger effect on HDPE than on CP#2. This may be due to a negative effect of the heteroatoms and trace metals contained

in CP#2. For degradation of CP#2 under hydrogen, the general trends of non-catalytic and catalytic reactions were like those under nitrogen (Table 1, Figure 1).

Plastic-Derived-Liquids Used as Solvents for Coal Liquefaction. Table 2 shows the effects of different solvents on liquefaction of DECS-6 coal at 400°C, 2000 psig H_2, for 60 minutes. Compared with the non-solvent reaction, reactions in the presence of A-1, A-2, A-7, and A-8 oil gave higher total conversions and gas+oil yields. However, A-4, A-5, A-10, and A-11 oil, which were derived from degradation of CP#2, had slightly negative effects on total conversion although increased gas+oil yields. In the presence of waste oil, total conversion increased to some extent, with slightly increasing gas+oil yield. The positive effect of waste oil may be due to a higher content of metals, which may behave as catalysts at reaction conditions [19]. Tetralin, an excellent hydrogen donor solvent, gave the highest conversion and gas+oil yield. The difference in conversion corresponding to different solvents is significant, with 81.4% for tetralin, 57.1% for waste oil, 39.9-48.4% for Plastic-Derived-Liquids, and 44.0% for the non-solvent reaction.

In Table 3, the catalytic results, using PDL as solvents, are compared with those when tetralin and waste oil were used, and when no solvent was used. Compared with thermal reactions (Table 2), the trend of the effects of solvents on conversion and yields for catalytic runs is the same. A-1, A-2, A-7, and A-8 oil were active for catalytic coal liquefaction, increasing both total conversion and yields, while A-4, A-5, and A-11 oil (obtained from CP#2), decreased total conversion slightly, although enhanced the gas+oil yields greatly. Compared with thermal reactions, the difference in conversion corresponding to different solvents decreased in the presence of catalyst. From Tables 1 and 2, at a catalyst loading of 1.12%, the difference in coal conversions between tetralin and PDL is only about 2-10 percentage points, while the difference in thermal conversions for these solvents is about 33-41 percentage points. This implies that PDL can be used with this Fe catalyst, and results obtained are nearly the same as those obtained from tetralin, an expensive hydrogen donor for coal liquefaction. Compared with the thermal reactions, the total conversions and yields were higher in the presence of iron catalyst for each solvent used. This shows that the Fe catalyst was active for the reaction system at conditions used.

For thermal reactions (Table 4), compared with oil from the non-solvent run, the oil products obtained from the reactions with PDL as solvent contained higher amounts of lower-boiling fractions (gasoline, kerosene, and gas oil), except for A-7 oil, which was produced from degradation of HDPE under hydrogen. It is notable that A-7 oil gave highest conversion and oil+gas yield among PDL (Table 2). The lightest oil was from reaction with A-2 oil as solvent, with 92.1% lower-boiling fractions (b.p. up to 325°C). The quality of oil products obtained from reaction with waste oil as solvent was very poor, although the total conversion was increased to some extent. The lower-boiling fractions (b.p. up to 325°C) was only 14.0%. This indicated that further severe upgrading of the oil products would be required.

For catalytic reactions (Table 5), addition of each PDL improved the quality of oil products, producing more lighter components in oil fractions. The oil product with best quality was obtained with A-8 oil, produced from decomposition of HDPE using HZSM-5 as catalyst under hydrogen. This oil contains 59.6% gasoline fraction (<200°C), 24.3% kerosene fraction (200-275°C), and 7.9% gas oil fraction (275-325°C).

Compared with the corresponding thermal reactions, catalytic reactions gave heavier oil products except for the reaction using A-8 oil as solvent. For example, for the non-solvent reaction, the oil products contain 67.5% and 48.1% lower-boiling fractions (b.p. up to 325°C) for thermal and catalytic reactions, respectively. The same numbers for the reaction with A-1 oil as solvent were 78.4% and 70.3% for thermal and catalytic reactions, respectively. This indicated that the total conversion and gas+oil yield increased for catalytic reactions at the expense of oil quality, although the quality just slightly decreased and conversion greatly improved.

Taking into consideration conversion, oil quality, process economics, and process safety, a reasonable senario is: in the first stage, HDPE or CP#2 is degraded under nitrogen; in the second stage, oil products obtained from the first stage (A-1 oil from HDPE and A-4 oil from CP#2) are used as solvents for liquefaction of iron loaded DECS-6 coal. With A-1 oil as solvent, the total conversion of coal was 85.0%, and oil products contained 26.9% gasoline (<200°C), 27.5% kerosene (200-275°C), 15.9% gas oil (275-325°C), 16.6% gas heavy gas oil (325-400°C), and 13.1% vacuum gas oil (400-538°C). The coal conversion was 77.9% in the presence of A-4 oil, and oil products contained 72.0% lower-boiling fractions (b.p. up to 325°C).

CONCLUSIONS

- HDPE and CP#2 can be thermally or catalytically depolymerized under either nitrogen or hydrogen at 435°C. Thermal reactions gave better results with nitrogen than with hydrogen, while catalytic reactions (HZSM-5 used as catalyst) produced oil products with higher quality under hydrogen than under nitrogen.

- The oil from degradation of HDPE or CP#2 can be used as coal liquefaction solvents. In the presence of the impregnated iron catalyst, the Plastic-Derived-Liquids (oil obtained from decomposition of HDPE at 435°C, 0 psig initial nitrogen pressure, 1 hour) produced similar gas+oil yield and total conversion as did tetralin. The resulting oil contained 70.3% lower boiling fractions (b.p. up to 325°C).

- The bench-scale experiments showed that two-stage coprocessing is a feasible and promising method for utilization of plastic waste. In the first stage, plastics can be degraded alone under nitrogen at 435°C; the resulting liquids can be utilized as solvent for liquefaction of Fe loaded coal at 400°C in the second stage.

ACKNOWLEDGMENT

The authors gratefully acknowledge the funding support from the U.S. Department of Energy through the Consortium for Fossil Fuel Liquefaction Science.

REFERENCES

1. Vernon, L.W. (1980), Fuel, **59**(2), 102.
2. Clarke, J.W., Rantell, T.D., Snape, C.E. (1984), Fuel, **63**, 1476.
3. Mochida, I., Takayama, A., Sakata, R., Sakanishi, K. (1990), Energy and Fuels, **4**, 398.
4. Bedell, M.W. and Curtis, C.W. (1991), *ibid*, **5**, 469.
5. Tagaya, H., Takahashi, K., Hashimoto, K., Chiba, K. (1989), *ibid*, **3**, 345.
6. Takemura, Y., Saito, Y., Okada, K., Koinuma, Y. (1989), *ibid*, **3**, 342.
7. Winschel, R.A., Robbins, G.A., Burke, F.P. (1986), Fuel, **65**, 526.
8. Yuen, W.H. (1994), Dissertation, University of Utah.
9. Okamoto, S., Kitajima, A., Taniguchi, H., Ikenaga, N., Suzuki, T. (1994), Energy and Fuels, **8**, 1077.
10. Anderson, R.K., Armstrong, B.T., Givens, E.N., Derbyshire, F.J. (1994), Preprints of ACS, Div. Fuel Chem., **39**(4), 1093.
11. Huffman, G.P., Ganguly, B., Zhao, J., Rao, K.R.P.M., Shah, N., Feng, Z., Huggins, F.E., Taghiei, M.M., Lu, F., Wender, I., Pradhan, V.R., Tierney, J.W., Seehra, F.E., Ibrahim, M.M., Shabtai, J., Eyring, E.M. (1993), Energy and Fuels, 7, 285.
12. Pradhan, V.R., Hu, J., Tierney, J.W., Wender, I. (1993), Energy and Fuels, 7, 446.
13. Eklund, P.C., Stencel, J.M., Bi, X.X., Keogh, R.A., Derbyshire, F.J. (1991), Preprints of ACS, Div. Fuel Chem., **36**(2), 551.
14. Derbyshire, F.J. (1988), in Catalysis in Coal Liquefaction, IEACR/08, IEA Coal Research: London, UK, p69.
15. Ding, W., Tuntawiroon, W., Liang, J. and Anderson, L.L. (1996), Fuel Proc. Tech., in press.
16. U.S. Patent 4,250,345.
17. Kanai, J., Martens, J.A. and Jacobs, P.A. (1992), J. of Catalysis, 133:527.
18. Anders, G., Burkhardt, I., Illgen, U., Schulz, I.W. and Scheve, J. (1990), Applied Catalysis, 62:272.
19. Tarrer, A.R., Kuo, C.H., Mulgaonkar, M.S., Parkash, K.R., Wimberly, J.D. (1994), Proceedings of Contractors' Review Conference, Coal Liquefaction and Gas Conversion (Pittsburgh), p539.

Table 1. Yields of Products Obtained from Thermal and Catalytic Degradation of HDPE or CP#2 in a 150-cm^3 Autoclave at 435°C, 60 Minutes, 800 rpm (0.4 g HZSM-5 was used as catalyst for 20.0 g HDPE or CP#2)

Initial Pressure	Run Number	Reaction System	Gas Yield, wt%	Oil Yield, wt%	Solid Yield, wt%
0 psig N_2					
	A-1	HDPE	7.3	87.2	5.5
	A-2	HDPE+2% HZSM-5	16.5	82.1	1.4
	A-4	CP#2	9.3	86.2	4.5
	A-5	CP#2+2% HZSM-5	12.5	83.4	4.1
1000 psig H_2					
	A-7	HDPE	3.1	81.8	15.1
	A-8	HDPE+2% HZSM-5	21.2	77.8	1.1
	A-10	CP#2	7.5	83.7	8.8
	A-11	CP#2+2% HZSM-5	17.6	76.2	6.2

Table 2. Yields (refer to coal alone) of Products Obtained from Liquefaction of DECS-6 Coal with Plastic-Derived-Liquids as Solvents in a 27-cm^3 Tubing Reactor at 400°C, ~2000 psig H_2, 60 Minutes, 160 rpm (solvent : dry coal = 1:1, weight)

Solvent	Gas+Oil Yield, wt%	Asphaltenes+ Preasphaltenes Yield, wt%	Conversion, wt%
None	24.4	19.5	43.9
Tetralin	40.2	41.2	81.4
Waste Oil	26.6	30.5	57.1
A-1 Oil (1st stage: HDPE, N_2)	28.9	18.6	47.5
A-2 Oil (1st stage: HDPE+2% HZSM-5, N_2)	31.2	17.2	48.4
A-4 Oil (1st stage: CP#2, N_2)	30.5	9.4	39.9
A-5 Oil (1st stage: CP#2+2% HZSM-5, N_2)	27.5	13.9	41.4
A-7 Oil (1st stage: HDPE, H_2)	34.1	14.3	48.4
A-8 Oil (1st stage: HDPE+2% HZSM-5, H_2)	28.5	18.6	47.1
A-10 Oil (1st stage: CP#2, H_2)	28.4	13.2	41.6
A-11 Oil (1st stage: CP#2+2% HZSM-5, H_2)	25.8	17.0	42.8

Table 3. Yields (refer to coal alone) of Products Obtained from Liquefaction of Fe Loaded DECS-6 Coal (Fe:dry coal =1.12:100, in weight) with Plastic-Derived-Liquids as Solvents in a 27-cm^3 Tubing Reactor at 400°C, ~2000 psig H_2, 60 Min., 160 rpm (solvent : dry coal = 1:1, weight)

Solvent	Gas+Oil Yield, wt%	Asphaltenes+ Preasphaltenes Yield, wt%	Conversion, wt%
None	29.6	49.6	79.2
Tetralin	41.8	45.1	86.9
Waste Oil	37.9	42.1	80.0
A-1 Oil (1st stage: HDPE, N_2)	39.1	45.9	85.0
A-2 Oil (1st stage: HDPE+2% HZSM-5, N_2)	36.1	48.6	84.7
A-4 Oil (1st stage: CP#2, N_2)	42.5	35.4	77.9
A-5 Oil (1st stage: CP#2+2% HZSM-5, N_2)	36.5	41.1	77.6
A-7 Oil (1st stage: HDPE, H_2)	39.8	42.7	82.5
A-8 Oil (1st stage: HDPE+2% HZSM-5, H_2)	42.3	38.4	80.7
A-10 Oil (1st stage: CP#2, H_2)	37.9	42.0	79.9
A-11 Oil (1st stage: CP#2+2% HZSM-5, H_2)	35.2	41.1	76.3

Table 4. Boiling Point Distribution (numbers in weight percent) of Final Oil Products Obtained from Two-Stage Coliquefaction of DECS-6 Coal with HDPE or CP#2 (in the first stage, HDPE or CP#2 was degraded in a 150-cm^3 autoclave at 435°C, 1 hour, 800 rpm, under N_2 or H_2; in the second stage, DECS-6 coal was liquefied with Plastic-Derived-Liquids obtained from the 1st stage as solvents in 27-cm^3 tubing reactors at 400°C, ~2000 psig H_2, 60 minutes, 160 rpm (solvent : dry coal = 2:1, weight ratio))

Solvent	Gasoline (<200°C)	Kerosene (200-275°C)	Gas Oil (275-325°C)	Heavy Gas Oil (325-400°C)	Vacuum Gas Oil (400-538°C)	Vacuum Residue (>538°C)
None	12.6	33.2	21.7	17.0	15.4	0.1
Waste Oil	2.9	5.0	6.1	23.0	47.2	15.8
A-1 Oil	29.6	31.5	17.3	14.6	7.0	0.0
A-2 Oil	49.4	31.4	11.3	6.0	1.9	0.0
A-4 Oil	36.9	31.4	15.5	11.6	4.6	0.0
A-5 Oil	39.4	25.2	12.7	13.5	9.2	0.0
A-7 Oil	24.0	22.6	16.0	16.9	17.3	3.2
A-8 Oil	54.1	23.7	9.1	8.4	4.7	0.0
A-10 Oil	32.7	30.1	16.7	14.0	6.5	0.0
A-11 Oil	46.6	31.2	12.0	7.9	2.3	0.0

Table 5. Boiling Point Distribution (numbers in weight percent) of Final Oil Products Obtained from Two-Stage Coliquefaction of Fe Loaded DECS-6 Coal (Fe: dry coal = 1.12:100, weight ratio) with HDPE or CP#2 (in the first stage, HDPE or CP#2 was degraded in a 150-cm^3 autoclave at 435°C, 1 hour, 800 rpm, under N_2 or H_2; in the second stage, DECS-6 coal was liquefied with Plastic-Derived-Liquids obtained from the 1st stage as solvents in a 27-cm^3 tubing reactor at 400°C, ~2000 psig H_2, 60 minutes, 160 rpm (solvent : dry coal = 2:1, weight ratio))

Solvent	Gasoline (<200°C)	Kerosene (200-275°C)	Gas Oil (275-325°C)	Heavy Gas Oil (325-400°C)	Vacuum Gas Oil (400-538°C)	Vacuum Residue (>538°C)
None	8.2	24.0	15.9	19.7	30.7	1.5
Waste Oil	3.0	5.3	5.7	22.7	47.0	16.3
A-1 Oil	26.9	27.5	15.9	16.6	13.1	0.0
A-2 Oil	42.6	28.0	12.3	11.4	5.7	0.0
A-4 Oil	31.3	26.0	14.7	16.1	11.9	0.0
A-5 Oil	35.0	27.1	14.1	14.1	9.7	0.0
A-7 Oil	22.3	22.6	14.2	17.5	16.9	6.5
A-8 Oil	59.6	24.3	7.9	5.6	2.6	0.0
A-10 Oil	26.5	22.3	13.8	17.8	18.0	1.6
A-11 Oil	38.0	25.2	12.8	13.7	10.3	0.0

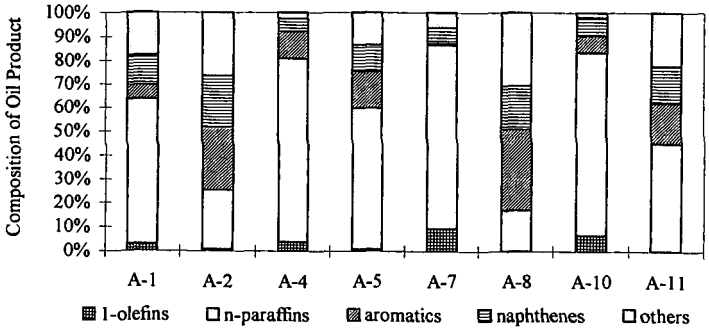

Figure 1. Effects of Catalyst (HZSM-5) and Reaction Atmosphere (N_2 or H_2) on Composition of Oil Products Obtained from Degradation of HDPE or CP#2 in a 150-cm^3 Autoclave at 435°C, 800 rpm, for a Reaction Time of 60 Minutes

LIQUEFACTION OF COMMINGLED WASTE PLASTICS CONTAINING PVC

G.P. Huffman, Zhen Feng, Dan Bailey, Jeff Rockwell, Jianmin Zhao, and F.E. Huggins, CFFLS, 533 S. Limestone St., Room 111, University of Kentucky, Lexington, KY 40506

ABSTRACT

Direct liquefaction studies were conducted on a washed, commingled waste plastic(CWP), as received from the American Plastics Council and after addition of 5 wt.% of polyvinyl chloride (PVC). Both non-catalytic and catalytic experiments were performed; the catalytic experiments utilized 1 wt.% of HZSM-5. The experiments on the CWP-PVC mixture were conducted with and without the addition of 5 wt.% of calcium hydroxide. The effect of PVC on product yields was evaluated. Oil quality was examined by GC simulated distillation. The forms of occurrence of chlorine in the liquefaction products were determined by x-ray absorption fine structure(XAFS) spectroscopy utilizing the X-ray absorption near edge structure(XANES).

INTRODUCTION

Previous research[1-11] has demonstrated that direct liquefaction of waste plastics is a very promising recycling option as well as a significant potential new oil resource. As discussed elsewhere, waste plastics can be liquefied at low hydrogen pressure[5,8] and no solvent is needed,[5-11] although waste automotive oil and petroleum resid[9,10] can serve as excellent solvents, if desired. Solid acid catalysts, such as HZSM-5[3-5,8] and sulfated zirconia[7] are very active for plastic liquefaction and metal-promoted solid acid catalysts have been demonstrated to improve the oil product substantially.[7,11] The coliquefaction or coprocessing of coal with plastics also looks promising.

An aspect of plastics liquefaction that has not been adequately studied is the liquefaction of plastics containing realistic amounts of polyvinyl chloride (PVC). Several groups, including our own, have worked with a washed commingled waste plastic(CWP) provided by the American Plastic Council (APC) that contains very little chlorine, due to the fact that PVC has a higher specific gravity than most other resins and separates out during washing. In the current study, we have investigated the liquefaction of the APC CWP with and without the addition of PVC, calcium hydroxide, and HZSM-5.

EXPERIMENTAL

Liquefaction: The liquefaction experiments were conducted in "tubing bomb" reactors with a volume of 50 ml, which were heated in a fluidized sand bath for 60 minutes while being shaken at a rate of 400 rpm. The reactors were charged with 10 g of plastic, with all combinations of additions of 5 wt.% of PVC and $Ca(OH)_2$ and 1 wt.% of HZSM-5. No solvent was used and hydrogen gas was added at low pressure (200 psig, cold). The HZSM-5 was a commercial catalyst[12] with average particle sizes of 40-50 Å and a Si/Al = 4.[8]

At the end of each run, the reactor was cooled rapidly to room temperature in a second sand bath. Gas products were then collected and analyzed by gas chromatography. The other products were removed from the reactor with tetrahydrofuran (THF) and extracted in a Soxtech apparatus for 2 hours. Total THF conversion was determined from the amount of insoluble material that remained (residue). All insoluble materials were dried at 80°C overnight before weighing. Any added catalyst was subtracted from the residue sample weight. The THF solubles were subsequently separated into pentane soluble (oils) and pentane insoluble (preashpaltenes + ashpaltenes(PA + AS)) fractions. The experimental errors for total conversion and oil yield are approximately ±3%.

The oil fraction was analyzed by GC - simulated distillation. The GC operating parameters were as follows: column - Petrocol B, 20" x 1/8" packed column; temperature - 0 - 360 °C with 10 °C/min ramp; detector - FID at 380 °C; flowrate - 35 ml/min He. The simulated distillation method is described in ASTM D-2887. The oil product was categorized into three fractions: gasoline (B.P. < 200 °C); kerosene (B.P. - 200-275 °C); and heavy oil (B.P. - 275 - 550 °C).

Cl XAFS Spectroscopy: XAFS spectroscopy was carried out at beamline X-19A at the National Synchrotron Light Source at Brookhaven National Laboratory. Spectra were obtained at the chlorine K absorption edge (at ca. 2825 eV) from the oils, asphaltenes + pre-asphaltenes, and IOM residues separated from the products of the liquefaction runs. Some of the fractions were also examined at the calcium K absorption edge (at ca. 4038 eV). The samples were suspended in the X-ray beam in ultrathin polypropylene bags in a Lytle fluorescent detector.[13] The x-ray beam path

was flushed with helium to minimize x-ray absorption by air. Spectra were collected from 75 eV below the chlorine edge to about 300 eV above the chlorine edge, at which point the K absorption edge arising from argon at 3107 eV was encountered. Over the near-edge or XANES region (from about 10 eV below the edge to 50 eV above the edge), the spectra were acquired with a step width of only 0.2 eV/point. The maximum in the derivative of the Cl XAFS spectrum of NaCl was taken as the zero point of energy for the Cl XAFS spectra and all spectra were calibrated with respect to this point. Most samples were sufficiently rich in chlorine to obtain an adequate spectrum with a counting time of 1 sec/point; however, multiple spectra were run and summed to give a single spectrum with improved signal/noise ratio if the chlorine content was relatively low.

XAFS spectral analysis consisted of (i) calibration of the XAFS spectrum relative to the NaCl standard spectrum, (ii) subtraction of the pre-edge slope from the XAFS spectrum, and (iii) division of the spectrum into two distinct regions for the X-ray absorption near-edge structure (XANES) and the extended X-ray absorption fine structure (EXAFS). In this report, only the XANES data will be described.

RESULTS AND DISCUSSION

Liquefaction results: The liquefaction results are briefly summarized in Figures 1 and 2. Chemical compositions of the feedstock (CWP + PVC), the IOM samples and the oil products are given in Table 1. Two points should be noted regarding Figure 1. First, the yields are given as oil + gas, as the gas yields of all experiments was not determined. However, for most of the samples the gas yield was determined and found to be ≤5%. Second, the yields indicated for the CWP alone and the CWP + 1% HZSM-5 are for experiments that utilized a cold hydrogen pressure of 800 psig rather than 200 psig. It is seen that neither the oil + gas yields nor the total conversion were much affeeted by the presence of either PVC or HZSM-5 at 445 °C. Furthermore, the oil quality as reflected by the relative fractions of gasoline, kerosene and heavy oil does not vary dramatically. In general, there is some increase in both the quantity and quality of the oil produced with the addition of HZSM-5; at this relatively high temperature, however, the results of the thermal runs are almost as good as those of the catalytic runs. Perhaps the most significant result is the fact that the presence of 5% PVC does not appear to have any significant damaging effect on either oil yields or quality.

The distribution of the most critical elements(C, H, Ca, and Cl) in the IOM and oil samples is given in Table 1. It is seen that the addition of calcium hydroxide increased the amount of Cl retained in the IOM significantly, and somewhat more for the case where 1% HZSM-5 was added than for the thermal run. Similarly, the oil samples exhibited a decrease in Cl content when Ca was present. However, the decrease was larger for the thermal run than for the catalytic run. It should be emphasized that *none* of the oils would be acceptable in most refineries because of their relatively high Cl contents.

Cl XANES spectra: As shown in Figure 3, quite different chlorine XANES spectra were obtained from the oil and IOM fractions. Strong chlorine XANES spectra were also obtained from the AS+PA fractions, but they were closely similar to the IOM spectra obtained from the baseline situation (no catalyst, no Ca additive). The Ca additive appears to have little effect on the appearance of the Cl XANES spectra of the oil and AS+PA fractions; these spectra show relatively little variation. However, the Ca additive clearly did affect the appearance of the Cl XANES spectra of the IOM fractions. As shown in Figure 3, the sharp peak at -4.8 eV is much reduced in intensity when the Ca additive is present. The presence or absence of the HZSM-5 catalyst had relatively little effect on the appearance of the spectra.

The chlorine spectrum of the oil clearly arises from organochlorine species. The peak position of the first prominent sharp peak at -1.45 eV is consistent with data in the literature for organic chlorides[14], with the possible exception of aryl chlorides, which tend to have a more positive peak position in the range -1.0 to -0.5 eV. Furthermore, a similar sequence of three increasingly broader and weaker peaks at about -1.5 eV, 4 eV, and 12 eV is observed in a number of organochlorine compounds. In contrast, the chlorine spectrum of the IOM with the Ca additive is largely consistent with inorganic occurrences of chloride anions, and we have observed similar spectra from hydrated calcium chlorides. The prominent sharp peak observed at -4.8 eV observed in the spectra of all of the AS+PA fractions and of the two IOM fractions without Ca additive, however, is difficult to explain at this time and indicates a complication that cannot be explained by a simple separation of the PVC-derived chlorine into organic and inorganic chlorides. The width of the peak is narrow and

very similar to that observed for the organochlorine occurrence in the oil, but the remainder of the spectrum appears to be more like that of an inorganic chloride. Possibly, a chlorine occurrence based on the hypochlorite molecular anion (OCl^-) may offer an explanation for this peak.

It is also worth comparing the results obtained here with data obtained earlier[15] on coliquefaction of PVC-doped waste plastics with a North Dakota lignite. In those experiments, no organochlorine compounds were found in the oil; rather the chlorine XANES spectrum obtained from the oil was consistent with a hydrochloride adduct attached to presumably a quaternary nitrogen functionality in the oil derived from the coal. In the present coal-absent system, there is virtually no nitrogen to form such HCl adducts. Also, the Cl XANES indicated the formation of significant NaCl in the lignite/waste plastics/PVC experiments, suggesting that sodium may be a better sink for chlorine than calcium.

Acknowledgment

This research was supported by the U.S. Department of Energy through DOE contract No. DE-FC22-93-PC93053 as part of the research program of the Consortium for Fossil Fuel Liquefaction Science. We are grateful to Richard Anderson of the University of Kentucky Center for Applied Energy Research for assistance with liquefaction experiments and to Fulong Lu of the CFFLS for assistance with the XAFS experience.

References

1. B.O. Strobel and K-D. Dohms, *Proc. Int. Conf. Coal Sci, II*, 536-539(1993).
2. L.L. Anderson and W. Tuntawiroon, *Prepr.Pap.-Am. Chem. Soc., Div. Fuel Chem., **38(4)**,* 816-822(1993).
3. M.M. Taghiei, F.E. Huggins, and G.P. Huffman, *Prepr.Pap-Am. Chem. Soc., Div. Fuel Chem., **38(4)**,* 810-815(1993).
4. M.M. Taghiei, Zhen Feng, F.E. Huggins, and G.P. Huffman, *Energy & Fuels,* 1228-1232(1994).
5. G.P. Huffman, Zhen Feng, V. Mahajan, P. Sivakumar, H. Jung, J.W. Tierney, and I. Wender, *Prepr.Pap.-Am. Chem. Soc., Div. Fuel Chem.*, **40(1)**, 34-37(1995).
6. E.C. Orr, W. Tuntawiroon, W.B. Ding, E. Bolat, S. Rumpel, E.M. Eyring, and L.L. Anderson, *Prepr.Pap.-Am. Chem. Soc., Div. Fuel Chem.*, **40(1)**, 44-50(1995).
7. X. Xiao, W. Zmierczak, and J. Shabtai, *Prepr.Pap.-Am. Chem. Soc., Div. Fuel Chem.,* **40(1)**, 4-8(1995).
8. Z. Feng, J. Zhao, J. Rockwell, D. Bailey, and G.P. Huffman, "Direct Liquefaction of Waste Plastics and Coliquefaction of Coal-Plastic Mixtures," to be published in *Fuel Processing Technology.*
9. H.K. Loo and C.W. Curtis, "Catalytic Coprocessing of Plastics with Coal and Petroleum Resid using $NiMo/Al_2O_3$," to be published in *Energy & Fuels.*
10. M.S. Luo and C.W. Curtis, "Thermal and Catalytic Coprocessing of Illinois No. 6 Coal with Model and Commingled Waste Plastics," to be published in *Fuel Processing Technology.*
11. W.B. Ding, W. Tuntawiroon, J. Liang and L.L. Anderson, "Depolymerization of Waste Plastics with Coal over Metal-Loaded Silica-Alumina Catalysts," to be published in *Fuel Processing Technology.*
12. United Catalysts Inc., Post Office Box 32370, Louisville, KY 40232.
13. F. W. Lytle, R. B. Greegor, D. R. Sandstrom, E. C. Marques, Joe Wong, C. L. Spiro, G. P. Huffman, and F. E. Huggins, Nuclear Instruments & Methods, 226, 542-8 (1984).
14. F.E. Huggins and G.P. Huffman, *Fuel*, **1995**, *74*, 556-569.
15. F.E. Huggins, M.M. Taghiei, and G.P. Huffman, *Proceedings, Emerging Technologies in Hazardous Waste Management VI (Atlanta, GA)*, D.W. Tedder, Ed., American Chemical Society, Washington D.C., **1994**; pp. 993-996.

Table 1. Chemical composition of oils and IOM samples (wt. %).

IOM Samples	C	Ca	Cl
CWP-PVC	63	1.2	3.4
CWP-PVC-Ca	51	31	5.5
CWP-PVC, HZSM-5	45	0.7	3.9
CWP-PVC-Ca, HZSM-5	39	32	7.0
Oil Samples	C	H	Cl
CWP-PVC Feedstock	83	14	2.8
CWP-PVC	82	13	0.07
CWP-PVC-Ca	82	13	0.4
CWP-PVC, HZSM-5	84	12	0.1
CWP-PVC-Ca, HZSM-5	87	12	0.08

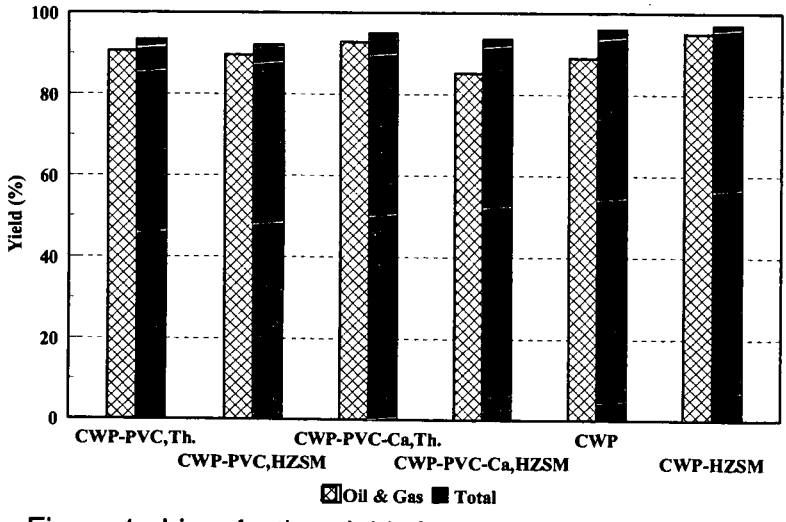

Figure 1. Liquefaction yields for the commingled waste plastic with and withoutadditions of PVC(5%), calcium hydroxide(5%), and HZSM-5(1%).

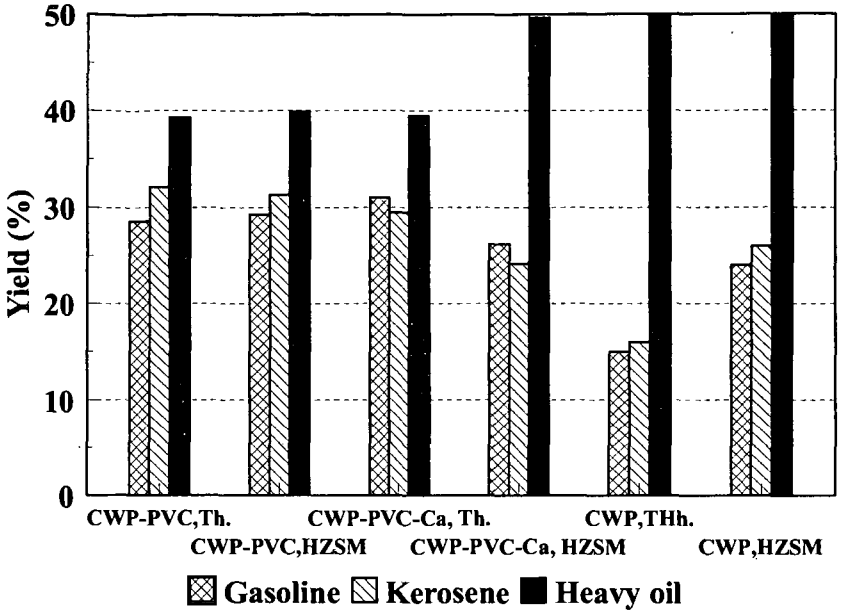

Figure 2. Simulated distillation analysis of the oil product from liquefaction of CWP with and without addition of PVC, calcium hydroxide, and HZSM-5.

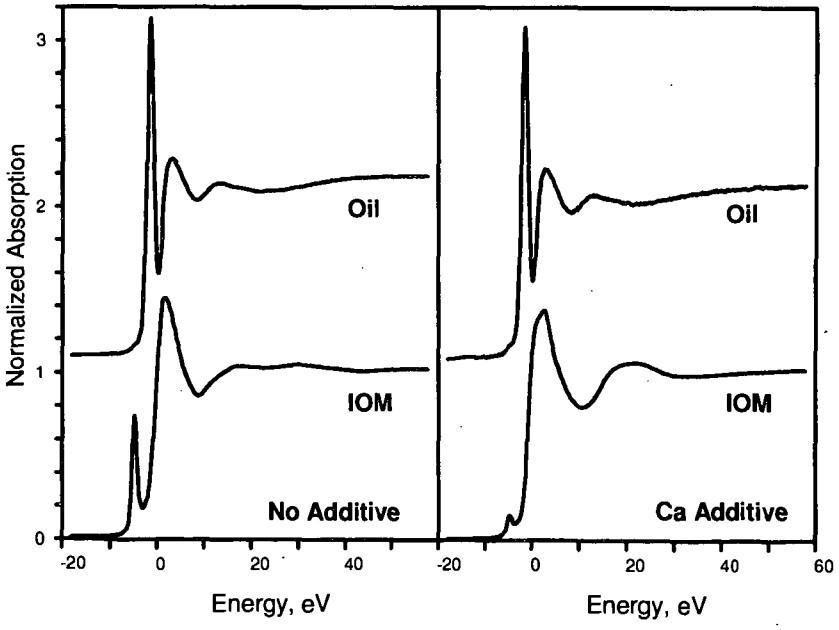

Figure 3. Chlorine K-edge XANES spectra of IOM and oil samples with and without calcium hydroxide additive.

COPROCESSING OF WASTE PLASTICS WITH COAL AND PETROLEUM RESID USING DIFFERENT CATALYSTS

Hyun Ku Joo and Christine W. Curtis
Chemical Engineering Department
Auburn University, AL 36849

Keywords: Coprocessing, petroleum resid, coal, waste plastics

INTRODUCTION

Waste plastics are a source of hydrocarbons that are currently not being used effectively. Only ~2% of the plastics are being recycled (Smith, 1995), and the remainder is being disposed of in landfills. Waste plastics are produced from petroleum and are composed primarily of hydrocarbons but also contain some antioxidants and colorants (Leidner, 1981). A number of problems are associated with the recycling effort, including convincing consumer households of the necessity to recycle, separating the waste plastics effectively for primary recycling of the plastic back to the monomer, and having sufficient waste plastic for processing, particularly in areas a far distance from the population centers. Tertiary recycling that results in the production of fuels and chemical feedstocks from waste plastics will provide an additional source of hydrocarbon fuels and chemical feedstocks. The addition of other hydrocarbon sources such as our most abundant U.S. hydrocarbon resource, coal, will provide a constancy of supply as well as an additional source of hydrocarbon fuels and feedstocks.

The direct coprocessing of coal and waste plastics is difficult because of chemical and processing incompatibility of the two materials (Luo and Curtis, 1996 a, 1996 b; Joo and Curtis, 1995, 1996). Typical household plastics waste consists of ~ 63% polyolefins (high and low density polyethylene (HDPE, LDPE)), 11% polypropylene, ~11%polystyrene, ~7% PET and 7% (Erwin and Henley, 1990), causing the wastes to be highly aliphatic. By contrast, coal is ~70% aromatic. These differences in chemistry result in the two materials being incompatible. Joo and Curtis (1996) have shown that heavy petroleum resid acts as an effective bridging solvent that when added to coal and waste plastics provides a medium for their mutual dissolution (Joo and Curtis, 1995, 1996).

The current research evaluated the effect of three different catalysts on the conversion and product distributions obtained from the coprocessing of coal, heavy petroleum resid, and waste plastics. The plastic used in this study was LDPE since it and its higher density form has been shown to be especially difficult to coprocess with coal (Luo and Curtis, 1996a). A hydrogenation catalyst with some hydrocracking activity is needed to convert coal and upgrade coal liquids and petroleum resid and a hydrocracking catalyst is required to break apart the bonds and make shorter chains of LDPE. Therefore, three different catalysts having these selectivities were employed in this study: presulfided $NiMo/Al_2O_3$, presulfided NiMo/zeolite, and Zeolyst Z-753, a hydrocracking catalyst. The addition of 10 wt % hydrocracking catalyst Z-732 to presulfided $NiMo/Al_2O_3$ was also examined to determine if adding some hydrocracking capacity to the system would increase the conversion and hexane soluble production of the plastics.

EXPERIMENTAL

Materials. The model plastic, low density polyethylene (LDPE), was obtained from Aldrich Chemical Co. and used as received. Blind Canyon DECS-17 bituminous coal was used in the study and obtained from the Penn State Coal Sample Bank. The proximate analysis of the coal is 45% fixed carbon, 45% volatile matter, 6.3% ash and 3.7% moisture. The ultimate analysis of the coal is 82.1% C, 6.2% H, 0.4% S, 1.4% N, and 0.12% Cl. The resid used was Manji obtained from Amoco. The analysis of the Manji resid is 85.1% C, 10.8% H, 0.7% N, 2.6% S, 231 ppm V, 220 ppm Ni and 23 ppm Fe. The solvents used for fractionation of the reaction products were HPLC grade hexane, toluene, and tetrahydrofuran (THF) from Fisher Scientific. Hexane solubles (HXs) were dissolved in carbon disulfide (CS_2) for simulated distillation.

The catalysts tested in this study were $NiMo/Al_2O_3$, NiMo/zeolite, and Zeolyst Z-753. The $NiMo/Al_2O_3$ catalyst from Shell was composed of 2.72 wt % Ni and 13.16 wt % Mo while the NiMo/Zeolite from Akzo was <25 wt % of molybdenum oxide and 1-10 wt % of nickel oxide with ultrastable zeolite. The Zeolyst Z-753 from Shell was composed of <60 wt % of amorphous silica, <15 wt % of tungsten oxide, <5 wt % of nickel oxide, <1 wt % of sodium oxide, and balanced alumina.

Reactions and Procedures. The reaction systems, LDPE, coal plus LDPE, and coal plus Manji plus LDPE, were studied to evaluate the activity of selected catalysts in coprocessing. Two sets of reactions were conducted: one set was performed with each of the two individual catalysts except $NiMo/Al_2O_3$ (Table 1) and the other with combined catalysts of $NiMo/Al_2O_3$ and Z-753. Reactions using a single catalyst and the same charging method as ones with combined catalyst were also performed for LDPE, coal/LDPE, and coal/Manji/LDPE systems to evaluate the effect of the catalyst combination (Table 2). For all reactions, reactants were charged at 1.0 g each for coal and polymer and 1.5 g for resid, giving resid to polymer and resid to coal ratios of 3:2 in the binary

systems and coal to resid to polymer ratios of 2:3:2 in the ternary systems. All reactions were performed using 1 wt % of powdered, presulfided $NiMo/Al_2O_3$ and NiMo/zeolite, and pretreated Z-753 on a total charge basis.

All reactions were performed in ~20 cm^3 stainless steel tubular microreactors at 400 °C or 430 °C for 30 or 60 min with 8.3 MPa of H_2 introduced at ambient temperature. The microreactors were agitated horizontally at 450 rpm in a fluidized sand bath and were immediately quenched in water after reaction. The coal was stored in a vacuum desiccator before being used.

The procedure for presulfiding $NiMo/Al_2O_3$ and NiMo/zeolite began with predrying $NiMo/Al_2O_3$ with N_2 for one hr at 300 °C. Then, 10 vol % H_2S/H_2 gas mixture was flowed over the catalyst at 225 °C for one hr, at 315 °C for one hr, and 370 °C for two hr. In the final step N_2 was flowed N_2 at 370 °C over $NiMo/Al_2O_3$ for one hr and turning off the furnace to room temperature. The pretreatment procedure for Z-753 involved heating the catalyst for two hr at 204 °C, and then increasing the temperature to 538 °C for two hr. After this, it was cooled down to room temperature. During the entire procedure, the catalyst was kept under a flow of N_2. All catalysts were stored in vacuum desiccator prior to use.

The reaction products were determined by using solvent fractionation and by weighing the gaseous products. The liquid products were fractionated using a series of solvents into hexane soluble materials (HXs); toluene soluble, hexane insoluble material (TOLs); and THF soluble, toluene insoluble material (THFs), and THF insoluble material or IOM which is defined as insoluble organic matter that is moisture and ash-free. The definition for conversion used in this study is the conversion of the reactant to THF soluble material.

$$\% \text{ conversion} = \left[1 - \frac{g\ IOM}{g\ maf\ total\ reactant} \right] \times 100 .$$

The coal is a solid at room temperature and is essentially insoluble in THF; LDPE is solid at room temperature and has limited solubility in THF (3.1%), while resid is a semi-solid at room temperature and are totally soluble in THF. The boiling point distribution of HXs were analyzed using ASTM D-2887 method. Detailed procedure can be referred to in the previous work (Joo and Curtis, 1996).

RESULTS AND DISCUSSION

The investigation of coprocessing waste plastics with coal and heavy petroleum resid was performed using two different sets of reactions: a set of reactions was performed in which LDPE was reacted at four different reaction conditions with presulfided NiMo/zeolite and Z-753 catalysts, and a second set was performed in which coal, resid, and LDPE were coprocessed with the two above mentioned catalysts and presulfided $NiMo/Al_2O_3$, as well as with a combination of 10 wt % Z-753 with presulfided $NiMo/Al_2O_3$. The measures that were used to evaluate the efficacy of the catalysts were conversion of the solids to THF solubles, product distribution in terms of HXs and THFs. The boiling point distributions of the products obtained in the HXs fractions were also determined and compared for the different catalytic systems.

Individual Reaction Systems. The conversion and product distributions of LDPE reactions with the two catalysts are given in Table 1 for Z-753 and presulfided NiMo/zeolite catalysts. The reaction conditions used were 430 °C, 60 min; 430 °C, 30 min; 400 °C, 60 min; and 400 °C, 30 min. A composite of the conversion and product distribution data for the two sets of catalytic LDPE reactions is given in Figure 1. Increased reaction time and temperature resulted in higher conversions for LDPE for both the Z-753 and presulfided NiMo/zeolite catalysts. For example, with Z-753 a conversion of 35.7% was achieved at 400 °C and 30 min but increased to 94.2% when 430 °C and 60 min was used. The highest production of hexane solubles yielding 69.7% also occurred at 430 °C and 60 min. Similar LDPE reaction behavior was observed for presulfided NiMo/zeolite catalyst, although its hydrocracking activity was higher than Z-753 as evidenced by the higher conversion to gases at all reaction conditions. LDPE conversion and hexane soluble production decreased somewhat with longer reaction time at the lower temperature for both catalysts, although the gas make remained fairly constant. Recoveries were low at the highest severity condition of 430 °C which was caused by the high volatility of the reaction products.

An experimental design analysis of a 2^k factorial which involved 3 factors (temperature, time, and catalyst) with each two levels (400 °C and 430 °C, 30 min and 60 min, Z-753 and NiMo/zeolite), respectively, was performed for this set of experiments to determine the factor that most affected the product distribution obtained (Table 2). For production of gas, the catalyst and reaction temperature were equally strong-effect factors. The yield of hexane solubles from LDPE as well as the conversion to THF solubles, was affected by temperature as the predominant effect factor but was also affected by a two-factor interaction of reaction temperature and time. This analysis clearly demonstrated the importance in selecting reaction temperature with proper catalyst and reaction time to obtain maximum amount of desirable product from LDPE liquefaction.

Coprocessing Reactions. Individual reactions of LDPE and coprocessing reactions with coal/LDPE and coal/Manji/LDPE were performed with the three previously described catalysts and with the combination of presulfided $NiMo/Al_2O_3$ with 10 wt % Z-753. The conversions and product

distributions for these systems at reaction conditions of 430 °C and 60 min are given in Table 3. These high severity conditions were selected on the basis of the LDPE liquefaction results from Table 1 and of the results previous reactions containing both coal and LDPE and in some cases resid which indicated that this severity was necessary to coprocess all three materials simultaneously (Joo and Curtis, 1995, 1996; Luo and Curtis, 1996 a, b).

The catalysts directly influenced the reactivity of the LDPE liquefaction and coprocessing systems although the composition of the systems also had a strong influence on both conversion and hexane soluble yield. The LDPE conversions and product distributions obtained were directly related to the hydrocracking propensity of the catalysts. The conversions increased from 69.6% for $NiMo/Al_2O_3$ to 76.2% with the 10 wt% Z-753 hydrocracking catalyst present. When hydrocracking catalysts were used exclusively, the reactions with Z-753 and NiMo/zeolite produced 94.2 and 93.1% conversion, respectively. Similarly, gas production increased with hydrocracking activity with the NiMo/zeolite yielding the highest amount. The Z-753 catalyst produced the highest hexane soluble yields and conversion while the stronger hydrocracking catalyst NiMo/zeolite produced more gas and less hexane solubles.

By contrast, the coal/LDPE reactions were not influenced by catalyst type. All of the catalysts gave very similar conversions, ranging from 41.3% to 43.5%. Similarly, the amount of gas produced and hexane soluble yields were similar for all of the catalysts. The catalysts appeared to be ineffectual in the system; however, results in our laboratory have indicated that increasing the time of the LDPE/coal reaction has a significant effect on the both conversion and product distribution (Joo, 1996). Extended reaction time experiments are currently being performed to determine the effect of these catalysts on this system.

Coprocessing reactions of coal/Manji/ LDPE were influenced by the catalyst type during the 60 min reaction time as was the LDPE system. The conversion increased from 61.7% for $NiMo/Al_2O_3$ to 69% for 10 wt% for Z-753 in $NiMo/Al_2O_3$ while 100% Z-753 gave a similar conversion of 68%. The highest conversion of 74.9% obtained was with NiMo/zeolite. The results from using the NiMo/zeolite catalyst showed the advantage of having the hydrocracking selectivity from the zeolite and the hydrogenation activity from the NiMo. The different catalysts did not have any differential effect on production of the hexane solubles from the three component coprocessing reactions. All of the catalysts with hydrocracking activity resulted in similar amounts. Only slight differences were observed in the gas production.

Simulated distillation of the hexane soluble fraction from each of these reactions was performed to determine the boiling point distribution of the products produced. The fractions that were determined were gasoline (~180 °C), naphtha (170 to 290 °C), heavy oil (260 to 350 °C), and lubricant (~300 to 370 °C) as shown in Table 4. The reaction of LDPE alone produced the largest amount of material boiling less than 370 °C while the reactions with LDPE and coal produced the lowest weight percent. The type of catalyst employed affected the weight percent of material boiling less than 370 °C for LDPE with the hydrocracking catalysts yielding the highest amounts, but catalyst type had little effect on the products produced from the other two types of reactions.

CONCLUSIONS

The coprocessing of LDPE with coal and petroleum resid was affected by catalyst type. The presence of hydrocracking selectivities during reaction increased conversion and production of hexane soluble materials in the LDPE reaction. Reaction temperature also strongly affected the conversion and the product slate in the LDPE reactions. None of the catalysts affected either the conversion or product distribution from the coal/ LDPE system at the reaction conditions used. Longer reaction time experiments are currently underway to determine if these catalysts influence the two component reaction to any appreciable extent. Simultaneous reactions of LDPE/resid and coal also responded to the different selectivities of the different catalysts. At reaction conditions of 60 min and 430 °C, catalysts with substantial hydrocracking activity yielded higher levels of conversion and hexane soluble material than did the reaction with $NiMo/Al_2O_3$. Catalysts, like NiMo/zeolite and the 10% Z-753 in $NiMo/Al_2O_3$, with combined hydrogenation and hydrocracking selectivities, affected the three component system most positively, producing the highest yields of hexane solubles and conversion to THF soluble materials.

REFERENCES

1. Erwin, L.; Healy, L.H., Jr. "Packing and Solid Waste Management Strategy" American Management Association, New York, 1990.
2. Joo, H. K., personal communication, 1996.
3. Joo, H. K.; Curtis, C. W. *Energy and Fuels*, in press, 1996.
4. Joo, H. K.; Curtis, C.W. *ACS Fuel Chem. Div. Prep.* 1995.
5. Leidner, J. "Plastics Waste," Marcel Dekker, Inc. 1981
6. Luo, M; Curtis, C. W. *Fuel Process. Techno.*, in press, 1996a.
7. Luo, M; Curtis, C. W. *Fuel Process. Techno.*, in press, 1996b.
8. Smith, R. Presentation at the Consortium for Fossil Fuel Liquefaction Science, Ninth Annual Meeting, Pipestem, WV, August 1995.

Table 1. Effect of Reaction Temperature and Time on Reactions with Different Catalysts[a]

Catalyst[b]	Product Distribution (%)					Conversion (%)	Recovery (%)
	gas[c]	HXs	TOLs	THFs	IOM		
430 °C, 60 min							
LDPE with Z	24.5±1.3	69.7±1.2	-	-	5.8±2.1	94.2±2.1	55.6±2.3
LDPE with NZ	37.1±1.2	56.0±1.3	-	-	6.9±2.6	93.1±2.6	54.9±2.8
430 °C, 30 min							
LDPE with Z	19.6±1.1	22.6±1.4	-	-	57.8±1.9	42.2±1.9	91.5±1.9
LDPE with NZ	28.5±0.8	23.7±1.6	-	-	47.9±1.8	52.1±1.8	84.6±0.7
400 °C, 60 min							
LDPE with Z	20.2±0.4	5.1±1.4	-	-	74.6±1.1	25.4±1.1	94.2±1.5
LDPE with NZ	22.1±0.7	6.5±0.9	-	-	71.5±2.0	28.5±2.0	92.1±1.7
400 °C, 30 min							
LDPE with Z	19.2±2.1	16.5±0.7	-	-	64.3±0.7	35.7±0.7	89.7±1.1
LDPE with NZ	22.7±1.7	9.4±1.1	-	-	67.9±1.4	32.1±1.4	94.1±2.4

[a] Reaction conditions : 8.3 MPa H_2 1g of reactant. 1 wt% catalyst of total feedstock.
[b] Z = Zeolyst 753 catalyst, NZ = NiMo/zeolite
[c] gas = gaseous products; HXs = hexane solubles; TOLs = toluene solubles; THFs = THF solubles; IOM = insoluble organic matter which is calculated on an ash-free basis.

Table 2. Factorial Design Analysis for LDPE Reaction with Two Different Catalysts

		A[a]	B	C	AB	AC	BC
gas	0	84.2	90.0	83.5	103.5	105.0	98.0
	1	109.7	103.9	110.4	90.4	88.9	95.9
	delta[b]	25.5	13.9	26.9	13.1	16.1	2.1
HX	0	37.5	72.2	113.9	151.6	101.3	101.6
	1	172.0	137.3	95.6	57.9	108.2	107.9
	delta	134.5	65.1	18.3	93.7	6.9	6.3
Conversion	0	121.7	162.1	197.5	255.1	206.3	199.5
	1	281.6	241.2	205.8	148.2	197.0	203.8
	delta	159.9	79.1	8.3	106.9	9.3	4.3

[a] A=temperature, B= time, and C=catalyst.
[b] The higher the **delta** is, the stronger effect that factor has.

Table 3. Effect of Catalyst Combination on Selected Coprocessing[a] Systems

Reaction Combination	Catalyst N, Z, or NZ[b]	Product Distribution (%)					Conversion (%)	Recovery (%)
		gas[c]	HXs	TOLs	THFs	IOM		
430 °C, 60 min								
LDPE	N	19.1±1.0	50.5±2.2	-	-	30.4±1.6	69.6±1.6	93.9±3.3
	10% Z in N	21.0±0.9	55.3±1.8	-	-	23.7±2.0	76.2±2.0	82.6±2.5
	Z	24.5±1.3	69.7±1.2	-	-	5.8±2.1	94.2±2.1	55.6±2.3
	NZ	37.1±1.2	56.0±1.3	-	-	6.9±2.6	93.1±2.6	54.9±2.8
Coal/LDPE	N	9.8±0.8	25.3±0.6	3.4±0.3	4.3±1.5	57.1±1.3	42.9±1.3	96.3±1.2
	10% Z in N	9.7±1.5	23.7±0.9	4.2±1.1	3.7±1.1	58.7±1.4	41.3±1.4	98.3±2.2
	Z	9.8±1.1	24.5±1.1	4.2±0.7	5.0±0.4	56.5±0.6	43.5±0.6	97.4±1.0
	NZ	10.7±1.9	23.9±0.8	3.5±0.6	4.2±0.5	57.7±2.8	42.3±2.8	97.7±1.1
Coal/Manji/LDPE	N	7.4±1.2	38.3±0.8	8.9±2.1	7.1±1.1	38.3±2.2	61.7±2.2	98.4±0.9
	10% Z in N	7.7±1.7	45.3±0.3	8.3±1.3	7.6±0.3	31.0±0.9	69.0±0.9	96.5±1.1
	Z	8.5±0.8	43.7±0.4	8.7±2.2	7.1±1.1	32.0±1.1	68.0±1.1	97.7±1.2
	NZ	8.4±0.4	45.2±2.1	9.5±1.1	11.8±0.9	25.1±2.3	74.9±2.3	96.5±2.4

[a] Reaction Conditions : 430 °C, 60min, and 8.3 MPa H_2 introduced at ambient temperature. Reactant loading : 1g of coal (Blind Canyon DECS-17), 1g LDPE, 1.5 g resid (Manji).
[b] N = Presulfided $NiMo/Al_2O_3$, Z = Pretreated Z-753, NZ=NiMo/Zeolite. 1 wt% catalyst loading on total charge basis.
[c] gas = gaseous products; HXs = hexane solubles; TOLs = toluene solubles; THFs = THF solubles; IOM = insoluble organic matter which is calculated on an ash-free basis.

Table 4. Simulated Distillation of Hexane Solubles from Coprocessing Reactions[a]

Catalyst[b]		Weight %					
		SIMREC[c]	Gasoline[d]	Naphtha	Heavy oil	Lubricant	Total with gas
LDPE	N	73.7	1.7±0.9	6.8±1.3	7.9±1.4	6.8±1.3	42.3±1.4
	10% Z in N	74.3	2.5±1.0	7.1±1.4	8.7±1.6	7.4±1.4	46.7±1.6
	Z	65.3	2.4±1.1	8.7±1.7	13.1±2.0	10.0±1.8	58.7±2.0
	NZ	52.5	2.1±0.8	5.4±1.2	7.6±1.4	5.6±1.2	57.8±1.4
Coal/ LDPE	N	51.4	0.9±0.4	2.1±0.6	3.0±0.7	2.3±0.6	18.1±3.0
	10% Z in N	59.9	0.8±0.4	2.3±0.6	3.5±0.8	2.7±0.7	19.0±3.5
	Z	57.8	0.9±0.4	2.6±0.6	3.4±0.7	2.6±0.6	19.2±0.7
	NZ	64.1	0.7±0.4	3.2±0.7	3.8±0.8	2.9±0.7	21.3±0.8
Coal/ LDPE/ Manji	N	63.8	1.2±0.6	5.1±1.0	5.7±1.1	4.6±1.0	24.0±1.1
	10% Z in N	65.0	1.7±0.8	5.7±1.2	6.5±1.2	5.4±1.1	27.1±1.2
	Z	65.5	1.2±0.7	6.1±1.2	7.0±1.3	5.6±1.1	28.3±1.3
	NZ	70.3	1.4±0.8	6.1±1.2	7.7±1.4	6.2±1.2	29.7±1.4

[a] 430 °C, 60 min. 8.3 MPa H_2. 1 wt % catalyst loading on the total charge basis. Reactant roading : 1g of coal (Blind Canyon DECS-17), 1g of LDPE, and 1.5g of Manji resid.
[b] N = NiMo/Al_2O_3, Z = Z-753, NZ = NiMo/Zeolite.
[c] SIMREC = Simulated distillation recovery.
[d] Gasoline ~180 °C, 170 °C < Naphtha < 290 °C, 260 °C < Heavy oil < 350 °C, 300 °C < Lubricant < 370 °C.

Figure 1. Product Distribution Trends for LDPE Reaction

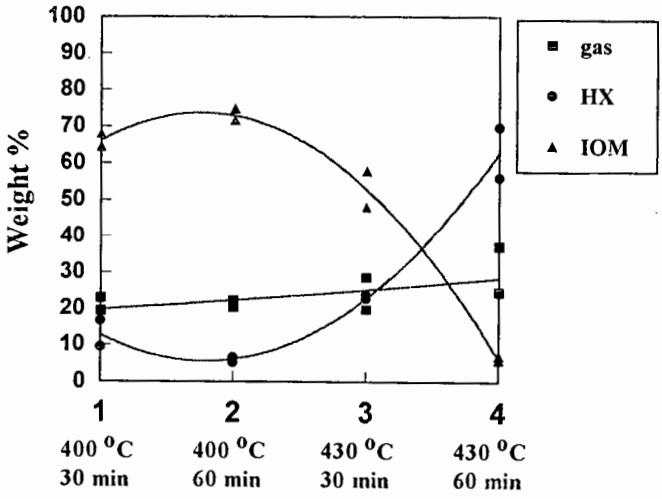

A KINETIC MODEL FOR CO-PROCESSING OF COAL AND WASTE TIRE

Dady B. Dadyburjor, Ramesh K. Sharma, J. Yang and John W. Zondlo
Department of Chemical Engineering
West Virginia University
P.O. Box 6102, Morgantown WV 26506-6102

Keywords: Kinetics, coal liquefaction, co-liquefaction.

ABSTRACT
Liquefaction of waste (recycled) tire and coal was studied both separately and using mixtures with different tire-to-coal ratios. Temperatures from 350-425°C were used. The data were analyzed using a model with a second-order consecutive reaction scheme (liquefaction to asphaltenes to oil and gas) for coal; a second-order conversion of tire to oil and gas; and an additional synergism reaction forming asphaltenes, first order in both coal and tire, when both are present. The agreement between the model and experiment was good.

INTRODUCTION

Disposal of used tires is a major environmental problem. Liquefaction of such tires in conjunction with coal has been suggested as an alternative to their disposal [1-3]. Farcasiu and Smith [1] studied the co-liquefaction of tire and Illinois #6 coal at 425°C and observed a synergistic effect of tire on coal conversion. Similar results were obtained at 400°C by Liu et al. [2] for the liquefaction of DECS-6 coal with a tire sample prepared from an used Goodyear Invicta tire. In all these studies a complete conversion of the volatile matter of the tire was obtained.

In this work, co-liquefaction of DECS-6 coal and a waste tire sample was studied at 350-425°C. Runs were made with tire and coal separately as well as by using mixtures with tire/coal ratios of 0-4. The hydrogen pressure was kept at 1000 psi (cold). The data were analyzed using a second-order consecutive reaction scheme for the liquefaction of coal to asphaltenes and then to oil and gas.

EXPERIMENTAL

The coal used was DECS-6 which is a high-volatile-A bituminous coal from the Blind Canyon seam in Utah. The tire sample was obtained from the University of Utah Tire Bank and represented mixed recycled tires ground to -30 mesh. The proximate and ultimate analyses showed that the coal contained 49% volatile matter (on a dry, ash-free basis) and 51 wt% fixed carbon. The amounts of volatile matter and fixed carbon in tire were 71 wt% and 29 wt%, respectively. The fixed carbon essentially represents the content of carbon black in the tire.

The details of the experimental equipment, run procedures and analytical techniques have been described earlier [4]. A stainless-steel tubing bomb reactor with a volume of 27 ml was used for the liquefaction. The reactor was loaded with the feed, purged and pressurized with H_2 to 1000 psi (cold). The feed consisted of tire or coal or a mixture of the two in different ratios. The gaseous products were collected and analyzed by gas chromatography. The solid and liquid products in the reactor were washed and extracted with tetrahydrofuran (THF) for 24h. The THF-insoluble material (TI) was separated by filtration. The conversion is calculated from the amount of THF-insoluble material. After the removal of THF by rotary evaporation, the THF-solubles were extracted with hexane for 2h. The extract was separated into hexane-insoluble (HI) and hexane-soluble (HS) fractions by filtration. The THF-soluble/ hexane-insoluble fraction, i.e. the HI fraction, represents asphaltenes. The HS fraction was the 'oil'. The oil yield was obtained by difference. In many cases, the combined oil + gas yield was calculated by difference. Most runs were made in duplicate and the experimental error was ±2.5%.

In the co-liquefaction runs, the overall conversion and the yields of asphaltenes and oil + gas fractions were calculated as above. However, in order to get a better insight, the results were also analyzed in terms of incremental conversion and yields, based on coal, which were calculated as follows;

$$X_{cm} = (X_{ov} - w_t X_t)/w_c \qquad (1)$$

where X_{ov} is the total conversion and w_t and w_c are the weight fractions of tire and coal in the feed, respectively. In equation (1), X_{cm} is the conversion of the mixture on a coal-alone basis and X_t is the conversion of tire alone under the same conditions. The yield of asphaltenes on a coal-alone basis was calculated similarly. The oil+gas yield from coal was calculated by difference.

RESULTS AND DISCUSSION

Effect of R_{TC} and Temperature

Figure 1 shows the effect of tire-to-coal ratio (R_{TC}) on conversion and oil+gas yield at 375°C. The results are presented on a coal-alone basis, i.e., the contribution of the tire has been subtracted. The conversion increases from 30% (at R_{TC}=0) to about 40% at R_{TC}=4. This indicates that the addition of tire has a synergistic effect on coal conversion. The synergistic effect is mainly towards the asphaltenes since the oil+gas yield is essentially unaffected by the addition of the tire.

The results at 400°C, presented in Figure 2, indicate a significant effect of R_{TC} on conversion, especially at low values of R_{TC}. The conversion of coal alone increases from 35% (without tire) to 49% when R_{TC}=1. At higher R_{TC} values, the addition of tire has only a small effect on coal conversion. There seems to be slight maximum in the conversion at R_{TC}~3, where the conversion is 54%. The decrease in conversion at high R_{TC} may be due to a low concentration of coal in the reaction mixture. The oil+gas yield decreases more-or-less linearly with increase in R_{TC}.

Similar observation are made from the results obtained at 425°C (Figure 3). In this case, the maximum conversion is over 70% at R_{TC}=1. The oil+gas yields at 425°C are also higher than those at 400°C.

Data Analysis

Since oil and gas are the major products of tire liquefaction, the liquefaction of tire (TR) is essentially represented by:

$$TR \xrightarrow{k_{tr}} OG \qquad (2)$$

For coal liquefaction, the experimental data suggest a predominantly consecutive reaction scheme with liquefaction of coal (C) to asphaltenes (A) and oil+gas (OG).

$$C \xrightarrow{k_t} A \xrightarrow{k_a} OG \qquad (3)$$

In the presence of the tire (TR), the conversions increase due to the synergism by the free-radical reactions between coal and tire. The synergism is mainly towards asphaltenes and is represented by:

$$C + TR \xrightarrow{k_s} A \qquad (4)$$

Now, the rates of conversion of tire (r_{tr}) and coal (r_c), and the rate of asphaltenes formation (r_a) are:

$$r_{tr} = k_{tr}C_{tr}^2 + k_sC_{tr}C_c \qquad (5)$$

$$r_c = k_tC_c^2 + k_sC_{tr}C_c \qquad (6)$$

$$r_a = k_tC_c^2 + k_sC_{tr}C_c - k_aC_a^2 \qquad (7)$$

where C_{tr}, C_c and C_a are the mass fractions of tire, coal and asphaltenes, respectively. In order to minimize the correlation between the activation energy and the pre-exponential factor, the rate constants were reparametrized to the form:

$$k = k(M)\ \exp[E\{1/T(M)-1/T\}/R] \qquad (8)$$

with k and k(M) being the values of the rate constant at T and T(M); E and R represent the activation energy and universal gas constant. The results are presented in Table 1. The rate constant for the liquefaction of tire (k_{tr}) is higher than that for the coal (k_t), as expected. The activation energies for both the liquefaction of coal and tire are low indicating a possible pore diffusion effect. The activation energy (E_a) for k_a was found to be not significantly different from zero indicating that the rate of asphaltene-to-oil+gas reaction is not dependent on temperature.

The experimental values of the overall conversion (of coal+tire) and overall yield (of oil+gas) are compared in Figure 4 with values calculated from the parameters of Table 1. The comparison seems satisfactory, considering the complexity of coal/tire co-liquefaction.
The model shows that the synergistic effect of tire is strongly dependent on the process conditions. Both the observed and predicted conversions decrease above 400°C when R_{TC} is 2. The oil+gas yields are governed mainly by the concentration of asphaltenes, increasing with an increase in asphaltene concentration.

CONCLUSIONS

1. The conversion and product yields from coal and tire are strongly dependent on temperature.
2. The co-liquefaction of tire with coal has a considerable synergistic effect on the conversion and asphaltene yield from coal. The synergism increases with an increase in tire/coal ratio, at least up to a tire/coal ratio of 1.
3. A consecutive reaction scheme for the conversion of coal to asphaltenes and oil+gas represents the data reasonably well at various temperatures and tire/coal ratios. The model uses second-order kinetics for the separate liquefaction of coal and tire and an overall second-order rate expression for the co-liquefaction (synergism reaction).

ACKNOWLEDGEMENT. This work was conducted under U.S. Department of Energy Contract No. DE-FC22-90PC90029 under the cooperative Agreement to the Consortium for Fossil Fuel Liquefaction Science.

REFERENCES

1. Farcasiu, M. and Smith, C.M. Prepr. Pap.- Am. Chem. Soc., Div. Fuel Chem. 1992, 37(1), 472.
2. Liu, Z., Zondlo, J.W. and Dadyburjor, D.B. Energy & Fuels 1994, 8(3), 607.
3. Tang, Y. and Curtis, C.W. Fuel Process Technol. 1996, 46, 195.
4. Sharma, R.K., Yang, J., Zondlo, J.W. and Dadyburjor, D.B. Fuel submitted.

Table 1. Summary of Kinetic Results[a]

Rate Constant	k(M)* [Min^{-1}]	Activation Energy [kJ.mole^{-1}]
k_{tr}	4.0±1.1	24.4±6.9
k_t	1.0±0.4	35.7±7.2
k_a	6.8±1.8	0
k_s	3.6±0.6	83.8±27.4

[a]±represents 95% confidence limits; *k at 673K.

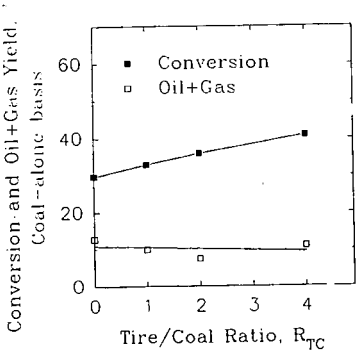

Figure 1. Effect of R_{TC} on co-processing of coal and waste tire at 375°C. Other conditions: 30 min, 1000 psi H_2 (cold).

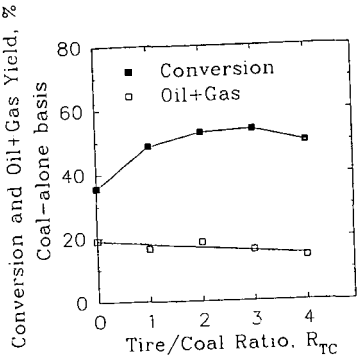

Figure 2. Effect of R_{TC} on co-processing of coal and waste tire at 400°C. Other conditions same as in Figure 1.

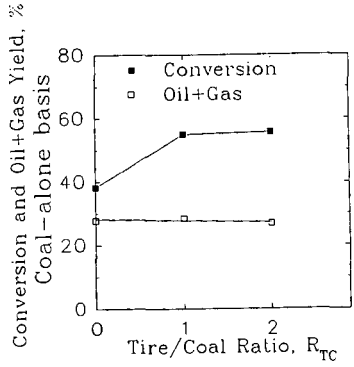

Figure 3. Effect of R_{TC} on co-processing of coal and waste tire at 425°C. Other conditions same as in Figure 1.

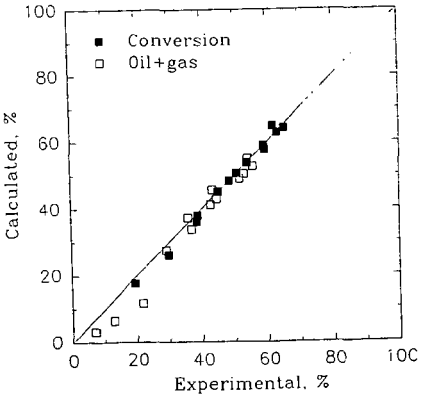

Figure 4. Comparison of the experimental and calculated values of the conversions and oil+gas yields from coal/tire co-processing

TWO STAGE COPROCESSING OF WASTE TIRES AND COAL

Ying Tang and Christine W. Curtis
Chemical Engineering Department
Auburn University, AL 36849-5127

Keywords: waste tires, coal, coliquefaction, coprocessing

INTRODUCTION

Waste tires present an insidious waste disposal problem since piles of waste tires often attract rodents and other varmints and frequently burn. Recent use of ground waste tires as a fill material for roads has resulted in oil being released from the tire after weathering and the tire fill erupting into flames. Therefore, safe and healthy disposal of waste tires is necessary and needs immediate attention since the Department of Energy has reported that 350 million waste tires are disposed of each year in the United States. A number of safe and useful waste tire processing technologies have been developed as alternatives to disposing in landfills. Waste tires have been used as fuel to generate electricity [1], as filler in asphalt road pavement,[2] and as raw material for secondary product production. [3] Waste tire pyrolysis [4-6] and liquefaction [7-12] are two technologies that can be applied to waste tires to produce fuels and chemical feedstock, thereby recycling the hydrocarbon base.

Several pyrolysis methods are being developed at pilot or industrial scale.[4] Cypres et al. [4] investigated the effect of pyrolysis conditions on the liquid product and found an increase of naphthalene and benzene with a decrease of the liquid fraction as the residence time increased. Merchant et al. [5] recovered solid material, primarily consisting of carbon black, from waste tire pyrolysis, activated the material, and used it for waste water treatment. Recently, Conesa et al.[6] examined gas production from scrap tires pyrolysis in a fluidized sand bed reactor. The yield of total gas was reported to increase in the range of 600-800 °C from 6.3 to 37.1%.

Waste tire liquefaction has been actively investigated in recent years. Farcasiu et al.[7] indicated that coprocessing waste tire with coal was beneficial for enhancing coal conversion. Liu et al.[8] investigated the liquefaction of coal and waste tire individually and compared the results to that of simultaneously coprocessing the two materials. The conversion obtained from the coprocessing reactions was greater than that achieved from combining the individual reactions. Orr et al. [9] also observed synergism in reactions where there was a 10 to 30% loading of waste tires to coal and the reaction occurred at 350 °C and in reactions at 430 °C at almost all loadings levels of waste tires. Tang and Curtis [10] performed thermal and catalytic coprocessing of waste tires and coal using waste tires from two sources and coals of three different ranks. The bituminous coals yielded higher conversions than either subituminous coal or lignite when coprocessed with waste tire. Catalytic coprocessing of waste tires with coal using slurry phase hydrogenation catalysts increased conversion of the total system and the coal within the system compared to the conversions obtained in thermal reactions. Orr et al. [11] coprocessed Blind Canyon coal with ground waste tire particles and vacuum pyrolyzed tire oil (PTO), respectively. Coprocessing of coal with PTO yielded higher coal conversion than coprocessing with ground waste tire particles. Badger et al. [12] evaluated hydrogen transfer in coal/oil coprocessing by coprocessing coal with heavy oil (petroleum) distillates (HOD) and pyrolyzed tire oil (PTO). HOD, being highly aliphatic, did not show any H-donation capability. By contrast, PTO, being highly aromatic and containing substantial phenanthrenes and substituted phenanthrenes but very little hydroaromatic compounds, could be induced to transfer hydrogen by hydrogen shuttling. PTO was more effective for dissolving coal after being prehydrogenated and, thereby, containing more hydroaromatic compounds.

The objective of the current research was to investigate the effect of two stage processing of waste tires and coal. The first stage served as a reaction medium by which waste tires were converted to liquids and the solids and where carbon black and other minerals can be removed from the system. In the second stage, the liquefied waste tire served as a solvent for coal and was coprocessed with coal under reaction conditions that were favorable for liquefying of coal and upgrading of coal liquids. Reaction conditions for producing high quality products from both reactions were examined. Both slurry phase and supported catalysts were used.

EXPERIMENTAL

Materials. Two stage reactions were performed by dissolving waste tires in waste oil in the first stage. The carbon black was removed from the liquid by filtration. The waste tire/oil liquid was used as the solvent for coal in the second stage. The waste tire used was supplied by Rouse Rubber industries, Vicksburg, MS. The waste oil was provided by Auburn Waste Oil Reprocessing Lab. The two coals utilized in this research were Beulah Zap lignite and Wyodak Anderson subituminous coal, both of which were obtained from the Argonne Premium Coal Sample Bank.

Catalytic reactions were performed using slurry phase hydrotreating catalyst, molybdenum naphthenate (MoNaph)(6% Mo), obtained from Shepherd Chemical. Elemental sulfur obtained from Aldrich was added to the catalytic reactions with MoNaph. A supported hydrotreating catalyst, $NiMo/Al_2O_3$ (SNiMo), supplied by Shell, was also used in this research. The catalyst was presulfided

prior to reaction by purging the catalyst with N_2 at 300 °C for 1 hr, then subjecting the catalyst to 10.1% H_2S/H_2 with a flow rate of 60 ml/min at 225 °C for 1 hr, followed by 315 °C for two hr, and then 370 °C for 1 hr.

Reaction Procedures. The first stage coliquefaction reactions of waste tires with waste oil were performed in approximately 60 cm^3 stainless steel tubular microreactors at 400 °C for 30 min. H_2 or N_2 was introduced at 6.9 MPa at ambient temperature. The total charge to the reactor was 12 g with the waste tire to waste oil ratio being 5:1 or 1:1. In the first stage catalytic coliquefaction reactions, MoNaph was charged at 1000 ppm of active metal per total reactor charge. Elemental sulfur was added to the catalytic reaction with MoNaph in a 3 to 1 stoichiometric ratio of sulfur to metal using the assumption that MoS_2 was formed. For the reactions with SNiMo, the catalyst loading was at 1.5 wt% of SNiMo powder on a total charge basis.

The second stage coprocessing reactions of coal with THF solubles obtained from the first stage reactions were conducted in approximately 20 cm^3 stainless steel microreactors at 400 °C for 30 min. The total charge to the reactor was 5 g with a solvent to moisture and ash free (maf) coal ratio being 1 to 1. In the second stage catalytic coprocessing reactions, the type and loading of the catalysts were the same as the first stage catalytic coliquefaction reactions.

Several reactions were performed by combining waste tire, waste oil, and coal in a single stage reaction at 400 °C for 30 min with initial H_2 pressure at 6.9 MPa. Rouse waste tire and waste oil were added to the reactor with tire to oil ratio at 5 to 1 or 1 to 1 in an amount that would produce 2 g THF solubles when the tire and oil were coliquefied without coal. In catalytic one stage reactions, SNiMo was charged to the reactor together with waste tire, waste oil, and coal at 1.5 wt% of the catalyst on a total charge basis.

Analysis. After reaction, gaseous products were determined by weighing the tubular microreactor before and after releasing gaseous products. The liquid and solid products were analyzed by solvent fractionation using sequential extractions of hexane and THF. The organic material that was not soluble in THF was defined as insoluble organic matter or IOM which was ash free.

RESULTS AND DISCUSSION

Two stage coprocessing of coal and waste tires was investigated to determine if more coal conversion and hexane soluble products could be produced if the waste tire was liquefied prior to contact with coal and the carbon black was removed. The first stage was a coliquefaction of waste tires with waste oil, the waste oil providing a dissolving medium for the tires. Two ratios of waste tires to waste oil, 5:1 and 1:1, were used. At the reaction conditions of 400 °C for 30 min, high conversions to THF soluble materials of the convertible material were obtained regardless of whether the atmosphere was H_2 or N_2. After reaction, the unconverted material, including carbon black and other mineral constituents in the tire, were removed. The THF soluble liquid was then used as the solvent for the second stage coal reaction.

Thermal Coprocessing Reactions Using First Stage Liquids as Solvents. Thermal reactions of Beulah Zap lignite and Wyodak subbituminous coal were performed with first stage liquids as well as waste oil, waste tire, and two hydroaromatic solvents, including tetralin and dihydroanthracene (DHA) as given in Table 2. The reactions with waste tire and/or waste oil were performed in H_2 while the reactions with tetralin and DHA were performed in N_2. The product distributions and the conversion of the materials were the measure by which the effectiveness of the solvent for liquefaction was determined. The total product distribution and total conversion measured the reactivity of the total system both the solvent and coal. By contrast, the product distribution on a coal basis and the coal conversion removed the effect of the solvent on these two measures, thereby describing how the coal itself reacted in the solvent.

The total conversions obtained for Beulah Zap lignite and Wyodak coal second stage reactions with first stage waste tire and oil solvents were similar and ranged from 64.2 to 67.3% for Beulah Zap and 63.9 to 69.2% for Wyodak. The total conversions with DHA and tetralin as solvents were somewhat higher but also similar and gave values of 74.6 and 72.8%, respectively. The total product distribution yields for gases, hexane solubles, and THF solubles were also similar for all of the reactions with waste tire and waste oil first stage liquids. However, tetralin yielded the highest hexane solubles, while DHA yielded the lowest. The reaction with DHA gave the largest amount of THF solubles of any of the reactions.

Coal conversions and, particularly, product distributions based on coal with the solvent effect removed showed more variability than those from the total values. Factors that affected coal conversion included type of coal used, atmosphere used in the first stage reaction, and ratio of waste tires to waste oil used in the first stage. The amount of hexane soluble and THF soluble material produced was also dependent on these factors. For lignite, coal conversion with solvents consisting of 5:1 ratio of waste tires to waste oil was greater than the 1:1 ratio regardless of the type of atmosphere used in the first stage reaction. Coal conversion was also higher when a H_2 atmosphere was used in the first stage rather than a N_2 atmosphere regardless of ratio. The coal conversion ranged from 34.2% for a 5:1 tires to oil ratio in the first stage reacted in H_2 to a low of 25.7% when a 1:1 ratio was reacted in a N_2 atmosphere. The ratio of waste tire to waste oil also strongly affected

the amounts of hexane solubles and THF solubles obtained with a given atmosphere. The higher ratio resulted in less hexane solubles and more THF solubles.

The factors that affected the second stage lignite thermal reaction also affected the Wyodak second stage reaction. Higher conversion was observed with first stage having a 5:1 ratio and when reacted in H_2. Reactions were performed with the individual reactants as well. Waste tires as a solvent gave a Wyodak conversion of 40.2 % while waste oil yielded 34.1%. The hexane solubles based on coal were higher with the higher ratio of 5:1 and a H_2 atmosphere in the first stage reaction.

Hydrogen donation to coal by solvents derived from waste tires during liquefaction is feasible since these solvents contain aromatic oil that can be hydrogenated to form hydroaromatics during coprocessing. Badger et al. (1994) evaluated H-donation to coal using solvent produced from the pyrolysis of waste tires. The pyrolyzed oil itself was ineffectual in converting coal even in a H_2 environment. Prehydrogenating the waste tire liquids was effectual for H-donation if the extent of prehydrogenation was not too great, since too much hydrogenation decreases the hydrogen donor capability of the solvent. (Badger et al., 1994; Curtis et al., 1981) In the current study, hydrogen donation from liquefied waste tires to coal was evaluated by comparing the coal conversion obtained in a liquefied waste tire/waste oil solvent to that obtained with tetralin and DHA in a N_2 atmosphere. The highest coal conversions, 48.7 and 44.5%, respectively, were achieved with these hydrogen donors, thereby indicating that the waste tire/waste oil solvents were much inferior hydrogen donors.

Catalytic Two Stage Coprocessing. The low total and coal conversions obtained from thermal two stage coprocessing clearly showed the need for introducing catalysts into one of the stages. Table 3 presents the conversions and product distributions from two stage reactions with catalysts being introduced separately in the first and second stage. Sulfided $NiMo/Al_2O_3$ and MoNaph plus excess S catalysts were each added to the second stage of the two stage reaction using Wyodak coal. The total conversion for the SNiMo catalyst ranged from 79.7 to 86.5% while higher total conversions were observed for the second stages with MoNaph + S, ranging from 94.5 to 95.2%. The coal conversion using SNiMo catalysts resulted in higher conversion, which ranged from 61.5 to 73.1%, than the thermal reaction which ranged from 25.6 to 40.5%. The MoNaph was even more effective since reactions with MoNaph + S and coal resulted in coal conversion which ranged from 89.8 to 91.2%. Reactions performed with solvents of the 5:1 ratio of waste tires to waste oil that had been liquefied in a H_2 atmosphere yielded the highest conversions with each catalyst. However, when either catalyst was added to the first stage, neither was effectual resulting in low total conversions of ~68% and coal conversion of ~40 to 41 %. These low two stage conversions showed that adding the catalyst to the first stage resulted in conversion values that were similar to thermal reactions. These results strongly indicated that the catalysts were deactivated by contact with the waste tires while they were being liquefied.

Comparison of One and Two Stage Coprocessing. A comparison of one and two stage coprocessing reactions is given in Table 4 where thermal and catalytic reactions of Wyodak coal performed under equivalent conditions but using different staging are given. The catalyst used in the comparison is SNiMo. The separation of the tire liquefaction reaction from the coal liquefaction reaction dramatically improved the efficacy of the catalyst. At a 5:1 ratio of waste tire to waste oil, the thermal conversion was higher in the single stage reaction than in the two stage reaction. However, the addition of the catalyst in the single stage reaction resulted in only minimal improvement of less than 2% conversion, while a substantial increase in conversion (32.6%) was observed when the catalyst was added to second stage of the two stage reaction. In addition, the observation can be made that the less contact between liquefying waste tire and catalyst, the better the overall conversion obtained. The single stage conversions with the catalyst with a waste tire to waste oil ratio of 1:1 were higher than the reactions with ratios of 5:1. These results emphasize the detrimental effect on catalytic activity that resulted from direct contact between the liquefying waste tire and the hydrotreating catalysts.

SUMMARY AND CONCLUSIONS

The advantage of two stage coprocessing of waste tires with coal was most apparent when a catalyst was used. The introduction of a hydrotreating catalyst in the second stage resulted in improved overall conversion and coal conversion. The slurry phase Mo naphthenate catalyst was more effective than the supported $NiMo/Al_2O_3$ catalyst when added to the second stage. In the second stage, the catalyst contacted waste tire that had been already liquefied and whose carbon black and mineral constituents had been removed, and, hence, the catalyst suffered less deactivation.

The waste tire itself was a reasonably effective solvent for coal dissolution but did not provide much H-donor capability. The result was clearly observed when the conversions obtained with liquefied waste tires were benchmarked against these obtained with known H-donors. Increased reactivity of the waste tire solvent for coal dissolution may be possible by pyrolyzing and prehydrogenating the waste tire. This research is currently underway.

REFERENCES

1. Tesla, M.R., *Power Engineering*, 1994, May, 43-44.
2. *Paul J. Kirk-Othmer Encyclopedia of Chemical Technology*, Wiley, New York, 1982, Vol198, 1002-1010.
3. Orgasawara, S.; Kuroda, M.; and Wakao, N., *Ind. Eng. Chem. Res., 26*, 1987, 2552-2556.
4. Cypres, R.: Bettems, B. in Pyrolysis and Gasification, Ferrero, G.L.; Maniatis, K.; Buekens, A.; Bridgwater, A.V., Editors, Elsevier Applied Science, London, 1989, p 209.
5. Merchant, A.A.; Petrich, M.A., AICHE J. 1993, 39(8), 1370.
6. Conesa, J. A.; Font, R.; Morcilla, A., *Energy and Fuels*, 1996, 10, 134-140.
7. Farcasiu, M.; Smith, C.M., *ACS Fuel Chem Div Prepr., 37,1,* 1992, 472-479.
8. Liu, Z.; Zondlo, J.W.; Dadyburjor, D.B., Energy Fuels, 8(3), 1994, 607-12.
9. Orr E.C.; Tuntawiroon, W.: Anderson, L.L., Eyring, E.M., *ACS Fuel Chem Div Prepr.,39,* 1994, 1065-1072.
10. Tang, Y., Curtis, C. W., *Fuel Processing Technology, 46,* 1996, 195-215.
11. Orr, E.C.; Burghard, J. A.; Tuntawiroon, W.; Anderson, L. L.; Eyring E. M., *Fuel Processing Technology,* 1996, in press.
12. Badger, M.W.; Harrison, G.; Ross, A.B., Presentation at 208th National Meeting, ACS, Washington, D.C.,1994, August 21-26.
13. Curtis, C.W.; Guin, J.A.; Jeng, J.F.; Tarrer, A.R. *Fuel, 60,* 677-783, 1981.

Table 1. Thermal Coliquefaction of Waste Tires with Waste Oil[a]

Reactants	Ratio (wt)	THF Solubles (wt%)		Conversion (wt%)	
		Total	Tire	Total	Tire
6.9 MPa of H_2 at ambient temperature					
RWT/WO[b]	5:1	94.2±1.2	93.1±1.6	96.2±1.3	95.7±1.4
RWT/WO	1:1	95.5±0.4	92.4±0.5	97.5±0.8	93.5±0.9
6.9 MPa of N_2 at ambient temperature					
RWT/WO	5:1	93.0±1.4	91.5±1.8	95.5±1.5	93.9±1.9
RWT/WO	1:1	94.7±0.9	90.2±1.2	96.6±1.0	91.3±1.0

[a] Coliquefaction reaction conditions: 400°C, at 6.9 MPa H_2 and N_2, for 30 min, total charge 12 gram with ratio of waste tire to waste oil being 5 to 1 and 1 to 1.
[b] RWT=Rouse waste tire provided by Rouse Company, WO=waste motor oil provided by Auburn Waste Oil Reprocessing Lab.

Table 2. Thermal Coprocessing Reactions of Coals with the Liquids Obtained by First Stage Coliquefaction of Waste Tire and Waste Oil[a]

Liquid Source	Coal	Product Distribution (wt%)						Conversion (%)	
		Total			Coal				
		GAS	HEXS[b]	THFS[b]	GAS	HEXS	THFS	Total	Coal
WO[b]	BZ[b]	3.9±0.3	51.1±1.0	12.3±1.1	5.3±0.6	4.8±2.9	24.6±2.7	67.3±2.2	34.7±1.3
RWT/WO 5/1 H_2[c]		4.9±0.5	44.0±0.8	16.6±1.0	6.9±0.9	3.2±2.3	24.1±2.5	65.5±2.0	34.2±1.1
RWT/WO 1/1 H_2		4.3±0.2	50.1±1.1	10.1±1.3	6.0±0.5	11.3±3.0	13.0±3.2	64.5±2.5	30.3±1.4
RWT/WO 5/1 N_2		4.6±0.4	47.3±0.6	13.2±0.9	6.6±0.8	5.8±1.8	18.1±2.3	65.1±1.7	30.5±0.9
RWT/WO 1/1 N_2[c]		4.8±0.6	54.0±1.3	5.4±0.6	7.2±1.1	15.1±3.4	3.4±1.5	64.2±1.9	25.7±1.6
Tetralin with N_2	WY[b]	2.1±0.4	63.1±1.6	9.2±0.9	2.3±0.4	28.0±2.0	18.4±1.7	74.6±2.7	48.7±3.4
DHA with N_2		3.0±0.6	45.4±1.4	24.4±1.1	4.2±1.1	37.6±1.8	2.7±1.3	72.8±2.9	44.5±3.2
RWT		3.2±0.2	51.1±1.0	14.3±0.9	3.8±0.4	16.7±2.3	19.7±1.8	68.6±1.8	40.2±1.9
WO		3.5±0.4	54.9±1.4	8.1±0.8	4.4±0.8	13.8±1.5	15.9±2.0	66.5±2.4	34.1±2.0
RWT/WO 5/1 H_2		3.4±0.2	54.0±0.7	11.8±0.3	4.1±0.5	21.4±0.9	15.0±0.5	69.2±1.0	40.5±1.4
RWT/WO 1/1 H_2		3.8±0.3	52.1±1.0	8.4±1.0	5.0±0.5	15.4±1.0	9.5±1.9	64.3±2.0	29.9±2.9
RWT/WO 5/1 N_2		3.0±0.2	52.5±0.8	11.7±0.8	3.4±0.5	19.7±1.3	14.7±0.9	67.2±1.9	37.8±2.0
RWT/WO 1/1 N_2		3.6±0.5	52.5±1.2	7.8±0.8	4.6±0.8	12.5±1.1	8.5±1.5	63.9±1.6	25.6±2.5

[a] Reaction conditions: 400°C, 30 min, 6.9 MPa H_2 at ambient temperature, 2 g maf coal, maf coal:solvent=1:1.
[b] HEXS=hexane solubles; THFS= THF soluble and Hexane insolubles;
BZ=Beulah-Zap lignite; WY=Wyodak subbituminous coal; RWT= Rouse waste tire provided by Rouse Company;
WO= waste motor oil supplied by Auburn Waste Oil Reprocessing Lab.
[c] RWT/WO 5/1 H_2 = the liquid(THF solubles) obtained by first stage coliquefaction of Rouse waste tire and waste oil at 400 °C, in 6.9 MPa initial H_2, at waste tire:waste oil=5:1, for 30 min, then extracting the product with THF;
RWT/WO 1/1 N_2 = the liquid(THF solubles) obtained by first stage coliquefaction of Rouse waste tire and waste oil at 400 °C, in 6.9 MPa initial N_2 at waste tire:waste oil=1:1, for 30 min, then extracting the product with THF.

Table 3. Coprocessing Reactions of Wyodak Coal with the Liquids Obtained by Coliquefying Waste Tires and Waste Oils Thermally and Catalytically[a]

Liquid Source	Catalyst	Product Distribution (wt%)						Conversion (%)	
		Total			Coal				
		GAS	HEXS[b]	THFS[b]	GAS	HEXS	THFS	Total	Coal
Catalyst added in the second stage but not in the first stage									
RWT/WO 5/1 H_2[c]	SNiMo	4.8±0.8	50.0±1.7	31.7±1.2	7.0±1.6	11.3±3.2	54.8±2.3	86.5±2.8	73.1±3.3
RWT/WO 5/1 N_2		2.7±0.3	52.7±1.6	24.3±0.6	2.9±0.6	20.1±1.8	38.5±0.8	79.7±1.8	61.5±2.6
RWT/WO 1/1 H_2		3.9±0.7	52.0±1.6	26.0±1.1	5.1±1.3	18.1±2.8	42.6±2.1	81.9±2.6	65.8±2.9
RWT/WO 5/1 H_2	MoNaph+S	4.0±0.6	48.6±1.3	42.6±0.9	5.0±1.0	14.6±2.4	71.6±1.7	95.2±2.1	91.2±2.5
RWT/WO 5/1 N_2		2.6±0.4	53.7±1.9	38.2±1.1	2.8±0.7	23.1±3.4	63.9±1.9	94.5±3.0	89.8±3.4
RWT/WO 1/1 H_2		3.5±0.7	55.1±1.5	36.3±1.0	4.3±1.3	22.0±2.8	63.8±1.8	94.9±2.6	90.1±3.0
Catalyst added in the first stage but not in the second stage									
RWT/WO 5/1 H_2	SNiMo	3.2±0.3	52.1±1.2	12.8±1.0	3.6±0.7	20.0±2.3	16.6±1.8	68.1±2.2	40.3±3.0
RWT/WO 5/1 H_2	MoNaph+S	3.4±0.7	50.5±0.9	15.0±0.7	4.1±1.2	17.0±1.7	20.7±1.5	68.9±1.6	41.8±2.8

[a] Coprocessing Reaction conditions: 400°C, 30 min, 6.9 MPa H_2 and N_2 at ambient temperature, 2 g maf Wyodak coal, maf coal:solvent = 1:1, SNiMo 1.5wt%; MoNaph 1000 ppm Mo, S:Mo=6:1.

[b] HEXS=hexane solubles; THFS= THF soluble and hexane insolubles.
RWT= Rouse waste tire provided by Rouse Company.
WO=waste motor oil supplied by Auburn Waste Oil Reprocessing Lab.

[c] RWT/WO1 5/1 in H_2=the liquid(THFS) obtained by coliquefying Rouse waste tire and waste oil at 400 °C, in 6.9 MPa initial H_2, at waste tire:waste oil=5:1, for 30 min, then extracting the product with THF. For catalytic coliquefaction, SNiMo(1.5 wt%) and MoNaph+S(1000 ppm, S:Mo=6:1).

Table 4. Comparison of Single and Two Stage Thermal and Catalytic Coprocessing Reactions of Wyodak Coal with Waste Tire and Waste Oil[a]

Reactants	Catalyst	Product Distribution (wt%)						Conversion (%)	
		Total			Coal				
		GAS	HEXS[b]	THFS[b]	GAS	HEXS	THFS	Total	Coal
Two Stage Reaction									
WY+(RWT/WO 5/1/H_2)[c]	None	3.4±0.2	54.0±0.7	11.8±0.3	4.1±0.5	21.4±0.9	15.0±0.5	69.2±1.0	40.5±1.4
WY+(RWT/WO 5/1/H_2)	SNiMo	4.8±0.8	50.0±1.7	31.7±1.2	7.0±1.6	11.3±3.2	54.8±2.3	86.5±2.8	73.1±3.3
WY+(RWT/WO 1/1/H_2)	None	3.8±0.3	52.1±1.0	8.4±1.0	5.0±0.5	15.4±1.9	9.5±1.9	64.3±2.0	29.9±2.9
WY+(RWT/WO 1/1/H_2)	SNiMo	3.9±0.7	52.0±1.6	26.0±1.1	5.1±1.3	18.1±2.8	42.6±2.1	81.9±2.6	65.8±2.9
One Stage Reaction									
WY+RT+WO(T/O 5/1)[c]	None	5.8±0.5	41.0±1.1	24.0±1.2	5.5±0.6	1.4±0.3	40.9±2.4	70.7±1.3	47.8±2.0
WY+RT+WO(T/O 5/1)	SNiMo	6.7±0.6	44.7±1.7	22.1±1.4	7.1±1.0	2.4±0.4	39.9±2.1	73.5±1.7	49.5±1.9
WY+RT+WO(T/O 1/1)	None	5.5±0.2	42.4±1.5	25.5±1.8	5.0±0.8	6.0±0.5	44.6±2.7	73.3±1.9	50.2±2.8
WY+RT+WO(T/O 1/1)	SNiMo	6.2±0.4	48.0±1.8	22.8±1.5	6.5±1.2	4.6±0.4	42.5±2.1	77.0±2.0	53.6±2.7

[a] Reaction conditions: 400°C, 30 min, 6.9 MPa H_2 at ambient temperature, 2 g maf Wyodak coal, maf coal:solvent(THF solubles) = 1:1.

[b] WY=wyodak coal;
RWT=Rouse waste tire;
WO=waste oil from Auburn Waste Oil Reprocessing Lab;
HEXS=hexane solubles;
THFS= THF solubles;
SNiMo= presulfided $NiMo/Al_2O_3$

[c] For two stage reactions, (RT/WO 5/1 H_2)= THF Solubles obtained from the first stage reaction with Rouse waste tire to waste oil ratio of 5 to 1 in H_2; For one stage reactions, RT+WO(T/O 5/1)= Rouse waste tire with waste oil at tire to oil ratio of 5 to 1 in an amount that would produce 2 g THF solubles.

POLYETHYLENE DEGRADATION IN A COAL LIQUEFACTION ENVIRONMENT

Kurt S. Rothenberger, Anthony V. Cugini, and Robert L. Thompson
U.S. Department of Energy, Pittsburgh Energy Technology Center,
P.O. Box 10940, Pittsburgh, PA 15236

KEYWORDS: polyethylene, liquefaction, waste coprocessing.

INTRODUCTION

The coprocessing of coal with waste materials such as plastic has shown promise as an economical means to recover the inherent value of the wastes while producing useful products. Polyethylene (PE) is one of the dominant plastic materials; recent statistics indicate that low- and high-density PE together make up about half of all municipal plastic waste.[1] The degradation of PE in a pyrolysis environment has been well studied,[2] and pyrolysis-based methods for the conversion of PE to fuels have been published.[3] However, recent studies have shown that PE is among the most difficult plastics to convert in the traditional liquefaction environment, particularly in the presence of coal and/or donor solvents.[4] The coal liquefaction environment is quite different than that encountered during thermal or catalytic pyrolysis. Understanding the degradation behavior of PE in the liquefaction environment is important to development of a successful scheme for coprocessing coal with plastics.

In this paper, a novel analytical method has been developed to recover incompletely reacted PE from coprocessing product streams. Once separated from the coal-derived material, gel permeation chromatography, a conventional polymer characterization technique, was applied to the recovered material to ascertain the nature of the changes that occurred to the PE upon processing in a bench-scale continuous liquefaction unit. In a separate phase of the project, 1-L semi-batch reactions were performed to investigate the reactivity of PE and coal-PE mixtures as a function of temperature.

EXPERIMENTAL SECTION

Materials. Liquefaction experiments were conducted using -200 mesh Black Thunder mine coal (Wyodak-Anderson seam, Campbell County, WY). High-density polyethylene (PE; T_m = 135 °C, d = 0.96 g/mL) was supplied by Solvay Polymers. Polystyrene (PS; T_m = 95 °C, d = 1.0 g/mL) was supplied by BASF. Polypropylene (PP; T_m = 176 °C, d = 0.94 g/mL) was supplied by Amco Plastics. The same plastics were used in both the semi-batch experiments and the bench-scale continuous run. All plastics were supplied as 3.2 mm (0.125 in) extruded pellets. A mildly hydrogenated petroleum-derived oil, containing small amounts of coal derived liquid, was used as a solvent in the semi-batch coprocessing tests. The bench scale continuous unit run was started up on a similar solvent but then operated in a recycle mode. An aged Ni-Mo catalyst supported on alumina in the form of 1/16" extrudates (AO-60) was supplied by Akzo and used in the semi-batch tests. Both molybdenum and iron based catalysts were used in the bench-scale continuous run. Tetrahydrofuran (THF) and dichloromethane (CH_2Cl_2) solvents used in work up and/or extraction procedures were obtained in bulk grade and used without further purification. Decane fraction (bp 171-177°C), used in the PE recovery procedure, was obtained from Fluka Chemie AG and used without further purification.

Reactions. Semi-batch tests were performed in a 1-L stirred-tank reactor system.[5] Sample work-up and feed conversions were calculated by a procedure described previously.[6] Samples were obtained from a bench scale continuous mode run performed on a close-coupled, two-stage, catalytic reactor system, and operating as part of the U.S. Department of Energy's coal liquefaction program. A simplified schematic diagram of the continuous unit configuration is shown in Figure 1. Samples were obtained from the following points, identified in Figure 1: (1) feed slurry, (2) first reactor, (3) second reactor, (4) atmospheric still bottoms, (5a) vacuum still overhead, and (6a) vacuum still bottoms, or (5b) pressure filter liquid, and (6b) pressure filter solids. Samples were taken during three different coprocessing run conditions, identified by the feed type: (1) coal mixed plastics in a 2:1 ratio (67% coal, 13% PE, 11% PP, 9% PS), (2) coal:PE in a 2:1 ratio, and (3) coal:plastics in a 1:1 ratio (50% coal, 20% PE, 16.5% PP, 13.5% PS).

Extraction of Incompletely Reacted PE from Bench Scale Continuous Unit Process Streams. In order to more thoroughly investigate the behavior of PE in a coal liquefaction system, a general method was devised to recover incompletely reacted PE

from coal liquefaction process streams. The method is diagrammed in Figure 2. The first step involved a cold THF wash to remove as much soluble coal-derived material as possible without affecting the incompletely reacted PE. In fact, this step alone was sufficient to isolate PE from a tarry stream that contained no insoluble coal matter (e.g., a non-ashy recycle stream).[7] The THF insolubles were then subjected to a hot decane extraction; the decane fraction dissolved the incompletely reacted PE, but left the coal derived solids behind. After the hot decane was filtered and concentrated, a dichloromethane wash was used to remove any remaining coal derived materials and aid in formation of an beige, powdery solid. The method also removes other polyolefins, such as PP. The method was applicable to a wide range of process streams including tars, solids, and multi-phase mixtures.

The process samples containing unreacted PE existed either as solids or as viscous tars. If solid, the sample was crushed in a mortar and pestle prior to the extraction procedure. If tar, the sample was heated in an oven at low temperature (<100°C) and poured into a reaction flask. The procedure began by digesting the solid co-processing residue in THF. The sample (5-25 g) was placed into a Whatman cellulose Soxhlet thimble (25 mm od x 100 mm), submerged in THF (ca. 250 mL) within a beaker and sonicated for about 1 hr at ambient temperature. At this point the THF solution had turned dark brown with soluble coal-derived material. After the THF was removed, the thimble was placed in a Soxhlet extraction apparatus and exhaustively extracted with another 500 mL of fresh THF. This extraction typically required 24 hr before the washings become colorless.

The THF insoluble material (at this point typically 1-10 g) were vacuum dried inside the extraction thimble in an oven at 50°C to evaporate any residual THF, then transferred to a 500 mL flask along with ca. 300 mL decane fraction (bp 171-177°C), used as received from Fluka Chemie AG. The mixture was refluxed under flowing nitrogen (preventing atmospheric oxygen from coming into contact with the hot decane solution) for 1 to 2 days to digest the PE. The *boiling hot* decane solution was then filtered through a fresh cellulose Soxhlet thimble (43 mm od x 125 mm) to give a black solid and a viscous yellow filtrate containing the incompletely reacted PE. The decane was evaporated under reduced pressure on a rotary evaporator at 70°C to yield a yellow to yellow-brown filmy residue which adhered to the walls of the flask.

After addition of ca. 300 mL CH_2Cl_2, the residue was then scraped from the walls of the flask and sonicated at ambient temperature for 1 hr. After sonication the CH_2Cl_2 had become yellow and the residue had formed flocculent particles and flakes. The mixture was filtered through a medium-porosity glass frit to give a light beige to tan solid and yellow CH_2Cl_2 filtrate. The beige incompletely reacted PE product was vacuum dried in an oven at 50°C until constant weight.

Gel Permeation Chromatography (GPC). GPC of the recovered PE samples was performed by Jordi Associates, Inc., of Bellingham, MA. Samples were dissolved in trichlorobenzene at 145°C, and analyzed on a Waters 150C high pressure liquid chromatograph, equipped with a mixed bed linear column (prepared at Jordi) and refractive index detector. Calibration was done with polystyrene standards. Molecular weight distribution parameters M_n, the number average molecular weight, and M_w, the weight average molecular weight, were provided by the data acquisition and handling software at Jordi. For convenience in interpreting samples with bimodal molecular weight distributions, the maximum points in the distribution curves (i.e., the most frequently occurring molecular weight values) were calculated at PETC.

RESULTS AND DISCUSSION

The efficacy of a coal liquefaction procedure is generally measured in terms of conversion, usually defined in terms of solubility in a given solvent or distillation at or below a given endpoint. Although this is a functional way of evaluating a set of processing parameters, it reveals little about the chemical nature of the species involved in the reactions. The ability to isolate and recover unconverted PE from a coal-plastics coprocessing stream affords the ability to characterize it withour the complexity of the coal and coal derived products. This yields a significant opportunity to understand the degradation of PE in the coal liquefaction environment.

The PE recovery method was developed at PETC according to the procedure diagrammed in Figure 2 and described in the Experimental Section. The method was

tested on a sample of virgin PE (M_n = 15,000; M_w = 100,000) of the same source as was used as feed in the semi-batch and bench-scale continuous runs. The percentage of original PE recovered, and the GPC data for the virgin PE before and after the extraction procedure is shown in the first two lines of Table I. None of the initial PE was left behind; the recovery of 86% represents losses that occurred upon the filtration step due to rapid cooling of the decane solution. A better hot filtration method is currently being implemented to improve quantitation of the technique. The slightly higher molecular weight values of the PE obtained after extraction may indicate the occurrence of condensation reactions during extraction; this observation is currently being investigated.

The PE extraction technique was also tested by examining a coprocessing sample (containing both coal and PE) before and after PE extraction, using solid state nuclear magnetic resonance (NMR) spectroscopy done by Ronald Pugmire and Mark Solum at the University of Utah.[9] Before extraction, the aliphatic portion of the spectrum consisted of a single sharp peak in the CH_2 region superimposed on a broader signal due to coal-derived material. After extraction, the recovered PE yielded only the sharp CH_2 signal; the coal-derived residue materials showed only the broader signal.[9] Thus it is reasonable to assume that, except for filtration losses, the method removes essentially all of the incompletely reacted PE and no coal derived material.

The extraction technique was used to recover PE from a series of sampling streams during three different feed conditions of a coprocessing operation on a bench scale continuous unit. The percentage of each sample stream recovered, as well as the molecular weight distribution parameters obtained from GPC of the recovered material, are listed in Table I. Molecular weight distribution curves, obtained from GPC data for the 2:1 coal:PE feed condition, are shown in Figure 3a-e. For comparison, a GPC trace of the unreacted PE after extraction is shown in Figure 3f.

The most dramatic observation from Figure 3 is the presence of two peaks in the samples taken from the feed slurry (Figure 3a) and first reactor (Figure 3b). The two peak maxima occur at molecular weight values of approximately 2,000 and 50,000 amu. The larger maximum in Figure 3a (and 3b) strongly resembles the unreacted, extracted PE in Figure 3f. Therefore, the larger, or higher molecular weight peak in Figure 3a (and 3b) can be assigned to fresh PE feed. The smaller, or lower molecular weight peak in Figure 3a (and 3b) resembles the PE recovered from the sampling points downstream in the process (Figure 3d,e). In particular, the PE-containing pressure filter liquid stream (Figure 3e) constituted the recycle vehicle during the 2:1 coal:PE operating condition of the continuous unit. Therefore the peak at about 2,000 amu in Figure 3a (and 3b) can be attributed to PE that had been recycled back to the feed slurry after having been through the process. In the other two feed conditions listed in Table I, the sample from the feed slurry (and first reactor) also exhibits bimodal distributions. The feed slurry and first reactor samples also contain unreacted PP, but the same conclusions are valid. This is the first time that a method exists to unambiguously distinguish PE that has been recycled through the process to that has been freshly added to the feed.

Downstream of the feed slurry, the distribution of recovered PE remains bimodal into the first reactor (Figure 3b, Table I). However, by the sampling point for the second reactor (Figure 3c), the bimodal distribution is gone. The GPC molecular weight distribution shows only a single peak, with a maximum and an M_n value approaching that found in the downstream samples (Figure 3d, Table I). This observation confirms that most of the PE breakdown occurs in the reactor zones, i.e., between the sampling points for the first and second reactors. A gradual narrowing of the lineshape from the second reactor (Figure 3c) to the atmospheric still bottoms sample (Figure 3d) and pressure filter liquid (Figure 3E) with accompanying reduction in molecular weight seen in Table I is indicative that some PE breakdown continues past the reactor section of the unit. The same argument can be made for the 2:1 coal:plastics and 1:1 coal:plastics feed conditions (Table I). Thus, it appears that most, but not all, of the PE degradation takes place in the reactor zone.

An important point that should not be overlooked in this finding is that virtually all of the PE feed material *has* undergone some degree of reaction. Because conventional solubility tests or distillation procedures in coprocessing experiments have indicated that PE is difficult to convert, it is easy to make the erroneous assumption that the unconverted PE is also unreacted. These experiments show conclusively that such is not the case. The molecular weight of the PE feed has been reduced by a factor of 10 to 30, depending on what parameter is used to characterize the molecular weight

distribution. The recovered PE has simply not reacted sufficiently to be considered to be converted by traditional coal liquefaction measures.

Two different methods of solids separation were used on the atmospheric still bottoms stream during the continuous run. During the 2:1 coal:plastics feed condition, vacuum distillation was employed. In this configuration no PE was found in the vacuum still overhead material; it all went with the solids. Therefore, a recycle stream produced from only vacuum distilled material would be free of incompletely reacted PE. (In actuality, the recycle stream during the 2:1 coal:plastics condition was a combination of vacuum still overhead and atmospheric still bottoms; hence the PE in the recycle stream.) During the 2:1 coal:PE and 1:1 coal:plastics feed conditions, pressure filtration was employed on the atmospheric still bottoms. In this configuration, most of the unconverted PE went with the filtrate; only a small, approximately constant amount was recovered with the solids. The pressure filtration was done at a temperature above the melting point of PE so most of the PE passed through the filter as liquid or in solution; a small amount became entrained and trapped in the filter cake. Therefore, a recycle stream produced from pressure filtered material would be high in incompletely reacted PE. In this way, the method of solids separation could be tailored to retain or exclude incompletely reacted PE from the recycle stream.

In a separate aspect of the project, 1-L semi-batch reactions were performed to investigate methods for optimizing PE conversion and overall feed conversion in coal-plastics coprocessing. The effect of temperature on the conversion three different feed mixtures to <850°C distillable products is illustrated in Figure 4. The results from a 1:1 ratio of coal:mixed plastics, a 1:1 ratio of coal:PE, and PE feed alone are compared at 430°C, 445°C, and 460°C. The conversion of 1:1 coal:mixed plastics increases from 430°C to 445°C, then levels out from 445°C to 460°C. The conversion of 1:1 coal:PE increases fairly steadily across the entire temperature range. The conversion of the PE only feed shows the most significant increase between 445°C and 460°C. Although the conversion of all three feed mixtures increase with temperature, the PE, at least when used without coal or other plastics, seems to be influenced most by increasing the temperature from 430°C to 460°C. The results suggest that temperature is an important parameter in processing of PE under coal liquefaction conditions. This study will be continued by applying the PE extraction method discussed earlier to the incompletely reacted PE from these semi-batch runs, in order to determine how the temperature or feed composition influences the nature of the PE left unconverted.

Summary. A novel method has been developed to isolate and recover incompletely reacted PE from coal-plastics coprocessing product streams. The method has been applied to samples obtained from a bench scale continuous unit and the recovered material has been characterized by gel permeation chromatography. The method has conclusively established that virtually all PE undergoes some reaction in the coal liquefaction environment, with an average reduction in molecular weight distribution for the "unconverted" material of 10 to 30. The method can definitively distinguish between fresh (feed) and recycled PE in the process stream, and has established that most of the PE degradation occurs in the reactor zone. Vacuum distillation and pressure filtration have dissimilar effects on the incompletely reacted PE present in the atmospheric still bottoms process stream. Finally, semi-batch studies demonstrate the influence of temperature on the distillate conversion of various coal and plastics feed combinations.

Acknowledgements. The authors acknowledge Dr. Gary Robbins of Consol, Inc., and Dr. Vivek Pradhan of Hydrocarbon Technologies, Inc., whose information that PE could be isolated from a deashed coprocessing recycle stream on the basis of THF insolubility led us to develop the generalized PE recovery method reported here. The authors acknowledge Professor Ron Pugmire and Dr. Mark Solum at the University of Utah for solid state NMR to confirm the efficacy of the extraction method. The work of one of the authors (RLT) was performed under an appointment to the U.S. Department of Energy Postgraduate Research Training Program at the Pittsburgh Energy Technology Center administered by the Oak Ridge Institute for Science and Engineering.

DISCLAIMER

REFERENCES

1. Smith, R.A. "Overview of Feedstock Recycling of Commingled Waste Materials," Ninth Annual Technical Meeting, Consortium for Fossil Fuel Liquefaction Science, Pipestem, WV, August 15-18, 1995.
2. Madorsky, S.L. "Thermal Degradation of Organic Polymers," Polymer Reviews Volume 7, Mark, H.F., Immergut, E.H., Eds.; Wiley-Interscience: New York, 1964; pp 93-129.
3. Ng, S.H. Fuel, **1995**, 9, 735-742.
4. (a) Palmer, S.R.; Hippo, E.J.; Tandon, D.; Blankenship, M. Prepr. Pap. - Am. Chem. Soc., Div. Fuel Chem., **1995**, 40(1), 29-33. (b) Huffman, G.P.; Feng, Z.; Mahajan, V.; Sivakumar, P.; Jung, H.; Tierney, J.W.; Wender, I. Prepr. Pap. - Am. Chem. Soc., Div. Fuel Chem., **1995**, 40(1), 34-37.
5. Cugini, A.V.; Krastman, D.; Lett R.G.; Balsone, V.D. Catal. Today, **1994**, 19(3), 395-408.
6. Cugini, A.V.; Rothenberger, K.S.; Ciocco, M.V.; McCreary, C. In Coal Science, Proceedings of the Eighth International Conference on Coal Science, Volume II, Pajares, J.A.; Tascon, J.M.D., Eds.; Coal Science and Technology Series, Volume 24; Elsevier: Amsterdam; 1995; pp 1299-1302.
7. Robbins, G.; Pradhan, V., personal communication
8. Pugmire, R.; Solum, M., personal communication

Figure 1: Simplified diagram of continuous unit configuration.

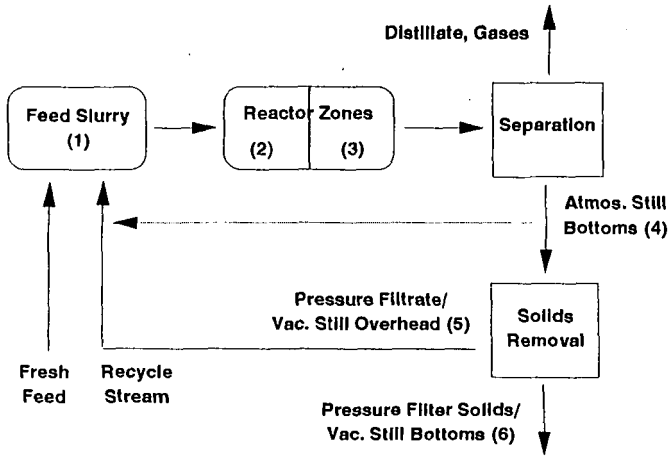

Figure 2: Scheme for recovery of incompletely reacted PE.

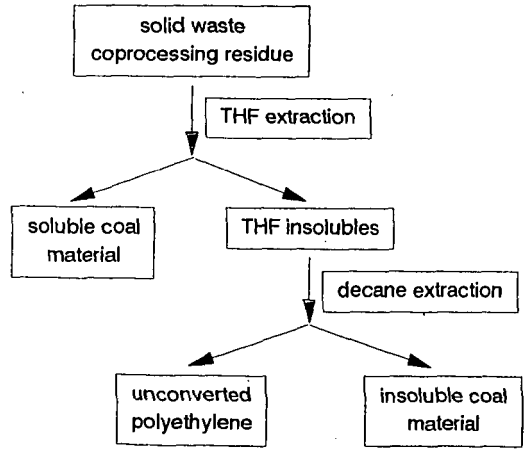

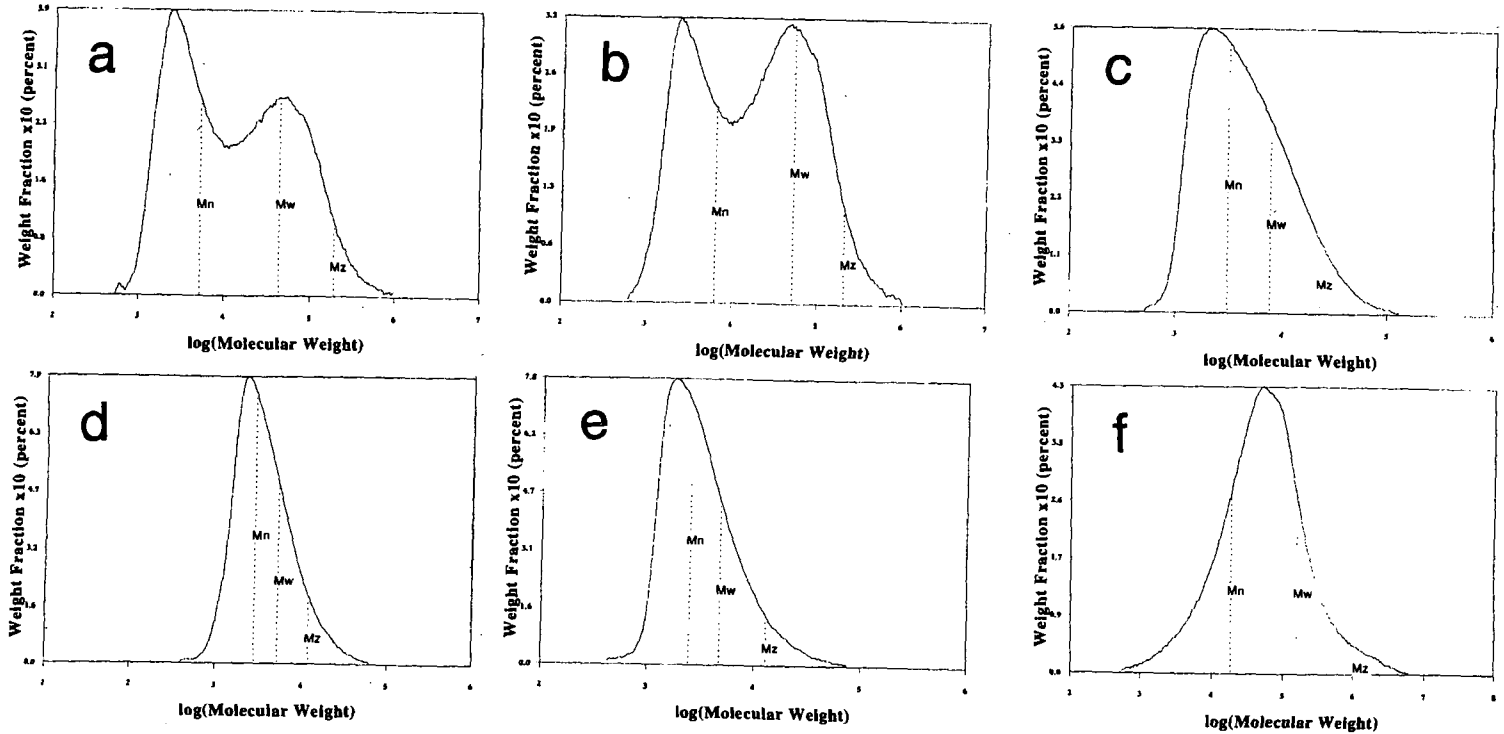

Figure 3: GPC data for 2:1 coal:PE feed condition. (a) feed slurry [sample stream **1**], (b) first reactor **[2]**, (c) second reactor **[3]**, (d) atmospheric still bottoms **[4]**, (e) pressure filter liquid **[5b]**, (f) unreacted, extracted PE.

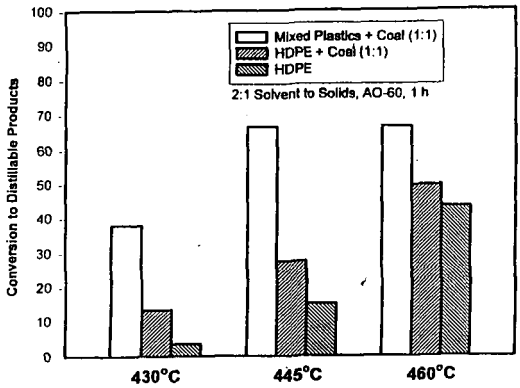

Figure 4: Effect of Temperature on Conversion to Distillable Products (Semi-Batch Studies)

Table I. GPC Results for PE Recovered from Continuous Bench Scale Unit.

Sample Description	PE yield[a]	Max[b]	M_n[b]	M_w[b]
Unreacted Polyethylene (PE)				
PE before extraction	----	46,000	15,000	100,000
PE after extraction	86 %	54,000	19,000	150,000
2:1 coal:plastics condition				
(1) feed slurry	8 %	2,500; 85,000	9,700[c]	230,000[c]
(2) reactor #1	8 %	1,900; 96,000	8,000[c]	200,000[c]
(3) reactor #2	3 %	2,400	3,400	8,000
(4) atmospheric still bottoms	3 %	2,000	2,500	4,100
(5a) vacuum still overhead	0 %	-----	-----	-----
(6a) vacuum still bottoms	12 %	1,500	1,900	3,100
2:1 coal:PE condition				
(1) feed slurry	11 %	2,500; 47,000	5,000[c]	42,000[c]
(2) reactor #1	14 %	2,500; 50,000	6,200[c]	51,000[c]
(3) reactor #2	12 %	2,200	3,000	7,500
(4) atmospheric still bottoms	12 %	2,500	2,800	5,100
(5b) pressure filter liquid	18 %	1,800	2,400	4,800
(6b) pressure filter solids	2 %	1,400	1,900	3,500
1:1 coal:plastics condition				
(1) feed slurry	16 %	2,600; 76,000	3,000[c]	160,000[c]
(2) reactor #1	17 %	2,200; 80,000	2,700[c]	120,000[c]
(3) reactor #2	NA	NA	NA	NA
(4) atmospheric still bottoms	9 %	2,000	2,300	4,100
(5b) pressure filter liquid	10 %	1,300	1,300	1,500
(6b) pressure filter solids	2 %	1,300	1,700	2,900

a. This value represents the amount of PE reclaimed based on the total mass of the sample, not on the amount of PE originally located in the sample.
b. All data points except unreacted PE represent an average of two determinations. Unreacted PE value is based on a single determination.
c. Single M_n and M_w values were calculated by the GPC software based on the composite bimodal lineshape. Maxima were determined for each individual peak when more than one peak was present.

DETERMINATION OF UNCONVERTED HDPE IN COAL/PLASTICS CO-LIQUEFACTION STREAM SAMPLES

Gary A. Robbins, Richard A. Winschel, and Francis P. Burke

CONSOL Inc.
Research & Development
4000 Brownsville Road
Library, PA 15129

KEYWORDS: coal liquefaction, coal/waste coprocessing, analysis

INTRODUCTION

In several coal/plastics liquefaction runs performed by Hydrocarbon Technologies, Inc. (HTI), a substantial amount of incompletely converted high-density polyethylene (HDPE) was present in ash-free recycle resid streams when either the ROSE-SR unit was used in Run POC-2, or the pressure filter unit was used in Runs CMSL-8 and CMSL-9. This indicates that the HDPE is less reactive than coal at the liquefaction conditions used.[1-4] In these ash-free streams, there is no solid organic or inorganic material arising from the coal, and the incompletely converted HDPE can be recovered by extraction and filtration with tetrahydrofuran (THF) at room temperature. The HDPE (or HDPE-like material, which could also consist of heavy waxes) is THF insoluble. However, in ashy streams, there are both inorganic ("ash") and organic (unconverted coal) components present from liquefaction of the coal, that interfere with an easy and clean separation of the HDPE from the coal/plastics liquefaction stream sample. Therefore, CONSOL developed an analytical procedure for HDPE in the ashy stream samples based on extraction of HDPE from the sample using hot (150 °C) decalin (decahydronaphthalene), in which the HDPE is soluble. The decalin extraction is both preceded and succeeded by extractions and washes with THF at room temperature, to remove the coal-derived components from the sample.

EXPERIMENTAL

HDPE Solubility and Filtration Tests. The first tests were performed to identify a suitable solvent and temperature for dissolution and recovery of the HDPE feedstock used in several HTI liquefaction runs. These experiments were conducted by heating beakers containing HDPE/solvent mixtures on a hot plate. The virgin HDPE, consisting of clear pellets, was supplied to HTI by Amco plastics, manufactured by BASF, mp 135 °C, and density 0.96 g/cc.[5] It is essentially devoid of ash, sulfur, nitrogen, and oxygen.[1] The decahydronaphthalene (decalin) was obtained from Aldrich Chemical Co., as anhydrous, 99+% purity, consisting of a mixture of cis- and trans- isomers, and with bp 189-191 °C.

In mixed cresol at ≈150 °C, HDPE (2 g/25 mL cresol) melted, but did not dissolve. The HDPE readily dissolved in decalin at 125 °C (2 g HDPE/50 mL decalin), forming a colorless solution. The HDPE-decalin solution at 125 °C was pressure-filtered (about 7 psig nitrogen) through a Whatman no. 42 paper in a filtration apparatus which was heated to 145 °C. Hot decalin was used to rinse the beaker and filter paper, but some precipitated HDPE adhered to the beaker. The filtrate was cooled to room temperature. It then was pressure-filtered through Whatman no. 42 paper and washed with fresh, cool decalin. The filtrate was clear, and slightly yellow in color. The filter cake was dried in a vacuum oven at 60 °C. After drying, it still had a faint decalin odor. 91.6% of the original HDPE was recovered as a hard white solid.

Tests of Extraction Sequence. It was expected that a THF wash would be needed to distinguish HDPE from other materials that may be extracted in hot decalin, since HDPE is completely insoluble in THF at room temperature. However, it was uncertain whether or not the decalin extraction step also should be preceded by THF-extraction to remove distillate and coal-derived residual components. A test was conducted in which aliquots of one sample were extracted using both test sequences. In the decalin-first procedure: 1) the sample was extracted and filtered with hot decalin, 2) the decalin extract was cooled to room temperature, 3) the precipitated solid HDPE was filtered and dried, 4) the tan-colored filter cake was washed with THF, and 5) all fractions were dried in the vacuum oven to remove solvent. In the THF-first procedure, the sample was extracted and filtered with THF at room temperature, and then steps 1 through 5 were followed. In this sequence, both the THF-soluble fractions obtained prior to and after decalin extraction were combined before solvent removal. Results of the extraction sequence tests are described below.

RESULTS AND DISCUSSION

Method Development and Validation. The solubility and filtration tests demonstrated that unreacted feed HDPE could be dissolved, filtered, and recovered in high yield (>90% recovery). The results obtained using the two extraction sequences are quite similar (Table 1). Yields of the fractions were 34 to 39 wt % HDPE (decalin-soluble, THF-insoluble), 58 to 62 wt % THF solubles, and 3 wt % THF and decalin insolubles. The similarity of the results provided overall validation of the method, and indicated that either method was probably adequate for routine analysis. HDPE products from both extractions had a similar tan color and coarse powdery appearance. However, the THF-first procedure minimizes the possibility of interferences, and the HDPE product was cleaner in appearance. FTIR spectra (not shown) indicated that the recovered HDPE fractions obtained by

the two extraction sequences are similar to each other, and to the feed HDPE. Thus, these recovered decalin solubles appear to be essentially pure HDPE (or heavy n-paraffins, which may be indistinguishable from HDPE). The THF-first procedure requires an additional extraction step, but the total time required for the extraction steps is only about four hours. It was adopted as the routine method, a flow chart for which is shown in Figure 1. Solvent removal steps are not shown in the flow chart. This method was found to be easy to perform in a routine manner. Combined recoveries of the three fractions (THF solubles, HDPE, and THF/decalin insolubles) ranged from 98% to 105%, averaging 102% in 19 tests using the method (this includes the decalin-first test described above). It is presumed that recoveries are biased high because of the difficulty in removing solvents (THF or decalin) from the recovered fractions. For routine use, the fraction percentages are reported on a normalized basis. Additional validation information was developed in conjunction with application of the extraction method to authentic samples from HTI Runs CMSL-8 and CMSL-9, and is described in sections to follow.

Application to Runs CMSL-8 and CMSL-9. The HDPE extraction method was applied to selected samples from HTI Runs CMSL-8 and CMSL-9 to characterize the samples and determine the fate of HDPE.[2-4] The data were used for four purposes: 1) determine the amount of HDPE in the pressure filter cake (PFC) samples from periods in which coal and plastics were fed, 2) determine the degree of analytical interference from HDPE-like material produced from the coal, 3) determine the HDPE conversion for each of the periods of coal/plastics operation, and 4) develop a HDPE material balance around the solids separation unit (vacuum still or pressure filter, depending on run and operating period).[2,4] The conditions in Runs CMSL-8 and CMSL-9 relevant to this discussion are given in Table 2. Solids separation operations in the HTI bench unit are conducted using either pressure filtration or vacuum distillation; characteristics of the bottoms and overhead streams from these two operations differ greatly. Sample streams relevant to this discussion are: 1) continuous atmospheric still bottoms (CASB), the flashed bottoms product of liquefaction and the feed to the solids separation device in use; 2) pressure filter liquid (PFL), the solids-free recycle stream; 3) pressure filter cake (PFC), the corresponding filter solids containing rejected insolubles; 4) vacuum still overheads (VSOH), the 524 °C$^-$ distillate; and 5) vacuum still bottoms (VSB), the rejected 524 °C$^+$ resid and ash.

The extraction results (not shown) for Conditions 8-1 and 9-6 (coal feed only) show that little coal-derived material reports as "HDPE" using this method. In samples of resid from CASB and of PFC from Condition 8-1 and 9-6, only 0.06 to 0.32 wt % of each sample reported as "HDPE".[2,4] Extraction results from the coal/plastics operating periods show that with pressure filtration, little HDPE goes out in the PFC stream; instead, most of the HDPE is recycled in the PFL stream. During coal/plastics periods of Run CMSL-8 there was about 5 wt % HDPE in the PFC stream, and 16 to 37 wt % HDPE in the PFL stream. During coal/plastics periods of Run CMSL-9 there was about 2 wt % HDPE in the PFC stream, and about 23 wt % HDPE in the PFL stream.[4] CASB 454 °C$^+$ resids from Conditions 8-2 through 8-5 were found to contain 15 to 62 wt % HDPE; those from Conditions 9-7 through 9-9 were found to contain 9 to 35 wt % HDPE. In Condition 9-7, there was 11 wt % HDPE in the VSB sample (it is presumed that none is in the corresponding VSOH sample).

Material balances (based on a combination of CONSOL analytical results with HTI material balance data) for HDPE around the solids separation operations gave generally poor results (not shown, results ranged from 32% to 374% in Runs CMSL-8 and CMSL-9). Corresponding ash balances based on CONSOL analytical data from the same samples ranged from 102% to 1264%, i.e., more than twelve-fold over recovery. The poor ash balances indicated that the problem was not an analytical problem with the HDPE method, per se. We had observed that some CASB samples from Runs CMSL-8 and CMSL-9 were inordinately low in ash, and the sample integrity was suspect. We examined the percent total THF insolubles (THFI) obtained from two extraction procedures on two CASB sample types (whole or resid). Assuming robust extraction procedures, the THFI contents determined by different extraction procedures on the same sample should agree well. Using Method 1, (the decalin extraction method), the THFI content is the sum of THF/DI (THF and decalin insolubles) and HDPE fraction weight percentages. Using Method 2 (the THF extraction procedure that is our normal work-up procedure for liquefaction samples), the THFI content is the sum of unconverted coal and ash component weight percentages. As shown in Figure 2, the amount of THFI obtained by the two methods on two sample types (CASB 454 °C$^+$ resid and whole CASB), shows considerable scatter for samples representing a particular run condition. These data thus confirm that a major problem may lie in obtaining good data from the CASB samples from coal/plastics operations at HTI. In contrast, we find that percent THF insolubles obtained by the decalin extraction method of VSB and PFC are very similar to those obtained by THF extraction of the same samples (Figure 3). These results indicate that there may be little problem with use of the decalin extraction data obtained from the VSB and PFC samples.

HDPE Conversion During Runs CMSL-8 and CMSL-9. Our original procedure for estimating HDPE conversions during Run CMSL-8 employed the simplifying assumption that the PFC contained no unconverted HDPE.[2,3] At the time, we had no way of measuring the concentration of unconverted HDPE in solids-containing streams. We can now make these measurements directly with the hot decalin extraction procedure. The HDPE extraction results described above for samples from Runs CMSL-8 and CMSL-9 generally validate the original assumption that the PFCs contain no HDPE, because little HDPE (1 to 6 wt %) was found in the PFC samples.

Both overall and single-pass conversions of HDPE are given by:

Conversion = [Mass of HDPE In - Mass of HDPE Out] x 100 / [Mass of HDPE In],

where the masses of HDPE in and out are defined differently for overall conversion than for single-pass conversion. For overall conversion, the "mass of HDPE in" is the HDPE in the fresh feed, and the "mass of HDPE out" is summed from HDPE in any net product streams, such as PFL and PFC or VSB. For single-pass conversion, the "mass of HDPE in" is the sum of HDPE in the fresh feed and all recycle streams (such as CASB, PFL, and PFC or VSB), and the "mass of HDPE out" is the sum of HDPE in all of the gross product streams (such as CASB, PFL, and PFC or VSB). The results presented here for Run CMSL-8 differ from those given previously,[2,3] in that HDPE can be accounted for in more streams, whereas previously it could only be accounted in the fresh feed and PFL streams. Note that CASB can be accounted directly (if the HDPE content of CASB is measured), or it can be accounted as both PFL and PFC (or as VSB). Thus, it is possible to measure single-pass HDPE conversion with CASB as a recycle or product stream, even if the HDPE content of the CASB is not measured directly. Problems described above with use of the CASB data suggests that it may be better to use the PFL/PFC accounting approach, since the HDPE concentrations of PFC samples seem to be more reliable than those of CASB samples.

In Figure 4, the overall and single-pass conversions of HDPE in each period of Runs CMSL-8 and 9 that were evaluated are compared. The overall conversion of HDPE ranged from 69-86% during Run CMSL-9, comparable to those obtained for periods Conditions 8-2, 8-4, and 8-5. This was accomplished in spite of operation at a higher space velocity and without benefit of supported catalyst, but at higher liquefaction temperatures in Run CMSL-9. A high space velocity led to operating problems and low HDPE conversion in Condition 8-3. Higher conversion of HDPE in Condition 9-7, in which vacuum distillation and ashy recycle were used, relative to Conditions 9-8 and 9-9, in which pressure filtration and ash-free recycle were used, suggests that use of ashy recycle may increase HDPE conversion. In Figure 5, the overall HDPE conversions based on this direct measurement method for Run CMSL-9 periods are compared with those estimated by HTI[6] based on measured total feed conversions, and assumed fixed conversions of 88% for the coal, and 100% for all of the non-HDPE plastics. These two sets of results show fair to good overall agreement, for the overall run and for individual periods. HTI's model assumptions thus appear to apply to the combination of coal and plastics tested in Run CMSL-9.

CONCLUSIONS

A HDPE extraction method was developed that can be routinely applied to ashy coal/plastics co-liquefaction stream samples. The method requires about four hours of operator and extraction time, with several hours of additional time needed for solvent removal from recovered fractions. The HDPE extraction method shows little interference from coal-derived material. Results from the HDPE extraction method show that during coal/plastics operations with pressure filtration, little HDPE goes out in the PFC stream; instead, most of the HDPE is recycled in the pressure-filter liquid (PFL) stream. HDPE extraction results were combined with material balance data to calculate HDPE balances and conversions during Runs CMSL-8 and CMSL-9. HDPE extraction results obtained from PFC and VSB samples appear to be reliable, but those from CASB samples are generally poor, either from sampling or analytical inconsistencies. The overall conversion of HDPE ranged from 69-86% during Run CMSL-9, comparable to those obtained for most periods of Run CMSL-8. Run CMSL-9 results suggest that ashy recycle may increase HDPE conversion. Overall HDPE conversions determined by CONSOL are consistent with those estimated by HTI for Run CMSL-9.

FUTURE WORK

The HDPE concentration data provided by this method can provide a basis for consideration of kinetics of HDPE conversion, and in development of improved processing strategies. In runs following CMSL-9, HTI's feedstocks for co-liquefaction have included municipal solid waste (MSW) plastics and petroleum resid, in various combinations with and without coal. The HDPE extraction method provides a potential means to determine HDPE concentration in mixed MSW feeds. A potential difficulty for the method is interference from petroleum resid. Since heavy waxes may behave like HDPE in terms of solubilities in decalin and THF, it may be more difficult to distinguish petroleum resid and HDPE than to distinguish coal-derived material and HDPE. We will continue to apply this characterization method to samples from appropriate streams in subsequent runs in which HDPE was fed.

ACKNOWLEDGMENTS

Samples and other information were provided by Dr. Vivek Pradhan of HTI. This work was sponsored by the U.S. Department of Energy under contract no. DE-AC22-94PC93054.

REFERENCES

1. Robbins, G. A.; Brandes, S. D.; Winschel, R. A.; Burke, F. P. "A Characterization and Evaluation of Coal Liquefaction Process Streams, Quarterly Technical Progress Report October 1 through December 31, 1994", DOE/PC 93054-10, May 1995.

2. Robbins, G. A.; Brandes, S. D.; Winschel, R. A.; Burke, F. P. "A Characterization and Evaluation of Coal Liquefaction Process Streams, Quarterly Technical Progress Report April 1 through June 30, 1995", DOE/PC 93054-18, September 1995.

3. Robbins, G. A.; Brandes, S. D.; Winschel, R. A.; Burke, F. P. "Characteristics of Process Oils from HTI Coal/Plastics Co-Liquefaction Runs", Proceedings of the DOE Coal Liquefaction and Gas Conversion Contractors Review Conference, August 29-31, 1995, Pittsburgh, PA.

4. Robbins, G. A.; Brandes, S. D.; Winschel, R. A.; Burke, F. P. "A Characterization and Evaluation of Coal Liquefaction Process Streams, Quarterly Technical Progress Report October 1 through December 31, 1995", DOE/PC 93054-25, May 1996.

5. Comolli, A. G. "Results of Recent POC Run at HRI on Waste/Coal Coprocessing", Proceedings of the PETC/DOE Workshop "Waste/Coal Coprocessing", Pittsburgh, PA, September 9, 1994.

6. V. R. Pradhan, personal communication, and HTI reports covering Runs CMSL-8 and CMSL-9 under DOE Contract No. DE-AC22-93PC92147.

TABLE 1. TEST OF THF AND DECALIN EXTRACTION SEQUENCE IN A TEST SAMPLE

Fraction	Fraction Wt % of Sample (454 °C⁺ Resid from CAS Bottoms Sample, Period 38 of Run CMSL-9)	
	Decalin Extraction First - Unnormalized (Normalized)	THF Extraction First - Unnormalized (Normalized)
THF/Decalin Insolubles	2.91 (2.77)	3.59 (3.46)
THF Solubles	61.0 (58.2)	64.3 (62.1)
Decalin Solubles/THF Insolubles (HDPE)	40.9 (39.0)	35.7 (34.4)
Recovery	104.8 (100.0)	103.6 (100.0)

TABLE 2. SUMMARY OF CONDITIONS FROM COAL AND COAL/PLASTICS OPERATIONS IN HTI RUNS CMSL-8 AND CMSL-9

Run and Condition Number	Run Period	% Plastics in Fresh Feed (Remainder is Coal)	% HDPE in Fresh Feed	Recycle/Solids Separation Methods
CMSL-8 (227-85) Coal: Crown II Mine, Ill. 6 Seam Mixed Plastics: HDPE, PS, PET Catalysts: Shell 317/1st Reactor, Dispersed Mo (100-200 ppm) and Fe (10000 ppm) Temperatures: T_1/T_1 + ca. 15 °C in 1st/2nd Liquefaction Reactors				
8-1	6	0	0.0	Ash-Free/Pres. Filt.
8-2	11	25 (mixed)	12.5	Ash-Free/Pres. Filt.
8-3	16	25 (mixed)	12.5	Ash-Free/Pres. Filt.
8-4	20	33 (mixed)	16.5	Ash-Free/Pres. Filt.
8-5	22/23	33 (HDPE)	33.0	Ash-Free/Pres. Filt.
CMSL-9 (227-87) Coal: Black Thunder Mine, Wyodak & Anderson Seams Mixed Plastics: HDPE, PP, PS Catalysts: Dispersed-Only, Mo (100-300 ppm) and Fe (10000 ppm) Temperatures: T_2/T_2 + ca. 10 °C in 1st/2nd Liquefaction Reactors, $T_2 > T_1$ in CMSL-8				
9-6	29	0	0	Ashy/Vac. Still
9-7	34	33 (mixed)	13	Ashy/Vac. Still
9-8	38	33 (HDPE)	33	Ash-Free/Pres. Filt.
9-9	41	50 (mixed)	20	Ash-Free/Pres. Filt.

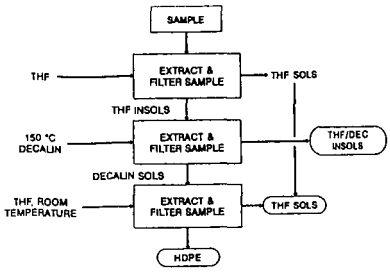

Figure 1. Flow Chart of Hot Decalin Extraction Method to Recover HDPE from Coal/Plastics Co-Liquefaction Samples.

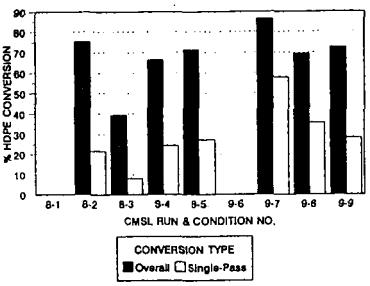

Figure 4. Overall and Single-Pass Conversion of HDPE in HTI Runs CMSL-8 and CMSL-9.

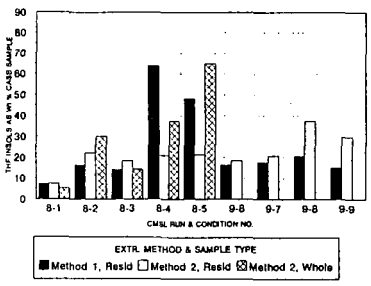

Figure 2. THF Insolubles Concentration in CASB Samples from HTI Runs CMSL-8 and CMSL-9 as Measured by Two Extraction Procedures, Showing Poor Agreement.

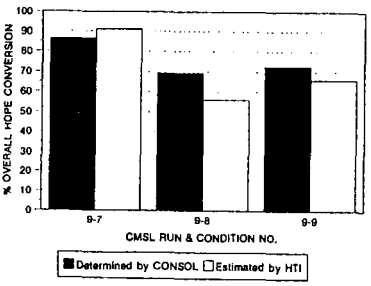

Figure 5. A Comparison of CONSOL (Determined) and HTI (Estimated) Overall Conversion of HDPE in HTI Run CMSL-9.

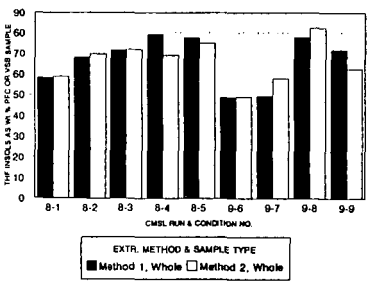

Figure 3. THF Insolubles Concentration in PFC and VSB Samples from HTI Runs CMSL-8 and CMSL-9 as Measured by Two Extraction Procedures, Showing Good Agreement.

CONVERTING NATURAL AND METHANE GASES DIRECTLY INTO LIQUIDS

: Quentin J. Adams
Earth Resources Technology Services
3208 N. 37th St. #9, Phoenix, AZ 85018-6333

Keywords: liquefaction, Coal-bed Methane Gas Feeedstock, Synthetic Fuels

INTRODUCTION

The recent increase in Crude 0il, gasoline and natural gas prices, dried-up reserves and the petroleum industry's reluctance in increasing petroleum production and drilling any new wells have brought **ECONOMICS** back as a major player in the development of synthetic (alternate) fuels.

Petroleum experts state that there are approximately 30 to 40 years of crude oil and natural gas left, after all of the enhanced recovery technologies have been utilized. **There are about 200 years of coal left.** This time line can be increased if we drill into and remove the coalbed methane gas instead of mining the coal.

DOE's Clean Coals Technology Programs has spent **$7 Billion** to date for joint venture industry/government investment in a new generation of clean coal technology. Plus millions of dollars have gone into DOE's programs for improving the technologies for coal liquefaction and gas conversion. Some of the programs included revising and modifying versions of the classical Fisher-Tropsch process developed just prior to Word War II and used by the Germans to provide Synthetic Diesel fuel for their Panzer Tanks..

Sasol Ltd. of South Africa and Haldor Topsoe AS of Lyngby, Denmark, have signed a technology cooperation agreement to promote Sasol's Slurry Phase Distillate technology together with Topsoe's natural gas conversion technology for the production of high quality diesel fuels from natural gas.

It is anticipated that this combination will allow the economic conversion of natural gas from any viable source world-wide to high quality environmentally friendly diesel fuels, with the additional potential to produce petrochemicals.

U.S. DOE's Pittsburgh Energy Technology Center's (PETC) let a contract with the Bechtel Group for a Baseline Design/Economics using Advanced Fisher-Tropsch Technology. The plant design includes all process equipment necessary to convert coal to gas and gas to the desired transportation fuels (i.e., gasoline and diesel fuel). In addition, Bechtel has developed an aspen process simulation model to perform additional process sensitivity studies in the future.

DOE/PETC has also issued an amendment to the above study that includes modifying the design model and that the modifications should include the development of an enhanced computer model that incorporates **coalbed methane and natural gas feedstocks.**

A Synfuels plant provides owners of Coalbeds producing **methane** Gas.(**40%** of the gas produced in Alabama that goes into the Interstate Gas Pipeline is Coalbed Methane Gas) plus natural gas reserves, City and County Landfills, Sewer Treatment plants with Digestors and any thing that can produce methane gas, provides an opportunity to capitalize on previously unprofitable resources

As stated in the abstract t"The development of synthetic (alternate) fuels was motivated by the 1990 Clean Air Act Amendment. .

The mission for Synfuels is from the Office of Mobile sources, Motor vehicles and Urban buses (extracts from Pages 4 and 5)..

1994 - Truck and buses must meet stringent diesel particulate emission standards, equivalent to 5% of the uncontrolled level. All buses in service in cities with populations of 750,000 or more, to be operated on clean alternate fuels.

1996 - Establishes a new program, initially in California and required in 1996, to require the sale of 150,000 ultra-clean vehicles in the state, increasing in 1999 to 300,000 annually.

Clean Fuels, An Overview, What are Clean Fuels?, The most familiar transportation fuels in this county are gasoline and diesel fuel, but any number of energy sources are capable of powering motor vehicles. These include grain, wood and coal alcohol, electricity, natural and methane gases (including coalbed methane) and propane. Some vehicle fuels because of physical or chemical properties, create less pollution than do to days gasoline. These are called "clean fuels".

Synthetic diesel fuels derived from methane gas emits, at a minimum, 18% less particulate, 15% less hydrocarbons, and 14% less carbon monoxide than No. 2 diesel fuel. Environmentally friendly synthetic fuels, lubricants and waxes. Synthetic diesel fuel are the cleanest fuel available, and unlike other alternate fuels, does not require any special equipment or engine alterations.

A number of process technologies that convert coal-derived syngas into liquid fuels have been demonstrated at DOE's Alternate Fuels Development Unit (AFDU), located in LaPorte, Texas. U.S. DOE's Pittsburgh Energy Technology Center's (PETC) is presently managing a number of programs for improving the technologies for coal liquefaction and gas conversion.

Gas-to-Liquids Conversion Technologies

Coupling of two methane molecules to higher hydrocarbons is not thermodynamically feasible because the energy of formation is not favorable. However, in the presence of a co-reactant, such as oxygen, the reaction path can be altered, and methane conversion reactions can be successfully carried out. Natural gas (primarily methane) can be upgraded to higher hydrocarbons either by direct conversion routes (single-step or staged), or via synthesis gas (a mixture of carbon monoxide and hydrogen). The important process considerations for commercially viable natural gas upgrading operations are methane conversion rate and selectivity to preferred products.

Based on chemistry, the processes for natural gas upgrading include 1) partial oxidation to oxygenates, such as methanol, 2) oxidative coupling to higher hydrocarbons, such as ethylene, 3) derivatization, such as oxyhydrorochlorination to chlorinated hydrocarbons, which are subsequently converted to higher hydrocarbons, and 4) pyrolysis to aromatic and/or higher hydrocarbons.

In the indirect process, natural gas is first converted to synthesis gas, followed by catalytic hydrocarbon of the carbon monoxide in a synthesis reactor to a variety of higher hydrocarbon fuels. Fisher-Tropsch (FT) synthesis and its variants are important synthesis reactions, involving **low-pressure conversion of synthesis gas to gasoline, diesel fuel, wax, and oxygenates.** The products of reaction depend on the temperature, pressure, and catalyst used in the synthesis reactor.

PETC's Gas-To-Liquids Program

The goals of PETC's Gas-To-Liquids Program can be summarized as follows:

- Discover new chemistry and catalysts for the conversion of methane and other light hydrocarbon gases to value-added, easily transportable fuels and chemicals
- Obtain necessary design and engineering information to develop prototype technologies for demonstration and commercial deployment.
- Pursue cost-shared, risk-shared, industry-driven R&D, demonstration, and technology transfer to ensure pay-off of Federal R&D investments.

- Contribute to energy policy goals by selecting investments consistent with the four major policy thrusts:
  - Energy security
  - Economic growth
  - Environmental quality improvement
  - Enhancing scientific foundations.

Some of the Synfuel development milestones:

1 DOE Contract No. DE-AC-911PC90027 with the Bechtel Group, This Advanced Fisher-Tropsch indirect Liquefaction Study is for the conversion of Coal to gas and the gas into liquids:

The present indirect liquefaction technology is the base for Bechtel's baseline design study, the PFS model, developed for a wide range of plant capabilities and operating parameters, is a research tool for evaluation of future technology advances. This effort was a logical continuation of Bechtel's baseline design study and will provide additional capabilities to the model for future use with the appropriate modifications of the current baseline design and computer mode, any hydrocarbon feedstock can be used.

2 PETC has amended Bechtel Group's contract for the modification of Bechtel's baseline design study to include an economic analysis for natural gas and coalbed methane gas as feedstock.

Capital and operating costs are called for in the contract, this will also include individual plant costs for the alternative cases.

An ASPEN/SP Process Flowsheet (PFS) model and an economic spreadsheet model. Sensitivity studies have been performed to demonstrate the effects of key independent process variables and economic assumptions.

Some Synfuel Plants in Operation

A 14,500 BPD natural gas-to-gasoline plant started operating in New Zealand in 1985 and is on stream producing 87 octane unleaded gasoline. In this process, natural gas was first converted to methanol via synthesis gas, followed by conversion of methanol to gasoline using a novel catalyst developed by Mobil in the 1970s.

In April 1993, Exxon announced its AGC-SA Advanced Gas Conversion Technology for converting natural gas to high quality refinery feedstock. Olefin-based transportation fuels from natural gas is produced in the Mossgas plant in South Africa.

The Shell Middle Distillate Synthesis (SMDS) process is by now well known as Shell's development to broaden the basis of natural gas utilization.

This technology is now being applied by Shell MDS (Malaysia) Sendirian Berhad in a first full scale application of 12,500 bbl/day, which was started in Bintylu, Sarawak in 1993. The plant produces automotive fuels of exceptional quality, and , in addition to this, special chemicals and waxes. Flexibility in the process operation allows for a wide range of product selection, which is a valuable asset in a variable market.

Because of these excellent properties, which are in particular far in excess of the market minimum specifications for smoke point and cetane number, these products make excellent blending components for upgrading of lower quality stock derived from conventional crude oil processing or catalyst and thermal cracking operations e.g. cycle oils The linear blending characteristics of Shell MDS gasoil, shows that the addition of some 35 per cent (35%) of SMDS gasoil to a typical naphthionic gasoil is sufficient to raise the cetane number from 33 to the required specification of 47..

There are other Synfuel Plants, a operating Industrial demonstration plant in Shanxi province, China and a plant by Intevap in Venezuela

Due to the nature of the feedstock, products do not contain any sulfur or nitrogen and conform to the new EPA Clean Air Act regulations with respect to particulate emissions, sulfur and aromic content. Distillates from this process are finding a premium value in the market .

The MITRE Corp., McLean VA, a DOE consultant is analyzing a number of Synfuels plant technologies resulting in lowering plant cost and operating reductions. MITRE Corp. DOE contract is to review the development of any technologies that can reduce the costs in Bechtel's technoeconomic analysis

An extensive report prepared November, 1991 by the MITRE Corp., McLean, VA (under a DOE contract) in the form of a technoeconomic analysis for The Great Plains Synfuels plant in Beulah, North Dakota that is developing a Hybrid Plant Coal Liquefaction Concept for a 2,000 barrel per day Synfuels plant.

The report analyzed a number of liquefaction processes and found that the Rentech, Inc. process is rated one of the best economically. Ref. to Page 50 Figure #8-1 Rentech - 1 Indirect shows 640 BPSD times Incremental Capital = $6.8 Million.

Incremental Capital costs of $6.8MM (Million) to produce 640 Total Liquids (BPSD) - Barrels (26,880 gallons) per day. In the Report's Section 8.2 "Economic Evaluations" shows the varies rates of return. What it does not show is the fact that Synfuel plants can eliminate approximately 60% of the front-end cost of using direct coal liquefaction technologies in their design/build process.

Other products produced by a Synthetic Fuels Plant.

Wal Mart is selling a Biodegradable Motor oil for approximately $3.00 a Quart. (You can buy Regular Motor oil from Auto Zone or Checker for $.85 to $1.25 a quart). Wal-Marts supplier is Synthetic Oil Services International (SOS), McLean, VA. SOS also offers a synthetic low smoke biodegradable motor oil formulated for outboard marine use. .

WAXES

Waxes produced from Synfuels plants are known as Fisher-Tropsch (F-T) waxes, and have the potential to be refined to compete with F-T waxes currently produced in South Africa. They have a very high molecular weight, melting point, and have excellent hardness. F-T waxes are similar to petroleum hydrocarbon waxes with the exception that they have a higher proportion of higher melting, linear molecules.

The United States alone consumes approximately 25 - 30 million pounds of F-T waxes each year. However, until now, no F-T waxes was produced in the United States. About one-half of the waxes consumed in the U.S. are used in hot melt adhesives, 25 - 30 percent in inks and coatings, mainly as micro pulverized materials, and the balance in a large variety of applications as:

* Candles
* Crayons
* Lipsticks
* Textiles
* Resin-wax polish formulations
* Paste and emulsion polishes for floor ,furniture and automobiles
* Anticorrosion coatings
* Internal lubricants and mold-release agents for plastics

NAPHTHA

Naphtha produced by the Synfuels process can be used as a feedstock for chemical processing or refined to be used in the following products:

Varnish maker and paints
Type IV mineral spirits
Petroleum ether
Textile spirits and ink oil

While Liquid Hydrogen is the fuel of choice for a space-launch vehicle that accelerates quickly out of the atmosphere, studies have shown that liquid methane is better for an aircraft cruising at Mach 5 to Mach 7.

Methane (either natural gas or coalbed methane gas) is widely available, provides more energy than jet fuels, and can absorb five times as much heat as kerosene. Compared with liquid hydrogen , it is three times denser and easier to handle. This is the fuel used by the U.S. hypersonic spy plane, Aurora SR-71.

CONCLUSIONS:

As seen in table 1, by converting Natural gas or Coalbed methane Gas extracted from the Coalbeds directly into liquids can save a total of 72% compared to Coal liquefaction.

The environmentally friendly products produced from a Synthetic fuels plant, such as biodegradable motor oil, marine oil, lubricating oils can save millions of dollars now being spent in oil clean-up costs of used motor oils and petroleum based lubricants.

As stated earlier, Synfuels plants provides owners of Coalbeds producing methane Gas plus natural gas reserves, City and County Landfills, Sewer Treatment plants with Digestors and any thing that can produce methane gas, provides an opportunity to capitalize on previously unprofitable resources

REFERENCES

1 Gerald N. Choi, Sheldon J. Kkramer and Samuel S. Tam (Bechtel Corporation San Francisco, CA) Joseph M. Fox III Consultant) "SIMULATION MODELS AND DESIGN FOR ADVANCED FISHER-TROPSCH TECHNOLOGY", DOE CONTRACT NUMBER DE-AC22-DE-AC22-91PC90027

2 Hugh D. Guthrie, Gary J. Stiegel, Rodney D. Malone "Gas-to-Liquids Program Overview" Presented at the 1995 Coal Liquefaction and Gas Conversion Conference August 29-31, 1995

3 Publication - The Shell Middle Distillate Synthesis Plant in Bintulu, Malaysia, 20 Pages, May, 1992

4. Publication - Large-scale Conversion of Natural Gas to Liquid Fuels by, Haldor-Topsoe A/S

5 Jan H. Fourie General Manager Sasol Limited "The Sasol Slurry Phase Distillate Process: An alternative to LNG projects" Presented at the Fourth Annual Middle East Petroleum & Gas Conference, Bahrain, January 1996 .

6 Peter J.A. Tijm, J. M Marriott, H. Hasenack, M.M.G. Senden, Th. Van Herwijnen "The Market for Shell Middle Distillate Synthesis Products", presented at the ALTERNATE ENERGY '95 Vancouver, Canada, May 2-4, 1995

7 David Grey, Glen C. Tomlinson, Abdel ElSawy "Hybrid Plant Coal liquefaction Concept at the Great Plains Synfuels Plant", Report prepared for Basin Cooperative Services November 1991

Table 1. Element of cost - Bechtel Design costs in a indirect coal liquefaction baseline plant where further reductions in costs may be possible.

	%	OMIT
Coal Handling	6	OMIT
Gasification	32	OMIT
Oxygen Plant	14	OMIT
Byproduct Recovery	3	
Fisher-Tropsch Synthesis	7	
Syngas Recycle Loop	12	
Product Refining	6	
Field Cost	20	OMIT
TOTAL	100	

FISCHER-TROPSCH INDIRECT COAL LIQUEFACTION DESIGN/ECONOMICS - MILD HYDROCRACKING VS. FLUID CATALYTIC CRACKING

Gerald N. Choi, Sheldon J. Kramer and Samuel S. Tam
(Bechtel Corporation, San Francisco, CA)
Joseph M. Fox III (Consultant)
William J. Reagan (Amoco Oil Company, Naperville, IL)

Keywords: Fischer-Tropsch, Economics, Fluid Catalytic Cracking

In order to evaluate the economics of Fischer-Tropsch (F-T) indirect coal liquefaction, conceptual plant designs and detailed cost estimates were developed for plants producing environmentally acceptable, high-quality, liquid transportation fuels meeting the Clean Air Act requirements. The designs incorporate the latest developments in coal gasification technology and advanced (F-T) slurry reactor design. In addition, an ASPEN Plus process simulation model was developed to predict plant material and energy balances, utility requirements, operating and capital costs at varying design conditions. This paper compares mild hydrocracking and fluid catalytic cracking as alternative methods for upgrading the F-T wax.

FISCHER-TROPSCH PLANT DESIGN

Plant Configurations

Figure 1 is a block flow diagram showing the overall process configuration for the original design using mild hydrocracking. The plant contains three main processing areas. Area 100 generates a clean syngas from Illinois No. 6 coal from the Burning Star mine. Area 200 is the Fischer-Tropsch (F-T) synthesis area, and Area 300 is the product upgrading and refining area. Areas 100 and 200 are identical for both the mild hydrocracking and fluid catalytic cracking (FCC) cases. Utility plants and storage requirements in the offsites were estimated, but they are not detailed here.

1. Area 100 - Syngas Production -- Synthesis gas is generated in Shell gasifiers from ground, dried coal. Processing of the raw synthesis gas from the gasifiers is conventional, with Wet Scrubbing followed by single-stage COS/HCN Hydrolysis and Cooling, Acid Gas Removal by inhibited amine solution and Sulfur Polishing. Sour Water Stripping and Sulfur Recovery units are included in this area.

2. Area 200 - The Fischer-Tropsch Synthesis Loop -- This area includes the Fischer-Tropsch Synthesis, CO_2 Removal, Recycle Gas Compression and Dehydration, Hydrocarbon Recovery by deep refrigeration, Hydrogen Recovery and Autothermal Reforming. The Hydrocarbon Recovery unit includes deethanization, depentanization, fractionation and an oxygenates wash column. At low H_2/CO ratios, CO_2 is the primary byproduct of the F-T reaction (using a iron based catalyst) so a large CO_2 removal unit is required. The Autothermal Reformer converts the unrecovered light hydrocarbons to additional syngas which is recycled back to the F-T synthesis reactors.

3. Area 300 - Product Upgrading
   Hydrocracking Design -- Figure 2 is a block flow diagram of Area 300 of the mild hydrocracking design. This area contains eight processing steps; 1) wax hydrocracking, 2) distillate hydrotreating, 3) naphtha hydrotreating, 4) naphtha reforming, 5) C4 isomerization, 6) C5/C6 isomerization, 7) C3/C4/C5 alkylation, and 8) saturated gas processing and product blending. The hydrocracked and hydrotreated naphthas are catalytically reformed to produce an aromatic gasoline blending component. The lighter materials are isomerized and alkylated to produce a high quality gasoline blending stock. Purchased butanes are required to alkylate all the available C3/C4/C5 olefins.

   Fluid Catalytic Cracking Cases -- Figure 3 is a block flow diagram of Area 300 for the Fluid Catalytic Cracking (FCC) cases. Two FCC upgrading cases are considered; one uses a beta zeolite cracking catalyst, and the other uses an equilibrium USY cracking catalyst. In these cases, the wax hydrocracker is replaced by a FCC unit, a MTBE (methyl-tertiary-butyl ether) plant, and a NExTAME (mixed C5/C6/C7 ethers) plant. The other seven processing plants are unchanged.

The F-T slurry reactor is a bubble column reactor in which the slurry phase is a mixture of liquid hydrocarbons (molten wax) and catalyst. Synthesis gas provides the agitation necessary for good mixing and mass transfer of the reactants and products between the two phases. The slurry bed reactor design was chosen over a fixed bed reactor design based on an earlier DOE sponsored Bechtel study[1,2]. The reactor design is based on Mobil's two-stage, slurry reactor pilot plant studies[3]. These results were the basis for the yield correlations contained in the F-T slurry bed reactor computer model used in this study[4]. Details concerning the overall design basis, process selection, and costs have been reported[5].

Product and Byproduct Yields

A Fischer-Tropsch liquefaction facility can produce a wide variety of products of various qualities depending on the method used to upgrade the F-T wax.

In the mild hydrocracking case, the facility produces C3 LPG, an upgraded C5-350 °F naphtha and a 350-850 °F distillate. Liquid sulfur also is produced by the syngas production area. The hydrocarbon products have no measurable sulfur or nitrogen contents. Oxygen is removed to less than 30 ppmv. There are virtually no aromatics in the distillate. Both the naphtha and distillate products have low

rcsidual olefin concentrations. The diesel fraction has a very high cetane number. The jet fuel and heavy distillate fractions have low smoke points. The naphtha product is a mixture of C3/C4/C5 alkylate, C5/C6 isomerate and catalytic reformate. It is basically a raw gasoline with a clear (R+M)/2 octane of about 88.

In the FCC upgrading cases, the facility produces a propylene product in addition to those produced in the hydrocracking case. Methanol is purchased and reacted with the tertiary C4, C5, C6 and C7 olefins to produce MTBE and a mixed C5/C6/C7 ethers stream from the NExTAME etherification plant. The ether streams are mixed with the C5-350 °F naphtha to form an oxygenated gasoline blending component which contains significant amounts of olefins and has higher octane numbers than in the mild hydrocaracking case. Except for a lower pour point, the distillate fraction has about the same properties as that produced in the hydrocracking case.

PROCESS SIMULATION MODEL

The ASPEN Plus process flowsheet simulation model predicts the effects of key process variables on the overall material and utility balances, operating requirements and capital costs. It was developed as a planning/rcsearch guidance tool for use by the DOE and its subcontractors to explore, evaluate and define additional promising areas for future research in the production of liquid transportation fuels. The model is not a detailed plant design tool although it contains some design features. The F-T synthesis loop design is modeled in some detail, and Bechtel's slurry bed F-T reactor sizing and yield models have been incorporated into the ASPEN model. For the other plants, only overall yield, utility requirements and capital costs are estimated. Individual plant costs are prorated on capacity using cost-capacity exponents in conjunction with minimum and maximum single train capacity limits.

All plants in the three main processing sections are simulated either by stand-alone user Fortran blocks or a combination of ASPEN Plus process blocks and user Fortran blocks. Material balances, as well as utility consumptions, operating personnel requirements and ISBL costs for each plant are generated. The offsites, engineering and contingency costs are estimated as a percentage of the processing plant costs to generate the total installed cost of the facility. Detailed discussions of the ASPEN model development and simulation results have been presented in three separate papers[6-8]; the last of which discusses the beneficial effect of treating the F-T reactor vapor products in a close-coupled ZSM-5 reactor as an alternative product upgrading scheme.

A linear programming (LP) model of a typical PADD II refinery was developed using Bechtel Corporation's proprietary Process Industry Modeling System (PIMS) to assess the values of the F-T products from the mild hydrocracking case[9]. With the ASPEN and LP model results, a discounted-cash-flow analysis was carried out under a given set of financial assumptions to calculate the cost of F-T production for a 15% return on investment. Results are presented in terms of a Crude Oil Equivalent (COE) price which is defined as the hypothetical break-even crude oil price at which the liquefaction products are competitive with those produced from crude oil. Table 1 summaries the overall simulation model results for the mild hydrocracking case and the two FCC upgrading cases; one of which uses a beta zeolite cracking catalyst, and the other uses an equilibrium USY cracking catalyst.

FLUIDIZED-BED CATALYTIC CRACKING OF F-T WAX

Fischer-Tropsch wax can be readily cracked in a FCC unit under normal petroleum feedstock operating conditions, as demonstrated by the Amoco Oil Company[10]. The product is rich in C4 to C7 reactive olefins which are valuable for oxygenates production. The hydrocracking design and the ASPEN Plus simulation model were modified to use FCC instead of mild hydrocracking for upgrading the F-T wax. In addition, both a MTBE plant and a NExTAME (mixed C5/C6/C7 ethers) plant were included in Area 300. Both ether plants contain an associated selective hydrogenation unit to saturate diolefins in the feed.

Based on the Amoco data, two FCC cases were considered; a beta zeolite catalyst case and an equilibrium USY catalyst case. Although not in widespread commercial use, beta zeolite catalyst was selected for comparison with an equilibrium USY catalyst since it produces more olefins which can be converted to ethers for use as reformulated gasoline blending components. The propylene is purified and sold. The butenes are sent to the MTBE (methyl-tertiary-butyl ether) plant in which the isobutene is converted to MTBE, and the normal butenes are passed through to the alkylation unit. The C5, C6 and C7 olefins are sent to a NExTAME unit which converts most of the C5 olefins, less of the C6 olefins, and still less of the C7 olefins to ethers. This design produces significantly more gasoline blending components at the expense of distillate production than the hydrocracking design.

Amoco found that the F-T wax cracks so easily in a FCC unit that it does not produce enough coke to maintain the unit in heat balance. One solution to this problem is to supply additional fuel, sometimes called torch oil, to the regenerator to heat the regenerated catalyst to a high enough temperature to sustain the cracking operation. In a conventional petroleum refinery whenever torch oil is required, a low-value heavy material is used. However, in this stand-alone situation, no high-boiling low-valued streams are available from sources other than the FCC unit. Therefore, the heaviest portion of the potential distillate product is used as torch oil and burned in the regenerator to maintain the FCC unit heat balance.

Table 1 compares the model results for the wax hydrocracking case with those for the two FCC wax upgrading cases. In the hydrocracking case, approximately 3100 bbls/day of butanes are purchased and

isomerized for alkylation unit feed since the F-T reaction does not produce a sufficient amount to alkylate all the C3/C4/C5 olefins. The two FCC cases produce more olefins for alkylation unit feed, and as a result, still more butanes have to be purchased. Both FCC cases produce significantly more gasoline than the hydrocracking case. This additional gasoline is produced at the expense of distillate production which is reduced by over 60% resulting in gasoline to distillate ratios of over 4/1 compared to a 0.97/1 ratio for the wax hydrocracking case. In addition, the gasoline products are of better quality. They now contain oxygenates and have higher octanes, lower Reid vapor pressures, and contain less aromatics.

ECONOMIC COMPARISON

The predicted installed cost of each case is just under 3 billion dollars in mid-1993. The FCC upgrading cases have somewhat higher capital costs because of a larger alkylation plant, and the cost of the FCC plant and two etherification plants are more than the hydrocracker. These are preliminary cost estimates and have an accuracy range of +/- 30%. Most of the cost is in the syngas preparation and F-T synthesis areas. For the hydrocracking case, the entire product upgrading and refining area accounts for less than 8% of the ISBL cost.

A discounted-cash-flow economic comparison of the three cases was made using the spreadsheet program with previously reported economic assumptions[8]. Inflation projections are those of the Energy Information Administration[11]. Results are reported in terms of a Crude Oil Equivalent (COE) price which is the hypothetical break-even crude oil price at which the F-T liquefaction products are competitive with those produced from crude oil in an average PADD II refinery.

The hydrocracking case has an expected COE price of 35.4 $/bbl. The expected COE prices for the two FCC upgrading cases are the same at 34.5 $/bbl. These COE prices were calculated using the same margins for the gasoline and diesel blending stocks that were calculated for the hydrocracking case at the typical PADD II refinery. The gasoline blending stocks produced in these two FCC upgrading cases are of better quality than those from the hydrocracking case and should be more valuable. However, the COE calculations for the two FCC cases did not account for this expected increased value. Thus, the calculated COE prices for both FCC cases are conservative in the sense that they are somewhat higher than they should be because the products probably are undervalued. In order to accurately evaluate these two FCC upgrading cases, additional refinery LP modeling studies are required to assess the value of these blending stocks properly, and they will be done under another DOE contract.

In addition, there is another significant difference between the beta zeolite and equilibrium USY catalyst cases which can influence the choice between them. Both FCC upgrading cases consume methanol and produce a propylene product; whereas neither component is present in the hydrocracking case. The beta zeolite catalyst case consumes about 54% more methanol and produces about 57% more propylene than the equilibrium USY catalyst case. For 1995, propylene prices have ranged between 350 and 495 $/s-ton, and methanol prices have ranged at least between 0.47 and 1.35 $/gal (141 to 406 $/s-ton)[12]. The above expected COE prices were calculated using the average propylene price of 422.5 $/s-ton and the average methanol price of 0.91 $/gal (273 $/s-ton). The following table shows the effect of these variations in the methanol and propylene prices on the COE price for the two FCC upgrading cases.

	Most Optimistic	Average	Most Pessimistic
Propylene price, $/ton	495	422	350
Methanol price, $/ton	141	273	406
COE Prices, $/bbl			
Beta zeolite catalyst FCC upgrading case	33.2	34.5	35.8
Equilibrium USY catalyst FCC upgrading case	33.7	34.5	35.3

Thus, the COE price for the beta zeolite catalyst FCC upgrading case can vary between 33.2 and 35.8 $/bbl, a range of 2.6 $/bbl. For the equilibrium USY catalyst case, the COE price can vary between 33.7 and 35.3 $/bbl, a smaller range of only 1.6 $/bbl. This leads to the conclusion that with all other factors being the same, the equilibrium USY catalyst FCC upgrading case is less risky based on recent prices since it minimizes the effect of price variations on the expected COE price.

In conclusion, FCC upgrading of the F-T wax appears to be preferable to upgrading it by mild hydrocracking. Recent wide variations in methanol and propylene prices have been shown to cause significant fluctuations in the COE price of the F-T liquefaction products. Additional petroleum refinery modeling studies are needed to determine more accurately the values of the FCC upgraded products and to define a more reliable COE price for both of the FCC indirect F-T liquefaction cases. It is expected that this will improve the economics of upgrading the F-T wax by fluid catalytic cracking.

ACKNOWLEDGMENT

Bechtel, along with Amoco who was the main subcontractor for a major portion of this study, expresses our appreciation to the DOE/Pittsburgh Energy Technology Center for both technical guidance and financial funding under Contract No. DE-AC22-91PC90027

REFERENCES

1. Fox, J. M., "Slurry vs. Fixed-Bed Reactors for Fischer-Tropsch and Methanol", DOE Contract No. DE-AC22-89PC89876, Final Report, June 1990.
2. Fox, J., M., "Fischer-Tropsch Reactor Selection", *Catalysis Letters* 7 (1990) 281-292.
3. Kuo, J. C., "Slurry Fischer-Tropsch/Mobil Two-Stage Process of Converting Syngas to High Octane Gasoline", DOE Contract No., DE-AC22-80PC30022, Final Report, June 1983; and "Two-Stage Process for Conversion of Synthesis Gas to High Quality Transportation Fuels", DOE Contract No. DE-AC22-83PC60019, Final Report, October, 1985.
4. Fox, J. M. and Tam, S. S., "Correlation of Slurry Reactor Fischer-Tropsch Yield Data", *Topics in Catalysis* 2,(1-4), 285-300 (1995).
5. Choi, G. N., Tam, S. S., Fox, J. M., Kramer, S. J. and Marano, J. J., "Baseline Design/ Economics for Advanced Fischer-Tropsch Technology", DOE/Proceedings of The Coal Liquefaction and Gas Conversion Contractors' Review Conference, September 27-29, 1993.
6. Choi, G. N., Tam, S. S., Fox, J. M., Kramer, S. J. and Rogers, S., Process Simulation Model for Indirect Coal Liquefaction using Slurry Reactor Fischer-Tropsch Technology", Symposium on Alternative Routes for the Production of Fuels, ACS National Meeting, Washington, D. C., August 21-26, 1994.
7. Choi, G. N., Tam, S. S., Fox, J. M., Kramer, S. J. and Marano, J. J., "Process Design Simulation Models for Advanced Fischer-Tropsch Technology", DOE/Proceedings of The Coal Liquefaction and Gas Conversion Contractors' Review Conference, September 7-9, 1994.
8. Choi, G. N., Kramer, S. J. Tam, S. S. and Fox, J. M., "Simulation Models and Design for Advanced Fischer-Tropsch Technology", DOE/Proceedings of The Coal Liquefaction and Gas Conversion Contractors' Review Conference, August 29-31, 1995
9. Marano, J. J., Choi, G. N. and Kramer, S. J., "Product Valuation of Fischer-Tropsch Derived Fuels", Symposium on Alternative Routes for the Production of Fuels, ACS National Meeting, Washington, D. C., August 21-26, 1994.
10. Reagan, W. J., Nicholas, J. J., Hughes, R. D., and M. M. Schwartz, "The Selective Catalytic Cracking of Fischer-Tropsch Liquids to High Value Transportation Fuels", DOE Contract No. DE-AC22-91PC90057, Final Report, August 1994.
11. U.S. Department of Energy, Energy Information Administration, "Annual Energy Outlook 1995", January 1995.
12. Propylene prices are from the Chemical Marketing Reporter. Methanol prices are from Hart's Oxy-Fuel News, Vol. VII, No. 6, Sept. 4, 1995

TABLE I

Comparison of Mild Hydrocracking and Fluid Catalytic Cracking Upgrading of Fischer-Tropsch Wax

	Method of Upgrading the F-T Wax		
	Hydrocracking	FCC 1	FCC 2
Wax Upgrading Mode	Hydrocracking	FCC	FCC
FCC Catalyst Type	--	Beta Zeolite	Equilibrium USY
Plant Input:			
ROM Coal, TSD (MF)	18575	18575	18575
Methanol, TSD	0	321	209
Mixed Butanes, BSD	3110	5204	4327
Electric Power, Mwatts	54	58	56
Plant Output:			
Gasoline, BSD	23943	39723	39950
Distillate, BSD	24686	9764	9347
Propylene, BSD	0	5060	3215
Liquid Propane, BSD	1922	1573	1584
Sulfur, TSD	560	560	560
Slag, TSD (MF)	2244	2244	2244
Total Net C5+ Production, BSD	48629	49487	49297
Total Net C4+ Production, BSD	45519	44283	44970
Blended Gasoline Properties:			
Research Octane Number	90.9	96.8	95.8
Motor Octane Number	86.1	88.9	87.8
(R+M)/2 Octane Number	88.5	92.8	91.8
Reid Vapor Pressure, psi	5.0	4.7	4.7
Benzene, wt%	0.3	0.1	0.1
Aromatics, wt%	28.1	11.0	13.9
Olefins, wt%	0.0	12.7	15.5
Oxygen, wt%	0.0	3.3	2.1
Blended Distillate Properties:			
Pour Point, °F	- 28	- 40	- 40
Cetane Index	74	74	74
Installed Plant Cost, MM$ in mid-1993	2964	2987	2978

Figure 1
Indirect Coal Liquefaction Baseline Study
Overall Process Configuration

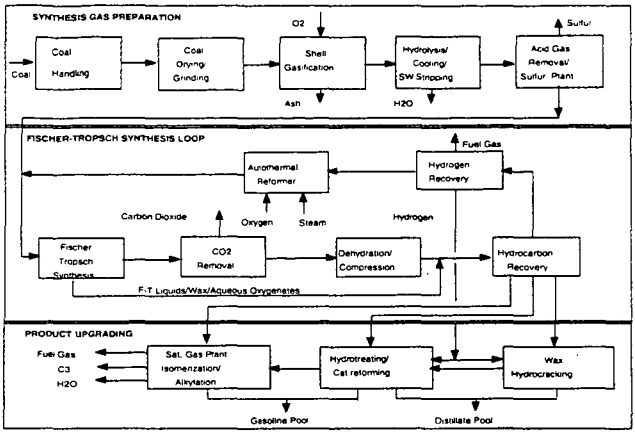

Figure 2
Area 300 Block Flow Diagram - Baseline Design With Wax Hydrocracking

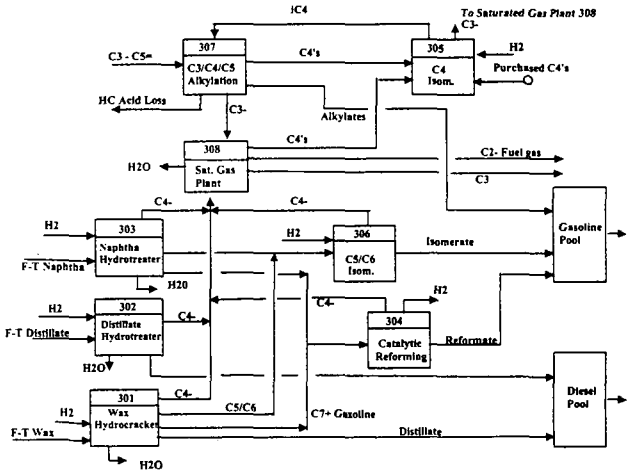

Figure 3
Area 300 Block Flow Diagram - Fluid Catalytic Cracking

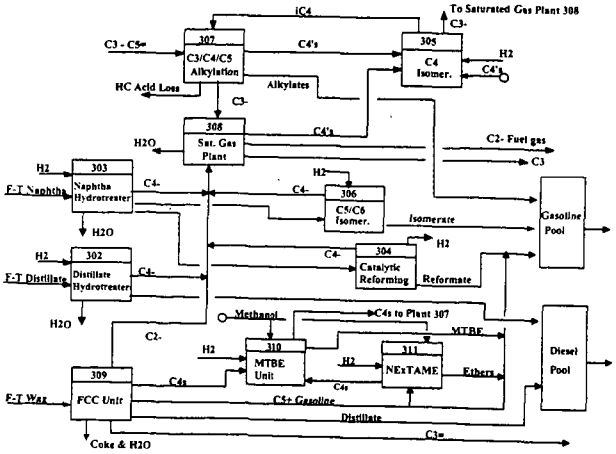

DECARBOXYLATION OF COAL MODEL COMPOUNDS UNDER LIQUEFACTION CONDITIONS: DOES DECARBOXYLATION LEAD TO RETROGRADE REACTIONS?*

Thomas P. Eskay, Phillip F. Britt, and A. C. Buchanan, III
Chemical and Analytical Sciences Division, Oak Ridge National Laboratory
P.O. Box 2008, MS-6197, Oak Ridge, Tennessee 37831-6197

Keywords: Decarboxylation, Liquefaction, Cross-Linking, Model Compounds.

Introduction

In recent years, it has become clear that oxygen functional groups in low-rank coals are major actors in retrograde reactions which inhibit their efficient thermochemical processing. In the pyrolysis and liquefaction of low-rank coals, low-temperature cross-linking reactions have been correlated with the loss of carboxyl groups and the evolution of CO_2 and H_2O [1,2]. Pretreatments such as *methylation, demineralization,* or *ion-exchange* of the inorganic cations reduce cross-linking and CO_2 evolution in pyrolysis [2a,3a]. In pyrolysis and liquefaction, the exchange of Na^+, K^+, Ca^{++}, or Ba^{++} into demineralized coal increases cross-linking and CO_2 evolution [3,4]. Cross-linking reactions also have a deleterious effect on liquefaction yields and the distribution of oils, preasphaltenes and asphaltenes [3,4]. These results suggest that decarboxylation may occur by a pathway that initiates retrograde (cross-linking) reactions in the coal polymer independent of the reaction conditions. However, the decarboxylation pathways in liquefaction and pyrolysis of low-rank coals are not known, and it is not clear how decarboxylation leads to cross-linking. Radical recombination or radical addition reactions have been suggested as being involved in retrograde reactions. However, the involvement of radical pathways in thermal decarboxylation reactions has recently been brought into question. We have presented evidence that in the pyrolysis of several bibenzyls containing aromatic carboxylic acids, radical pathways are not involved in thermal decarboxylation reactions and no cross-linking or coupling products are formed [5]. Further, Manion et al. observed that decarboxylation of benzoic acid derivatives in tetralin yielded only small amounts of aryl-aryl coupling products [6]. To gain a better understanding of the role decarboxylation plays in cross-linking reactions during liquefaction in low-rank coals, we have studied the thermal decomposition of several bibenzyls containing aromatic carboxylic acids, and their salts, in the presence of a hydrogen donor solvent (tetralin) and a nondonor solvent (naphthalene). The structures currently under investigation are 1,2-(3,3'-dicarboxyphenyl)ethane (**1**), 1-(3-carboxyphenyl)-2-(4-biphenyl)ethane (**2**), and the di-potassium salt of 1,2-(4,4'-dicarboxyphenyl)ethane (**3**).

Experimental

1,2-(3,3'-dicarboxyphenyl)ethane (**1**) was synthesized as described previously [5]. The synthesis of 1-(3-carboxyphenyl)-2-(4-biphenyl)ethane (**3**) and di-potassium 1,2-(4,4'-dicarboxyphenyl)ethane (**2**) are described below. Tetralin (Aldrich) was purified by washing with concentrated H_2SO_4 until the acid layer was colorless, washing with dilute aqueous $NaHCO_3$, followed by fractional distillation under reduced pressure (purity 99.4 % by GC). Naphthalene (Aldrich , 99.9 %) was used without further purification. THF (J.T. Baker HPLC Grade) was distilled from K before use. Gas chromatography analysis was performed using a Hewlett-Packard 5890 Series II gas chromatograph equipped with a J&W Scientific 30 m x 0.25 mm id, 0.25 μm film thickness DB-1 column and a flame ionization detector. Mass spectra were obtained at 70 eV on a Hewlett-Packard 5972 GC/MS equipped with a capillary column identical to that used for GC analysis.

Dipotassium 1,2-(4,4'-dicarboxyphenyl)ethane (3). 1,2-(4,4'-dicarboxyphenyl)ethane [7] (0.498 g, 1.85 mmol) was placed in DMF (10 mL) and aqueous KOH (1.0 M) was added dropwise until the solution became homogeneous. Ethanol (175 mL) was added to precipitate the salt, and the salt was collected by vacuum filtration (0.601 g, 94 %) and dried over P_2O_5 in a vacuum.

Diethyl 3-bromobenzylphosphonate. Into an oven-dried 100 mL flask equipped with a reflux

* Research performed at Oak Ridge National Laboratory, managed by Lockheed Martin Energy Research Corp. for the Division of Chemical Sciences, Office of Basic Energy Sciences, U.S. Department of Energy under contract DE-AC05-96OR22464.

condenser was placed 3-bromobenzyl bromide (20.01 g, 80 mmoles) and triethyl phosphite (13.8 mL, 80 mmol). The mixture was heated under argon to 140 °C with stirring for 2 h and then cooled to room temperature. The reflux condenser was replaced with a still head and the mixture was slowly reheated to 170 °C to distill off ethyl bromide and unreacted triethyl phospite. After cooling, the liquid (24.2 g, 99 %) was stored under argon. GC-MS retention time 17.9 min, *m/z* (relative intensity) 308 (M^+, 26), 306 (26), 171 (89), 169 (100), 138 (95).

1-(3-bromophenyl)-2-(4-biphenyl)ethene. Sodium hydride (3.2 g, 60 % mineral oil dispersion, 0.080 moles) was suspended in THF (100 mL) in a 250 mL oven-dried flask under a positive pressure of argon. A solution of diethyl 3-bromobenzylphosphonate (24.5 g, 80 mmol) in THF (100 mL) was transferred to the flask by cannula, and the mixture was stirred for 0.5 h. A solution of 4-biphenylcarboxaldehyde (14.6 g, 80 mmol) in THF (50 mL) was added dropwise over a period of 1 h, and the solution was refluxed for 2 h. The reaction was quenched with H_2O (200 mL) and a white solid was collected by vacuum filtration (19.4 g, 78 %). GC-MS retention time 26 min, *m/z* (relative intensity) 336 (M^+, 98), 334 (100), 255 (21).

1-(3-carboxyphenyl)-2-(4-biphenyl)ethene. 1-(3-bromophenyl)-2-(4-biphenyl)ethene (12.0 g, 35.8 mmol) was weighed into an oven-dried flask under an atmosphere of argon and THF (300 mL) was added. The stirred solution was cooled to -78°C and *n*-BuLi (14.5 mL, 2.5 M solution in hexane, 35.8 mmol) was added over a period of 0.25 h and the solution was stirred for 0.5 h. Carbon dioxide (produced from warming dry ice and passed through a $CaSO_4$ drying tube) was bubbled through the solution for 1.5 h. The solution was warmed to room temperature and quenched with 10 % H_2SO_4 (100 mL) and H_2O (300 mL). The THF layer was collected and the aqueous layer was extracted with THF (2 x 200 mL). The combined organic layers were washed with H_2O (100 mL) and dried over Na_2SO_4 . The THF was removed under reduced pressure to produce 10.1 g (93 %) of a white solid. GC-MS, analyzed as the trimethyl silyl ester, retention time 27.8 min, *m/z* (relative intensity) 372 (M^+,100), 357 (32), 283 (20).

1-(3-carboxyphenyl)-2-(4-biphenyl)ethane (2). Crude 1-(3-carboxyphenyl)-2-(4-biphenyl)ethene (3.02 g, 10.1 mmol), 10 % Pd/C (0.30 g), and EtOH (50 mL) were placed into a Parr hydrogenation bottle and shaken under 50 psi of H_2 until 1-(3-carboxyphenyl)-2-(4-biphenyl)ethene could no longer be detected by GC analysis (72 h). The solution was vacuum filtered and the Pd/C was washed with CH_2Cl_2. The solution was evaporated to dryness producing a white solid (3.10 g, 99%). GC-MS, analyzed as the trimethylsilyl ester, retention time 25.5 min, *m/z* (relative intensity) 374 (M^+, 9), 359 (6), 207 (3), 167 (100). The product was recrystallized 4 times from isopropyl alcohol (GC purity 99.9 %) and dried in vacuum with P_2O_5 prior to use in pyrolysis.

Pyrolyses. Pyrolyses in tetralin were performed by weighing the carboxylic acid and tetralin into a pyrex glass tube. The sample was frozen in liquid N_2, evacuated (10^{-4} Torr), backfilled with argon, and allowed to warm to room temperature. This process was repeated 7 times, the sample was frozen, the tube was evacuated (ca. 10^{-5} Torr), and sealed. Pyrolyses in naphthalene were performed by loading pyrex tubes with the appropriate amounts of carboxylic acid and naphthalene and conducting 3 freeze-pump-thaw cycles prior to sealing the tube at 10^{-5} Torr. The neat acid was pyrolyzed in sealed pyrex tubes (sealed at ca. 10^{-5} Torr). The pyrolyses were performed in a Tecam fluidized sandbath at 400 $\pm$ 1.5 °C. Following the pyrolysis, the samples were quickly removed from the sandbath and cooled in liquid N_2. The tubes were cracked open, and the solid products were removed with a 2:1 mixture of pyridine:N,O-bis(trimethylsilyl)trifluoroacetamide (BSTFA). Internal standards (2-phenylbenzoic acid and 2,4,6-trimethylbenzoic acid for (**1**) or 3,5-dimethylbenzoic acid for (**2**)) were added and the reaction mixtures analyzed by GC and GC-MS. For toluene analysis, the solids from the pyrolysis were extracted with CH_2Cl_2, internal standards (cumene and those mentioned above) were added, and the sample was analyzed by GC. The CH_2Cl_2 was blown off under argon, and the sample was dissolved in BSTFA:pyridine and reanalyzed. The identities of products from the thermolysis of **1** and **2** were determined by GC-MS analysis and were further confirmed by comparison with commercially available or synthesized authentic materials.

Results and Discussion

Thermolysis of 1 and 2 in Tetralin and Naphthalene

Previously, we have studied the pyrolysis of neat **1** at 400 °C [5]. The major products in the pyrolysis are shown in equation 1, and a typical product distribution for a 30 min pyrolysis is given in Table 1, entry 1. Excellent mass balances were observed in these thermolyses (97 % at 67 % conversion) and no coupling or high molecular weight products were observed by GC or HPLC analysis. From these results, we proposed that decarboxylation occurs by an acid-promoted, ionic mechanism as shown in equation 2. We have now extended our study of thermal decomposition of

aromatic carboxylic acids to include "liquefaction" conditions. In this study, a mono-carboxybibenzyl (**2**) was also investigated to provide an additional example of decarboxylation, and to confirm the diacid does not decompose by a unique pathway. Thermolysis of **1** and **2** in tetralin and in naphthalene were conducted at 400 °C in sealed pyrex tubes and the products were analyzed by GC and GC-MS.

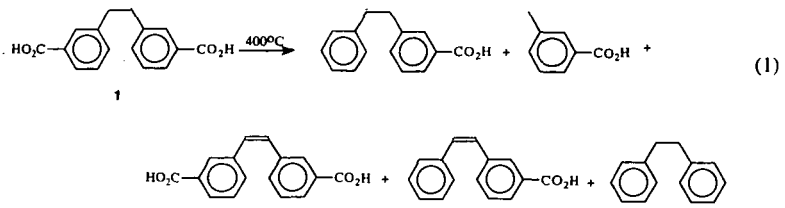

(1)

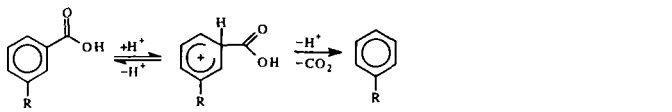

(2)

The major products from the thermolysis of **1** and **2** are shown in equation 1 and 3, respectively, and the product distributions at various time intervals are given in Tables 1 and 2. Several other products

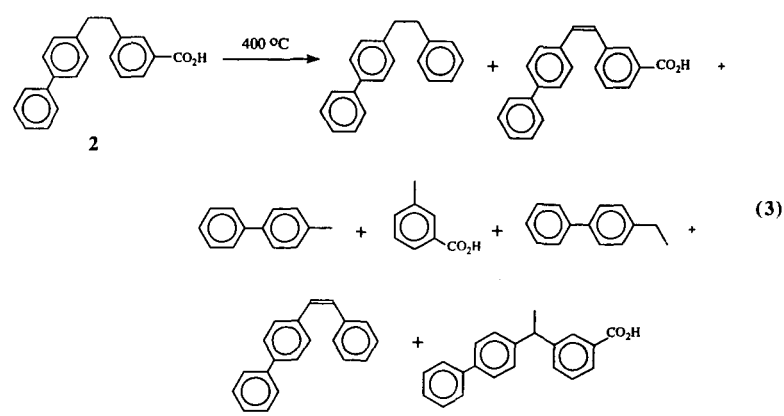

(3)

are formed in the pyrolysis that have not been identified, but based upon the GC peak area and the good mass balance, the amount of these products are small (<5 % mole % at conversions >30 % for **1** and <2 mole % at conversions of 14 % for **2**).

The results of the thermolysis of **1** and **2** in a hydrogen donor and nondonor solvent at 400 °C show that decarboxylation is a major reaction pathway. Despite the large amount of decarboxylation, no cross-linked products are detected. The good mass balances suggest that decarboxylation does not lead to any significant amounts of undetected coupling or cross-linking products. Compared to the pyrolysis of the neat acids, dilution with either a hydrogen donor solvent or a nondonor solvent increases the mole % of toluene products formed and decreases the amount of decarboxylation. This trend is due to a decrease in the rate of decarboxylation with dilution. The rate of unimolecular C-C homolysis, which leads to the toluene products, is unaffected by dilution. On the basis of the similar effect of dilution by a hydrogen donor and nondonor solvent, we propose that decarboxylation is occuring by an acid-promoted, ionic mechanism (eq 2) under "liquefaction" conditions. The source of acid for this decarboxylation is believed to be a second molecule of carboxylic acid and a second-order process is supported by the observation that the rate of decarboxylation decreases when compounds **1** and **2** are diluted in napthalene or tetralin. Additional

investigations into the reaction order for decarboxylation are currently in progress. Furthermore, we have established that a substituent effect is present that supports the mechanism in equation 2. The rate of decarboxylation of 1,2-(4,4'-dicarboxyphenyl)ethane (**5**) is roughly a factor of 2 faster than **1** neat or diluted in diphenyl ether. If the rate-determining step is *ipso*-protonation of the aromatic ring, as shown in equation 2, the *para*-alkyl substituent in **5** would stabilize the carbocation intermediate while the *meta*-alkyl substituent in **1** would not. McMillen has also observed that benzoic acids containing electron donating substituents (-OH and -OMe) decarboxylate faster than benzoic acid at 400 °C in tetralin [6]. This enhanced rate with activated benzoic acids in tetralin provides additional evidence that supports the acid-promoted ionic decarboxylation pathway shown in equation 2.

The results in Tables 1 and 2 also show that in tetralin, the formation of stilbene products is suppressed. The toluic acid and stilbene derivatives are formed by a free-radical reaction analogous to that reported for the thermolysis of bibenzyl [8,9]. Homolysis of **1** produces 2 ($HO_2CPhCH_2\bullet$), which can form toluic acid by hydrogen abstraction from tetralin or **1** to form $HO_2CPhCH_2CH(\bullet)PhCO_2H$ (**4**) (Scheme 1, the same pathway will also occur with **2**). Because

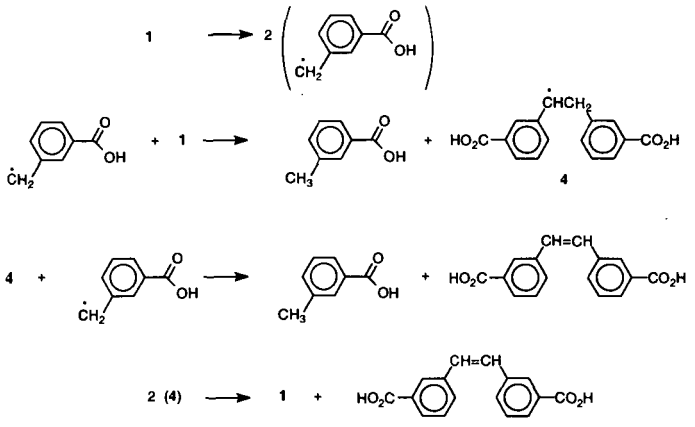

Scheme 1

tetralin is in large excess (10-fold), it quenches most of the free-radicals and any **4** produced will hydrogen abstract from tetralin before undergoing disproportionation to form stilbene. Also, stilbenes have been shown to react with tetralin at 400 °C to produce bibenzyl [10].

Thermolysis of 3 in Tetralin and Naphthalene

The exchange of inorganic cations, such as Na^+, K^+, Ca^{++}, or Ba^{++}, into demineralized low-rank coals can significantly decrease the liquefaction yields. For example, in the liquefaction (400 °C, 30 min, tetralin, H_2) of Zap lignite coal, exchange of potassium cations into an acid demineralized coal increases retrogressive reactions and decreases the liquefaction yields 40 % compared to the demineralized coal [3]. For Wyodak and a North Dakota lignite, ion exchange of potassium cations into the coal decreases the liquefaction yields 25 % compared to an acid demineralized coal [4]. Thermolysis of the dipotassium salt (**3**) was investigated in tetralin and naphthalene at 400°C for 0.5 h. No products were detected in either solvent and **3** was recovered unreacted (>99 % by GC analysis of the reaction mixtures). In addition, we have found that the neat salts are stable at 400 °C for times up to 2 h. The dipotassium salt is relatively stable at 400 °C under the liquefaction and inert solvent conditions and the salt remained solid during the thermolysis. These preliminary results suggest that the salts of aromatic carboxylic acids do not readily undergo decarboxylation that might lead to cross-linking reactions. Further investigation of the decarboxylation of inorganic salts of carboxylic acids is planned using the carboxy salts of **1** and **2** under liquefaction conditions.

Summary and Conclusion

The thermolysis of two aromatic carboxylic acids **1** and **2** and a dipotassium salt of a carboxylic acid (**3**) have been investigated at 400 °C as models of carboxylic acids in low rank coals under liquefaction and inert solvent conditions. Thermolysis of acids **1** and **2** leads to a large amount of decarboxylation products, but no evidence for the occurrence of retrograde reactions associated

with the decarboxylation process. It is proposed that the decarboxylation occurs by an acid-promoted, ionic pathway and further investigation of this reaction mechanism under liquefaction conditions is in progress. The dipotassium carboxy salt, **3**, is relatively stable at 400 °C and decarboxylation is not observed under liquefaction or inert solvent conditions. This preliminary result suggests that formation of carboxy salts in low-rank coals does not contribute to the retrograde chemistry. Overall, the results of both the acids and salt suggest that decarboxylation does not contribute to retrogressive reactions during the thermal processing of low-rank coals under liquefaction conditions. The evolution of CO_2 from low rank coals during thermal processing may well be coincidental with the chemistry occuring that results in cross-linking.

References

1. Suuberg, E.M.; Lee, D.; Larsen, J.W. *Fuel* **1985**, *64*, 1668.
2. (a) Solomon, P.R.; Serio, M.A.; Despande, G.V.; Kroo, E. *Energy and Fuels* **1990**, *4*, 42. (b) Ibarra, J.V.; Moliner, R.; Gavilan, M.P. *Fuel* **1991**, *70*, 408.
3. (a) Serio, M.A.; Kroo, E.; Chapernay, S.; Solomon, P.R. *Prepr. Pap.-Am. Chem. Soc. Div., Fuel Chem.* **1993**, *38(3)*, 1021. (b) Serio, M.A.; Kroo, E.; Teng, H.; Solomon, P.R. *Prepr. Pap.-Am. Chem. Soc., Div. Fuel Chem.* **1993**, *38(2)*, 577.
4. Joseph, J.T.; Forria, T.R. *Fuel* **1992**, *71*, 75.
5. (a) Eskay, T.P; Britt, P.F.; Buchanan, A.C. III *Prepr. Pap.-Am. Chem. Soc., Div. Fuel Chem.* **1996**, *41(2)*, 739. (b) Eskay, T.P; Britt, P.F.; Buchanan, A.C. III, submitted for publication in *Energy and Fuels.*
6. Manion, J.A.; McMillien, D.F.; Malhotra, R. *Prepr. Pap.-Am. Chem. Soc., Div. Fuel Chem.* **1992**, *37(4)*, 1720.
7. Britt, P.F.; Buchanan, A.C., III, Hoenigman, R.L. *Coal Science* Pajares, J.A. and Tascon, J. M. D. Eds.; Coal Science and Technology 24; Elsevier Science B.V.: Amsterdam, Netherlands, 1995, 437.
8. Stein, S.E.; Robaugh, D.A.; Alfieri, A.D.; Miller, R.E. *J. Am. Chem. Soc.* **1982**, *104*, 6567.
9. Poutsma, M. L. *Fuel* **1980**, *59*, 335.
10. King, H-H., Stock, L.M. *Fuel* **1984**, *63*, 810.

Table 1. Product Distributions Observed from the Thermolysis of *m,m*-$HO_2CPhCH_2CH_2PhCO_2H$ Diluted 10:1 (Molar Ratio) with Tetralin or Naphthalene at 400°C for Various Time Intervals.

Entry	1	2	3	4	5	6
Products (mole %)[b]	30 min (neat)	45 min Naph	45 min Tet	90 min Tet	225 min Naph	225 min Tet
$PhCH_3$	0[a]	0[a]	0[a]	0[a]	13.1	12.7
$PhCO_2H$	0.1	0	0	0	0	0
m-CH_3PhCO_2H	8.4	28.2	42	34	20.2	21.4
m-$CH_3CH_2PhCO_2H$	1.5	2.3	0	0	1.1	0.3
$PhCH_2CH_2Ph$	0.2	0	0	0	3.1	3.5
PhCH=CHPh	0	0	0	0	0.1	0
m-$HO_2CPhCH_2CH_2Ph$	77.1	62.5	58	66	55.1	59.7
m-HO_2CPhCH=CHPh	0.5	0.3	0	0	2.2	0
m,m-$HO_2CPhCH_2PhCO_2H$	0	0	0	0	0.3	0
m,m-$HO_2CPhCH(CH_3)PhCO_2H$	4.3	0.6	0	0	1.3	1.8
m,m-HO_2CPhCH=$CHPhCO_2H$	7.7	5.4	0	0	2.9	0
Conversion[b]	9.6	6.6	5.7	14.1	34.0	35.2
Mass Balance	99.1	97.1	99.4	96.2	95.0	93.0

a-Analysis for toluene not performed.
b-Based on products identified.
Tet=Tetralin; Naph=Naphthalene

Table 2. Product Distributions Observed from the Thermolysis of *m*-$HO_2CPhCH_2CH_2Ph$-Ph Diluted 10:1 (Molar Ratio) with Tetralin and Naphthalene at 400°C.

Entry	1	2	3
Product (mole %)[b]	60 min Neat	90 min Tet	90 min Naph
$PhCH_3$	0[a]	5.6	1.1
$PhCO_2H$	1.1	0	0
m-CH_3PhCO_2H	12.9	34.3	28.2
m-$CH_3CH_2PhCO_2H$	0.6	0	0.76
p-Ph-$PhCH_3$	14.6	38.7	30.7
p-Ph-$PhCH_2CH_3$	4.0	0	0
p-Ph-$PhCH(CH_3)Ph$	0.4	0	0.13
p-Ph-$PhCH_2CH_2Ph$	42.4	21.3	24.1
p-Ph-PhCH=CHPh	1.8	0	0
p-Ph-$PhCH_2Ph$-*m*-CO_2H	0.78	0	0.40
p-Ph-$PhCH(CH_3)Ph$-*m*-CO_2H	5.14	0	3.0
p-Ph-PhCH=CHPh-*m*-CO_2H	16.1	0	11.4
Conversion %[b]	14.4	11.6	14.2
Mass Balance	95.3	103	99.5

a-Toluene analysis not performed.
b-Based on products identified.
Tet=Tetralin; Napb=Naphthalene

UNIQUE FRACTIONATION OF BIOMASS TO POLYOLS PROVIDES INEXPENSIVE FEEDSTOCK FOR LIQUID FUELS PROCESS

J. Michael Robinson*, Caroline E. Burgess, Hari D. Mandal,
Chris D. Brasher, Kevin O'Hara, and Preston Holland
Science and Mathematics Department/Chemistry Faculty
The University of Texas of the Permian Basin
4901 E. University Blvd., Odessa, TX 79762

Keywords: biomass fractionation, coal liquefaction, coal hydrolysis

INTRODUCTION

Previous work in this laboratory established a unique process that converts C_5 and C_6 polyols (straight-chain hydrocarbons with a hydroxyl group on each carbon) to hydrocarbons using hydroiodic acid and phosphoric acids.[1] Polyols, such as sorbitol and xylitol, are commercially available from highly purified glucose and xylose but are expensive. To use less costly and renewable biomass resources as feedstock for this process, the biomass must first be fractionated (e.g. by steam explosion [2]) for cellulose and/or hemicellulose recovery; these polysaccharides can then be hydrolyzed and reduced to polyols. We are investigating a one-step Russian method [3] to directly convert raw "biomass-to-polyols" (BTP) to determine more definitive optimum reaction conditions and the economics of this method for comparison to using steam-exploded cellulose. In the Russian method, biomass is subjected to simultaneous dilute acid hydrolysis and catalytic hydrogenation at ~170 °C and ~50 atm H_2 (cold), thus trapping the incipient aldoses as their corresponding, but less reactive, polyols (alditols).

At this point, the main limitation to the effectiveness of the Russian method is the recycle of the catalyst, as using ruthenium/carbon (Ru/C) once-through is costly. In this process, the solid phase by-product lignin remains separate from the solution of polyols as the latter is formed from cellulose/hemicelluloses. The solid, with the catalyst, are simply filtered from solution. A major milestone in our investigation is separation of the lignin from the catalyst either by (1) base-extracting the lignin or (2) reacting it further at higher temperature and pressure in base. As the Russian paper suggests, clean catalyst can be recovered at 280-320 °C and ~50-70 atm H_2 (cold).[3]

As lignite has structural features similar to cellulose and lignin, we anticipated these reaction conditions could also convert a high percentage of coal into smaller moieties. Coal has been converted to liquids using many different solvents, temperatures, catalysts, and gas atmospheres.[4-6] However, few researchers have done acid or base hydrolysis/hydrogenation, particularly at such low severity conditions. Base extraction is used to remove humic acids, typically about 10-20 % of lignite.[7] Some of the original coal liquefaction reactions were done at low temperature by Berthelot where he heated coal with hydroiodic acid in a sealed glass tube to 250°C.[8] The bituminous coal was converted into a semi-liquid material with an oil content of 60 %. However, other research suggests that this conversion to oil would have contained a high iodide content.[9] In more recent work, lignite had high hexane-soluble yield using sodium aluminate and molybdenum/nickel catalysts at ~360°C.[10] Ruthenium catalysts have also been used successfully in coal liquefaction reactions at 400 °C and 50 atm of H_2, with a total conversion of Australian Yallourn brown coal of 96.5 % to THF-solubles/gas and an oil yield of 57.8 %.[11]

We describe in this paper the results for the BTP conversion at our typical reaction conditions, the cleaning of the ruthenium catalyst and how well the clean catalyst performed. We also include some preliminary experiments on a Texas coal at each of the reaction conditions of our BTP, possibly in stages, to see if indeed lignite can be converted under such low severity reaction conditions.

EXPERIMENTAL

Materials

The sawdust used was an oak hardwood. The catalyst was purchased from Aldrich Chem. Co., 5 % ruthenium on carbon (5% Ru/C). Phosphoric acid, sodium hydroxide, and methylene chloride are reagent grade. Lignite coal was obtained from COPL at Pennsylvania State University, sample DECS-1, with an ultimate analysis (dry) of %C - 62.5, %H - 4.8, %N - 1.2, %S - 1.0, %O - 14.7, % ash - 15.8.

Reaction Conditions

The reactions are done in a 3 L stirred autoclave that is heated by electric coils on the outside and cooled by water-cooled coils inside the reactor. The heater is temperature-controlled by computer. The reaction conditions for the BTP process are 180 °C, 2h, 50 atm H_2 (cold). The acid is a 0.8 % solution of phosphoric acid, and enough Ru/C is added for a 0.5% metal loading (~200g sawdust to 20g of 5% Ru/C catalyst). After reaction, the solid material is filtered from the liquid product by vacuum filtration and rinsing with water. The remaining solid is not dried. For the coal reaction, only 50 g (dry) coal and 5g of catalyst are used, the reaction was done twice using 0.8 % solution of phosphoric acid and sulfuric acid each, and the remaining solid after filtration is extracted with methylene chloride by ultrasonicating for 10 min and filtering the remaining solid.

For the sawdust reactions, initial experiments were done to determine if the lignin/catalyst could be run again without separation, but deactivation already occurred. Two methods were tried to remove the lignin from catalyst. The first involved base extraction of the catalyst to remove the lignin at atmospheric conditions. Using a 5 % solution of NaOH, the catalyst/base mixture was heated to 100 °C for 2-6 h, then filtered and rinsed repeatedly with water to remove the base.[2] The second method, described in the Russian literature [3] was to mix the catalyst with a 1.5 % solution of NaOH in the stirred autoclave to a temperature of 235-250 °C, 2 h, 44 atm H_2 (cold), then filtered and rinsed repeatedly with water.

The reaction conditions for a second lignite reaction are 235 °C, 2 h, 44 atm H_2 (cold) while in a 1.5 % solution of NaOH, which is then filtered and rinsed repeatedly with water. Only 50 g (dry) coal and 5g of catalyst are used, and the remaining solid after filtration is extracted with methylene chloride by ultrasonicating for 10 min and filtering the remaining solid. The results of these experiments and the process are explained in the next section.

RESULTS AND DISCUSSION

Figures 1-3 contain schematics of the processes used for these experiments. Figure 1 is a schematic of the entire process, each box representing a key step in our process and each circle representing a small step in our process that must be done in order to make our process economical. As described in previous publications,[1] the first step of our process is to convert either raw biomass or steam exploded biomass to polyols, followed by a second step to reduce the polyols to hydrocarbons using HI/H_3PO_3, and then finally to eliminate iodine from the hydrocarbons by using NaOH to produce hexene. The focus of this paper is Step 1, the BTP method, which is shown in the white box and highlighted in Figures 2 and 3.

BTP Method

As discussed in the introduction, the BTP method is used to convert the raw biomass to polyols using 0.7 % phosphoric acid, Ru/C catalyst at 180 °C, 50 atm H_2 (cold) for 2 h. Several different reaction conditions were tried as the Russian literature explained a range of reaction conditions,[3] but we found with these parameters the greatest yield of polyols, about 70 % of the wood, and about 30% of the remaining wood is lignin, as expected. These results are reproducible. However, in the process of separating the polyols from the lignin and catalyst, the lignin and catalyst are solids that are not easily separated, and without the separation of the lignin and catalyst, the catalyst cannot be recycled as it becomes deactivated. Without being able to recycle the catalyst and the loss of potentially sellable product lignin, the process is not very economical. So a major milestone for using this method is to separate lignin from the Ru/C catalyst.

Separation of Lignin and Catalyst

Two methods to accomplish this separation have been tried. The first method was to extract the lignin using hot sodium hydroxide; this is a well-known method to extract lignin from plants. This facile method has significant potential to remove most if not all of the lignin and has much less severe conditions than the alternative method. After six hours, about 75 % of the lignin is extracted. The yield of polyols in subsequent BTP reactions using the cleaned catalyst was reduced to 58 % upon the first recycle reaction and 51% upon the second recycle reaction indicating some deactivation of the catalyst.

The second method is from the Russian literature.[3] It is claimed that clean catalyst is obtained after reaction of the catalyst/lignin at 280-320 °C, 50-70 atm H_2, and 1.5 % NaOH solution, the product being phenolic compounds. At this time, mechanical problems have kept us from completing these reactions. Another reactor has been acquired to complete this study.

Coal Reactions

As discussed in the introduction, we felt both of these mild reaction conditions could significantly alter the structure of lower rank coal, so we have some preliminary results from these reactions. When reacting the coal at the 180 °C reaction condition in acid, we converted ~40 % of the coal to methylene chloride-solubles with little of the H_2 consumed during the process. When reacting the coal in base at 250 °C (the temperature did reach 250 °C for about 20 min, but fell to about 235 °C over a period of 80 min) and an initial H_2 pressure of 44 atm, we converted ~20 % of the coal to water-solubles; however, as these are intial experiments, we plan to continue to vary these reaction conditions. The pressure profile for this reaction was unusual in comparison to the reactions at lower temperature and could indicate the reaction ran at supercritical conditions.

For low temperature reactions using a hydrogenation catalyst (reactions < 320 °C), usually conversions are quite low, typically < 20 % of the coal reacts.[6, 10, 12] Most researchers believe the controlling mechanism of coal liquefaction is the depolymerization of the coal which does not significantly occur until 350 °C.[6] Exceptions to these data are acid-catalyzed reactions, such as Berthelot using HI [8] and other researchers using $ZnCl_2$ and $SnCl_2$,[6] as these catalysts are known to crack C-C bonds.

REFERENCES

1. (a) Robinson, J.M. *Amer. Chem. Soc. Division of Fuel Chemistry Preprints*, **1995**, *40*(3), 729, (b) U.S. Patent No. 5516960, May, **1996**.
2. Heitz, M., Capek-Menard, E., Koeberle, P.G., Gagne, J., Chornet, E, Overend, R.P., Taylor, J.D., and Yu, E. *Bioresource Tech.*, **1991**, *35*, 23.
3. Sharkov, V.I. *Angew. Chem. I.E.E.*, **1963**, *2*(8), 405.
4. Gorin, E., in *Chemistry of Coal Utilization*, **1981**, M.A. Elliott, Editor. John Wiley & Sons: New York, p1845-1918.
5. Donath, E.E., in *Chemistry of Coal Utilitzation*, **1963**, H.H. Lowry, Editor. John Wiley & Sons: New York, p1041-1080.
6. Derbyshire, F.J., *Catalysis in Coal Liquefaction*, **1988**, IEA Coal Research, London, IEA CR/08.
8. Berthelot, P.E.M., *Bull. Soc. Chim.*, **1869**, *11*, 278.
9. Geerards, J. J. Th. M., van Krevelen, D.W., and Waterman, H.I., Brenn.-Chemie, **1958**, *39*, 11.
10. Hulston, C.J.K., Redlich, P.J., and Marshall, M., *Fuel*, **1995**, *74*, 1870.
11. Suzuki, T., Yamada, H., Yunoki, K., and Yamaguchi, H. *Energy & Fuels*, **1992**, *6*, 352.
12. Redlich, P., Jackson, W.R., and Larkins, F.P. *Fuel*, **1985**, *64*, 1383.

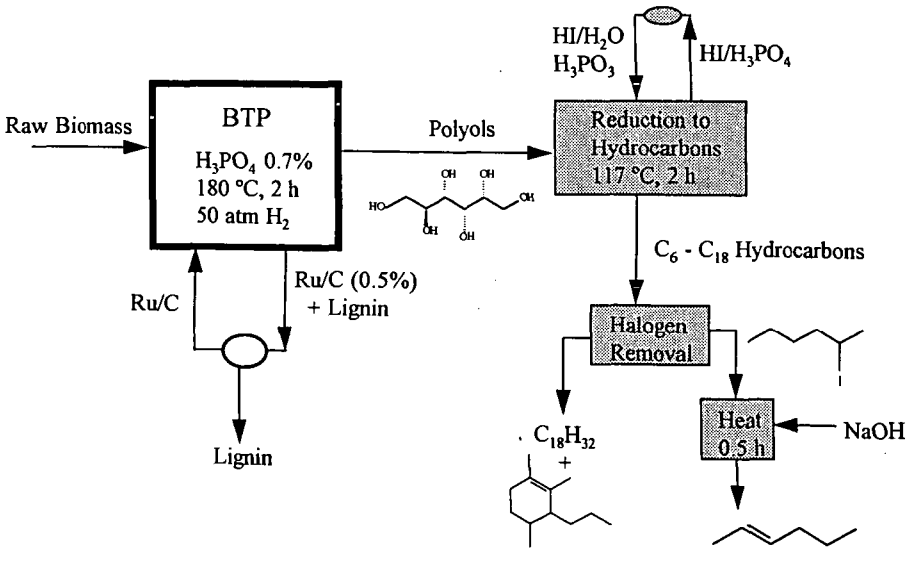

Figure 1: Schematic of Overall Biomass-to-Hydrocarbon Process

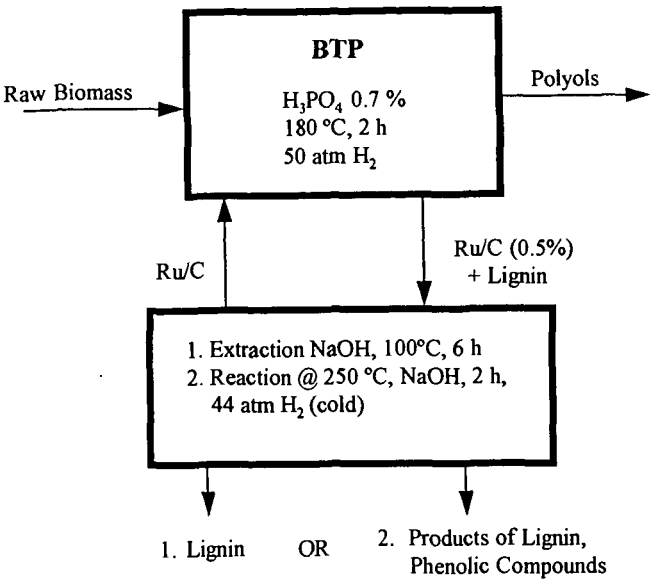

Figure 2: Schematic of BTP Process and Possible Processes to Separate Lignin and Ru/C for Recycle

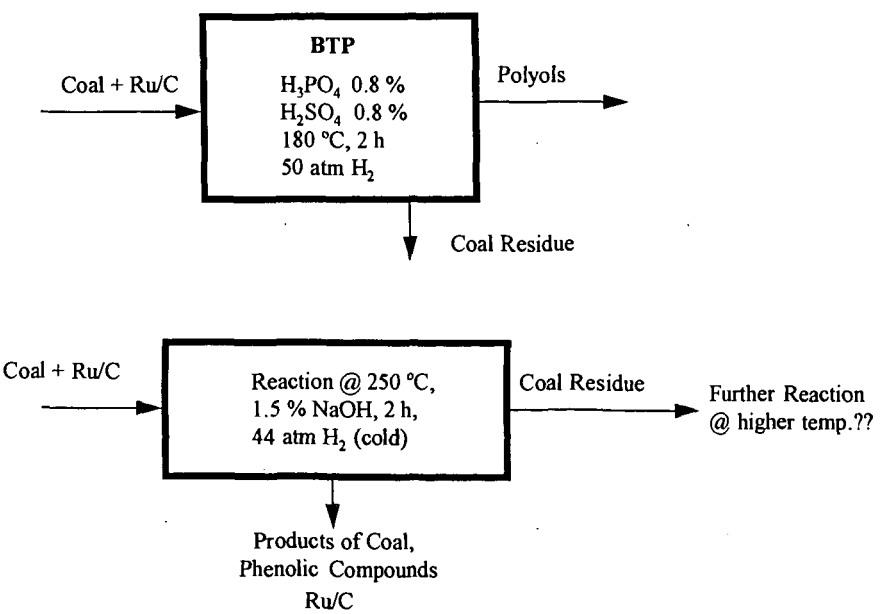

Figure 3: Schematic of BTP Process and Lignin Reaction Process Applied to Coal

CHANGES IN MOLECULAR ACCESSIBILITY IN APCS COAL OXIDIZED IN THE PRESENCE OF SUNLIGHT

R. Ding, L.D. Kispert and A.S. Jeevarajan
Department of Chemistry, Box 870336
The University of Alabama
Tuscaloosa, AL 35487-0336

KEYWORDS: Coal, Accessibility, Weathering, Spin Probes, EPR

ABSTRACT

Weathering changes the properties of coal and its utilization through oxidative and moisture loss processes. Using an EPR-spin probe method, it has been shown that the regions in Illinois # 6 coal accessible to spin probes upon *O*-alkylation increase if the coal is first exposed to sunlight in air rather than to air in the absence of sunlight. Analysis reveals that an increase in oxidation products and microporosity has occurred. One plausible cause for the increase is the formation and reaction of singlet oxygen. A study of Pocahontas #3, Lewiston-Stockton and Wyodak-Anderson coal in which the oxygen content varies from 2% to 17% shows that the accessibility of spin probes in toluene swelled oxidized coal depends also on the percent oxygen present and time of exposure to sunlight

INTRODUCTION

An EPR spin probe method developed in this lab[1] has been used to determine micropore size distribution and acid/base character during swelling[2-4], changes in pore structure and wall chemistry upon swelling at different temperatures and with solvents of various polarities[5,6], the break-up of the hydrogen bonding between the bedding planes[7], and the accessible nature of the covalently cross-linked materials during swelling[8]. This technique has been used successfully to follow changes in the micropore structure during weathering, oxidation, dehydration, and short term oxidation [9-12] of APCS coal.[13] Upon weathering the lower ranked coals (Beulah-zap and Wydak-Anderson) were observed to undergo structural collapse which precluded retention of even the smallest probes, while medium ranked coals exhibited improved retention.[9]

PREVIOUS STUDIES ON COAL OXIDATION

Eight vacuum dried APCS coals were oxidized in a pure O_2 environment as well as weathered in air so the effect of oxidation alone on coal structure could be determined.[10,11] It was shown that the removal of water was primarily responsible for the structural collapse observed in low ranked coal and for the increase in retention of polar spin probes in medium ranked coals.[10] Coals oxidized in a pure oxygen environment showed an increase in retention by as much as a factor of five.[11] Even the higher ranked coals showed significant retention of polar spin probes after four days exposure to oxygen. Short term exposure[12] of Illinois #6 to dry argon or oxygen showed a dramatic change in the coal structure in as little as thirty seconds. Long term weathering for as long as six months was carried out[14] to show that for Beulah-Zap, Illinois #6, and Upper Freeport coals little change occurs after weathering for thirty-six days. However, this is not true for Wyodak Anderson, Blind Canyon and Lewis-Stockton coals which undergo changes throughout the six months weathering period.

It has also been established that the inclusion of spin probes into the macromolecular structure of coal increases in a dramatic oscillatory manner by spiking a "poor" swelling solvent (toluene) with as little as 100 ppm of a strong swelling solvent (pyridine).[15] This has been explained in terms of four different processes: (1) disruption of weak hydrogen bonds which isolate the interconnected micropore system; (2) disruption of weak hydrogen bonds which protect individual micropores; (3) competition of pyridine for the active sites involved in the hydrogen bonds or the "poisoning" of sites; and (4) disruption of stronger hydrogen bonds within the macromolecules which causes an opening of the structure.

These processes were confirmed when the hydroxyl substituents were derivatized[16] with *n*-butyl groups in the absence of oxygen and light. The dramatic cyelic variation was eliminated due to the decrease in hydrogen bonding. It was also shown that a dramatic increase in spin probe retention occurred upon alkylation due to the existence of a more open structure (increasing microporosity) as a result of a decrease in attractive forces, and it was noted that the microporosity increased with increasing rank. In particular, upon O-alkylation, the relative value of the spin probe concentration increased by a factor of 4 for Beulah-Zap lignite (19.1% O), 2.5 for Wyodak-Anderson subbituminous (16.9% O), 5 for Illinois #6 (10.1% O), 3 for Blind Canyon (10.9% O), 1.3 for Pittsburgh #8 (6.9% O), 5.4 for Lewiston-Stockton high volatile bituminous coal (6.7% O), 10 for Upper Freeport medium volatile bituminous (4.7% O) and 6 for Pocahontas #3 low volatile bituminous (1.5% O). Previously published work by Liotta, Rose, and Hippo[17] indicated that an increase in microporosity occurs upon alkylation and that this increase is more pronounced in higher than lower ranked coals. Our measurements confirm these results. We also observed that the increase in microporosity depends on the structure of

each coal; Pittsburgh #8 and Lewiston-Stockton have almost identical oxygen content (6.9% vs. 5.7%) yet exhibit a large difference in the change in microporosity upon *O*-alkylation (1.3% vs. 5.4%). A similar effect was also observed for Illinois #6 and Blind Canyon (5% vs. 3%), although the difference is smaller for these coals which contain a higher percentage oxygen.

Oxidation processes of the coal have been studied by other methods as well. The oxygen content of coal has been determined by neutron activation analysis[18] and by XPS analysis of the coal surface.[19,20] Oxidation has also been measured by noting the relative changes in the FTIR signatures,[21] pH,[22] Gieseler fluidity,[23,24] pyrolysis response,[25,26] and free swelling index.[27] Low temperature oxidation must be quantified even though the amount of solid oxidation products is small.[28] XPS measurements in conjunction with GC analysis of the gaseous products and thermal gravimetric analysis (GA) of the fuels[29] have been useful in determining the oxidation process. Oxidation-induced structural changes of APCS at 120 °C were observed by differential scanning calorimetry (DSC) and solvent swelling.[30] The changes in the free radical character of Alberta coals upon air oxidation between 20-250 °C have been studied[31] as a function of mineral, moisture, and exinite macerate content. Water was also found to be a suitable probe molecule for the detection and measurement of coal oxidation.[32] Although a number of studies have been carried out, the influence of sunlight on the weathering process has not been studied and is the subject of this paper.

EXPERIMENTAL

The coal samples were irradiated by sunlight in the air on a clear day (30-40 °F) when the relative humidity was about 40%. A portion of the samples was swelled in toluene after exposure to sunlight, another was alkylated after exposure according to published methods[17] and a third portion was kept in the dark and then swelled.

A 40 mg unmodified sample of each APCS coal was added to a 10^{-3} M solution of the nitroxide spin probe in the swelling solvent. A spin probe was selected (in this study, VII; Tempamine[15]) depending on the dimensions (approximately spherical) of the coal pores to be studied or the substituents (amine) on the nitroxide molecule required to interact with various functionalities present in the coal.

Each coal and spin probe mixture was stirred vigorously under a nitrogen atmosphere at room temperature. After 18 hours, the mixture was filtered by suction, and residual solvent coating the coal was removed under reduced pressure at room temperature to collapse the coal around the nitroxide spin probe. The resulting material was washed with cyclohexane to remove any spin probe attached to the surface or trapped in large open pores of the coal, and the mixture was filtered and vacuum dried to remove the residual cyclohexane. The coal sample was packed into an EPR sample tube, evacuated, and sealed. The prepared spin probe-doped coal sample was stored at 77 K to prevent the slow 2-3 week decay of the nitroxide spin probe EPR signal at 300 K. EPR powder spectra were recorded on a Varian E-12 EPR spectrometer. Because of the presence of a large central signal due to radicals always present in coal, only the A_{zz} nitrogen hyperfine coupling was deduced. The magnetic field was calibrated using proton NMR markers, and the microwave frequency was measured with a frequency counter. The relative spin concentration per weight of undoped coal was determined by integrating the low field EPR line and comparing it to the integrated EPR spectrum of a frozen solution of the nitroxide spin probe under study. The absolute spin concentration was determined by comparison to a Cr(III) standard from the National Bureau of Standards.

RESULTS AND DISCUSSION

Changes in the Accessible Regions of Coal after Oxidation in Sunlight followed by Alkylation

The spin probe retention as a function of swelling solvent is plotted (Figure 1) for samples of swelled Illinois #6 O-alkylated (A) under a nitrogen atmosphere, in the absence of sunlight, (B) O-alkylated in air and in the absence of sunlight, and (C) after the coal was exposed to sunlight for 1.5 hours in air and then alkylated in air. The increase (37%) in the retained spin probe concentration upon alkylation reflects the increase in accessible regions of the coal as the coal becomes oxidized and is then alkylated. The effect of sunlight is striking. The spin probe tempamine (VII) is a base approximately spherical in shape that contains an amine substitutent capable of forming strong hydrogen bonds. Since upon alkylation the hydrogen-bonding OH substituents are converted to OR groups, the possibility of binding a trapping of tempamine by such hydrogen-bonding is excluded. The fact that nevertheless considerably greater amount of the spin probe are trapped (Figure 1 C) implies that micropores similar in size to spin probe VII are formed after alkylation of the coal that was oxidized in the presence of sunlight and air, and that the spin probe is not removed by the cyclohexane rinsing.

It was also noted that for toluene swelled Wyodak-Anderson (Figure 2), a decreasing spin probe retention occurred with increasing time of exposure to sunlight in the presence of air. In the case of toluene swelled Lewiston-Stockton (Figure 3), no dependence on spin probe concentration was found on time of exposure to air and sunlight; however, for toluene swelled

Pocahontas #3 (Figure 4), the spin probe concentration increased with increasing exposure to air and sunlight. It is apparent that an increase in OH groups occurs in high rank Pocahontas #3 upon air oxidation in the presence of sunlight, i.e., that addition sites for hydrogen bonding for spin probe VII are formed. However, the opposite trend occurs for coals with high oxygen content. In oxygen rich coal, cross-linking can occur by the combination of hydroperoxide radicals with existing radicals in the coal, reducing the microporosity with increasing exposure to sunlight. As the oxygen content decreases, the cross linking mechanism decreases in importance. Thus, it is expected that no dependence on sunlight will be observed for Lewiston-Stockton, a coal with 6.7% oxygen where the presence of cross-linking is balanced by the presence of hydrogen bonding as the exposure to sunlight is increased.

Sunlight Oxidation Mechanism

A clue to the reason for the increased numbers of OH (and perhaps carbonyl) groups in samples of coal exposed to sunlight in an air atmosphere was provided by the following observation. Upon irradiating a Blind Canyon coal suspension in dichloromethane, with filtered light (λ = 300 - 390 nm) from a 200 watt Hg cw lamp, a very intense phosphorescence peak was observed at 1277 nm. This emission is known to occur in the decay of singlet oxygen to the triplet ground state. Further such a signal was not observed upon irradiating dichloromethane (CH_2Cl_2 does not absorb above 240 nm) or a coal suspension in cyclohexane (a non-swelling solvent for coal). The formation of singlet oxygen is a result of energy transfer from the exited state (D_2 or D_1) of the radicals present in undoped coal, (Figure 5) to the excited singlet S_1 state of oxygen which then undergoes decay to the T_0 state producing the observed phosphorescence. The coal based phenoxyl and naphthalene anion radicals, for example, absorb at 390 and 340 nm, respectively. Thus, one plausible cause for the increase in oxidized products formed in coal upon exposure to sunlight is the formation and reaction of singlet oxygen. It is also possible to generate singlet oxygen by energy transfer from irradiated toluene which absorbs at 300 nm, so the choice of solvent is crucial.

CONCLUSION

Sunlight plays an important role in the weathering process. An increase in the number of OH groups in Illinois #6 occurs upon exposure to sunlight in the presence of air or oxygen. After subsequent alkylation, the micropore structure increases by 37%. One possible reason is the formation of singlet oxygen by energy transfer from excited singlet states of the radicals. The increase in microporsity decreases with time of exposure to sunlight for coals (not alkylated) with high (17%) oxygen content. For Lewiston Stockton coal not alkylated with medium (6.7%) oxygen content, there is no dependence on sunlight but for high rank coal (2%), Pocahontas #3 (not alkylated), there is an increase in microporosity with exposure to sunlight. The formation of singlet oxygen could possibly account for the increase in oxidation products in high rank coals as a function of sunlight.

ACKNOWLEDGMENT

This investigation was supported by the United States Department of Energy, University Coal Grant Program, Grant No. DE-FG22-93PC93202. Dr. Chignell at the National Institute of Environmental Health Sciences (NIEHS), Research Triangle Park, NC, is thanked for use of his equipment to measure the singlet oxygen phosphorescence from irradiated coal suspension and Dr. Elli Hand for discussions.

REFERENCES

1. Wuu, S.K.; Kispert, L.D. *Fuel* **1985**, *64*, 1681.
2. Goslar, J.; Kispert, L.D. *Energy and Fuels* **1989**, *3*, 589.
3. Goslar, J.; Cooray, L.S.; Kispert, L.D. *Fuel* **1989**, *68*, 1402.
4. Goslar, J.; Kispert, L.D. *Fuel* **1990**, *69*, 564.
5. Spears, D.R.; Kispert, L.D.; Piekara-Sady, L. *Fuel* **1992**, *71*, 1003.
6. Spears, D.R.; Sady, W.; Kispert, L.D. *Prepr. Pap. Am. Chem. Soc.,Div. Fuel Chem.* **1991**, *36*, 1277.
7. Spears, D.R.; Sady, W.; Kispert, L.D. *Fuel* **1993**, *72*, 1225.
8. Spears, D.R., Sady, W.; Tucker, D.; Kispert, L.D. *Energy and Fuels* **1993**, *7*, 1001.
9. Sady, W.; Kispert, L.D.; Spears, D.R. *Prepr. Pap. Am. Chem. Soc., Div. Fuel Chem.* **1992**, *37*, 1151.
10. Sady, W.; Tucker, D.; Kispert, L.D.; Spears, D.R. *Prepr. Pap. Am. Chem. Soc., Div. Fuel Chem.* **1993**, *38*, 1323.
11. Tucker, D.; Kispert, L.D. *Prepr. Pap. Am. Chem. Soc., Div. Fuel Chem.* **1993**, *38*, 1330.
12. Tucker, D.; Kispert, L.D.; *Prepr. Pap. Am. Chem. Soc., Div. Fuel Chem.* **1993**, *38*, 1335.
13. Vorres, K.S. *Energy and Fuels* **1990**, *4*, 420.
14. Kispert, L.D.; Tucker, D.; Sady, W. *Prepr. Pap. Am. Chem.Soc., Div. Fuel Chem.* **1994**, *39*, 54.
15. Ding, R.; Tucker, D.; Kispert, L.D. *Prepr. Pap. Am. Chem. Soc.,Div. Fuel Chem.* **1995**, *40*, 590.
16. Ding, R.; Tucker, D.; Kispert, L.D. *Prep. Pap. Am. Chem. Soc., Div. Fuel Chem.*

1995, *40*, 425.
17. Liotta, R.; Rose, K; Hippo, E. *J. Org. Chem.* **1981**, *46*, 277.
18. Ehmann, W.D.; Koppenaal, D.W.; Hamrin, C.E., Jr.; Jones, W.C.; Prasad, M.N.; Tian, W.Z. *Fuel* **1986**, *65*, 1563.
19. Perry, D.L.; Gint, A. *Fuel* **1983**, *62*, 1029.
20. Clark, D.T.; Wilson, R. *Fuel* **1983**, *62*, 1034.
21. Fredericks, P.M.; Moxon, N.T. *Fuel* **1986**, *65*, 1531.
22. Yun, Y.; Hoesterey, B.; Meuzelaar, H.I.C.; Hill, G.R. *Prepr., Pap. Am. Chem. Soc., Div. Fuel Chem.* **1987**, *32*,302.
23. Huffman, G.P.; Huggins, F.E.; Dunmyre, G.E.; Pignocco, A.J.; Lin, M. *Fuel* **1985**, *64*, 849.
24. Grint, A.; Perry, D.L. *Proc. Int. Conf. Coal Sci. 1985*, 879.
25. Ignasiak, B.S.; Clugston, D.M.; Montgomery, D.S. *Fuel* **1972**, *51*,76.
26. Iyuhara, H.; Tanibata, R.; Nishida, S. *Proc. Conf. Coal Sci.* **1985**, 491.
27. Larsen, J.W.; Dee, D.; Schmidt, T; Grint, A. *Fuel* **1986**, *65*, 595.
28. Gethner, J.S. *Fuel* **1987**, *66*, 1091; Isaacs, J.J.; Liotta, R. *Energy & Fuels* **1987**, *1*, 349.
29. Kilemen, S.R.; Freund, H. *Prepr. Pap. Am. Chem. Soc., Div. Fuel Chem.* **1988**, *33*, 706.
30. Yun, Y.; Sunberg, E. *Prepr. Pap. Am. Chem. Soc., Div. Fuel Chem.* **1992**, *37*, 1184.
31. Kudynska, J.; Buckmaster, H.A. *Fuel* **1992**, *71*, 1127.
32. Petit, J.C. in "1991 International Conference on Coal Science Proceedings," Edt. by International Energy Agency Coal Research, Butterworth-Heinemann, Oxford, 1991, p. 186.

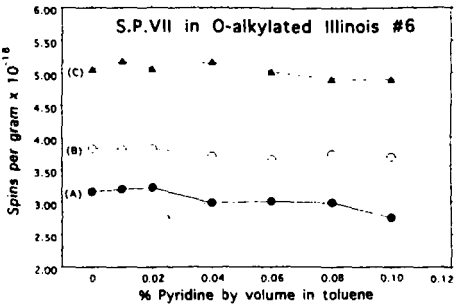

Figure 1: Spin probe VII retention concentration in O-butylated Illinois #6 versus percent pyridine by volume in toluene.

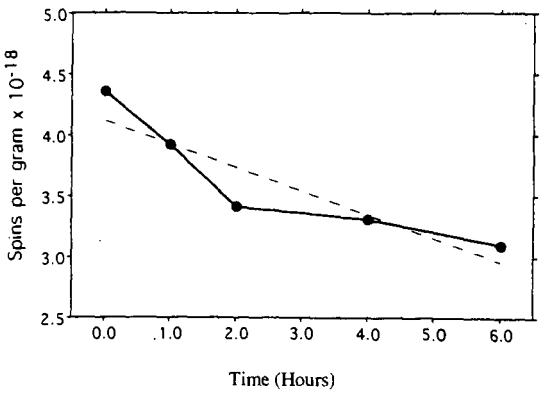

Figure 2: Toluene Swelled Wyodak-Anderson: Time of exposure to sunlight in the presence of air versus spin probe retention concentration

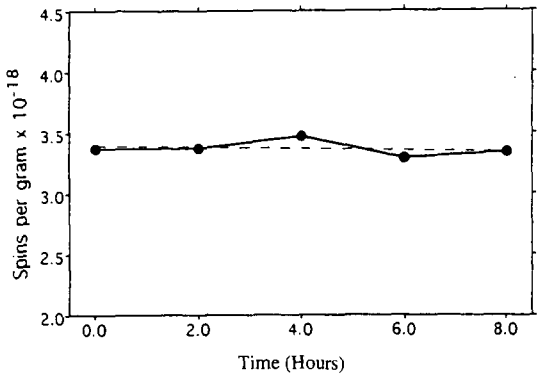

Figure 3: Toluene Swelled Lewiston-Stockton: Time of exposure to sunlight in the presence of air versus spin probe retention concentration

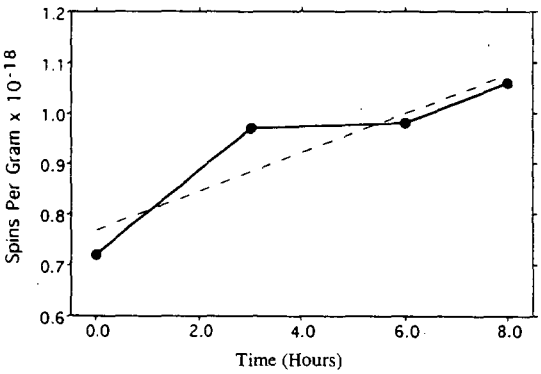

Figure 4: Toluene Swelled Pocahontas # 3: Time of exposure to sunlight in the presence of air versus spin probe retention concentration

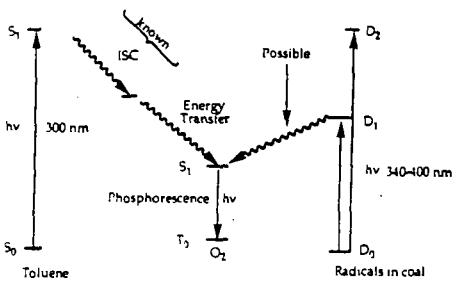

Figure 5: Energy diagram for singlet oxygen formation upon excitation of the naturally occurring radicals in coal

HIGH CONVERSION (98%) FOR THE HYDROGENATION OF 1-METHYLNAPHTHALENE TO METHYLDECALINS

Belma Demirel
U.K. Center for Applied Energy Research
3572 Iron Works Pike, Lexington, KY 40511-8433, USA
and
Wendell H. Wiser
University of Utah, Chemical and Fuels Engineering
Salt Lake City, UT 84112, USA

Keywords: Hydrogenation, 1-methylnaphthalene, methyldecalin

ABSTRACT

This work presents results from the hydrogenation of 1-methylnaphthalene. Aromatics are undesirable because of their toxicity, poor combustion characteristics and environmental impact. Saturated cyclic hydrocarbons with one or two rings show great promise for use in fuels. Methyldecalins were used as feed in the second step of a two-stage operation for the production of high octane gasoline components from 1-methylnaphthalene, which represents coal derived liquids. Experiments were conducted in a stirred batch reactor with commercial as well as previously tested non-commercial catalysts under different reaction conditions. The data shows that a NiMo catalyst supported on titania-alumina produced high yields of methyldecalins at 325°C and 1000 psi. The products were analyzed by GC/MS and ^{13}C-NMR spectroscopy. The conversion to methyldecalins were 98%. Previous methods yielded considerably lower conversion.

INTRODUCTION

It is widely agreed that the availability of petroleum in international trade is likely to diminish in the future. Research is being undertaken to develop economically competitive process for the conversion of coal, oil shale, tar sands and petroleum residues into liquid fuels. Although there has been significant advances both in improving the technology for converting coal to liquid fuels as well as in improving economics, the cost is still higher than for fuels produced from petroleum. Several of these coal liquefaction processes rely on the use of a catalyst.

Coal liquefaction processes generally involve a number of mechanical and chemical steps. Catalytic hydrogenation and cracking of the coal liquids take very important place in the development of coal liquefaction technology. The catalyst is believed to bring about the conversion of various species to molecules which are capable of cracking or depolymerizing coal particles by hydrogen transfer.

Coal liquids are very complex mixtures, mostly containing ring-type molecules, both aromatics and hydroaromatics, with various types of functional groups attached. 1-Methylnaphthalene (1-MeNAPH) was selected as a model compound representing coal-derived liquids. The immediate objective of this part of the project is to convert 1-MeNAPH to methyldecalins. Methyldecalins were in this study used as feed in the second stage of a two-stage operation for the production of high octane gasoline components from 1-MeNAPH, but they can also be used directly as a component in jet fuels.[1-6]

EXPERIMENTAL

Catalyst Preparation. NiMo/TiO_2-Al_2O_3 and NiMo/SiO_2-Al_2O_3 catalysts were prepared by incipient impregnation method. The support TiO_2-Al_2O_3 or SiO_2-Al_2O_3 was calcined in air at 540°C for 16 h, ground and sieved to -100 mesh. All prepared catalysts contained 25 mmol of Ni and 77 mmol of Mo per 100 g of support. A weighed sample was first impregnated with an aqueous solution of ammonium molybdate ($(NH_4)_6Mo_7O_{24}.4H_2O$, Alfa Product). The impregnated sample was oven-dried at 120°C for 16 h and then impregnated with a salt solution of nickel nitrate ($Ni(NiO_3)_2.6H_2O$, Fischer Scientific Co.).

NiW/TiO_2-Al_2O_3 and NiW/Al_2O_3 was impregnated in a single step with an aqueous solution containing calculated amounts of ammonium meta tungstate($(NH_4)_6H_2W_{12}O_{40}.3H_2O$, Cerac inc.) and nickelous nitrate followed by drying at 120°C for 16 h. The resulting material contained 88.9 mmol of Ni and 165.6 mmol of W per 100 g of TiO_2-Al_2O_3 or 100 g of Al_2O_3. Each catalyst was finally calcined in air at 540°C for 16 h.

NiW/SiO_2-Al_2O_3 (Harshaw Catalysts), Pt/REX and Pd/REX (proprietary) are commercial catalysts used for the experiments.

Presulfidation. All catalysts except Pt/REX and Pd/REX were sulfided in a tubular reactor prior to use. Nitrogen with a flow rate of 60 ml/min purged the sulfidation reactor to remove the air. The catalyst was heated to 400°C under nitrogen flow and kept at this temperature and inert conditions for an hour. The gas flow after this desorption step was changed to 10% (by wt) hydrogen sulfide in hydrogen. The reactor was maintained at 400°C at the same flow rate for 2 h. Subsequently, it was purged with nitrogen at the same conditions for an hour to remove the residual amount of hydrogen sulfide and then cooled to ambient temperature.

Reaction Experiments. Reaction experiments were conducted in a 300 cc batch reactor equipped with a magnetic drive stirrer, heating assembly, gas inlet and gas collector. Weighed amount of 1-MeNAPH (Aldrich Chemicals, 98%) and the sulfided catalyst in a feed to catalyst ratio of 10 to 1 were quickly dumped into the reactor. The sealed reactor was repeatedly purged with nitrogen and subsequently hydrogen to replace the air, and then pressurized with hydrogen and heated to a reaction temperature over about 20 minutes at slow stirring rate (80 rpm). Once the desired temperature was reached, the stirring speed was increased to 800 rpm and the reactor was remained at reaction temperatures for 1-10 h. Sulfided fresh catalyst was added to reaction mixture after first 5 h.

Product Analysis. Liquid products were identified by GC and GC/MS (Hewlett Packard 5890 Series II GC with a HP 5971 Mass Selective Detector). DB-5 column (30mx0.25mm i.d.x1.0μm, J&W Scientific) with a temperature program from 40 to 260°C. Gas products were analyzed by a Shimadzu GC-14A gas chromatograph, equipped with a flame ionization detector (FID) and Chromosorb 102 80/100 column (6'x1/8"x0.0085", Supelco). The column temperature ranged from 40 to 200°C. Scotty standard gases were used for calibration.

Methyldecalins from the hydrogenation of 1-MeNAPH were also identified by ^{13}C-NMR spectroscopy (VXR-400).

RESULTS AND DISCUSSION

Initial experiments were performed at 325°C and 1000 psi for 10 h with a feed to catalyst ratio of 10 to 1 by weight. The results are given in Figure 1. All conditions remained the same for all experiments, changing only the catalyst. The total conversion was defined as

$$\%\text{Total Conversion} = 100 \times \frac{\text{Feed - Feed in product}}{\text{Feed}}$$

Liquids were weighed just after completion of the reaction, and gas amounts were calculated from gas chromatograms. Liquid product distribution was calculated based on converted material. The products can be subdivided into four different groups.

(1) Cycloalkanes (*methyldecalins*, *cyclohexanes* and *cyclopentanes* which are mostly alkyl substituted and *'other cycloalkanes'* which include decalins, octahydroindenes, bicycloheptanes, etc.)
(2) Alkanes (*normal* and *branched*)
(3) Alkenes and cycloalkenes
(4) Aromatics (*Methyltetralins*, and *'other aromatics'* which include bigger than one ring aromatics)

Near 100% conversion was achieved with each catalyst but product distribution i.e. the depth of ring hydrogenation varies widely (Figure 1). $NiMo/TiO_2$-Al_2O_3 exhibited by far the highest hydrogenation activity followed by NiW/Al_2O_3 and NiW/TiO_2-Al_2O_3. Pt/REX and Pd/REX exhibited high cracking activity with a product dominated by aromatics. NiW/SiO_2-Al_2O_3 gave a mixture of hydrogenation and cracking products. Conclusively, the most effective catalyst in hydrogenation of 1-MeNAPH is $NiMo/TiO_2$-Al_2O_3 catalyst with a 97.2% conversion to methyldecalins at 325°C and 1000 psi.

Figure 2 shows the effect of temperature on the yield and distribution of liquid products from 1-MeNAPH using $NiMo/TiO_2$-Al_2O_3. The total conversion slightly decreased when the temperature was increased from 350°C to 450°C. The yield of methyltetralins and methyldecalins also showed a reverse temperature dependence. Conversion to one ring compounds, given under 'other aromatics', was observed as a result of cleavage reactions of tetralins at high temperatures.

Since reactions at higher temperatures result in cracking, the temperature was decreased to 325°C using $NiMo/TiO_2$-Al_2O_3 catalyst. Figure 3 summarizes the results under different reaction conditions, keeping only the temperature constant at 325°C. A total conversion of 100% was achieved, and the yields of methyldecalins were over 92% for each experiment. The yield of

methyldecalins only changed from 97.2 % to 98.6% as pressure was increased from 1000 psi to 1500 psi. When only the feed/catalyst ratio was changed from 10/1 to 5/1 at 1000 psi for 10 h reaction time, the conversion to methyldecalins reached to 99.5%,

Mass balances were closed with 4 to 13% error. The amount of gas products was 0.1-8.4% depending on reaction conditions. The gaseous fractions analyzed by GC were predominantly composed of methane at 325°C with $NiMo/TiO_2$-Al_2O_3, NiW/TiO_2-Al_2O_3 and NiW/Al_2O_3 catalysts because these catalysts have higher hydrogenation activities compared to NiW/SiO_2-Al_2O_3, Pt/REX and Pd/REX catalysts. The latters exhibited higher yields of C_3-C_4 hydrocarbons. The temperature effect on the distribution of gas products from hydrogenation of 1-MeNAPH at 350-450°C with $NiMo/TiO_2$-Al_2O_3 catalyst showed that the yields of C_1-C_2 hydrocarbons increased with temperature whereas those of C_3-C_4 hydrocarbons decreased.

Verification of Methyldecalin Synthesis. Primary identification of methyldecalins, separated by gas chromatography, was done by mass spectrometry and comparisons with database cracking patterns.[7] The results from GC/MS are given in Figure 4. Secondary identification was given by matching retention times with published boiling points. Figure 5 compares the present results with those of Weitkamp et al.[7-9] Filled circles represent retention times for eight isomers as measured in the present work and by Weikamp et al. Open circles represent two more isomers identified as methyldecalins by mass spectrometry in the present study and extrapolated values in Weitkamp's work. Additional support for the identification of these compounds as 9-methyldecalins was given by boiling points. Finally, consistency between different spectra was verified by comparisons with a compiled list of retention times for all identified compounds within the present project. Some uncertainties still persist for the distinction between different isomers except in the case of methyldecalins, where full agreement exists with literature.[7, 8,10-12]

Figure 6 shows the ^{13}C-NMR spectrum of the product from hydrogenation of 1-MeNAPH. The signals were integrated into two groups: (a) aliphatic carbons; chemical shift, δ=15-55 ppm, and (b) aromatic carbons; δ=125-160 ppm. It was observed that the aromaticity was about 2% and that the isomers have eleven carbon atoms in different proportions.

CONCLUSION

High conversions of methyldecalins (up to 99.5%) were obtained from the hydrogenation of 1-MeNAPH using $NiMo/TiO_2$-Al_2O_3 catalyst at 325°C and 1000 psi for 10 h reaction time. The hydrogenation processes consist of a complex array of kinetic steps involving a serious of intermediates producing methyldecalins simultaneously. The intermediate products are mixtures of methylnaphthalenes, methyltetralins and methyldecalins.

When reaction temperatures were increased, hydrocracking reactions set in as observed in Figure 4.3. The results from the present study agree with the work of Weitkamp et al.[7, 8, 13] They studied the hydrogenation of alkylnaphthalenes using a broad variety of catalysts. With most catalysts, yields of methyldecalins up to 90% range were obtained from individual methylnaphthalenes after 30-40 h reaction time over $Pt(0.6\%)/Al_2O_3$ catalyst at 200°C.

REFERENCES

1. Groot, C. K., de Beer, V. H. J., Prins, R., Stolarski, M. and Niedzwiedz, W. S. *Ind. Eng. Chem. Prod. Res. Dev.* **1986**, 25, 522
2. Patzer, II J. F., Ferrauto, R. J. and Montagna, A. A. *Ind. Eng. Chem. Process Des. Dev.* **1979**, 18, 625
3. Rosal, R., Fernando, V. D. and Herminio, S. *Ind. Eng. Chem. Res.* **1992**, 31, 1007
4. Sapre, A. V. and Gates, B. C. *Ind. Eng. Chem. Process Res. Dev.* **1981**, 20, 68
5. Gollis, M. H., Belenyessy, L. I., Gudzinowicz, B. J., Koch, S. D., Smith, J. O. and Wineman, R. J. *J. Chem. Eng. Data* **1962**, 7, 311
6. Donath, E. and Hess, M. *Chem. Eng. Progress* **1960**, 56 (4), 68
7. Weitkamp, A. W., Banas, E. M. and Johnson, G. D. *Preprints Amer. Chem. Soc. Div. Petr. Chem.* **1962**, 7, C-139
8. Weitkamp, A. W., in 'Advances in Catalysis, Volume 18', (Eds D. D. Eley, H. Pines and P. B. Weisz), Academic Press, New York, **1968**, p.1
9. Banas, E. M., Weitkamp, A. W. and Bhacca, N. S. *Analytical Chemistry* **1966**, 38 (12), 1783.
10. Meyerson, S. and Weitkamp, A. W. *Org. Mass Spectr.* **1969**, 2, 603
11. Bagrii, E. I., Musarev, I. A., Kurashova, E. K., Dolgopolova, T. N. and Sanin, P. I. *Neftekhimiya* **1968**, 8, 818
12. Stukanova, L. N., Shan'gina, T. N. and Petrov, A. A. *Neftekhimiya* **1969**, 9, 196
13. Shaptai, J., Nag, N. K. and Massoth, F. E. 'Proc. 9th International Congress on Catalysis', Calgary, **1988**, p.1

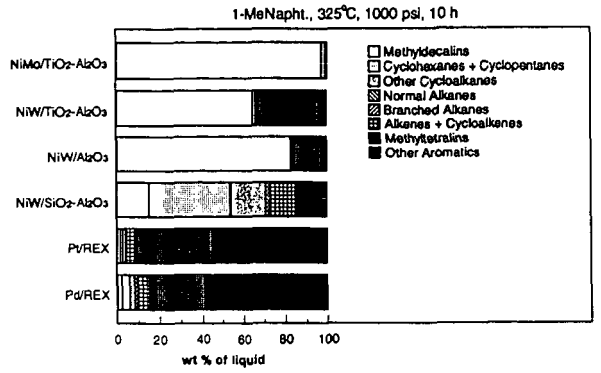

Figure 1. Yield and distribution of liquid products from hydrogenation/hydrocracking of 1-MeNAPH using different catalysts. Difference to 100% is the unconverted material. Feed/catalyst ratio is 10/1.

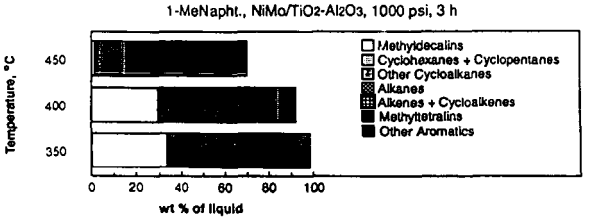

Figure 2. Effect of temperature on the yield and distribution of liquid products from hydrogenation/hydrocracking of 1-MeNAPH. Difference to 100% is the unconverted material Feed/catalyst ratio is 10/1

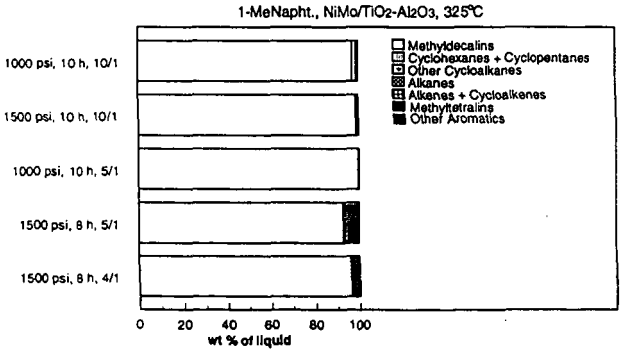

Figure 3. Effect of variable combinations on the yield and the distribution of liquid products from the hydrogenation of 1-MeNAPH using $NiMo/TiO_2$-Al_2O_3 catalyst. 10/1, 5/1 and 4/1 define feed to catalyst ratios.

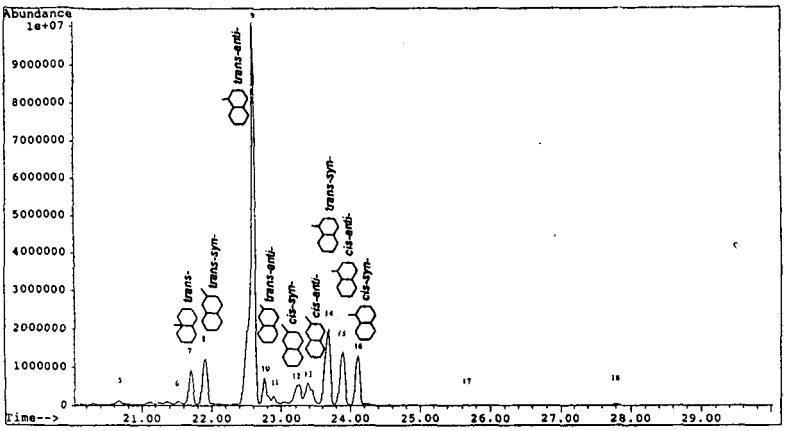

Figure 4. Identification of methyldecalins by GC/MS.

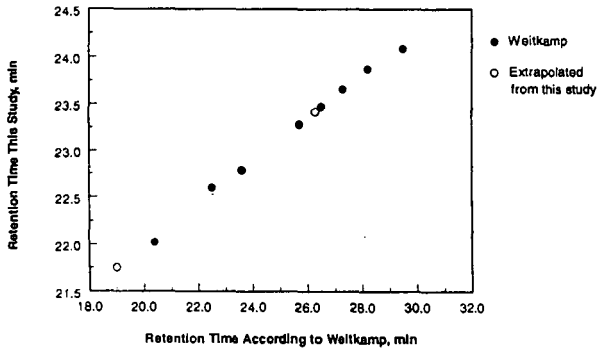

Figure 5. Identification of isomers of methyldecalins by comparison with published GC retention times.

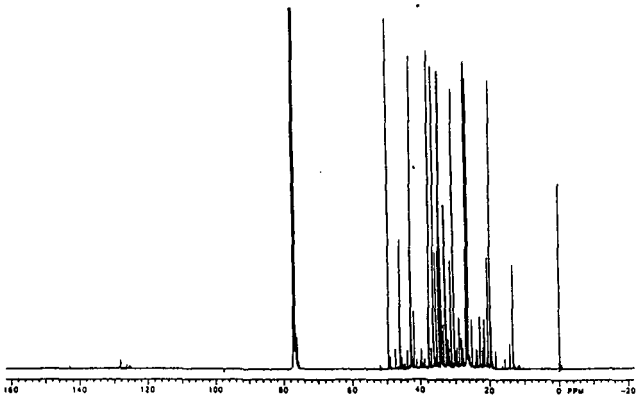

Figure 6. ^{13}C-NMR spectrum of the product from hydrogenation of 1-MeNAPH.

COMBUSTION PROPERTIES OF ILLINOIS COAL-CHAR BLENDS

Joseph A. DeBarr[1], Massoud Rostam-Abadi[1] and Steven A. Benson[2]
[1]Illinois State Geological Survey, 615 E. Peabody Dr., Champaign, IL 61820
[2]Energy & Environmental Research Center, P.O. Box 9018, Grand Forks, ND 58202

Keywords: Coal-char blends, combustion, SO_2 emissions reduction

INTRODUCTION AND BACKGROUND

The principal product (about 60-70 percent by weight) of mild gasification (MG) processes is a partially devolatilized coal (hercin referred to as char) that must be effectively utilized to help the overall economics of the process. The loss of volatile matter (VM) indicates loss of hydrocarbon materials from the coal that are desirable for ignition, carbon burn-out and flame stability. In addition, the chars produced from processing high-sulfur Illinois coals still contain a high residual sulfur content which, when burned directly, would exceed the years 1995 and 2000 emissions limits of 2.5 and 1.2 lbs SO_2/MMBtu.

Recent research suggests that MG of a high-sulfur Illinois coal followed by a low temperature oxidation step may produce a low-sulfur char with considerable VM [1-3]. One potential use of a low sulfur-char is as a compliance fuel burned in a boiler designed to burn low-volatile fuels. The char could also be burned in conventional pulverized coal (PC) boilers with or without an auxiliary fuel such as methane or by blending with high-sulfur Illinois coal or low-sulfur Western coal. However, the combustion characteristics of low-sulfur chars have not been researched extensively. Previous results obtained at the Illinois State Geological Survey (ISGS) indicate that the char derived under MG conditions, when mixed with coal to make a 25% VM blend, can be burned with an acceptable combustion efficiency in PC boilers [3]. This paper describes our efforts to prepare a low-sulfur char from Illinois coal, blend this char with the parent coal, and determine the combustion properties of the char and coal-char blends.

EXPERIMENTAL

The chars used in this work were prepared in a continuous-feed rotary tube kiln (RTK) from an Illinois No. 2 hvCb coal, sample IBC-102 of the Illinois Basin Coal Sample Program [4]. Details of experimental methods are given elsewhere [5]. Preoxidation of -48 mesh coal was done at 150°C for 30 min in air using a feed rate of about 0.9 kg/h. The preoxidized coal was fed at 0.5 kg/h and pyrolyzed in N_2 at 600°C for 30 min. Low temperature oxidation (LTO) was done to remove sulfur from the char. Char was fed at 0.4 kg/h and oxidized at 430°C for 10 min in 17% O_2, balance N_2 during LTO.

The feasibility of decreasing SO_2 emissions during combustion tests by blending calcium-based sorbents with coal prior to charring was investigated. The coal was blended with either an ISGS high-surface area hydrated lime (HSAHL) [6, 7] or a commercially available hydrated lime (COMHYD). Coal-hydrated lime blends were prepared with 68% coal and 32% hydrated lime by weight. A continuous feed charring oven (CFCO) was used for char production [5]. The coal-hydrated lime blends were pyrolyzed in the CFCO using a feed rate of about 2 kg/h, a bed depth of 15 mm, a maximum temperature of 600°C and a residence time of about 16 min.

Five different blends were prepared from the available samples. All samples were ground to 70% -200 mesh prior to blending. The samples prepared were: 1) RTK blend - 62% (by weight) coal + 38% of the RTK char; 2) RTK_{HSAHL} blend - 92% RTK blend + 8% HSAHL; 3) $CFCO_{HSAHL}$ blend - 75% coal + 25% CFCO char (prepared from a coal/HSAHL mix); 4) $CFCO_{COMHYD}$ blend - 75% coal + 25% CFCO char (prepared from a coal/COMHYD mix); 5) $Coal_{HSAHL}$ blend - 90% coal + 10% HSAHL.

Combustion tests were done at the U.S. EPA in their Innovative Furnace Reactor (IFR) by maintaining a constant flow rate of primary, secondary and tertiary air and adjusting the fuel feed rate to achieve a constant oxygen level of about 8.0% in the effluent. This fuel feed rate corresponded to a firing rate of about 39,000 to 42,000 Btu/h. Sorbent was added downstream at a constant injection temperature of about 1200°C and at Ca/S molar ratios between 0 and about 2.4.

Selected samples were tested at the University of North Dakota Energy and Environmental Research Center (UNDEERC) in an optical access drop-tube furnace (DTF) to determine deposit growth factors, deposit strengths, and deposit compositions. Initial slagging temperatures were determined using the test conditions described elsewhere [5]. Coal was combusted at 50% excess air using a feed rate corresponding to about 0.007 g/min of ash, until a deposit of 0.6-1.0 cm had grown on the probe. The temperature was increased at 5°C/min until the deposit began to slump and consolidate (initial slagging temperature). Deposit growth factors are the ratio of deposit weight to the weight of ash fed. Fouling tests were done using conditions that simulate the environment in a boiler convective pass. Feed rates and excess air were the same as for slagging conditions. Deposit crushing strengths were determined by measuring the pressure required to crush the main portion of each deposit following removal from the DTF.

RESULTS AND DISCUSSION

Analyses of the -48 mesh samples prepared from IBC-102 in the RTK are shown in Table 1. The only significant difference between the raw coal and the preoxidized coal appears to be the slightly lower hydrogen and higher oxygen content of the preoxidized sample. During preoxidation, two processes occur concurrently, that is the gain of oxygen, and removal of hydrogen, carbon and oxygen from the coal as CO, CO_2 and water. The latter process becomes of increasing importance as the temperature is increased [8].

Table 1. Analyses of samples prepared in the RTK and CFCO (moisture free).

	IBC-102	Preoxidized IBC-102	MG char	RTK char	CFCO $Char_{HSAHL}$	CFCO $Char_{COMHYD}$
Moisture	10.96	1.57	0.79	3.42	0.73	0.74
Proximate						
Volatile Matter	40.43	39.47	15.53	19.93	32.29	33.58
Fixed Carbon	53.38	54.39	75.39	69.86	27.18	27.13
H-T Ash	6.19	6.14	9.08	9.49	40.53	39.29
Ultimate						
Carbon	74.42	74.38	80.97	77.77	45.23	46.74
Hydrogen	4.81	3.73	0.99	0.92	2.74	3.37
Nitrogen	1.38	1.33	1.76	1.85	0.97	0.99
Oxygen	9.31	9.57	3.43	7.07	8.46	7.39
Sulfate Sulfur	0.56	0.51	0.07	0.14	---	---
Pyritic Sulfur	1.45	1.48	0.18	0.17	---	---
Organic Sulfur	1.31	1.29	1.85	1.17	---	---
Total Sulfur	3.32	3.28	2.11	1.48	2.08	2.22
Btu/lb	13,330	13,225	13,284	12,499	7,271	7,830
lb SO_2/MMBtu	4.98	4.96	3.18	2.37	5.72	5.67

The pyritic sulfur content decreases and the organic sulfur content increases during devolatilization of the preoxidized coal (Table 1). Typically, 30-60% of the organic sulfur is released at pyrolysis temperatures below about 550°C [2, 9, 10]. However, Huang and Pulsifer [11] found that during pyrolysis in the presence of the gases derived from coal, only 25-33% of the organic sulfur is removed. Conditions in the RTK would be similar to those of Huang and Pulsifer because the nitrogen sweep gas flowed counter current to both to the gases released from the coal and the solid sample as it moved through the reactor. It has also been found that a significant amount of the sulfur released during pyrite decomposition can be retained in the char or react with the organic portion of the coal to form carbon-sulfur bonds [2, 11, 12].

After LTO, the VM content of the char is higher than that of the precursor char due to the chemisorption of oxygen, which is also shown by the increase in oxygen content (Table 1). These stable carbon-oxygen complexes evolve at a higher temperature than the inherent VM, and would not be expected to contribute to the flammability characteristics of the chars. The pyritic sulfur content remains constant while the organic sulfur content decreases substantially compared to the precursor char. This is unexpected, as previous researchers have found that LTO removes mainly pyritic sulfur [2, 11, 13]. The decrease in organic sulfur content may be due to the removal of sulfidic and/or elemental sulfur, which is included in the organic sulfur fraction during determination of the forms of sulfur in the char.

The SO_2 emissions of the RTK char are significantly higher than for a similar char prepared in a fluidized bed reactor (FBR) [5]. Smaller particle diameters and better gas-solid contact in the FBR may help explain this trend [5]. In addition, because the gases flowed countercurrent to the solid flow in the RTK, the SO_2 produced during oxidation may have accumulated to the point where the back reaction of SO_2 with Fe and/or the carbonaceous matrix would be thermodynamically favorable. Based on estimates of the SO_2 concentrations in the RTK during LTO, the major iron-containing product of this system would be $Fe_2(SO_4)_3$ not Fe_2O_3. This would result in lower sulfur removal than in the FBR, where the SO_2 produced is rapidly removed from the system by the fluidizing gas. A recent study found that while using a multi-step process involving oxidation, about 57% and 87% of the sulfur was removed from an Illinois coal in a fixed-bed and a fluidized-bed reactor, respectively [1].

The results of analyses of the chars prepared in the CFCO are shown in Table 1. The samples prepared with the two different hydrated limes are almost identical according to these results. The VM content of the samples includes the decomposition of $Ca(OH)_2$ and $CaCO_3$ that were present from the hydrated lime. Methods were developed to discern the portion of VM due to decomposition of calcium compounds and that due to VM remaining from the coal [5]. Overall, the VM content of the chars derived from the original coal fraction is estimated to be about 13% and 14.5% for the HSAHL and COMHYD chars. The HSAHL and COMHYD chars contained 29.9% and 29.4% CaO. Assuming that all of the sulfur released during pyrolysis

was captured by the Ca-based sorbent, the amount of free calcium available in the char/lime blends for sulfur capture during combustion was 17.7% by weight.

Analyses of the coal-char blends prepared are shown in Table 2. The four samples that have Ca-based sorbents added exhibit higher ash contents, as expected. It is unclear why the total sulfur contents of these samples are also higher, but could be due to the formation of either $CaSO_4$ or CaS and their subsequent decomposition during tests to determine total sulfur contents.

Table 2. Analyses of coal-char blend samples prepared from IBC-102 (moisture free).

	RTK blend	RTK_{HSAHL} blend	$CFCO_{HSAHL}$ blend	$CFCO_{COMHYD}$ blend	$Coal_{HSAHL}$ blend
Moisture	8.95	7.78	10.21	10.61	12.62
Proximate					
Volatile Matter	31.31	33.05	39.28	38.14	40.12
Fixed Carbon	60.80	48.15	39.31	40.63	38.70
H-T Ash	7.89	18.80	21.41	21.23	21.17
Ultimate					
Carbon	76.12	70.25	65.80	66.15	65.16
Hydrogen	4.11	3.91	4.49	4.63	6.59
Nitrogen	1.49	1.39	1.27	1.25	1.20
Oxygen	7.81	3.32	4.01	3.77	2.83
Sulfur	2.59	2.33	3.02	2.96	3.05
Btu/lb	12,894	11,800	11,480	11,647	11,799
lb SO_2/MMBtu	4.02	3.95	5.26	5.08	5.17

Combustion Tests

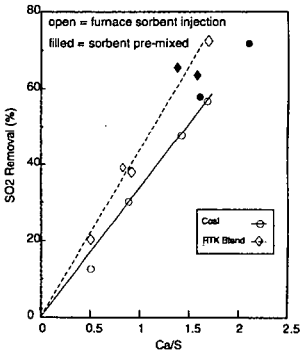

Figure 1. SO_2 removal efficiencies during IFR tests.

The SO_2 removal efficiencies for various Ca/S ratios during combustion of coal and RTK blend samples tested in the IFR are shown in Figure 1. The sorbent (HSAHL) was either physically pre-mixed with the samples or injected about 104 cm downstream (furnace sorbent injection (FSI)) of the fuel injection point. Surprisingly, the method of incorporating sorbent into the furnace does not determine SO_2 removal efficiencies. Similar results were obtained for other fuel and fuel/HSAHL mixtures, but are not shown to allow clarity. Typically, lower temperatures are used during FSI to minimize sintering of the sorbent which would decrease calcium utilization and SO_2 removal. The gas temperature at the FSI point was estimated to be about 1200°C. The temperature at the point of fuel injection was not measured during these tests. However, previous suction pyrometry data 41 cm from the burner tip for tests conducted on a Pittsburgh No. 8 coal at about the same firing rate as the present study indicated a temperature of 1250-1350°C. This suggests that the temperature difference between the two HSAHL injection points is not significant enough to affect SO_2 removal efficiencies.

The SO_2 removal efficiencies for Ca/S of 1.5 were about 52% and 66% for the coal and RTK blend fuels. The result for coal is comparable to the 50% SO_2 removal obtained with FSI of HSAHL in utility boiler tests [6, 7]. Figure 2 shows the general trend for all the samples tested in the IFR. The SO_2 removal efficiencies are greater for fuels which contain char blended with the coal. All types of chars tested enhanced the efficiency of SO_2 removal during tests. It is hypothesized that the presence of char moderates flame temperature, decreasing sintering of the sorbent, which leads to increased sorbent utilization. Ash samples collected downstream during tests using the RTK blend with and without injection of HSAHL contained about 10.8 and 5.5% carbon, respectively. It is difficult to explain the amount of residual carbon in the ash. The calculated residence time of the fuel in the heated zone (>900°C) was about 3.6 seconds with an oxygen concentration of at least 8%. Previous studies by the authors have shown that a char comparable to the RTK char achieved >90% carbon conversion at 1300°C in 6% oxygen for a residence time of 0.8 seconds [3]. The possibility that increased SO_2 removal for coal/char blends was due to incomplete char combustion was accounted for by assuming that the amount of sulfur released from the fuel corresponds directly to the amount of carbon consumed, and calculating the feed rate of fuel based on exhaust gas concentrations. The calculated feed rate was used to determine a predicted concentration of SO_2 in the gas based on analyses of the fuel. The SO_2 removal efficiency was then obtained as the difference between predicted and measured gas concentrations.

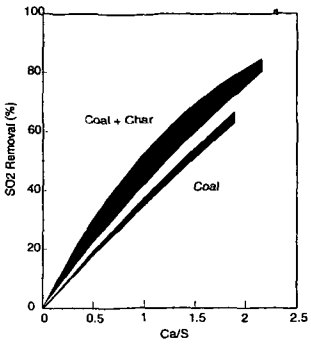

Figure 2. SO_2 removal efficiencies during IFR tests.

Figure 3 shows the emissions produced by combustion of selected fuels in the IFR. The coal produces about 4.4 lbs SO_2/MMBtu with no sorbent added. This is close to that predicted from fuel analyses (Table 1). The $CFCO_{HSAHL}$ and $CFCO_{COMHYD}$ (not shown) blends exhibit emissions similar to that for the parent coal. Due to the presence of sorbent during char preparation, the sulfur released from the coal is retained as CaS and concentrated in a smaller sample (by weight). The total sulfur content of fuels is determined at 1400°C in 100% oxygen, which decomposes the $CaS/CaSO_4$ present, allowing the entire amount of sulfur in the sample to be determined. However, in the IFR, the lower temperature (1200°C) and much shorter residence time mean that the decomposition of $CaSO_4$ is much less significant, and that sulfur present as $CaS/CaSO_4$ is not released. Since SO_2 removal efficiencies are based on total sulfur measurements, the calculated SO_2 removal efficiencies for the CFCO blends are higher than for coal (Figure 2), but because of the increased sulfur content of the blends, the overall emissions are similar.

The RTK blend and coal exhibit emissions of about 1.3 and 2.1 lbs SO_2/MMBtu at a Ca/S of 1.5 (Figure 3). This is true whether FSI is used or the sorbent is physically mixed with the samples prior to combustion. A series of tests was also done by replacing 10% of the higher heating value of the RTK blend with methane. Surprisingly, although the Btu value attributed to the methane would not be expected to have any sulfur associated with it, the RTK blend exhibits the same emissions with or without methane. The results in Figure 3 suggest that under the conditions present in the IFR, the best method of those studied to reduce the emissions of high-sulfur coals to year 2000 levels of 1.2 lbs SO_2/MMBtu would be to blend the coal with a low-sulfur char, then mix a calcium-based sorbent with the blend at a Ca/S of about 1.5.

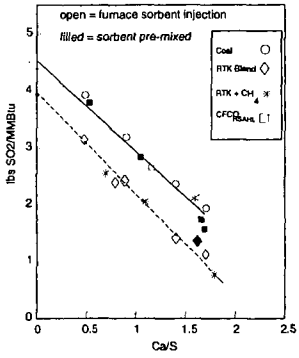

Figure 3. Emissions of fuels in IFR.

Samples tested at UNDEERC for ash deposition characteristics were IBC-102 (coal), the RTK blend and the $CFCO_{HSAHL}$ blend. The initial slagging temperatures (IST) were 1255°C for the coal, 1275°C for the RTK blend, and 1220°C for the $CFCO_{HSAHL}$ blend. The increase in IST for the RTK blend reflects the increased amount of silicon-rich species found in the deposit by scanning electron microscopy point count (SEMPC) analysis [14]. The high calcium content of the $CFCO_{HSAHL}$ blend accounts for its low IST. The deposit morphology also shows the $CFCO_{HSAHL}$ blend slagging deposit to be sintered into a nearly amorphous mass, as compared with the coal and RTK blend deposits in which individual ash particles are discernable.

Deposit growth factors for the coal and char blends were determined under both fouling and slagging conditions. Under slagging conditions, growth factors were 0.53, 0.61 and 0.64 for the coal, $CFCO_{HSAHL}$ blend and RTK blend. Under fouling conditions, growth factors were 0.46, 0.53 and 0.61 for the coal, $CFCO_{HSAHL}$ blend and RTK blend. Both blends form deposits more rapidly than the parent coal. Crush strengths of fouling deposits were 10, 29, and 0.2 psi for the coal, $CFCO_{HSAHL}$ blend and RTK blend, respectively. The high calcium content of the $CFCO_{HSAHL}$ blend, which formed a well sintered, dense deposit, accounts for its high crush strength. The RTK blend ash deposit, with more silicon-rich species and higher IST, is less consolidated than either the $CFCO_{HSAHL}$ blend or coal deposits. Although the RTK blend had the highest growth factor, the fouling deposit had a very low crush strength, indicating that it should be easily removed by soot-blowing. Conversely, the $CFCO_{HSAHL}$ blend fouling deposit had a crush strength three times that of the parent coal, indicating that the deposits will be quite consolidated and probably difficult to remove.

Behavior of the three fuels and their resultant deposits was predicted based on chemical composition data. Viscosities of the liquid phases expected to be present in each fouling deposit at 1200°C were calculated from the SEMPC results. The $CFCO_{HSAHL}$ blend deposit contained the greatest proportion of low-viscosity material, indicating a greater tendency to flow at 1200°C. The coal deposit and the RTK blend deposit had similar viscosity distributions, with less low-viscosity material than the $CFCO_{HSAHL}$ blend deposit sample. Thermal chemical equilibrium computational code that is utilized at UNDEERC to predict mineral phases and viscosities based on bulk composition data, was run for the coal and blends. The $CFCO_{HSAHL}$ blend ash exhibited a significantly lower viscosity at lower temperatures than the coal and RTK blend ashes, which are higher and nearly identical in viscosity. However, the predicted weight percentage of liquid phases in the $CFCO_{HSAHL}$ blend ash was very low at these lower temperatures, much lower than that of the coal and

RTK blend ashes. This presented two competing effects: higher-viscosity material present in significant amounts and low-viscosity material present in small amounts. However, the very-low-viscosity material present, coupled with the high ash content of the $CFCO_{HSAHL}$ blend ash, indicated that the deposition behavior would be significantly more severe than for the other two ashes.

Coal composition data were entered into an in-house EERC program that produces a fouling and slagging index. The chars were not evaluated with the program. The coal showed a potential for significant slag formation in the radiant section of a conventional PC boiler similar to that for other Illinois Basin coals. The magnitude of the index (85) is such that it may be controllable using standard remediation techniques, such as wall blowers. Severe slagging coals usually have values of 100-200. One of the main causes for the slagging potential of the ISGS coal is the high pyrite content. However, the potential for slag formation is not as high as it could be. In order to form a good low-viscosity slag, the iron from pyrite requires significant quantities of aluminosilicate clay material present, but the clay content of the IBC-102 coal is fairly low. The potential for high-temperature fouling, such as in the secondary superheater and reheater regions of the convective pass, and low-temperature fouling, such as in the economizer, should be low to nonexistent.

CONCLUSIONS

Based on results presented for the fuels in this study, the RTK blend would be the most attractive boiler feedstock because of its lower slagging and fouling potential and lower sulfur content. The best method to reduce emissions of high-sulfur coals appears to be to blend the coal with a low-sulfur char, then mix a calcium-based sorbent with the coal-char blend prior to combustion. Further studies are necessary to determine if the observed reduction in emissions by physically mixing sorbent prior to combustion is real, or an artifact of the experimental system. The results of that study would have direct implications whether to blend high-volatile, high-sulfur coals with lower-volatile, low-sulfur coals to reduce SO_2 emissions.

ACKNOWLEDGMENTS

This work was sponsored by the Illinois Department of Energy and Natural Resources through the Illinois Coal Development Board and Illinois Clean Coal Institute, and the United States Department of Energy. The assistance of Dr. Brian K. Gullett is greatly appreciated. Discussions with Dr. Carl Kruse and Dr. John Lytle were also insightful.

REFERENCES

1. Alvin, M. A., D. H. Archer and M. M. Ahmed, 1987. "Pyrolysis of Coal for Production of Low-sulfur Fuel." EPRI Final Report AD-5005, Project No. 2051-2.
2. Hackley, K. C., R. R. Frost, C-L. Liu, S.J. Hawk and D. D. Coleman, 1990. "Study of Sulfur Behavior and Removal During Thermal Desulfurization of Illinois Coals." Illinois State Geol. Survey Circ. #545, Champaign, IL.
3. DeBarr, J. A., M. Rostam-Abadi, R. D. Harvey, C. Feizoulof, S. A. Benson, and D. L. Toman, 1991. "Reactivity and Combustion Properties of Coal-Char Blend Fuels." Final Technical Report to the Center for Research on Sulfur in Coal. September, 1991, Carterville, IL.
4. Kruse, C. W., C. Chaven, H. P. Ehrlinger III, J. M. Lytle, L. B. Kohlenberger, D. M. Rapp and K. S. Vorres, 1992. "Illinois Basin Coal Sample Program." Final Technical Report to the Center for Research on Sulfur in Coal. September, 1992, Carterville, IL.
5. DeBarr, J.A., M. Rostam-Abadi, B.K. Gullett, and S.A. Benson, 1993. "Integrated Methods for Production of Clean Char and its Combustion Properties." Final Tech. Report to the Illinois Clean Coal Institute, 12/93.
6. Keen, R.T., C.C. Hong, J.C. Opatrny, T.M. Sommer, B.A. Folsom, R. Payne, and J.M. Pratapas, 1993. "Gas Reburning-Sorbent injection Demonstration Results." 1993 EPRI SO_2 Control Symposium, Volume 2: Sessions 5A, 5B, 6A, 6B, Boston, Massachusetts, August 24-27.
7. Miller, C.L., 1993. "Reduction of NO_x and SO_2 Using Gas Reburning, Sorbent Injection, and Integrated Technologies." Clean Coal Technology Topical Report No. 3, U.S. DOE
8. Maloney, D. J., R. G. Jenkins and P. L. Walker, Jr., 1982. "Low-temperature Air Oxidation of Caking Coals. 2. Effect on Swelling and Softening Properties." Fuel, 61(2), pp 175-81.
9. Oh, M. S., A. K. Burnham and R. W. Crawford, 1988. "Evolution of Sulfur Gases During Coal Pyrolysis." Paper prepared for submittal to American Ceramics Society Meeting, June 5-12, Toronto, Canada.
10. Khan, M. R., 1989. "Prediction of Sulphur Distribution in Products During Low Temperature Coal Pyrolysis and Gasification." Fuel, 68(11), pp 1439-1449.
11. Huang, E. T. K. and A. H. Pulsifer, 1977. "Coal Desulfurization During Gaseous Treatment." Coal desulfurization, ACS Symposium Series 64, Wheelock (ed.), pp 290-304.
12. Yergy, A. L., F. W. Lampe, M. L. Vetal, A. G. Day, G. J. Fergusson, W. H. Johnston, J. S. Snyderman, R. H. Essenhigh and J. E. Hudson, 1974. Ind. Eng. Chem, 13(13), pp 233-240.
13. Sinha, R. K. and P. L. Walker, 1972. "Removal of Sulphur from Coal by Air Oxidation at 350-450°C." Fuel, 51(4), pp 125-129.
14. Kalmanovitch, D.P., G.C. Montgomery and E.N. Steadman, 1987. "Computer Controlled Scanning Electron Microscope Characterization of Coal Ash Deposits." In: Presented at Joint Power Generation Conference, Miami FL, October: 1987, p. 87-JPGC-Fact-4, 8p.

REACTIVITY OF COLOMBIAN COALS TOWARD COMBUSTION

Rincón J. M. , Escallón M. , Baquero M. C., Moreno G. Ortiz P. and Diaz J. J.
Laboratorio de Investigación en Combustibles, *Departamento de Química*
Universidad Nacional, Bogotá, Colombia S.A

Keywords: Burning profile, Combustion behavior, TGA,Combustion coal blending

With the new world wide environment regulations, special attention is given to combustion efficiency in the electric utilities. Colombian coals are of cretaceous origen and the behavior towards combustion is different to the European and North American coals. The increase of international coal market has also created new power station operational problems in the areas of ignition, ash properties and residual carbon in ash (1) so the charaterization of coal toward combustion behavior is increasily important.. The study of pulverized coal char reactivity has been done by Drop tube reactor and Wire mesh tests. However these equipments are not common in most laboratories and easier methods must been suitable. Cumming (2) has done burning profile test to assessing the coal reactivity by DTG output from thermobalance system.. This combustion profile test has been subsecuently used by different authors (3)(4)(5)(6) as a method for characterization of coal burning properties. Pisupati (5) has found a good correlation between the Drop tube reactor test and the ignition temperature. Zhan (7) has also found that the reactivity estimated from the burn out measurement on stainless steel plate at 800°C and DTG technique in the higher temperature range match quite well.

The Martin del Corral Power Station localized near to Bogotá, is burning medium to low volatile coal and the fly ash carbon content is surprisingly high between 18-30%. The objective of the present work is to evaluted the reactivty profile of the coals used in the utility and to compare with the industrial test done in a boiler.

Experimental

Fresh samples of coals localized in the zone of influence of the Power Station were characterized and evaluated its combustibility by the combustion profile method using TGA non isotherm method.The differential thermogravimetric (DTG) test were carried out using a Perkin Elmer TGA equipment. About 5mg of pulverized sample, less than 75µm was spread into the crucible and the system was heated at a heating rate of 20 °C min^{-1} until 900 °C. A residence time at 120 °C for 5 minutes was fixed to permit the release of moisture. In the burnig profile, figure 1, three points can be clearly define; the initial temperature (IT) is defined as the temperature at which the rate of weigt loss excess 0.1% after the moisture peak., the peak temperature (TP) is defined as the temperature at which the rate of weight loss was a maximun and the burnout temperature (BP) is the temperature at which the rate loss decreased less than 1.0% min^{-1}.

FIGURE 1. COMBUSTION PROFILE

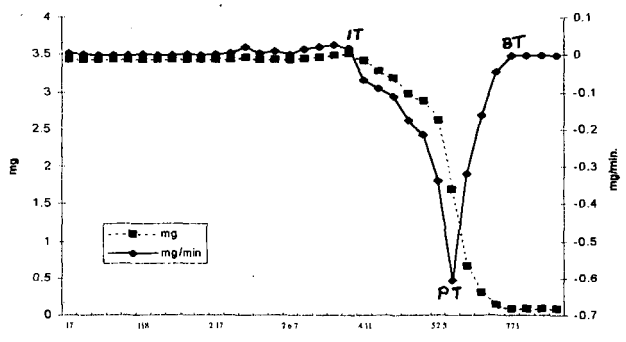

At the thermoelectric plant three coals were fired during the test in a 343.000 lb steam/h boiler. A tipical blend of the medium volatile bituminous coals a single low volatile bituminous coal and a single high volatile bituminous coal.

Results and discussion.

Table 1 shows the analytical data of the coal used. The rank of coal goes from low volatile to high volatiles bituminous C. Figure 1 shows a tipical burning profile of the coal used. The region of weight gains between 200-300°C indicates chemisorption of oxygen. Some peaks and shoulders observed before TP are believed to be due to quick release of volatile matter or to the evolution of trapped material into the macromolecular structure of coal.

In the burning profile, IT indicates the temperature at which start the evolution of small moities of organic matter and can be related with the rank of the coal used. Figure 2, shows that there is an increase of the IT as the rank of coal increases. The related curve has two breaks at 80%C and 87%C which correspond to the coalification jumps of the bituminous coals. Similar tendency can be observed for PT, figure 3. Not correlation was found for the BP. It is well known that the volatile matter content [VMC] is an indicative of the rank of coal and as expected a good linear relation with a 0.83 correlation factor, was found for the IT, as shown in the figure 4. The lower IT (297.10 °C) was found for the higest VMC (46.39%) while a IT of 348 °C was found for the lowest one (20.23%).

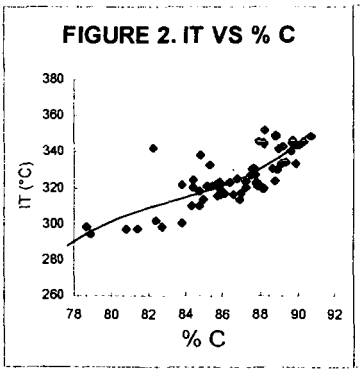

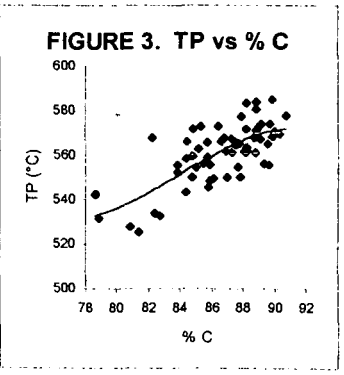

Pisupati (5) has found a good correlation betwen IT and the combustion efficience in an industrial scale demostration boiler. In this work a good correlation was found between IT and the VMC, indicating that it is a good index for study the behavior of coal during combustion and this criteria was used for the selection of the industrial test. Table 2 shows the analytical data of the coal used in the industrial scale test. The boiler efficience the three coals were: 80.89 for the coal with the lower VMC; 84.74 for the coal with the highest VMC and 83.70 for the industrial blend.

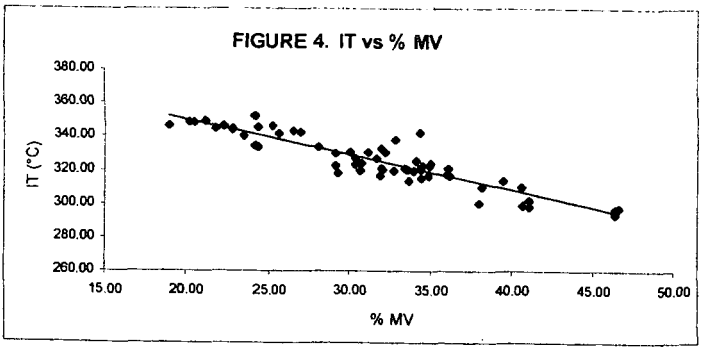

Table 1. Analytical data of the coal used.

Sample No	%H_20 (a)	%Ash (a)	%V.M (b)	%C (b)	%H (b)	%N (b)	%S (a)
1	0.89	8.05	30.35	86.39	5.49	1.83	0.81
2	1.02	10.03	30.68	87.25	5.60	2.00	0.92
3	0.85	14.12	34.14	86.79	5.63	2.25	0.89
4	1.94	6.90	32.71	88.21	5.71	2.04	1.17
5	1.22	4.55	22.77	89.65	5.00	1.78	0.58
6	0.97	12.82	25.60	89.02	5.31	1.96	0.45
7	1.40	14.48	21.81	88.21	4.97	1.64	0.35
8	1.40	5.15	22.38	89.71	4.62	1.77	0.51
9	0.95	3.64	23.50	89.56	5.08	1.80	0.69
10	0.90	20.51	33.55	84.43	5.92	1.79	0.88
11	1.04	22.61	34.33	82.28	5.53	1.96	7.15
12	1.10	25.87	35.04	84.40	5.86	1.93	1.47
13	0.93	9.64	36.12	85.46	5.83	2.05	1.24
14	0.80	20.67	32.78	84.82	5.65	2.08	4.34
15	1.04	5.96	32.16	88.68	5.63	1.82	1.03
16	2.24	9.30	46.63	80.80	6.31	1.79	1.33
17	0.99	4.76	18.99	90.31	4.71	1.71	0.44
18	1.14	8.37	38.13	84.77	5.89	2.01	0.76
19	1.16	12.84	34.51	85.70	5.67	1.93	1.59
20	0.96	5.53	24.31	89.87	5.19	1.87	0.45
21	0.79	13.24	29.17	88.89	5.64	1.99	0.79
22	0.68	5.70	24.32	88.20	5.27	1.86	0.65
23	1.18	14.92	40.61	84.36	6.05	1.91	0.68
24	1.48	10.86	41.02	82.42	5.85	1.76	1.84
25	1.11	13.14	34.41	83.84	5.71	1.88	2.06
26	1.16	11.10	39.42	84.99	5.82	1.80	0.99
27	2.26	18.52	46.39	81.42	6.46	1.75	1.64
28	2.61	14.09	46.43	78.90	6.31	1.79	2.98
29	1.88	19.72	40.66	78.66	6.02	1.67	0.59
30	0.92	21.57	29.31	84.78	5.86	1.86	1.10
31	1.12	15.81	36.01	86.96	5.93	1.94	0.39
32	2.15	5.54	41.06	82.74	6.03	1.79	0.81
33	0.92	16.24	33.40	85.18	5.79	1.87	0.93
34	0.85	12.18	34.40	85.68	5.70	2.15	1.09
35	0.68	21.23	25.27	87.91	5.17	1.66	2.04
36	2.26	3.33	38.03	83.83	5.79	1.82	0.52
37	1.03	9.03	34.83	86.11	5.71	2.00	1.10
38	1.26	6.06	36.16	85.88	5.76	1.82	0.70
39	0.76	20.50	24.17	88.23	5.17	5.97	1.20
40	0.98	6.33	34.42	87.27	5.55	1.89	0.49
41	1.08	5.48	34.91	85.84	5.66	1.92	1.02
42	1.29	7.82	31.99	87.85	5.55	1.86	0.65
43	0.93	11.52	29.16	87.79	5.60	2.00	2.03
44	1.18	4.77	33.98	85.82	5.70	1.85	0.71
45	1.57	4.70	33.62	86.88	5.54	1.93	0.48
46	1.09	6.08	31.69	87.70	5.59	1.87	1.03
47	1.35	5.45	31.91	86.60	5.52	1.92	0.44
48	0.70	6.42	31.16	87.62	5.52	1.93	0.65
49	0.96	4.86	32.01	88.05	5.65	1.83	0.89
50	1.01	3.75	31.99	85.31	5.38	1.90	0.53
51	1.13	6.18	30.02	87.57	5.47	1.87	1.21
52	0.86	10.13	26.96	89.18	5.46	1.97	1.14
53	0.95	5.14	30.38	87.49	5.61	1.83	0.81
54	0.90	4.72	30.71	88.77	5.46	1.90	0.45
55	1.17	3.96	30.66	88.14	5.41	1.72	0.39
56	0.78	5.09	28.04	89.11	5.45	1.75	0.71
57	0.66	4.28	26.57	90.04	5.31	1.75	0.55
58	0.98	9.96	21.21	88.84	4.93	1.79	0.49
59	0.81	7.78	22.80	89.87	5.11	1.75	0.50
60	0.70	4.18	24.16	89.31	5.08	1.72	0.45
61	0.73	7.68	20.53	88.87	4.83	1.78	0.50
62	0.79	4.69	20.23	90.71	4.73	1.70	0.53

Where:(a), as determined; (b), moisture ash free basis

Table 2. Analytical data of the coal used in the industrial boiler test.

Sample	%H_2O (a)	%V. M (a)	%Ash (b)	%C (b)	%H (b)	%N (b)	%S (a)
003	2.04	30.03	19.38	84.63	4.20	1.65	1.48
163	1.37	26.65	16.91	87.78	4.06	1.95	0.96
mixture	1.53	27.89	20.12	85.55	4.08	1.70	1.57

Where:(a), as determined; (b), moisture ash free basis

This results shows that when working with bituminous coal the VMC is a good approach for the design of the burning coal blend. To have high volatile coal in the blend is important since its ignition temperature is lower and it will be the first ones in burning, given full speed in the burning of the other coals.

Acknowledgments

This work was partly supported by FONIC (Ecocarbón-Colciencias) and EEB. This support is gratefully acknowledged

References.

1-Cai H. Y., Guell A. J., Chatzakis Y. N., Lim J. Y., Dugwell D. R., and Kandiyoti R.,Fuel 75, 15, (1996)
2-Cumming, J. W. Fuel, 63, 1436 (1984)
3- Smith S. E., Neavel R. C., Hippo E. J., and Miller R N, Fuel 60, 458 (1981)
4- Morgan, P. A., Robertson, S. D., and Unsworth, J. F., Fuel 65, 1546 (1986)
5- Pisupati S. V., Preprints 21th ACS National Meeting Vol 41 No1, 13 (1996).
6- Escallón M. M. Thesis, Quimico U.N (1996)
7- Zhang D., Wall T. F. and Tate A. G., Fuel 71, 1247 (1992)

A LABORATORY ASSESSMENT OF THE SLAGGING PROPENSITY OF BLENDED COALS

Nicholas J. Manton and Jim Williamson
Department of Materials, Imperial College of Science, Technology and Medicine,
London SW7 2BP, UK
and
Gerry S. Riley
National Power plc, Windmill Hill Business Park, Swindon SN5 6PB, UK

Keywords: boiler slagging, ash formation, CCSEM analysis.

ABSTRACT

This paper presents the results of an experimental study to assess the slagging propensity of blends of UK coals with world traded coals when burned under low NOx conditions. Coals ground to pulverised coal grade were blended in a laboratory mixer. Ash deposits were formed by passing the coals through an entrained flow reactor designed to simulate the time-temperature conditions which pulverised coal particles are subjected to in a large utility boiler. The deposits were collected on a ceramic probe at approximately 1250°C. The slagging propensity of the coal ash was assessed from a CCSEM chemical and microstructural characterisation of mounted and polished cross-sections of each deposit. The CCSEM data was used to obtain an estimate of the fraction of the deposit which would have been fluid enough for viscous flow sintering to have occurred, producing fused and bonded portions of the slags. The results indicate that the slagging propensity of a coal blend may be a non-linear function of the composition, showing both positive and negative deviations from a simple additive relationship. The findings are discussed in terms of the mineral matter transformations which occur in forming ash particles and boiler wall deposits.

INTRODUCTION

The efficient operation of modern pulverised coal-fired boilers is dependent on fuel quality, high conversion efficiencies and a high availability of plant. The nature and quantity of mineral matter in a coal can have a profound effect on the operation and performance of the boiler. Boiler slagging not only reduces the thermal efficiency of a boiler but can give rise to other problems, such as high exit gas temperatures leading to increased fouling of superheaters and economisers. The formation of large wall deposits on water walls and superheaters can lead to blocked ash hoppers and fractured boiler tubes.

Fuel technologists have long sought reliable methods for predicting the slagging propensity of a coal ash (1). Conventional methods of assessment based on ash fusion tests, viscosity of coal ash melts and empirical indices related to the chemical composition of the ash (2) all fail to reflect the complex mineral matter decompositions and reactions which occur at the combustion temperatures. In addition, the short residence times for ash particles within the burner region (1-2 sec) frequently do not allow the larger mineral particles to reach chemical equilibrium. Advanced microstructural analysis, combined with chemical analysis of individual ash particles obtained using computer controlled scanning electron microscopy (CCSEM), has demonstrated the diverse chemical nature of ash particles and the lack of chemical homogeneity (3). Thus, to obtain reliable data, fuel technologists have developed combustion test facilities which closely simulate the conditions in large pulverised coal boilers. The results obtained with these facilities still require validation with full scale boiler trials, as recently reported by Gibb et al (4). The cost of such trials, and the need to obtain objective assessments of the slagging propensity of a coal ash provided the stimulus for the design and construction of a laboratory entrained flow reactor (EFR) at Imperial College (5) to simulate ash formation and deposition phenomena.

The EFR was designed to closely simulate the conditions which pf and ash particles experience in large utility boilers. The reactor consists of a vertical multi-zoned furnace, approximately 5m in length, with an internal diameter of 100mm. Four independently controlled furnaces heat the reactor, providing a temperature gradient from 1650°C at the top of the reactor to 1200°C or less at the bottom. A series of sample ports at approximately 1m intervals down the length of the reactor allow ash and char samples to be withdrawn from the combustion atmosphere, or for deposition probes to be inserted . Pulverised coal is introduced at the top of the furnace at a rate of 50-200g hr^{-1}, the chosen feed rate largely depending on the ash content of the coal or blend under investigation. Gas flow rates of approximately 70 l min^{-1} (STP) , equivalent to 450 l min^{-1} at 1650°C entrain all particles with a density of 5 g cm^{-3} or less and a particle size of < 80μm. Under these conditions, particle residence times from top to bottom of the reactor are approximately three seconds. The reactor is shown schematically in Fig.1, with the position of the sample ports. Gas temperatures at the top sample port are approximately 1400°C and 1250°C at the second port.

Both air-cooled metal deposition probes and uncooled ceramic probes have been used to collect ash deposits. Deposits collected at 1400°C at the first port must be collected on a ceramic probe, as it has not been possible to provide sufficient cooling of a metal probe at this port to prevent the probe from melting. The deposits are generally of a highly fused nature and give little indication of the likely slagging propensity of the coal. However, when deposits are collected at 1250°C on an uncooled ceramic probe, they range from a thin covering of lightly sintered ash particles to well-bonded and coherent deposits, the nature of the deposit depending on the proportions of the mineral matter present in the coal. These deposits most closely resemble those which form on the platten superheaters of large utility boilers and are therefore suitable for characterisation.

The ceramic probe used in this study was of simple construction, consisting of a mullite tube or coupon, 16mm OD and 12.5mm ID, and 200mm in length. The coupon is held in place over a longer (approximately 1m) mullite tube of 12mm OD. The coupon is held in place with a small amount of a high alumina cement mixed with a sodium silicate solution. The same cement was used to block the open end of the 12mm tube, thus preventing gas leakage into or out of the reactor. An aluminium holder with an "O" ring seal is used to hold the probe in position in the sample port.

CHARACTERISATION OF DEPOSITS

Over a 1-2hr period, the deposits varied in thickness from 2-8mm depending on the ash content and mineral matter in the coal and the feed rate. A small sample of the deposit is first removed for X-ray powder diffraction analysis to establish the crystalline phases present, while the remainder of the deposit is left undisturbed on the coupon. The deposit is then coated in a low viscosity epoxy resin, which penetrates the open porosity of the sample, but when set gives stability to even the most fragile deposits. Sections through the deposit are cut with a diamond saw, perpendicular to the surface, to give samples approximately 5mm in length. These samples are then set in resin blocks so that a cross-section through the deposit from the interface with the probe to the surface of the deposit may be examined. The samples are ground and polished to a 0.25μm diamond finish, and coated with carbon for SEM examination. At low magnification (10x) a series of backscattered images (BSI) is first obtained to give an overall view of the microstructure of the deposit. More detailed examination is then made of selected areas at higher magnifications, typically 50-100x. Quantitative chemical and image analysis data is then acquired using a Tracor Noran low element detector and Tracor Noran Voyager software. Typically, a chemical analysis is acquired using a 16x16 matrix of analysis points, giving 256 separate analyses. Quantitative EDS analyses are obtained from this data using Proza corrections. The porosity of the microstructure, which gives a strong indication of the amount of viscous flow sintering which has occurred, may be obtained from a grey scale digital image which differentiates between the ash and the resin (i.e. the filled pores) or from the fraction of analysis points reporting oxide analyses, where the criteria used for this are that analyses with $\Sigma(CaO+Fe_2O_3+Al_2O_3+SiO_2) > 80$wt% can reasonably be assumed to be an oxide particle. The chemical and microstructural data is collected from a number of areas within each section and from samples taken at intervals along the coupon length. Typically, the number of analysis points exceeds 1000, thus giving sufficient data for reliable statistical variations to be established.

An assessment of the slagging propensity of the ash is made by a consideration of the analysis and the chemical variations shown by the ash particles and the bonding phase(s). The four main oxides which make up the ash composition are CaO, Fe_2O_3, Al_2O_3 and SiO_2, and the chemical data may be analysed by normalising each ash composition to two ternary systems, i.e. CaO-Al_2O_3-SiO_2, and Fe_2O_3-Al_2O_3-SiO_2. Only those analyses where $\Sigma(CaO+Al_2O_3+SiO_2)$ or $\Sigma(Fe_2O_3+Al_2O_3+SiO_2)$ exceeds 80 wt% are taken, since the normalisation of compositions totaling less than this could lead to substantial errors. The data obtained may then be plotted on a ternary diagram, see for example Fig.2. Each plot shows not only the range of chemical compositions obtained by analysis, and thus the degree of chemical inhomogeneity in the sample, but also indicates the degree of interaction between the decomposed mineral residues, i.e. the clays (kaolinite and illites), pyrite, calcite, quartz etc.

The quartz and decomposed clays can be considered as relatively refractory materials at the combustion temperatures. Indeed, coals which contain only these minerals give few problems with regard to boiler slagging. Any ash which forms on the boiler walls is little more than a friable dust with no mechanical strength. Slagging problems arise if the mineral matter contains additional minerals such as pyrite (FeS_2), calcite ($CaCO_3$), dolomite ($Ca.Mg(CO_3)_2$), siderite ($FeCO_3$), and ankerite ($Ca.Fe(CO_3)_2$. Each of these minerals decomposes to give the respective oxide, which acts as a strong fluxing agent for the aluminosilicate phases, lowering both the liquidus temperature and the viscosity of the melt. On a mole for mole basis, FeO is a more powerful fluxing agent than CaO, since the Fe^{2+} ion is smaller in size than the Ca^{2+} ion, enabling the aluminosilicate anions to move over each other more readily. Aluminosilicate ash particles which

have been fluxed with either FeO or CaO, or both, have the potential to form sticky ash particles which will not only adhere to a surface (water wall or deposit) but will bond together the more refractory ash particles. Exactly how much FeO or CaO is required to form a sticky ash particle remains open to debate, but lower limits of 5-10 wt% would be considered a reasonable estimate. At higher concentrations of FeO or CaO, a reverse of the fluxing role of these oxides is observed. In the case of FeO, a solubility limit is reached, and the excess iron oxide is precipitated from solution in the form of iron oxide dendrites (magnetite or haematite). Ash particles with more than 50 wt% Fe_2O_3 are therefore more than likely to be mainly solid crystalline iron oxides and thus of relatively low slagging propensity. CaO, which itself is refractory oxide, lowers the liquidus temperature and the viscosity of aluminosilicates, with a maximum effect on coal ash compositions at 25-30 wt% of added CaO. Further increases lead to increasing liquidus temperatures and a reduction in the amount of liquid phase present (6). Ash particles with 40% or more of CaO may similarly be considered as non-slagging particles, at least in the early stages of the formation of deposits. An EFR slagging index has therefore been established by determining the fraction of ash particles which contain 10-50 wt% of Fe_2O_3, or 5-40 wt% CaO.

COAL BLENDS

Two UK power station coals (coals 1 and 2) were chosen for blending with a Colombian coal (coal 3), two US coals (coals 4 and 5) and a South African coal (coal 6). The ash content and ash composition for each of these coals is shown in Table 1. Coals were each ground separately to pf grade, i.e. 70% less than 75μm. The coals were then blended in a laboratory mixer in batches of 1-2 kg. Coal were dried at 110°C for several hours before feeding to the EFR for the ash deposition studies. Failure to dry the coals sufficiently resulted in uneven flow rates of pf from vibratory hopper, which in turn caused blockages of the pf in the water-cooled injection probe at the top of the reactor.

RESULTS AND DISCUSSION

The results of blending coal 1(UK) with coal 3(Colombian) are shown in Fig.3. In order to assess the sensitivity of the EFR slagging index, the CCSEM data has been analysed here using three sets of compositional limits in determining the fraction of ash particles which would be deemed to be of a fluxed nature and a low viscosity. The conditions chosen were as shown below.

Conditions	CaO (wt%)	Fe_2O_3 (wt%)
A	5-40	10-50
B	5-45	5-55
C	10-35	15-45

In all three cases, the variations in slagging propensity with the addition of coal 3 are similar, with initially an increase in slagging propensity which shows a significant positive deviation from a simple law of mixtures. Conditions B, which provide the widest compositional limits give the highest values for the EFR slagging index, while conditions C, with the narrowest range give the lowest values. Conditions C also show the smallest variations and thus the least sensitivity to compositional changes and related microstructural changes. Fig. 4 shows the variations in slagging indices obtained on blending the two UK coals with the overseas coals. In each case , major deviations were observed from a simple linear relationship between the slagging index and the blend composition. The data shown in Fig. 4 was obtained using the compositional limits A in each case. These conditions were chosen as giving the optimum measure of the compositional variations in each deposit. In each case, the addition of the overseas coal initially gave a marked increase in the slagging propensity, with a maximum value in the range 25-50 wt% of added overseas coal. Above 50 wt% of the added coal, the slagging propensity decreased, in two cases with negative deviations from a linear relationship.

In a blended pf, there are basically two types of mineral matter. Most of the adventitious mineral matter present in the original coal is liberated as discrete mineral particles during the grinding process, while the finely distributed inherent minerals remain within the coal particles. It is generally assumed that the discrete mineral particles exhibit little interaction during the ash formation processes, reacting only with other ash particles on deposition. Inherent minerals interact and coalesce during the combustion of the char and are responsible for the wide range of aluminosilicate compositions observed for ash particles. Synergistic effects between ash particles suggests that complex interactions between particles must occur, and these are most likely to take place following deposition to form the slag.

REFERENCES
1. Couch,G. " Understanding Slagging and Fouling in PF Combustion", IEA Coal Research IEACR/72, 1994.
2. Raask,E., " Mineral Impurities in Coal Combustion", Hemisphere Publishing Corp., Washington, 1985.
3. Wigley, F. and Williamson, J. in "The Impact of Ash Deposition in Coal-Fired Plants" ed by J. Williamson and F. Wigley, Taylor and Francis, Washington, 1994, pp 385-398.
4. Gibb, W.H., Jones, A.R. and Wigley, F. in "The Impact of Ash Deposition in Coal-Fired Plants" ed by J. Williamson and F. Wigley, Taylor and Francis, Washington, 1994, pp 3-18.
5. Hutchings,I.S., West,S.S. and Williamson. J., Engineering Foundation Conf. "Applications of Advanced Technology to Ash-Related Problems", New Hampshire, 1995, in press.
6. Williamson,J., West,S.S. and Laughlin,M.K., Fuel 72, 697, 1993.

Table 1 Coal ash compositions (wt%) and ash contents

Coals	1	2	3	4	5	6
wt% ash	9.8	16.0	8.6	8.7	8.5	14.8
SiO_2	41.9	56.0	63.5	50.0	48.2	40.7
Al_2O_3	24.3	26.4	19.9	25.6	21.1	32.7
Fe_2O_3	20.9	6.5	8.5	14.6	16.5	2.4
CaO	7.1	1.9	2.6	4.5	4.4	9.3
MgO	3.3	1.7	1.7	1.0	1.0	2.5
Na_2O	0.1	1.5	0.6	0.8	1.4	0.4
K_2O	1.0	4.0	2.2	2.0	2.2	0.7
P_2O_5	0.2	0.1	0.2	0.4	0.3	1.4
TiO_2	1.0	1.0	0.9	1.2	1.2	1.7
MnO	0.2	-	0.1	<0.1	-	-

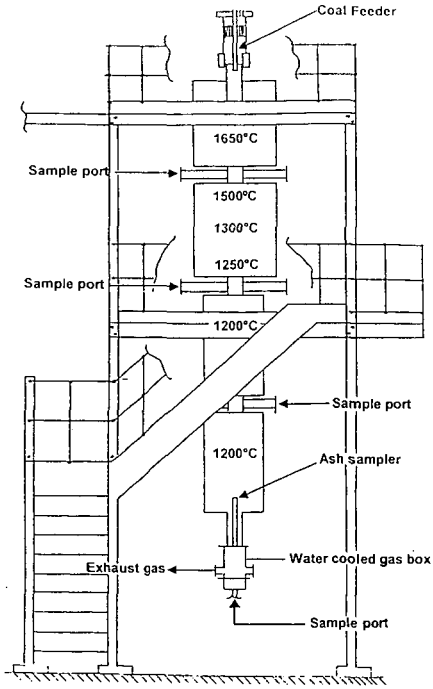

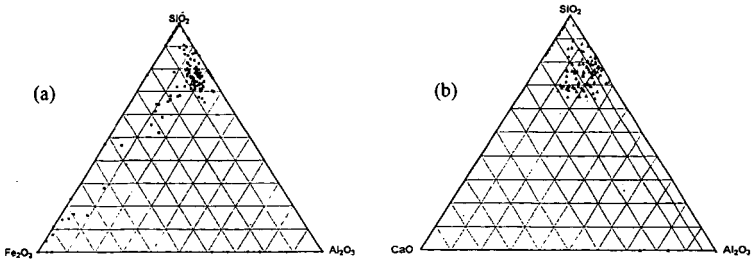

Fig. 2. Chemical inhomogeneity of slags as shown by EDS point analysis of polished cross-sections. Each composition has been normalised to (a) Fe_2O_3+Al_2O_3+SiO_2, and (b) CaO+Al_2O_3+SiO_2 for plotting. Shaded areas are compositions deemed to be slagging.

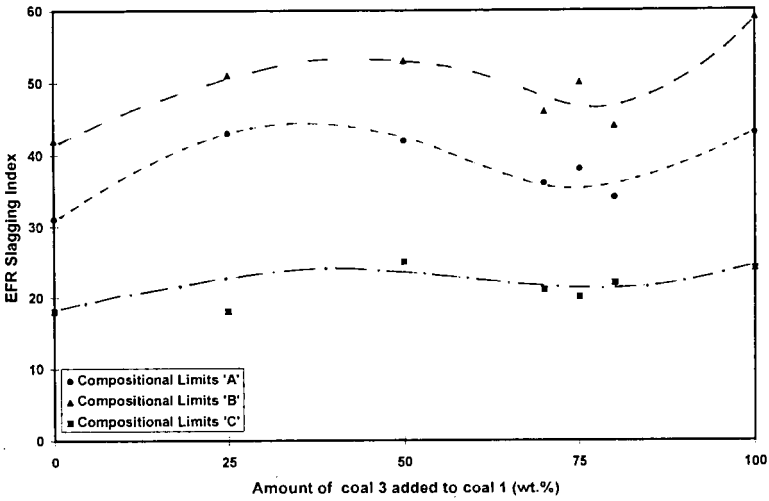

Fig. 3. Variation in EFR slagging index obtained with blends of coal 1(UK) with coal 3 (Colombian). Compositional limits A,B and C represent different concentrations of Fe_2O_3 and CaO in fluxed ash particles, see text for full details.

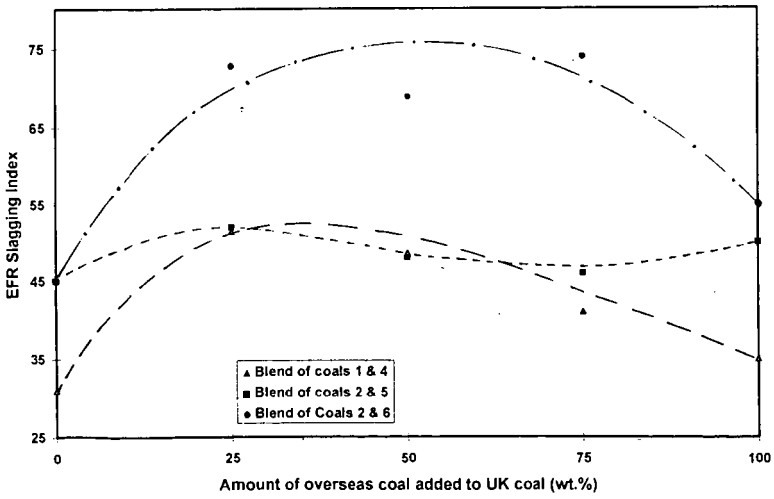

Fig. 4. EFR slagging indices for blends of UK coals 1 and 2, with overseas coals 4, 5 and 6.

CLASSIFICATION OF INDIAN COALS FOR COMBUSTION

V.GOPALAKRISHNAN,
Additional General Manager, Bharat Heavy Electricals Limited,
Tiruchirappalli - 620014, INDIA

DR. R. VASUDEVAN,
Director, School of Energy, Bharathidasan University,
Khajamalai Campus, Tiruchirappalli- 620024, INDIA

Key Words: "Indian Coals" "Classification" "Principal Component Analysis"

1. INTRODUCTION

In annual coal production India ranks fourth in the world, behind China, USA and Russia, with an estimated production of 225 million tons in 1995-96. The utilities burn nearly 60% of the mined coal while industries consume 25-30% of the coal for captive power generation and process heat. The remaining 10-15% goes for the production of coke and miscellaneous applications. Combustion is thus the most important use of coal in India or for that matter, anywhere in the world.

Countries like USA have national coal sample banks and databases. The Pennsylvania state (PENN) coal sample bank and database are well known, which are also used by the US Department of Energy(DOE). The Argonne National Laboratory has used 200 samples from the PENN coal database and using cluster analysis, has identified 8 representative samples among American coals. Similar exercises have been carried out by Illinois Coal Development Board, US DOE's Pittsburgh Energy Technology Center and several universities. The need for a similar coal data bank/database for India and the lack of it at present have been highlighted by Nandakumar and Gopalakrishnan (1988). Especially, for the design of combustion equipment, it will be highly helpful if one can come up with a set of typical Indian coals.

Classification schemes have similar objectives. However, a classification system meant exclusively for combustion applications or for Indian coals does not exist nor is it likely to be developed with the present approaches. Many classification schemes restrict themselves to two or three coal properties but the picture is not complete. If too many properties are involved, classification gets complicated and ends up as a coding scheme. In general, rank, calorific value, proximate and ultimate analyses, fuel and atomic ratios and petrography seem to be the most important variables for characterizing a coal's combustion behaviour. They are highly inter-related, as revealed in the literature. Is it possible to develop a classification system using all these properties and still achieve a reasonably simple grouping? Principal component analysis (PCA) offers a solution, under certain conditions.

2. PCA METHODOLOGY

Principal Component Analysis(PCA) consists of finding an orthogonal transformation of the original variables to a new set of uncorrelated variables, called principal components (PCs), which are derived in decreasing order of importance (Chatfield and Collins, 1980). The usual objective of the analysis is to see if the first few components account for most of the variation in the original data. If they do, then the dimensionality of the problem is reduced. With two PCs, plotting the values in a graph can reveal some patterns in the data.

To validate this proposition, a reference dataset, preferably non-Indian (to avoid biases) and fairly well structured, is needed. Hensel (1980) has used a reference table of US coals for studying combustion and classification and this table will be used for the comparisons. Leaving out lignite-B, of which there are no known reserves in USA or Canada, Hensel has selected eight to eleven coals for each of the remaining 12 groups in the ASTM ranks containing a total of 119 samples. The table contains the Calorific value (Cvd), proximate analysis (Fd and Vd) and ultimate analysis (Cd, Hd, Od, Nd, Sd) on a dmmf basis, to which F/V, C/H and CH/O will be added. Petrographic information is not available and hence is left out for the present exercise. Thus the table serves a dual purpose - it covers the entire spectrum of ranks (except lignite-B) and will serve as a good background for the Indian data. It will also help to compare the Indian and US coals.

The analysis can now be gone through in stages. First, one has to decide about the variables. Since Fd and Vd are complementary, one will do. The variables have to be standardised to have unit variance. The correlation matrix is computed next (Table-1). Of the 10 variables listed, Nd and Sd show poor correlation with the other variables. Nd and Sd are relatively outsiders and hence were left out of the analysis.

Table-1 Correlation matrix between variables

	Cvd	Fd	Cd	Hd	Nd	Sd	Od	F/V	C/H	CH/O
Cvd	1.00	0.71	0.89	−0.30	0.11	0.14	−0.95	0.30	0.40	0.71
Fd	0.71	1.00	0.93	−0.84	−0.34	−0.12	−0.85	0.74	0.84	0.93
Cd	0.89	0.93	1.00	−0.65	−0.16	−0.05	−0.97	0.63	0.73	0.90
Hd	−0.30	−0.84	−0.65	1.00	0.55	0.19	.51	−0.90	−0.96	−0.78
Nd	0.11	−0.34	−0.16	0.55	1.00	0.04	.04	−0.53	−0.53	−0.29
Sd	0.14	−0.12	−0.05	0.19	0.04	1.00	−0.13	−0.16	−0.17	−0.05
Od	−0.95	−0.85	−0.97	0.51	0.04	−0.13	1.00	−0.50	−0.60	−0.85
F/V	0.30	0.74	0.63	−0.90	−0.53	−0.16	−0.50	1.00	0.97	0.73
C/H	0.40	0.84	0.73	−0.96	−0.53	−0.17	−0.60	0.97	1.00	0.81
CH/O	0.71	0.93	0.90	−0.78	−0.29	−0.05	−0.85	0.73	0.81	1.00

The eigen values of the reduced correlation matrix are calculated (Table-2).

Table - 2 Eigen values

	1	2	3	4	5	6	7	8
value	6.26	1.41	0.17	0.09	0.03	0.02	0.01	0.00
%	78.24	17.64	2.17	1.13	0.37	0.29	0.12	0.04
cumulative%	78.24	95.88	98.06	99.19	99.56	99.84	99.96	100.00

The first two eigen values alone are significant and account for nearly 96% of the information. The eigen vectors were next worked out and used to transform the variables to principal components (PC). The PCs corresponding to the first two eigen values for all the samples were plotted in a graph (Figure-1a). **Alphabets are used as symbols and follow the rank**. Thus 'A' refers to meta-anthracite and 'L' refers to lignite-A.

This curve is comparable to the Seyler graph in the sense that with two (pseudo) properties, it enables one to compare several coals. It has in fact captured the essence of all the eight chosen coal properties. The clustering of coals of the of same rank is clearly visible in the figure as also the smooth transition from meta-anthracite at one end to the lignites at the other end. Anthracites and low volatile bituminous coals fall on one side. The high volatile coals and lignites fall on the other side. The medium volatile bituminous coals are near the peak. **This is a new discovery and has not been reported in literature so far.** The graph does not change if mean values alone are used (Figure-1b)

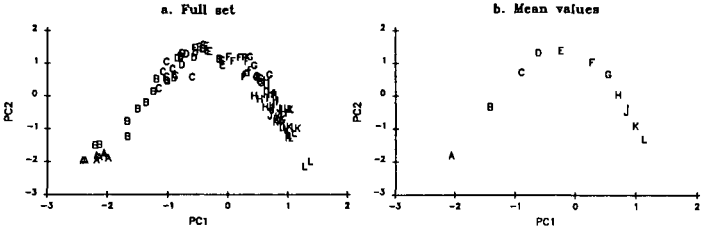

Figure - 1. Principal Components - ASTM Coals

To explore the relationship between PCs and the variables, PC1 and PC2 were plotted against the other variables. The graphs display a rank based continuity and the inescapable conclusion is that the PCs represent the rank in essence. Variation of Cv, Cd and F/V with PCs alone are shown to illustrate the point (Figure- 2 & 3).

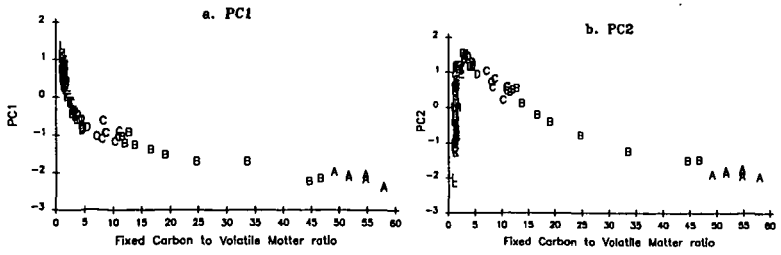

Figure - 2. Principal Components and Fuel Ratio

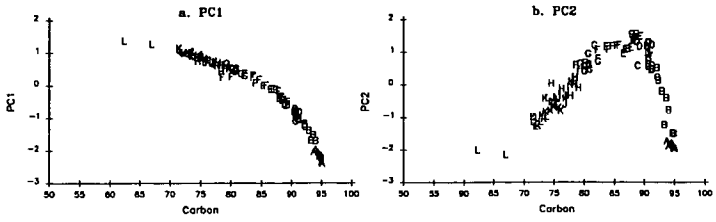

Figure - 3 Principal Components and Carbon

To explore the matter further, the correlations between the original variables and PCs were worked out (Table-3). PC1 is well correlated with all the variables. PC2 however correlates well only with Cvd, Hd, Od, F/V and to some extent with C/H. Significantly, PC3 and the rest show poor correlation with the variables, justifying PCA

Table - 3 Correlation matrix between variables and PCs

	PC 8	PC 7	PC 6	PC 5	PC 4	PC 3	PC 2	PC 1
CV	0.00	0.01	-0.04	0.12	-0.03	-0.11	0.65	-0.74
Fd	0.01	-0.01	-0.09	-0.05	-0.10	0.19	0.01	-0.97
Cd	-0.02	0.07	0.03	-0.07	-0.04	-0.03	0.29	-0.95
Hd	0.02	0.02	-0.05	-0.07	0.11	-0.14	0.50	0.84
Od	0.00	0.06	-0.06	0.06	0.02	0.07	-0.46	0.88
F/V	-0.02	-0.01	-0.06	-0.02	0.07	-0.25	-0.51	-0.82
C/H	0.04	0.02	0.04	0.02	-0.03	-0.10	-0.43	-0.89
CH/O	0.00	0.00	0.01	0.02	0.25	0.17	0.05	-0.95

After a few trials, it was realised that there was a good correlation between PC2 and Hd-Od/8 (HO/8) as well, which appears in the Dulong formula and which can be taken as a measure of the free hydrogen in coal. So, taking HO/8 as an additional variable, step-wise regression analysis between the PCs and the rest of the variables including HO/8 were carried out. The summarised results are presented in Table-4.

Table-4 Step-wise regression analysis

PC1		PC2	
Variable	Multiple Correlation	Variable	Multiple Correlation
Fd	0.971	HO/8	0.956
F/V	0.982	Cvd	0.967
Cd	0.997	F/V	0.999

Function1 = 0.1560 x Fd + 0.1511 x Cd + 0.1317 x F/V
Function2 = 0. 2050 x HO/8 + 0.4603 x Cvd - 0.3621 x F/V

PCs were plotted against the functions which are made up from a combination of the variables appearing in step-wise regression (Figure- 4 a & b).

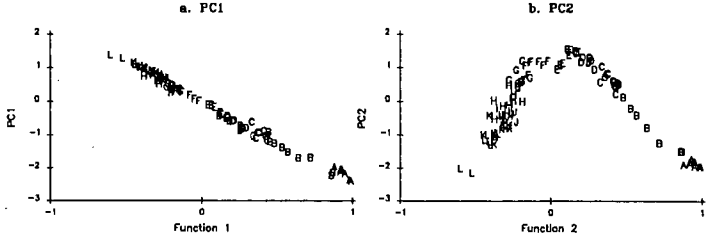

Figure - 4. Principal Components - Correlations

PC1 correlates very well with all the variables but seems to fit best with Fd and Cd. PC2 is highly influenced by HO/8. It is also related to Cvd and F/V to a lesser extent. PC2 vs Function2 resembles the graph PC1 vs PC2. It can be inferred that PC1 and PC2 probably represent Fd/Cd and the available hydrogen. Stated in a different way, it can be inferred that they represent the char and the volatile matter in coal. To probe further into this matter, Seyler's graph was plotted for the original data (Figure-5a) and a modified Seyler's graph was drawn using **Hd-Od/8** (HO/8) instead of Hd (Figure-5b). The shape of the graphs obtained clearly demonstrate that this is the **missing link between the original Seyler graph and the PC graph.** This brings the PCA to an end.

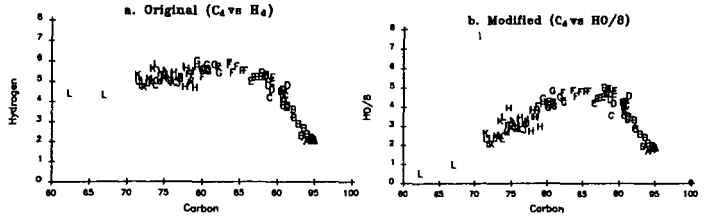

Figure - 5. Seyler Graph - ASTM Coals

3. PCA FOR INDIAN COALS

Twenty major Indian coal fields, based on their reserves were chosen and a statistical sample consisting of nearly 400 records was chosen from the publications of Central Fuel Research Institute's publications (CFRI,1978). The mean properties alone are given in Table-5 for each of these fields.

Table-5 Indian Coals - mean values

Field	Sym bol	Cvd	Fd	Cd	Hd	Nd	Sd	Od	F/V	C/H	CH/O	Reserve Million Tons	% to Total
Bisrampur	○	7913	65.7	82.9	4.7	1.6	0.5	10.2	1.9	17.6	9.1	520	0.3
Bokaro	+	8565	70.4	88.2	5.0	2.0	0.6	4.5	2.4	17.7	19.3	9701	5.5
Godavari	⊠	7879	62.0	81.8	4.9	1.7	0.4	11.2	1.7	16.7	7.8	10771	6.1
Ib-River	⊕	7936	62.5	82.8	4.8	1.6	0.5	10.3	1.7	17.2	8.6	20757	11.7
Jharia	▽	8723	74.2	90.1	4.8	2.1	0.6	3.1	3.0	18.7	20.8	19417	11.0
Kamptee	△	7547	62.6	79.9	4.6	1.6	0.3	13.6	1.7	17.4	6.3	1372	0.8
Korba	⧖	7884	63.7	82.8	4.8	1.6	0.5	10.2	1.8	17.4	8.8	8021	4.5
N. Karanpura	▽	8049	63.8	84.1	5.0	1.9	0.7	8.1	1.8	16.8	11.7	13578	7.7
Pench-Kanyan	⧓	8437	63.6	86.0	5.3	1.9	0.5	6.4	1.7	16.1	14.9	1955	1.1
Rajmahal	□	7520	58.9	78.9	4.8	1.7	0.6	13.9	1.4	16.6	5.3	10404	5.9
Ramgarh	⬡	8326	63.0	85.2	5.3	1.9	0.6	7.0	1.7	16.2	11.7	970	0.5
Raniganj	⋎	8090	58.8	82.1	5.4	2.1	0.4	9.8	1.4	15.2	8.6	27245	15.4
Singarauli	⧗	7606	60.6	79.8	4.9	1.6	0.6	13.2	1.5	16.4	6.3	9207	5.2
Sohagpur	⍓	8181	65.2	84.4	5.0	1.8	0.5	8.3	1.9	16.9	11.0	2145	1.2
S. Karanpura	⊠	7932	62.4	82.5	5.0	2.1	0.6	9.7	1.7	16.3	8.4	5148	2.9
Talcher	✳	7831	57.7	80.8	5.3	1.7	0.5	11.7	1.4	15.4	7.3	23547	13.3
Wardha	×	7493	59.5	78.7	4.7	1.7	0.4	14.4	1.5	16.6	5.9	4212	2.4
Others	⍒	7772	63.5	81.8	4.7	1.7	0.5	11.3	1.8	17.3	7.9	3700	2.1
Tertiary coals	☆	8226	65.9	83.7	5.3	1.3	1.9	8.2	2.9	16.1	15.5	862	0.5
Neyveli lignite	◇	6673	44.1	71.4	5.2	1.1	1.8	22.6	0.8	13.5	3.6	3300	1.9

A similar procedure(normalisation, calculation of correlation matrix, eigen values and eigen vectors) was carried out on the Indian coals. The first two eigen values accounted for more than 90% of the variance (after removal of Sd and Nd). The analysis was carried out on an air-dried basis as well as on a dmmf basis on the 390 random values as well as the 20 mean values. PCs for the Mean values alone are plotted in Figure-6.

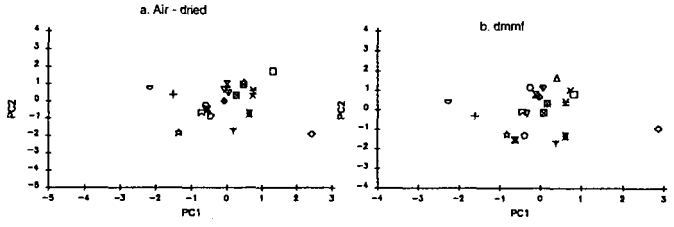

Figure - 6. Principal Components - Indian Coals - Mean Values

Jharia and Bokaro coals and the lignites stood out in both the cases. Rajmahal and tertiary coals looked different on air dried basis but came closer to the other coals on a dmmf basis. It means that their ash and moisture contents are significantly different from the rest. The rest of the samples, in both cases, fell into one small patch. A finer grouping has been done using cluster analysis but that is outside the scope of the present paper. The rest of the analysis and the results were similar to that of the US coals.

4. COMPARISON OF US AND INDIAN COALS

The Indian and US coals were analysed together next. It is worth stressing again that the US data covers almost all the (ASTM designated) ranks and hence serves as a

good background. Comparisons are done at two levels- 119 US samples against the 390 Indian random samples at one level and the 12 US (rank-wise) mean values against the 20 Indian (field-wise) mean values at the other level. The same procedure was adopted and the PC graphs are shown in Figure-7. The graphs are exactly similar to Figure -1a and 1b.

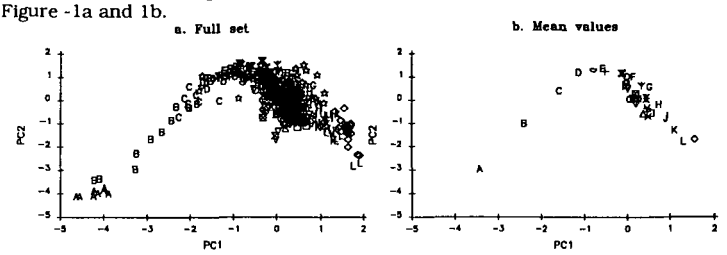

Figure - 7. Principal Components - US and Indian Coals

The 390 Indian samples fall into a small black patch in Figure-7a. A few lignite samples and Tertiary coal samples alone are visible in this graph. In Figure-7b, the Indian lignites fall with the US lignites. Bokaro and Jharia coals have the highest rank among Indian coals. Indian coals fall below the main line for the lower ranks.

The original and modified Seyler graphs were plotted for the 32 mean values (Figure - 8a and 8b). The Indian fields lie below the main graph which dips to the left. The higher oxygen content of Indian coals leads to a corresponding reduction in carbon and hydrogen contents.

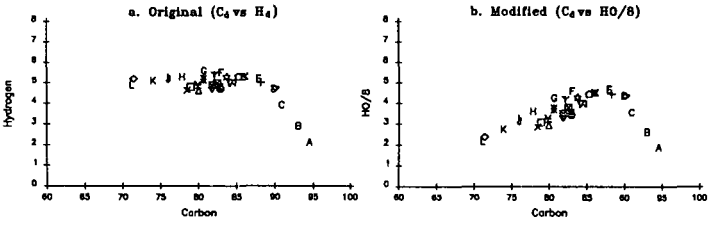

Figure - 8. Seyler Graph - US and Indian Coals - Mean Values

6. CONCLUSIONS

A graph of the principal components can be the new Seyler's graph for coal classification. The PCs seem to represent the rank. The graph shows a peak for the middle ranks. PC1 correlates best with Cd (and Fd) and PC2 with 'Hd- Od/8' (and Vd). PC1 and PC2 seem to represent the carbon and the available hydrogen in coal or broadly, the char and the volatiles of the coal. Among Indian coals, Jharia, Bokaro / Rajmahal/ Tertiary coals/Lignites look different and the rest show little variation. Cluster analysis can reveal a finer distinction.

The PCs are pseudo variables and not physical quantities. The choice of the variables is critical. The graphs at this stage can be used for comparative analyses. The stress is on methodology and the analysis can be repeated for other combinations of variables. There is a good potential for further research.

BIBLIOGRAPHY

CFRI (1978) INDIAN COALS (Volumes 1-8), Central Fuel Research Institute, P.O. Fuel Research Institute, Dhanbad Dt. 828108, Bihar, India

Chatfield C, Collins AJ (1980) INTRODUCTION TO MULTIVARIATE ANALYSIS, Chapman and Hall Ltd, 11, New Fetters Lane, London, EC4P 4EE 246 pp

Hensel R P (1980) COAL CLASSIFICATION, CHEMISTRY AND COMBUSTION : Coal-fired industrial boilers workshop, Dec 10-11, 1980, Raleigh, North Carolina, USA

Nandakumar K, Gopalakrishnan V (1988) TOWARDS A COMPUTERISED DATA BANK FOR INDIAN COALS All India seminar on Coal Technology, The Institution of Engineers, India and Bharat Heavy Electricals Limited, Tiruchi, India 16-17,Sep 1988 I2.01-2.14

ACKNOWLEDGEMENT

The author wishes to thank the management of Bharat Heavy Electricals Limited, Tiruchirappalli, for permitting him to present the paper.

INFLUENCE OF MACERAL COMPOSITION IN THE COMBUSTIBILITY OF SOME COLOMBIAN COALS.

Rincón J. M., Valderrama G*. and Viasus J.
Laboratorio de Investigación en Combustibles, Departamento de Química
Universidad Nacional, Bogotá, Colombia S.A

*INGEOMINAS, Bogotá, Colombia

Keywords: Combustion, Macerals concentrate, TGA, buning profile.

The increase of international coal market has created new power operational problems and the need to reduce the carbon levels in ash below around 6% in order to render the pulverized fuel ash saleable as well as mantain the combustion efficieny (1).

Compared with the Northern hemisphere coals, many Gondwana coals contain high levels of maceral of the inertinite group. The inertinite maceral group is commonly regarde as the main source of unfused chars (2) and this can increase problems with carbon carryy-over in the fly ash, leading to less overall efficience and cost are incurred in its disposal.

Since coal is a very heterogeneous material consisting of different organic substances (macerals) and mineral matter to know the behavior of the different macerals in the combustion is important. The propose of the present work was to investigate the influence of maceral association in the burning profile of coal.

EXPERIMENTAL

Three samples of coal were crushed and analized by conventional ASTM method. The elemental analysis were carried out using Leco CHN-600 equipment and sulfur determinator Leco SC-132 equipment.

The demineralization of the coals were done by HF/HCl digestion as described by Radovic et al, (3). The demineralized sample were separated into different fractions using density gradient separation. The coal was placed in a vessel filled with density-gradient aquous CsCl ranging from 1.0-1.6 g/ml at 25°C. The density gradient method was developed using a glass colum of 1.5cm of id by 50 cm long. as show in the Figure 1. The solution was added into the column handly with care to avoid mixture. The order of addition was first the solution with the higher density in the sequence shown in the Figure 1.

Sample of 0.1-0.3 g of the demineralized coal was mixed with 0.5ml of Brij-35, a non ionic surfactant, as described by Dyrakacz and co-workers (4). The mixed sampled is fixed at the top of the colum with care and left for 90 minutes to permit the diffusion of the coal macerals according to their specific density. After the maceral separation the samples were filtered and the solution density was measured by refractometry index. Finally the coal sample were washed with destillated water and the maceral concentration was essesed using a microscop Leitz MPV-SP.

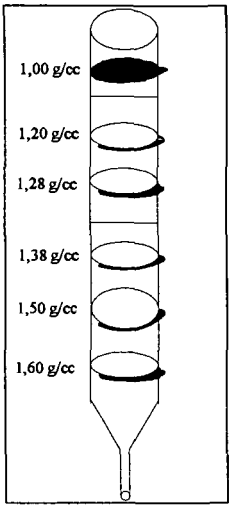

The combustiblity profile of the coals and macerals concentrated were done according to the method described in previous work (5). About 5mg of pulverized sample, less than 75μm was spread into the crucible and the system was heated at a heating rate of 20 °C min^{-1} until 900 °C. A residence time at 120 °C for 5 minutes was fixed to permit the release of moisture. Three points can be clearly define; the initial temperature (IT) is defined as the temperature at which the rate of weigt loss excess 0.1% after the moisture peak., the peak temperature (TP) is defined as the temperature at which the rate of weight loss was a maximun and the burnout temperature (BP) is the temperature at which the rate loss decreased less than 1.0% min^{-1}.

Figure 1: Sequence and density of the solution used.

RESULTS AND DISCUSSION

The analytical data of the coal used is presented in table 1. The samples belong to

Table 1. Analytical date of the coal used

Sample	H_20	Ash a)	V.M (a)	%C (b)	%H (b)	%S (b)	%V (a)	%E	%I	R_o
GB-093	3.07	11.98	39.80	82.28	5.88	1.81	58.7	21.0	18.3	0.64
GB-148	3.24	18.50	37.21	82.46	6.97	1.59	61.1	18.3	8.2	0.68
Cerrejon	8.30	1.51	41.38	81.40	6.01	0.87	78.6	6.8	11.7	0.60

Where:(a), as determined; (b), moisture ash free basis, V, vitrinite, E, exinite, I, inertinite; R_o, reflectance.

bituminous coals. The density of the solution can be estimated by the refractive index, the straight line equation that relates density (X) with the refractive index (Y) was Y=0.079747X + 1.2384 with a correlation factor of 0.9996 The exinite was concentrate in the lower density solution while the inertinite concentrate in the higher density solution, Table 2. For all the samples vitrinite was the easier maceral to concentrate and in Cerrejon the vitrinite concentrated was +99%. Exinite and inertinite were difficult to separate indicating that the agregate of this macerals are presented in very fine particle.

The combustibility as measured by the burning profile method and using the IT index (6) shows (Table 3) that the mineral matter content has a negative effect upon combustion for the first two samples but in Cerrejón sample the mineral matter present a positive influence indicating that the mineral matter in this coal acts as catalyst during the combustion process.

Table 2: Maceral concentration in the different density gradient .

Sample No	Density	Maceral concentration			
		%V	%E	%I	%MM
DGB-093	1.19	44.0	**48.0**	7.5	0.5
	1.27	**88.0**	8.0	4.0	--
	1.33	47.8	2.1	**49.5**	0.6
DGB-148	1.13	74.5	**23.5**	1.5	0.5
	1.26	**95.8**	2.1	1.6	0.5
	1.31	78.5	0.9	**20.0**	0.6
Dcerrejon	1.16	54.0	**39.0**	6.9	0.1
	1.23	**99.4**	0.3	0.2	0.1
	1.36	50.6	1.0	**48.2**	0.2

Where: D, demineriliz ed; % in volumetric; V, vitrinite; E, exinite
I, Inertinite.

Table 3 shows that exinite is the maceral easer to burn as shown by the burning profile peak index. The inertinite peacks shows that the burnout temperature is allways higher that the other two macerals and in the IT is also at higher temperature. According to this results the order for the combustibility facility of the macerals is: exinite>vitrinite>inertinite. The relative high concentration of inertinite in the Cerrejon coal may explain the operational problems that have been presented when using this coal directly in the utility it also conclude that some mineral matter is needed in this coal for better combustion.

Table 3. Combustion profile peaks of the origi coals, demineriliz ed coals and their maceral concentrates.

Sample	IT	PT	BT
GB-093	293.6	673.4	787.6
DGB-093	261.5	619.3	782.1
GB-148	311.1	685.1	815.0
DBG-148	275.7	629.9	821.1
Cerrejon	306.0	591.4	758.8
Dcerrejon	334.5	620.6	819.5
Exinite concentrate GB-093	221.5	578.2	737.1
Vitrinite conentrate GB-093	294.4	651.9	750.0
Inertinite concentrate GB'093	262.2	620.2	752.5
Exinite concentrate GB-148	217.0	571.2	671.4
Vitrinite conentrate GB-148	240.4	594.6	715.6
Inertinite concentrate GB-148	255.8	610	766.0
Exinite concentrate Cerrejon	285.3	571.5	521.2
Vitrinite conentrate Cerrejon	293.3	579.5	738.7
Inertinite concentrate Cerrejon	317.8	603.8	791.1

Where: IT, Initial temperature; PT, Peak temperature or temperature of maximun burning rate; BT, Burnout temperature; D, demineriliz ed coal.

It can be conclude that maceral composition has a great influence in the reactivity of coal. The order of reactivity found was exinite>vitirinite>inertinite. The contend of mineral matter has also a great influence in the combustibility parameters.

Acknowledgments

This work was partly supported by FONIC (Ecocarbón-Colciencias) and INGEOMINAS. This support is gratefully acknowledged

References.

1-Cai H. Y., Guell A. J., Chatzakis Y. N., Lim J. Y., Dugwell D. R., and Kandiyoti R.,Fuel 75, 15, (1996)
2- Thomas C. G., Shibaoka M., Gawronski E., Gosnell M. E., Brunckhorst L. F., and Phong-anant D., Fuel 72, 905 (1993)
3- Radovic, L. R., Wlaker P. L., and Jenkins, R. G. Fuel, 61, 209 (1983)
4- Dyrkacz G. R., Bloomquist C. A. A. and Ruscic, Fuel 63, 1166 (1984)
5- Escallón M. M. Thesis, Quimico U.N (1996)
6- Pisupati S. V., Preprints 21th ACS National Meeting Vol 41 No1, 13 (1996).

CHLORINATED ORGANIC COMPOUNDS EVOLVED DURING THE COMBUSTION OF BLENDS OF REFUSE-DERIVED FUELS AND COALS

Xiaodong Yang, John Napier, Brian Sisk, Wei-Ping Pan, John T. Riley, and William G. Lloyd

Materials Characterization Center
Department of Chemistry
Western Kentucky University
Bowling Green, KY 42101

Keywords: Thermal analysis, evolved gas analysis, refuse derived fuels

ABSTRACT

The objective of this study was to examine the possible formation of chlorinated organic compounds during the combustion of blends of refuse derived fuels (RDF) and coal under conditions similar to those of an atmospheric fluidized bed combustion (AFBC) system. A series of experiments were conducted using a TGA interfaced to FTIR and MS systems. Additional experiments using a tube furnace preheated to AFBC operating temperatures were also conducted. The combustion products were cryogenically trapped and analyzed with a GC/MS system. The chlorination of phenols and the condensation reactions of chlorophenols were investigated in this study. A possible mechanism for the formation of chlorinated organic compounds such as dibenzodioxins and dibenzofurans, by chlorination and condensation reactions involving phenols, was proposed.

INTRODUCTION

The amount of municipal solid waste (MSW) generated in the United States each year has risen to nearly 200 million tons. The amount of waste generated and the rapidly declining availability of landfill space has forced municipalities to evaluate alternative waste management technologies. Incineration of unprocessed MSW is an area of concern since polychlorinated dibenzodioxins (PCDDs) and polychlorinated dibenzofurans (PCDFs) have been reported as products of MSW combustion.[1]

Lindbauer and coworkers[2] reported that co-firing MSW with 60% coal drastically reduced PCDD/PCDF levels. Gullett and Raghunathan[3] found that sulfur hindered PCDD and PCDF formation even at a sulfur/chlorine ratio of 0.64. The mechanism thought to be responsible for the inhibition is as follows:

$$SO_2 + Cl_2 + H_2O \rightarrow SO_3 + 2HCl \qquad (1)$$

This mechanism, and several others that have been proposed, recognize the existence of molecular chlorine (and not HCl) as an important precursor to the formation of chlorinated hydrocarbons during combustion. Although the presence of molecular chlorine is thought to be a key starting material, the conclusive reports in the literature about the possible formation of PCDDs and PCDFs in combustion systems are often contradictory and confusing.[4]

In previous work TG/FTIR/MS studies of the organic compounds evolved during combustion of blends of coal and refuse derived fuels revealed the production of phenols, furans, and various other organic materials during the combustion of paper and other cellulosic materials blended with coals.[5,6] The production of molecular chlorine during the combustion of polyvinyl chloride was also observed. Phenol, furan, and molecular chlorine could provide the important precursors for the formation of PCDDs and PCDFs in combustion processes. TG/FTIR/MS studies done by Lu[5] showed that more hydrocarbons are evolved at a fast heating rate due to incomplete combustion. These studies indicated there is a greater likelihood for the formation of chlorinated organic compounds at the fast heating rates, due to the concurrent evolution of HCl (which may be converted to molecular chlorine) and hydrocarbons, especially aromatics. Thus, chlorinated organic compounds may be formed at high heating rates, whereas products such as organic acids and alcohols are generally observed at slower heating rates.

A mechanism being proposed for the formation of chlorinated organics and possibly PCDDs and PCDFs is given in equations 2-4:

$4HCl + O_2 \leftrightarrow 2H_2O + Cl_2$ (Deacon reaction) (2)

$C_6H_5OH + Cl_2 \rightarrow$ chlorophenols (3)

condensation of chlorophenols $\rightarrow$ PCDDs and PCDFs (4)

This paper reports results from a series of studies designed to prove, or disprove, this proposed mechanism.

EXPERIMENTAL

Apparatus and Reagents - The TG/FTIR/MS system consisted of a TA Instruments SDT 2960 Simultaneous DTA-TGA system interfaced with a Perkin-Elmer 1650 Fourier Transform Infrared Spectrometer and a Fisons Instruments model VG Thermolab Mass Spectrometer. A Shimadzu QP 5000 system with a NIST/EPA/NIH 62,000 compound database was used for the GC/MS analysis. A twelve-inch Sola Basic Lindberg tube furnace was used for the preheated tube experiments. Reagents used include MC&B reagent grade phenol, EM Scientific HPLC grade dichloromethane, while 2,4-dichlorophenol, 4-chlorophenol, 2-chlorophenol and dibenzofuran were 99+% grade from Aldrich.

To closely simulate conditions in an AFBC combustor, studies were conducted using a preheated quartz tube in the Lindberg tube furnace. The evolved gases were trapped in methylene chloride, concentrated, and analyzed using the GC/MS system. Combustion products of phenol and chlorophenols were also investigated. The detailed experimental conditions are outlined in the following paragraphs.

To examine the possibility of producing molecular chlorine via the Deacon reaction, as illustrated in equation 2, a mixture of air and 10% HCl in N_2 (air:HCl volume ratio of 2:1) was introduced into the quartz tube preheated to different temperatures in the tube furnace. The product gases were trapped in a phenol-methylene chloride solution and the solution analyzed for chlorophenols using the GC/MS system.

To examine the gas phase chlorination of phenol, as illustrated in equation 3, 100 mg portions of phenol were placed in a heated tube and evaporated in the presence of a constant flow 0.5% Cl_2 in N_2. Chlorination took place in the gaseous phase and the products were trapped in an aqueous solution of $NaHSO_3$, extracted by CH_2Cl_2, and analyzed using the GC/MS system.

The combustion of chlorinated phenols, which may lead to the reaction illustrated in equation 4, was examined by heating 100 mg portions of 2,4-dichlorophenol in the presence of air in the tube furnace. The combustion products were adsorbed by CH_2Cl_2 and identified using the GC/MS system. The reaction was also studied in a series of experiments in which 10 mg portions of 2,4-dichlorophenol were heated in air at a rate of 10°C/min in the TGA and the evolved gases were monitored (on-line) using the FTIR and MS spectrometers.

RESULTS AND DISCUSSION

The production of molecular chlorine by heating HCl in air followed by the chlorination of phenol in solution is an indication that the Deacon reaction (equation 2) takes place in the heated tube. Figure 1 shows the GC/MS results from these experiments conducted at different temperatures. The chromatograms indicate that the higher temperatures favor an increase in the production of chlorophenols. This indicates the Deacon reaction is favored at higher temperatures, which is consistent with thermodynamic calculations that show the Deacon reaction is favored above 590°C.

The gas phase chlorination of phenol (equation 3) experiments produced 2-chlorophenol, 4-chlorophenol, 2,4-dichlorophenol, 2,6-dichlorophenol and 2,4,6-trichlorophenol, as identified by NIST library matches and GC retention times of the pure materials. The chlorination of phenol began at temperatures around 250°C. At higher temperatures, dibenzofuran was produced. At still higher temperatures near 600°C, naphthalene was produced.

To examine the possible condensation of chlorophenols during combustion reactions, as is illustrated by equation 4, the compound 2,4-dichlorophenol was heated in air inside the tube furnace. The combustion products were trapped in methylene chloride, concentrated, and analyzed by GC/MS. Figure 2 shows examples of chromatograms for the combustion products. The products are indicated to be mainly 2,4,6-trichlorophenol, tetrachlorodibenzofuran, and dichlorodibenzodioxin, as identified by NIST library searches. The TG/MS experiments indicated the products of combustion include CO_2 (m/z = 44), H_2O (m/z = 18), HCl (m/z = 36) and trichlorophenol (m/z = 196), as is illustrated

by the mass spectra profiles shown in Figure 3. This profile also shows the formation of chlorinated hydrocarbons at relatively low temperatures, which begins around 200°C. The small amount of material used, the slow heating rate, and the 300 amu limitation of the TG/MS system made it impossible to observe any larger chlorinated hydrocarbon product in this particular experiment. FTIR analysis of the evolved gases confirmed the emission of CO_2, CO and H_2O, and HCl, as labeled on the three dimensional plot in Figure 4.

CONCLUSIONS

Based on the information presented in this paper summary statements that can be made include:

- The Deacon reaction for the production of molecular chorine is generally favored at temperatures over 600°C.
- The gas phase chlorination of phenol is generally favored at temperatures over 600°C.
- Tetrachlorodibenzofuran, dichlorodibenzodioxin, and other chlorinated organic compounds are formed during the combustion of 2,4-dichlorophenol.
- The proposed three-step mechanism appears to be a possible pathway for the production PCDDs and PCDFs in combustion processes.

ACKNOWLEDGMENTS

The financial support for this work received from the U.S. Department of Energy (Contract No. DE-FG22-94PC94211) and from the Huntsman Thermal Analysis Fellowship is gratefully acknowledged.

REFERENCES

1. Liberti, A.; Goretti, G.; Russo, M.V. *Chemosphere*, **1983**, *12*, 661.
2. Lindbaurer, R.; Wurst, F.; Prey, T. *Chemosphere*, **1992**, *25*, 1409.
3. Gullett, B.K.; Raghunathan, K. "The Effect of Coal Sulphur on Dioxin Formation", Final Technical Report for the Illinois Clean Coal Institute, Carterville, IL, 1993.
4. Purushothama, S.; Lloyd, W.G. "Organic Coproducts of Coal Combustion," *J. Coal Quality*, (in press).
5. Lu, H. "A Study of the Combustion of Coal with RDF Using Thermal Analytical Techniques," M.S. thesis, Western Kentucky University, December 1995.
6. Purushothama, S.; Lu, H.; Yang, X.; Hyatt, J.; Pan, W.-P.; Riley, J.T.; Lloyd, W.G. *Prepr. Pap.--Amer. Chem. Soc., Div. Fuel Chem.*, **1996**, *41(1)*, 56-61.

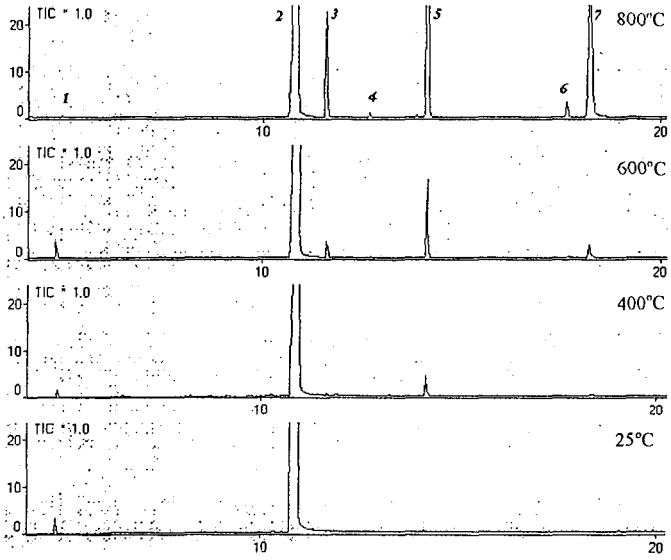

Figure 1. Chromatograms of the products from the reaction of HCl heated in air and trapped in a CH_2Cl_2 solution of phenol, concentrated, and analyzed by GC/MS. The MS assignments (NIST library matches) are as follows: 1 = cyclohexane, 2 = phenol, 3 = 2-chlorophenol, 4 = 2-chlorocyclochlorocyclohexanol, 5 = *trans*-1,2-dichlorocyclohexene, 6 = 2,4-dichlorophenol, and 7 = 4-chlorophenol.

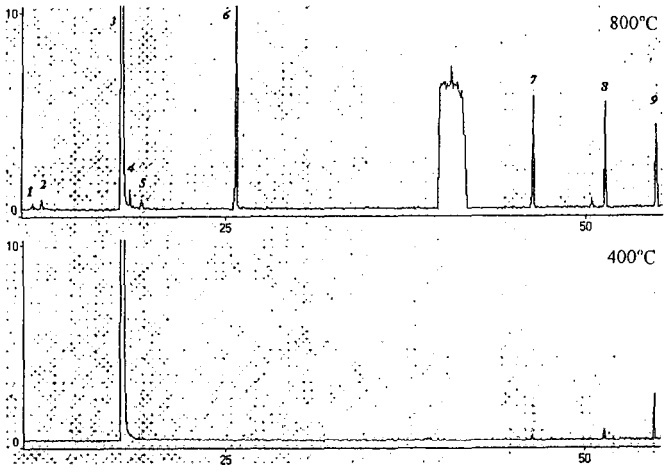

Figure 2. Chromatograms of the reaction products from the combustion of 2,4-dichlorophenol, which were trapped in CH_2Cl_2, concentrated, and analyzed by GC/MS. The MS assignments (NIST library matches) are as follows: 1 = 2-chlorophenol, 2 = dichlorobenzene, 3 = 2,4-dichloro-phenol, 4 = trichlorobenzene, 5 = 2,6-dichlorophenol, 6 = 2,4,6-trichlorophenol, 7 = dichloro-dibenzodioxin, 8 = trichlorodibenzodioxin, 9 = tetrachlorodibenzofuran.

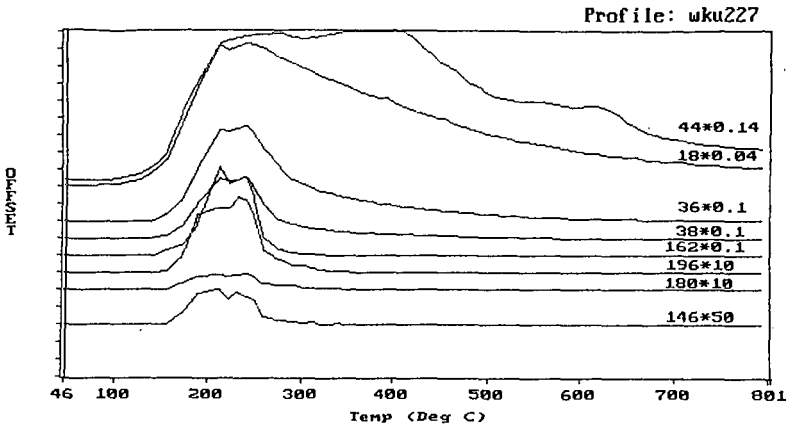

Figure 3. Mass spectra profiles for the combustion products of 2,4-dichlorophenol.

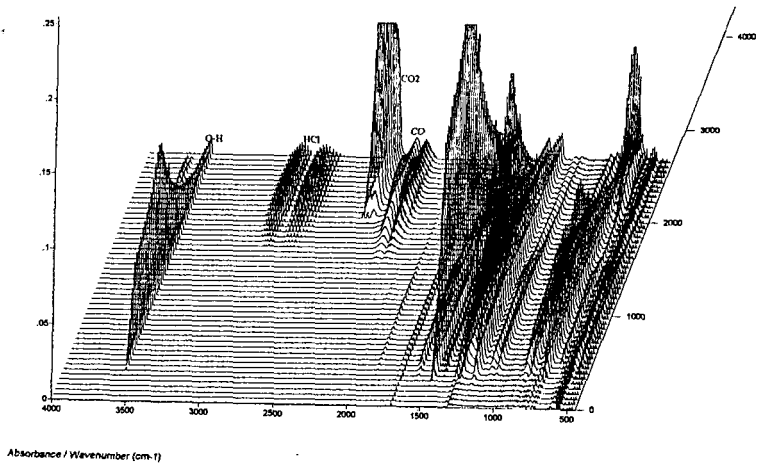

Figure 4. Three-dimensional FTIR spectra of the combustion products of 2,4-dichlorophenol.

COMBUSTION PROPERTIES OF COAL-CHAR BLENDS: NO_x EMISSION CHARACTERISTICS

Massoud Rostam-Abadi[1], Latif Khan[1], Joseph A. DeBarr[1]
L. D. Smoot[2], G. J. Germane[2], and C. N. Eatough[2]

[1]Illinois State Geological Survey, Champaign, IL 61820
[2]Advanced Combustion Engineering Research Center
Brigham Young University, Provo, UT 84602

Key words: Combustion, NO_x Reduction, Coal-Char Blend

INTRODUCTION

Nitric oxide formation in hydrocarbon flames occurs primarily through three mechanisms; thermal NO (the fixation of molecular nitrogen by oxygen atoms produced at high temperatures), fuel NO (the oxidation of nitrogen contained in the fuel during combustion), and prompt NO (the attack of a hydrocarbon radical on molecular nitrogen). Of these three mechanisms, fuel NO is by far the most significant source of NO in practical coal flames [1].

It has been suggested that NO_x produced early in pulverized coal flames is subsequently reduced to N_2 by char/NO_x interactions [1]. NO_x can be both produced and reduced by heterogeneous char reactions. For some cases, as much as half of the fuel nitrogen remains in the coal after devolatilization [2]. The amount retained apparently is a function of the reactor stoichiometry [3]. Heterogeneous NO_x often accounts for 20-30 percent of the total NO_x formed [4, 5, 6]. The exact amount appears to be dependent on the temperature and extent of devolatilization. The rate of heterogeneous NO_x reduction has been investigated by many researchers [1, 7, 8, 9]. Essentially, char reduction of NO_x begins only after oxygen is locally depleted in the reactor [10]. The heterogeneous destruction reactions have been determined to be significant in fuel-lean conditions for char combustion, but for fuel-rich coal combustion, the reduction reactions in the gaseous phase appears to control reaction rate [11]. CO enhances NO_x reduction due to surface catalysis of the NO/CO reaction [1, 7]. In the absence of CO, the char-NO_x reduction rate is controlled by the dual-site mechanism of absorbed NO_x [12]. In the presence of CO, the controlling step is the reaction of gaseous NO_x and absorbed NO_x at an active site to form N_2, CO_2, and an oxide complex. Water and O_2 were reported to inhibit the reaction due to the buildup of a chemisorbed layer of oxygen on the char surface [1,12].

The primary goal of this study was to investigate the concept of lowering NO_x emissions by co-firing pulverized Illinois coal with char in a practical flame. A summary of the results obtained is presented in this paper.

EXPERIMENTAL

Coal-Char Blends - A continuous feed charring reactor was used for producing char samples from an Illinois No. 6 coal (38% volatile matter, dry basis). Char samples were pulverized to 70% minus 200 mesh. Pulverized coal (70% minus 200 mesh) was mixed with either the char or powder activated carbon (Calgon Carbon Company) to prepare the following blends:

Blend 1: 125 pounds of 12.5% char - 87.5% coal
Blend 2: 500 pounds of 25% char - 75% coal
Blend 3: 125 pounds of 50% char - 50% coal
Blend 4: 125 pounds of 12.5% activated carbon-87.5% coal

Proximate and ultimate analyses of the fuels and pore area and pore volume of the coal, char, and activated carbon were determined.

Combustion Tests - Combustion tests were performed with the coal and blends in a 0.5-1.0 Mbtu/hr combustor located at Brigham Young University (BYU) Advanced Combustion Engineering Research Center (ACERC). The combustor, referred to as a controlled profile reactor (CPR), is a cylindrical, down-fired reactor with an inside diameter of 0.80 m and a length of 2.40 m [13]. The burner consists of a central fuel injection tube surrounded by a swirling annular jet of secondary air. The secondary air is preheated to about 500 F and passes through a moveable-block swirl generator capable of varying secondary swirl number from 0 to 5.

Thirteen combustion tests were performed. The first three test were to establish base combustion conditions of the coal only, with no char addition. Tests 4 and 5 were performed to investigate the in situ capture of SO_2 by a high surface area hydrated lime. The remaining tests were designed to determine the ability to reduce NO_x by the coal-char blends. In all combustion tests, effluent gas and solid samples were collected and analyzed.

RESULTS AND DISCUSSION

Properties of Coal-Char Blends- Table 1 compares the proximate analyses of the coal, char (mixture of all char samples ground to -200 mesh), and the blends. The volatile matter (VM) and H-T ash contents of the char were 16.2 and 16.7 wt% (dry basis) compared to 38 and 12.4 wt% for the coal. The VM contents of the blends ranged from 27.3 wt% for the coal-activated carbon blend to 35.6 wt% for the 12.5% char - 87.5% coal blend. As summarized in Table 2, sulfur and nitrogen contents and Btu/lb values of the coal and blends were comparable (3.17 to 3.41% S; 1.20 to 1.33% N; and 12,047 to 12,182 Btu/lb).

The nitrogen-BET pore area of the char was 15.7 m^2/g compared to 1012 m^2/g for the powder activated carbon, Table 3. The pore area of the coal was 18.8 m^2/g indicating that during charring some of the macropores were blocked or destroyed. Nevertheless, char should have micropore area of about 100-400 m^2/g. Micropore area is measured by CO_2 adsorption which was not performed in this study.

Combustibility of Coal-Char Blends- The combustion test matrix is shown in Table 4. Flame temperatures were recorded for the base test condition noted as test 1 and for tests 8-10, 12 and 13. An axial temperature profile was made during test 1. Peak centerline flame temperature was recorded at the 28 cm axial location. Therefore, subsequent characteristic centerline flame temperatures were measured during tests 8-10 and 12, 13 at the 28 cm axial location. The flame temperature measurements are shown in Figure 1.

The effect of char addition to the coal on carbon burnout is shown graphically in Figure 2. Carbon burnout increased with initial increase in percent char in the fuel and decreased slightly with additional char. Visually the flame was stable but became more detached from the burner and flickered at the highest char percentage. Volatile content of the fuel is important to flame stability and therefore burnout. By increasing the char content, the volatile content is decreased resulting in greater flame instability.

Figure 3 shows the measured increase in effluent NO_x concentrations with increasing combustion temperature for the combustion tests performed for this study. Effluent NO_x concentrations in combustion systems is known to increase with combustion temperature [14, 15] due mainly to the increase in thermal NO_x production.

Figure 4 shows the effect that increasing stoichiometry has on effluent NO_x values. Since conversion of fuel nitrogen to NO depends on the availability of oxygen atoms, an increase in effluent NO_x values with increasing stoichiometric ratio was expected. The reason for the stronger dependance noticed for the 0% compared with the 25% char case deserves further investigation.

In order to determine the effect of NO_x reduction on char surfaces during combustion, other NO_x producing or reducing factors must be accounted for. For example, if NO_x is noticed to decrease with increasing char in the fuel, is the effect due to the addition of more NO_x reduction sites on the char surfaces, or from the decrease in burnout and therefore release of fuel nitrogen, or from the decrease in flame temperature and subsequent decrease in the production of thermal NO_x. In coal combustion, fuel nitrogen is certainly the dominant source of NO_x [16]. Since it has been shown that fuel nitrogen evolves from coal particles at approximately the same rate as carbon is consumed [16, 17], the fuel nitrogen release and therefore production of fuel NO_x can be corrected for burnout. Thermal NO_x contributions can be subtracted from total NO_x if the temperature dependence is known. Previous natural gas combustion tests performed using the CPR provided thermal NO_x concentrations as a function of flame temperature [8]. This correlation indicates that only about 10% of the effluent NO_x values measured during these combustion tests originated as thermal NO_x.

Figure 5 shows the effect of increasing percentage of char in the fuel on effluent NO_x concentrations. In order to reduce other NO_x producing and reducing effects as much as possible, these NO_x values have been corrected for burnout as well as thermal NO_x. The trends show a slight initial increase in NO_x with addition of char in the fuel but subsequently NO_x decreases with additional char.

NO_x levels are shown to increase with addition of small amounts of char to the fuel stream. However, an almost linear reduction in NO_x values is noted with increasing char above 12.5%. The reason for the initial increase in NO_x values is not well understood. It is likely that the addition of char extends the reaction zone allowing for greater mixing of fuel and combustion air so that a greater percentage of fuel nitrogen is released in a more oxygen rich environment causing amine radicals to oxidize to NO rather than molecular nitrogen. This explanation is substantiated by the observation that the 12.5% activated carbon-coal blend produced slightly higher effluent NO_x levels than the 12.5% char-coal blend. The low volatile content of activated carbon, and hence, low reactivity, would cause it to lengthen the reaction zone to a greater extent than the addition of 15% volatile content char.

Establishing additional carbon sites by blending char with the coal in the feed stream, along with increasing the NO-carbon contact time, may enhance the effectiveness of the NO reactions. This may account for the measured decrease in NO with additional char. Additional near burner testing or modeling of the combustion system may provide insight into this phenomenon.

SUMMARY AND RECOMMENDATIONS

Blending char with parent coal may have some merit as a viable NO_x reduction scheme for high values of char addition (ie, above 40%). It is recommended that future work be aimed at using high surface area char and increasing the stability of high char content fuels by studying the effect of parameters such as air preheat, burner geometry, and gas or oil assist. The effect of different types of char and injection location (temperature) on the effluent NO_x concentration should also be investigated.

The increase in effluent NO_x concentration with low levels of char blended with coal is not well understood. It is recommended that fuel nitrogen partitioning studies be performed to determine the separate relationships between volatile and char nitrogen on effluent NO_x. It is also recommended that near burner combustion tests be performed to study the fate of NO_x precursors in coal and coal-char flames.

ACKNOWLEDGMENTS

This work was sponsored by the Illinois Department of Energy and Natural Resources through the Illinois Coal Development Board and Illinois Clean Coal Institute, and the United State Department of Energy.

REFERENCES

1. Levy, J. M., L. K. Chan, F. Sarofim, and J. M. Beer, "NO/Char Reactions at Pulverized Coal Flame Conditions," 18th Symposium (International) on Combustion, The Combustion Institute, Pittsburgh, PA, p. 111 (1981).
2. Pershing, D. W. and J.O.L. Wendt, "Relative Contributions of Volatile Nitrogen and Char Nitrogen to NO_x Emissions from Pulverized Coal Flames," Ind. Eng. Chem. Process Des. Dev., 18,1 (1979).
3. Glass, J. W., and J.O.L. Wendt, "Mechanisms Governing the Destruction of Nitrogenous Species During the Fuel Rich Combustion of Pulverized Coal," 19th Symposium (International) on Combustion, The Combustion Institute, Pittsburgh, PA, p. 1243 (1982).
4. Pohl, J. H., and A. F. Sarofim, "Fate of Coal Nitrogen During Pyrolysis and Oxidation," EPA Symposium on Stationary Source Combustion, Atlanta, GA, (September, 1975); Proceedings of the Stationary Source Combustion Symposium, I, EPA 600/2-76-152a, June (1976).
5. Heap, M. P., T. M. Lowes, R. Walmsley, H. Bartelds, and P. LeVaguerese, "Burner Criteria from NO_x Control: Influence of Burner Variables on NO_x in Pulverized Coal Flames," U.S.E.F.T.S., EPA-600/2-76-061a (1976).
6. Pershing, D. W., and J. O. L. Wendt. 1977. "Pulverized Coal Combustion: The Influence of Flame Temperature and Coal Composition on Thermal and Fuel NO_x." Paper presented at the 16th International Symposium on Combustion, p. 389, Pittsburgh, PA.
7. Shelef, M and K. Otto, "Simultaneous Catalytic Reaction of O_2 and NO with CO and Solid Carbon", Jrn of Coll. and Interface Science, 31:1,73 (1969).
8. Song, Y.H., D.W. Blair, V.J. Siminski, and W. Bartok, "Conversion of Fixed Nitrogen to N_2 in Rich Combustion," Eighteenth Symposium (International) on Combustion, The Combustion Institute, Pittsburgh, PA, 53 (1981).
9. Glass, J. W., and J.O.L. Wendt, "Mechanisms Governing the Destruction of Nitrogenous Species During the Fuel Rich Combustion of Pulverized Coal," Western States Section/Combustion Institute, University of Utah, Salt Lake City, UT (1982).
10. Wendt, J.O.L., D. W. Pershing, J. W. Lee, and J. W. Glass, "Pulverized Coal Combustion: NO_X Formation Mechanisms Under,Fuel Rich and Staged Combustion Conditions," 17th Symposium (International) on Combustion, The Combustion Institute, Pittsburgh, PA, p.77 (1979).
11. Glass, J.W. and J.O.L. Wendt, "Advanced Staged Combustion Configurations for Pulverized Coal: Fuel Nitrogen Conversion During Fuel Rich Combustion of Pulverized Coal and Char," U.S. Department of Energy Topical Report No. 1, DOE/ET?15184-1152 (1981).
12. Sheppard, W.M., "A Kinetic Study of the Reaction of Nitric Oxide and Active Carbon, " Doctoral Dissertation, Clemson University.
13. Eatough, C.N., Controlled Profile Reactor Design and Combustion Measurements, Ph.D. Dissertation, Department of Mechanical Engineering, Brigham Young University, Provo, UT, 1991.
14. Boardman, R.D., C.N. Eatough, G.J. Germane, and L.D. Smoot, "Comparison of Measurements and Predictions of Flame Structure and Thermal NO_x in a Swirling, Natural Gas Diffusion Flame," Combustion Science and Technology, vol. 93, 1993, pp. 193-210.
15. Zel' dovich, Y.B., P.Y. Sadovnikov, and D.A. Frank-Kamentskii, "Oxidation of Nitrogen in Combustion," (translated by Shelef), Academy of Sciences of USSR, 1947.
16. Smoot, L.D., (Editor), Fundamentals of Coal Combustion for Clean and Efficient Use, Elsevier, New York, NY, 1993.
17. Chen, J.C., and S. Niksa, "Suppressed Nitrogen Evolution From Coal-Derived Soot and Low-Volatility Coal Chars," 24th Symposium, International, on Combustion, The Combustion Institute, Pittsburgh, PA, 1992, pp. 1269-1276.

Table 1. Proximate analyses of fuels (wt %, dry basis)

	Coal	Blend 1	Blend 2	Blend 3	Blend 4	Char
moisture	12.5	10.4	8.8	6.4	11.7	2.11
volatile matter	38.0	35.6	32.9	27.3	34.7	16.2
fixed carbon	49.6	51.3	53.7	58.3	54.2	67.1
H-T ash	12.4	13.2	13.4	14.4	11.1	16.7

* minus 200 mesh samples

Table 2. Analysis of fuels (wt%, dry basis)

	Coal	Char	Blend 1	Blend 2	Blend 3	Blend 4
Nitrogen	1.33	1.46	1.30	1.34	1.42	1.29
Sulfur	3.41	2.83	3.31	3.27	3.09	3.17
Btu/lb	12,182		12,138	12,169	12,047	12,480

Table 3. Pore area and pore volume data

	Coal	Char	Activated Carbon
Pore area (m^2/g)	18.8	15.71	1012
Pore volume (cc/g)	0.0342	0.145	

Table 4. Combustion Test Matrix.

Test No.	Description	Fuel Feed Rate (kg/hr)	Air Feed Rate (kg/hr)	Stoichiometric Ratio[1]
1	Coal	11.4	96.4	1.08
2	Coal	11.4	110.0	1.24
3	Coal	11.4	93.5	1.05
4	Hydrated Lime Injection	11.4	96.4	1.08
5	Activated Carbon Injection	11.4	96.4	1.08
6	Coal - 25% Char	11.4	100.9	1.09
7	Coal - 25% Char	11.4	93.5	1.01
8	Coal - 25% Char	11.4	114.5	1.23
9	Coal - 25% Char	18.2	160.1	1.08
10	Coal - 25% Char	11.4	79.4	0.85
11	Coal - 12.5% Char	11.4	100.9	1.08
12	Coal - 12.5% Activated Carbon	11.4	102.0	1.09
13	Coal - 50% Char	11.4	103.2	1.08

[1] Stoichiometric ratio is actual A/F divided by stoichiometric A/F.

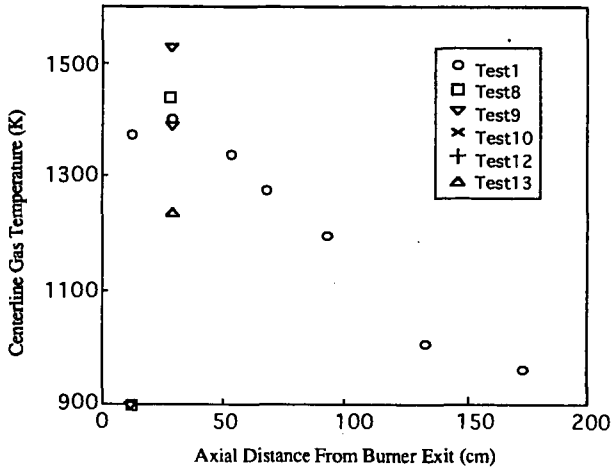

Figure 1. Gas temperature measurements for selected CPR combustion tests.

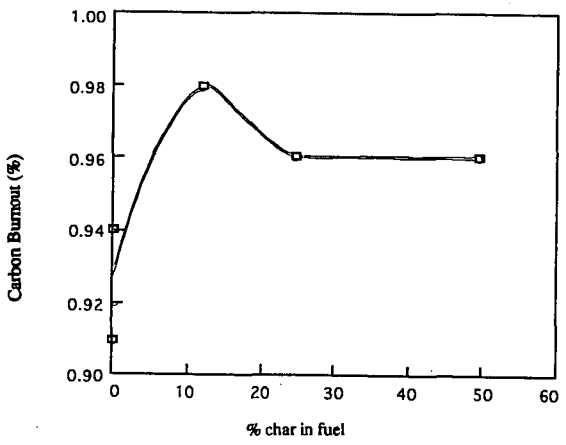

Figure 2. Effect of char concentration in the fuel on carbon burnout.

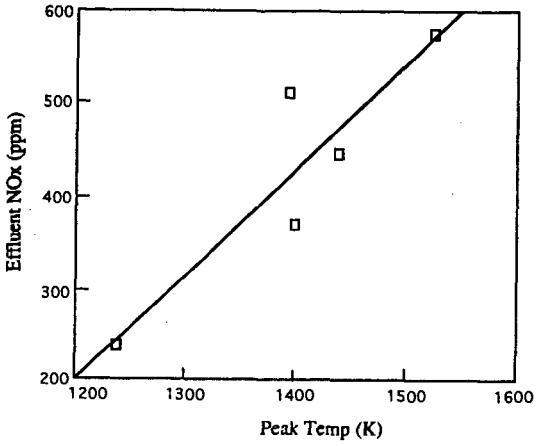

Figure 3. Relationship of peak flame temperature with measured effluent Nox concentration.

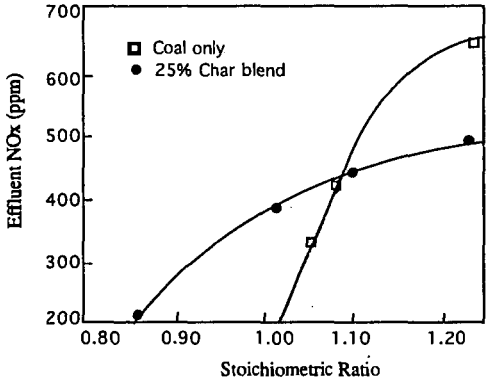

Figure 4. Effect of stoichiometric ratio on effluent Nox (Fuel feed 11.4 kg/hr).

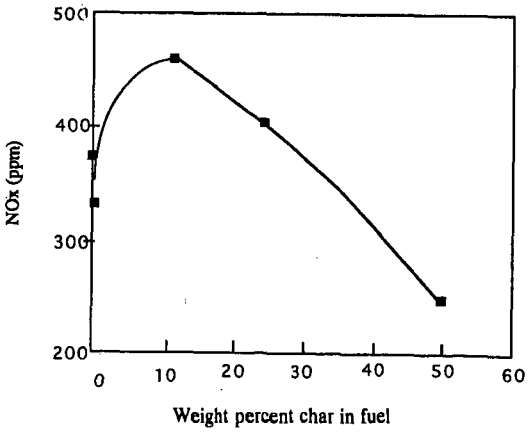

Figure 5. Effect of char concentration on effluent Nox emissions (corrected for burnout and thermal Nox; fuel feed 11.4 kg/hr, SR = 1.08).